

A NOVEL GENE-BASED THERAPY FOR GLAUCOMA

From discovery to preclinical development



**Trinity
College
Dublin**

The University of Dublin

A thesis submitted to the University of Dublin for
the degree of Doctor of Philosophy

Jeffrey O'Callaghan

February 2018

Declaration

I declare that this thesis has not been submitted as an exercise for a degree at this or any other university and it is entirely my own work, except where otherwise stated.

I agree to deposit this thesis in the University's open access institutional repository or allow the Library to do so on my behalf, subject to Irish Copyright Legislation and Trinity College Library conditions of use and acknowledgement.

Signed

Jeffrey O'Callaghan

February 2018

Acknowledgements

Foremost, I would like to thank my supervisor, Professor Pete Humphries for giving me the opportunity to undertake this project, the guidance throughout, and the support to see it through. I would also like to thank Dr. Mathew Campbell, Dr. Lawrence Tam, Dr. Ester Reina Torres, Dr. Sophie Kiang, and Dr. Marian Humphries for their assistance with various techniques and experimental design. I am grateful to our collaborators Charles Murray, Dave Flynn, Caroline Woods, Professor Darryl Overby, Professor Dan Stamer, Professor Colm O'Brien, Professor Elke Lütjen-Drecoll, Dr. Cassandra Flügel-Koch, Dr. Kristin Perkumas, and Dr. Joseph Sherwood, without whom very few techniques would have been possible.

Special thanks are reserved for Dr. Paul Cassidy and Dr. Darragh Crosbie, who were of paramount significance in the progression of this project, from developing experimental plans to assisting with weekend animal work, and for making this experience more enjoyable overall. I am thankful for all those in the lab, the extended department, and close friends for their contributions to my sanity. I am especially appreciative of my family who have been a limitless source of support and motivation, and of my girlfriend Orla for her unwavering encouragement and remarkable ability to put up with me.

Funding

Glaucoma research at the Ocular Genetics Unit at the University of Dublin, Trinity College has been supported by the European Research Council [ERC-2012-AdG 322656-Oculus], together with an equipment grant from Science Foundation Ireland [12/ERC/82539]. Non-human primate studies were conducted with the assistance of Enterprise Ireland and the St. Kitts Biomedical Research Foundation.

Publications

Arising from this work

- O’Callaghan, J., *et al.* (2017) Open-angle glaucoma: therapeutically targeting the extracellular matrix of the conventional outflow pathway. *Expert Opinion on Therapeutic Targets*, **21**, 1037-1050 (Appendix 3).
- O’Callaghan, J., *et al.* (2017) Therapeutic potential of AAV-mediated MMP-3 secretion from corneal endothelium in treating glaucoma. *Human Molecular Genetics*, **26**, 1230-1246 (Appendix 4).
- O’Callaghan, J., *et al.* (2018) Intracameral Injection of AAV2.9 for Gene Delivery to Corneal Endothelium *in press* (Appendix 5).

Related contributions

- Tam, L.C., *et al* (2017) Enhancement of Outflow Facility in the Murine Eye by Targeting Selected Tight-Junctions of Schlemm’s Canal Endothelia. *Scientific Reports*, **7**, 40717 (Appendix 6).
- Campbell, M., *et al* (2018) Manipulating ocular endothelial tight junctions: Applications in treatment of retinal disease pathology and ocular hypertension. *Progress in Retinal and Eye Research*, **62**, 120-133 (Appendix 7).

Related patents

- Glaucoma gene therapy, *application under review*.

Contents

Declaration.....	I
Acknowledgements.....	II
Funding	II
Publications.....	III
Contents	IV
Glossary of Abbreviations	X
Summary	XIII
Chapter 1: Choosing a Target	1
1.1 Introduction.....	1
1.2 Anatomy of the eye.....	2
1.3 Aqueous humour flow dynamics	5
Aqueous humour production.....	6
Outflow resistance generation at the outflow tissues.....	7
1.4 Glaucoma	11
Clinical Presentation	12
Types of glaucoma.....	13
Epidemiology and risk factors	15
Glaucoma as a neurodegenerative disease	16
Genes associated with POAG	18
1.5 The ECM as a therapeutic target.....	20

ECM composition within the outflow tissues	20
ECM in outflow resistance	24
Modulation of ECM turnover	25
1.6 Traditional treatments in the management of glaucoma	26
Topical medications.....	26
Surgical interventions	28
1.7 Emerging medications	30
New classes of drug.....	30
On the development of genetic therapies	35
1.8 Conclusion.....	37
1.9 Aims	40
Chapter 2: Selecting a Viable Therapeutic	41
2.1 Introduction	41
2.2 Results	43
SC monolayer permeability in response to cytokines	43
Cytokines modulate expression of MMPs.....	45
The cytokine to MMP signalling cascade	51
MMP in Aqueous Humour	52
2.3 Discussion.....	52
Chapter 3: Validation as a Potential Therapy.....	55
3.1 Introduction	55
MMP structure and function.....	55

Therapeutic design	56
AAV vector design and delivery.....	57
3.2 Results.....	60
Effects of glaucomatous aqueous humour on SC endothelial and TM cell monolayers.	60
Treatment of outflow cell monolayers with recombinant human MMP-3 increases permeability with concomitant reductions in TEER.....	63
Active, recombinant murine MMP-3 increases outflow facility in murine eyes	65
Treatment of SCEC and HTM monolayers with active recombinant human MMP-3 induces remodelling and degradation of ECM components	66
Intracameral inoculation of AAV-2/9 expressing a CMV-driven MMP-3 gene efficiently transduces corneal endothelium and results in elevated levels of MMP-3 in aqueous humour	70
Intracameral inoculation of AAV-2/9 expressing an MMP-3 gene increases outflow facility and reduces IOP in murine eyes	74
Controlled periodic activation of MMP-3.....	78
Ultrastructural analysis of AAV-MMP-3 treated eyes	79
Latanoprost increases outflow facility using iPerfusion	82
3.3 Discussion	83
Chapter 4: Efficacy of AAV-iMMP-3 in Glaucoma Models.....	91
4.1 Introduction.....	91
Glaucoma Models	91
Dexamethasone model	93
Myocilin model.....	94

Non-human primate.....	95
4.2 Results	96
Validation of Dexamethasone as a model	96
Effect of MMP-3 on IOP in a DEX model.....	96
Effect of DEX and MMP-3 on Facility	100
Ultrastructural analysis of Dexamethasone-treated eyes.....	102
Effect of AAV-iMMP-3 on IOP in a MYOC model.....	104
Effect of AAV-iMMP-3 on outflow facility in a MYOC model.....	107
AAV2/9-eGFP transduction of the corneal endothelium in a NHP	110
4.3 Discussion.....	114
Chapter 5: Conclusion	118
Discussion of AAV-MMP-3 as a potential therapy.....	118
Comments on procedures and experimental design	121
Clinical relevance	123
Future directions and optimisation	125
Chapter 6: Materials and Methods.....	128
6.1 Cell culture.....	128
6.2 Animals.....	129
6.3 Patient aqueous humour samples	130
6.4 Transendothelial Electrical Resistance (TEER) measurement	131
6.5 Permeability assessment by FITC-Dextran flux.....	131
6.6 RT-PCR	132

6.7	Fluorescent-activated cell sorting (FACS)	133
6.8	Cell Viability	133
6.9	Immunocytochemistry	134
6.10	Western Blotting	135
6.11	Zymography.....	136
6.12	AAV.....	137
6.13	Intracameral Injection	138
6.14	Immunohistochemistry (murine eyes)	139
6.15	Immunohistochemistry (NHP eyes)	140
6.16	Viral purity and estimations of titre.....	141
6.17	Total MMP-3 quantification	142
6.18	MMP-3 Activity Assay (FRET)	143
6.19	Measurement of Outflow Facility.....	144
	IOP	145
6.20	IOP method for Chapter 3	145
6.21	IOP method for Chapter 4	145
6.22	Analysis of central corneal thickness	147
6.23	Transmission Electron Microscopy (TEM)	148
6.24	Osmotic Pump Implantation	150
6.25	Statistical Analysis.....	151
	References	152
	Appendix	200

Appendix 1: Supplementary Figures	200
Appendix 2: MATLAB code for IOP analysis.....	203
Appendix 3: Open-angle glaucoma: therapeutically targeting the extracellular matrix of the conventional outflow pathway	
Appendix 4: Therapeutic potential of AAV-mediated MMP-3 secretion from corneal endothelium in treating glaucoma	
Appendix 5: Intracameral Injection of AAV2.9 for Gene Delivery to Corneal Endothelium	
Appendix 6: Enhancement of Outflow Facility in the Murine Eye by Targeting Selected Tight-Junctions of Schlemm's Canal Endothelia	
Appendix 7: Manipulating ocular endothelial tight junctions: Applications in treatment of retinal disease pathology and ocular hypertension	

Glossary of Abbreviations

AAV	Adeno-associated virus
AAV-eGFP	AAV constitutively expressing GFP
AAV-iGFP	Inducible AAV expressing GFP
AAV-iMMP-3	Inducible AAV expressing MMP-3
AAV-MMP-3	AAV constitutively expressing MMP-3
AAV-NULL	AAV expressing a nonsense sequence
ACAID	Anterior chamber associated immune deviation
ADAM	A disintegrin and metalloproteinase
ADAMTS	A disintegrin and metalloproteinase with thrombospondin motifs
AH	Aqueous Humour
AV	Adenovirus
BSA	Bovine serum albumin
CAT	Cataract
CI	Confidence interval
CP	Ciliary process
ECM	Extracellular matrix
ELISA	Enzyme-linked immunosorbent assay
ER	Endoplasmic reticulum
FA	Focal adhesion
FACS	Fluorescent-activated cell sorting
FBS	Fetal bovine serum
FD	FITC-conjugated dextran

FITC	Fluorescein isothiocyanate
FRET	Fluorescent resonance energy transfer
GFP	Green fluorescent protein
GWAS	Genome-wide association studies
HPRA	The health products regulatory authority
HSV	Herpes simplex virus
HTM	Human trabecular meshwork
IL-1 α	Interleukin 1 alpha
IL-1 β	Interleukin 1 beta
IOP	Intraocular Pressure
IW	Inner wall
JCT	Juxtacanalicular
L-ITR	Left inverted terminal repeat
MAD	Median absolute deviation
MMP	Matrix metalloproteinase
MMP-1	Matrix metalloproteinase 1
MMP-2	Matrix metalloproteinase 2
MMP-3	Matrix metalloproteinase 3
MMP-9	Matrix metalloproteinase 9
MYOC (-)	Negative for the myocilin transgene
MYOC (+)	Positive for the myocilin transgene
MYOC	Myocilin
NHP	Non-human primate
ONH	Optic nerve head
P	Pressure
PACG	Primary angle-closure glaucoma

Papp	Apparent permeability
PBS	Phosphate-buffered saline
POAG	Primary open-angle glaucoma
Q	Flow
RFU	Relative fluorescent unit
R-ITR	Right inverted terminal repeat
ROCK	Rho-associated protein kinase
SC	Schlemm's Canal
scAAV	Self-complementary adeno-associated virus
SCEC	Schlemm's canal endothelial cells
SLT	Selective laser trabeculoplasty
TEER	Trans-endothelial electrical resistance
TEM	Transmission electron microscopy
TIGR	Trabecular meshwork glucocorticoid response
TIMP	Tissue inhibitor of metalloproteinase
TJ	Tight junction
TM	Trabecular Meshwork
TNF- α	Tumor necrosis factor alpha
TYR437HIS	Mutation of tyrosine to histidine at point 437
WT	Wild type
Y437H	Mutation of tyrosine to histidine at point 437

Summary

Glaucoma is one of the major causes of blindness worldwide, currently estimated to affect ~70 million people. Glaucoma is a multifactorial condition characterised by elevated intraocular pressure, reduced aqueous humour outflow from the eye, retinal ganglion cell death, reduced visual fields and, if left untreated, blindness. First line clinical management of glaucoma is the use of topical pressure-reducing eye drops. These formulations have been available as a treatment for glaucoma since the 1970's, and whilst they have been slowly improving in efficacy and safety over the years, they have never been side-effect free. In addition, a significant proportion of patients are sub-optimally responsive to these treatments, which may in part be attributed to patient compliance. As a second line of treatment, a variety of surgical interventions have been developed. In an attempt to meet the continuing demand for more effective therapies, several new treatments for glaucoma are currently undergoing clinical trials. These new therapies primarily target the conventional outflow pathway of aqueous removal, contrary to traditional medications. In response to the as yet unmet need for more effective glaucoma treatment options, concepts for genetic therapies are beginning to emerge to challenge molecular medications in the hope of superseding them with greater efficacy and more precise treatment targets.

The premise of this body of work was to design such a genetic-based therapeutic approach to reduce the early phenotypic manifestations of glaucoma, namely elevated intraocular pressure and diminished outflow facility. The tissues of the conventional outflow pathway were deemed to be the most attractive target for therapeutic intervention, based on the sites of outflow resistance generation and by the mechanisms of current medications (Chapter 1). MMP-3 was identified as an attractive protein molecule for secretion into the anterior chamber due to its upregulation in concentration, but not activity, in response to cytokine imbalance and for the observed increases in cell monolayer permeability after treatment (Chapter 2/3). A mechanism

of delivery and proof of concept was ascertained *in vivo* to assess the viability of such a therapeutic approach (Chapter 3). Intracameral inoculation of AAV-2/9 containing a CMV-driven MMP-3 gene (AAV-MMP-3) into wild type mice resulted in efficient transduction of corneal endothelium and an increase in aqueous concentration and activity of MMP-3. Most notably, AAV-mediated expression of MMP-3 increased outflow facility and decreased IOP through ultrastructural changes in the outflow tissues. Further exploration of therapeutic potential was assessed in well-characterised models of glaucoma, along with the first steps to investigating feasibility in a primate species (Chapter 4). Controlled expression using an inducible promoter activated by topical administration of doxycycline achieved reduced IOP with a concomitant increase in outflow facility in these models. Chapter 5 consists of the materials and methodology used to facilitate this project.

Together, the following data shows that the AAV-mediated induction of MMP-3 expression in the corneal endothelium can reduce ocular hypertension and increase outflow facility by way of extracellular matrix degradation at the outflow tissues in glaucomatous murine models. These results indicate that periodic induction, via use of an eye drop, could have therapeutic potential for those cases of glaucoma that are sub-optimally responsive to conventional pressure-reducing medications.

Chapter 1

Choosing a Target

1.1 Introduction

The eye provides us with probably the most important of our senses: sight. It is the most complex sensory organ in the body and is involved in the perception of most sensory impressions, reflecting that vision is the most developed sense in humans. Humans are reliant on sight as the dominant sense and are very capable visual sensors due the intricacy of both the eye and the brain. The eye is considered an extension of the brain, facilitating learning, memory and understanding of the surrounding world. It is therefore unsurprising that loss of sight results in a severe handicap to a species so reliant upon it. Difficulties including depression, social contact, and academic performance are only some of the correlated psychosocial implications of blindness or impaired vision. It is essential that development of treatments progress for the multitude of pathologies leading to vision loss. Preservation of sight is crucial, as vision is central to our quality of life, from keeping our minds sharp to providing awareness of the dangers around us.

1.2 Anatomy of the eye

The eye can be largely divided into three major segments: the anterior, posterior and vitreous chambers (Figure 1.1). The anterior chamber is characterised as the area from the cornea on its anterior limit to the iris on its posterior limit, and the posterior chamber consists of the narrow space between the suspensory ligaments of the lens and the peripheral part of the iris. The cornea consists of collagen fibres arranged in such a way that it remains translucent, refracting light entering the eye onto the lens. The iris regulates light entering the eye, with muscular contractions determining the size of the pupil, the circular opening in the centre of the iris where light passes through to the lens. The crystalline lens is fixed behind the iris by suspensory ligaments and fibres and is involved in the focusing of light onto the retina. The anterior chamber is entirely avascular and relies on aqueous humour (AH) for nutrients. The AH fills the space of the anterior chamber providing structural support to the eye by maintaining intraocular pressure (IOP) and is produced at a high rate of turnover at the ciliary body. Where the cornea meets the iris is referred to as the iridocorneal angle and is the site of the outflow tissues. This comprises the Schlemm's canal (SC), trabecular meshwork (TM), collector channels and episcleral veins, and facilitates drainage of the AH from the eye.

The posterior pole most notably contains the lens and the retina, supplied by the choroid layer of blood vessels, and is also fluid filled by the vitreous humour. The sclera forms the protective, external white surface of the vitreous segment, and binds the six extraocular muscles required for rotating the eye about its axes. Lining the rear of the eye lies the retina, composed of the photoreceptors and associated neural cells necessary to convert light into an electrical signal. The macula is a region at the centre of the retina, containing photoreceptors responsible for high acuity central vision perception, and the fovea forms a small indentation at the centre of the macula, containing the greatest concentration of cone cells: the photoreceptor subtype responsible for colour vision.

Anatomy of the Eye

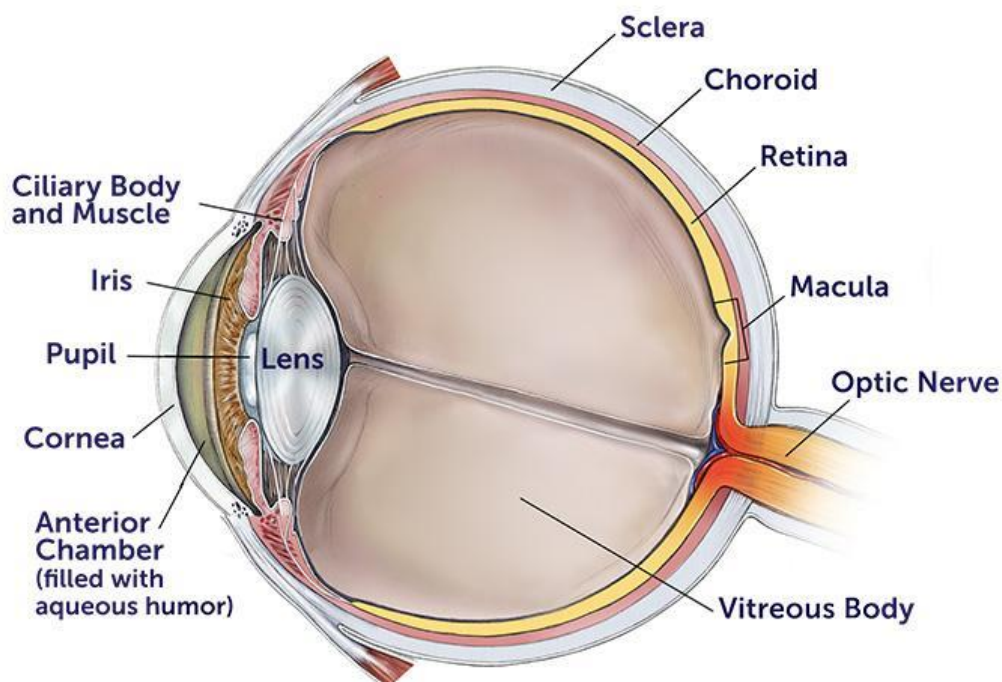


Illustration by Bob Morreale, provided courtesy of the BrightFocus Foundation



Figure 1.1: Anatomy of the eye

The anterior chamber (left) and vitreous body (right) of the human eye are depicted above, with the major tissues labelled. Image taken from BrightFocus Foundation.

The retina surrounds the interior surface of the vitreous chamber and is the primary ocular tissue responsible for vision. As part of the central nervous system, the retina contains a neural network responsible for transmitting the electrical activity of the photoreceptors to the brain in the form of action potentials. Light is absorbed by the pigments in the first neuronal cell type, the photoreceptors, of which there are rods and cones, inducing a cascade of events in the outer nuclear layer releasing neurotransmitters that are received by bipolar cells at their synapses in the outer plexiform layer. The cell bodies of the bipolar cells in the inner nuclear layer pass on

the electrical signal to the ganglion cells at the inner plexiform layer. The large axonal bodies of the ganglion cells form the optic nerve which relays the sensory information to the brain. Horizontal and amacrine cells allow lateral interactions across their respective plexiform layer allowing the system to maintain its sensitivity to different contrasts over a range of light intensities (1) (Figure 1.2).

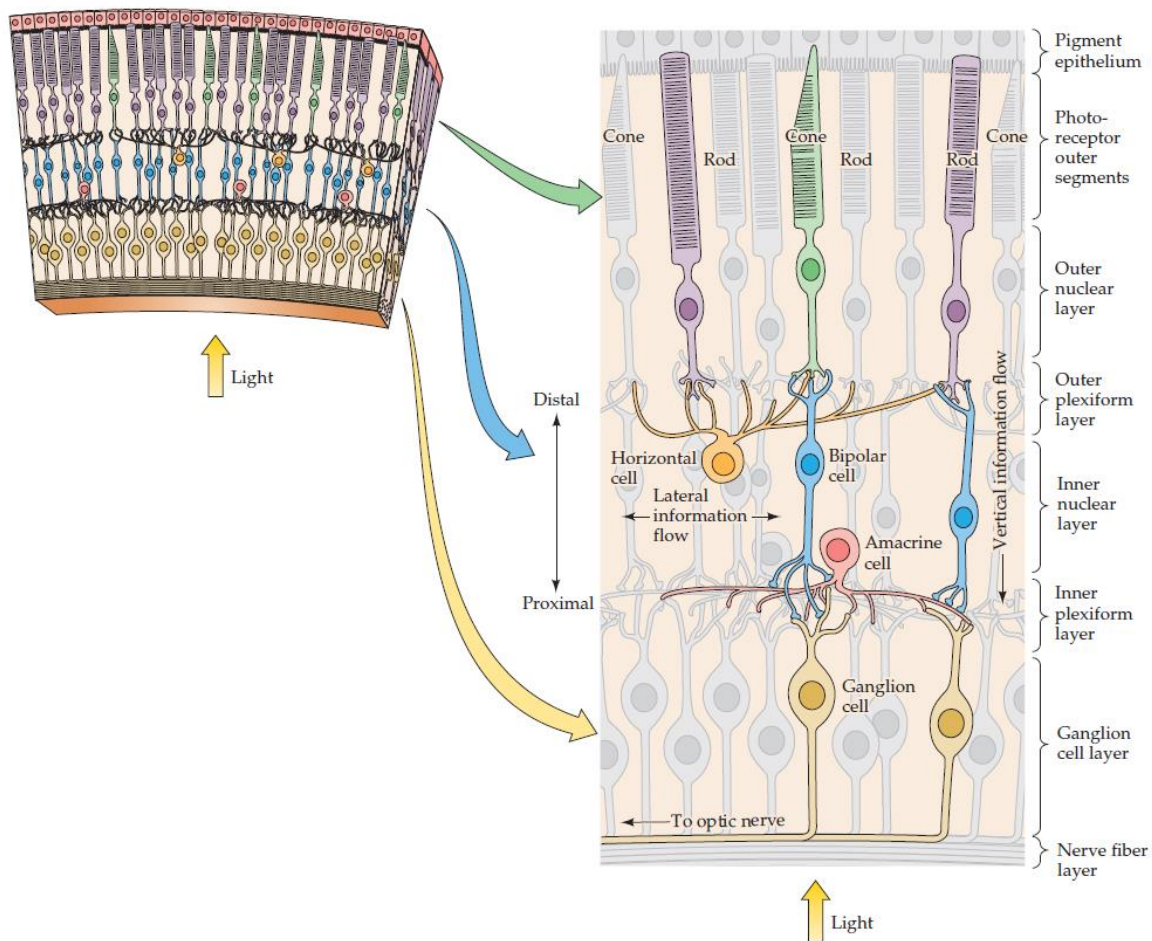


Figure 1.2: The structure of the retina

Section of the retina showing light entering from the anterior direction. The overall structure of the retinal circuitry is shown with the 5 neural cell types in their relative layers. Light is perceived by the photoreceptor and this information is relayed to the brain through the bipolar and ganglion cells. Lateral interactions are mediated by the horizontal and amacrine cells. Image taken from (1).

1.3 Aqueous humour flow dynamics

The AH is a key component of the anterior chamber, substituting a vascular system that supplies nutrients, growth factors and neurotransmitters, and clears metabolic byproducts as part of its primary homeostatic function (2). AH plays an important role in maintaining the structural integrity of the anterior chamber by sustaining IOP, which is generated through a balance of AH production and resistance to its removal from the eye. AH secreted from the ciliary body moves from the posterior chamber through the pupil and into the anterior chamber. From here it crosses the TM, its movement being facilitated by a pressure gradient, and is then directed towards the SC lumen. This pathway, known as the conventional outflow pathway, accounts for up to 90% of human aqueous drainage, especially in the elderly (2-4). AH enters the SC either transcellularly, through pores in giant vacuoles formed in the endothelial cells lining the inner wall of the canal, or paracellularly, through the pores between SC cells regulated by the inter-endothelial junctions (5-7). AH then exits the lumen through collector channels into aqueous veins that discharge into the episcleral venous circulation. AH can also leave the eye via the unconventional pathway, where it flows laterally through the TM, directly into the interstitial spaces of the ciliary muscle bundles into the supraciliary and suprachoroidal space (Figure 1.3).

In this pathway, transscleral drainage accommodates the removal of large proteins, while small molecules and water exit across the sclera by diffusion, to be absorbed by orbital veins (uveoscleral pathway). Osmotic forces drive AH removal in the choroid, and the uveovortex veins drain fluid into peripheral blood circulation (uveovortex pathway) (8). Both AH production and its clearance, modulated by changes in resistance at the outflow tissues, are central to the homeostasis of IOP, and any disruption to this equilibrium can lead to pathogenesis (9).

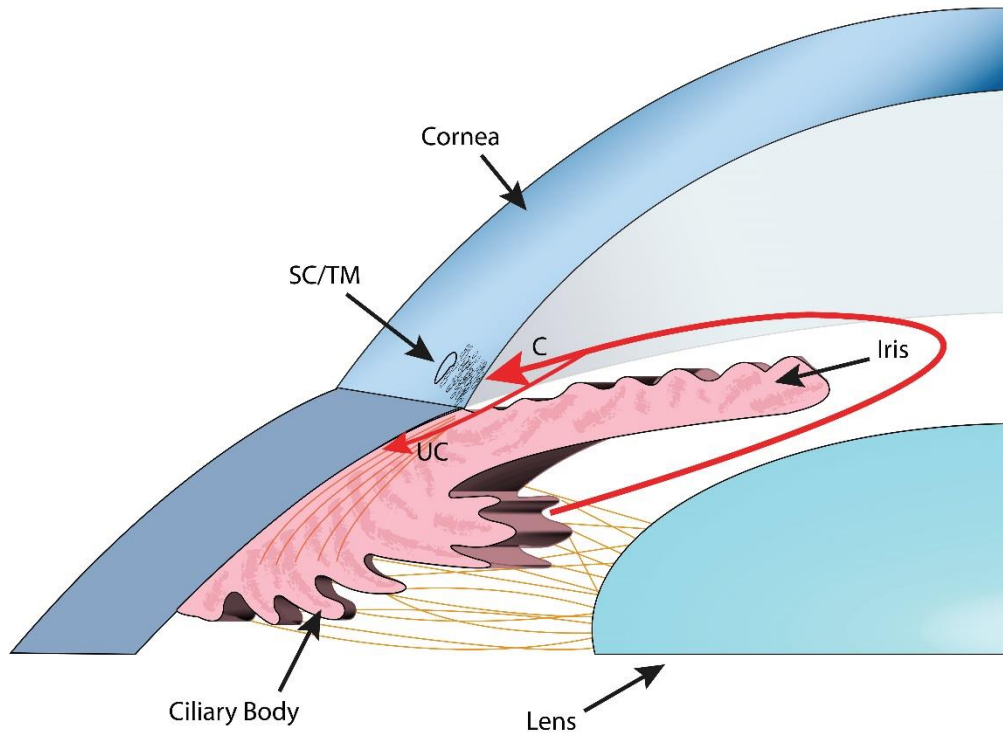


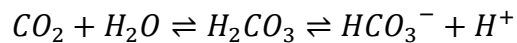
Figure 1.3: The route of aqueous humour.

Aqueous humour is secreted by the ciliary body and moves through the pupil, around the iris. A pressure gradient directs it toward the SC lumen, where most aqueous egresses (large, red arrow). This is termed the conventional pathway (C). The unconventional pathway (UC) involves the removal of aqueous through the fibres of the ciliary body into the supraciliary and suprachoroidal spaces. Image adopted from (10), O'Callaghan et al.

Aqueous humour production

AH formation occurs at the ciliary processes, consisting of layers of epithelial cells, a stroma and a capillary supply. The large surface area of the non-pigmentary epithelial cells that protrude into the posterior chamber are thought to be the site of AH production (11). Formation and secretion arises from three major processes: diffusion, ultrafiltration and active secretion. Diffusion involves the passive movement of solutes and ions across tissue membranes between the capillaries and posterior chamber. Ultrafiltration refers to movement of water and water soluble substances in response to a pressure gradient, where hydrostatic difference between

capillary pressure and IOP favours fluid movement into the ciliary stroma (12). These passive processes lead to the accumulation of blood plasma in the stroma, from which AH is derived. Active secretion is responsible for 80-90% of total AH formation (13). This consists of selective transcellular movement of ions across a concentration gradient, through the blood-aqueous barrier comprising junctional complexes that limit diffusion of ions and small solutes through paracellular spaces (14). Aquaporins (water channels) and protein transporters aid in secretion across an insufficient pressure gap. Carbonic anhydrase is an essential component of AH secretion, mediating the transport of bicarbonate across the ciliary epithelium according to the following equation:



This reversible hydration of carbon dioxide to form bicarbonate affects sodium ions, which are integral to supplying aquaporin channels with energy (15). The result is an AH with inorganic and organic ions, carbohydrates, urea, amino acids, proteins, oxygen, carbon dioxide, and fundamentally, water (2). AH has a 200-fold less protein concentration than that of plasma, reflected in its optical clarity and similar refractive index to that of water (1.335 vs 1.33).

Outflow resistance generation at the outflow tissues

The exact locus of AH outflow resistance has not been fully determined; however different structures in the anterior chamber have been confirmed to contribute to total resistance. These structures comprise the outflow tissues, most notably the SC and TM in the iridocorneal angle. The TM is divided into three regions: the uveal meshwork, the corneoscleral meshwork and the juxtacanalicular region (JCT) or cribriform region. The TM is a network of beams composed of connective tissue (lamellae) on which TM cells reside, forming irregular intertrabecular fenestrations (16). Lamellae are found on both the uveal and corneoscleral meshworks, the latter

also containing layers of TM cell-covered perforated sheets of fibres. Intertrabecular spaces become smaller in this region. These layers act as pre-filters, removing debris from AH before it enters the less porous JCT and SC (17). Numerous openings occur in these meshworks, with pores gradually getting smaller toward the distal layers of the TM (18), however the spaces in this region are so large that resistance is negligible (19). The JCT region, adjoining the innermost layer of the TM and the inner wall of the SC comprises cells resting on a basement membrane, surrounded by an amorphous ECM dispersed with open spaces, allowing aqueous egress (20, 21). This layer measures 2-20 μm thick and consists of discontinuous cell layers embedded in an ECM (22). The SC itself is a unique vessel in that it incorporates both blood and lymphatic endothelial cell phenotypes (23). It is a continuous endothelial layer on a discontinuous basement membrane that facilitates flow in the basal to apical direction, differing from other vessels (18). It is also distinct from other vessels in its ability to form giant vacuoles under high pressure and its unique tight junction profile including claudin-11 (24). These features have allowed for new therapeutic opportunities to arise, such as the use of the VEGF family in outflow facility modulation (24, 25). The SC contributes to resistance through its cell-cell contacts mediated by tight junctions. It also has one of the highest hydraulic conductivities in the body (26), explained through ultrastructural visualisation of the inner wall, shown to contain 1000 pores/ mm^2 (27).

A synergistic model of resistance generation has been proposed, in which both the JCT and SC are the primary contributors to resistance. This 'funnelling model' (Figure 1.4) describes AH converging on the discrete pores in the SC inner wall as it leaves the much wider JCT. This non-uniform flow results in an increased hydraulic resistance, predicted to be a 15-fold increase when both pore density and giant vacuoles are considered (18, 28). Calculating flow through this model suggests that the funnelling area is greater than that of giant vacuoles, indicating that the discontinuities of the basement membrane may be a controlling factor for pore density.

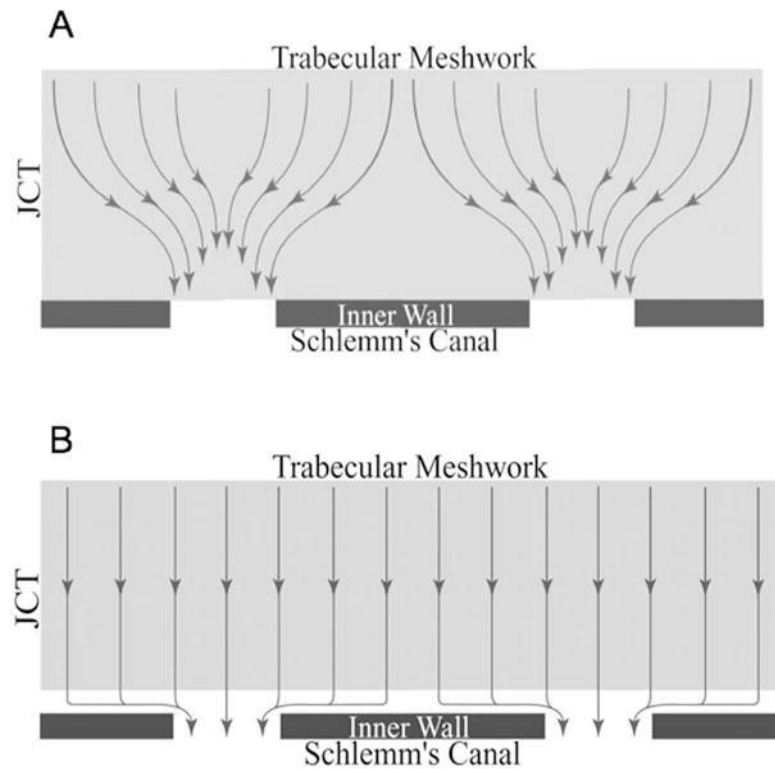


Figure 1.4: The Funnelling Model

(A) This schematic describes the phenomenon of funnelling through the JCT and the non-uniformly dispersed pores of the SC. (B) Funnelling is proposed to be uniform through the JCT once separation of the JCT-SC tether occurs. Image taken from (18).

If the JCT and SC inner wall were to separate, a uniform flow would be observed through the JCT due to the loss of the hydrodynamic influence of the SC. This effect known as ‘washout’ decreases outflow resistance over time in experimental studies, supporting the concept of the funnelling model (29). AH outflow is described as segmental, or non-uniform about the TM, as shown by tracer studies (30-32). Regions of high flow and low flow are present, ranging from hundreds of micrometres in size to millimetres, such that flow only occurs in a fraction of the available outflow tissue. The tethering of the JCT to the SC may also explain these segmental outflow patterns, with flow preferentially reaching regions of detachment. Treatment with a rho kinase inhibitor was shown to convert segmental outflow patterns to uniform flow across the TM, with concomitant increase in JCT-SC separation (33).

Downstream of the inner wall resides the lumen of the SC, collector channels, the aqueous veins and the system of episcleral and ocular veins, finally connecting to general circulation. Located at the apex of the iridocorneal angle, the SC lumen is a flattened circular vessel with an average meridional diameter of 233 μm in humans (34). The aqueous veins, averaging 50 μm , are distributed non-uniformly and occur most frequently in the inferior nasal quadrants (35). The lumens of these vessels are connected for direct flow routes. Stratification of AH and blood occurs at transition zones at the episcleral veins, visible on the surface of the conjunctiva (36). The composition of blood and AH changes with IOP and is sometimes an indicator of IOP modulation (37). At lower IOP, the cross-sectional area of the SC lumen is too large to generate any significant outflow resistance. While canal collapse is seen to occur at high IOP, the resistance increase generated by lumen narrowing is not nearly as high as that observed in glaucomatous eyes. This indicates that although canal collapse could worsen the glaucomatous condition (increased outflow resistance), it cannot be causative of it (38). Regions of high flow are further concentrated at collector channels, however as is the case with the SC lumen, collector channels should not contribute significantly to resistance as their relatively large diameters suggests that resistance is again negligible (26, 39). After trabeculotomy 25% of outflow resistance remains, implicating the collector channels as contributors to resistance generation, however such remaining resistance is not thought to be relevant to glaucoma as trabeculotomy also eliminates the elevated resistance observed in glaucoma (19, 40). This indicates that in glaucoma, the site of increased outflow resistance lies proximal to the collector channels, ruling out distal outflow pathway tissues as sites of outflow resistance generation or indeed potential therapeutic targets (19, 38, 41).

As well as the microanatomy of the outflow tissues, some processes may influence resistance to aqueous flow and ultimately IOP. Heart rate can contribute to outflow as it, in part, determines the AH pressure gradient. Elevated venous pressure can cause complications by leading to the obstruction of AH outflow or reflux of blood into the SC (42). Recent

developments have shown that reducing episcleral venous pressure may have additive effects with other IOP-lowering drugs (43). A mechanical pump is also assumed in the form of pulsating flow (37). Pulsating flow occurs as a result of transient IOP spikes during the cardiac cycle, blinking and eye movements. These transient spikes cause microscopic deformations of the drainage channel, the pulse wave forcing AH flow through the collector channels and aqueous veins, but move back to their original configuration when IOP drops again, leading to a reduction in pressure which induces the flow of AH into the SC lumen (36, 44).

Outflow resistance is not a fixed parameter of the conventional outflow pathway, rather it is a dynamic value dependant on the microanatomy of multiple tissues and the fluid dynamics within fluid vessels. Outflow resistance is certainly a key factor in determining IOP and is a property of interest especially when abnormal resistances become pathological.

1.4 Glaucoma

The eye is pressurised by a balance in the production of AH and resistance to its drainage through the TM and SC. Precise regulation of aqueous inflow together with outflow resistance are critical in maintaining an average IOP of approximately 16 mmHg in a normal functioning eye (45). Glaucoma is a disease characterised by a reduction in AH outflow, resulting in elevated IOP clinically defined as greater than 21 mmHg, a state which is referred to as ocular hypertension (46). Build-up of pressure in the anterior chamber exerts a force upon the retina and optic nerve head (ONH), leading to retinal ganglion cell degeneration. The ONH itself is the region at which retinal ganglion cell axons converge, inducing a depression in the retina (optic cup) and lead towards the brain through pores in the lamina cribrosa, the tissue which structurally supports the ONH. It is a blind spot in that no photoreceptors are present on this optic disc. The sclera is perforated at the OHN, exposed as a weak spot compared to the rest of the vitreous body during ocular hypertension. The increased pressure gradient causes the ONH to recede, further increasing the depth and area of the optic cup. (47). It is not fully understood

how axonal damage occurs but there are various mechanistic contributors. Firstly, retinal ganglion cell death may be a direct result of the mechanical deformation of the pores of the lamina cribrosa, reducing physical support to the axons (48). IOP may also have a negative impact on retrograde axonal transport. Consequently, a blockade of axonal protein transport forms at the lamina cribrosa, causing retinal ganglion cell death by trophic insufficiency (49). Other independent factors may also lead to ganglion cell death. Ischemia-induced hypoxia, immune dysregulation, impaired glutamate signalling and oxidative stress have all been reported as potential contributors to ONH damage (49). This damage, known as glaucomatous optic neuropathy, ultimately results in the progressive loss of visual fields if left untreated, and is the worldwide leading cause of irreversible vision loss.

Clinical Presentation

Glaucoma progresses and may appear symptomless until substantial neuronal damage has occurred. As a result of elevations in IOP, the ONH degenerates, visibly recognisable as receding, or ‘cupping’, of the optic disc. This can be observed in patients using optical coherence tomography or scanning laser polarimetry. Deformation of the lamina cribrosa and damage to the retinal ganglion cell axons that make up the optic nerve fibres eventually prevents signal transmission to the brain. Visual field loss begins in the mid-periphery and progresses in a centripetal manner until only central vision remains. Thus, visual field tests can be indicators of disease progression, or even establishing early diagnosis, however many ganglion cells may be lost before defects are detectable by visual field testing. Changes to the fibrous layer can be identified during ophthalmoscopic examination of the ONH, structural damage of the ONH being critical to disease diagnosis (50). Newer techniques involving laser scanning have further improved the early identification of the disease (51).

Types of glaucoma

Glaucoma encompasses a range of eye disorders including pigmentary-, secondary-, and normal-tension forms of disease, however the most prevalent are primary open-angle (POAG) and primary angle-closure glaucoma (PACG). POAG represents greater than 74% of all glaucoma cases (52). In this form, the narrow angle between the cornea and iris leading to the conventional outflow tissues remains open without physical obstruction, while the conventional outflow tissues themselves, the TM and SC, retain only partial AH drainage function as AH resistance is increased. The molecular basis for the pathology has not yet been fully elucidated, although many contributors to the glaucomatous reduction in AH outflow have been suggested. These include changes in pore density, increased ECM deposition, contractility and elasticity alterations, changes in cytoskeletal arrangement, disrupted IOP sensing mechanisms, segmental outflow regulation and oxidative damage to cells (53). A combination of these contributors may occur in any given patient, but it is unclear which, or any, of these are causative of the underlying pathology.

In contrast, while these outflow tissues remain functional in PACG, flow of AH through them becomes physically blocked by the narrowing of the iridocorneal angle, often due to deformity of the iris, whether it is acute or chronic. PACG can be caused by AH resistance through the pupil, where a build-up of pressure leads to the apposition of the iris against the cornea obstructing fluid flow, called an iris bombe. Other contributing factors to PACG include an anteriorly positioned lens, peripheral iris thickness and iris curvature, all relating to the proximity of the lens to the corneal endothelium at the iridocorneal angle (54). Thus, in both forms of disease, AH drainage becomes restricted, leading to elevated IOP and optic neuropathy (55). An anatomical comparison between POAG and PACG is presented in figure 1.5.

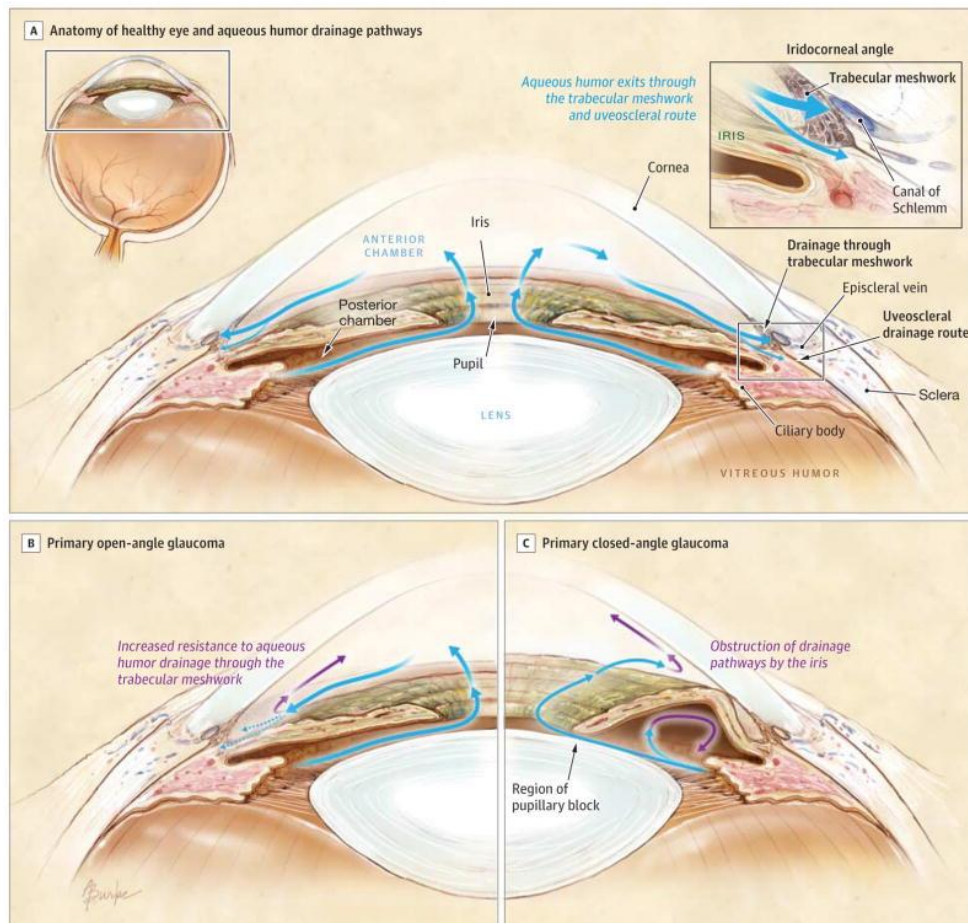


Figure 1.5: Physical comparison of POAG and PACG in the anterior chamber

(A) Anterior chamber and AH flow route (blue) in a healthy eye. (B-C) Abnormal fluid flow and anatomical deformities as seen in POAG and PACG respectively. Figure adapted from (47).

Other forms of glaucoma are less prevalent but result in a similar loss of vision. Normal tension glaucoma is similar to POAG in that the angle remains open however there is no elevation in IOP, yet optic neuropathy still occurs. This could be structural abnormalities in the connective tissue supporting the optic nerve, or low blood pressure could increase the pressure gradient at the ONH, or through loss of sufficient ocular perfusion (56). Secondary glaucoma further encompasses its own subclasses, and refers to any form of glaucoma where there is a known cause of elevated IOP, leading to optic nerve damage (47). Pseudoexfoliative glaucoma occurs in those with pseudoexfoliative syndrome and is also a class of POAG. Fibrillar, proteinaceous material is produced at high concentrations throughout the body, but it may accumulate in the

anterior chamber. These deposits become lodged in the conventional outflow tissue and physically block AH outflow. Elevations and fluctuations in IOP follow, leading to glaucomatous progression. Degeneration of the iris, lens and cornea may also contribute to this disease state (57). Pigment dispersion glaucoma arises as a result of the breakdown of the iris. Pigments become disturbed and result in a physical blockage of the outflow pathway, similar to that of pseudoexfoliative glaucoma, leading to ocular hypertension (58). Other secondary forms include uveitic glaucoma, caused by infection, inflammation or disease; traumatic glaucoma, resulting from physical damage to the eye; lens related, due to lens particle disruption; surgery-related; or from elevated episcleral venous pressure. All these forms of glaucoma are derived from underlying syndromes, of which should be the target for primary treatment. POAG remains the most prevalent form of glaucoma, with the greatest demand for treatment, and is therefore the focus for the rest of this study.

Epidemiology and risk factors

Glaucoma, in its various forms, is one of the most common causes of visual handicap in the world, rivalling cataract and infection. Glaucoma currently affects an estimated 70 million people, with projections showing an increase to 76-79 million people in 2020 and nearly 120 million by 2040 (52, 59). This projected increase is based upon the trend towards increasingly aged populations, as age is one of the primary risk factors of glaucoma. Worldwide, approximately 10% of those suffering from glaucoma are bilaterally blind (52, 60), with fewer than 50% of patients in developed countries being aware of having the disease until visual fields become significantly reduced (61). Ocular hypertension is recognised as the major disease risk factor for vision loss in glaucoma, along with age, lifestyle, and gender (59, 62). Ethnicity can correlate with a prevalence of glaucoma; those of African descent have an increased prevalence of POAG (5.4%) versus the global average (3.1%) (59). Other baseline factors that may indicate a future glaucomatous optic neuropathy may include large optic cup-to-disc ratio, optic disc

cup area and thin central corneas. Other risk factors for glaucoma include thin corneas, family history of glaucoma, myopia, eye injury, high blood pressure, corticosteroid use (63). Environmental factors primarily include diabetes, of which proliferative diabetic retinopathy or neovascular glaucoma can occur (64), and smoking (65). Risk factors for normal-tension glaucoma include cardiovascular disease, family history of glaucoma, low eye pressure and Japanese ethnicity. Angle-closure contributing factors include age, family history, farsightedness, eye injury/surgery and east Asian and Inuit ethnicities (63, 66).

Glaucoma as a neurodegenerative disease

As mentioned, IOP is the major risk factor for glaucoma. This does not mean it is causative of the condition, rather, if it was controlled then there would be a reduced chance of developing the disease. Many of these factors are all contributory, yet it is a combination of them, mainly elevated IOP along with vision loss, that defines the disease. This is because in some cases, with reduced IOP, progressive vision loss among glaucoma patients is still common. IOP does not address the underlying susceptibility of RGCs to degeneration. Thus, glaucoma is often classified as a neurodegenerative disorder (67).

Several neuroprotective agents have been used in the treatment of glaucoma, and have been successful, however the effect size of these drugs has been quite small, and may benefit from parallel strategies or polypharmacy. As mentioned, ischemia, ROS, defective axonal transport, excitotoxicity and trophic factor withdrawal may all be initiating mechanisms in the death of RGCs in glaucoma. Ultimately, no matter the pathophysiology, RGCs primarily die by apoptosis (68). Several neuroprotective agents have been used to slow or prevent the death of neurons in order to retain their function. A glutamate receptor agonist typically used for Alzheimer's has been tested in glaucoma patients although primary efficacy endpoints were not met (69). Alpha adrenergic receptors have also been used in neuroprotection, although their

efficacy in RGC protection can't be studied independently from its IOP lowering effect. Other approaches include an siRNA-based caspase inhibitor, nitric oxide synthesis inhibition and activity-dependant neurotrophic factors. RGC protection may be sufficient in some diseases in which temporary survival is required, however optic nerve axon regeneration is encouraged to rebuild the connections from the eye to the brain. Strategies to enhancing RGCs intrinsic growth ability such as ROCK inhibitors, Kruppel-like factors and activating the pro-regeneration activities of mTOR and CNTF could provide therapeutic approaches to promote axon regeneration (69-71). Neuroenhancement, the short-term improvement in RGC function, could also be employed to enhance function and improve vision in RGCs that are dysfunctional, but not dead. This could encompass neurotrophic factors that may act at the synaptic level to enhance function, or citicoline which has demonstrated improvement in glaucoma patients (72). While IOP lowering is a successful neuroprotectant in itself, complementary approaches hold promise for maintaining a patient's visual fields. There is a need for molecular biomarkers of glaucomatous neurodegeneration to further the research in this area, but animal models of neurodegeneration and prospective human studies will contribute to this (73). As such, there is a great potential for neuroprotective and regenerative therapies with improved efficacy in future glaucoma treatment.

Axonal energy is generated primarily through oxidative phosphorylation in the mitochondria, and energy disruption is proposed as an early contributor to pathology in a variety of neurodegenerative conditions (74). Energy depletion can occur through ischemia, mitochondrial dysfunction or a loss of axon support factors among others. Studies have shown the importance of the mitochondria in axonal function and preventing degeneration (75, 76). In glaucoma, mitochondria isolated from patients exposed to high IOP with absent pathology demonstrated high efficiency, suggesting that mitochondrial function could be a potential biomarker for those with high IOP (74). Mitochondrial function may be impaired in glaucoma

as a result of age, mechanical stress, hypoperfusion due to elevated IOP or by oxidative stress. Mitochondrial pathogenesis at the optic nerve may include oxidative phosphorylation defects, increased reactive oxygen species and altered mitochondrial dynamics, resulting in an energy depletion that negatively impacts RGC function (77). Glaucoma is increasingly treated as a neurodegenerative disorder, and viewing it as such opens new avenues of therapeutic intervention targeting aspects such as mitochondrial biogenesis, regeneration or improved function.

Genes associated with POAG

POAG is a classically multifactorial disease in that, while there are familial tendencies, the vast majority of cases are of adult onset and are not inherited in a Mendelian sense. However, rare hereditary forms of disease do exist that segregate in families in an autosomal dominant fashion, and through genetic linkage studies, genes involved in such forms of disease were localised and characterised. Recent association studies have also highlighted an array of genes with moderate correlation to POAG (78-83).

The first gene to be identified through genetic linkage encoded a TM glucocorticoid response protein (TIGR), now known as myocilin. Most ocular tissues produce myocilin, but it is only secreted by some, including the TM (84, 85). Myocilin interacts with ECM components including fibronectin, laminin and decorin (86, 87), however the function of such interactions remains unknown. Current evidence suggests that mutant myocilin protein misfolds and aggregates in cells of the TM, rather than being secreted (88), leading to endoplasmic reticulum (ER) stress and dysfunction of TM cells. In TM cells expressing a dominant human Myocilin (Tyr437His) mutation there is an intracellular build-up of ECM components and a decrease in secretion of matrix metalloproteinases (89). Transgenic animals expressing this mutation exhibit elevated IOP and reduced outflow facility, characteristic of glaucoma (89, 90).

The second gene to be mapped in POAG using genetic linkage studies encoded Optic neuropathy-inducing protein, or optineurin. The gene is expressed in the TM, non-pigmented ciliary epithelium, retina, brain and in other tissues (91). Optineurin may play a neuroprotective role against TNF- α mediated cytolysis, and translocates to the membrane in response to oxidative stress (91-93). Most commonly associated with normal tension glaucoma and motor neurone disease (94), optineurin mutations have also been linked to POAG (95). Evidence suggests that optineurin is involved in the accumulation of damaged mitochondria and is associated with mitochondrial dysfunction in RGC degeneration in synergy with other factors (96). Together, mutations within the optineurin and myocilin genes have been encountered in up to 5% of adult-onset cases of POAG (97).

In regard to adult-onset disease, genome-wide association studies (GWAS) have implicated caveolins CAV1 and CAV2 in POAG. These proteins appear to affect the organization of collagen matrix fibres in lung tissue (98, 99) and fibronectin, collagens and α -SMA in murine mammary tumours (100), all of which are perturbed during fibrosis. Reduced expression of caveolins in glaucomatous tissues may be indicative of a pathological role for caveolins in POAG, such as their role in suppressing TGF- β 2 transcription, a known inducer of ECM expression (101, 102). Interestingly, it has recently been shown that lack of caveolae in the TM of mice results in ocular hypertension, with cells of the outflow tissues having a greater susceptibility to rupture through mechanical stress, indicating a possible genetic and functional link to glaucoma (103). GWAS have resulted in the elucidation of additional glaucomatous or IOP-related susceptibility loci. Primary candidate genes related to both IOP and POAG include TMCO1, ABCA1 and GAS7 (79, 104, 105). Their contributions to the pathogenesis of glaucoma are still unclear, however basic functionalities have been established. TMCO1 encodes a transmembrane protein that functions as a calcium channel in response to excess calcium levels in the endoplasmic reticulum (106). ABCA1 belongs to a family of transporters

and functions as a cholesterol efflux pump, and *GAS7* may promote maturation and differentiation of neurons. Proteins encoded by these genes have been shown to be expressed in human ocular tissues (105). Systems genetics has also recently identified *CACNA2D1*, which modulates IOP (107).

While some of these high-penetrance glaucoma-causing genes are known to encode proteins that interact with ECM components, no genetic variants in ECM genes have as yet been significantly linked to POAG. There are, however, several genetic variants within the collagen genes that are significantly associated with glaucomatous endophenotypes such as maximum vertical cup-disc ratio, increased optic disc cup area and altered central corneal thickness (108-110). Other mutations within fibrillin 1, latent-transforming growth factor beta-binding protein 2 and versican genes have been associated with glaucoma in humans (111-115). These proteins constitute large ECM fibrils that have roles in cell adhesion within the matrix. Mutations in genes involved in the remodelling of the ECM, such as the disintegrin and metalloproteinase with thrombospondin motifs (ADAMTS) proteins and other members of the matrix metalloproteinase (MMP) family, are associated with increased vertical cup-disc ratio and reduced central corneal thickness (108, 110, 116). Collectively, these data support the concept that genetic variations affecting ECM homeostasis may be related to the development of glaucomatous endophenotypes.

1.5 The ECM as a therapeutic target

ECM composition within the outflow tissues

The ECM of the conventional outflow tissues not only provides structural support but is also involved in the regulation of a variety of cellular processes and functions. ECM within this region is comprised of a heterogeneous group of fibrous and matrical materials, including proteoglycans, collagens, fibronectin, laminin, elastin and others, all of which contribute to it

tensile strength and complex function (Figure 1.6). The basement membrane is a fibrous layer of ECM material separating the endothelium from underlying connective tissues. It is discontinuous around the canal circumference tethering SC cells against large pressure gradients. As with other vascular endothelia, the basement membrane incorporates a lattice of collagen IV and laminin-511 along with collagen I, dystroglycans and other laminin chains. Although these components are found throughout the ECM of the JCT, they are critical to basement function, in particular, the heterotrimer of laminin subunits with arms containing binding sites for SC cell surface receptors, integrins and proteoglycans (117). Co-localisation studies show an overlap of laminin-511 and the integrin $\alpha 6$, expressed at the SC endothelial periphery and not the TM, indicating that this focal adhesion complex is involved in basement membrane-endothelial adhesion (118).

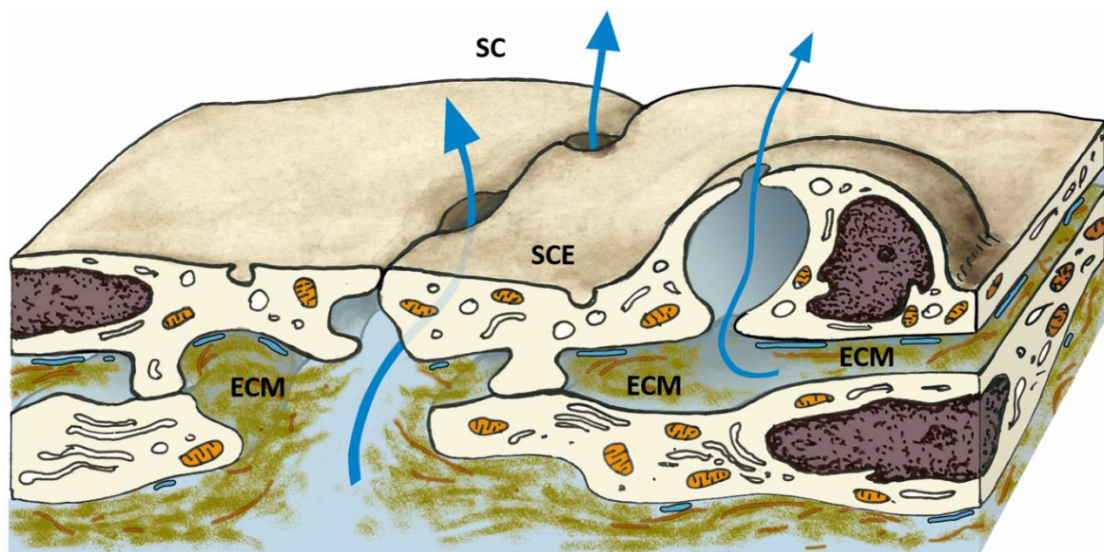


Figure 1.6: The ECM of the conventional pathway

Oblique diagram illustrating the route of AH through ECM of the conventional pathway. ECM material is highly expressed in this region, and areas void of ECM give rise to fluid channels in both the transcellular and paracellular routes of flow (blue arrows). ECM = Extracellular matrix, SC = Schlemm's Canal, SCE = Schlemm's Canal Endothelium. Image contributed by Prof. Elke Lütjen-Drecoll.

The ECM is formed by complex proteinaceous meshworks in the extracellular spaces throughout the JCT, which are regularly remodelled to retain porosity. Collagen fibres are irregularly orientated within the matrix of the JCT, which may provide an explanation as to why JCT cells are stationary while other cells in regularly orientated collagen matrices are migratory (20). Fibronectin is a major ECM component, with the protein organising into interwoven repeating chains that form extensible fibrils involved in the contractility of the TM in response to IOP. Alternative splicing of fibronectin occurs in the TM, and POAG patients are more likely to express key exons that promote assembly of fibronectin matrices which may decrease outflow facility (119). Elastin is one of the core elements of the JCT, with elastin fibres forming the cribriform plexus, which runs tangential to the inner wall endothelium joining the basement material of the SC with the ciliary muscles. Elastin and its associated proteins react to muscle tension and thus induce widening or contraction of the SC lumen in response to IOP elevation (120). The binding of ECM to cell membranes is facilitated by integrin-ECM interactions at sites referred to as focal adhesions (121). Transmembrane integrin subunits interact with the Arg-Gly-Asp domains of ECM proteins, while the cytoplasmic domain connects to actin-binding proteins (122-124). Interaction between these proteins and the actin cytoskeleton reflect the importance of focal adhesions in regulating cellular function and response to environmental cues. In conjunction with integrins, inter-endothelial junctions maintain endothelial cell-cell adhesion, regulating paracellular transport channels. These features are summarised in Figure 1.7.

The TM expresses MMP-2, tenascin-C and α -SMA at consistently high levels, normally only expressed highly in cells undergoing remodelling, suggesting a constant remodelling process at the TM to maintain open flow channels (117). TGF- β 2 is a cytokine with an important regulatory role at the TM, inducing the expression of collagens, α -SMA, fibronectin and PAI-1 among others. TGF- β 2 signalling is mediated by elastic microfibrils, specifically the fibrillin component that confers ECM elasticity, which is critical to sequestration and activation of TGF-

$\beta 2$ complexes (125). Induction of ECM cross-linking by TGF- $\beta 2$ bears similarities to the cross linking observed in glaucomatous tissues and may be a contributing factor to disease pathogenesis. Matricellular proteins are those described as non-structural glycoproteins enabling communication between the cell and the surrounding ECM such as CTGF, SPARC, tenascin-C, thrombospondin and others. These proteins are upregulated in response to TGF- β signalling, the levels of which are upregulated in POAG AH, and are associated with fibrosis and ECM deposition (126).

The ECM of glaucomatous tissues bears similarities to fibrotic tissue, particularly excessive accumulation of ECM components such as α -SMA, progressing to a hardening or scarring of connective tissues (127, 128). The ECM at the glaucomatous JCT displays some hallmarks of fibrosis in the form of sheath-derived plaques, i.e. an increase in elastic fibril sheath size due to increased adherence of fibrils and other ECM components to the sheath, particularly in the ageing TM (20, 129).

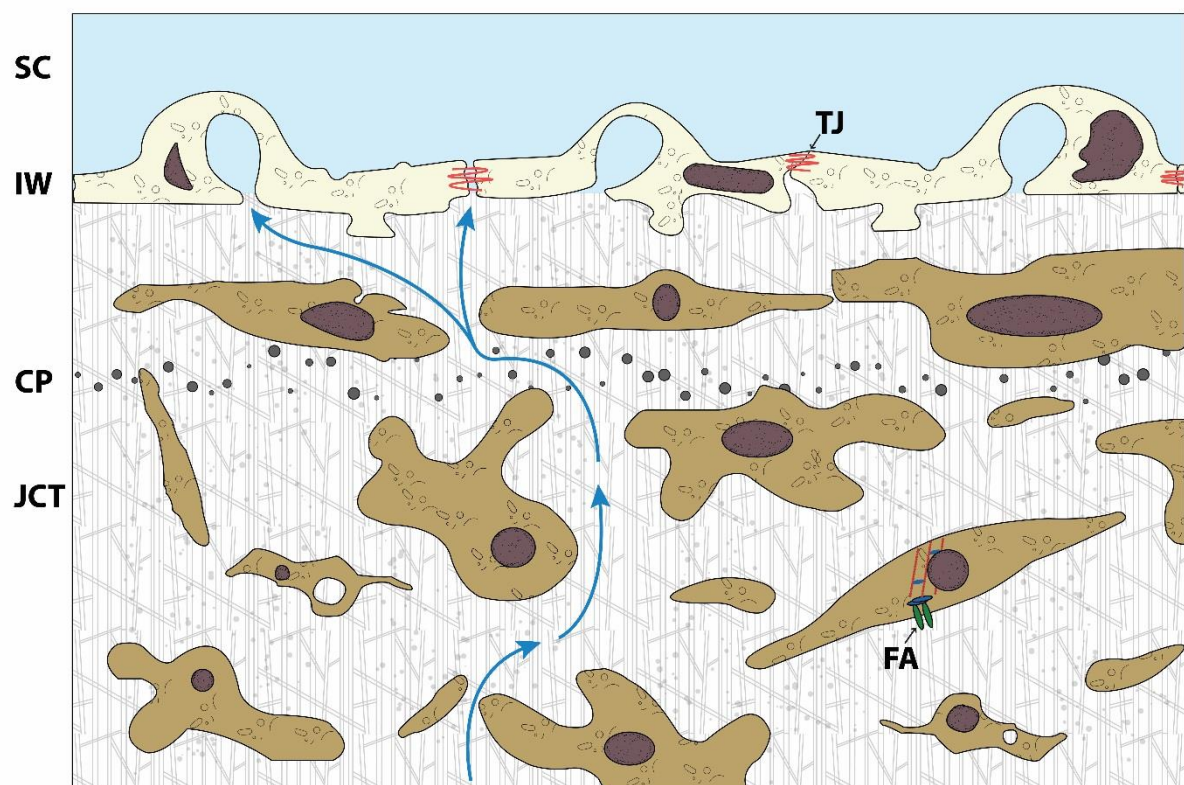


Figure 1.7: An expanded view of the JCT region.

Diagram depicting a cross section of the conventional outflow tissues including various extracellular matrix (ECM) elements. AH traverses the TM, exiting the juxtacanalicular region (JCT) through the inner wall (IW) into the lumen of the Schlemm's canal (SC), via either the transcellular route, through transendothelial pores in giant vacuoles, or the paracellular route, through paracellular pores controlled by tight junctions (TJ). Cells are embedded in a structured ECM and adhesion to the matrix is facilitated by focal adhesion (FA) sites where integrins bind both extracellular material and the intracellular actin cytoskeleton (red). The cribriform plexus (CP) comprising elastin sheaths is predominantly found underlying the first sub-endothelial layer. Image taken from (10), O'Callaghan et al.

ECM in outflow resistance

It is generally accepted that the majority of outflow resistance is generated at the JCT region (18, 26), in particular, at the ECM of the JCT (112, 130-132). Porous spaces within the ECM of this region allow the AH to reach the endothelial lining of SC, however proteoglycans, glycosaminoglycans and other large ECM constituents can fill these spaces, further increasing resistance to AH outflow (18, 133-136). Obstruction of AH flow through ECM components reducing ECM porosity is more likely in aged and glaucomatous tissue (134). AH funnels from the full expanse of the TM/JCT to discrete pores in SC endothelium, leading to generation of outflow resistance through a bottleneck effect. As ECM accumulates in this region, the extracellular space close to SCEC becomes more tortuous, leading to increased outflow resistance (18). The effect that this ECM has on outflow resistance alone is difficult to measure, however recent developments in measuring and modelling of perfusion data may lead to more accurate estimations of outflow facility (137). In general, changes in ECM composition and turnover in the TM play an important role in outflow resistance, including dynamic reactions to environmental cues, such as mechanosensation of IOP (117, 138).

Modulation of ECM turnover

Homeostatic ECM turnover plays an important role in the regulation of outflow resistance, turnover being triggered, for example, by stretch or distortion of TM cells, often as a result of elevated IOP (139). JCT cells constitutively express a range of ECM proteins, with exposure to environmental stresses, synthetic agents, or laser trabeculoplasty surgeries invoking alterations in ECM gene expression profiles (140-143). High gene expression levels reflect the fact that regular ECM turnover, facilitated by proteinases that target ECM components, is essential to homeostasis (141). Homeostatic proteinases include zinc-dependant proteinases - classical matrix metalloproteinases (MMP's), adamalysins (ADAM and ADAMTS proteins), and other proteinases involved in plasminogen activation (144). The MMP group of proteinases is secreted extracellularly in their inactive form and require further processing for activation (145, 146). MMPs are constitutively expressed throughout the TM, expression profiles responding to various stimuli (147-149). Tight regulation of proteinase expression within the ECM is required for effective control of outflow resistance. To this end, tissue inhibitors of metalloproteinases (TIMPs) are expressed in a manner similar to that of MMPs, while the ratios of MMP:TIMP determine the extent of ECM modulation (129, 150). Such ratios tend to be imbalanced in POAG (151-154), and may be indicative of dysfunctional ECM turnover. MMP proteins are often upregulated in glaucomatous AH, however the activity of these proteins is reduced in comparison to cataract controls, likely reflective of MMP:TIMP imbalance (151, 155-157). Perfusion of ocular tissues with MMPs or MMP-activating compounds results in increased outflow facility, possibly the most convincing demonstration of ECM involvement in regulating outflow resistance (158-161). Furthermore, recent studies on ECM characteristics, such as stiffness resulting from crosslinking, or caveolin-mediated matrix endocytosis, also highlight ECM influence on outflow facility (162, 163).

ADAMs proteins have a similar domain structure to those of classic MMPs and also associate with ECM proteins and integrins (164). As a result of MMP-related proteolysis, ECM

remodelling can induce changes at the sites of focal (cell-matrix) adhesions. Disruption or inhibition of integrin-ECM linkages binding cells to the ECM, or ECM receptor inhibition has been associated with increases in endothelial permeability and transendothelial transport (123, 165-167). ECM remodelling at focal adhesions alters migration of fibres within the actin cytoskeleton, allowing F-actin and α -actin to act as indicators of ECM turnover (119, 168, 169). It is also worthy of note that ECM proteinases affect inter-endothelial SC junctions, providing an additional avenue for modulation of outflow resistance. (24, 170-172).

Newly emerging treatments, detailed below, have a greater focus on the conventional pathway, representing the major site of outflow resistance, often with direct or indirect effects on the ECM. This more targeted approach to glaucoma treatment will hopefully allow for the development of a new class of drugs that may prove to be more efficacious in arresting disease progression.

1.6 Traditional treatments in the management of glaucoma

Topical medications

Lowering IOP remains the only effective treatment for POAG. The primary standard of care for patients with open angle glaucoma involves topically-administered eye drops, surgery, or both, with the annual cost of such interventions in the US having recently been estimated to amount to \$1.9 billion, 38-52% of which is related to topical pressure reducing medications (173). Glaucoma management involves either reducing AH production at the ciliary body or increasing AH outflow. A recent meta-analysis has confirmed that prostaglandin analogues are the most effective in lowering IOP, a reflection of the fact that these compounds are the most commonly prescribed eye-drop (174). Significant increases in unconventional outflow (175), and to a lesser extent, conventional outflow (176, 177), are observed with such analogues. Prostaglandins are endogenously expressed in many tissues and throughout the anterior

chamber (178), such expression being influenced by bioactive molecules, laser treatments, mechanical stress, or glucocorticoids, indicating their importance in homeostasis (179). Extensive studies have demonstrated prostaglandin-related decreases in TM cell contractility and outflow resistance of organ-cultured anterior segments (180-182). The overall mechanisms through which prostaglandins enhance AH outflow remain to be fully elucidated, however it is widely accepted that remodelling of the ECM plays a part (183-186), and it is of note that upregulation in MMP expression, through activation of prostaglandin receptors, may be involved (148, 187). However, the unique receptor profile for each analogue may induce ECM modulation via different cascade pathways. One EP4 receptor agonist in particular has been shown to induce an increase in conventional outflow facility specifically (188). Comparisons have been made between the effects of laser treatment and prostaglandins in SC monolayer permeability. Cells treated by laser, media conditioned from lasered cells, or prostaglandins all show a reduction in levels of tight junctions and a concomitant increase in cell conductivity (189). Modulation of SC permeability by prostaglandins further indicates an effect on enhancement of outflow through the conventional pathway.

Second line medications include carbonic anhydrase inhibitors and β -blockers, however the latter may have potentially dangerous off-target side effects. β -blockers inhibit either β 1-, or both β 1- and β 2-adrenoceptors (190). Since these receptors are abundantly expressed in the ciliary processes, this may result in an excess of noradrenaline, which may, in turn, induce vasoconstriction and decreases in blood supply to the ciliary body, aiding in the reduction of AH production (191). Alpha2-adrenergic receptor agonists work in a similar way but are not often used as topical medications owing to their side effects. These agents cause an initial decrease in aqueous production, and an increase in unconventional outflow after chronic exposure, likely due to elevated prostaglandin expression (192, 193). Carbonic anhydrase inhibitors also decrease AH production through chemical inhibition of bicarbonate formation (56).

Cholinergic drugs represent third line medications that have seen a reduction in clinical use in recent years, primarily due to the frequency with which they need to be instilled (3-4 times per day). These drugs increase conventional outflow and decrease IOP (194, 195) by inducing ciliary muscle contraction, increasing SC lumen area, in turn allowing for increased aqueous fluid transport across SC endothelial cells (196). As previously mentioned, elastin fibres are responsible for the connection of the ciliary body to SC and associated muscle contractions. The ciliary muscles express cholinergic nerve terminals facilitating contraction, and it is presumed that the muscle is pulled back again by a recoil of the elastin net (195, 197).

It is important to emphasise that these widely-used topical medications predominantly target unconventional outflow and mostly only influence the conventional pathway by means of secondary or indirect responses. It is of interest to note however, that administration of alpha/ β -blockers, alpha1-blockers, alpha2-agonist- and prostaglandin derivatives all upregulate MMPs and downregulate TIMPs, in contrast to the effects of β -blockers, suggesting at least some role in ECM modulation for these anti-glaucoma drugs (198).

It should be noted that for the most commonly used prostaglandin analogues, between 25 and 50% of patients are sub-optimally responsive, commonly defined as not achieving more than a 20% reduction in IOP (199, 200). Consequently, there continues to be a need for improved medications, particularly targeting the conventional pathway.

Surgical interventions

As is the case with many medications, there will always be a percentage of patients that do not respond to the treatment. Several studies note non-responders to beta blockers, but then often demonstrate successful IOP reduction in response to a prostaglandin (201, 202). Surgical management is indicated when there is an inadequate lowering of IOP, or if visual degeneration persists despite treatment (47). Surgeries have similar approaches to that of topical medications

such as increasing conventional outflow, reducing AH production or increasing outflow by alternative means (203).

Selective laser trabeculoplasty (SLT) (succeeding argon laser trabeculoplasty) is a repeatable, cost-effective and efficient treatment for those with a high pre-treatment IOP. SLT can maintain a reduction in IOP for a number of years however its effectiveness decreases over time (204-207), with a mean survival time of about 2 years (208). A 3 nanosecond laser burst is sufficient to open fluid channels via selective absorption of laser energy by pigmented TM cells. Minimal structural damage is observed after SLT, with some disruption of trabecular beams and SC endothelia (209, 210). Because of this, it is suggested that the mechanism of SLT occurs at the cellular level without mechanical or thermal indications (206, 211). These could be due to a combination of oxidative stress or cytotoxic effects (212), tight junction disassembly as previously mentioned (189), or proliferative responses (213). A significant biological implication is the release of chemotactic and vasoactive agents, primarily cytokines (214). Such cytokines are known to recruit monocytes and induce MMP expression, both of which can be used to remodel the ECM of the surrounding tissue (211, 215-217).

Traditional incisional surgeries that increase conventional outflow include trabeculectomy and aqueous shunts but are associated with marked risk profiles (218). A trabeculectomy involves the physical removal of a section of TM and SC inner wall, creating a path for AH to directly enter the collector channels from the anterior chamber, whereas a shunt bypasses the TM, allowing AH to flow into the lumen of the shunt and into the SC, or allows for dilation of the SC. Shunts are similar to canaloplasty in that it involves the insertion of a microtubule, but in canaloplasty this suture is pushed through the entire circumference of the SC and tensioned to pull the TM inwards, enlarging the SC (219). Endocyclophotocoagulation represents a safe and effective way of reducing IOP through the reduction of aqueous production, where a laser

endoscope probe is inserted through a corneal wound. Ciliary processes are laser treated to the point of tissue shrinkage and blanching (220, 221).

Surgically increasing outflow in an unconventional-type manner comprises the insertion of shunts that drain AH from the anterior chamber into the suprachoroidal or subconjunctival space. The development of mini-shunts has become the attention of industry as of late, which has traditionally only been used for complicated glaucoma surgeries or where primary standard trabeculectomy has failed. Greater emphasis has been put on the usage of shunts or stents in patients undergoing cataract surgery to achieve further support for IOP lowering. Hypotony is prevented by the consideration that the inner diameter of the microtubes are narrow to the point that enough outflow resistance is generated without the need for valves or tight sutures as with older models (203, 222). As these mechanisms are a result of mechanical alteration to the structure of the anterior chamber, they will not be discussed further. It is important to note however that although each surgical intervention mentioned has acceptable degrees of efficacy, they are not without side effects and may require secondary procedures or reoperation (218, 223-225). Limitations exist which include limited quality and duration of evidence, lack of cost-effective data, lack of study standardization, unknown long-term outcomes, the inability to directly compare surgical types due to varied study design, risk of late failure due to scarring, and the fact that most trials include cataract surgery which is known to reduce IOP in itself (203, 226, 227). Hence, improved treatment methods are still in demand, capable of increasing outflow facility and reducing IOP for patients with POAG.

1.7 Emerging medications

New classes of drug

A collective objective in developing new formulations is to increase conventional outflow via targeting of the JCT or cytoskeleton of cells of the outflow tissues. Rho kinase inhibitors, marine macrolides, adenosine- and prostanoid-receptor agonists together with siRNA

formulations are all currently under evaluation. Arguably, the most advanced of these are rho kinase (ROCK) inhibitors that have already been approved for use in Japan and have completed phase III trials in the US. IOP decrease in response to ROCK inhibitors is associated with enhanced outflow facility caused by expansion of the TM, JCT and episcleral veins and increases in SC cross-sectional area (228, 229). Studies using a rho kinase inhibitor in conjunction with a norepinephrine transport inhibitor demonstrated similar results, but with the advantage of a dual mechanism of action that also decreases AH production (230). Rho family GTPases are seen to be elevated in glaucomatous ONHs, activating effector kinases to polymerize actin fibres and regulate smooth muscle contraction (231-234). Decreases in myosin light chain phosphorylation were observed in ROCK inhibitor-treated TM tissue, suggesting that outflow enhancement was facilitated by actomyosin cytoskeletal disorganisation at the JCT/inner wall assembly (33, 235). ROCK effectors also indirectly stabilise filamentous actin, reducing cell migration and interact with actin-binding proteins. Depolymerisation of filaments by ROCK inhibitors may further widen the empty spaces in the JCT and increase SC vacuoles, thereby increasing outflow facility (236, 237). Similarly, Rho GTPase inhibition via expression of exoenzyme C3 transferase has been shown to disrupt actin bundles in human TM cells, correlating with increased outflow facility in primates. Focal adhesions, as visualised through vinculin staining (involved in integrin-actin binding) were distinctly reduced, as was β -catenin, indicating a loss of intercellular junctions, reflected in the decrease in cellularity (238).

Marine macrolides, isolated from aquatic sponges, have antifungal, cytotoxic and antiproliferative properties. Interactions of these compounds with actin are similar to those of the ROCK inhibitors. Macrolides have established functions in: 1) severing polymeric actin (F-actin) and stabilising dimeric actin, disrupting the cytoskeleton (swinholid A); 2) sequestering actin monomers (G-actin) preventing their use in polymerisation, thus disrupting filament organisation as is the case with latrunculin-B; 3) competing for actin binding to induce and stabilise its polymerisation (jasplakinolide) (239-242). Macrolides have been shown to increase

aqueous outflow facility in primate eyes, with the greatest focus appearing to have been placed on latrunculin-B. (239, 243-245). Topical administration of latrunculin-B is sufficient to increase aqueous outflow facility and lower IOP (244), while in treated eyes, noticeable changes have been observed in the JCT region, including increased intercellular space and dilated SC, but with normal and intact corneoscleral regions (246). Inter-endothelial junctions of primate SC endothelia appeared intact, although there was a loss of ordered alignment and integrity in actin filaments. Similar studies in human eyes have shown some focal SC inner wall separation from the ECM of the JCT (245). Increased central corneal thickness and transient increase of corneal endothelium permeability was observed in one study, raising questions of safety issues in using macrolides in the anterior chamber (247). Phase I trials have been conducted however, and have reported few clinically significant adverse effects (248).

Adenosine receptor agonists have been shown to increase conventional outflow and lower IOP, with a similar mechanism to those of cholinergic agonists. A₃ agonists reduce AH flow by inhibiting chloride ion channels in ciliary epithelial cells (249). An A₁ agonist in phase III trials has demonstrated favourable toxicity profiles, possible neuroprotective effects, and efficacious IOP lowering (250, 251). Receptor activation has also been shown to induce the secretion of MMPs, particularly MMP-2, probably the cause of reduced outflow resistance (252, 253). Increases in facility were negated by the addition of an MMP inhibitor, implicating ECM remodelling along with cell volume shrinkage as mediators of outflow enhancement (254, 255). Developments on prostanoid receptors have yielded agonists specific to individual receptor subtypes. Further understanding of the mechanism of action of the prostaglandin pathway has resulted in the development of drugs that include nitric oxide-donating prostaglandin F₂-analogues, which strongly increase fluid drainage across both pathways. Relaxation of TM cells due to a reduction of actin stress fibres and vinculin localisation at focal adhesions was observed using such analogues (256). Interest is increasing in the development of EP₂ and EP₄ receptor agonists for the treatment of POAG, with one such EP₂ agonist having been shown to reduce

IOP by increasing both unconventional and conventional flow, facilitated by the relaxation of SC and by decrease in contractility and collagen deposition at the TM (257-259). These effects are similar to those of traditional FP receptor agonists, however these, in contrast, may increase TM contractility. Furthermore, selective EP₄ agonists have also been shown to be efficacious in treatment of POAG. Both SC and TM cells express EP₄ receptors, and hypertension lowering effects are believed to be primarily localised to the conventional pathway (188, 260). EP₄ receptors alone induce expression of early growth response factor-1, mediated by extracellular signal-regulated kinases (261), while these kinases are also known to influence MMP expression (262). These observations illustrate the unique modes of action of prostanoid receptors, and the potential that these drugs can be tailored to have greater specificity and efficacy.

A number of siRNA therapies are in clinical trial for glaucoma, some functioning in a similar manner to that of β -blockers, inhibiting the B₂-adrenergic receptors at the ciliary body, thereby reducing AH production. Tolerability and safety profiles indicate that siRNA was only present in ocular tissues, providing a possible alternative form of therapy for patients that may have asthma or congestive heart failure where the use of traditional, nonselective beta blockers is limited (263, 264). It is also interesting to note that a recent study in rodents using siRNA targeting the tight junctions of the SC reported increased outflow facility corresponding to additional open clefts, indicating increased paracellular transport (24). This study, undertaken at this Unit and having input from myself, is presented in Appendix 6.

Since patient compliance is a major issue, the development of longer-lasting medications could provide great benefit to patients. Strategies for enhanced delivery include drug re-formulation into nanocapsules or nanospheres, reducing the amount of preservatives (which may illicit side effects (265)), or modulation of solution viscosity by incorporation of polymers, collagen shields, gels or liposomes. Such engineering allows greater cell-specificity and retention of stability. Slow release implants are also in development, including those designed for sustained

release of prostaglandin by an implant introduced into the eye via intracameral injection. Other devices include plugs or rings to deliver traditionally topical medications into the punctum or conjunctival fornices respectively (266, 267). A summary of traditional and emerging formulations is provided in Table 1.

Table 1. Comparison of traditional vs emerging formulations in glaucoma treatment

Class of Medication	Clinical Prevalence Today	Primary Mode of Action	Mechanism	References
Traditional				
Prostaglandin F2 α Analogue	1 st line- Common	Increases unconventional and conventional outflow	Ciliary muscle relaxation, ECM remodelling by MMPs	124 - 127
B-blockers	2 nd line - Uncommon	Reduces AH production	Block β 1/ β 2 adrenoceptors, vasoconstriction at ciliary body	131, 132
Carbonic Anhydrase inhibitors	2 nd line - Uncommon	Reduces AH production	Inhibit bicarbonate formation	135
Cholinergics	3 rd line - Uncommon	Increases conventional outflow	Ciliary muscle contraction	136 - 138
A2-adrenergic receptor agonists	Rarely used due to side effects	Reduces AH production, increases unconventional outflow	Block α 2-adrenergic receptors, elevate prostaglandin expression	133, 134
Emerging				
ROCK inhibitor	Approved in Japan, phase III trials in US	Increases conventional outflow	Cytoskeletal disorganisation, promotes cell migration	143, 144
Macrolides	Phase I trials	Increases conventional outflow	Disruption of actin cytoskeleton	155-164
Adenosine receptor agonists (A ₁)	Phase III trials	Increases conventional outflow	ECM remodelling by MMPs	165-170
siRNA	Phase II trials	Reduces AH production	Inhibit β 2-adrenergic receptors at ciliary body	178, 179
AAV	Preclinical development	Increases conventional outflow	ECM remodelling by MMPs	194, 98

Table taken from (10), O'Callaghan et al.

On the development of genetic therapies

Adenoviral (AV), Herpes simplex (HSV), Lentiviral and Adeno-associated viral (AAV) vectors have all been used in targeting experimental gene therapies to the TM. There have also been a

limited number of early reports on the use of HSV vectors in transfection of the TM, however, limited reporter gene expression and significant inflammatory responses were observed (268, 269). Long-term expression in TM cells and in rodents has been achieved with lentivirus following a single intracameral inoculation (270, 271). The first demonstration of efficient lentiviral transduction in primates reported well tolerated, extensive viral expression with a mild inflammatory response (272). In early AV studies, gene expression was obtained in TM cells of mice for up to 14 days following intracameral inoculation of a replication-deficient AV vector expressing a LacZ gene (273). In practice however, the feasibility of using AV as a gene therapy vector is extremely limited owing to its immunogenicity and the non-sustainability of viral expression, however AV has been a useful vector in demonstrating proof of principle of gene therapy strategies (274-276). In this regard, an AV system in which MMP-1 expression could be activated by a glucocorticoid-responsive promoter has been developed. Corticosteroid treatments can result in elevations in IOP in a significant number of individuals, thus steroid induced expression of MMP-1 within the TM will result in a reduction in collagen type I, potentially preventing an increase in IOP (277). This approach was subsequently extended to sheep, where steroid-induced expression of MMP-1 resulted in a decrease in IOP (278), and later deployed in a scAAV system more appropriate to human intervention (279).

AAVs are widely used in gene therapy vector systems today. AAV is an innate human virus, integrated into the human genome on chromosome 19, and will only replicate in the presence of AV helper functions. In some studies, AAV has been shown to have little immunogenicity such as in the CNS, however immunogenicity via systemic administration is apparent (280, 281). Animal models have not always successfully predicted the T-cell response to AAVs in humans, although recent developments have generated mouse models for the T cell response to capsid proteins that mimics that of humans (282). Moreover, AAV has been used extensively in human trials of gene therapy for retinopathies, particularly for Leber congenital amaurosis and retinitis pigmentosa. Conventional AAVs have a single stranded DNA genome, which

requires second strand synthesis by host DNA polymerases. By incorporating a second self-complementary DNA strand into these vectors (scAAV), these viruses have been shown to be significantly more efficient in transducing target cells, with the disadvantage of a reduction in the size of their DNA handling capacity (283). While standard AAV constructs transfect but do not appear to be expressed in cells of the conventional outflow pathway, highly efficient expression has been demonstrated via the use of scAAV (284). Rapid and widespread transfection of the TM has been demonstrated following intracameral inoculation of GFP-expressing scAAV2 constructs in both rats and non-human primates, with expression lasting in rats for greater than 3.5 months and in monkeys for at least 2.35 years.

In the case of glucocorticoid inducible expression of MMP-1 previously mentioned, IOP was successfully reduced in sheep following intracameral inoculation of the AAV virus, with no localized or systemic negative effects (279). This study was the first in which the feasibility of a gene therapy approach for steroid induced IOP was demonstrated with a virus that could be deployed as a human therapy. Given the safety profile of AAV and its wide use in ocular gene therapy, having progressed through Phase III trials for Leber congenital amaurosis and Leber hereditary optic neuropathy (285), AAV systems in which proteinases can be periodically induced as indicated by IOP hold substantial promise as gene medicines.

1.8 Conclusion

The ECM is a dynamic structure capable of enhancing outflow resistance at the JCT region of the conventional outflow tissues. Normal responses to elevated IOP allow this structure to expand and alter its configuration to facilitate increased outflow facility, thus alleviating ocular hypertension. In open-angle glaucoma however, hypertension remains through as of yet incompletely elucidated mechanisms. As lowering IOP remains the primary treatment for patients with this disease, medications and surgeries aim to do so via a variety of biological and mechanical interventions. New strategies in development target the conventional outflow

pathway more specifically, many of which employ remodelling of the ECM. Re-organisation of matrix components using MMPs, inhibition of focal adhesions, depolymerisation of the actin cytoskeleton and deterioration of inter-endothelial junctions are such examples that provide a means by which AH outflow facility can be increased, ultimately leading to a reduction in IOP. Novel targeting approaches, together with advanced delivery systems and combination therapies, may assist in improving patient compliance, long term cost, chronic reductions in IOP, and ultimately a reduction in vision loss.

That the bulk of AH outflow is through the conventional pathway and that most of the medications in current clinical use do not primarily target this pathway will be a matter of intrigue to most non-specialists. However, while many of the new formulations in development target pathological disease processes which are primarily located in the anterior part of the eye, death of the retina's output sensory neurons, the ganglion cells, is the final determinant of vision loss caused by elevated IOP. It is therefore not unreasonable to speculate that combinatorial therapies, simultaneously targeting outflow together with ganglion cell survival, may prove more highly efficacious than attempting to lower IOP singularly. Mediators of the cytoskeleton, focal adhesions, intercellular junctions and ECM can all alter the architecture of the outflow tissues, including alterations in cell geometry, contractility, and migration, among other functions, leading to changes in outflow resistance. However, it remains to be determined whether such morphological changes are transient, and whether treated tissues will remain in their remodelled state if treatment is discontinued. To date, the underlying mechanisms by which current first line medications act remain to be fully elucidated, although significant steps have been made in recent years. Emerging knowledge has led to the development of new formulations showing greater efficacy and safety than conventional medications, with many of these are currently in clinical trial. Many drugs, both old and new, target the conventional outflow pathway, in particular the ECM and cytoskeletal structures, but this is often secondary or indirect to their primary mode of action. Remodelling of the ECM has been shown to

influence outflow resistance greatly, giving strength to the hypothesis that the ECM at the JCT contributes substantially to outflow resistance. Perfusion with compounds that activate matrix modulators, such as MMPs, or even traditional medications, have been shown to increase outflow facility with simultaneous elevations in MMP expression. It is not surprising however, that perfusion with purified MMP's alone significantly alters conventional outflow, in both its morphology and AH dynamics. Recent developments have demonstrated the efficacy of introducing MMP genes into the anterior chamber via AAVs. Implementing proteases directly modulating the ECM reduces the potential for unwanted off-target and downstream adversities in comparison to activators or inducers of such proteases, however MMPs themselves also have downstream signalling cascades, thus selection of specific proteases is important and further development may see an even more specific use of metalloproteinases. For example, MMP-1 was chosen for glucocorticoid-induced expression as it is a well-documented MMP with a large target profile. Similar selection must be undertaken for other drugs in development. ECM modulation by metalloproteinases should in theory be effective in targeting secondary glaucoma, including pseudoexfoliative, pigmentary and uveitic glaucoma, which involve physical blockage of drainage channels. AAV used as a vector for gene delivery has an excellent safety and tolerability profile. External inducers of viral expression are avenues in themselves, response elements currently ranging from glucocorticoid responsive promoters to tetracycline responsive promoters. The tetracycline-inducible systems have been widely used in AAV expression, however with them comes their own limitations including leaky promoters and potential toxicity of the inducer. In this regard it is of note that doxycycline is commonly used as an antibiotic and is also approved for inhibition of select MMP expression. Topical doxycycline is used to treat dry eye, showing efficacy in mouse models in decreasing gelatinolytic activity in corneal epithelia and improving surface regularity and barrier function (286). Doxycycline is both anti-microbial and anti-inflammatory, and a low dose regimen has been shown to be efficacious and tolerable in dry eye with mild side effects including upset

stomach, yeast infections and photosensitivity (287). Alternative tetracycline derivatives could prove more efficacious, or the design of unique inducible elements may generate new means of controlling expression in disease states. Such therapies are still in proof of concept stages however, and pre-clinical functional validation and safety in non-human primates will be required.

There is clearly an unmet need for novel glaucoma therapeutics which sufficiently demonstrates long term reduction of IOP with minimal side effects. Further elucidation of the exact mechanisms of open angle glaucoma, and its treatments, may lead to medications that directly target the causative site, arresting disease progress and restoring function to existing tissues.

1.9 Aims

The primary aim for the work reported in this thesis is to design an AAV-mediated gene therapy to reduce IOP by reducing outflow resistance. The proposed mechanism involved for such a therapy encompasses ECM degradation by means of a protease secreted by AAV delivered by an intracameral injection. The nature of this protease must first be determined *in vitro* via permeability assays before incorporation into an AAV. Proof of efficacy will be determined using rebound tonometry and ocular perfusions along with initial safety and morphology by transmission electron microscopy (TEM). The end goal of this body of work is to show efficacy of a gene therapy in a murine model of glaucoma.

Chapter 2

Selecting a Viable Therapeutic

2.1 Introduction

Cytokines, small signalling molecules affecting the behaviour of cells, have the potential to be used as biomarkers for POAG. Tear films were taken from POAG patients who had not undergone eye drop treatment, and it was found that the levels of 8 pro-inflammatory cytokines were reduced compared to controls (288). Non-invasive methods that can accurately quantify cytokine levels from low protein concentrations, such as the example above, may lead to the identification of novel diagnosis biomarkers for POAG. Cytokine levels in the vitreous humour were analysed and shown to be significantly elevated in acute PACG but were not in chronic PACG or POAG (289). The AH of glaucomatous patients has also been studied for any imbalance in cytokine levels. Recent studies show elevations in IL-8, TGF β 1, TNF- α , SAA, IP-10, MCP-1, MIP-1 β and INF- α in POAG AH versus cataract control AH, along with the reduction in IL-6 and IL-12 concentrations in some studies, contradictory to other studies. (290-292). Not only is this imbalance present in the fluids of the eye in glaucoma, but also in the outflow tissues. The TM of POAG patients has been shown by immunohistochemistry to express prominent elevations in IL-6, TNF- α and IL-1 β (293). These findings indicate that

macrophages within the TM secrete cytokines, leading to an acute inflammatory reaction and the recruitment of other immune cells. It is apparent that cytokines play an important role in the pathogenesis of glaucoma, although this role remains elusive. These studies suggest that anti-inflammatory treatments are necessary for controlling IOP in glaucoma. It is also of interest to note that biomarkers of neurodegeneration are present in POAG AH, which along with cytokines, may contribute to TM injury (294). Such biomarkers include cathepsin D: known to play a role in neurodegenerative diseases along with its substrates; the cell adhesion molecule NCAM: an influencer of axonal outgrowth and synaptogenesis, the levels of which are altered in the cerebral spinal fluid of patients with Alzheimer's disease, multiple sclerosis and schizophrenia; and VCAM-1: an factor that can indicate endothelial activation or dysfunction and has been suggested to be a marker for dementia in Parkinson's disease (294, 295).

Cytokines form the basis of intercellular signalling by binding to receptors on the cell surface, initiating complex transduction pathways, and are components of a vast range of biological processes. Some such processes include immunity, inflammation, differentiation, development, phosphorylation, growth and migration, and are therefore considered the controllers of cells. Due to their tight regulation and potency, they can be used as markers for toxicity (296). As is the case for POAG, cytokines are upregulated by unconfirmed means, resulting in an imbalance, no doubt affecting several homeostatic processes. Positive feedback may occur in which high cytokine concentration results in the expression of more cytokines, leading to what is called a 'cytokine storm', negatively impacting adjacent tissues further. Simultaneously, the expression of a plethora of proteins may be affected, as is the case in post-mortem TM tissue (297, 298).

Specific examples of TM homeostatic regulation by cytokines are numerous in the literature. Evidence exists suggesting that ECM remodelling and cytoskeletal alterations may occur in the TM in response to IL-6, TNF- α and IL-1 β (293). IL-6 reduces outflow resistance in porcine eyes and was elevated in TM cells as a result of oxidative stress (299, 300). Along with IL-6, TNF- α regulates endothelial tight junction modulation, through cytoskeletal rearrangement

(301). Further, it is known that cytokines impact outflow of AH and cell monolayer permeability, in the case of IL-6 and IL-8 (302, 303).

There is, however, little evidence in the literature stating whether cytokines can influence the SC, its endothelia, and ultimately its contribution to outflow resistance. The following sets of experiments confirm some previous observations but also expand them to SC cells and multiple members of the MMP protein family. By treating cells of the outflow tissue such as SC cells with a range of cytokines, we may be able to predict how these cells function in a glaucomatous environment (high cytokine concentration). As outlined in Chapter 1, modulating ECM expression via MMPs could be an attractive avenue for a therapy, and it has also been shown that cytokines upregulate MMPs (304). Thus, cytokines may play an indirect role in glaucoma, initiating signal cascades that induce proteins (such as the MMP family) that subsequently result in a homeostatic or pathogenic effect. How SC cells respond to cytokines may be useful in determining how MMP expression itself is regulated in an environment comparable to glaucoma. Transcription, translation and activity are important factors in MMP homeostasis, and will be observed in and SC cells treated with cytokines, to simulate that of control and glaucomatous human AH.

2.2 Results

SC monolayer permeability in response to cytokines

Cell monolayer permeability is determined by flux assay (method 6.5) and transendothelial electrical resistance (TEER) values (method 6.4). These assays determine any changes in paracellular macromolecular and ionic permeability respectively.

SC endothelial cells treated with cytokines at 10 ng/ml (method 6.1) showed alterations in paracellular permeability. Each of IL-1 α , IL-1 β , and TNF- α increased paracellular flux across the monolayer, however only IL-1 α resulted in a significant increase of 6.9 [4.1, 9.6] Papp

(mean [95% confidence intervals (CI)]) compared to the PBS vehicle control ($p = 0.0002$, $n = 3$, 1way ANOVA with Tukey's multiple comparison test, Figure 2.1).

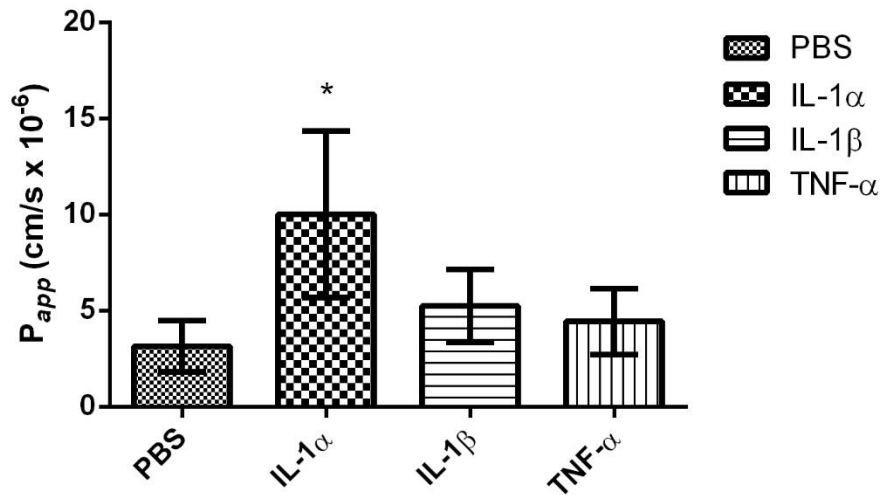


Figure 2.1: Dextran flux in response to cytokines

SC cells treated with cytokines IL-1 α , IL-1 β , and TNF- α were tested for enhanced permeability by FITC-dextran flux assay using a 70kDa dextran and show an increase in the coefficient of permeability compared to a vehicle control.

TEER values were taken at both 24 and 48 hours post-treatment. 2way ANOVA with multiple comparisons (Bonferroni in this case) allows for comparison between both treatments, and timepoints. From this analysis, each cytokine significantly reduced TEER at 24 hours, but there was no significant difference at 48 hours (Figure 2.2). At the 24 hour timepoint, each of IL-1 α , IL-1 β , and TNF- α treated at 10 ng/ml significantly reduced TEER by 6.1 [2.2, 10.0] $\Omega\cdot\text{cm}^2$ ($p < 0.001$), 5.8 [1.9, 9.7] $\Omega\cdot\text{cm}^2$ ($p < 0.001$) and 3.9 [0.1, 7.8] $\Omega\cdot\text{cm}^2$ ($p < 0.01$) respectively. At 48 hours, TEERs were non-significantly reduced by 1.3 [-2.6, 5.1] $\Omega\cdot\text{cm}^2$, 0.6 [-3.3, 4.4] $\Omega\cdot\text{cm}^2$ and 2.4 [-1.5, 6.3] $\Omega\cdot\text{cm}^2$ respectively ($n = 3$ in all cases). In accordance with the 2way ANOVA format, the difference between timepoints and treatments were significantly different at $p =$

0.0023 and $p = 0.0003$ for each parameter. This suggests that cytokines eventually become sequestered or degraded over time, and permeability modulations are transient.

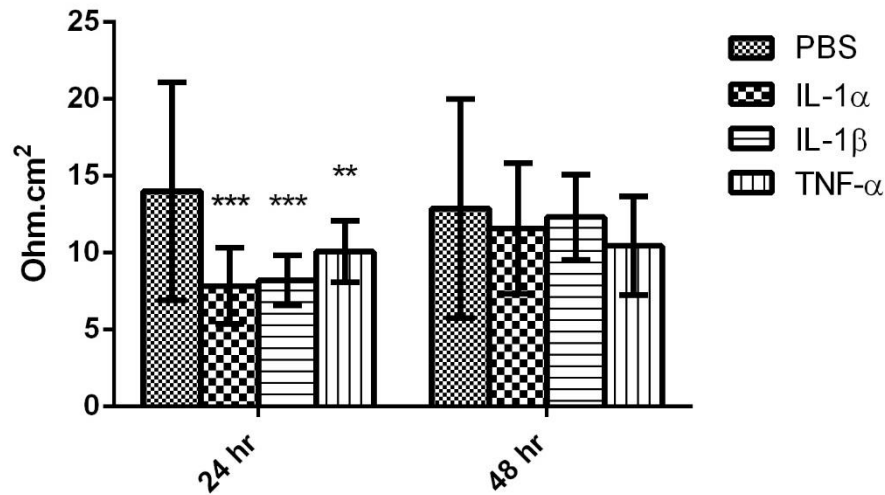


Figure 2.2: Transendothelial electrical resistance in response to cytokines

SC cells treated with cytokines IL-1α, IL-1β, and TNF-α at 10 ng/ml each were tested for their electrical resistance as a measure of permeability. All treatments show significant reduction in TEER at 24 hr and the effect is reversed by 48 hr.

Cytokines modulate expression of MMPs

The literature assumes that upregulation of regulatory factors is responsible for the changes in monolayer permeability by cytokines, presumed to be MMPs. Each of these cytokines acts on MMP-3 induction in different ways, for example IL-1α increased monolayer permeability the most, however IL-1β increases MMP-3 expression to a greater extent at the 24-hour timepoint, as denoted by the literature (149). This early timepoint allows for time savings, and choosing IL-1β as a single treatment makes it easier to screen a variety of inhibitors and combinations. To address which MMPs are upregulated, RT-PCR was conducted to determine mRNA levels of MMP-2, MMP-3 and MMP-9 (method 6.6). $\Delta\Delta CT$ calculations determined fold change expression in MMP mRNA. SC cells were treated with combinations of cytokine, MMP and

inhibitors to best determine the dynamics of MMP transcriptional regulation. Fold change results were normalised to the vehicle control (PBS), and a 1way ANOVA was used to test for significance. No combinations of IL-1 β significantly increased MMP-2 or MMP-9 expression in SC cells. Similarly, addition of MMP-3 or TIMP-1 (the MMP inhibitor with the greatest affinity for MMP-3 inhibition) to cell media did not significantly affect expression levels. Conversely, addition of IL-1 β to SC cells greatly increased MMP-3 RNA expression by 46-fold, n = 3 versus controls. IL-1 β + TIMP-1 showed similar significance at a 45-fold increase (Figure 2.3). This is as expected as TIMP-1 only inhibits MMP-3 in its protein state, by inactivation, and has little influence on its transcription in the presence of IL-1 β .

On its own, TIMP-1 appears to somewhat inhibit the expression of MMP-2. Addition of MMP-3 however highlights a trend of reduced expression for all MMPs tested. This suggests a form of autoregulation, or a negative feedback loop, where the abundance of MMP-3 prevents further MMPs being expressed until high MMP-3 concentrations are reverted to basal levels. Interestingly, the same trend is observed when cells are treated with both MMP-3 and IL-1 β . Although these trends are not significant, it indicates that the repression of MMP-3 is downstream, or more potent, than the activation of transcription via cytokine signalling pathways.

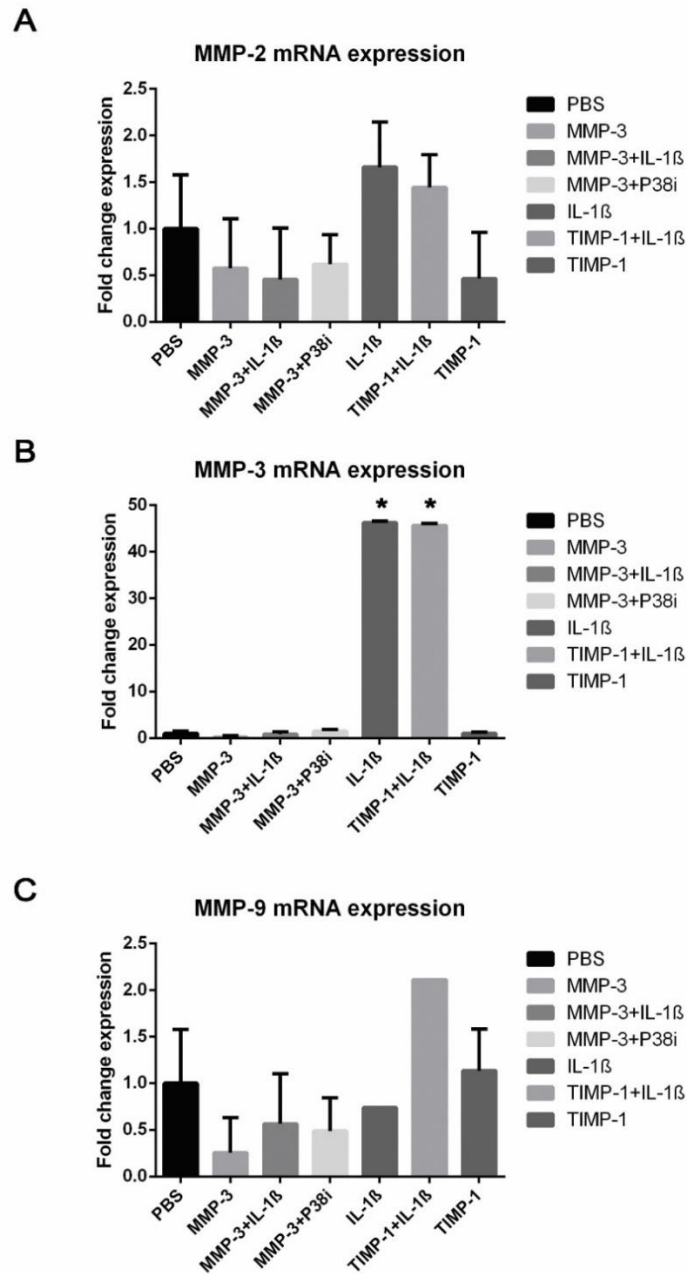


Figure 2.3: Induced MMP expression profiles

RNA was extracted from SC cells treated with various cytokine and protein combinations to determine the expression patterns of MMP-2 (A), MMP-3 (B) and MMP-9 (C). A significant increase in MMP-3 transcription compared to vehicle control (PBS) is seen upon induction with IL-1 β or IL-1 β + TIMP-1.

Due to this dramatic increase in expression, it was of interest to look more closely at the transcriptional dynamics. As such, SC cells were treated with 10 ng/ml of cytokines and RNA

was extracted at 6, 18 and 24 hours post-treatment (method 6.6). Using the same analysis method as before, 2way ANOVA suggests that MMP-3 mRNA expression is significantly elevated at 18 hours post-treatment of IL-1 β (28.2 [8.6, 47.8] fold increase, $p < 0.001$, $n = 3$) and in combination with IL-1 α and TNF- α (54.9 [35.2, 74.5] fold increase, $p < 0.001$, $n = 3$, Figure 2.4). The synergistic effects of cytokines on transcription are well documented and were therefore expected to produce the greatest MMP-3 expression (149). Expression levels are returned to baseline at the 24 hour time-point, reflecting the transience observed in Figure 2.2.

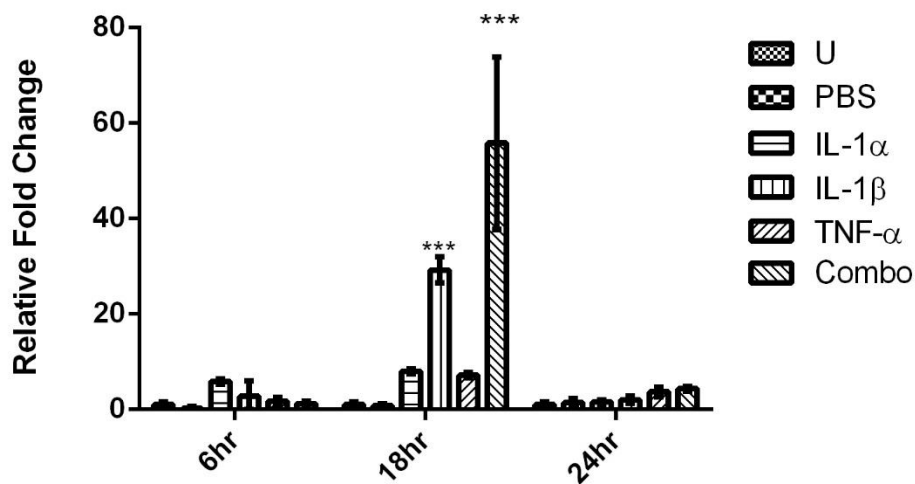


Figure 2.4: mRNA expression of MMP-3 over time

Treating SC cells with various cytokines singly or combined (combo) results in elevated MMP-3 mRNA. Elevation is significant at 18 hours post-treatment of IL-1 β and a combination of IL-1 α , IL-1 β , and TNF- α .

Hence, it follows to view protein expression. SC cells treated with cytokines were lysed at 24 post-treatment. This time point was chosen based on Figure 2.4, as it was expected to have the greatest change in protein expression. Western blot experiments were performed on both cell lysates and cell media (method 6.10). Samples were probed for MMP-3 and normalised to β -actin (Figure 2.5). Similar to mRNA expression, cellular MMP-3 was increased most noticeably

in IL-1 α , IL-1 β and in combination. From cell media samples, it was observed that MMP-3 was abundantly present extracellularly, especially in IL-1 β - and combined cytokine-treated samples. Basal secretion levels were not visualised in control samples, likely due to the high intensity of treated samples requiring shorter exposure times. This indicates that MMP-3 is not only generated within the cell and is secreted extracellularly, correlating with the literature, but vast amounts are secreted into the extracellular space upon induction by cytokines. Normalisation to β -actin in media lysates was not possible as β -actin is non-secretory and are therefore visualised in pixel density instead of fold expression.

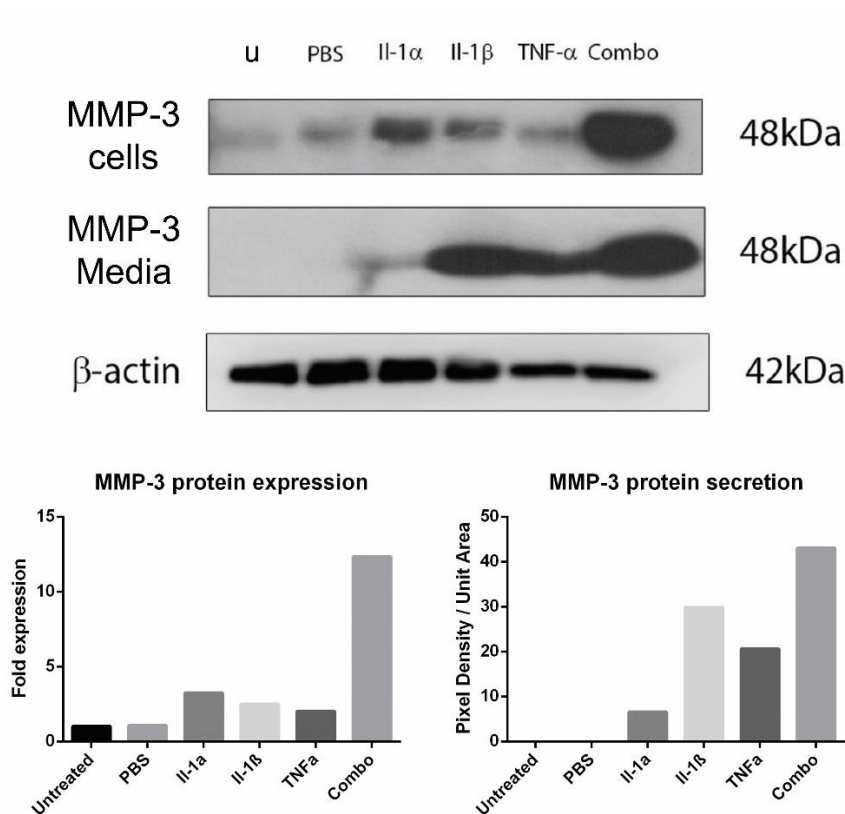


Figure 2.5: SC protein expression of MMP-3 in response to cytokines

Western blot experiments show that treatment of cytokines results in the upregulation of MMP-3 protein. MMP-3 protein is detected in both the cell lysate samples and in the cell media. Expression is strongest when SC cells are treated with numerous cytokines.

It was also of interest to determine if cytokine-mediated secreted MMP was in its active state or in its latent form. Gelatin zymography is routinely used to semi-quantitatively assess the activity of MMP-2 and MMP-9. Casein zymography has been shown to allow detection of MMP-3 activity (305), however this is not a sensitive assay as MMP-3 does not readily cleave casein, thus zymography was only used to evaluate MMP-2 and MMP-9 activities (method 6.11). SC and TM cells were treated with either IL-1 α or IL-1 β . Media samples were run on polyacrylamide gels and were compared to controls after renaturing and developing. In TM cells, MMP-9 was observed to have a greater activity after treatment with both cytokines, and MMP-2 activity appeared unchanged. In SC cells, however, MMP-2 had brighter bands in treatment lanes and MMP-9 intensities remained constant post-treatment (Figure 2.6). The use of both SC and TM cells provides the advantage of determining the presence cell-specific dynamics such as different signalling pathways or concentration levels. This experiment was performed in duplicate and the following figure is representative of both.

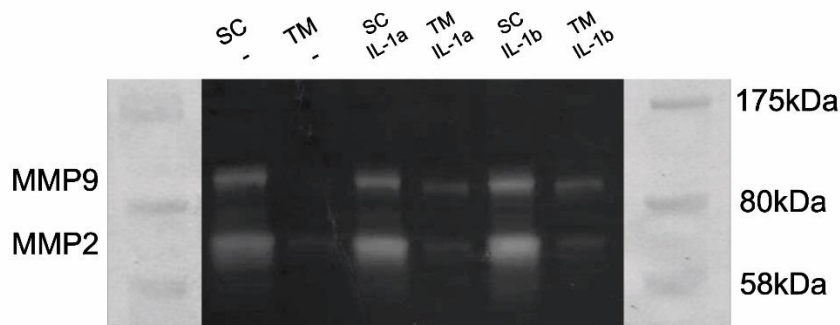


Figure 2.6: Gelatinase activity in cells of the outflow tissue

Media from both SC and TM cells treated with cytokines was assayed using gelatinase zymography. MMP-9 bands are more intense in TM-treated samples and MMP-2 bands are more intense in SC-treated samples indicating greater activity in these cases.

The cytokine to MMP signalling cascade

Several steps in the typical cytokine signalling cascade were confirmed to be active in SC cells that would help to highlight the pathway by which MMPs are upregulated. Firstly, both SC and TM cells express the cytokine receptor protein, IL-1R, along with increased expression in glaucomatous SC cells. SC cell lysates were taken up to 60 minutes after treatment with IL-1 β . P-ERK and P-p38, the phosphorylated state of the ERK and p38 proteins, were probed for and found to be elevated from as early as 5 minutes post-treatment (method 6.10). Phosphorylation of these proteins suggests the involvement of the ERK and MAPK pathways, which are responsible for the transmission of signals from the cell surface to the nucleus (Figure 2.7).

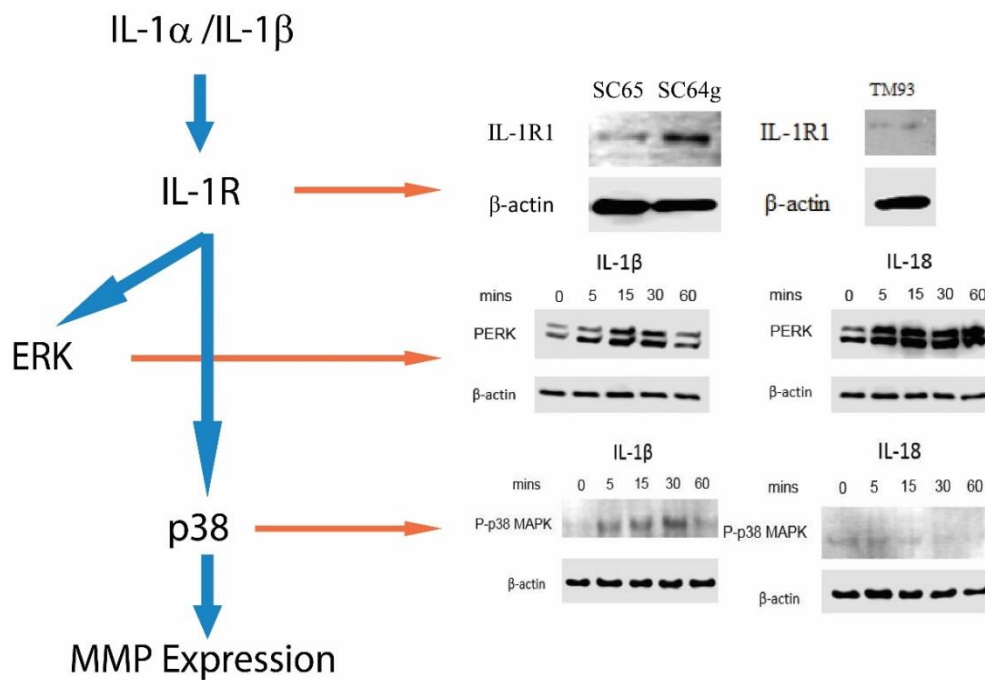


Figure 2.7: Signalling pathway leading to MMP-3 expression.

Several markers were assayed for in western blots to demonstrate that they are being phosphorylated upon treatment with cytokines. The IL-1R receptor, the ERK and MAPK pathways appear to be implicated in the signalling cascade necessary for MMP expression.

MMP in Aqueous Humour

It has already been established that levels of MMPs, along with TIMPs, differ in glaucomatous AH and TM tissue as compared to those from normotensive individuals (151, 152). It has also been shown before that although MMP-2 is upregulated, its activity is still less than that of cataract controls (151). This was confirmed by zymography (method 6.11). MMP-2 activity was significantly reduced in POAG patient AH samples (-0.91 [-1.2, -0.62], $p = 0.0009$, $n = 3$, students t -test, Figure 2.8 left). To determine if this was the case for MMP-3, fluorescent resonance energy transfer (FRET, method 6.18), allowed for the accurate measurement of MMP-3 activity, and, although not significant, a trend towards reduced MMP-3 activity was observed in POAG AH samples (-9.8 [-41.7, 22.3] mU/ml, $p = 0.45$, $n = 4$, Figure 2.8 right). These data suggest a deprivation of MMP proteolysis in the anterior chamber, further implicating the ECM in POAG pathogenesis.

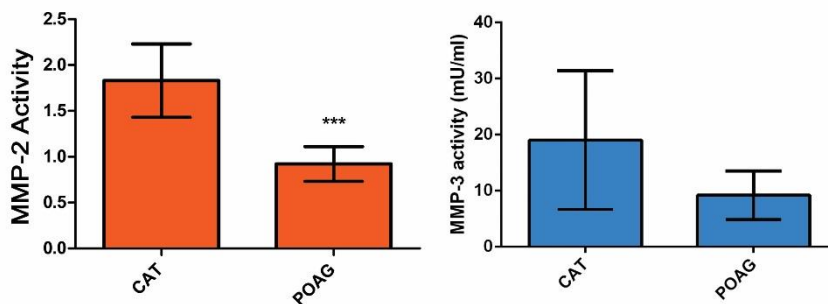


Figure 2.8: MMP activity in human Aqueous

Zymography shows that MMP-2 has a reduced activity in POAG human AH compared to cataract (CAT) control AH (left). To determine MMP-3 activity, FRET (right) was performed. A non-significant reduction in aqueous MMP-3 activity is observed in POAG samples.

2.3 Discussion

Cytokines clearly influence the permeability of SC monolayers (Figures 2.1, 2.2), with different cytokines possibly having different magnitudes of effect. This mechanism of action has been

pointed out before, and molecules that were responsible for initiating the signalling process to modulate permeability were referred to as 'ligands' (303). There is extensive literature stating how tight junctions can regulate ionic, macromolecular and water barriers to modulate paracellular permeability in cell monolayers (24, 306-308). Therefore, tight junctions cannot be ruled out as contributors to the observed increase in permeability in response to cytokines. It is also evident that cytokines have the ability to induce the transcription of many genes, including to a large degree MMP-3, implicating the ECM as another contributor to monolayer permeability regulation (Figures 2.3, 2.4). Why then, does an imbalance of cytokines in POAG AH not result in elevated levels of active MMP-3? As MMP-3 total protein is indeed increased, perhaps there is a prevention of its transformation into active protein. TIMP inhibitors are also upregulated in POAG AH, and it is likely that this increase sequesters any active MMP molecules, reducing overall activity without affecting concentration. The MMP: TIMP ratio is sensitive and tipping the balance in any way could result in large differences in proteolytic activity (151, 154, 309). This could be attributed to Figures 2.3 and 2.6, where a non-significant increase in MMP-2 was observed in response to cytokines, yet an increase in protein activity is apparent. Perhaps this non-significant increase was enough to favour increased MMP-2 activity, or perhaps MMP-2 is activated by cytokines through an unknown mechanism. It must also be considered that elevated MMP levels in AH could be attributed to the treatment undertaken by the patient from which the AH was retrieved. It is known that Latanoprost, for example, increases MMP expression (148), but the extent to which MMP elevation seen in POAG AH resulting from such treatment is unclear. Because of this, it was decided that any results arising from assaying patient AH directly could be partly confounding due to treatments. It was still of interest to determine the effect of a diseased AH on a healthy cell population however, and monitor how these cells respond (method 6.1). This is discussed further in Chapter 3.

The isolation of mouse SC endothelial cells was also attempted through fluorescent-activated cell sorting (FACS, method 6.7). There are no commercially available murine SC endothelial

cell lines, and performing assays on mouse cells may better predict any outcomes in the transition to a murine *in vivo* system. To this end, corneas were dissected from the eyes of mice in such a way that the outflow tissues would remain attached. Corneas were dissociated in a cocktail of proteases over several hours. Dissociated cells were incubated with fluorophore-conjugated CD-31 and VEGF-R3 antibodies. Repeated FACS analysis revealed that cell counts were very low for the amount of tissue processed. It was also very difficult to identify positive and negative populations. This was attempted 3 times varying the number of corneas and dissociation time, however it was clear that this analysis would require significant optimisation and was therefore not pursued. A sample FACS gating strategy from one of these attempts is provided in Appendix 1, Supplementary Figure 1.

The biological relevance of these results is still somewhat unclear. In ocular homeostasis, an increase in IOP induces mechanical stress on the TM, resulting in increased cytokine and MMP expression, thus relieving pressure by increasing outflow facility (139, 302). In a glaucomatous state, this MMP may not be activated to increase outflow. Conversely, cytokines generated by injury processes, such as excessive oxidative stress (310) may also attribute to reduced MMP activity, resulting in a lack of ECM degradation at the outflow tissue, increasing outflow resistance. Although it is not obvious whether the MMP activity issue is a cause or a result of ocular hypertension, the preliminary data would suggest that the process converting latent MMP into active MMP is impeded.

It follows that addition of active MMP on to healthy SC monolayers should induce the same effect as cytokines on permeability. Should it be observed that MMP is the downstream molecule responsible for the effects on monolayer permeability, it would be preferred over cytokines as a potential therapeutic drug, due to the inflammatory properties of cytokines, their potency, and involvement in many processes resulting in off target effects. This is explored further in Chapter 3.

Chapter 3

Validation as a Potential Therapy

3.1 Introduction

MMP structure and function

As previously mentioned, reduction in ECM turnover within the TM and JCT region as a result of an imbalanced latent-to-activated MMP ratio can be a contributing factor to increased outflow resistance, as observed in glaucoma. It is therefore evident that increasing ECM turnover in outflow tissues may have therapeutic significance by reducing outflow resistance. Topical pressure reducing medications primarily increase the rate of aqueous outflow through the unconventional pathway, or reduce aqueous production (55). The unmet clinical need for improved methods of disease treatment prompted the design of an MMP-3-based therapeutic (defined in Chapter 2 as a promising target). These secreted proteases are responsible for degradation of ECM proteins and cell proliferation, and are thus key components in ECM remodelling and outflow tissue homeostasis (311). MMPs are secreted as inactive protein precursors and are activated when cleaved by extracellular proteinases and other MMPs (145). ProMMP-3, the inactive precursor, typically consists of the propeptide itself, a catalytic domain, a linker peptide and a hemopexin domain. Initially, the preproprotein synthesised intracellularly contains a signal sequence which may be involved in secretion. This domain

becomes cleaved upon secretion, resulting in an extracellular propeptide. The propeptide region interacts with the hemopexin domains directly and the catalytic domain via a 'cysteine switch', rendering the protein in a 'closed' configuration, preventing an essential water-zinc interaction in the catalytic domain required for catalysis, hence it is in an inactive state. A 'bait' region in the pro-domain allows for the interaction of general proteinases to cleave part of the proprotein. A configuration now exists where other MMP's or MMP intermediates complete the removal. This is known as 'stepwise activation' (312). MMP-3 in particular has the ability to autoactivate, performing the second step in this cleavage process itself. The catalytic domain now allows binding of a substrate, which docks into a 'pocket' at the substrate binding site. The depth of this pocket is variable between MMP's and is therefore a factor in substrate specificity. The water in the previously mentioned water-zinc reaction becomes displaced, one of its protons are drawn to the active site and a nucleophilic attack occurs on the water molecule of the carbonyl group of the peptide bond, and thus, substrate cleavage has occurred (313). The hemopexin domain plays a role in collagenolytic activity. It is necessary in order to unwind the triple helix configurations of collagens, otherwise only non-collagenous proteins would undergo proteolysis (314).

Therapeutic design

Deploying MMP-3 as a therapy raises some challenges, as this protein needs to act within the anterior chamber. It would be inappropriate to develop MMP-3 in an eye drop formulation as it may not actively negotiate the corneal layers and may induce off target effects at this site. Repeated intracameral injections of MMP-3 into the anterior chamber may prove effective; however such invasiveness is not attractive in a therapeutic. Here, an approach to develop a gene-based therapy for the delivery of MMP targeting the conventional outflow tissues was undertaken, with the primary aim of reducing both outflow resistance and IOP. Of the many classes of MMPs, MMP-3 (stromelysin-1) presents itself as an attractive candidate for targeting

the ECM of outflow tissues. MMP-3 possesses a vast proteolytic target profile including type IV collagen, fibronectin, laminin, elastin, and proteoglycans, all of which are present in the meshwork and JCT regions of the outflow tissues, making this MMP of particular interest (315-319). Additionally, MMP-3 has the advantages of possessing a secretory domain and can also activate other MMPs, including MMP-1 and MMP-9 (145, 320-322), further assisting in the remodelling of ECM components (170, 172, 323).

AAV vector design and delivery

Efficient gene delivery into the anterior segment of the eye is feasible through the use of adenoviral and AAV vectors. In particular, self-complementary AAV vectors have been shown to have such capability (278, 279, 284, 324). Owing to the fact that MMP-3 is a secretory enzyme synthesised in the endoplasmic reticulum, transduction of tissues of the anterior segment with AAV expressing MMP-3 will result in secretion of the protein into the AH. Any existing MMP-3 negative feedback loops will not affect vector expression due to the independent expression system of the vector. This will subsequently enable MMP-3 to be delivered into outflow tissues via conventional aqueous flow, potentially facilitating targeted degradation of ECM components and thus increasing aqueous outflow.

AAV is the most investigated gene delivery vehicle, having been initially discovered as a contaminant in adenoviral preparations. It is generally considered that up to 5 Kb for an expression cassette is the maximum viable size to retain production yields (325). After delivery to the nucleus, the single stranded DNA must be converted to double stranded DNA, which can be considered a limiting factor in the initiation of transgene expression. Self-complementary AAV can be used to bypass this process as it forms the double strand independently (283). The CMV promoter may perhaps be the most commonly used promoter in AAV constructs, allowing expression in all cell types except in the central nervous system (326). A strong, constitutive promoter such as this is preferred for high expression levels. Promoters may also

be selected for tissue-specific expression, particularly if the AAV is delivered systemically. Codon engineering is recommended to optimise the codon sequence of the gene of interest, contributing to protein production, tissue specificity, and to reduce innate immune responses to foreign DNA (327). For the experiments below, the CMV promoter was used for the reasons outlined above. For inducible control vectors, the U6 promoter is one of the most commonly used promoters for shRNA expression as it is well characterised, is active in all cell types, induces a high level expression of shRNAs and is in routine use in this laboratory {Roelz, 2010 #429}.

Cell type of interest must also be considered. AAV transgenes can form circular concatemers that persist as episomes in the nucleus of transduced cells, and not integrate into the genome (328). This may cause issues as there is no replication mechanism for the vector, and subsequently protein product will be diluted over time. Cell turnover rates will determine the rate of transgene loss. AAV enters cells through interactions with carbohydrates on the cell surface (329). Sugar binding preferences, encoded within the capsid sequence, can influence the transduction of a particular recipient cell type (330). Secondary receptors can also confer cell or tissue specificity (331). Hence, an AAV capsid variant is chosen for its preference in infecting a certain cell or tissue type. Mutated and engineered capsids are also in development for greater control over tropism and specificity (332, 333). Directed evolution is a powerful approach that is used to generate AAV vectors with specific capabilities to overcome delivery limitations. Emulating natural evolution, this high-throughput molecular engineering technique involves repeated genetic diversification and selection to accumulate mutations or modifications that improve function. For capsid genes, a library of viral particles comprising of capsid variants is generated, and selective pressure is applied to promote the emergence of a variant to overcome given barriers. Successful variants are recovered and further enriched for improved variants. This can result in the discovery of a capsid that can transduce specific tissue or cell types, cross physical or cellular barriers, or develop the ability to evade neutralising

antibodies (334, 335). Further optimisation is achieved through improved methods of AAV production and purification to enrich for capsids with full vector genomes along with the elimination of empty vectors. Purification is typically achieved through variations on affinity or ion-exchange chromatography (336). Much trial and error takes place in developing optimal constructs, from both design aspects and translatability from *in vitro* to *in vivo* or even cross species from model organism to human (337).

AAV is typically less immunogenic than other viruses, since certain AAVs do not efficiently transduce antigen-presenting cells, and a recombinant AAV contains no viral genes that would amplify an immune response (338, 339). The capsid proteins and transgene sequence however, may induce immune activity. Adaptive responses may pre-exist in those that have been exposed to AAV variants in the past, reducing the clinical efficacy of subsequent reinfections (340). AAV is well tolerated in the retina with minimal immunogenicity with injections having been successful in the second eye after transduction in the first eye. The anterior chamber is more immunogenic than the sub-retinal space however, and future studies will require detailed analysis of immunogenic responses to AAV. AAV particles have been shown to remain intact in the retina in primates and dogs for over 6 years post administration (341).

The most successful ocular AAV gene therapy study was for Leber's congenital amaurosis, with the gene replacement for *RPE65*. Four separate phase I-II clinical trials were conducted, with variations in design with respect to promoter use, sub-retinal injection volume and surgical protocol, the data collectively demonstrates the safety of AAV2 delivery to the retina (342). A phase III trial (ClinicalTrials.gov Identifier: NCT00999609) was conducted with subretinal administration of the virus, indicating an increase in visual acuity with no serious adverse events (343). This treatment, named Luxterna, was approved by the FDA in December 2017. This is a significant milestone as it would mark the first approved gene therapy for inherited conditions if it were to be approved in early 2018. The first gene therapy sold in the United States, named Kymriah (Novartis) was approved in late 2017 for the treatment of acute lymphoblastic

leukaemia (344). The pioneering results of the trials for this *ex vivo* gene therapy have led to the initiation of trials for other forms of retinopathies. Gene replacement therapies for *MERTK* and *REPI* associated retinal diseases, Stargardt disease, Usher syndrome, achromatopsia, X-linked progressive retinal atrophy, *PDE6 β* associated retinitis pigmentosa and many others are all examples of undergoing trials, many of which use the AAV2 genome (342). To date there are no records of interventional gene therapies for the treatment of glaucoma (clinicaltrials.gov). The approval and initiation of new gene therapies will in turn raise the reputation and public opinion of gene therapies and make them more attractive for both the pharmaceutical industry to pursue, and patients to undergo treatment. Improved efficacy and safety of gene therapies will also render them more popular for doctors and patients when side effects of conventional drugs are considered. Awareness still has to be raised to increase public knowledge of gene therapies, genetically modified organisms, and genetic engineering in general before these non-conventional means of treatment become mainstream.

3.2 Results

Effects of glaucomatous aqueous humour on SC endothelial and TM cell monolayers.

Cultured human SCEC monolayers were treated with human glaucomatous (POAG) or control (cataract) AH for 24 hours (method 6.1), and levels of total secreted and activated MMP-3 in culture media were quantified. This was achieved by performing an ELISA and FRET assay, to monitor the degree of cleavage of an MMP-3 specific substrate, on cell media 24 hours post-treatment (methods 6.17, 6.18). A significant increase was not observed in the level of total (latent and active forms) secreted MMP-3 in culture media following treatment with POAG aqueous, with an increase of 0.15 [-0.35, 0.66] ng/ml ($p = 0.45$, $n = 3$, Figure 3.1A) over controls. However, activity assays indicated that the MMP-3 secreted in response to POAG aqueous had less enzymatic activity than that of cataract control AH, with an average change

of -0.15 [-0.28, -0.02] mU/ml ($p = 0.024$, $n = 9$ cataract, $n = 7$ POAG, Figure 3.1B). These observations corroborate results obtained involving other members of the MMP family in POAG aqueous (151) in that the amount of secreted MMP may remain relatively unchanged but its proteolytic activity is reduced.

Effects of glaucomatous AH on permeability of Schlemm's canal endothelial cells (SCEC) and human TM (HTM) monolayers were determined by TEER and FITC-dextran flux assays (methods 6.4, 6.5). Treatment of cultured SCEC monolayers with POAG AH resulted in increased TEER by an average of 102 % after 24 hour treatment compared to control AH (-7 %), displaying an average absolute increase of 19.82 [15.82, 23.81] $\Omega \cdot \text{cm}^2$ ($p < 0.0001$, $n = 6$ cataract, $n = 12$ POAG, Figure 3.1C). Similarly, HTM responded with an increase of 9.79 [5.55, 14.05] $\Omega \cdot \text{cm}^2$ in response to glaucomatous AH, ($p = 0.0002$, $n = 8$, Figure 3.1D). Glaucomatous AH also reduced SCEC paracellular flux, as measured by the permeability co-efficient (P_{app}), to dextrans of 70 kDa as compared to cataract controls, with a mean difference of 0.14 [0.05, 0.22] $\text{cm/s} \times 10^{-8}$ ($p = 0.009$, $n = 3$ cataract, $n = 3$ POAG, Figure 3.1E). A reduction in HTM permeability was also observed with a mean difference of 0.17 [0.09, 0.23] $\text{cm/s} \times 10^{-9}$ ($p = 0.005$, $n = 8$ cataract, $n = 7$ POAG, Figure 3.1F).

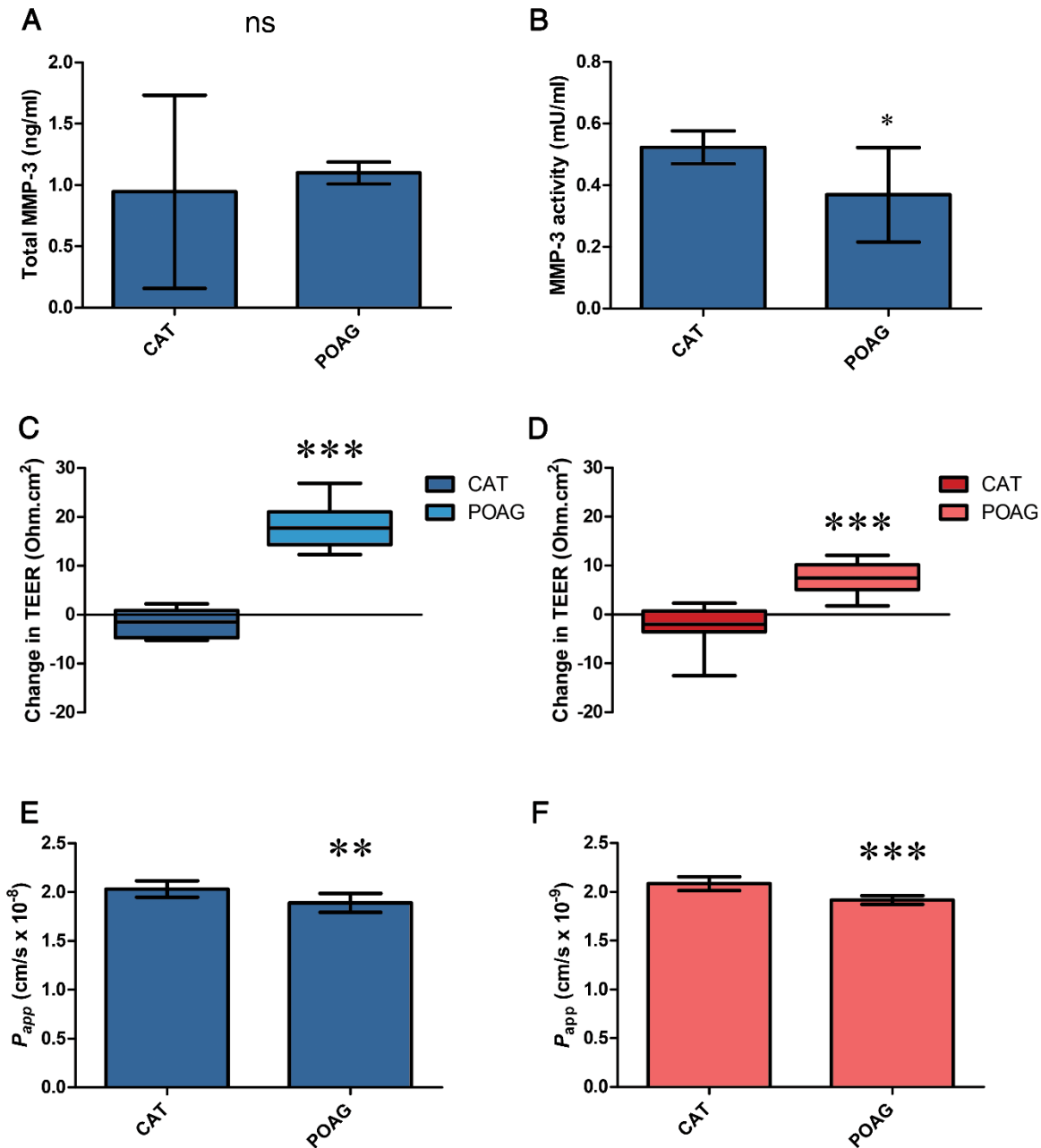


Figure 3.1: MMP-3 concentration and permeability modulations in glaucomatous AH-treated SCEC and HTM monolayers.

(A) MMP-3 concentrations in the media of SCEC monolayers treated with either cataract (control) or POAG human AH showed no significant difference after 24 hours. (B) POAG aqueous-treated SC media samples from (A) were found to have an average change in MMP-3 proteolytic activity of -0.15 [-0.28 , -0.02] mU/ml compared to control media. (C) Addition of POAG aqueous humour onto SC monolayers resulted in an average increase in TEER of 102 % compared to controls. (D) Treatment of HTM cells with human aqueous also increased TEER value. (E-F) SCEC and HTM subjected to AH were tested for cellular permeability using a

*FITC-Dextran flux assay respectively. Decreased permeability to a 70 kDa dextran was observed in response to POAG rather than cataract AH. Graphs show mean with 95% CI error bars. CAT = cataract, POAG = primary open-angle glaucoma. Figures A-F were analysed with a Student's t-test. NS = non-significant. Symbols *, ** and *** denote P values of < 0.05, < 0.01 and < 0.001 respectively.*

Treatment of outflow cell monolayers with recombinant human MMP-3 increases permeability with concomitant reductions in TEER.

In contrast to the negative effects of glaucomatous AH on SCEC and HTM permeability and resistance, it was observed that treatment of cultured monolayers with 10 ng/ml of active recombinant human MMP-3 reduced TEER values on average by 5.62 [2.92, 8.32] $\Omega\cdot\text{cm}^2$ greater than inactivated MMP-3 controls over the course of 24 hours for SCEC ($p < 0.0001$, $n = 8$, Figure 3.2A) and by 4.29 [0.11, 8.48] $\Omega\cdot\text{cm}^2$ for HTM ($p = 0.0137$, $n = 8$, Figure 3.2B) respectively. Permeability assays complemented these data as increases in paracellular flux of 70 kDa FITC-dextran by 0.14 [0.12, 0.18] $\text{cm/s} \times 10^{-9}$ ($p < 0.0001$, $n = 8$, Figure 3.2C) were observed in SCEC, and 0.04 [0.01, 0.06] $\text{cm/s} \times 10^{-9}$ ($p < 0.01$, $n = 8$, Figure 3.2D) in HTM monolayers when comparing treatments of MMP-3 to its inactivated counterpart control: TIMP-1 incubated with MMP-3. To rule out cytotoxicity as a reason for the observed changes in paracellular permeability, a cell viability assay was undertaken (method 6.8). Based on data shown in Figure 3.2E, for concentrations below 36 ng/ml MMP-3, the average SCEC viability for $n = 3$ will exceed 85%. Greater tolerability was observed in HTM cases, retaining an average viability of at least 85% for MMP-3 concentrations up to 151 ng/ml ($n = 3$, Figure 3.2F).

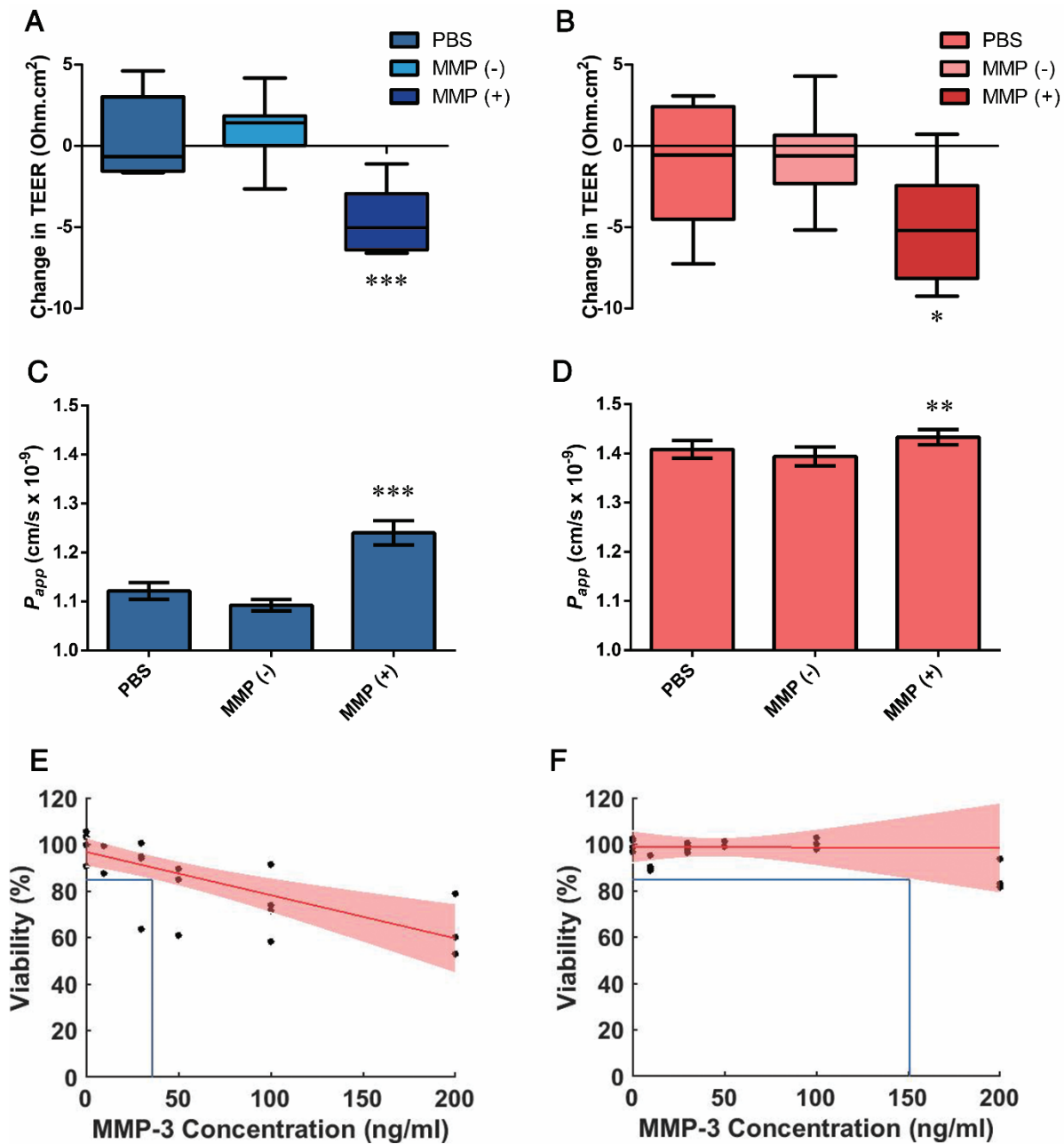


Figure 3.2: Effect of recombinant human MMP-3 on paracellular permeability in HTM and SCEC cell monolayers

SCEC and HTM cells were treated with 10 ng/ml recombinant MMP-3 for 24 hours, using PBS and inactivated MMP-3 (incubation with TIMP-1, MMP(-)) as vehicle and negative controls respectively. (A) SCEC and (B) HTM both show reductions in TEER values after treatment of 4.6 [2.9, 6.2] and 5 [2.2, 7.8] Ohms.cm² respectively. Permeability to a 70 kDa dextran was increased in treated cells (MMP (+)) in both (C) SCEC and (D) HTM. (E) An average viability of 85% was expected for SCEC with MMP-3 concentrations up to 36 ng/ml. (F) 85% viability

is retained on average in HTM cells at concentrations up to 151 ng/ml MMP-3. A, C and E in blue represent SCEC data, whereas B, D and F in red represent HTM data.

Active, recombinant murine MMP-3 increases outflow facility in murine eyes

A pilot study was conducted to determine if MMP-3 could affect outflow resistance in mouse eyes, and if that difference could be detected. 2 μ l of a 100 ng/ml solution of active recombinant, murine MMP-3 was intracamerally injected into one eye of 4 mice. The contralateral eye was injected with 2 μ l of PBS to serve as a control (method 6.13). 24 hours post-injection, eyes were enucleated and cannulated within the iPerfusion system (method 6.19). Analysis by this system indicates that MMP-3 is able to increase outflow facility, by reducing outflow resistance. In this experiment, facility is increased by 3.2 [1.1, 5.4] nl/min/mmHg in MMP-3 treated eyes ($p = 0.016$, $n = 4$, Students t -test, Figure 3.3). This result was sufficient to confirm that MMP-3 can modulate outflow resistance, correlating with the literature (158), and did not warrant further animal testing, rendering a Students t -test adequate for this data set.

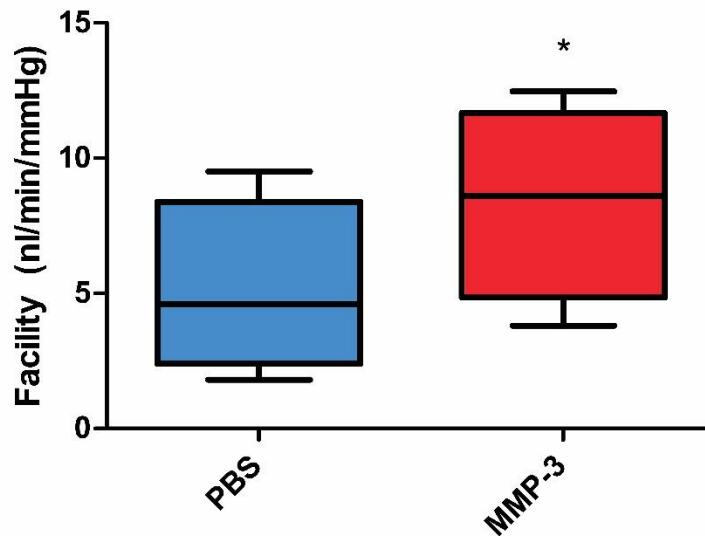


Figure 3.3: Intracamerally injected MMP-3 increases outflow facility

Pilot study involving the intracameral injection of recombinant, active, murine MMP-3 into mice with PBS as a contralateral control. 24 hours after injection, enucleated eyes were perfused. Outflow facility is increased on average by 3.2 nl/min/mmHg in MMP-3 injected eyes.

Treatment of SCEC and HTM monolayers with active recombinant human MMP-3 induces remodelling and degradation of ECM components

In order to attribute increases in permeability to the ECM remodelling effects associated with MMP-3, SCEC and HTM monolayers were both treated as above with 10 mg/ml MMP-3 for 24 hours (method 6.1). Following treatment, there were observational changes in the staining pattern and intensity of a number of ECM proteins by immunocytochemistry (method 6.14). Specific collagen IV staining was localised to perinuclear areas and cytoplasm in both SCEC and HTM cells (Figure 3.4A-B). In particular, a decrease in the staining intensity around perinuclear areas in treated cells was observed as compared to controls. A-SMA fibres facilitating cell-cell contacts in SCEC localised specifically to the cytoplasm and cytoskeleton, and MMP-3 treatment led to an attenuation of fibre bundles with thinning of intercellular

connections (Figure 3.4C). Fluorescent images of F-actin in HTM monolayers also revealed constricted actin bundles and a reduced tendency for bundle crossovers (Figure 3.4D). Immunofluorescence staining of laminin in SCEC and HTM cells showed diminished cytoplasmic localisation and reduced network complexity and multiplicity in MMP-3 treated cells as compared to control staining intensity of laminin (Figure 3.4E-F). To visualise fibronectin clearly without cellular interference, decellularisation was performed after MMP-3 treatment to isolate the ECM scaffold from the cell monolayer. Fluorescent images show significant perturbation of fibronectin networks in treated cells as opposed to the linear cellular organisation observed in control cells (asterisk, Figure 3.4G-H). 4 images were taken across random points in the wells of the chamber slide for every treatment, protein of interest and cell type. Thus Figure 3.4 represents a total of 64 images. To quantitatively demonstrate remodelling of these proteins, western blot analysis was performed on both cell lysate and media fractions of SC and HTM cell monolayers (Figure 3.5, method 6.10)). Specific bands were observed at 300 kDa for collagen IV, 42 kDa for α -SMA, 220 kDa for laminin and 290 kDa for fibronectin. Significant reductions of collagen IV ($p = 0.01$, $p = 0.01$) α -SMA ($p = 0.04$, $p = 0.04$) and laminin ($p = 0.04$, $p = 0.03$) were observed in SC and HTM whole cell lysate samples respectively ($n = 4$ for all cases). Collectively, these data clearly illustrate that MMP-3 mediates remodelling of ECM components in both SCEC and HTM cell monolayers.

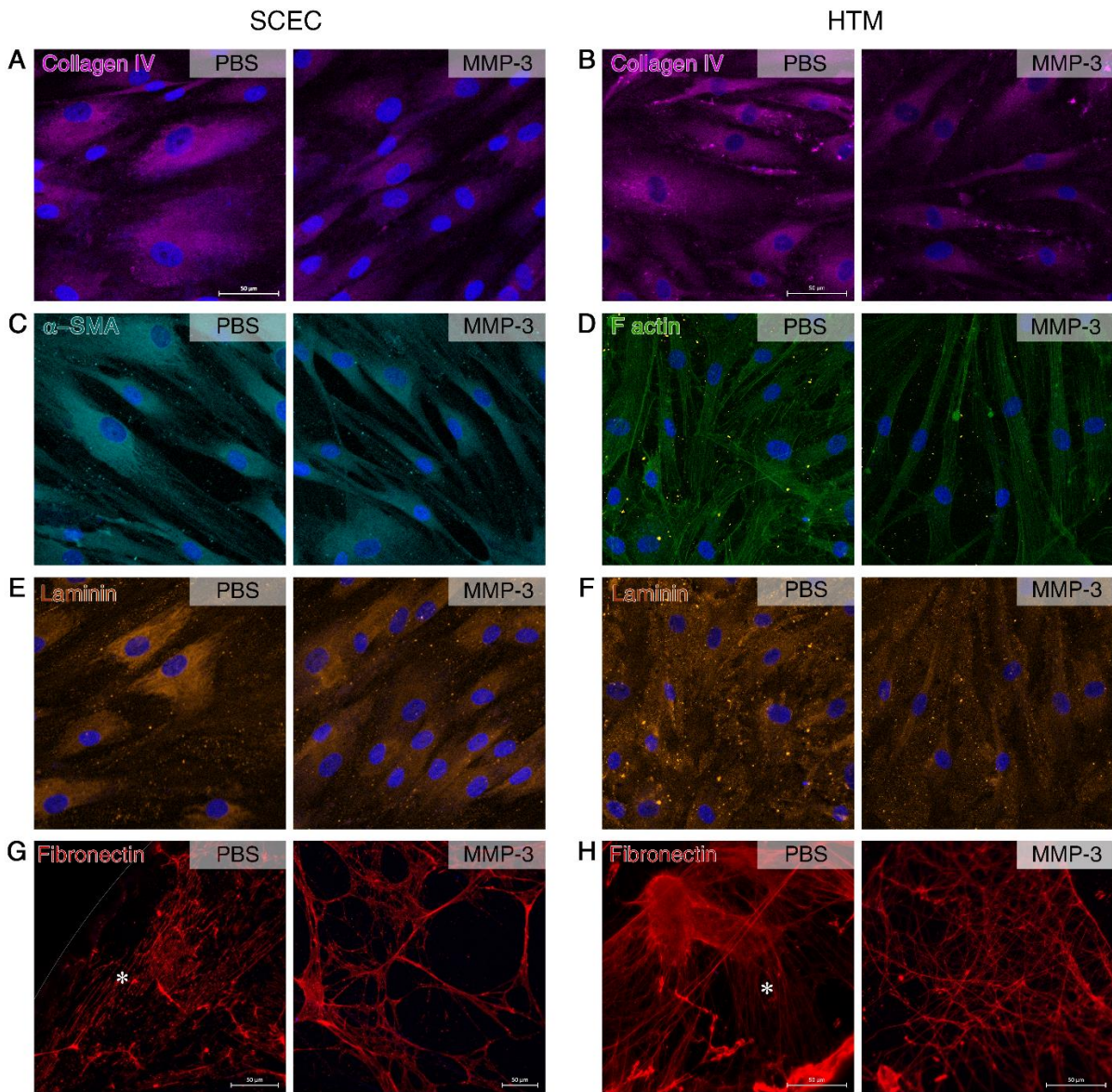


Figure 3.4: Remodelling of ECM components in SCEC and HTM cell monolayers

Immunocytochemistry shows various remodelling artefacts on core ECM components in SCEC and HTM cells in response to MMP-3 treatment. (A-B) Collagen IV appears to have reduced intensity in both cell types after treatment. Collagen IV is concentrated around cells in controls but shows reduced spread after treatment, fibrils barely protruding past the cell nuclei. (C) Alpha smooth muscle fibres extend the width of the cell towards a neighbouring cell. Treated samples show that these fibre bundles have constricted, leading to multiple thin connections between cells. (D) HTM F-actin staining depicts a slight thinning of filament bundles and a reduction of filament branching post MMP-3 treatment. (E-F) Laminin expression exhibits a modest reduction in staining intensity in both cell types, and a reduction in network complexity in TM cells. (G-H) Fibronectin was visualised after decellularisation, depicting linear and

organised strands in PBS controls, as denoted by an asterisk. Treatment groups lacked a linear network, and instead showed a disjointed, porous network. Scale bars represent 50 μm . Left column pairs = SCEC, right column pairs = HTM.

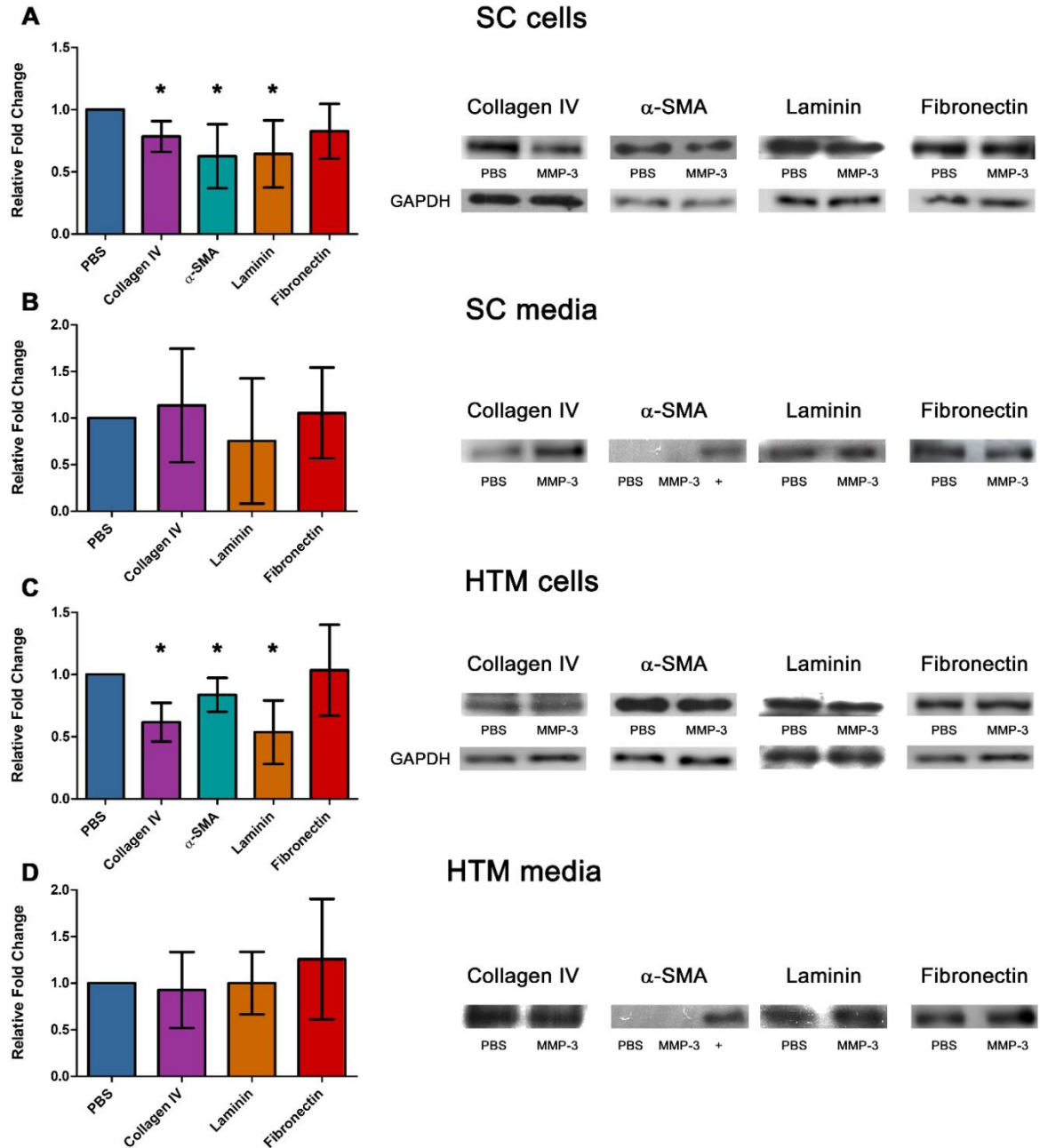


Figure 3.5: Quantification of ECM remodelling and degradation.

Western blot analysis was performed on PBS and MMP-3 treated samples of (A) SC cells, (B) SC media, (C) HTM cells and (D) HTM media. Significant degradation of collagen IV, α -SMA and laminin is apparent in cell lysates only. No α -SMA was detected in media samples. '+'

denotes a positive control lane containing a cell lysate sample. Bars represent mean fold change with 95% confidence intervals.

Intracameral inoculation of AAV-2/9 expressing a CMV-driven MMP-3 gene efficiently transduces corneal endothelium and results in elevated levels of MMP-3 in aqueous humour

AAV-mediated transduction of corneal endothelium could, in principle, serve as an efficient means of expressing and secreting MMP-3 into AH. The advantage of such an approach is that the natural flow dynamics of AH will allow transportation of secreted MMP-3 towards the outflow tissues (Figure 3.6A). We evaluated the efficiency of a number of AAV serotypes with either single stranded or self-complementary genomes to transduce the anterior chamber (Appendix 1, Supplementary Figure 2). 4×10^9 viral genomes of each serotype (a titre of 2×10^{12} vg/ml), expressing a CMV-driven eGFP reporter gene (Figure 3.6B, methods 6.13, 6.14) were intracamerally inoculated into wild-type C57BL/6 mice in a volume of 2 μ l and eyes examined via fluorescent microscopy at 3 weeks post-inoculation. Extensive expression of the reporter gene was observed in the corneal endothelium of eyes injected with non-self-complementary AAV-2/9 (Figure 3.6C top), with no fluorescence being detectable in the outflow tissues themselves using this construct. Hence, the eGFP cDNA from AAV-2/9 was exchanged with murine MMP-3 cDNA to generate AAV-MMP-3, and similar inoculation resulted in MMP-3 expression that was prominently detected in the corneal endothelium and not in AAV-Null controls (Figure 3.6C, bottom) AAV-Null contains the same viral backbone and capsid but does not express any protein. No significant difference in central corneal thickness was detected following AAV inoculation between treated (116.7 [112.5, 120.9] μ m) and control eyes (116.4 [113.6, 119.1] μ m) (n = 4, Figure 3.6). Corneas also appeared clear with no signs of cataracts upon visual inspection, and central corneal thicknesses appeared unaffected by MMP-3 treatment (Figure 3.7, method 6.22). In order to predict in which direction MMP-3 would

secrete from the corneal endothelial cells, SCEC and HTM monolayers were treated with cytokines to induce MMP-3 expression (Figure 3.8). It is clear that in these cells, MMP-3 is preferentially secreted in the apical direction, which is used as a prediction for corneal endothelia also.

The level of total MMP-3 in the AH of twelve inoculated animals was quantified using enzyme-linked immunosorbent assay (ELISA, method 6.17), and a significant average increase in total MMP-3 protein of 56%, 1.37 [0.89, 1.84] ng/ml was observed as compared to 0.87 [0.59, 1.12] ng/ml for AAV-Null control ($p = 0.016$, $n = 12$, Figure 3.6D). Activity of AAV-mediated production of MMP-3 was also assessed using FRET (method 6.18), and a significant increase in activity of 34 [6.86, 61.14] % was observed, on average, in AAV-MMP-3 treated eyes compared to contralateral controls ($p = 0.0164$, $n = 17$, Figure 3.6E).

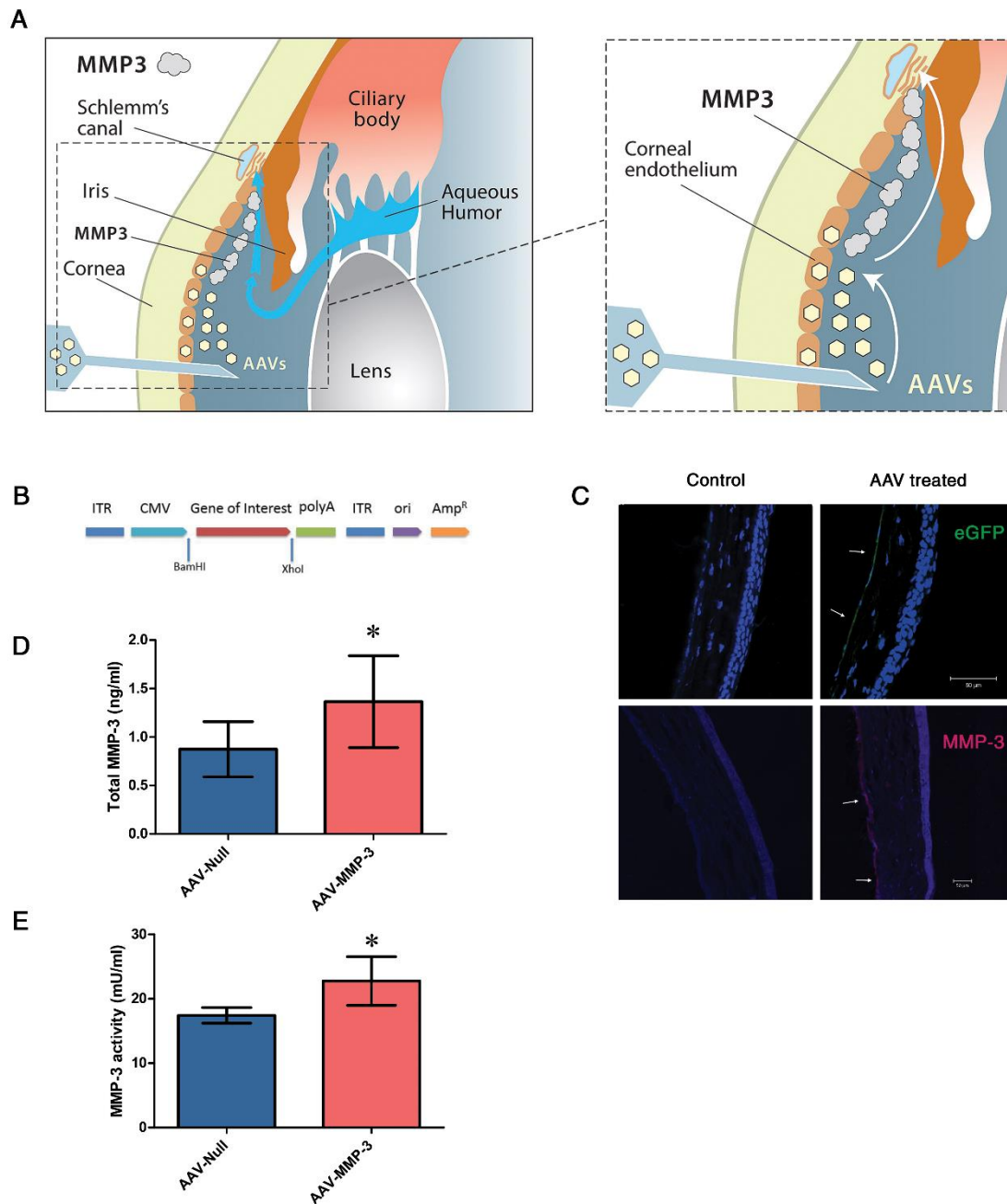


Figure 3.6: AAV-2/9 mediated MMP-3 expression in the corneal endothelium

(A) Diagrams illustrating the therapeutic concept addressed in this study. AAV-2/9 transduces the corneal endothelium upon intracameral inoculation (left). MMP-3 molecules are secreted into the AH from this location and are transported toward the outflow tissue by the natural flow of the aqueous (right). (B) A schematic diagram of the AAV-2/9 vector used for the expression of either eGFP or MMP-3. Murine MMP-3 cDNA was sub-cloned into the pAAV-MCS plasmid and constitutively driven by a CMV promoter (AAV-MMP-3). (C) Immunohistochemistry images of corneas from WT murine eyes intracamerally inoculated with AAV-2/9 expressing eGFP. AAV virus containing a CMV promoter demonstrates transduction and expression at the

corneal endothelium (marked with arrows). Using the AAV-MMP-3 virus, MMP-3 was detected at the corneal endothelium in treated eyes only, denoted by arrows. (D) ELISA was performed on murine AH 4 weeks post injection of virus. MMP-3 concentrations had increased by an average of 0.49 [0.11, 0.87] ng/ml in AAV-MMP-3 treated eyes (paired Student's *t*-test). (E) Aqueous MMP-3 activity was significantly increased by an average of 5.34 [1.12, 9.57] mU in AAV-MMP-3 treated eyes. Scale bars represent 50 μm . Asterisk symbol denotes a *p* value of < 0.05.

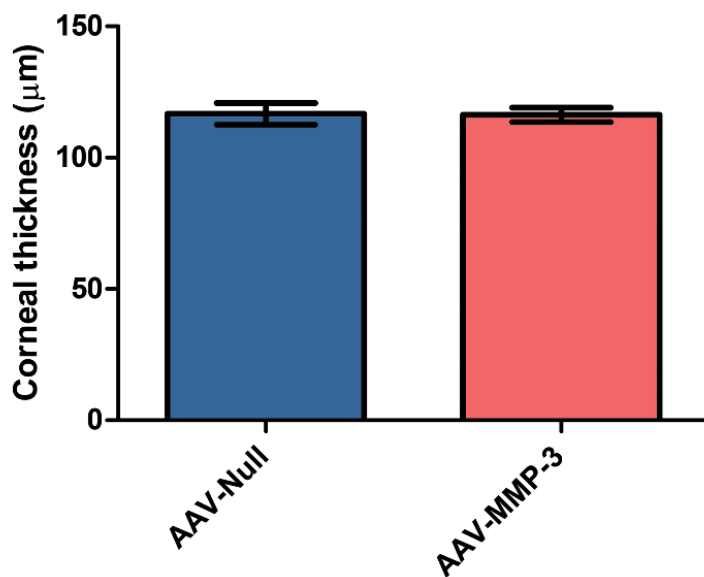


Figure 3.7: Analysis of central corneal thickness.

Central corneal thickness was quantified between AAV-MMP-3 injected eyes versus control. Average central corneal thickness (μm) between treatments was statistically compared by a paired Student's *t*-test. Error bars denote 95% CI. (*n* = 4 pairs of eyes).

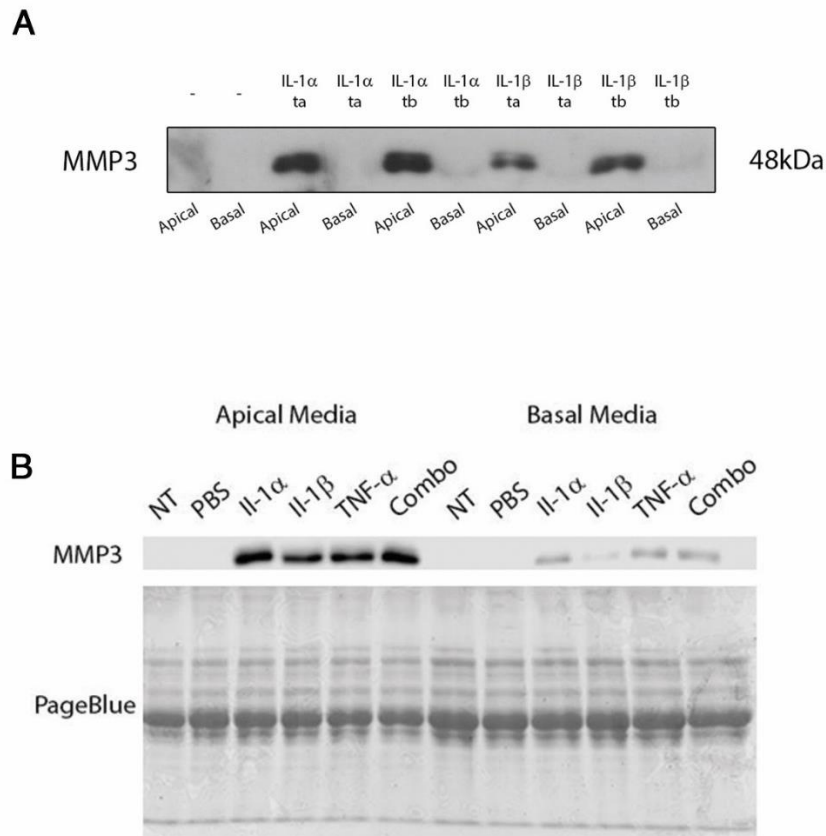


Figure 3.8: MMP-3 secretion characteristics

(A) *IL-1 α and IL-1 β -mediated induction of MMP-3 secretion in human SCEC monolayers. Human SCEC monolayers were treated with IL-1 α and IL-1 β apically or basally, and only apical secretion of MMP-3 was detected. “ta” = treated apically, “tb” = treated basally. (B) Human TM monolayers were treated with IL-1 α , IL-1 β , TNF- α , and in combination, and MMP-3 was only detected in apical samples.*

Intracameral inoculation of AAV-2/9 expressing an MMP-3 gene increases outflow facility and reduces IOP in murine eyes

In order to determine the effect of AAV-mediated expression of MMP-3 from the corneal endothelium on aqueous outflow, conventional outflow facility was measured using the recently developed *iPerfusion* system designed specifically to measure conventional outflow facility in mice (137). Wild type mice were intracamerally injected with 1.2×10^{11} viral genomes of AAV-MMP-3, and contralateral eyes received 1.2×10^{11} viral genomes of AAV-Null (a titre of 6×10^{13} vg/ml in both cases, method 6.13, Appendix 5). Four weeks post-inoculation, eyes

were enucleated and perfused in pairs over incrementing steps in applied pressure (method 6.19). A representative flow-pressure plot provided in Figure 3.9A describes the relationship between flow rate (Q) at each pressure (P) step in both AAV-MMP-3 (red) and AAV-Null (blue) eyes. This is further explained by Appendix 1, Supplementary Figure 3, which portrays the data generated by iPerfusion. Furthermore, the relative percentage difference in facility within each data pair is depicted in Figure 3.9B (left). The resulting facility data presented in Figures 3.10A-B clearly illustrate that control eyes have an average facility of 8.44 [6.14, 11.60] nl/min/mmHg with treated eyes having an average facility of 11.73 [8.05, 17.08] nl/min/mmHg. There is, therefore, an average increase in outflow facility of 39 [19, 63] % in pairs, between treated eyes and their contralateral controls ($p = 0.002$, $n = 8$ pairs).

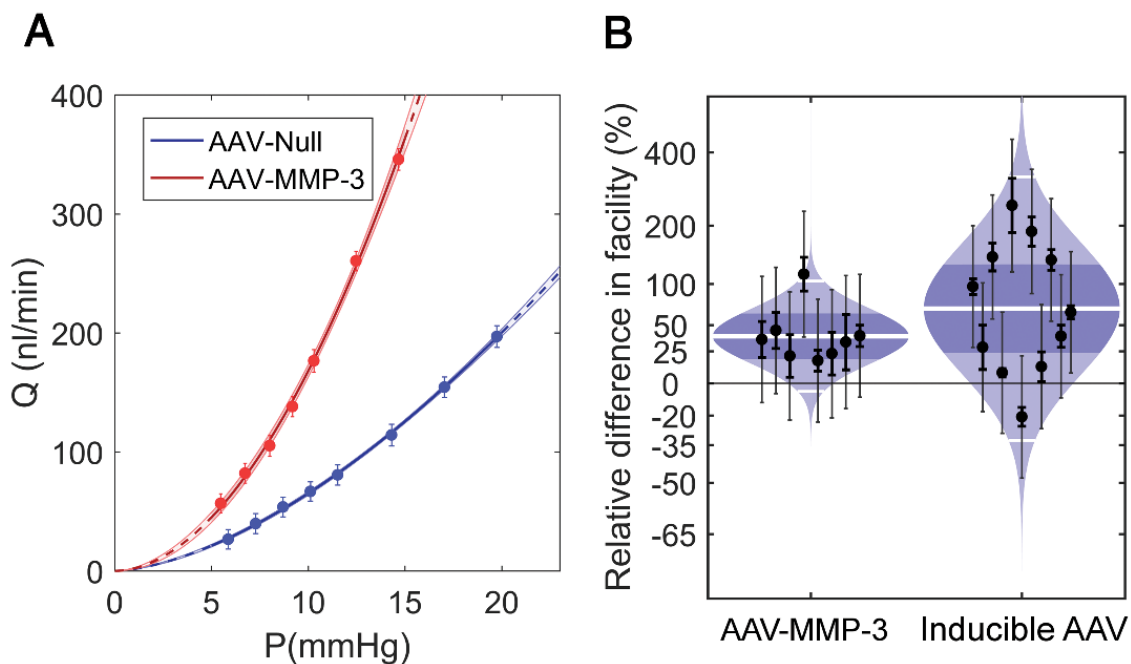


Figure 3.9: Perfusion representations.

(A) Plot depicting the relationship between flow (Q) and pressure (P) in a standard perfusion. As applied pressure increases, flow rate through the eye also increases. AAV-MMP-3 treated eyes have a greater response in flow to pressure increases compared to AAV-Null controls. (B) Relative differences in facility for paired eyes in both the constitutive and inducible viruses are depicted in the cello plot.

As the major pathology in POAG is IOP elevation, and an increased outflow facility was observed, tonometric IOP measurements were taken both immediately before (pre), and four weeks after (post) intracameral injection of AAV-2/9 expressing MMP-3 or a null vector in the case of the control (6.20). Differences between pre- and post-injection IOP were calculated using the non-parametric Wilcoxon matched-pairs signed rank test. Eyes treated with AAV-Null had no significant change in IOP -0.5 ± 2.9 mmHg (median \pm median absolute deviation (MAD), $p = 0.61$, $n = 7$, Wilcoxon signed-rank test with a theoretical median IOP change of 0) after treatment. In comparison, when treated with AAV-MMP-3, median IOP significantly decreased by 3.0 ± 2.9 mmHg ($p = 0.022$, $n = 7$, Figure 3.10C). The IOP difference in AAV-MMP-3 treated eyes was significantly greater than the IOP difference in the contralateral AAV-Null treated eyes by 2.5 ± 0.7 mmHg ($p = 0.034$, $n = 7$, Figure 3.10C).

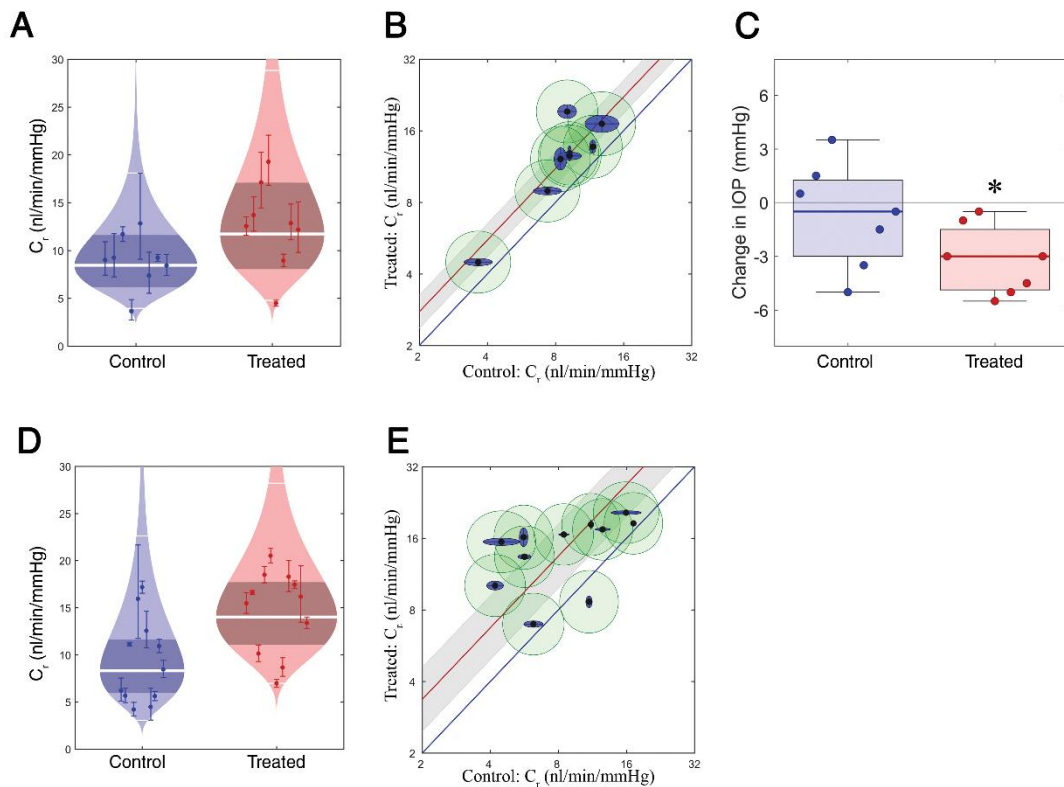


Figure 3.10: Effect of ECM remodelling on outflow facility and IOP

(A) 'Cello' plot depicting individual outflow facility values for eyes at 8 mmHg (C_r) and statistical distribution of both control (AAV-Null) and experimental (AAV-MMP-3) groups. Each point represents a single eye with 95% CI on C_r . Log normal distribution is shown, with the central white band showing the geometric mean and the thinner white bands showing two geometric standard deviations from the mean. The shaded region represents the 95% CI on the mean. (B) Paired outflow facility plot. Each inner point represents an eye pair, with log-transformed facilities of the control eye plotted on the x axis, and treated eye on the y axis. Outer blue and green ellipses show uncertainties generated from fitting the data to a model, intra-individual and cannulation variability respectively. Average increase is denoted by the red line, enclosed by a grey 95% CI, indicating significantly increased facility (does not overlap the blue unity line). (C) Box plots showing the change in IOP in treated and control eyes. Boxes show interquartile range and error bars represent the 5th and 95th percentiles. A significant reduction in IOP is observed in AAV-MMP-3 treated eyes (Wilcoxon signed-rank test). (D-E) Cello and paired facility plots for inducible AAV data sets.

Controlled periodic activation of MMP-3

To incorporate a control mechanism for the secretion of MMP-3 from corneal endothelium, AAV-2/9 expressing eGFP under the control of a tetracycline-inducible U6 promoter (pTIGHT TRE-U6) was first introduced into the anterior chambers of both eyes of wild type mice (method 6.12). After 3 weeks, mice were treated with a regime of 1 drop of 0.2% doxycycline (a tetracycline derivative) 2 times per day (approx. 8 hours between each application) for 10-16 days in one eye only (method 6.12). PBS was administered onto the contralateral eye as a control. As illustrated in Figure 3.11, extensive expression of the reporter gene was observed only in the corneal endothelium, and no expression was observed in the contralateral control. Following this, the reporter cDNA was replaced with murine MMP-3 cDNA and the resulting inducible AAV (AAV-iMMP-3) was injected into the anterior chambers of animals at 1.24×10^{10} viral genomes per eye (4 μ l at a stock titre of 3.1×10^{12} vg/ml). Using the inducible eGFP virus (AAV-iGFP) as a contralateral control, expression was induced by administering doxycycline (as above) to both eyes. Contralateral eyes were perfused as above, the control group exhibiting an average facility of 8.30 [5.75, 11.26] nl/min/mmHg and the MMP-3 treatment group resulting in a facility of 14.01 [11.09, 17.72] nl/min/mmHg. Paired, these eyes exhibit an average increase in outflow facility of 68 [24, 128] % ($p = 0.004$, $n = 11$, Figure 3.10D-E, method 6.19). The relative difference in facility within individual pairs is presented in Figure 3.10B (right). This observation strongly supports the concept that MMP-3 expression could be induced in a controlled and reversible manner, with periodic IOP measurements utilised to guide induction of expression. Vectors were designed by Dr. Marian Humphries and incorporated into AAVs by Vector Biolabs (method 6.12).

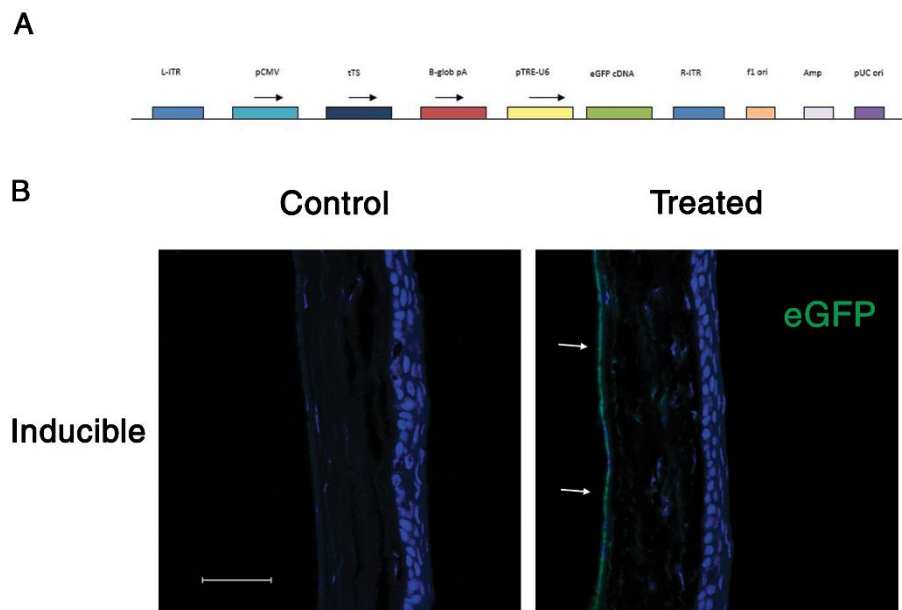


Figure 3.11: Doxycycline induced expression of eGFP from corneal endothelium.

(A) Illustration of the inducible vector construct. (B) AAV2/9 containing a tetracycline inducible promoter expressing eGFP was intracamerally inoculated into the anterior chamber. Expression patterns were similar to those obtained with constitutive expression of eGFP. Scale bar represents 50 μ m. Immunohistochemistry for this image was performed by Darragh Crosbie.

Ultrastructural analysis of AAV-MMP-3 treated eyes

In order to evaluate whether the AAV-MMP-3 treatment affects the morphology of the eye and the TM including the inner wall of SC, ultrastructural investigation was performed in four pairs of mouse eyes (method 6.23). Corneas appeared translucent and healthy on visual inspection during enucleation. Semi-thin sections clearly demonstrated that there were no signs of an inflammatory reaction, either in the TM or in the cornea, uvea or retina (Figure 3.12A-B). Ultrastructural analysis of control eyes revealed normal outflow structural morphology, cell-matrix attachments and cell-cell connections between the SC and TM. The inner wall endothelial cells formed foot-like connections with subendothelial TM cells, as well as connections to underlying elastic fibres and discontinuous basement membrane (Figure 3.12C). However, in some regions of treated eyes, especially those with a prominent SC lumen and

scleral spur-like structure typical of the nasal quadrant (195), there appeared to be more optically empty space directly underlying the inner wall endothelium of SC, compared to AAV-Null controls (Figure 3.12D). In these optically empty spaces, foot-like extensions of the inner wall to the sub-endothelial layer were absent or disconnected from the subendothelial cells or elastic fibres (Figure 3.12D-E). Occasionally, we observed an accumulation of ECM clumps beneath the inner wall that were not observed within the controls (Figure 3.12F) and may represent remnants of digested material.

We quantified the optically empty length directly underlying the inner wall of SC (method 6.23). In control eyes, the percent optically empty length in any one region ranged from 19 – 49% with an average of 37%. In the treated eyes, the equivalent range was 39 – 76% with an average of 59% (Figure 3.12G). The differences between control and experimental eyes for each pair ranged from 16 – 26%, which corresponded to a statistically significant increase in the proportion of open space underlying the inner wall with AAV-MMP-3 relative to AAV-Null ($p = 0.002$, $n = 4$; paired Student's t -test). These data indicate that reduced ECM material in the TM and along the inner wall of SC is associated with AAV-MMP-3 treatment and may explain the enhanced outflow facility and IOP reduction. Furthermore, these morphological changes, because they were absent from controls, could not be attributed to an inflammatory or lytic response to AAV alone.

Electron microscopy experiments were carried out independently by Prof. Elke Lütjen-Drecoll and Dr. Cassandra Flügel-Koch of the University of Erlangen-Nürnberg, Germany. The number of sections and images taken is described in the methods section 6.23.

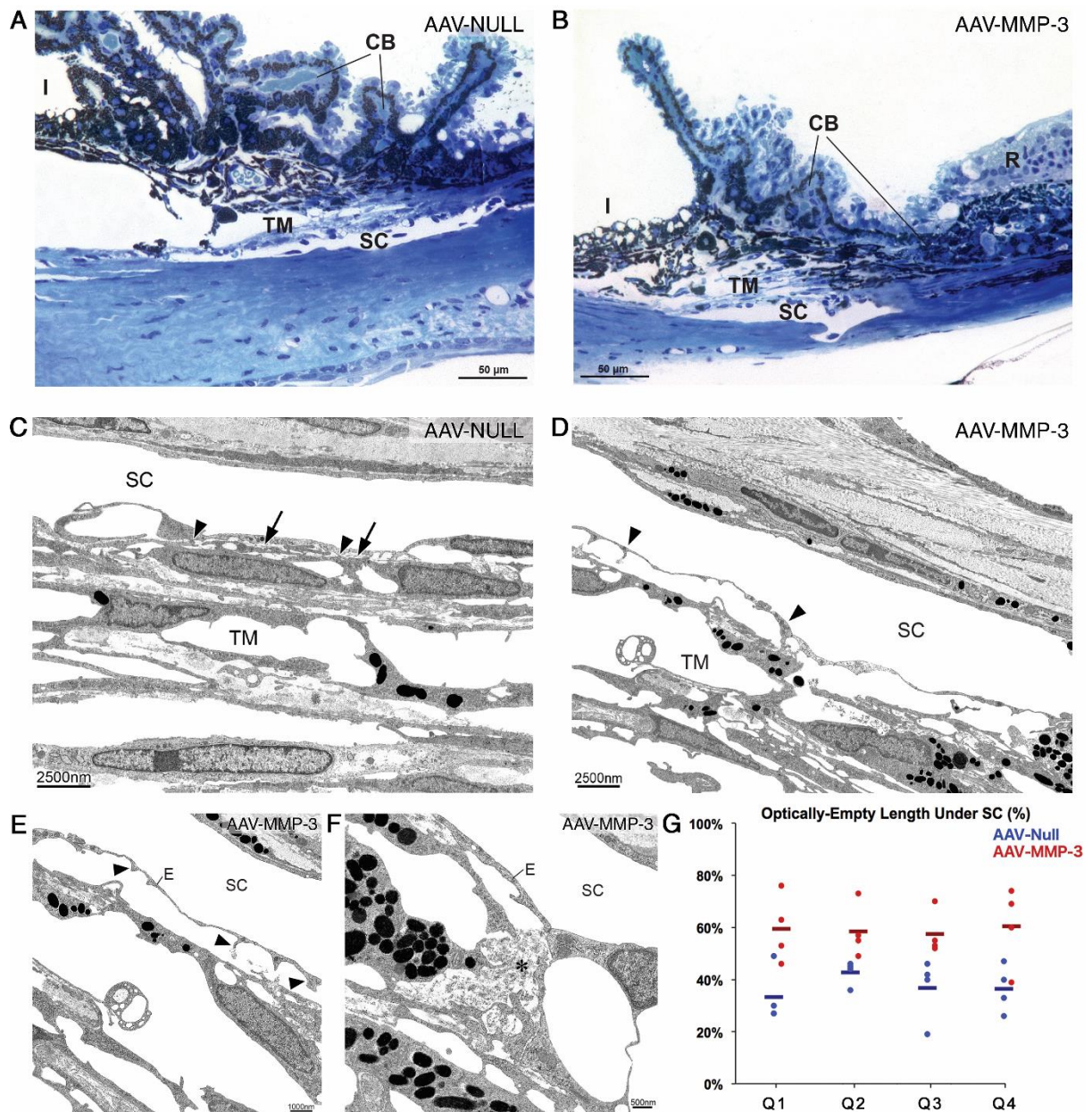


Figure 3.12: TEM analysis of ECM remodelling in outflow tissues.

Semi-thin sections of the iridocorneal angle in mouse eyes treated with either (A) AAV-Null or (B) AAV-MMP-3. AAV-MMP-3 treated eyes show greater inter-trabecular spaces in outer trabecular meshwork (TM) than controls. Scale bar denotes 50 μm . (C-D) Transmission electron micrograph of the inner wall of Schlemm's Canal (SC) and the outer TM. (C) Control eye illustrating normal attachment between foot-like extensions of the inner wall endothelium and subendothelial cells (arrowheads), as well as with the discontinuous basement-membrane material underlying the inner wall endothelium (arrows). (D) Representative TEM image of an MMP-3 treated eye showing a disconnection of the inner wall endothelium from the subendothelial cells and the ECM (arrowheads). The widened subendothelial region lacks

basement-membrane material and other ECM components. (E-F) Higher magnification of the inner wall of a treated eye. (E) Foot-like extensions of the inner wall endothelium (E) have disconnected from the subendothelial cells and the ECM (arrowheads), and the lack of ECM in this region is shown. (F) In other regions of treated eyes, clumps of presumably degraded ECM-material are localised underneath the inner wall of SC (asterisk). Such clumps of ECM are not present in controls. Scale bars are denoted on each image. CB = ciliary body, I = iris, R = retina. (G). Morphometric measurements of the optically empty space immediately underlying SC from 4 regions of contralateral eyes treated with AAV-MMP-3 (red data points) or AAV-Null (blue data points). The four regions, or quadrants, are denoted by Q1-Q4 and represent the superior, inferior, temporal and nasal quadrants. Bars indicate average values for each eye. Contralateral eyes are presented immediately next to one another.

Latanoprost increases outflow facility using iPerfusion

A pilot study was undertaken to determine the effect of Latanoprost on outflow facility using the iPerfusion system, the topical prostaglandin of choice for glaucoma treatment, allowing for the comparison of efficacy between Latanoprost and MMP-3. Animals were dosed in one eye with Latanoprost drops in the evening for two evenings (345). The following day, eyes were enucleated and perfused (method 6.19). Facility is on average 47 [-7, 132] % greater in contralaterally treated eyes. At $n = 6$, this data is non-significant at $p = 0.083$, Figure 3.13.

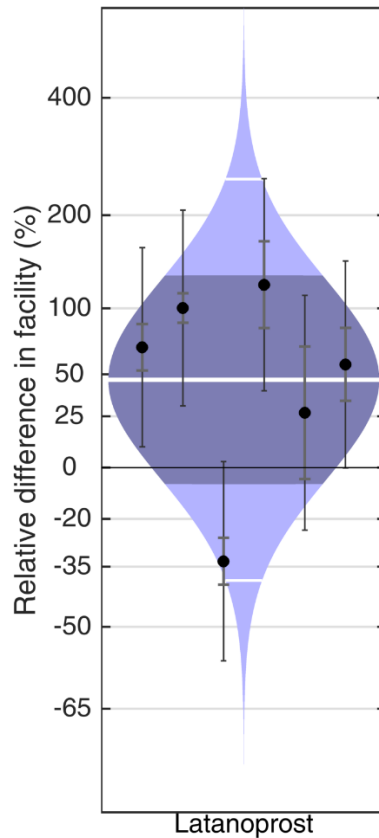


Figure 3.13: Latanoprost increases outflow facility

Data points show the average increase in outflow facility between each pair of eyes, one of which was treated with Latanoprost. An average increase of 47% in facility is observed in response to Latanoprost.

3.3 Discussion

Matrix metalloproteinases are key regulators in the remodelling of extracellular matrices in the JCT region of the TM. Dysregulation of MMP expression and loss of MMP/TIMP homeostasis in glaucomatous AH have been associated with abnormal fibrillary ECM accumulation in the JCT region of POAG eyes (154, 309, 346-348). Furthermore, perfusion of anterior segments with purified MMPs increased outflow facility, while the use of metalloproteinase inhibitors

(TIMP, minocycline) reduced outflow rates (158). Consistent with these findings, upregulation of MMPs following clinical laser treatment has been associated with the ocular hypotensive effect of trabeculoplasty (216, 349). It is therefore apparent that reduction in ECM turnover within the outflow tissues contributes to increased outflow resistance, and strategies specifically targeting outflow ECM may be effective in reducing outflow resistance. This study was focused on the development of a gene-based therapy for the delivery of MMP-3 into outflow tissues to facilitate aqueous outflow and reduce IOP.

It has been reported that the activity of a range of regulatory cytokines and growth factors found in AH directly impacts permeability in the outflow tissue, and many of these are known to be dysregulated in POAG AH (292, 350). In particular, cytokines such as IL-1, TGF and TNF are known to influence the expression and secretion of ECM modulators, including MMPs in outflow tissues (149, 215, 297). It was therefore of interest to assess how POAG AH may affect MMP-3 secretion and their relative activity in outflow cell culture systems.

Permeability assays were performed on AH-treated SCEC and HTM monolayers to demonstrate that dysregulated MMP's in POAG AH influence monolayer permeability via ECM remodelling (166, 351). SCEC monolayers showed decreased permeability *in vitro* in response to glaucomatous AH, and this decrease was associated with a reduction in extracellular MMP-3 activity. HTM cells exhibited similar reductions in permeability (Figure 3.1, methods 6.1, 6.4, 6.5). Further, non-significant increases in total MMP-3 observed in glaucomatous AH-treated cell monolayers agree with published data of glaucomatous AH itself, further verifying this analytical strategy (Figure 3.1).

In contrast, treatment of cell monolayers exclusively with recombinant MMP-3 elevated monolayer permeability in comparison to controls, suggesting that MMP-3 could correct the permeability lowering effects of POAG aqueous (Figure 3.2, methods 6.1, 6.4, 6.5). As MMP-3 has previously been associated with apoptotic behaviour in Chinese hamster ovary cells and

osteoclasts (352, 353), the effect of a wide concentration range of MMP-3 on SCEC and HTM viability was evaluated. This way, there can be confirmation that increases in paracellular permeability were not related to an MMP-3 cytotoxic effect, but rather its proteolytic activities, which these data support. There is no literature on the endogenous levels of MMP-3 in human tissues, however the average AH concentration is 0.6 ng/ml in cataract AH and 0.9 ng/ml in POAG patients (151). More importantly, even lower concentrations of MMP-3 were detected *in vivo* in murine AH after AAV-mediated MMP-3 secretion (1.37 [0.89, 1.84] ng/ml, Figure 3.6D, method 6.17) than those used in *in vitro* experiments. Collectively, these results indicate that a plausible target for MMP-3 activity is likely to be the ECM of TM and the inner wall endothelium of SC. This further contributes to the body of evidence demonstrating that the molecular pathological effects of glaucomatous AH are due, in part, to dysregulation of MMP-mediated remodelling and that induced elevations in MMP-3 expression in outflow tissues should have an enhancing effect on increasing aqueous outflow.

Previously, perfusion of explants of human anterior segments with a mixture of MMP-3, -2, -9 has been shown to result in an increase in outflow facility to 160% of baseline level (158). It has also been demonstrated that increases in IOP lead to an up-regulation of MMP-2, -3 and -14 through mechanical stretching of the TM and a reduction in TIMP2 (139, 161, 354-357). Such observations support the concept that controlled expression of MMPs within the anterior chamber holds therapeutic potential in regard to facilitating aqueous outflow. The inner wall endothelium of SC along with its basement membrane and JCT modulate the resistance to outflow. The interconnections between all components responsible for outflow resistance generation is essential to maintain the homeostasis of outflow drainage (18). Thus, targeting the ECM for remodelling in the JCT region using MMPs may effectively increase permeability of surrounding cells, thus increasing AH outflow rate and lowering IOP.

Owing to the fact that MMP-3 is a secretory enzyme, transduction of the corneal endothelium with AAV-MMP-3 will result in the secretion and delivery of the protein to the outflow tissues by following the natural flow of AH in the anterior chamber. *Ex vivo* studies in human corneas or corneal fibroblasts have demonstrated the potential and efficiency of delivering AAV to this tissue type (358, 359). Successful transfection of different layers in the rabbit cornea by recombinant AAV further support the potential of recombinant/exogenous protein delivery from corneal cells (360). The corneal endothelium degenerates at a rate of approximately 0.5% per year (361). Cell loss is compensated for by the migration and enlargement of neighbouring cells, rather than regeneration (362). Cell proliferation is suppressed by TGF- β 2, which prevents entry into the S-phase of the cell cycle (363). This lack of replication becomes beneficial in that MMP-3 product from AAV will not be diluted over time. A single AAV inoculation could theoretically be sufficient for lifelong gene expression.

Thus, it is likely that secreted MMP-3, expressed by corneal endothelia, will be directed toward the outflow tissue and activated with the aid of existing endogenous MMP-3 after which it will then be available for remodelling a range of ECM components. Attaining exclusive AAV expression in the cornea was obtained by using a single stranded AAV-2/9. It has been reported that although single stranded AAV may enter other cells such as the TM, self-complementary viruses are required for sufficient DNA replication, and hence transduction of these cells (364). In a more recent study however, it has been discovered that a single stranded AAV with an engineered capsid can transfect the TM, allowing for larger transgene sequences to be packaged into the virus (365).

The current data provide a direct proof of concept that AAV-mediated expression of MMP-3 from corneal endothelium decreases IOP with a concomitant increase in the rate of AH outflow through the drainage channels *ex vivo* (Figure 3.10). A number of parameters will require further refinement in order to address the translational feasibility of this approach. Although

significant elevations in transient MMP-3 were found in murine AH post treatment with AAV-MMP-3, these were well within tolerable limits as defined by our *in vitro* experiments (Figure 3.2E-F). These MMP-3 elevations in AH (Figure 3.6D), visually translucent corneas of normal thickness (Figure 3.7), and estimations on secretory characteristics (Figure 3.8) suggest that MMP-3 is preferentially secreted apically into the AH with no detectable off target effects in the stroma layers of the cornea. MMP-3 expressed in the corneal endothelial cell layer is in the inactive form, which requires secretion for cleavage-induced activation, and is therefore unlikely to induce remodelling or damage to the endothelium itself. Activation is likely to occur in the AH after secretion, or extracellularly within the outflow tissues in the presence of other proteases. The observed elevation in aqueous MMP-3 activity indicates that activation at least begins in the AH (Figure 3.6E). However, sustained expression of MMP-3, as would occur following permanent transfection of cells of the anterior chamber, could result in off-target proteolysis over time. A potentially more effective approach will be to employ an inducible promoter to drive MMP-3 expression on a periodic basis once the virus has been introduced into the anterior segment tissues of the eye. It is of note that the use of glucocorticoid-inducible promoters has been explored in this regard in adenoviral and AAV delivery systems to express MMP-1 in tissues of the TM (279). However, the use of a steroid response promoter may not be ideally suited from a therapeutic standpoint in humans, as activation of the promoter would require continuous exposure to steroid components, which can lead to abnormal IOP elevation (366-368). Glucocorticoids have been shown to influence gene expression, which may play a pathogenic role in developing hypertension (369). Hence, the effectiveness of a tetracycline-inducible system to express MMP-3 from the corneal endothelia was explored, which allows for controllable and reversible activation by topically applied eye drops (method 6.12). It was noted that activation of AAV for over 10 days was sufficient to significantly increase outflow facility *ex vivo* in mice and suggest that incorporation of other tetracycline derivatives may further enhance the effectiveness of the promoter and hence MMP-3 production. An observed

increase in facility of 68 [24, 128] % rivals that of conventional prostaglandin analogues which are in current use to treat glaucoma, noted to have an increase of 56 [-4, 154] % in the case of PDA205, also using the iPerfusion system (137). Latanoprost is known to increase outflow facility, however it has not been demonstrated before on the iPerfusion system (370). Although a small pilot study with Latanoprost such as this doesn't comprise adequate sample numbers for statistical power, a 47 [-7, 132] % increase is observed, allowing for an indirect comparison to the MMP treatment (Figure 3.13). This indicates that the AAV-iMMP-3 approach may compare to, or rival, conventional treatments.

Studies utilising MMPs for increasing outflow or reducing IOP as previously mentioned tended not to propose a mechanism of action for MMP in this regard. Here it is shown that MMP-3-mediated remodelling of specific ECM components is likely responsible for increased outflow, and hence, decreased IOP. Reductions in intensity and distribution of core ECM materials including collagen IV and laminin were observed *in vitro*, along with the disorganisation of the fibronectin meshwork and constrictions in the actin skeleton (Figures 3.4, 3.5, methods 6.14, 6.10). These modifications suggest the development of a porous nature within the ECM of these monolayers. Semi-quantitation via western blot analysis coincides with these results, showing significant reductions in collagen IV, α -SMA and laminin proteins in the cell lysate fraction, where ECM proteins are likely to reside as no significant changes were displayed in media samples. It is reasonable to assume that these extracellular changes contribute to the observed alterations in electrical resistance and paracellular flux.

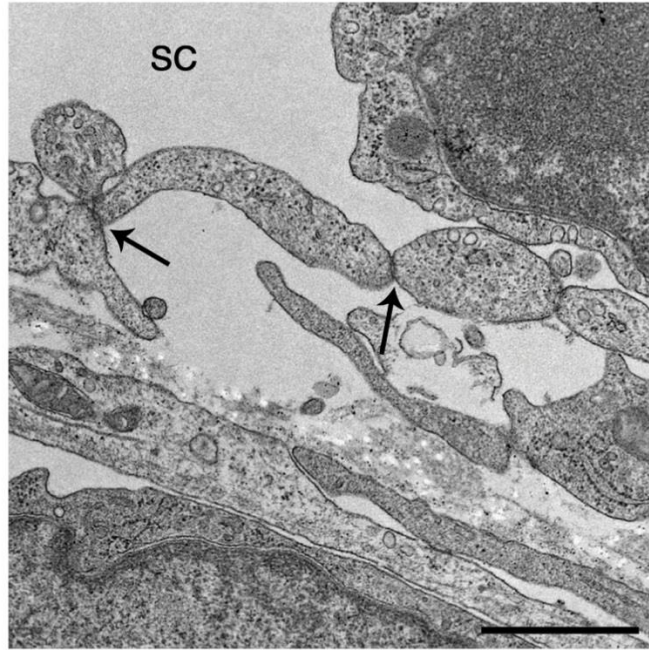


Figure 3.14: TEM analysis of endothelial junctions.

Ultrastructural analysis of Schlemm's Canal endothelium shows intact tight junctions between cells next to empty subendothelial regions in AAV-MMP-3 treated eyes. Scale bar represents 1 μ m.

Ultrastructural analysis of AAV-MMP-3 treated mouse eyes also showed reductions in ECM material at the sub-endothelial/JCT region, including areas of degraded ECM and widened inter-trabecular spaces (Figure 3.12, method 6.23). Upon quantification, these areas optically lacking ECM material were found to be consistently increased in response to MMP-3 both between regions of the anterior chamber and between treated eyes. Tight junctions remained intact after incubation with AAV-MMP-3 (Figure 3.12), contrary to previous studies which have shown tight junction degradation by MMPs (171, 371); validating that MMP-3 may primarily augment cell monolayer permeability via other mechanisms such as alteration of ECM components. These data indicate that a reduction in ECM material in the TM and inner wall of SC is responsible for the enhancement of outflow facility and consequently lowering of

IOP in the treated eyes. The data also show that the reduction in ECM is not due to an inflammatory response that secondarily induces lytic enzymes in the treated eyes but most likely to the induction of MMP-3 through the treatment directly.

Regarding the prospect of development of a gene therapy for glaucoma, we observed highly efficient transduction of corneal endothelial cells following a single intracameral inoculation of AAV-2/9 expressing MMP-3, and both levels and activity of MMP-3 were significantly elevated in mouse AH following such inoculation (Figure 3.6, method 6.13). It is shown here for the first time that a topical eye drop regime can control the expression of a gene therapy vector from the anterior chamber. Importantly, AAV-mediated expression of MMP-3 in corneal endothelium, either from a CMV-, or doxycycline-inducible promoter, resulted in a marked increase in outflow facility and reduction in IOP (Figure 3.10, methods 6.12, 6.19). These observations correlated with structural alterations in the ECM of the outflow tissues, suggesting a mechanism of action for MMP-3 in modulating outflow resistance. Hence, the current approach holds substantial potential as an effective human therapy should long-term safety and efficacy prove successful in non-human primates.

Chapter 4

Efficacy of AAV-iMMP-3 in Glaucoma Models

4.1 Introduction

The objective of data presented in this chapter was to assess the effect of the inducible MMP-3 virus on IOP and outflow facility in induced or genetically engineered models of glaucoma. These hypertensive models should reflect more accurately the degree to which MMP-3 might be effective in a glaucomatous environment. Testing the efficacy of a drug in a disease model is an integral part of early phase therapeutic development, resulting in the formation of a concept strategy for use in further pre-clinical studies.

Glaucoma Models

There are many models available for the different types of glaucoma varying in species with both spontaneous and induced forms of the disease. Rodents are the organism of choice, due to the small size, low cost, potential for experimental manipulation, short life span and an ocular structure and physiology that is similar to humans (372, 373). Structurally they have a lamellar TM and SC with both conventional and unconventional pathways, as with humans (374). Cyclical IOP fluctuations based on circadian rhythms occur in both mice and humans, and both have similar AH turnover rates. Similar mechanisms exist for AH production, IOP management

and response to drugs along with a lack of AH washout, making mouse ocular systems very similar to that of a human in terms of physiology (375). Differences from primate outflow pathways include a narrower anterior angle and a posteriorly placed TM with fewer trabecular beams (374). As such, the mouse is well suited to modelling and studying outflow dynamics in glaucoma.

As IOP is the major risk factor, and the primary target for glaucoma treatment, most models exhibit ocular hypertensive phenotypes. Models for studying RGC death have been developed through mechanical trauma, toxic insult, induction of retinal ischemia or genetic mutation. Most of these models however do not resemble a 'true' glaucomatous phenotype, as they do not involve all the processes leading to pathology or contain all of the hallmarks of glaucoma. As such, there is no ideal model for glaucoma, however existing systems allow for the study of different aspects of the disease and have successfully uncovered important aspects of the pathology. One of the most well characterised models is that of the DBA/2J mouse strain, a model of pigmentary glaucoma (376). Mutations in tyrosine-related and glycosylated transmembrane proteins results in pigment dispersion, iris atrophy and the consequential blockade of the outflow tissue (377). Other genetic models of ocular hypertension include the myocilin (MYOC) mouse expressing a mutated form of the human MYOC gene (Tyr437His), or another mouse containing a mutated version of the collagen type-1 $\alpha 1$ subunit which cannot be cleaved by MMPs. Glaucoma is a chronic disease, and therefore time consuming to model effectively, thus systems involving inducible hypertension have been developed. Acute ocular hypertension can be achieved through laser photocoagulation of the TM, episcleral injection of hypertonic saline, episcleral vein cauterisation, injection of IOP- elevating compounds and exposure to glucocorticoids (378-382). Other experimental models of induced retinal ganglion cell loss include optic nerve crush, introduction of excitotoxic agents, and ischemia-reperfusion insult (383-385). It is clear from the literature that many models of glaucoma exist; therefore it is important to select an appropriate model for experimentation. To this end both the MYOC

Tyr437His and glucocorticoid models were chosen. This allows for multiple hallmarks of glaucoma to be considered, such as genetic contribution, chronic disease development, cell stiffness, ocular hypertension, reduced outflow facility, retinal degeneration and visual field loss. Primarily, these models allow for ECM accumulation, which is a key element in testing the efficacy of MMP-3.

Dexamethasone model

Dexamethasone (DEX) is a well characterised glucocorticoid in the generation of a steroid-induced model of ocular hypertension. DEX typically increases IOP and reduces outflow facility, enhancing ECM material such as fibrils and plaques in areas such as the basement membrane and sub-endothelial layers (150). It is these regions that we have previously seen altered by MMP-3 expression, hence MMP-3 should remain viable to enhance outflow under DEX-treated conditions. DEX regulates outflow resistance by primarily upregulating ECM proteins, including a reorganization of the actin cytoskeleton to form cross-linked actin networks (CLANs) (386, 387). These CLAN structures within TM cells exhibit less migration, likely due to the increased stiffness of the cells themselves. Actin profiling has not been observed in SC cells up to this point, however. It follows that this upregulation and stabilisation of CLAN structures allows for further binding of scaffold proteins for tight junctions, such as ZO-1, which has been shown to be upregulated in SC cells treated with DEX (388). *In vivo*, the combined upregulation of ECM proteins, upregulated tight junctions, and reduced mobility due to cell stiffness lead to an increased outflow resistance, generating elevated IOP, as is seen in glaucoma. It is important to note, however, that DEX is known to inhibit the endogenous expression and activity of MMPs (389). This is achieved by regulating the ERK and MAPK pathways that would normally allow cytokines or other effectors of transcription to induce expression of MMPs (34, 390), and by upregulating TIMP inhibitors of MMPs (391). This

should not significantly impede the efficacy of the AAV-MMP-3 virus however, as the virus is driven by an exogenous promoter independent from this pathway, and there should be sufficient generation of MMP-3 molecules to overcome any TIMP-1 expression.

Myocilin model

As discussed in Chapter 1, MYOC is a causative gene for glaucoma in humans. Several models of individual MYOC mutations exist, however the Tyr437His (or Y437H) is the most common. Although the exact function of MYOC remains elusive, some aspects of its physiology have been elucidated. MYOC is expressed in most human cells as an intracellular glycoprotein. The highest MYOC expression is found at the TM, where it is uniquely secreted in vesicle-like structures, or endosomes, in response to AH (392). Mutant myocilin is not secreted from TM cells and gathers intracellularly, leading to an IOP increase through a gain-of-function mechanism. It is hypothesised that this accumulation leads to the dysfunction of cellular organelles, endoplasmic reticulum (ER) stress, and ultimately apoptosis (393). It is also postulated that TM cell stiffness and contractility play a role in the pathology, as MYOC can interact with the fibronectin and SPARC ECM proteins, potentially disrupting their function. A transgenic mouse containing the human Y437H variant was used as a model in this study, and has been extensively characterised (90). Accumulation of MYOC in the iridocorneal angle is correlated with an increase in IOP from 3-4 months of age onwards, along with a decline in retinal ganglion cell counts and mean axonal numbers. ER stress markers are shown to be activated, but glaucoma phenotypes are rescued with the use of a chemical chaperone to promote trafficking and secretion of MYOC (90). Induction of ER stress may be attributed to the abnormal intracellular accumulation of ECM proteins in response to mutant MYOC (89). As with the DEX model, ER stress can be initiated by an upregulation of fibronectin, particularly in the TM which is more prone to such stress (394). It is unclear as to the direct effect of the increased localisation of intracellular ECM, however it is also of note that MMP-

2 and MMP-9 activity were reduced in conditioned medium *in vitro* from TM cells expressing mutated MYOC (89). This model is not related to direct increases in iridocorneal ECM expression, like the DEX model, and so is an interesting addition to the study to determine if MMP-3 will still alleviate glaucoma phenotypes in a physiologically different environment.

Non-human primate

A logical step in the development process of any therapy is to begin pre-clinical assessment in a non-human primate (NHP). NHPs are typically used to bridge mouse studies with human clinical trials, especially with respect to safety and toxicity concerns. The close phylogenetic relationship of NHPs with that of humans renders them far superior to rodents in terms of validity of data. Aspects including behaviour, cognition, language, development, genetics, immunology, neurology and pharmacology are undoubtedly more translatable to humans in a NHP system than in a mouse model.

Experimental primate models of POAG exist where disease phenotypes can be induced by laser photocoagulation or injection of microspheres (395, 396). These interventions are somewhat invasive, and difficult to procure. Although not a model of glaucoma, African Green Monkeys have been extensively used as preclinical pharmacokinetic models to provide predictivity for human exposure, similar to cynomolgus or rhesus monkeys (397). In collaboration with the St. Kitts Biomedical Research Foundation, a small initial study to assess the ability of an AAV2/9 vector constitutively expressing human MMP-3 to transduce the anterior chamber was undertaken. A more careful consideration of safety, pharmacodynamics and efficacy are necessary in a pre-clinical setting. Thus, to adopt a small-scale study in a NHP, details of vector purity, efficacy of transduction, MMP-3 production efficiency and immunogenic responses are of initial concerns.

4.2 Results

Validation of Dexamethasone as a model

Although DEX is well characterised in terms of its use as a model, its effect on actin networks in SC cells has not yet been observed. Immunocytochemistry shows that α -SMA is upregulated in DEX-treated SC cells (method 6.9). Perinuclear area staining is increased, and branches leading to the ends of cells appear wider. This was then compared to the actin profile of SCg cells, cultured from patient donors with glaucoma. A similar expression pattern is observed, further validating the use of dexamethasone as a model for ocular hypertension (Figure 4.1). Each image represents 4 replicates.

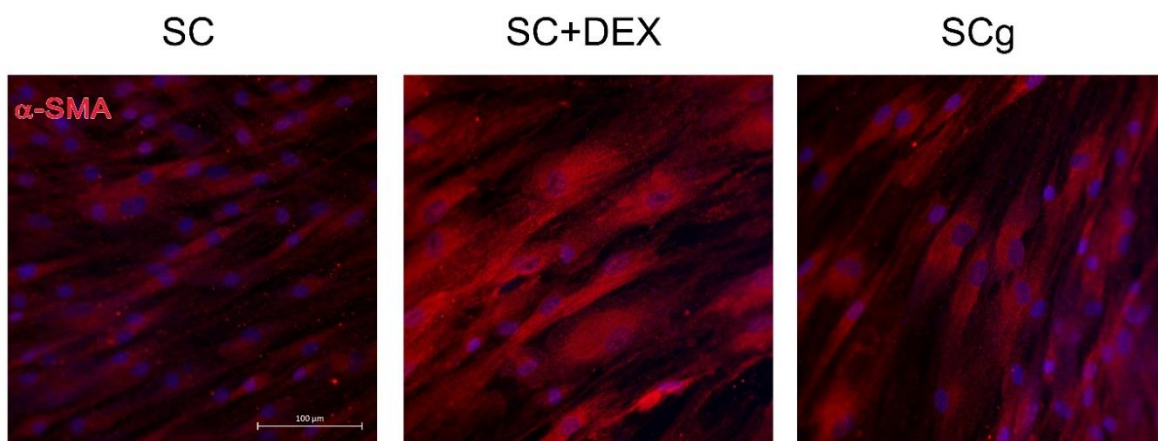


Figure 4.1: Actin organisation in Schlemm's Canal.

SC cells, SC cells treated with DEX and SCg cells were stained with alpha actin. Brighter intensity is observed in the DEX model and glaucomatous cells, along with greater perinuclear area staining. Scale bar represents 100 μ m.

Effect of MMP-3 on IOP in a DEX model

Animals were intracamerally inoculated with inducible AAV-iMMP-3 or contralateral AAV-iGFP as a control at 4 μ l of 3.1×10^{12} vector genomes per ml (method 6.13). 2 weeks later, animals were implanted with a micro-osmotic pump containing either cyclodextrin (control

group) or DEX at 2 mg/kg/day for 4 weeks (method 6.24). Virus was activated by topical administration of doxycycline eye drops (0.2%) 2 weeks after micro pump implantation. Tonometric IOP readings were taken every week and facility was measured ex vivo using iPerfusion 2 weeks after induction, at the experimental endpoint (methods 6.19, 6.21). MMP-3 impeded the increase in IOP observed in response to systemically-administered DEX. For the DEX cohort, DEX (+): in GFP-expressing eyes, IOP increased by 3.5 ± 1.9 mmHg (median \pm median absolute deviation) ($p = 0.0001$, $n = 10$, 1-sample Wilcoxon against a theoretical median of 0) over the 6 weeks, and in MMP-3-expressing eyes, IOP increased by 2.1 ± 1.4 mmHg ($p = 0.008$, $n = 14$) over the same period (Figure 4.2 and Figure 4.3). For the cyclodextrin control cohort, DEX (-): both control and treated eyes exhibited a non-significant change in IOP from baseline over the experimental period ($p = 0.3$ and $p = 0.2$, $n = 10$ respectively).

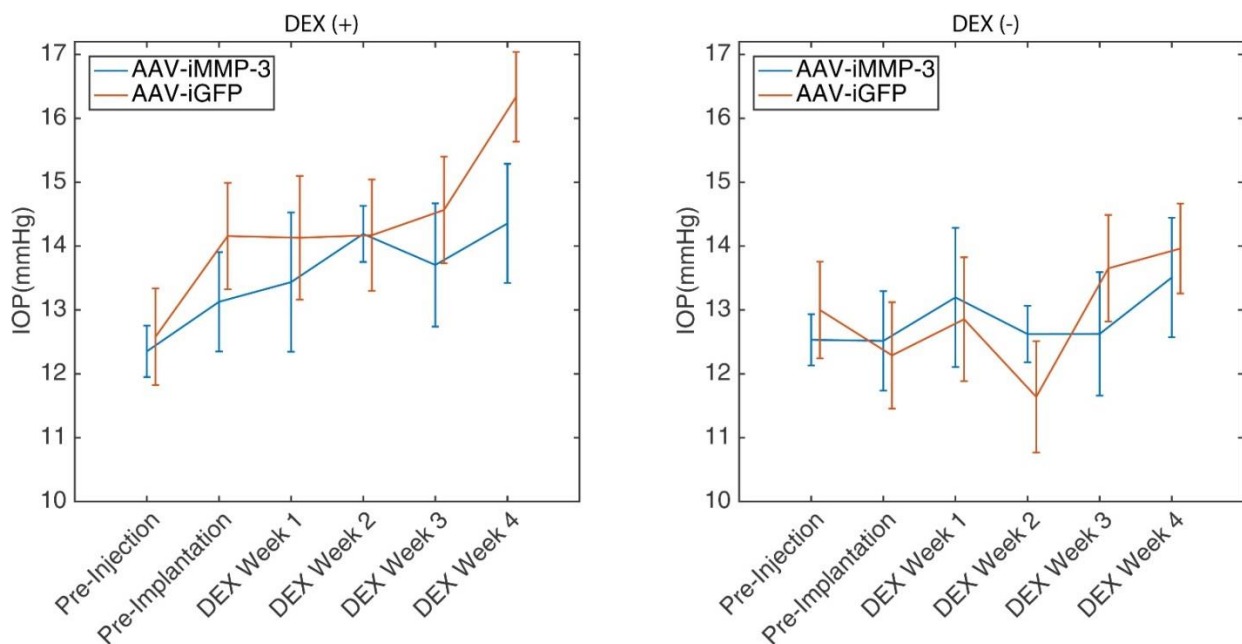


Figure 4.2: IOP over time in DEX animals and in response to MMP-3.

IOP measurements were taken weekly throughout the experiment. In DEX-treated animals (left) control eyes show steadily increasing IOP, whereas in the MMP-3 treated eyes, IOP stabilises after viral induction (DEX Week 2). In cyclodextrin control animals (right), IOP does not significantly change for either eye over the course of the experiment.

Between contralateral eyes of each cohort, the median reduction of IOP by AAV-iMMP-3 treatment over the 6 weeks was significant by 1.42 ± 0.5 mmHg, $p = 0.01$, $n = 14$ (Figure 4.3A) in DEX (+) animals, and non-significant in the DEX (-) cohort with a median change of 0.08 ± 0.8 mmHg, $p = 0.73$, $n = 10$ (Figure 4.3B).

At the experimental endpoint, IOP was on average 1.9 ± 0.1 mmHg lower in the MMP-3 treated eyes of the DEX (+) cohort ($p = 0.002$, $n = 14$, Figure 4.3C). IOP was not significantly different between eyes of the DEX (-) cohort 0.7 ± 0.3 mmHg ($p = 0.71$, $n = 10$, Figure 4.3D). It is also of note that by using unpaired median analysis (Wilcoxon rank sum test) to compare the final IOP of AAV-iGFP-treated eyes in both cohorts, IOP is significantly increased in the DEX (+) group (2.1 ± 0.02 mmHg, $p = 0.01$, $n = 14$ DEX (+) group, $n = 10$ DEX (-) group). Hence, DEX is elevating IOP in these animals, presenting an effective model of ocular hypertension.

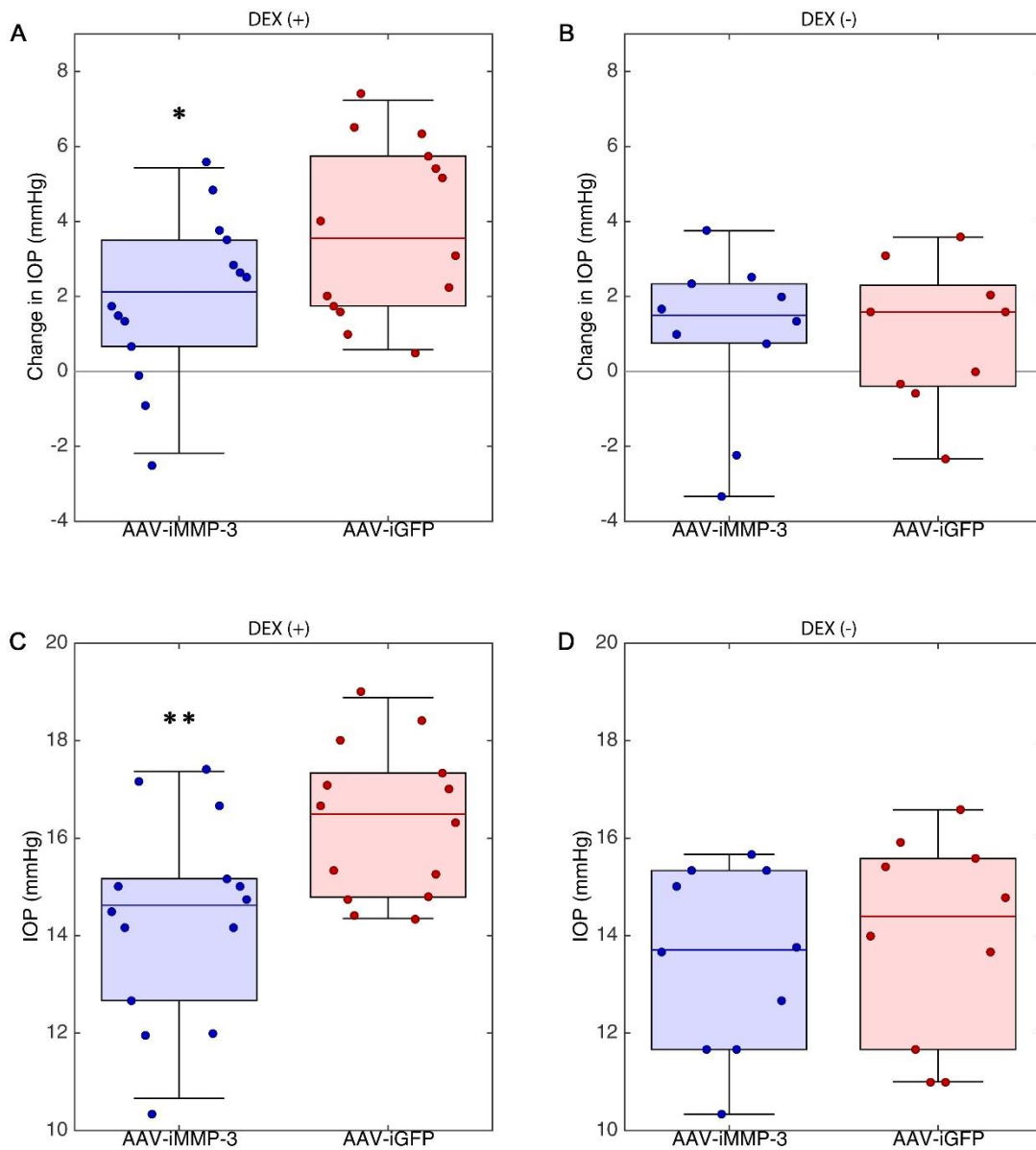


Figure 4.3: Total change in IOP.

(A-B) These dot-box plots depict the change in IOP from baseline (Pre-injection) to the final measurement (DEX Week 4), as denoted by Figure 4.2. Blue boxes represent AAV-iMMP-3 treated eyes, and red boxes the contralateral AAV-iGFP controls in both DEX treated (DEX (+), A) and the cyclodextrin control group (DEX (-), B). MMP-3 significantly reduces IOP in the hypertensive model only. (C-D) These plots represent the same groups, but only represent the final IOP timepoint from Figure 4.2. Similarly, MMP-3 significantly reduces IOP in the DEX (+) and not the (DEX -) cohort.

Effect of DEX and MMP-3 on Facility

Using unpaired analysis, it was observed that there was not a significant difference between facility of control eyes from both DEX (-) and DEX (+) cohorts, contrary to findings from the literature (150). Only a 1 [-23, 32] % change was found with $p = 0.9156$, $n = 8$, Figure 4.4, method 6.19).

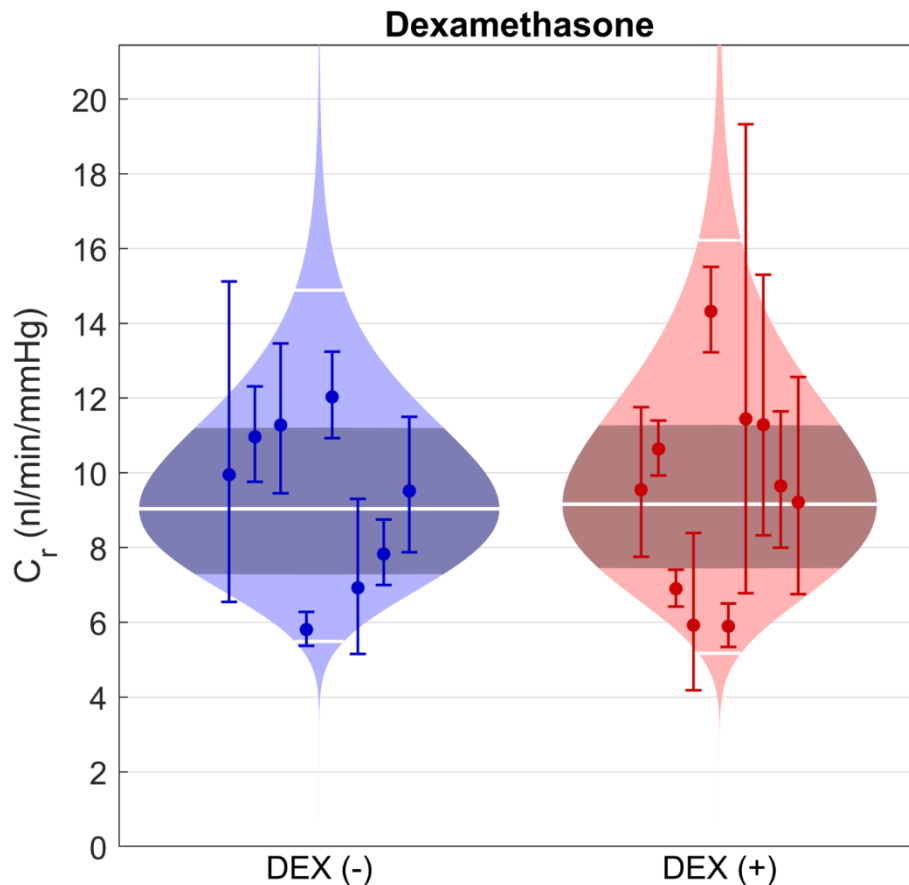


Figure 4.4: Dexamethasone does not decrease outflow facility

Absolute facility values of control eyes from both DEX (-) and DEX (+) cohorts are depicted above. These values fall within normal ranges, however facility in DEX (+) animals is not reduced as expected, even though IOP is increased as in Figure 4.2.

Facility in the AAV-iMMP-3 treated eyes was an average of 45 [18, 78] % ($p = 0.0049$, $n = 8$) higher than in AAV-iGFP-injected eyes for the DEX (+) cohort. For the control cohort, facility

in MMP-3-treated eyes was an average of 59 [26, 100] % ($p = 0.002$, $n = 8$) higher than GFP-treated eyes. GFP eyes in the DEX (+) cohort had a lower average facility (9.04 ± 1.24 nl/min/mmHg, mean \pm SEM) than the DEX (-) control cohort (9.59 ± 1.27 nl/min/mmHg) as expected, however this difference was not significant (Figure 4.5, method 6.19).

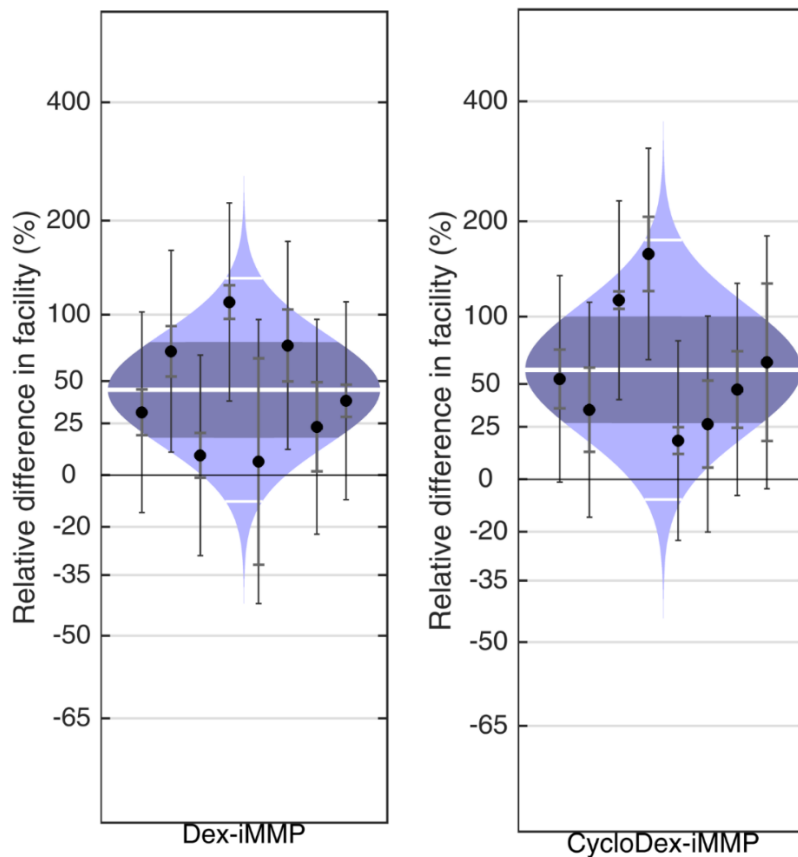


Figure 4.5: Outflow facility in response to dexamethasone and MMP-3.

Cello plots depicting paired analysis between AAV-iMMP-3 and AAV-iGFP treated eyes in both the DEX treated cohort (left) and the cyclodextrin control group (right). Average percentage facility difference is denoted by the white line, with the dark blue shading as the 95% CI of the mean. Individual data points are plotted along with their own 95% CIs. In the DEX model (left), MMP-3 treatment increases outflow facility by 45 [18, 78] %, and by 59 [26, 100] % in the control cohort (right).

Ultrastructural analysis of Dexamethasone-treated eyes

Examination of the outflow tissue was undertaken by transmission electron microscopy as in Chapter 3 (method 6.23). 4 pairs of non-perfused eyes, with one eye injected with AAV-iMMP-3 and contralateral eye with AAV-iGFP, were embedded in Karnovsky's fixative post DEX treatment and viral induction, replicating the methods above. Ultrastructural analysis shows, in general, that the sub-endothelial and TM regions are more ECM-dense and band-like than wild type counterparts, such as that in Figure 3.12C. Noticeably, collagen deposits and elastin fibrils are thicker and more abundant, but appear normal. In MMP-3 treated eyes, there is an obvious increase in empty spaces throughout the TM, with smaller, disturbed collagen fibres. In contrast to non-DEX treated eyes in Chapter 3, the inner wall endothelium is still in contact with the subendothelial region post-MMP-3 treatment. This is presumably due to ECM changes in response to DEX (Figure 4.6).

Quantification was performed, again looking at optically empty spaces around the circumference of the sub-endothelial region (method 6.23). In AAV-iMMP-3 treated eyes, the percentage of ECM-clear regions compared to ECM-containing regions was significantly higher than in AAV-iGFP eyes by 62.1 [45.4, 76.5] % (Figure 4.7). The number of pressure-sensing cilia at the inner wall were also counted, although there was no noticeable difference between treated and control eyes. The number of sections and images taken is described in the methods section 6.23.

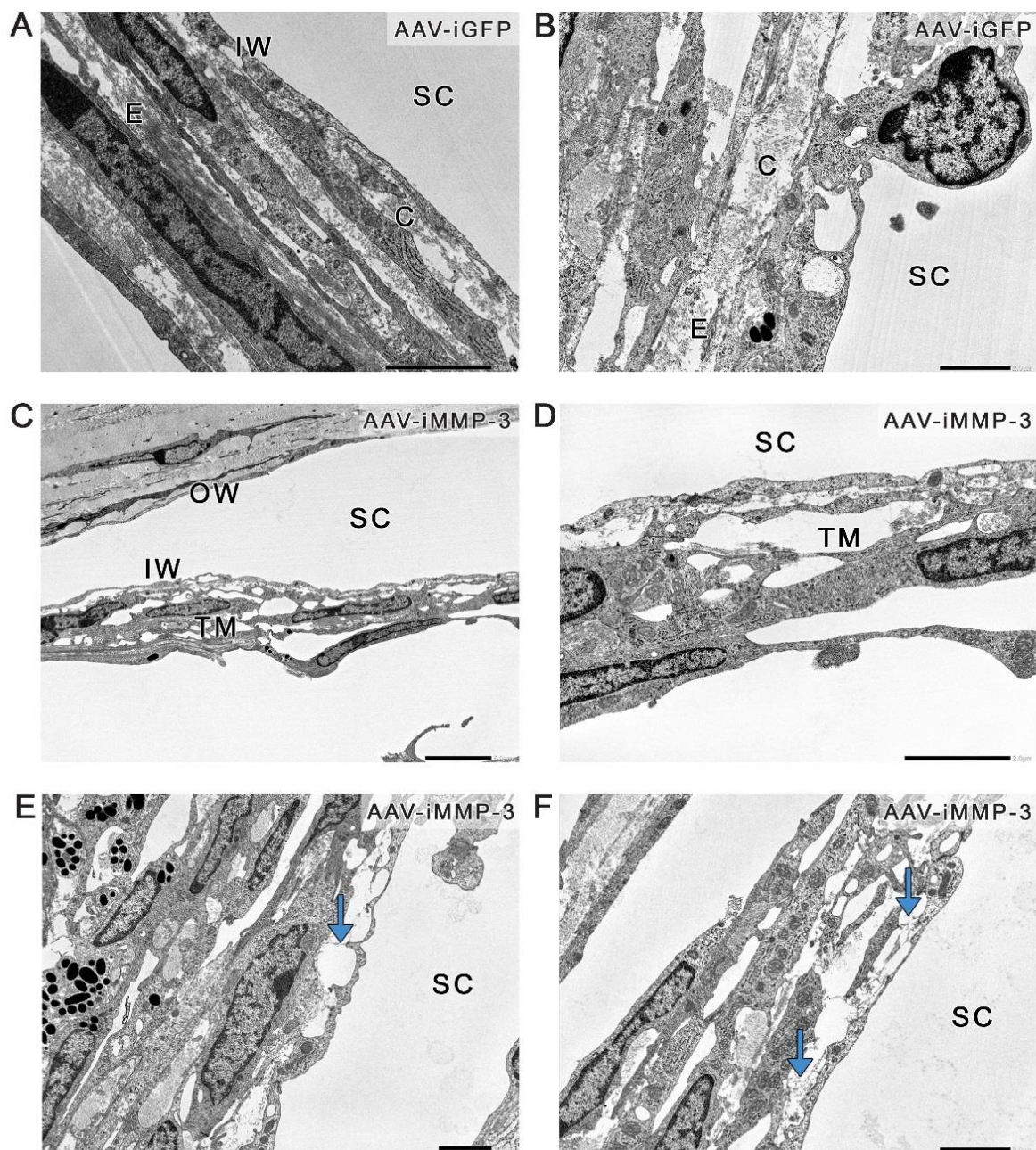


Figure 4.6: ECM changes in response to DEX and MMP-3.

(A-B) DEX (+) control eyes show dense TM and JCT regions, with prominent collagen and elastin deposits. (C-D) Upon treatment with MMP-3, the TM and JCT regions show less ECM-dense tissue, and greater empty spaces. (E) Foot like extensions on endothelial cells are still vaguely attached to the subendothelial region. (F) Sub-endothelial and JCT collagen fibres are much smaller and disturbed. Scale bar in panel C represents 5 μm but bars in other panels represents 2 μm . SC = Schlemm's canal, TM = trabecular meshwork, IW = inner wall, OW = outer wall, C = collagen and E = elastin.

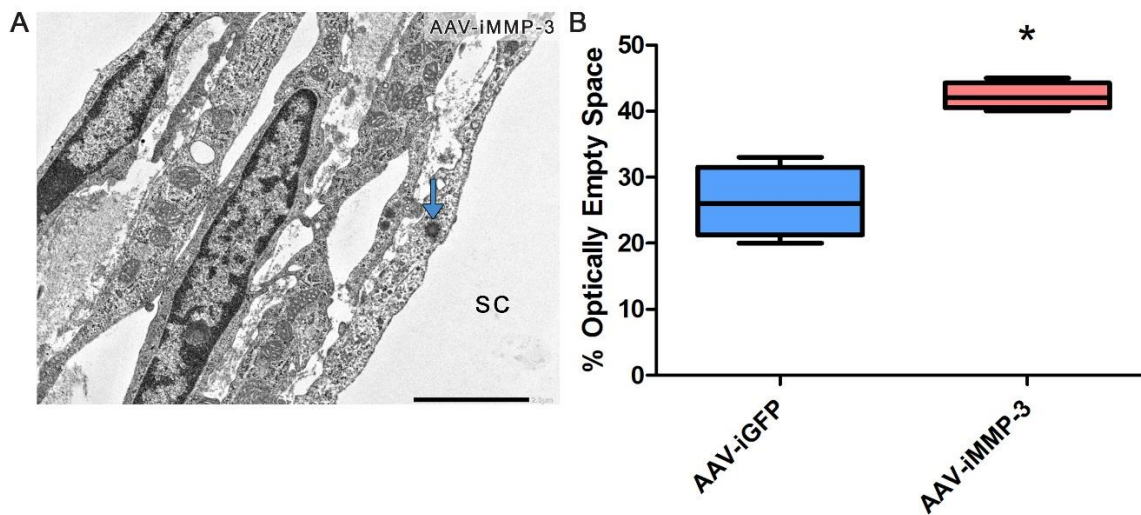


Figure 4.7: MMP-3 degrades ECM in DEX+MMP-3-treated eyes.

The sub-endothelial region of 4 contralateral pairs of eyes were analysed for cilia (A) and spaces void of ECM material (B). 6 different regions around the circumference of the SC were measured for ECM-containing and ECM-free spaces. In AAV-iMMP-3 treated eyes, the percentage of optically empty space was increased compared to controls.

Effect of AAV-iMMP-3 on IOP in a MYOC model

Animals positive for the myocilin transgene, MYOC (+), and those negative for the transgene, MYOC (-), were both used in this study, the latter serving as a control. Animals were injected with AAV-iMMP-3 in one eye, and with AAV-iGFP in the other as a control at 4 μ l of 3.1×10^{12} vector genomes per ml (method 6.13, Appendix 5). Viruses were given a two-week lead time before induction by doxycycline, as before. After a further two weeks of twice daily eye drops, animals were sacrificed and eyes were enucleated for ocular perfusions. IOP readings were taken immediately before injection, immediately before the initial dosage of doxycycline, and every week afterwards, with the final reading being taken 24 hours before perfusion to allow for recovery from anaesthesia (method 6.21, Appendix 2). In MYOC (+) animals, the IOP of control eyes (AAV-iGFP-treatment) increases over the course of the experiment. Treated eyes (AAV-iMMP-3) exhibit a reduction in IOP from the time of induction by doxycycline. In MYOC (-) eyes, there is no observable difference between the average IOPs of contralateral

eyes over time. A trend exists where control eyes in MYOC (+) animals have a greater increase in IOP over time compared to control eyes in MYOC (-) animals (Figure 4.8). These animals were 2-3 months of age at the time of injection, aging to 3-4 months by the final IOP timepoint and perfusions.

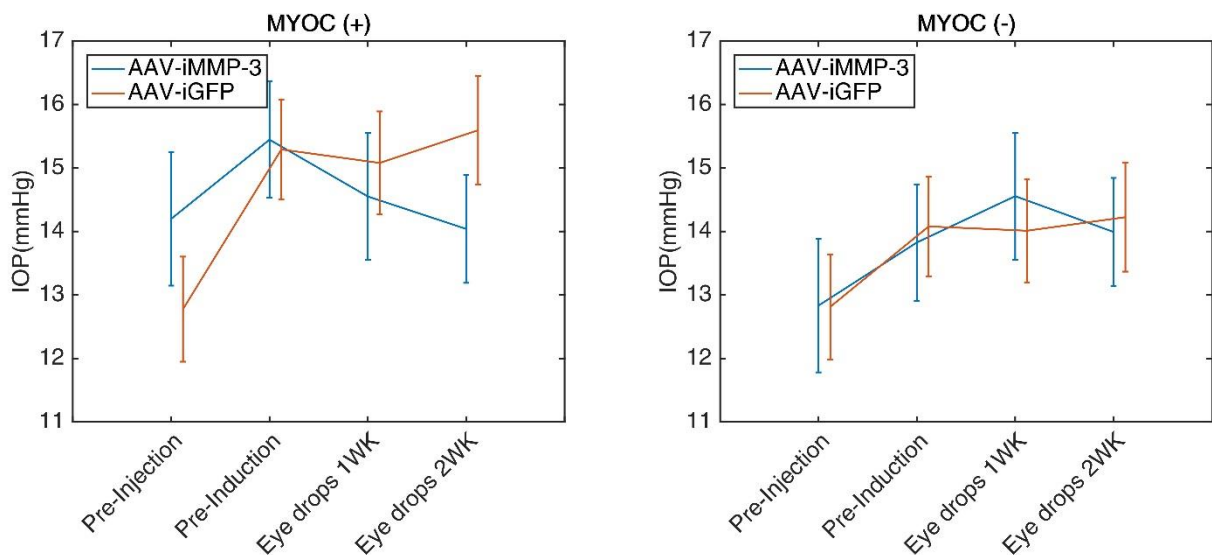


Figure 4.8: Effect of MMP-3 in MYOC (+) and MYOC (-) animals

IOP of AAV-iMMP-3 (blue) and AAV-iGFP (red) treated eyes in animals both positive (left) and negative (right) for the MYOC Y437H transgene. 4 IOP readings were taken over the course of the 1 month experiment. In MYOC (+) animals only, AAV-iMMP-3-treated eyes display a reduction in IOP after 2 weeks of induction by doxycycline.

For MYOC (+) animals: in GFP treated eyes, median IOP increased by 2.4 [1.1] mmHg (median [MAD]) over the course of the experiment, whereas the median IOP for MMP-3 treated eyes shows a change of -0.2 ± 1.3 mmHg. This represents a significant difference between contralateral eyes at $p = 0.0006$, $n = 16$, Wilcoxon signed-rank test, Figure 4.8A. For MYOC (-) animals: a median change of 2.3 ± 2 mmHg is observed in GFP treated eyes, and a change of 1.6 ± 1.6 mmHg is apparent from MMP-3 treated eyes over the course of the experiment. This

difference is non-significant between contralateral eyes at $p = 0.73$, $n = 9$, Wilcoxon signed rank test, Figure 4.9B. Additionally, a 1-sample Wilcoxon test was employed to test the significance of the median change of each eye versus a hypothetical median change of 0. This statistic tells us if the IOP of each eye strays significantly from its initial baseline value obtained from pre-injection IOPs. The only treatment to do so was the GFP treated eyes in the MYOC (+) group, with a significance of $p = 0.0003$, $n = 16$, suggesting that only MYOC (+) control eyes attain an elevated IOP over time (Figure 4.9A (red)).

At the final timepoint, 24 hours before enucleation and perfusion, the median final IOP of animals in the MYOC (+) group were 14.4 ± 1.0 mmHg for MMP-3 treated eyes and 16.1 ± 0.9 mmHg for GFP treated eyes. In MYOC (-) animals, final IOPs were 14.01 ± 1.6 mmHg for MMP-3 treated eyes and 14.2 ± 0.9 for GFP treated eyes. Final IOP reading between contralateral eyes were significant in MYOC (+) animals (1.7 ± 0.1 mmHg, $p = 0.0003$, $n = 16$, Figure 4.9C) but not in MYOC (-) animals (0.1 ± 0.2 mmHg, $p = 0.48$, $n = 12$, Figure 4.9D).

Using Wilcoxon rank-sum tests to compare the median final IOPs of unpaired eyes (between animal groups), it was found that control eyes of each cohort differed by 1.7 ± 0.3 mmHg, $p = 0.01$, $n = 16$ suggesting that IOP is increased in the mutant myocilin model compared to littermate controls. A non-significant difference is observed in MMP-3 treated eyes of MYOC (+) animals and GFP treated eyes of MYOC (-) animals ($p = 0.81$). This indicates that after MMP-3 treatment, IOP returns to a 'normal' value as determined by control eyes in the control group. A p -value of 0.018 is observed when comparing the GFP control eyes of both groups, indicating a significant increase in IOP between animal groupings, validating the MYOC (+) animals as an ocular hypertensive model.

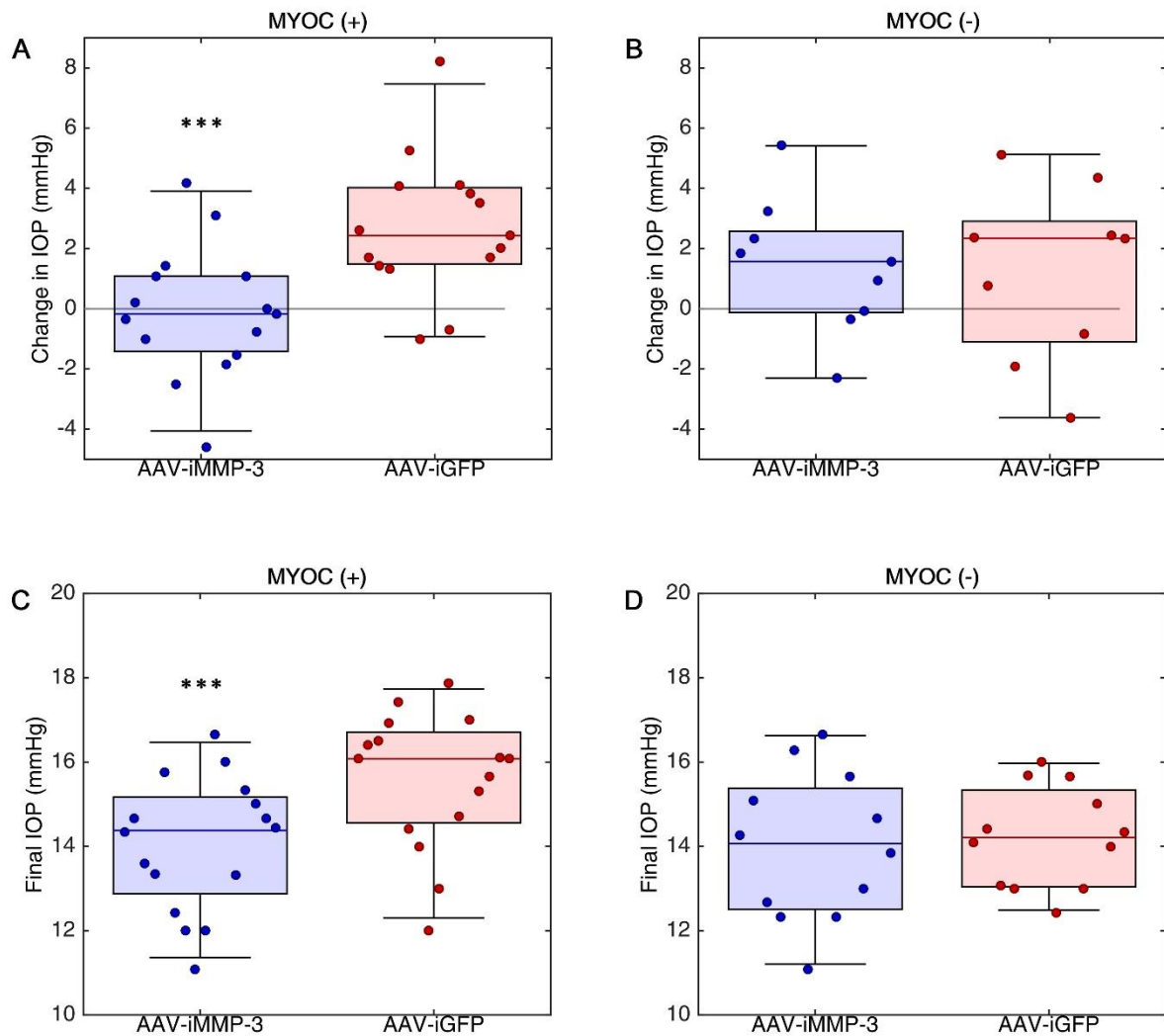


Figure 4.9: Total change in IOP in MYOC animals.

The median change in IOP of AAV-iMMP-3 and AAV-iGFP contralaterally treated eyes over the course of the experiment is presented in dot-box plots for the MYOC (+) group (A) and the MYOC (-) group (B). The final IOP readings are presented in (C) and (D) corresponding to MYOC (+) and MYOC (-) groups respectively.

Effect of AAV-iMMP-3 on outflow facility in a MYOC model

Using unpaired analysis, it was observed that there was a non-significant difference between facility of control eyes from both MYOC (+) and MYOC (-) cohorts. a 44 [-8, 126] % change

was found with $p = 0.1$, $n = 11$, Figure 4.10, method 6.19). This trend follows that of the IOP, and would likely be significant with a greater sample size.

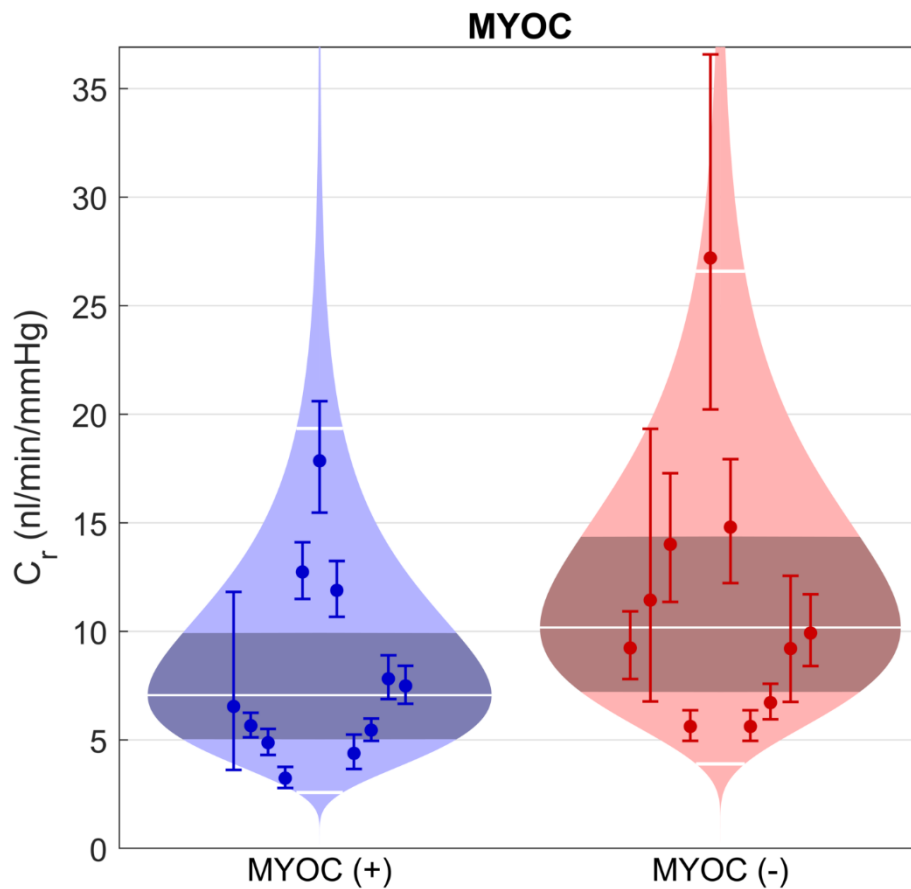


Figure 4.10: Transgenic myocilin does not decrease outflow facility

Absolute facility values of control eyes from both MYOC (+) and MYOC (-) groups are depicted above. These values fall within normal ranges, and facility is reduced in MYOC (+) animals although it is not significant.

Facility in MYOC (+) animals was increased on average by 49 [13, 97] % in response to AAV-iMMP-3 ($p = 0.0115$, $n = 9$, Figure 4.11 left, method 6.19). Facility in MYOC (-) eyes treated with AAV-iMMP-3 was similarly increased by 84 [53, 121] % compared to AAV-iGFP treated eyes ($p = 0.0003$, $n = 7$, Figure 4.11 right). A non-significant decrease is observed between

control eyes of the MYOC (+) group (7.65 ± 1.45 nl/min/mmHg) and control eyes of the MYOC (-) group (8.16 ± 1.40 nl/min/mmHg).

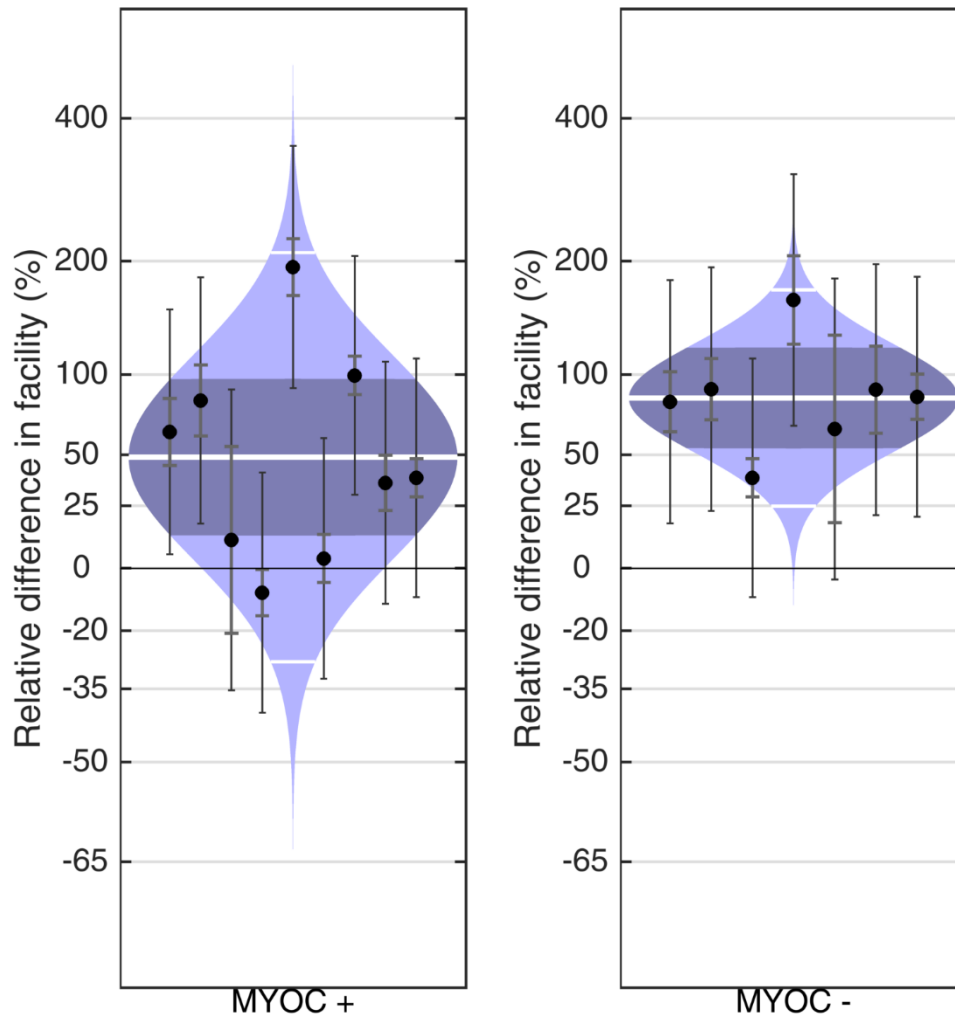


Figure 4.11: AAV-iMMP-3 increases outflow facility in MYOC animals

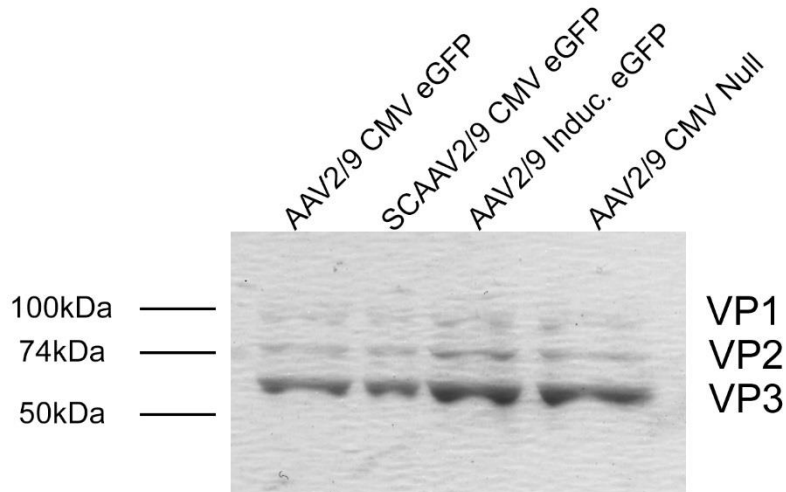
Facility is increased by 49% in MYOC (+) animals, and by 84% in MYOC (-) animals in eyes treated with AAV-iMMP-3 compared to control eyes treated with AAV-iGFP.

AAV2/9-eGFP transduction of the corneal endothelium in a NHP

In order to evaluate the efficacy of the AAV-MMP treatment in a NHP, it first had to be established if the virus was able to transfect the anterior chamber in this new species. This study also begins a 'pre-clinical' type setup in which more detailed pharmacodynamics are to be examined. It was determined that an AAV2/9, scAAV2/9 (self-complementary), and inducible AAV2/9 all expressing eGFP were to be tested, and were sent along with an AAV2/9-Null vector to the St. Kitts Biomedical Research Foundation. Aliquots were kept in order to test viral purity and to estimate real titre values, to compare to the original manufacturers titres. Coomassie blue staining of an SDS-PAGE gel loaded with virus shows 3 distinct bands corresponding to the capsid virion proteins. The lack of other bands indicates that these solutions are pure, and using the VP3 band, an estimation of titre can be determined (method 6.16). Both scAAV2/9 and the inducible construct exhibit similar titres to that stated by the manufacture, however the other two are approximately 3-fold lower (Figure 4.12). This could perhaps be attributed to a degradation of virus over time, or error in titre estimation. This is not an ideal method to determine viral titre, but serves as an estimation after the determination of viral purity while more robust assays are optimised (e.g. TaqMan qPCR).

50 µl of these viruses were injected into NHP eyes by Matthew Lawrence, Director of the St. Kitts Biomedical Research Foundation, the details and assignments of which were not disclosed until after image processing had occurred, ensuring that processing occurred in a blind fashion. Only 2 of the 6 eyes injected were determined to have a GFP-positive signal at the corneal endothelium (see method 6.15), and it was revealed that these eyes were injected with AAV2/9 constitutively expressing GFP (Figure 4.13). This correlates with previous murine studies with these same viruses (see Appendix 1, Supplementary Figure 2). Other regions of the anterior chamber such as the SC, TM, ciliary body/processes, iris, stoma and corneal epithelium did not show any GFP expression, thus, it is apparent that AAV2/9 is specific to the corneal

endothelium in both murine and NHP species. Eyes injected with the inducible virus were not included in this round of analysis.

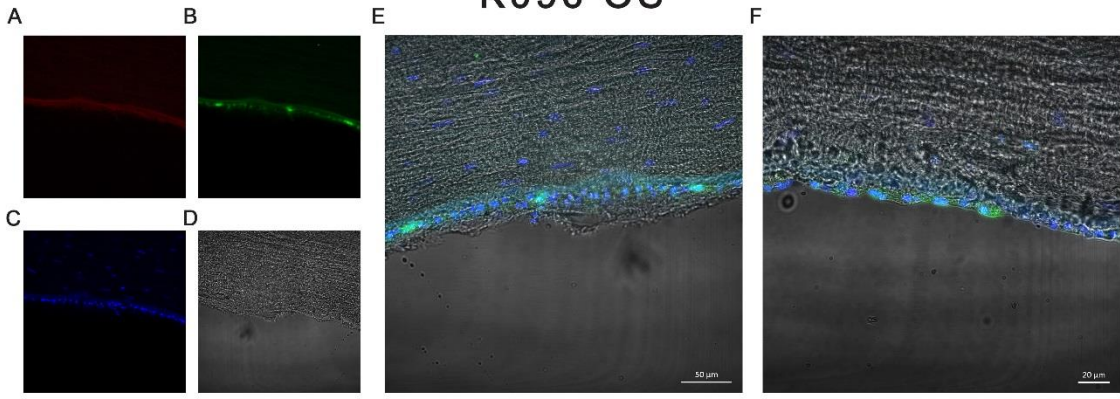


Virus	Observed Titre	Manufacturer Titre
AAV2/9 CMV eGFP	1.98E+13	6.0E13
SC AAV2/9 CMV eGFP	4.37E+13	3.3E13
AAV2/9 Induc. eGFP	3.49E+13	3.8E13
AAV2/9 CMV Null	3.40E+13	1.0E+14

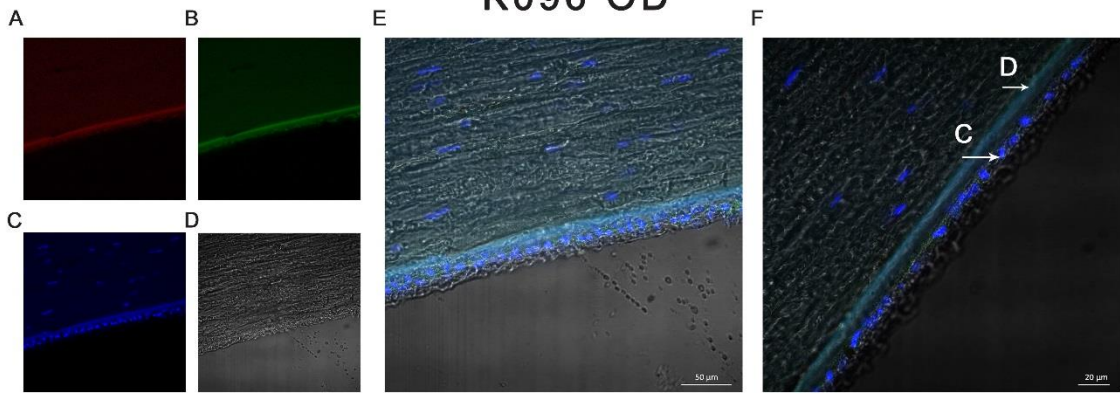
Figure 4.12: Viral purity and titre of selected constructs

Viruses were assayed for purity by SDS-PAGE, and demonstrate that the capsid proteins (VP1, 2, and 3) present bands of expected size and no other bands representing contamination were observed. Using bovine serum albumin (BSA), the titre of each virus was estimated and compared to the titre stated by the manufacturer, for confirmation.

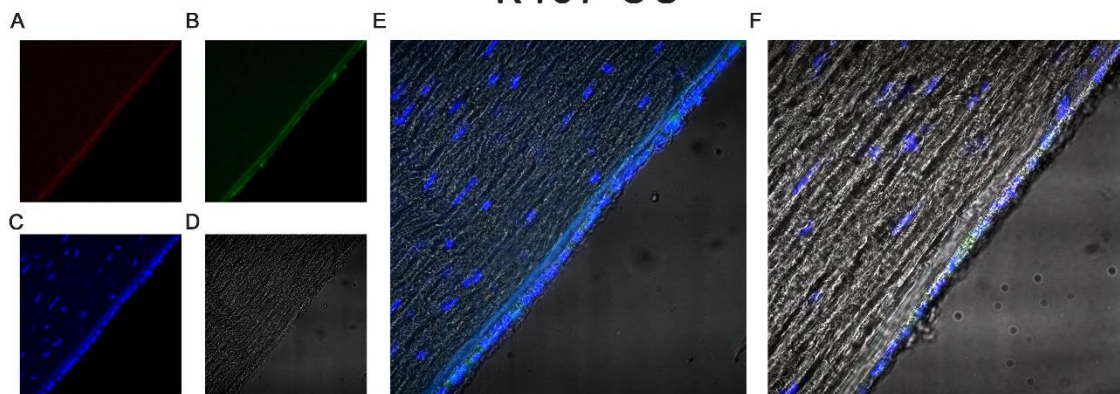
K096 OS



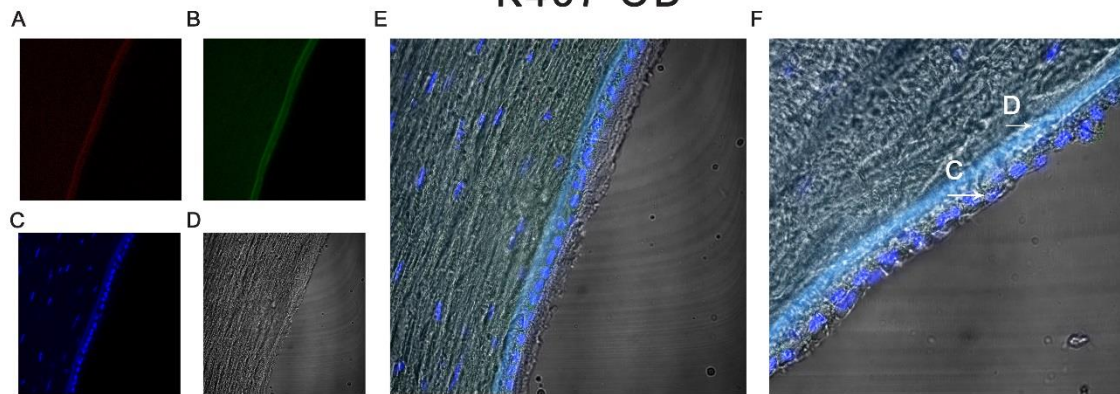
K096 OD



K457 OS



K457 OD



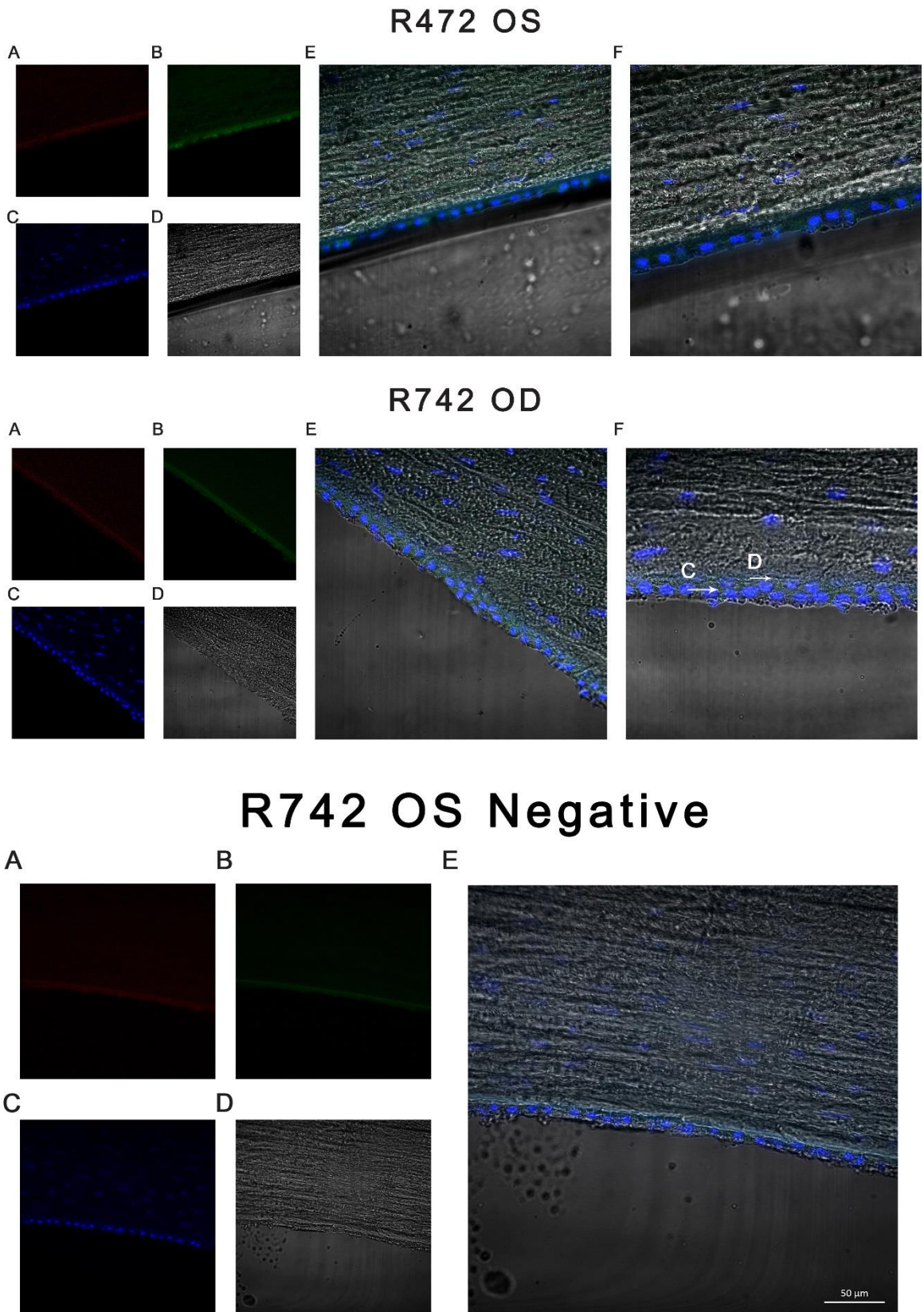


Figure 4.13: GFP expression in the corneal endothelium of NHPs.

Figure 4.13: GFP expression in the corneal endothelium of NHPs.

Images (A-F) represent the corneal endothelium of a single eye stained with Goat-Anti-GFP antibody conjugated to FITC fluorophore. (A) Red channel for autofluorescence comparisons. (B) Green channel for FITC-labelled GFP. (C) Nuclear material counterstained blue with DAPI. (D) Transillumination of the section. (E) Green/Blue/TL channels merged at 40X magnification. (F) Green/Blue/TL channels merged at 63X magnification. “R742 OS Negative” represents an unstained control. Scale bars are present on K096 images. C = Corneal endothelium. D = Descemet’s membrane.

4.3 Discussion

Dexamethasone is widely used and extensively characterised in modelling ocular hypertension. This has been further validated by comparing SC cells treated with DEX to SCg cells from glaucomatous patients (Figure 4.1, method 6.9). Changes to the actin cytoskeleton are similar to that found in SCg cells. SCg monolayers are thought to be transdifferentiated into myofibroblast-like cells. This mechanism is likely different with DEX treatment as it is reversible, however the effect is similar, adding to the consensus that DEX is an acceptable model of ocular hypertension and glaucoma. From the data, IOP was significantly increased upon exposure to dexamethasone, however facility was not significantly decreased (Figures 4.2, 4.4). A likely explanation is that unpaired analysis is not as strong as a paired analysis, i.e. measuring the difference between control eyes of different animals versus the contralateral eyes of the same animal. High variation in facility between animals will make unpaired analysis difficult without higher n numbers. iPerfusion, however, is sensitive enough to detect changes in facility in MMP-3 treated eyes regardless of whether the eyes were from a normotensive or hypertensive model (Figure 4.5, method 6.19). In both cases, MMP-3 increases facility by approximately 50%. Based on the confidence intervals, we cannot confidently say that this difference is greater in either cohort, yet it may be possible that TIMP-1 expression by DEX

could have led to a slightly reduced effectiveness in MMP-3's modulation of facility. Conversely, changes in IOP resulting from MMP-3 expression were only detected in the hypertensive model (Figure 4.3, method 6.21). This indicates that either MMP-3 does not change IOP in normotensive eyes, or rebound tonometry is not sensitive enough to detect changes at the pressure range of normotensive murine eyes. The latter is likely, given that tonometry has a large inherent variation and is dependent upon many factors including temperature, which was above the normal range during this experiment. The improved method for IOP in this chapter (6.21) was designed to minimise external variations arising from body temperature, anaesthesia, time since anaesthesia, animals stress and includes repeated measuring to account for tonometer variability. It does not account for factors such as central corneal thickness which may vary between animals and thus skew tonometry data. It must be considered that constitutive expression of MMP-3 is able to reduce IOP in normotensive eyes, as in Chapter 3 (Figure 3.10). This suggests that the inducible construct may not be expressing MMP-3 in quantities that are sufficient for normotensive reduction of IOP. This could be a factor of the eye drop regime, the different promoter, variations in injection volume or indeed the actual number of injected viral genomes. Facility is increased in the normotensive groups however, which further highlights that perfusions are a much more sensitive assay than rebound tonometry in murine eyes. Other methods of IOP measurement could have been introduced, such as an anterior chamber cannula connected to a pressure sensor, or goldman applanation tonometry which measures the force needed to flatten the surface of the cornea. These may prove more accurate and have less confounding variables than rebound tonometry, however they are either invasive or involved procedures with specialised equipment that were not feasible for this project.

Ultrastructural analysis shows that degradation of ECM components results in greater open spaces throughout the TM and JCT (Figure 4.6, method 6.23). This modulation is similar to that seen in naïve animals (Chapter 3, Figure 3.12), including the separation of the SC from the

sub-endothelial JCT layer. Although the foot-like extensions still appear to be attached to the sub-endothelial cells, there is a clear increase in optically empty space, indicating reduced outflow resistance. This supports the ‘funnelling model’ concept, in that the reduction of a bottleneck effect due to decreased ECM should lead to a decrease in outflow resistance, which is confirmed by perfusion. Quantification of optically empty spaces yields a similar result to that of naive animals in Chapter 3 (Figure 3.12, 4,7). Taken together, these data suggest that MMP-3 is effective in a model of steroid-induced glaucoma.

Observations are similar in the MYOC model. IOP increases over time as a confirmation of ocular hypertension, and reduction of IOP by MMP-3 is only observed in the positive cohort (Figure 4.8, 4.9, method 6.21). There is a non-significant decrease in outflow facility between control eyes of each group (Figure 4.10), and MMP-3 increases outflow facility in both groups (Figure 4.11). A trend exists where MMP-3 does not increase outflow facility in MYOC (+) animals to the same extent as in MYOC (-) animals, however this observation is also non-significant. At the time of writing, electron microscopy data is still ongoing, and thus conclusions on the structural analysis of the MYOC (+) TM and its response to MMP-3 cannot be made. It is presumed that a partial degradation of the TM will occur, however ECM material would still be modulated by MMP-3.

In both glaucoma models, IOP is significantly reduced by approximately 2 mmHg, and facility is increased by approximately 50% in response to MMP-3 treatment. In control cohorts, the same, if not a greater, increase in facility is observed, suggesting that IOP should be reduced. As this is not shown from the data, the most straightforward reason must be that rebound tonometry loses sensitivity or data resolution at lower IOPs. Nevertheless, the positive data from the DEX (+) and MYOC (+) animals suggests that MMP-3 can be effective in different glaucomatous environments, and may prove to slow disease progression.

Furthermore, these murine models are currently in use for the determination of efficacy of an siRNA-based approach in which tight junctions of the SC are transiently downregulated to

facilitate AH egress. siRNA molecules targeting both zonula-occludin-1 and tricellulin have been shown to increase the permeability of cell monolayers, and have further been shown to increase outflow facility when intracamerally injected into the anterior chamber of naïve mice. See Appendix 6 for the proof of concept paper for this approach.

Although the data from NHPs is still in its infancy, it is apparent that the same approach could be initiated in primate systems. GFP expression is rather discontinuous along the corneal endothelium, which will lead to the optimisation of such protocols including volume and titre of injected virus, capsid and codon optimisation, and processing technique. Based on the autofluorescence from the negative image, the red channel, and the signal intensity from Descemet's membrane, it appears that Descemet's membrane has a basal autofluorescence. Based on the 2.5D images (method 6.15), the presence of distinct peaks indicates positive GFP presence in the corneal endothelium. It is therefore apparent that K096 OS and K457 OS eyes express GFP, and any signal from R742 is likely background fluorescence (Figure 4.13). Self-complimentary viruses were injected into K096 OD and K457 OD eyes, however no GFP fluorescence is apparent. This was an unexpected result, however it agrees with that seen in murine eyes (Appendix 1, Supplementary Figure 2). Perhaps a technical issue or degradation of the vector occurred over time preventing infection and/or translation of anterior chamber tissues.

This conclusion matched the injection assignments, proving that performing the experiment blind was successful. The corneal epithelium, stroma, ciliary processes, ciliary body, trabecular meshwork, Schlemm's canal inner wall and lens did not appear to express GFP in these eyes. This generates promise for the pre-clinical development of this potential therapy, and if successful, to explore the feasibility of Phase 1 trials in human subjects.

Chapter 5

Conclusion

Glaucoma does not have a simple definition, nor are its mechanisms fully elucidated. There are many factors that contribute to glaucoma, including genetic and environmental factors from age to lifestyle. IOP is the main risk factor and is the most manipulatable and treated contributor, but is not necessarily causative of the disease. Significant advances in IOP lowering have demonstrated a prolonging of visual function, although as it is a neurodegenerative disorder, neuroprotection of RGCs is the primary goal of therapeutic intervention. Models of ocular hypertension are the focus of glaucoma research and further development on these will be crucial to the generation of new therapies, however it is important that these models also include RGC degeneration and loss of visual field to be true models of the disease.

Discussion of AAV-MMP-3 as a potential therapy

From the compiled data, it is clear that AAV-MMP-3 holds promise as a potential therapeutic approach in the treatment of glaucoma. By targeting the major site of aqueous outflow resistance, the JCT and in particular its ECM using MMP-3, we can simultaneously modulate a large proportion of the components that derive the ECM at this region. It was initially of interest to assess how cytokines would affect MMP expression in SC cells, in order to examine

the role cytokine imbalance plays in POAG AH. These results differ from those obtained by treating SC cells with POAG itself, indicating that although the cytokine imbalance upregulates total MMP expression, another factor remains that prevents this MMP from converting to its active form. It has been shown in this investigation that MMP-3 alters the structure and functionality of 4 major proteins involved in ECM and cytoskeletal composition: collagen IV, laminin, fibronectin and α -SMA (Figure 3.4). MMP-3's proteolytic profile extends further to proteoglycans, gelatins and elastin, also widely expressed in the JCT region. As the ECM network is a mesh of multiple protein types, degradation of a single subgroup of these proteins, such as the case would be with MMP-1, -2 or -9, may not be sufficient to produce a porous matrix and hence decrease outflow resistance. Collectively degrading these components with MMP-3 will be sufficient for reducing outflow resistance, and hence decreasing IOP. Additionally, modification of the ECM to this extent can indirectly modulate the actin cytoskeleton of the surrounding cells. This actin modulation is a mechanism of some glaucoma therapies and is known to reduce cell stiffness, reducing outflow resistance. In addition, MMP-3 can activate other members of the MMP family such as the gelatinase MMP-9 which may also be contributing to paracellular flux through gelatin, collagen or ZO-1 modulation. The ability of active MMP-3 to increase paracellular permeability while retaining cell viability proved it to be an attractive target. Studies utilising MMPs in organ-perfused cultures have previously shown that MMP activity is required to increase outflow facility and suggest the therapeutic potential of introducing compounds that increase activity (158, 159). One of the essential properties of the proposed AAV-MMP-3 therapy is that accumulation of latent MMP-3 results in an auto-activation cascade, rendering any further delivery of MMP-3-activation compounds unnecessary. This indicates that MMP-3 is the most obvious choice out of the entire MMP family, as most other secreted MMPs would also require some form of exogenous activation, which would be more challenging.

Transfection of the corneal endothelium and MMP-3 secretion by topical administration of doxycycline features a novel strategy for genetic delivery systems in the anterior chamber of the eye. The cells of the corneal endothelium, in humans, do not regenerate *in vivo* and instead neighbouring cells enlarge as compensation for endothelial cell loss (363, 398). Some species including rat, cat and rabbit however can somewhat regenerate endothelial cells, and regeneration can be induced in humans through corneal transplantation (399, 400). A lack of proliferation in these cells would indicate that the virus has the potential to persist for long periods, possibly for life in humans, obviating the need for follow-up injections. This poses an encouraging therapeutic timeframe for AAV-MMP-3, as an effect would likely be seen within a few days after injection, with expression lasting for a long time, likely many years, which would indicate a continuous management of IOP. Further optimisation of the eye drops could be achieved for the inducible system, such as the combination of doxycycline and a hydrogel to further increase availability to the corneal endothelium. Hydrogels have been used for tissue engineering and drug delivery to the anterior and posterior chambers and may be more effective than hydrophilic delivery (401). Drug delivery via contact lens provides high bioavailability, low compliance issues, reduces systemic loss of the drug and can provide a uniform release profile (402). Some processing and regulatory issues remain, however this could be an avenue for delivery in the future for viral-activating compounds, or perhaps even viruses themselves. Outflow facility and IOP data, especially those in models of ocular hypertension are indicative that AAV-MMP-3 is acting as intended, and could rival that of topical formulations currently in use in the clinic (Figures 4.2, 4.3, 4.5, 4.8, 4.9, 4.11). As demonstrated by EM experiments, ECM material is indeed being modulated and even degraded at the JCT region, specifically at the subendothelial cells underlying the SC (Figures 3.12, 4.6).

Comments on procedures and experimental design

Regarding the intracameral injection itself, infusion of a small volume into the anterior chamber often results in a transient pressure spike. Upon visual inspection, it is clear the eyes recover quickly and appear normal in the minutes after injection. This has been described previously and injected eyes exhibit normal tissue morphology (403). A slow infusion, perhaps over the course of 10 minutes, using an infusion pump would further reduce IOP spikes if they were a concern. Care was always taken to avoid superficial piercing of the cornea, along with preventing scratches or inducing cataracts. Contralateral control injections help to reduce confounding impacts from lens surface damage, additionally notes were taken on the quality of each injection and ocular health checks were performed post injection. Eyes were also checked for the absence of cataracts before each IOP reading and before perfusion. Withdrawal of virus into the Hamilton syringes was at a slightly different rate each time due to the position at which the needle was broken. Thus, it is possible that there were small variations in injection volume (method 6.13, Appendix 5). Viruses were not titred and the manufacturers titre was always assumed, however it should be considered that the manufacturers titre could include empty capsids. This could also result in inaccuracies, and together these variations in viral genome number could cause variations in MMP-3 expression and ultimately efficacy, and may be a factor in the variation observed in IOP and facility analyses. TaqMan qPCR titre assays are to be implemented in the future.

Constitutive expression of MMP-3 is likely to result in a negative feedback loop inducing expression of inhibitors such as TIMP-1. It is also possible that chronic exposure to MMP-3 may lead to apoptosis or other unwanted off target effects in some cells. Therefore, controlled regulation of MMP-3 expression would be preferable to prevent any negative effects in response to chronic over-expression. The incorporation of an inducible U6 promoter into the vector introduces this important control element. This is a well characterised and widely used promoter within the laboratory for the expression of shRNAs. In hindsight, this choice of

promoter may not have been optimal to mRNA expression as it recruits polymerase III for transcription as opposed to polymerase II which is typically used in eukaryotic mRNA expression. The most commonly used inducer of the tetracycline on/off system is doxycycline. 1 drop of doxycycline administered twice a day was sufficient to induce MMP-3 expression from the corneal endothelium, although less frequent administration has not been tested (method 6.12). Tetracyclines have been shown to inhibit MMP activity, particularly the gelatinase family (MMP-2 and -9), however little evidence points to MMP-3 inhibition. As reported by Hanemaaijer and colleagues, tetracycline has a weak to absent inhibition on MMP-3 (404). Regardless, it is unlikely that there would be sufficient amounts of doxycycline present in the anterior chamber to inhibit MMP-3 following topical administration. The eye drop is delivered at 0.2% doxycycline, the corneal availability of which is estimated to be <5% from an eye drop (405). The concentration of doxycycline would be considerably less in the anterior chamber following corneal layer penetration, and thus it would be difficult to assay for such a low concentration in the aqueous humour.

A glaucomatous environment is considerably different to that of a healthy one, in which novel therapies may have an entirely different response. This is somewhat overlooked in the literature as most experimentation is performed on healthy SC endothelial cells or naïve animals. In glaucoma, chronic fibrosis exists particularly in the anterior chamber, inducing transdifferentiation among multiple cells, for example, into mesenchymal or fibroblast-like cells. These cells exhibit different characteristics such as increased ECM deposition, actin cytoskeleton conformation, and a reduced ability to respond to their environment (406). Therefore, it could be presumed that a therapy targeting the outflow tissue, for example, may be less effective in a glaucomatous environment. This is somewhat observed in the DEX and MYOC animals injected with AAV-iMMP-3. Outflow facility is increased in response to MMP-3, as with controls, however the relative difference in facility is not as great as that of control animals (Figures 4.5, 4.11). Although the difference between the model and control

groups is non-significant, the trend is worth noting for the consideration of future trials and experimental design.

Were this work to be repeated or redesigned, a greater focus would be put on dose-response of both MMP-3 quantification in the AH and viral transduction and expression of MMP-3 for a number of reasons. Endogenous mechanisms could influence the conversion of latent MMP-3 into its active form such as endogenous MMP-3 levels, TIMP levels and cellular mechanisms enhancing AAV translation. As such, these factors could vary between glaucoma patients and may affect 'actual' dose. Dose is critical, especially in long term expression systems as with the constitutive promoter as there is the possibility that with excess MMP-3 levels, basement membrane material may be completely digested. Hypotony is not a concern as the remaining resistance generated by the intact SC would prevent such an outcome, however SC collapse is something to consider. Collapse in a regional sense would be well tolerated as AH would flow through remaining channels, however if the SC was to collapse around its entire circumference, this could lead to increases in IOP. Thus, dose response is an important aspect for study, even though translation of dose into humans poses its own challenge. A better selection in inducible promoter such as a mini CMV fused to the tetracycline response element, or perhaps a metallothionein-inducible promoter would be more favourable for the reasons outlined above. Murine models of glaucoma, specifically the DEX model have developed considerably since the initiation of this work, most noticeably with the delivery of DEX. Weekly subconjunctival injections of DEX nanoparticles have not only shown to be more effective in terms of increasing IOP (an increase of 6 mmHg), but are much less detrimental to animals as they are not systemic and can be continued for a much longer time period.

Clinical relevance

From both Chapter 3 and Chapter 4, a reduction in IOP of 2-3 mmHg seems insignificant at first in the context of glaucoma. It is important to recognise that the relationship between IOP

and RGC damage is not linear, and so it is impossible to define a threshold for adequate IOP lowering. In the case of POAG, the goal of surgical interventions is to achieve an IOP of 12-15 mmHg, and in normotensive glaucoma, to lower IOP from 14 mmHg to 8 mmHg. A favourable decrease in IOP is therefore approximately 6 mmHg, as is seen with some topical formulations. Of course, the physiologies of the mouse eye must be considered and scaled to the human eye. IOP can only be reduced so much, otherwise blood from the episcleral veins would reflux back into the anterior chamber. This limit is much lower in mice, and is referred to as the pressure drop or differential across the Schlemm's canal (calculated as IOP minus episcleral venous pressure). The most appropriate means of scaling to a human eye is to use the effect size of Latanoprost as a case study. The observed reduction in IOP from MMP-3 is comparable to that of previous studies involving latanoprost. These studies demonstrate that it is common to see an average decrease in IOP of 2-3 mmHg in mice treated with latanoprost (407). In an effort to see greater effect, some studies only measure IOP at night, when the IOP of a mouse is at its peak. Even so, a decrease of 3-4 mmHg is common even at the highest doses (408). We know that the effect of latanoprost scales in humans, studies showing an initial IOP decrease of 5 mmHg (409) and so there is confidence that in larger animal models with eyes accommodating higher IOP and pressure differentials, a greater IOP lowering effect would be observed with MMP-3. Therefore, the reductions in IOP as seen in these studies are clinically relevant and meaningful.

In terms of application in a clinical setting, a glaucoma patient would receive regular IOP measurements, and upon the recognition of high IOP (such as above the "normal" upper threshold of 21 mmHg) the patient would receive a single viral injection and given a prescription for doxycycline eye drops. After a certain time frame sufficient for IOP reduction, the patient would again receive an IOP measurement and if the reading is within a "normal" pressure range then topical administration would cease until a time where IOP increases again.

Immune responses to AAV may pose a challenge for this therapy. For sub-retinal injections of AAV2, minimal activation of T-cells was observed along with no neutralizing antibodies, especially at low doses. Some serum neutralising antibodies were observed in serum at higher doses however. Thus, at low doses, re-administration of AAV2 for transgene expression was achievable in this case (410). Different ocular compartments have different immune responses which would likely be different for each AAV serotype as well. For intravitreal injections targeting the retinal ganglion cells, a humoral immune response was generated blocking vector expression into the partner eye (411). This was not observed in subretinal injections, and so raises the question of tolerability in partner eyes and whether sympathetic effects would arise from intracameral injection. There is little information on AAV immunogenicity following intracameral injection in the literature, however this is an important aspect to consider when designing clinical trials. Previous experiences from key opinion leaders suggests that there is little to no neutralising antibodies expressed in response to AAV in the anterior chamber, but it is unclear if re-administration would be possible, if it were needed. Anterior chamber-associated immune deviation (ACAID) is a phenomenon where an injection into the anterior chamber induces TNF- α and monocyte chemoattractant protein 1 and an infiltration of circulating monocytes. These monocytes emigrate to the thymus and spleen where T cells are induced that inhibit the inductive or effector phases of a cell-mediated immune response. This immune privilege mechanism protects the eye from the damage induced by immune responses and also suppresses future damaging responses to infection (412). The sub-retinal space mirrors this ACAID response and so repeat injection may be possible in the anterior chamber, although this will need to be looked at closely for AAV9 (413).

Future directions and optimisation

There are many properties that have not been addressed with this strategy, including optimal titre and volume to deliver into the anterior chamber, optimal inducible system and/or inducer

(e.g. most effective tetracycline derivative), concentration, frequency and absorptivity of eye drop to be applied. Dose-response curves in cells can make a decent and cost-effective method to determine optimal tetracycline derivative, concentration and frequency. Absorption of the eye drop could be increased by dissolving in a carbomer instead of PBS. Proof of transduction in the corneal endothelium of a NHP is a first step toward toxicology and pharmacodynamic assessment, including biodistribution of the virus, assaying for TIMP-1 inhibitor levels in the AH, and TUNEL staining for *ex vivo* cell viability. A comparison between this therapy and conventional or emerging glaucoma medications would be of interest. AAV-MMP-3's effect on facility and IOP could be directly compared to that of Latanoprost and Rhopressa, a rho kinase inhibitor. As of yet, only an indirect comparison can be made (Figure 3.13) between animals treated with AAV-iMMP-3 and those treated with Latanoprost.

There remains a considerable amount of work required before validation of efficacy can occur in a clinical trial, such as a safety/toxicology study, anterior chamber immune responses, proof of efficacy in non-human primates, verification of the protection of retinal ganglion cells and their axons and further development of the vector therapy itself, all of which were not comprehensively assessed in this body of work. Future directions for this project to this end include the generation of codon optimised sequences for MMP-3 and the transduction efficiency of novel and proprietary AAVs to the corneal endothelium to attain the greatest expression of MMP-3. This is then to be titrated to a tolerated dose in detailed NHP studies. Quality control assays and pharmacodynamic studies will then be initiated on these vectors to assess their safety and then efficacy using tonometry, OCT, immunohistochemistry and TEM, along with repeated analyses of biomarkers and activity via aqueous taps. Indeed, the existence of an MMP3 inhibitor, TIMP-1 could be elevated in response to our overexpression. TIMP-1 elevation could be minimised by sequence optimised constructs, along with the fact that overexpression of MMP-3 by a viral system should out-compete any endogenous increases in TIMP-1, as this mechanism would not be as efficient as the viral promoter. Human anterior

segment perfusion with recombinant MMP-3 and AAV-MMP-3 will provide a good estimation of the translatability to humans, along with early toxicology into the cornea and outflow tissues. Upon successful determination of efficacy and dose, GMP grade material is to be manufactured for use with early phase I clinical trials. This will involve careful trial design including target population (likely those recommended for trabeculectomy where topical drops have failed) and comparative arms such as non-inferiority with timolol (gold standard for FDA regulated studies) or the newer ROCK inhibitors.

Until such a time that these issues can be systematically addressed (such studies have now been initiated), this project shows that secretion of MMP-3 from a topically induced AAV virus successfully increases outflow facility and reduces IOP in murine hypertensive models and holds promise for the future development of a gene therapy for glaucoma.

Chapter 6

Materials and Methods

All methodology was carried out by myself independently, unless otherwise stated.

6.1 Cell culture

Human SCEC were isolated, cultured and fully characterised according to previous protocols (414-416). Briefly, cells were isolated from the SC lumen of human donor eyes using a cannulation technique. Isolated cells were tested for positive expression of VE-cadherin and fibulin-2, but absence of myocilin induction upon treatment with 100 nM dexamethasone for 5 days. Confluent cells displayed a characteristic linear fusiform morphology, were contact inhibited and generated a net transendothelial electrical resistance greater than 10 Ω .cm². TEER values were confirmed again prior to MMP-3 treatments. SCEC strains used were SC82 and SC83 between passages 2 and 7. Dulbecco's modified eagle medium (Gibco, Life Sciences) 1% Pen/Strep/glutamine (Gibco, Life Sciences) and 10% foetal bovine serum (FBS) performance plus (Gibco, Life Sciences) was used as culture media in a 5% CO₂ incubator at 37°C. Cells were transferred to a media containing only 1% FBS a week prior to protein treatment. Cells were passaged with trypsin-EDTA (Gibco-BRL) and seeded into 12 well or 24 well transwell plates (Costar, Corning). Human trabecular meshwork (HTM) cells were isolated and fully characterised according to the procedures described in (417-420). TM tissue is

removed from human donor eyes using a blunt dissection technique, and TM cells are dissociated from the tissue using a collagenase digestion protocol as previously described (417). Isolated cells are characterised by their dramatic induction of myocilin protein following treatment with dexamethasone (100 nM) for 5 days as detailed before (414). HTM123 and HTM134 cells were cultured similar to SCEC's and matured for one week in 1% FBS media prior to treatment.

Human AH samples (detailed below) were added 1:10 to fresh media for cellular treatment for use with TEER and permeability assays as described below.

Cytokines (Gibco, Life Technologies) were added to cell monolayers at a concentration of 10 ng/ml in media. For combined cytokine treatment, each of IL-1 α , IL-1 β , TNF- α were mixed at 3.33 ng/ml each to a total of 10 ng of cytokines per ml before being added to the monolayers. Cytokine-treated media was incubated on cells for 24 hours.

Recombinant human active MMP-3 (ab96555, Abcam) was added to cell media at a concentration of 10 ng/ml for TEER, permeability assays, western blotting and immunocytochemistry as described below. Inactivated MMP-3 controls were achieved by incubating active MMP-3 (10 ng/ml) with recombinant human active TIMP-1 (100 ng/ml) in cell media for 1 hour prior to treatment.

6.2 Animals

Animals and procedures used in this study were carried out in accordance with regulations set out by The Health Products Regulatory Authority (HPRA), responsible for the correct implementation of EU directive 2010/63/EU. 8-11 week old male and female C57BL/6 mice were used in all experimentation outlined in this study. Animals were bred and housed in specific-pathogen-free environments in University of Dublin, Trinity College and all injections and IOP measurements complied with the HPRA project authorisation number AE19136/P017. 21 mice were used to calibrate the infusion pump for intracameral injections and optimise

perfusions with recombinant MMP-3. For the constitutive AAV-MMP-3 viral study, 70 animals were used for IOP, perfusions, TEM, aqueous MMP-3 concentration and activity experiments, immunohistochemistry and central corneal thickness experiments. 40 mice were injected with the inducible AAV-MMP-3 virus for IOP, perfusions, and the optimisation of intracameral injections and IOP. A total of 40 mice were used for the DEX study to include sufficient numbers for IOP, perfusions and TEM for both DEX (+) and DEX (-) cohorts. Regular health checks and daily care was given to these animals due to the severity of systemic DEX. Several animals did not survive the duration of the experiment, and some were sacrificed due to a weight loss of >20% of their initial body weight. For the myocilin study, a total of 37 mixed sex transgenic MYOC animals at the age of 3-3.5 months were used for IOP, perfusions and TEM. No adverse effects were observed. A total of 3 NHP were bred at, maintained and operated on at St. Kitts Biomedical Research Foundation and were used in accordance with the ARVO statement for the use of animals in ophthalmic and vision research.

6.3 Patient aqueous humour samples

Human aqueous was obtained from the Mater Misericordiae Hospital, Dublin, Ireland. Upon informed consent, AH samples were collected from both POAG and control patients undergoing routine cataract surgery by Dr. Colm O'Brien. The criteria for POAG was defined as the presence of glaucomatous optic disc cupping with associated visual field loss in an eye with a gonioscopically open anterior drainage channel, with an intraocular pressure > 21 mmHg (46). The samples were taken immediately prior to corneal incision at the start of the procedure using a method described previously (421). Frozen AH samples were delivered to Trinity College Dublin for *in vitro* experimentation. Human AH collection conformed to the WMA Declaration of Helsinki and was approved by the Mater Misericordiae University Hospital Research Ethics Committee.

6.4 Transendothelial Electrical Resistance (TEER) measurement

Electrical resistance values were used as a representative of the integrity of the endothelial cell-cell junctions. Cells grown on Costar transwell-polyester membrane inserts with pore size of 0.4 μ m were treated with 10ng/ml MMP-3 as described above. TEER readings were measured before and 24 hours after treatment. Plates were taken from the incubator and left in the laminar to adjust to room temperature for 10 minutes. Probes were cleaned in 70% ethanol and washed in dH₂O prior to use, and rinsed in dH₂O between groups of replicates. The electrical probe was placed into both the apical and basal chambers of the transwells and a current was passed through the monolayers, reported as a resistance in Ω .cm². A correction was applied for the surface area of the membrane (0.33 cm²) and for the electrical resistance of the membrane (blank transwell).

6.5 Permeability assessment by FITC-Dextran flux

The extent of monolayer permeability was assessed by the basal to apical movement of a tracer molecule through the monolayer. Measures of permeability were taken 24h after treatment immediately after TEER values, on transwell membranes, keeping experimental set-up identical to that of TEER readings. The permeability protocol was repeated as described in (307). A 70 kDa fluorescein isothiocyanate (FITC)-conjugated dextran (Sigma) was added to the basal compartment of the transwell. Fresh media was applied to the apical chamber and aliquots of 100 μ l were taken every 15 minutes for a total of 120 minutes, replacing with fresh media. Sample aliquots were analysed for FITC fluorescence (FLUOstar OPTIMA, BMG Labtech) at an excitation wavelength of 492 nm and emission wavelength of 520 nm. Relative fluorescent units (RFU) were converted to their corresponding concentrations by interpolating from a known standard curve. Corrections were made for background fluorescence and the serial dilutions generated over the experiments time course. P_{app} values were calculated

representing the apparent permeability coefficient for control (PBS) and treatment (10 ng/ml MMP-3). This was achieved via the following equation:

$$P_{app}(cm/s) = (dM/dT)/(A \times C_0),$$

Where dM/dT is the rate of appearance of FITC-dextran (FD) ($\mu\text{g/s}$) in the apical chamber from 0 to 120 minutes after introduction of FD into the basal chamber. A is the effective surface area of the insert (cm^2) and C_0 is the initial concentration of FD in the basal chamber.

6.6 RT-PCR

RNA was extracted from cells using the RNeasy mini kit (Qiagen) protocol. Briefly, cells were lysed, mixed with 70% ethanol and placed into a mini spin column. Columns were spun at 8000 $\times g$ for 15 seconds. Samples were washed once with 700 μl RW1 and twice with 500 μl RPE buffer to remove cellular material. Finally, 50 μl of RNase-free water was added to the column and centrifuged for 1 min at 8000 $\times g$ to elute the RNA. RT-PCR was carried out in accordance with the Quantitect SYBR Green RT-PCR handbook. SYBR Green, primers, RNA and RNase-free water were thawed and samples were kept on ice. 20 μl reactions were made consisting of 15 μl of master mix (270 μl SYBR Green, 27 μl of Primer mix, 4.32 μl of Quantitect RT mix and 103.68 μl RNase-free water for every 25 wells) and 5 μl RNA sample. Plates were mixed and placed into an Applied Biosystems StepOne Plus real time PCR system. The PCR cycle involved 30 minutes at 50°C for reverse transcription, 15 minutes at 95°C for PCR activation, and 30 cycles of 15 seconds of 94°C, 30 seconds of 60°C and 30 seconds of 72°C. Melting curve analysis was also performed for indications of primer suitability and contamination.

6.7 Fluorescent-activated cell sorting (FACS)

Mouse corneas were dissected by cutting around the circumference of the eye, just below the limbus, to ensure inclusion of the SC. The vitreous body, lens and iris were removed, except in the case of one attempt where the iris was included in case its removal was facilitating detachment of the outflow tissues. Corneas were pooled in a C-tube and incubated in a protease solution containing either collagenase 1, collagenase 1 and trypsin, or collagenase 1 and dispase, concentrations for each ranging from 0.1 to 5 mg/ml. Incubation was at 37 °C for one hour in constant rotation. Every 30 minutes afterwards, tubes were attached to a GentleMACS cell dissociator and dissociation programs were applied to physically disrupt cell-cell attachments. After a total of 4 hours, samples were centrifuged and filtered through a 70 µm filter. Cells were again centrifuged and resuspended in 1-2 mls of HBSS with 2% annexin binding buffer. 10 % of the sample was put aside for an unstained control. Primary antibodies (PECAM-1 conjugated to Alexa-Fluor 647 and VEGF-R3 conjugated to Alexa-Fluor 488) were added and samples were incubated for another 30 minutes. Propidium iodide was also added immediately prior to sorting to detect dead cells. Samples were then analysed using a flow cytometer and sorter (Aria Fusion Sorter). The sorting strategy was to isolate cells from debris using forward and side scatter, remove large clumps to obtain single cell populations, exclude cells positive for propidium iodide, and finally to visualise populations positive for both fluorophores and negative for both fluorophores. Cell counts were not favourable and no clear positive staining was observed, suggesting that the dissociation protocol required further optimisation (Appendix 1, Supplementary Figure 1).

6.8 Cell Viability

Cultured cells were treated with increasing concentrations of recombinant human MMP-3 (ab96555, Abcam) from 0-200 ng/ml. Cell viability was assessed 24 hours post treatment with

MMP-3 using a CellTitre 96[®] Aqueous One Solution Cell Proliferation Assay (Promega). Cell media was aspirated and a 1 in 6 dilution of the supplied MTS reagent in media was added to the cell surface. Cells were incubated at 37°C for 1 hour and the media/reagent was transferred to a 96-well plate for reading by spectrophotometry (Multiskan FC, Thermo Scientific) at 450 nm. Standard *in vitro* viability calculations fail to consider sample size and the biological significance of the data. Hence, a modified approach was taken to determine at which concentration SCEC's show a reduced tolerability to MMP-3. This was defined at an average of 85% viability over 3 cell samples. This conservative value ensures that a cell population would remain viable and still be able to proliferate. Anything lower should be regarded as MMP-3 intolerability i.e. reduced cell proliferation or cell death. Control samples (0 ng/ml MMP-3) were normalised to 100% viability and a linear model fitted to the normalised data. The MMP-3 concentration at which cells had an average of 85% viability was interpolated from the lower 95% confidence bound from this linear model. This value represents the concentration of MMP-3 at which the average of three cell samples would have a 97.5% chance of retaining a greater to or equal than 85% viability.

6.9 Immunocytochemistry

Immunocytochemistry was performed to visualise changes in ECM composition in response to MMP-3. Human SCEC and HTM were grown to confluency on chamber slides (Lab-Tek II) and treated for 24 hours with 10 ng/ml of recombinant, active, human MMP-3. Cells were then fixed in 4% paraformaldehyde (pH 7.4) for 20 min at room temperature and then washed with PBS for 15 min. Cell monolayers were blocked in PBS containing 5% normal goat serum (10658654, Fischer Scientific) and 0.1% Triton X-100 (T8787, Sigma) at room temperature for 30 min. Primary antibodies of collagen IV (ab6586, Abcam), α -SMA (ab5694, Abcam), laminin (ab11575, Abcam) and F-actin (A12379, ThermoFisher Scientific) were diluted at 1:100 in blocking buffer and incubated overnight at 4°C. Secondary antibodies (ab6939, Abcam) were

diluted at 1:500 in blocking buffer and then incubated for 2 hr at room temperature. Following incubation, chamber slides were mounted with aqua-polymount (Polyscience) after nuclei-counterstaining with DAPI. Fluorescent images of SCEC monolayers were captured using a confocal microscope (Zeiss LSM 710), and processed using imaging software ZEN 2012.

For clear fibronectin (ab23750, Abcam) staining, cells were grown on cover slips and subsequently decellularised, leaving only the ECM material. Round cover slips (15mm Diameter, Sparks Lab Supplies) were silanised before cell seeding to enhance binding to ECM products. This was achieved by initially immersing slips in 1% acid alcohol (1% concentrated HCL, 70% ethanol, 29% dH₂O) for 30 mins. Slips were washed in running water for 5 min, immersed in dH₂O twice for 5 minutes, immersed in 95% ethanol twice for 5 minutes and let air dry for 15 minutes. Cover slips were then immersed in 2% APES (3-aminopropyl triethoxysilane (A3648, Sigma) in acetone (Fisher Chemical)) for 1 minute. Slips were again washed twice in dH₂O for 1 minute and dried overnight at 37°C. Cells were grown to confluency on these cover slips and, following treatment, were decellularised. This was achieved by consecutive washes in HBSS, 20mM ammonium hydroxide (Sigma) with 0.05% Triton X-100, and finally HBSS again. Matrices were fixed and stained as described above with chamber slides. A total of 4 images were taken across random points in each well of each chamber slide.

6.10 Western Blotting

Cells were treated with 10 ng/ml MMP-3 for 24 hours in serum-free media. Media supernatants were aspirated and mixed 1:6 with StrataClean resin (Agilent). After centrifugation of 10,000 rpm for 15 minutes, the supernatant was removed and the pellet was resuspended in NP-40 lysis buffer containing 50 mM Tris pH 7.5, 150 mM NaCL, 1% NP-40, 10% SDS, 1X protease inhibitor (Roche). Cells were lysed using NP-40 lysis buffer for protein collection. Samples were centrifuged at 10,000 rpm for 15 minutes (IEC Micromax microcentrifuge) and

supernatant was retained. Protein samples were loaded onto a 10% SDS-PAGE gel at 30-50µg per well (20 µl max). Proteins were separated by electrophoresis over the course of 150 minutes at constant voltage (120 V) under reducing conditions and subsequently electro-transferred onto methanol-activated PVDF membranes at constant voltage (12 V). Gels intended for use with Collagen IV antibodies were run under native conditions. Membranes were blocked for one hour at room temperature in 5% non-fat dry milk and incubated overnight at 4°C with a rabbit primary antibodies to collagen IV, α -SMA, laminin and fibronectin as previously stated at concentrations of 1 in 1000 but 1 in 500 for laminin. Membrane blots were washed 3x5 min in TBS and incubated at room temperature for 2 hours with horse radish peroxidase-conjugated anti-rabbit secondary antibody (Abcam). Blots were again washed and treated with a chemiluminescent substrate (WesternBright ECL, Advansta) and developed on a blot scanner (C-DiGit, LI-COR). Membranes containing cell lysate samples were re-probed with GAPDH antibody (ab9485, Abcam) for loading control normalisation. Media samples were normalised against their total protein concentration as determined by a spectrophotometer (ND-1000, NanoDrop). A total of 4 replicate blots were quantified for each cell lysate sample antibody, and 2-3 replicates for a media sample. Band images were quantified using Image J software. Fold change in band intensity was represented in comparison to vehicle control treatments of PBS.

6.11 Zymography

10% zymogram gelatin protein gels cassettes were purchased from Novex, Invitrogen along with the recommended renaturing (LC2670), developing (LC2671), SimplyBlue (LC6060) and sample buffers (LC2676). Cassettes were removed from their pouches and rinsed in deionised water and then running buffer. Cassettes were inserted into the electrophoresis rig, which was filled with running buffer. Samples consisted of media supernatants from cells treated with cytokines, as above. These samples were mixed 1:1 with the sample buffer and 20 µl of each

were loaded into the wells of the gel. A protein marker (P7706s) was loaded in the first lane. Gels were run at 125 volts for 90 minutes. 100 ml of 1X renaturing and 1X denaturing buffer were made. After electrophoresis, gels were removed from their cassettes and placed into a container with the renaturing buffer and incubated for 30 minutes at room temperature with gentle agitation. Renaturing buffer was removed and replaced with developing buffer for 30 minutes at room temperature with gentle agitation. Developing buffer was replaced and incubated overnight at 37 °C. After this incubation, developing buffer was removed and the gel was rinsed 3 x 5 minutes with deionised water under gentle agitation at room temperature. The gel was placed into a clear polypropylene sheath (polypocket) and scanned for the position of the ladder. The gel was stained by addition of 20 ml of SimplyBlue SafeStain and incubated for 1 hour at room temperature with gentle shaking. The gel was de-stained by removing the stain and washing in deionised water for an hour. The gel was again placed into a plastic pocket and scanned. Image J quantification of bands was performed as before. Images were visualised in black and white by converting the image to 8-bit. Lanes were isolated and analysed to generate a profile plot for each band. Base lines were generated to completely enclose the peak area of interest. The area under the peak was quantified and expressed as a percentage of the total lane width.

6.12 AAV

AAV-2/9 containing the enhanced green fluorescent protein (eGFP) reporter gene (Vector Biolabs) was initially used to assess viral transduction and expression in the anterior chambers of wild type mice (C57/BL6). Murine MMP-3 cDNA was incorporated into Bam HI/XhoI sites of the pAAV-MCS vector (Cell Biolabs Inc) for constitutive expression of MMP-3. A null virus was used as contralateral control using the same capsid and vector. The inducible vector was designed by cloning MMP-3 or eGFP cDNA into a pSingle-tTS (Clontech) vector. This vector was then digested with BsrBI and BsrGI and the fragment containing the inducible system and

cDNA was ligated into the NotI site of expression vector pAAV-MCS, to incorporate left and right AAV inverted terminal repeats (L-IRT and R-ITR). AAV-2/9 was generated using a triple transfection system in a stable HEK-293 cell line (Vector Biolabs). This virus contains a pTIGHT TRE-U6 promoter, which consists of 7 TET operator elements fused to a mini-U6 promoter. For animals injected with the inducible virus, after a 3 week incubation period, 0.2% doxycycline (D9891, Sigma) in PBS was administered twice daily to the eye for 10-16 days to induce viral expression. A similar inducible virus expressing eGFP was used as a control in the inducible study. Plasmid constructs were generated and sub-cloned by Dr. Marian Humphries and were sent to Vector Biolabs for AAV synthesis, with which I was not involved.

6.13 Intracameral Injection

Animals were anaesthetised by intra-peritoneal injection of ketamine (Vetalar V, Zoetis) and domitor (SedaStart, Animalcare) (66.6 and 0.66 mg/kg respectively). Pupils were dilated using one drop of tropicamide and phenylephrine (Bausch & Lomb) on each eye. 2 µl of virus at a stock titre of 6×10^{13} vector genomes per ml was initially back-filled into a glass needle (ID1.0mm, WPI) attached via tubing (ID-1.02mm, OD-1.98mm, Smiths) to a syringe pump (PHD Ultra, Harvard Apparatus). An additional 1 µl of air was then withdrawn into the needle. Animals were injected intracamerally just above the limbus. Viral solution was infused at a rate of 1.5 µl/min for a total of 3 µl to include the air bubble. Contralateral eyes received an equal volume and titre of either AAV-MMP-3 or AAV-Null. The air bubble prevented the reflux of virus/aqueous back through the injection site when the needle was removed. Fucidic gel (Fucithalamic Vet, Dechra) was applied topically following injection as an antibiotic agent. To counter anaesthetic, Antisedan (atipamezole hydrochloride, SedaStop, Animalcare) was intra-peritoneally injected (8.33 mg/kg) and a carbomer based moisturising gel (Vidisic, Bausch & Lomb) was applied during recovery to prevent corneal dehydration.

This injection method was further optimised for injections requiring the inducible virus. Animals were anaesthetised by exposure to 3% isoflurane in oxygen. IOP readings were usually taken at this point for baseline readings (see below). Afterwards, pupils were dilated as before, and 4 µl of inducible virus at a stock titre of 3.1×10^{12} vector genomes per ml was initially back-filled into a glass needle connected to a Hamilton syringe. An additional 1 µl of air was then withdrawn into the needle. Animals were injected intracamerally just above the limbus with a glass needle to remove existing aqueous humour. Needles containing viral solution were guided towards the puncture site using a micromanipulator and virus was infused into the anterior chamber, including the air bubble. The needle was left in the eye for 2-3 minutes to allow for equilibration, before it was slowly withdrawn. Fucithalamic was again placed on the anterior surface and animals were allowed to recover. This improved method allows for greater injection volumes, greater injection precision and a smaller corneal wound site. The intracameral injection method is described in more detail in Appendix 5.

6.14 Immunohistochemistry (murine eyes)

Eyes were enucleated 4 weeks post injection of virus and fixed in 4% paraformaldehyde overnight at 4°C. The vitreous body was removed by dissection and anterior segments were washed in PBS and placed in a sucrose gradient of incrementing sucrose concentrations containing 10%, 20% and finally 30% sucrose in PBS. After overnight incubation in 30% sucrose, anterior segments were frozen in O.C.T compound (VWR Chemicals) in an isopropanol bath immersed in liquid nitrogen and cryosectioned (CM 1900, Leica Microsystems) at 12 µm thick sections. This was achieved by freezing the OCT block to the specimen mount and attaching it to the specimen block. A clean and smooth edge of the cutting blade and glass insert were lined up to the specimen block and the cutting wheel was rotated. Sections were gathered onto charged Polysine[®] slides (Menzel-Gläser) and stored at -20°C. An aqueous barrier was drawn onto slides using a pap pen and blocked for 1 hour with 5% normal

goat serum (10658654, Fischer Scientific) and 0.1% Triton X-100 in PBS. Slides were incubated overnight at 4°C in a humidity chamber with a 1:100 dilution of primary antibody. Antibodies used were MMP-3 (ab52915, Abcam) and GFP (Cell Signalling). Sections were washed three times in PBS for 5 minutes and incubated with a Cy-3 conjugated anti-rabbit IgG antibody (ab6936, Abcam) at a 1:500 dilution for two hours at 37°C in a humidity chamber. Slides were washed three times in PBS for 5 minutes again and counter stained with DAPI for thirty seconds. Slides were mounted using Aquamount (Hs-106, National Diagnostics) using coverslips (Deckgläser) that were gently placed onto the slides to prevent trapping air bubbles and visualised using a confocal microscope (Zeiss LSM 710).

6.15 Immunohistochemistry (NHP eyes)

NHP primate eyes were processed similarly to that of mouse eyes. A selection of constitutive (6×10^{13} vg/ml), inducible (3.8×10^{13} vg/ml), self-complementary (3.3×10^{13} vg/ml) and null (1×10^{14} vg/ml) viruses were sent for intracameral injection. 50 μ l of each virus was injected to maximise the number of viral genomes in each eye. Eyes were enucleated 2-3 weeks post injection, fixed in 4% PFA overnight and transferred to PBS with 0.01% azide by the St. Kitts Biomedical Research Foundation for shipping to Dublin. Here, with the support of Dr. Matthew Campbell, anterior segments were dissected and placed in a sucrose gradient, as above. Tissue was flash frozen for cryosectioning and cut at 50 μ m intervals. After inspection under a fluorescent microscope, sections were stained with an anti-GFP antibody conjugated with a FITC fluorophore after blocking as before. After overnight incubation at 4°C, slides were washed 3 times in TBS and counterstained with DAPI for 30 seconds. Slides were mounted and visualised as with murine sections. Approximately 20 images were taken of each eye. As images were processed blind, it was determined that the best approach was to determine if GFP signals were clearly stronger than that of the highly autofluorescent Descemet's membrane. Using histogram views, the Descemet's membrane layer was distinguished from the corneal

endothelium by DAPI staining. If signal peaks in the endothelium were much greater than the autofluorescent levels then that particular eye was labelled as GFP-positive (Figure 5.1).

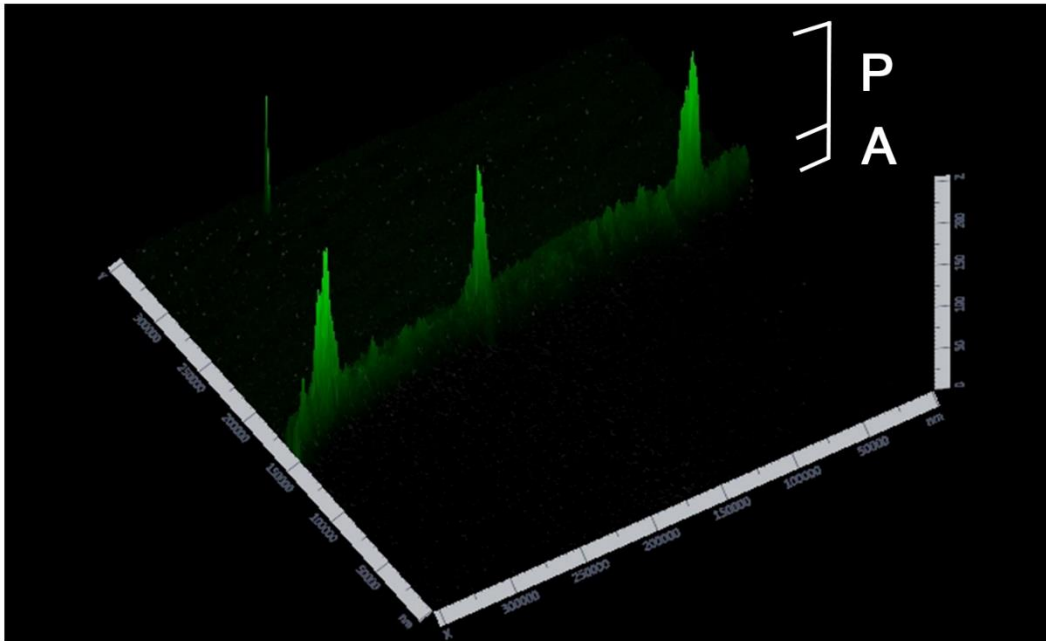


Figure 5.1: 2.5D view of the NHP cornea.

View depicts the stroma (faint signal at rear), the autofluorescence of the Descemet's membrane (A) and the GFP-positive peaks of cells in the corneal endothelial layer (P). Eyes in which $P > A$ were designated as GFP-positive.

6.16 Viral purity and estimations of titre.

12 μ l of AAV samples and 20 μ l of BSA serial dilutions were loaded onto an SDS-PAGE gel, as described in (422). The gel was run at 70V through the stacking gel and at 120V thereafter. The gel was washed twice in Coomassie prestaining solution (50% methanol, 10% acetic acid) for 5 minutes each wash. The gel was stained overnight in Coomassie blue stain. It was

destained the following day with a 40% methanol, 8% acetic acid solution for 4 hours. Subsequently, it was washed twice in dH₂O. Densitometry was performed on both standards and samples. The VP3 band of each virus was interpolated against the BSA standard curve. As described (422), the number of VP3 particles was calculated per AAV particle using the VP3 sequence and assumption of 50 VP3's per capsid. This gave the number of particles loaded per well, and when divided by loading volume, an estimation of viral titre was generated.

6.17 Total MMP-3 quantification

MMP-3 concentration was quantified using enzyme-linked immunosorbent assay (ELISA) kits for both human SC monolayers (DMP300, R&D Systems) and murine aqueous (RAB0368-1KT, Sigma) according to the manufacturer's protocol. SC monolayers were cultured and treated with a 1 in 10 dilution of human cataract and POAG AH, a method previously described (421). Media was taken from the monolayers 24 hours post treatment and assayed for total MMP-3.

To measure the secretion of MMP-3 by AAV-2/9 into the AH, animals were inoculated with virus as described previously via intracameral injection. 4 weeks post-injection, animals were sacrificed and AH was collected. This was achieved by the cannulation of the cornea with a pulled glass needle (1B100-6, WPI) and gentle pressing of the eye until it was deflated. Aqueous was expelled from the needle (approximately 5 µl) by the attachment of a 25ml syringe connected via barb fitting and tubing (Smiths Medical) and a gradual push of the syringe plunger. Aqueous was assayed using the previously mentioned ELISA kit.

ELISA kit reagents were brought to room temperature before use. A standard curve was generated and 100 µl of each standard and sample were placed into the wells of a pre-coated 96-well plate. Wells were covered and incubated for 2.5 hours at room temperature with gentle shaking. Wells were washed 4 times with 1X wash solution. After the final wash the plate was inverted against clean paper towels. 100 µl of 1X biotinylated detection antibody was added to

each well and incubated for 1 hour at room temperature with gentle shaking. The wash step was repeated and 100 μ l of HRP-streptavidin solution was added to each well. The plate was incubated for 45 minutes at room temperature with gentle shaking. The wash step was repeated. 100 μ l of colorimetric TMB reagent was added and incubated for 30 minutes in the dark. 50 μ l of stop solution was finally added to each well and the plate was read at 450 nm in a spectrophotometer. Mean absorbance minus blank was calculated for each well and samples were interpolated against the sigmoidal curve fitting the standards plotted as concentration vs absorbance.

6.18 MMP-3 Activity Assay (FRET)

Enzymatic activity of secreted MMP-3 was quantified using fluorescence resonance energy transfer (FRET). A fluorescent peptide consisting of a donor/acceptor pair remains quenched in its intact state. This peptide contains binding sites specific to MMP-3. Once cleavage occurs through MMP-3 mediated proteolysis, fluorescence is recovered by the transfer of energy from the donor to the acceptor, resulting in an increase in the acceptor's emission intensity. Cleavage of substrate, and therefore fluorescence, was monitored on a FLUOstar OPTIMA (BMG Labtech) over the course of 2.5 hours at 37°C, to allow ample time for substrate cleavage. Media samples were collected from treated SC monolayers and combined with a 1:100 dilution of an MMP-3 specific substrate (ab112148, Abcam). Levels of active MMP-3 were interpolated from a standard curve defined by ELISA. For murine aqueous MMP-3 activity, aqueous was retrieved four weeks post injection of AAV-MMP-3 or AAV-Null as described above. Aqueous samples were processed through an activity kit (abe3730, Source Bioscience), selected for its high sensitivity and specificity, according to the manufacturer's protocol.

Enzymatic activity was calculated as described in MMP-3 activity Assay Kit's (ab118972, Abcam) protocol:

$$\text{MMP-3 Activity (nmol/min/ml)} = \frac{B \times \text{Dilution Factor}}{(T_2 - T_1) \times V},$$

Where B is the level of MMP-3 interpolated from the standard curve, T1 is the time (min) of the initial reading, T2 is the time (min) of the second reading and V is the sample volume (ml) added to the reaction well. The units “nmol/min/ml” are equivalent to “mU/ml”.

6.19 Measurement of Outflow Facility

Animals were sacrificed for outflow facility measurement 4 weeks after injection of virus. Eyes were enucleated for *ex vivo* perfusion using the *iPerfusion*TM system as described in (137). Contralateral eyes were perfused simultaneously using two independent but identical *iPerfusion* systems. Each system comprises an automated pressure reservoir, a thermal flow sensor (SLG64-0075, Sensiron) and a wet-wet differential pressure transducer (PX409, Omegadyne), in order to apply a desired pressure, measure flow rate out of the system and measure the intraocular pressure respectively. Enucleated eyes were secured to a pedestal using a small amount of cyanoacrylate glue in a PBS bath regulated at 35°C. Perfusate was prepared (PBS including divalent cations and 5.5mM glucose) and filtered (0.2 µm, GVS Filter Technology) before use. Eyes were cannulated using a bevelled needle (NF33BV NanoFilTM, World Precision Instruments) with the aid of a stereomicroscope and micromanipulator (World Precision Instruments). Eyes were perfused for 30 minutes at a pressure of ~8 mmHg in order to acclimatise to the environment. Incrementing pressure steps were applied from 4.5 to 21 mmHg, while recording flow rate and pressure. Flow (Q) and pressure (P) were averaged over 4 minutes of steady data, and a power law model of the form

$$Q = C_r \left(\frac{P}{P_r} \right)^\beta P$$

was fit to the data using weighted power law regression, yielding values of C_r, the reference facility at reference pressure P_r = 8 mmHg (corresponding to the physiological pressure drop

across the outflow pathway), and β , a nonlinearity parameter characterising the pressure-dependent increase in facility observed in mouse eyes (137).

IOP

6.20 IOP method for Chapter 3

IOP measurements were performed by rebound tonometry (TonoLab, Icare) both prior to intracameral injection and 4 weeks post injection. Readings, which were the average IOP values after 5 tonometric events, were taken 10 minutes after the intra-peritoneal administration of mild general anaesthetic (53.28 mg/kg ketamine and 0.528 mg/kg domitor). Two readings were taken for one eye, then the other. This was repeated for a total of four readings per eye. Due to a minimum reading of 6 mmHg by the tonometer, a non-parametric approach was taken in the analysis of the readings. The median IOP was calculated for each eye, and MAD (median absolute deviation) values were used as a measure of dispersion. For comparing median values in a paired population, the Wilcoxon matched-pairs signed-rank test was employed to test for changes in IOP pre and post injection, and also for changes between contralateral eyes.

6.21 IOP method for Chapter 4

An improved method to measure IOP was devised for subsequent experiments. Many factors influence IOP, and these factors are often overlooked during tonometry. This is true for IOP measurements in Chapter 3 that may not be entirely reliable. A method was developed to best account for current limitations in IOP measurement. Such limitations include the effect of anaesthesia on IOP, IOP decay at the onset of anaesthesia, environmental stresses, body temperature, central corneal thickness, a minimum value of 6 mmHg readable by the Tonolab, and the inherent variation of tonometry itself. Temperature readings were monitored every day for a month leading up to, and for the duration of the experiment to ensure no major fluctuations

were observed. Animals were allowed to acclimatise for 3 weeks prior to experimentation. Animals were anaesthetised using 3% isoflurane in a chamber, and after 2 minutes were transferred to a head holder with inlets and outlets to the isoflurane vaporiser and scavenger. Tonometry measurements were taken every minute from minute 3 to minute 8, alternating between each eye every minute. Animals were measured in the OD eye first, but the first eye to be measured was alternated each week. Each tonometry measurement was the average of 5 individual readings, as determined by the Tonolab. A total of 3 measurements were taken at each minute timepoint. Values were imported to excel and all post-processing was performed through MATLAB. A Shapiro-Wilks test was implemented initially to test for normality, and a hampel filter was applied to exclude data drifting further than 4 median absolute deviations from the median (Figure 5.2). As the resulting distribution was non-normal, and to account for the non-parametric nature of the tonometer, central tendencies were determined by the median, and all statistical tests used were non-parametric tests. The median IOP for each time-point was calculated for each eye in all animals, and interpolated to 5 minutes.

To test whether IOP between MMP-3 and eGFP treatments were significantly different from each other, a Wilcoxon signed rank test was used to test paired median IOP changes over the course of the experiment, or on final IOP alone. To test whether either treatment resulted in a significant change from baseline IOP over the 6 weeks, a 1-sample Wilcoxon test was employed vs a hypothetical median IOP change of 0 mmHg. Unpaired comparisons between eGFP-treated eyes of the DEX and cyclodextrin control groups were made using a Wilcoxon rank sum test, to test the effect of DEX alone on IOP.

This new method allows for a much more robust and repeatable analysis of IOP in murine eyes, ensuring that influential variables are minimised and that the correct statistical tests are employed for the data. To reiterate, effects of anaesthesia are minimised by using isoflurane over ketamine, onset after anaesthesia is considered by interpolating each eye of each mouse to a timepoint of 5 minutes post-onset, temperature is monitored and a flask with warm water is

refilled periodically to retain the temperature, a heating pad was designed to further optimise this process but has not been implemented for this study yet, and unpaired analysis of a large sample size was used to account for the inherent variation of this procedure. The code generated to analyse IOP data is provided in Appendix 2.

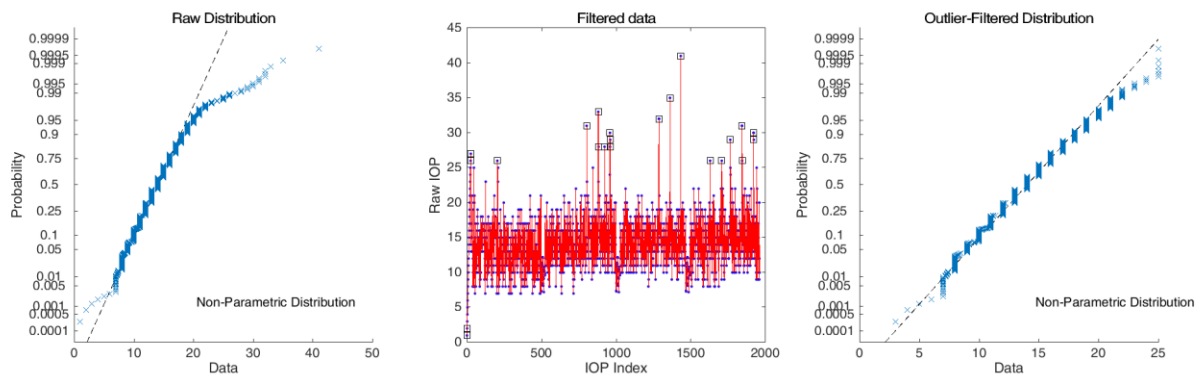


Figure 5.2: IOP distribution analysis

IOP data was collected and tested for normality using a Shapiro Wilks test and visualised on a probability plot (left). A hampel filter was applied to the data to remove obvious outliers, while retaining a conservative nature (middle). The resulting data was again tested for normality and found to still be non-parametric, determining the types of statistical tests for downstream analysis (right).

6.22 Analysis of central corneal thickness

Enucleated mouse eyes transduced with AAV-MMP-3 or its contralateral control, AAV-Null, were fixed overnight in 4% PFA and washed in PBS. Posterior segments were removed by dissection under the microscope and anterior segments were embedded in medium (Tissue-Tek OCT Compound). Serial sectioning was performed on each eye and five frozen sections (12 μ m) were transferred to a Polysine slide (Thermo Scientific) for staining with DAPI and mounted with aqua-polymount (Polyscience). Corneal sections were judged to be central by qualitatively taking the same distance from both iridocorneal angles. For quantitation, we

measured the corneal thickness of sections on five consecutive slides by light and confocal microscopy (Zeiss LSM 710). A total of 25 measurements were taken from each eye to represent mean central corneal thickness (μm) using NIH ImageJ software.

6.23 Transmission Electron Microscopy (TEM)

Ultrastructural investigation was performed by TEM in four pairs of treated mouse eyes. Four weeks after injection, the eyes were enucleated, and immersion fixed in Karnovsky's fixative (2.5% PFA, 0.1M cacodylate, 2.25% glutaraldehyde and dH_2O) for 1 hour. Eyes were then removed from fixative and the cornea pierced using a 30 gauge needle (BD Microlance 3, Becton Dickinson). Eyes were placed back into fixative overnight at 4°C , washed 3×10 min, stored in 0.1M cacodylate and sent to Erlangen.

Here the eyes were cut meridionally through the centre of the pupil, the lens carefully removed, and the two halves of each eye embedded in Epon. Semi-thin sagittal and then ultrathin sections of SC and TM were cut from one end of each half, and then the other approximately 0.2-0.3 mm deeper. The location of the superficial and deeper cut ends was alternated for the second half of the eye such that all 4 regions examined were at least 0.2 – 0.3 mm distant from one another. The ultrathin sections contained the entire anterior posterior length of the inner wall and the TM.

In 4 regions of each eye, the length of optically empty space immediately underlying the inner wall endothelium of SC was measured (Figure 5.3). The inner wall length in contact with ECM was also measured, including basement membrane material, elastic fibres, or amorphous material. The optically empty length divided by the total length (optically empty + ECM lengths) was calculated and defined as the percentage of optically empty length for that region. All measurements were performed at 10,000x magnification, with each region including approximately 100 individual lengths of ECM or optically empty space. The measurements

were performed blind by two independent examiners, Elke Lütjen-Drecoll and Cassandra Flügel-Koch.

For ultrathin sections, a pyramid is formed from each half of the eye. From one pyramid, around 15 ultrathin sections were obtained on 5 grids. For WT mice in Chapter 3 (Figure 3.12), another pyramid was generated. This gives 30 sections from each half, or 60 sections per eye. All sections were investigated however only 4 sections from each eye were used for quantification. With 4 mice, this gives 16 sections for each treatment group. The best sections (those free from folds or dirt) were used for quantification. From each ultrathin section, depending on the length of the SC, measurements of ECM material were taken from around 20 images at a magnification of 20,000X. This equates to 80 images per eye to account for the entire circumference of the SC, or 320 images per treatment group. For siRNA tight junction measurements, as in Appendix 6, there was twice this, i.e. 160 images per eye. For validation of intact tight junctions in response to MMP-3, approximately 20 images per eye were observed. For DEX-treated mice, the same amount of images were taken as wild-type mice.

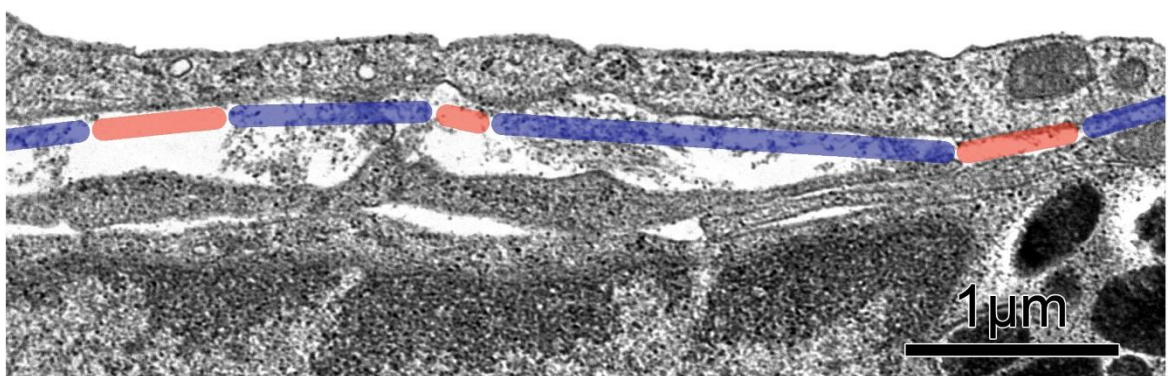


Figure 5.3: Morphometric analysis of the optically empty space underlying the inner wall endothelium of SC.

The anterior-posterior length of the inner wall was examined in 4 regions per eye at 10,000x magnification. Optically empty spaces (red zones) were identified, along with extracellular

matrix (ECM) where the inner wall cell contacted basement membrane material, elastic fibres or amorphous material (blue zones). The ratio of optically empty length to total length (optically empty + ECM length) was defined as the percentage optically open length, as shown in Figure 3.12G.

6.24 Osmotic Pump Implantation

For animals to be treated with dexamethasone, two weeks after intracameral inoculation of virus, animals were again put under anaesthesia, subcutaneously injected with 100ul Enrocare (antibiotic) and intramuscularly injected with 40ul Bupracare (painkiller). Animals were weighed the previous day and osmotic pumps were filled with reconstituted dexamethasone or cyclodextrin to account for a delivery of 2mg/kg/day and inserted subcutaneously into the lower back. This was achieved by an inch-long incision from the back of the neck downward. A blunt ended scissors was used to create a subcutaneous cavity where the pump was inserted. Care was taken to ensure that the pumps were as far from the incision site as possible. Skin was pinched together at the incision site and sealed using surgical glue. Mice were given Complian every second day to avoid weight loss. Mice were treated with dexamethasone for a total of 4 weeks, after which they were sacrificed for perfusions. Animals become dependent on the exogenous DEX at this time and would die as the pumps run out. Thus, this experimental timeframe (2 weeks after viral injection to see an increase in IOP, and 2 weeks after induction to see a reduction in IOP) was kept constant over all animal experiments. If a mouse lost greater than 20% of its body weight over the four weeks, or greater than 10% of its body weight in one week, it was euthanised for animal welfare reasons as this may have indicated a burst or leaky pump. As documented above, a total of 40 mice were implanted with osmotic mini pumps containing either dexamethasone or cyclodextrin.

6.25 Statistical Analysis

For TEER values, activity units (mU/ml) and concentrations (ng/ml), statistical differences were analysed by using unpaired two-tailed Student's *t*-tests. Differences in P_{app} values (cm/s) were determined by a one way ANOVA with Tukey's correction for multiple comparisons, where appropriate. ELISA standard curve concentrations were log-transformed and absorbance values were fitted to a sigmoidal dose response curve with variable slope for interpolation. Fold change of western blot data was log-transformed and investigated for significance using a one-sample *t*-test against a theoretical mean of 0. To measure MMP-3 concentration and activity in the AH of wild type (WT) mice, a paired two-tailed *t*-test was carried out for contralateral samples. Outflow facility was analysed using a weighted paired *t*-test performed in MATLAB as described in (137), incorporating both system and biological uncertainties. For IOP data, median values were obtained to reflect the non-parametric nature of the tonometer, and the Wilcoxon matched-pairs signed rank test was used to compare changes in paired populations. For morphology, the distribution of values representing the percent optically empty length was first examined using a Shapiro-Wilk and Anderson-Darling tests to detect for deviations from a normal distribution. The percent optically empty length between contralateral eyes was then analysed using a paired Student's *t*-test. Statistical significance was inferred when $P < 0.05$ in all experimentation. Results were depicted as 'mean, [95% Confidence Intervals]' unless otherwise stated in the results section.

References

- 1 Purves, D. (2004) *Neuroscience*. Sinauer Associates, Sunderland, Massachusetts U.S.A.
- 2 Goel, M., Picciani, R.G., Lee, R.K. and Bhattacharya, S.K. (2010) Aqueous humor dynamics: a review. *Open Ophthalmol J*, **4**, 52-59.
- 3 Alm, A. and Nilsson, S.F. (2009) Uveoscleral outflow--a review. *Exp Eye Res*, **88**, 760-768.
- 4 Stamer, W.D. (2012) The cell and molecular biology of glaucoma: mechanisms in the conventional outflow pathway. *Invest Ophthalmol Vis Sci*, **53**, 2470-2472.
- 5 Bill, A. and Svedbergh, B. (1972) Scanning electron microscopic studies of the trabecular meshwork and the canal of Schlemm--an attempt to localize the main resistance to outflow of aqueous humor in man. *Acta Ophthalmol (Copenh)*, **50**, 295-320.
- 6 Inomata, H., Bill, A. and Smelser, G.K. (1972) Aqueous humor pathways through the trabecular meshwork and into Schlemm's canal in the cynomolgus monkey (*Macaca irus*). An electron microscopic study. *Am J Ophthalmol*, **73**, 760-789.
- 7 Johnstone, M.A. and Grant, W.G. (1973) Pressure-dependent changes in structures of the aqueous outflow system of human and monkey eyes. *Am J Ophthalmol*, **75**, 365-383.
- 8 Johnson, M., McLaren, J.W. and Overby, D.R. (2017) Unconventional aqueous humor outflow: A review. *Exp Eye Res*, **158**, 94-111.
- 9 Kass, M.A., Hart, W.M., Jr., Gordon, M. and Miller, J.P. (1980) Risk factors favoring the development of glaucomatous visual field loss in ocular hypertension. *Surv Ophthalmol*, **25**, 155-162.
- 10 O'Callaghan, J., Cassidy, P.S. and Humphries, P. (2017) Open-angle glaucoma: therapeutically targeting the extracellular matrix of the conventional outflow pathway. *Expert Opinion on Therapeutic Targets*, **21**, 1037-1050.

- 11 Lawrence M. Levine, V.S.B., Michael H. Goldstein, Alon Kahana, William R. Katowitz, Simon K. Law, David A. Mackey, . (2015). Eurpoean Board of Ophthalmology, Vol. 2.
- 12 Civan, M.M. and Macknight, A.D. (2004) The ins and outs of aqueous humour secretion. *Exp Eye Res*, **78**, 625-631.
- 13 Mark, H.H. (2010) Aqueous humor dynamics in historical perspective. *Surv Ophthalmol*, **55**, 89-100.
- 14 Coca-Prados, M. (2014) The blood-aqueous barrier in health and disease. *J Glaucoma*, **23**, S36-38.
- 15 Maren, T.H. (1976) The rates of movement of Na⁺, Cl⁻, and HCO⁻³ from plasma to posterior chamber: effect of acetazolamide and relation to the treatment of glaucoma. *Invest Ophthalmol*, **15**, 356-364.
- 16 Lutjen-Drecoll, E., Futa, R. and Rohen, J.W. (1981) Ultrahistochemical studies on tangential sections of the trabecular meshwork in normal and glaucomatous eyes. *Invest Ophthalmol Vis Sci*, **21**, 563-573.
- 17 Abu-Hassan, D.W., Acott, T.S. and Kelley, M.J. (2014) The Trabecular Meshwork: A Basic Review of Form and Function. *Journal of Ocular Biology*, **2**.
- 18 Overby, D.R., Stamer, W.D. and Johnson, M. (2009) The changing paradigm of outflow resistance generation: towards synergistic models of the JCT and inner wall endothelium. *Exp Eye Res*, **88**, 656-670.
- 19 Grant, W.M. (1963) Experimental aqueous perfusion in enucleated human eyes. *Arch Ophthalmol*, **69**, 783-801.
- 20 Keller, K.E. and Acott, T.S. (2013) The Juxtacanalicular Region of Ocular Trabecular Meshwork: A Tissue with a Unique Extracellular Matrix and Specialized Function. *Journal of Ocular Biology, Diseases, and Informatics*, **1**, 3.

- 21 Fuchshofer, R., Welge-Lussen, U., Lutjen-Drecoll, E. and Birke, M. (2006) Biochemical and morphological analysis of basement membrane component expression in corneoscleral and cribriform human trabecular meshwork cells. *Invest Ophthalmol Vis Sci*, **47**, 794-801.
- 22 Tamm, E.R. (2009) The trabecular meshwork outflow pathways: structural and functional aspects. *Exp Eye Res*, **88**, 648-655.
- 23 Kizhatil, K., Ryan, M., Marchant, J.K., Henrich, S. and John, S.W. (2014) Schlemm's canal is a unique vessel with a combination of blood vascular and lymphatic phenotypes that forms by a novel developmental process. *PLoS Biol*, **12**, e1001912.
- 24 Tam, L.C., Reina-Torres, E., Sherwood, J.M., Cassidy, P.S., Crosbie, D.E., Lutjen-Drecoll, E., Flugel-Koch, C., Perkumas, K., Humphries, M.M., Kiang, A.S. *et al.* (2017) Enhancement of Outflow Facility in the Murine Eye by Targeting Selected Tight-Junctions of Schlemm's Canal Endothelia. *Sci Rep*, **7**, 40717.
- 25 Aspelund, A., Tammela, T., Antila, S., Nurmi, H., Leppanen, V.M., Zarkada, G., Stanczuk, L., Francois, M., Makinen, T., Saharinen, P. *et al.* (2014) The Schlemm's canal is a VEGF-C/VEGFR-3-responsive lymphatic-like vessel. *J Clin Invest*, **124**, 3975-3986.
- 26 Johnson, M. (2006) 'What controls aqueous humour outflow resistance?'. *Exp Eye Res*, **82**, 545-557.
- 27 Ethier, C.R., Coloma, F.M., Sit, A.J. and Johnson, M. (1998) Two pore types in the inner-wall endothelium of Schlemm's canal. *Invest Ophthalmol Vis Sci*, **39**, 2041-2048.
- 28 Grierson, I. and Lee, W.R. (1977) Light microscopic quantitation of the endothelial vacuoles in Schlemm's canal. *Am J Ophthalmol*, **84**, 234-246.
- 29 Overby, D., Gong, H., Qiu, G., Freddo, T.F. and Johnson, M. (2002) The mechanism of increasing outflow facility during washout in the bovine eye. *Invest Ophthalmol Vis Sci*, **43**, 3455-3464.

- 30 MacRae, D. and Sears, M.L. (1970) Peroxidase passage through the outflow channels of human and rhesus eyes. *Exp Eye Res*, **10**, 15-18.
- 31 de Kater, A.W., Melamed, S. and Epstein, D.L. (1989) Patterns of aqueous humor outflow in glaucomatous and nonglaucomatous human eyes. A tracer study using cationized ferritin. *Arch Ophthalmol*, **107**, 572-576.
- 32 Battista, S.A., Lu, Z., Hofmann, S., Freddo, T., Overby, D.R. and Gong, H. (2008) Reduction of the available area for aqueous humor outflow and increase in meshwork herniations into collector channels following acute IOP elevation in bovine eyes. *Invest Ophthalmol Vis Sci*, **49**, 5346-5352.
- 33 Lu, Z., Overby, D.R., Scott, P.A., Freddo, T.F. and Gong, H. (2008) The mechanism of increasing outflow facility by rho-kinase inhibition with Y-27632 in bovine eyes. *Exp Eye Res*, **86**, 271-281.
- 34 Yan, X., Li, M., Chen, Z., Zhu, Y., Song, Y. and Zhang, H. (2016) Schlemm's Canal and Trabecular Meshwork in Eyes with Primary Open Angle Glaucoma: A Comparative Study Using High-Frequency Ultrasound Biomicroscopy. *PLoS One*, **11**, e0145824.
- 35 Johnstone, M.A., Jamil, A., Martin, E. (2010) *Aqueous veins and open angle glaucoma*. Springer New York, New York.
- 36 Jabłońska, J., Lewczuk, K., and Rękas, M. (2016) Ichhpujani, D.P. (ed.), In *Glaucoma - Intraocular Pressure and Aqueous Dynamics*. InTech, InTech, in press.
- 37 Johnstone, M.A. (2004) The aqueous outflow system as a mechanical pump: evidence from examination of tissue and aqueous movement in human and non-human primates. *J Glaucoma*, **13**, 421-438.
- 38 Johnson, M.C. and Kamm, R.D. (1983) The role of Schlemm's canal in aqueous outflow from the human eye. *Invest Ophthalmol Vis Sci*, **24**, 320-325.

- 39 Rosenquist, R., Epstein, D., Melamed, S., Johnson, M. and Grant, W.M. (1989) Outflow resistance of enucleated human eyes at two different perfusion pressures and different extents of trabeculotomy. *Curr Eye Res*, **8**, 1233-1240.
- 40 Wise, J.B. and Witter, S.L. (1979) Argon laser therapy for open-angle glaucoma. A pilot study. *Arch Ophthalmol*, **97**, 319-322.
- 41 Swaminathan, S.S., Oh, D.J., Kang, M.H. and Rhee, D.J. (2014) Aqueous outflow: segmental and distal flow. *J Cataract Refract Surg*, **40**, 1263-1272.
- 42 Sit, A.J. and McLaren, J.W. (2011) Measurement of episcleral venous pressure. *Exp Eye Res*, **93**, 291-298.
- 43 Roy Chowdhury, U., Rinkoski, T.A., Bahler, C.K., Millar, J.C., Bertrand, J.A., Holman, B.H., Sherwood, J.M., Overby, D.R., Stoltz, K.L., Dosa, P.I. *et al.* (2017) Effect of Cromakalim Prodrug 1 (CKLP1) on Aqueous Humor Dynamics and Feasibility of Combination Therapy With Existing Ocular Hypotensive Agents. *Invest Ophthalmol Vis Sci*, **58**, 5731-5742.
- 44 Bill, A. (1975) Blood circulation and fluid dynamics in the eye. *Physiol Rev*, **55**, 383-417.
- 45 Lanza, M., Iaccarino, S., Mele, L., Carnevale, U.A., Irregolare, C., Lanza, A., Femiano, F. and Bifani, M. (2016) Intraocular pressure evaluation in healthy eyes and diseased ones using contact and non contact devices. *Contact Lens and Anterior Eye*, **39**, 154-159.
- 46 Siah, W.F., Loughman, J. and O'Brien, C. (2015) Lower Macular Pigment Optical Density in Foveal-Involved Glaucoma. *Ophthalmology*, **122**, 2029-2037.
- 47 Weinreb, R.N., Aung, T. and Medeiros, F.A. (2014) The pathophysiology and treatment of glaucoma: a review. *JAMA*, **311**, 1901-1911.
- 48 Fechtner, R.D. and Weinreb, R.N. (1994) Mechanisms of optic nerve damage in primary open angle glaucoma. *Surv Ophthalmol*, **39**, 23-42.
- 49 Weinreb, R.N. and Khaw, P.T. (2004) Primary open-angle glaucoma. *Lancet*, **363**, 1711-1720.

- 50 Medeiros, F.A., Alencar, L.M., Zangwill, L.M., Bowd, C., Sample, P.A. and Weinreb, R.N. (2009) Prediction of functional loss in glaucoma from progressive optic disc damage. *Arch Ophthalmol*, **127**, 1250-1256.
- 51 Medeiros, F.A., Zangwill, L.M., Bowd, C. and Weinreb, R.N. (2004) Comparison of the GDx VCC scanning laser polarimeter, HRT II confocal scanning laser ophthalmoscope, and stratus OCT optical coherence tomograph for the detection of glaucoma. *Arch Ophthalmol*, **122**, 827-837.
- 52 Quigley, H.A. and Broman, A.T. (2006) The number of people with glaucoma worldwide in 2010 and 2020. *Br J Ophthalmol*, **90**, 262-267.
- 53 Stamer, W.D. and Acott, T.S. (2012) Current understanding of conventional outflow dysfunction in glaucoma. *Curr Opin Ophthalmol*, **23**, 135-143.
- 54 Wang, N., Wu, H. and Fan, Z. (2002) Primary angle closure glaucoma in Chinese and Western populations. *Chin Med J (Engl)*, **115**, 1706-1715.
- 55 Grant, W.M. (1951) Clinical measurements of aqueous outflow. *Am J Ophthalmol*, **34**, 1603-1605.
- 56 Beidoe, G. and Mousa, S.A. (2012) Current primary open-angle glaucoma treatments and future directions. *Clin Ophthalmol*, **6**, 1699-1707.
- 57 Lee, R.K. (2008) The molecular pathophysiology of pseudoexfoliation glaucoma. *Curr Opin Ophthalmol*, **19**, 95-101.
- 58 Michelessi, M. and Lindsley, K. (2016) Peripheral iridotomy for pigmentary glaucoma. *The Cochrane Database of Systematic Reviews*, **2**, CD005655.
- 59 Tham, Y.C., Li, X., Wong, T.Y., Quigley, H.A., Aung, T. and Cheng, C.Y. (2014) Global prevalence of glaucoma and projections of glaucoma burden through 2040: a systematic review and meta-analysis. *Ophthalmology*, **121**, 2081-2090.
- 60 Quigley, H.A. (1996) Number of people with glaucoma worldwide. *Br J Ophthalmol*, **80**, 389-393.

- 61 Sommer, A., Tielsch, J.M., Katz, J., Quigley, H.A., Gottsch, J.D., Javitt, J. and Singh, K. (1991) Relationship between intraocular pressure and primary open angle glaucoma among white and black Americans. The Baltimore Eye Survey. *Arch Ophthalmol*, **109**, 1090-1095.
- 62 Actis, A.G., Versino, E., Brogliatti, B. and Rolle, T. (2016) Risk Factors for Primary Open Angle Glaucoma (POAG) Progression: A Study Ruled in Torino. *The Open Ophthalmology Journal*, **10**, 129-139.
- 63 McMonnies, C.W. (2017) Glaucoma history and risk factors. *J Optom*, **10**, 71-78.
- 64 Havens, S.J. and Gulati, V. (2016) Neovascular Glaucoma. *Dev Ophthalmol*, **55**, 196-204.
- 65 Perez-de-Arcelus, M., Toledo, E., Martinez-Gonzalez, M.A., Martin-Calvo, N., Fernandez-Montero, A. and Moreno-Montanes, J. (2017) Smoking and incidence of glaucoma: The SUN Cohort. *Medicine (Baltimore)*, **96**, e5761.
- 66 Brightfocus. (2018), In *Understanding your disease*, Vol. 2018.
- 67 Gupta, N. and Yucel, Y.H. (2007) Glaucoma as a neurodegenerative disease. *Curr Opin Ophthalmol*, **18**, 110-114.
- 68 Corredor, R.G. and Goldberg, J.L. (2009) Electrical activity enhances neuronal survival and regeneration. *J Neural Eng*, **6**, 055001.
- 69 Chang, E.E. and Goldberg, J.L. (2012) Glaucoma 2.0: neuroprotection, neuroregeneration, neuroenhancement. *Ophthalmology*, **119**, 979-986.
- 70 Moore, D.L., Blackmore, M.G., Hu, Y., Kaestner, K.H., Bixby, J.L., Lemmon, V.P. and Goldberg, J.L. (2009) KLF family members regulate intrinsic axon regeneration ability. *Science*, **326**, 298-301.
- 71 Park, K.K., Liu, K., Hu, Y., Smith, P.D., Wang, C., Cai, B., Xu, B., Connolly, L., Kramvis, I., Sahin, M. *et al.* (2008) Promoting axon regeneration in the adult CNS by modulation of the PTEN/mTOR pathway. *Science*, **322**, 963-966.

- 72 Rejdak, R., Toczolowski, J., Kurkowski, J., Kaminski, M.L., Rejdak, K., Stelmasiak, Z. and Grieb, P. (2003) Oral citicoline treatment improves visual pathway function in glaucoma. *Med Sci Monit*, **9**, PI24-28.
- 73 Ban, N., Siegfried, C.J. and Apte, R.S. (2018) Monitoring Neurodegeneration in Glaucoma: Therapeutic Implications. *Trends Mol Med*, **24**, 7-17.
- 74 Inman, D.M. and Harun-Or-Rashid, M. (2017) Metabolic Vulnerability in the Neurodegenerative Disease Glaucoma. *Front Neurosci*, **11**, 146.
- 75 Campbell, P.D., Shen, K., Sapio, M.R., Glenn, T.D., Talbot, W.S. and Marlow, F.L. (2014) Unique function of Kinesin Kif5A in localization of mitochondria in axons. *J Neurosci*, **34**, 14717-14732.
- 76 Rawson, R.L., Yam, L., Weimer, R.M., Bend, E.G., Hartweg, E., Horvitz, H.R., Clark, S.G. and Jorgensen, E.M. (2014) Axons degenerate in the absence of mitochondria in *C. elegans*. *Curr Biol*, **24**, 760-765.
- 77 Lee, S., Van Bergen, N.J., Kong, G.Y., Chrysostomou, V., Waugh, H.S., O'Neill, E.C., Crowston, J.G. and Trounce, I.A. (2011) Mitochondrial dysfunction in glaucoma and emerging bioenergetic therapies. *Exp Eye Res*, **93**, 204-212.
- 78 Abu-Amero, K., Kondkar, A.A. and Chalam, K.V. (2015) An Updated Review on the Genetics of Primary Open Angle Glaucoma. *Int J Mol Sci*, **16**, 28886-28911.
- 79 Burdon, K.P., Macgregor, S., Hewitt, A.W., Sharma, S., Chidlow, G., Mills, R.A., Danoy, P., Casson, R., Viswanathan, A.C., Liu, J.Z. *et al.* (2011) Genome-wide association study identifies susceptibility loci for open angle glaucoma at TMCO1 and CDKN2B-AS1. *Nat Genet*, **43**, 574-578.
- 80 Li, Z., Allingham, R.R., Nakano, M., Jia, L., Chen, Y., Ikeda, Y., Mani, B., Chen, L.J., Kee, C., Garway-Heath, D.F. *et al.* (2015) A common variant near TGFBR3 is associated with primary open angle glaucoma. *Hum Mol Genet*, **24**, 3880-3892.

- 81 Thorleifsson, G., Walters, G.B., Hewitt, A.W., Masson, G., Helgason, A., DeWan, A., Sigurdsson, A., Jonasdottir, A., Gudjonsson, S.A., Magnusson, K.P. *et al.* (2010) Common variants near CAV1 and CAV2 are associated with primary open-angle glaucoma. *Nat Genet*, **42**, 906-909.
- 82 van Koolwijk, L.M., Ramdas, W.D., Ikram, M.K., Jansonius, N.M., Pasutto, F., Hysi, P.G., Macgregor, S., Janssen, S.F., Hewitt, A.W., Viswanathan, A.C. *et al.* (2012) Common genetic determinants of intraocular pressure and primary open-angle glaucoma. *PLoS Genet*, **8**, e1002611.
- 83 Wiggs, J.L., Yaspan, B.L., Hauser, M.A., Kang, J.H., Allingham, R.R., Olson, L.M., Abdrabou, W., Fan, B.J., Wang, D.Y., Brodeur, W. *et al.* (2012) Common variants at 9p21 and 8q22 are associated with increased susceptibility to optic nerve degeneration in glaucoma. *PLoS Genet*, **8**, e1002654.
- 84 Hardy, K.M., Hoffman, E.A., Gonzalez, P., McKay, B.S. and Stamer, W.D. (2005) Extracellular trafficking of myocilin in human trabecular meshwork cells. *J Biol Chem*, **280**, 28917-28926.
- 85 Hoffman, E.A., Perkumas, K.M., Highstrom, L.M. and Stamer, W.D. (2009) Regulation of myocilin-associated exosome release from human trabecular meshwork cells. *Invest Ophthalmol Vis Sci*, **50**, 1313-1318.
- 86 Peters, D.M., Herbert, K., Biddick, B. and Peterson, J.A. (2005) Myocilin binding to Hep II domain of fibronectin inhibits cell spreading and incorporation of paxillin into focal adhesions. *Exp Cell Res*, **303**, 218-228.
- 87 Ueda, J., Wentz-Hunter, K. and Yue, B.Y. (2002) Distribution of myocilin and extracellular matrix components in the juxtacanalicular tissue of human eyes. *Invest Ophthalmol Vis Sci*, **43**, 1068-1076.
- 88 Jacobson, N., Andrews, M., Shepard, A.R., Nishimura, D., Searby, C., Fingert, J.H., Hageman, G., Mullins, R., Davidson, B.L., Kwon, Y.H. *et al.* (2001) Non-secretion of mutant

proteins of the glaucoma gene myocilin in cultured trabecular meshwork cells and in aqueous humor. *Hum Mol Genet*, **10**, 117-125.

89 Kasetti, R.B., Phan, T.N., Millar, J.C. and Zode, G.S. (2016) Expression of Mutant Myocilin Induces Abnormal Intracellular Accumulation of Selected Extracellular Matrix Proteins in the Trabecular Meshwork. *Invest Ophthalmol Vis Sci*, **57**, 6058-6069.

90 Zode, G.S., Kuehn, M.H., Nishimura, D.Y., Searby, C.C., Mohan, K., Grozdanic, S.D., Bugge, K., Anderson, M.G., Clark, A.F., Stone, E.M. *et al.* (2011) Reduction of ER stress via a chemical chaperone prevents disease phenotypes in a mouse model of primary open angle glaucoma. *J Clin Invest*, **121**, 3542-3553.

91 Rezaie, T., Child, A., Hitchings, R., Brice, G., Miller, L., Coca-Prados, M., Heon, E., Krupin, T., Ritch, R., Kreutzer, D. *et al.* (2002) Adult-onset primary open-angle glaucoma caused by mutations in optineurin. *Science*, **295**, 1077-1079.

92 De Marco, N., Buono, M., Troise, F. and Diez-Roux, G. (2006) Optineurin increases cell survival and translocates to the nucleus in a Rab8-dependent manner upon an apoptotic stimulus. *J Biol Chem*, **281**, 16147-16156.

93 Gemenetzi, M., Yang, Y. and Lotery, A.J. (2012) Current concepts on primary open-angle glaucoma genetics: a contribution to disease pathophysiology and future treatment. *Eye (Lond)*, **26**, 355-369.

94 Beeldman, E., van der Kooi, A.J., de Visser, M., van Maarle, M.C., van Ruissen, F. and Baas, F. (2015) A Dutch family with autosomal recessively inherited lower motor neuron predominant motor neuron disease due to optineurin mutations. *Amyotroph Lateral Scler Frontotemporal Degener*, **16**, 410-411.

95 Fuse, N., Takahashi, K., Akiyama, H., Nakazawa, T., Seimiya, M., Kuwahara, S. and Tamai, M. (2004) Molecular genetic analysis of optineurin gene for primary open-angle and normal tension glaucoma in the Japanese population. *J Glaucoma*, **13**, 299-303.

- 96 Shim, M.S., Takihara, Y., Kim, K.Y., Iwata, T., Yue, B.Y., Inatani, M., Weinreb, R.N., Perkins, G.A. and Ju, W.K. (2016) Mitochondrial pathogenic mechanism and degradation in optineurin E50K mutation-mediated retinal ganglion cell degeneration. *Sci Rep*, **6**, 33830.
- 97 Fingert, J.H. (2011) Primary open-angle glaucoma genes. *Eye (Lond)*, **25**, 587-595.
- 98 Tourkina, E., Gooz, P., Pannu, J., Bonner, M., Scholz, D., Hacker, S., Silver, R.M., Trojanowska, M. and Hoffman, S. (2005) Opposing effects of protein kinase Calpha and protein kinase Cepsilon on collagen expression by human lung fibroblasts are mediated via MEK/ERK and caveolin-1 signaling. *J Biol Chem*, **280**, 13879-13887.
- 99 Del Galdo, F., Lisanti, M.P. and Jimenez, S.A. (2008) Caveolin-1, transforming growth factor-beta receptor internalization, and the pathogenesis of systemic sclerosis. *Curr Opin Rheumatol*, **20**, 713-719.
- 100 Thompson, C., Rahim, S., Arnold, J. and Hielscher, A. (2017) Loss of caveolin-1 alters extracellular matrix protein expression and ductal architecture in murine mammary glands. *PLoS One*, **12**, e0172067.
- 101 Surgucheva, I. and Surguchov, A. (2011) Expression of caveolin in trabecular meshwork cells and its possible implication in pathogenesis of primary open angle glaucoma. *Mol Vis*, **17**, 2878-2888.
- 102 Razani, B., Zhang, X.L., Bitzer, M., von Gersdorff, G., Bottinger, E.P. and Lisanti, M.P. (2001) Caveolin-1 regulates transforming growth factor (TGF)-beta/SMAD signaling through an interaction with the TGF-beta type I receptor. *J Biol Chem*, **276**, 6727-6738.
- 103 Elliott, M.H., Ashpole, N.E., Gu, X., Herrnberger, L., McClellan, M.E., Griffith, G.L., Reagan, A.M., Boyce, T.M., Tanito, M., Tamm, E.R. *et al.* (2016) Caveolin-1 modulates intraocular pressure: implications for caveolae mechanoprotection in glaucoma. *Sci Rep*, **6**, 37127.

- 104 Ozel, A.B., Moroi, S.E., Reed, D.M., Nika, M., Schmidt, C.M., Akbari, S., Scott, K., Rozsa, F., Pawar, H., Musch, D.C. *et al.* (2014) Genome-wide association study and meta-analysis of intraocular pressure. *Hum Genet*, **133**, 41-57.
- 105 Hysi, P.G., Cheng, C.Y., Springelkamp, H., Macgregor, S., Bailey, J.N.C., Wojciechowski, R., Vitart, V., Nag, A., Hewitt, A.W., Hohn, R. *et al.* (2014) Genome-wide analysis of multi-ancestry cohorts identifies new loci influencing intraocular pressure and susceptibility to glaucoma. *Nat Genet*, **46**, 1126-1130.
- 106 Wang, Q.C., Zheng, Q., Tan, H., Zhang, B., Li, X., Yang, Y., Yu, J., Liu, Y., Chai, H., Wang, X. *et al.* (2016) TMCO1 Is an ER Ca(2+) Load-Activated Ca(2+) Channel. *Cell*, **165**, 1454-1466.
- 107 Chintalapudi, S.R., Maria, D., Di Wang, X., Bailey, J.N.C., consortium, N., International Glaucoma Genetics, c., Hysi, P.G., Wiggs, J.L., Williams, R.W. and Jablonski, M.M. (2017) Systems genetics identifies a role for *Cacna2d1* regulation in elevated intraocular pressure and glaucoma susceptibility. *Nat Commun*, **8**, 1755.
- 108 Lu, Y., Vitart, V., Burdon, K.P., Khor, C.C., Bykhovskaya, Y., Mirshahi, A., Hewitt, A.W., Koehn, D., Hysi, P.G., Ramdas, W.D. *et al.* (2013) Genome-wide association analyses identify multiple loci associated with central corneal thickness and keratoconus. *Nat Genet*, **45**, 155-163.
- 109 Springelkamp, H., Hohn, R., Mishra, A., Hysi, P.G., Khor, C.C., Loomis, S.J., Bailey, J.N., Gibson, J., Thorleifsson, G., Janssen, S.F. *et al.* (2014) Meta-analysis of genome-wide association studies identifies novel loci that influence cupping and the glaucomatous process. *Nat Commun*, **5**, 4883.
- 110 Iglesias, A.I., Springelkamp, H., Ramdas, W.D., Klaver, C.C., Willemsen, R. and van Duijn, C.M. (2015) Genes, pathways, and animal models in primary open-angle glaucoma. *Eye (Lond)*, **29**, 1285-1298.

- 111 Kloeckener-Gruissem, B., Bartholdi, D., Abdou, M.T., Zimmermann, D.R. and Berger, W. (2006) Identification of the genetic defect in the original Wagner syndrome family. *Mol Vis*, **12**, 350-355.
- 112 Keller, K.E., Bradley, J.M., Vranka, J.A. and Acott, T.S. (2011) Segmental versican expression in the trabecular meshwork and involvement in outflow facility. *Invest Ophthalmol Vis Sci*, **52**, 5049-5057.
- 113 Jelodari-Mamaghani, S., Haji-Seyed-Javadi, R., Suri, F., Nilforushan, N., Yazdani, S., Kamyab, K. and Elahi, E. (2013) Contribution of the latent transforming growth factor-beta binding protein 2 gene to etiology of primary open angle glaucoma and pseudoexfoliation syndrome. *Mol Vis*, **19**, 333-347.
- 114 Kuchtey, J., Chang, T.C., Panagis, L. and Kuchtey, R.W. (2013) Marfan syndrome caused by a novel FBN1 mutation with associated pigmentary glaucoma. *Am J Med Genet A*, **161A**, 880-883.
- 115 Kuchtey, J. and Kuchtey, R.W. (2014) The microfibril hypothesis of glaucoma: implications for treatment of elevated intraocular pressure. *J Ocul Pharmacol Ther*, **30**, 170-180.
- 116 Morales, J., Al-Sharif, L., Khalil, D.S., Shinwari, J.M., Bavi, P., Al-Mahrouqi, R.A., Al-Rajhi, A., Alkuraya, F.S., Meyer, B.F. and Al Tassan, N. (2009) Homozygous mutations in ADAMTS10 and ADAMTS17 cause lenticular myopia, ectopia lentis, glaucoma, spherophakia, and short stature. *Am J Hum Genet*, **85**, 558-568.
- 117 Vranka, J.A., Kelley, M.J., Acott, T.S. and Keller, K.E. (2015) Extracellular matrix in the trabecular meshwork: intraocular pressure regulation and dysregulation in glaucoma. *Exp Eye Res*, **133**, 112-125.
- 118 VanderWyst, S.S., Perkumas, K.M., Read, A.T., Overby, D.R. and Stamer, W.D. (2011) Structural basement membrane components and corresponding integrins in Schlemm's canal endothelia. *Mol Vis*, **17**, 199-209.

- 119 Faralli, J.A., Schwinn, M.K., Gonzalez, J.M., Jr., Filla, M.S. and Peters, D.M. (2009) Functional properties of fibronectin in the trabecular meshwork. *Exp Eye Res*, **88**, 689-693.
- 120 Rohen, J.W., Futa, R. and Lutjen-Drecoll, E. (1981) The fine structure of the cribriform meshwork in normal and glaucomatous eyes as seen in tangential sections. *Invest Ophthalmol Vis Sci*, **21**, 574-585.
- 121 Burridge, K., Fath, K., Kelly, T., Nuckolls, G. and Turner, C. (1988) Focal adhesions: transmembrane junctions between the extracellular matrix and the cytoskeleton. *Annu Rev Cell Biol*, **4**, 487-525.
- 122 Cheng, Y.F. and Kramer, R.H. (1989) Human microvascular endothelial cells express integrin-related complexes that mediate adhesion to the extracellular matrix. *J Cell Physiol*, **139**, 275-286.
- 123 Lampugnani, M.G., Resnati, M., Dejana, E. and Marchisio, P.C. (1991) The role of integrins in the maintenance of endothelial monolayer integrity. *J Cell Biol*, **112**, 479-490.
- 124 Geiger, B., Bershadsky, A., Pankov, R. and Yamada, K.M. (2001) Transmembrane crosstalk between the extracellular matrix--cytoskeleton crosstalk. *Nat Rev Mol Cell Biol*, **2**, 793-805.
- 125 Han, H., Wecker, T., Grehn, F. and Schlunck, G. (2011) Elasticity-dependent modulation of TGF-beta responses in human trabecular meshwork cells. *Invest Ophthalmol Vis Sci*, **52**, 2889-2896.
- 126 Wallace, D.M., Murphy-Ullrich, J.E., Downs, J.C. and O'Brien, C.J. (2014) The role of matricellular proteins in glaucoma. *Matrix Biol*, **37**, 174-182.
- 127 Mutsaers, S.E., Bishop, J.E., McGrouther, G. and Laurent, G.J. (1997) Mechanisms of tissue repair: from wound healing to fibrosis. *Int J Biochem Cell Biol*, **29**, 5-17.
- 128 Wight, T.N. and Potter-Perigo, S. (2011) The extracellular matrix: an active or passive player in fibrosis? *Am J Physiol Gastrointest Liver Physiol*, **301**, G950-955.

- 129 Tektas, O.Y. and Lutjen-Drecoll, E. (2009) Structural changes of the trabecular meshwork in different kinds of glaucoma. *Exp Eye Res*, **88**, 769-775.
- 130 Tanihara, H., Inatani, M., Koga, T., Yano, T. and Kimura, A. (2002) Proteoglycans in the eye. *Cornea*, **21**, 62-69.
- 131 Floyd, B.B., Cleveland, P.H. and Worthen, D.M. (1985) Fibronectin in human trabecular drainage channels. *Invest Ophthalmol Vis Sci*, **26**, 797-804.
- 132 Swaminathan, S.S., Oh, D.J., Kang, M.H., Ren, R., Jin, R., Gong, H. and Rhee, D.J. (2013) Secreted protein acidic and rich in cysteine (SPARC)-null mice exhibit more uniform outflow. *Invest Ophthalmol Vis Sci*, **54**, 2035-2047.
- 133 Keller, K.E., Bradley, J.M., Kelley, M.J. and Acott, T.S. (2008) Effects of modifiers of glycosaminoglycan biosynthesis on outflow facility in perfusion culture. *Invest Ophthalmol Vis Sci*, **49**, 2495-2505.
- 134 Gong, H., Freddo, T.F. and Johnson, M. (1992) Age-related changes of sulfated proteoglycans in the normal human trabecular meshwork. *Exp Eye Res*, **55**, 691-709.
- 135 Berggren, L. and Vrabec, F. (1957) Demonstration of a coating substance in the trabecular meshwork of the eye and its decrease after perfusion experiments with different kinds of hyaluronidase. *Am J Ophthalmol*, **44**, 200-208.
- 136 Francois, J. (1977) Corticosteroid glaucoma. *Ann Ophthalmol*, **9**, 1075-1080.
- 137 Sherwood, J.M., Reina-Torres, E., Bertrand, J.A., Rowe, B. and Overby, D.R. (2016) Measurement of Outflow Facility Using iPerfusion. *PLoS One*, **11**, e0150694.
- 138 Vranka, J.A. and Acott, T.S. (2017) Pressure-induced expression changes in segmental flow regions of the human trabecular meshwork. *Exp Eye Res*, **158**, 67-72.
- 139 Bradley, J.M., Kelley, M.J., Zhu, X., Anderssohn, A.M., Alexander, J.P. and Acott, T.S. (2001) Effects of mechanical stretching on trabecular matrix metalloproteinases. *Invest Ophthalmol Vis Sci*, **42**, 1505-1513.

- 140 Zhao, X., Ramsey, K.E., Stephan, D.A. and Russell, P. (2004) Gene and protein expression changes in human trabecular meshwork cells treated with transforming growth factor-beta. *Invest Ophthalmol Vis Sci*, **45**, 4023-4034.
- 141 Vittal, V., Rose, A., Gregory, K.E., Kelley, M.J. and Acott, T.S. (2005) Changes in gene expression by trabecular meshwork cells in response to mechanical stretching. *Invest Ophthalmol Vis Sci*, **46**, 2857-2868.
- 142 Lo, W.R., Rowlette, L.L., Caballero, M., Yang, P., Hernandez, M.R. and Borrás, T. (2003) Tissue differential microarray analysis of dexamethasone induction reveals potential mechanisms of steroid glaucoma. *Invest Ophthalmol Vis Sci*, **44**, 473-485.
- 143 Izzotti, A., Longobardi, M., Cartiglia, C., Rathschuler, F. and Sacca, S.C. (2011) Trabecular meshwork gene expression after selective laser trabeculoplasty. *PLoS One*, **6**, e20110.
- 144 Keller, K.E., Aga, M., Bradley, J.M., Kelley, M.J. and Acott, T.S. (2009) Extracellular matrix turnover and outflow resistance. *Exp Eye Res*, **88**, 676-682.
- 145 Nagase, H., Suzuki, K., Enghild, J.J. and Salvesen, G. (1991) Stepwise activation mechanisms of the precursors of matrix metalloproteinases 1 (tissue collagenase) and 3 (stromelysin). *Biomedica biochimica acta*, **50**, 749-754.
- 146 Chakraborti, S., Mandal, M., Das, S., Mandal, A. and Chakraborti, T. (2003) Regulation of matrix metalloproteinases: an overview. *Mol Cell Biochem*, **253**, 269-285.
- 147 Alexander, J.P., Samples, J.R., Van Buskirk, E.M. and Acott, T.S. (1991) Expression of matrix metalloproteinases and inhibitor by human trabecular meshwork. *Invest Ophthalmol Vis Sci*, **32**, 172-180.
- 148 Oh, D.J., Martin, J.L., Williams, A.J., Russell, P., Birk, D.E. and Rhee, D.J. (2006) Effect of latanoprost on the expression of matrix metalloproteinases and their tissue inhibitors in human trabecular meshwork cells. *Invest Ophthalmol Vis Sci*, **47**, 3887-3895.

- 149 Kelley, M.J., Rose, A.Y., Song, K., Chen, Y., Bradley, J.M., Rookhuizen, D. and Acott, T.S. (2007) Synergism of TNF and IL-1 in the induction of matrix metalloproteinase-3 in trabecular meshwork. *Invest Ophthalmol Vis Sci*, **48**, 2634-2643.
- 150 Overby, D.R., Bertrand, J., Tektas, O.Y., Boussommier-Calleja, A., Schicht, M., Ethier, C.R., Woodward, D.F., Stamer, W.D. and Lutjen-Drecoll, E. (2014) Ultrastructural changes associated with dexamethasone-induced ocular hypertension in mice. *Invest Ophthalmol Vis Sci*, **55**, 4922-4933.
- 151 Schlotzer-Schrehardt, U., Lommatzsch, J., Kuchle, M., Konstas, A.G. and Naumann, G.O. (2003) Matrix metalloproteinases and their inhibitors in aqueous humor of patients with pseudoexfoliation syndrome/glaucoma and primary open-angle glaucoma. *Invest Ophthalmol Vis Sci*, **44**, 1117-1125.
- 152 Ronkko, S., Rekonen, P., Kaarniranta, K., Puustjarvi, T., Terasvirta, M. and Uusitalo, H. (2007) Matrix metalloproteinases and their inhibitors in the chamber angle of normal eyes and patients with primary open-angle glaucoma and exfoliation glaucoma. *Graefe's archive for clinical and experimental ophthalmology = Albrecht von Graefes Archiv fur klinische und experimentelle Ophthalmologie*, **245**, 697-704.
- 153 Fountoulakis, N., Labiris, G., Aristeidou, A., Katsanos, A., Tentes, I., Kortsaris, A. and Kozobolis, V.P. (2013) Tissue inhibitor of metalloproteinase 4 in aqueous humor of patients with primary open angle glaucoma, pseudoexfoliation syndrome and pseudoexfoliative glaucoma and its role in proteolysis imbalance. *BMC Ophthalmol*, **13**, 69.
- 154 Ashworth Briggs, E.L., Toh, T., Eri, R., Hewitt, A.W. and Cook, A.L. (2015) TIMP1, TIMP2, and TIMP4 are increased in aqueous humor from primary open angle glaucoma patients. *Mol Vis*, **21**, 1162-1172.
- 155 Weinstein, W.L., Dietrich, U.M., Sapienza, J.S., Carmichael, K.P., Moore, P.A. and Krunkosky, T.M. (2007) Identification of ocular matrix metalloproteinases present within the

- aqueous humor and iridocorneal drainage angle tissue of normal and glaucomatous canine eyes. *Veterinary ophthalmology*, **10 Suppl 1**, 108-116.
- 156 Maatta, M., Tervahartiala, T., Vesti, E., Airaksinen, J. and Sorsa, T. (2006) Levels and activation of matrix metalloproteinases in aqueous humor are elevated in uveitis-related secondary glaucoma. *J Glaucoma*, **15**, 229-237.
- 157 O'Callaghan, J., Crosbie, D.E., Cassidy, P.S., Sherwood, J.M., Flugel-Koch, C., Lutjen-Drecoll, E., Humphries, M.M., Reina-Torres, E., Wallace, D., Kiang, A.S. *et al.* (2017) Therapeutic potential of AAV-mediated MMP-3 secretion from corneal endothelium in treating glaucoma. *Hum Mol Genet*, **26**, 1230-1246.
- 158 Bradley, J.M., Vranka, J., Colvis, C.M., Conger, D.M., Alexander, J.P., Fisk, A.S., Samples, J.R. and Acott, T.S. (1998) Effect of matrix metalloproteinases activity on outflow in perfused human organ culture. *Invest Ophthalmol Vis Sci*, **39**, 2649-2658.
- 159 Pang, I.H., Fleenor, D.L., Hellberg, P.E., Stropki, K., McCartney, M.D. and Clark, A.F. (2003) Aqueous outflow-enhancing effect of tert-butylhydroquinone: involvement of AP-1 activation and MMP-3 expression. *Invest Ophthalmol Vis Sci*, **44**, 3502-3510.
- 160 Webb, J.G., Husain, S., Yates, P.W. and Crosson, C.E. (2006) Kinin modulation of conventional outflow facility in the bovine eye. *J Ocul Pharmacol Ther*, **22**, 310-316.
- 161 De Groef, L., Van Hove, I., Dekeyster, E., Stalmans, I. and Moons, L. (2013) MMPs in the trabecular meshwork: promising targets for future glaucoma therapies? *Invest Ophthalmol Vis Sci*, **54**, 7756-7763.
- 162 Aga, M., Bradley, J.M., Wanchu, R., Yang, Y.F., Acott, T.S. and Keller, K.E. (2014) Differential effects of caveolin-1 and -2 knockdown on aqueous outflow and altered extracellular matrix turnover in caveolin-silenced trabecular meshwork cells. *Invest Ophthalmol Vis Sci*, **55**, 5497-5509.

- 163 Yang, Y.F., Sun, Y.Y., Acott, T.S. and Keller, K.E. (2016) Effects of induction and inhibition of matrix cross-linking on remodeling of the aqueous outflow resistance by ocular trabecular meshwork cells. *Sci Rep*, **6**, 30505.
- 164 Huovila, A.P., Turner, A.J., Pelto-Huikko, M., Karkkainen, I. and Ortiz, R.M. (2005) Shedding light on ADAM metalloproteinases. *Trends Biochem Sci*, **30**, 413-422.
- 165 Stickel, S.K. and Wang, Y.L. (1988) Synthetic peptide GRGDS induces dissociation of alpha-actinin and vinculin from the sites of focal contacts. *J Cell Biol*, **107**, 1231-1239.
- 166 Curtis, T.M., McKeown-Longo, P.J., Vincent, P.A., Homan, S.M., Wheatley, E.M. and Saba, T.M. (1995) Fibronectin attenuates increased endothelial monolayer permeability after RGD peptide, anti-alpha 5 beta 1, or TNF-alpha exposure. *Am J Physiol*, **269**, 248-260.
- 167 Wu, M.H., Ustinova, E. and Granger, H.J. (2001) Integrin binding to fibronectin and vitronectin maintains the barrier function of isolated porcine coronary venules. *J Physiol*, **532**, 785-791.
- 168 Tamm, E.R., Siegner, A., Baur, A. and Lutjen-Drecoll, E. (1996) Transforming growth factor-beta 1 induces alpha-smooth muscle-actin expression in cultured human and monkey trabecular meshwork. *Exp Eye Res*, **62**, 389-397.
- 169 Schlunck, G., Han, H., Wecker, T., Kampik, D., Meyer-ter-Vehn, T. and Grehn, F. (2008) Substrate rigidity modulates cell matrix interactions and protein expression in human trabecular meshwork cells. *Invest Ophthalmol Vis Sci*, **49**, 262-269.
- 170 Yang, Y., Estrada, E.Y., Thompson, J.F., Liu, W. and Rosenberg, G.A. (2007) Matrix metalloproteinase-mediated disruption of tight junction proteins in cerebral vessels is reversed by synthetic matrix metalloproteinase inhibitor in focal ischemia in rat. *Journal of cerebral blood flow and metabolism : official journal of the International Society of Cerebral Blood Flow and Metabolism*, **27**, 697-709.

- 171 Vermeer, P.D., Denker, J., Estin, M., Moninger, T.O., Keshavjee, S., Karp, P., Kline, J.N. and Zabner, J. (2009) MMP9 modulates tight junction integrity and cell viability in human airway epithelia. *Am J Physiol Lung Cell Mol Physiol*, **296**, 751-762.
- 172 Yamada, H., Yoneda, M., Inaguma, S., Watanabe, D., Banno, S., Yoshikawa, K., Mizutani, K., Iwaki, M. and Zako, M. (2013) Infliximab counteracts tumor necrosis factor-alpha-enhanced induction of matrix metalloproteinases that degrade claudin and occludin in non-pigmented ciliary epithelium. *Biochem Pharmacol*, **85**, 1770-1782.
- 173 Rylander, N.R. and Vold, S.D. (2008) Cost analysis of glaucoma medications. *Am J Ophthalmol*, **145**, 106-113.
- 174 Li, T., Lindsley, K., Rouse, B., Hong, H., Shi, Q., Friedman, D.S., Wormald, R. and Dickersin, K. (2016) Comparative Effectiveness of First-Line Medications for Primary Open-Angle Glaucoma: A Systematic Review and Network Meta-analysis. *Ophthalmology*, **123**, 129-140.
- 175 Mastropasqua, R., Fasanella, V., Pedrotti, E., Lanzini, M., Di Staso, S., Mastropasqua, L. and Agnifili, L. (2014) Trans-conjunctival aqueous humor outflow in glaucomatous patients treated with prostaglandin analogues: an in vivo confocal microscopy study. *Graefe's archive for clinical and experimental ophthalmology = Albrecht von Graefes Archiv fur klinische und experimentelle Ophthalmologie*, **252**, 1469-1476.
- 176 Toris, C.B., Gabelt, B.T. and Kaufman, P.L. (2008) Update on the mechanism of action of topical prostaglandins for intraocular pressure reduction. *Surv Ophthalmol*, **53 Suppl1**, S107-120.
- 177 Richter, M., Krauss, A.H., Woodward, D.F. and Lutjen-Drecoll, E. (2003) Morphological changes in the anterior eye segment after long-term treatment with different receptor selective prostaglandin agonists and a prostamide. *Invest Ophthalmol Vis Sci*, **44**, 4419-4426.

- 178 Goh, Y., Urade, Y., Fujimoto, N. and Hayaishi, O. (1987) Content and formation of prostaglandins and distribution of prostaglandin-related enzyme activities in the rat ocular system. *Biochim Biophys Acta*, **921**, 302-311.
- 179 Wan, Z., Woodward, D.F. and Stamer, W.D. (2008) Endogenous Bioactive Lipids and the Regulation of Conventional Outflow Facility. *Expert Review of Ophthalmology*, **3**, 457-470.
- 180 Bahler, C.K., Howell, K.G., Hann, C.R., Fautsch, M.P. and Johnson, D.H. (2008) Prostaglandins increase trabecular meshwork outflow facility in cultured human anterior segments. *Am J Ophthalmol*, **145**, 114-119.
- 181 Wan, Z., Woodward, D.F., Cornell, C.L., Fliri, H.G., Martos, J.L., Pettit, S.N., Wang, J.W., Kharlamb, A.B., Wheeler, L.A., Garst, M.E. *et al.* (2007) Bimatoprost, prostamide activity, and conventional drainage. *Invest Ophthalmol Vis Sci*, **48**, 4107-4115.
- 182 Thieme, H., Schimmat, C., Munzer, G., Boxberger, M., Fromm, M., Pfeiffer, N. and Rosenthal, R. (2006) Endothelin antagonism: effects of FP receptor agonists prostaglandin F2alpha and fluprostenol on trabecular meshwork contractility. *Invest Ophthalmol Vis Sci*, **47**, 938-945.
- 183 Weinreb, R.N., Toris, C.B., Gabelt, B.T., Lindsey, J.D. and Kaufman, P.L. (2002) Effects of prostaglandins on the aqueous humor outflow pathways. *Surv Ophthalmol*, **47 Suppl 1**, S53-64.
- 184 Schachtschabel, U., Lindsey, J.D. and Weinreb, R.N. (2000) The mechanism of action of prostaglandins on uveoscleral outflow. *Curr Opin Ophthalmol*, **11**, 112-115.
- 185 Ocklind, A. (1998) Effect of latanoprost on the extracellular matrix of the ciliary muscle. A study on cultured cells and tissue sections. *Exp Eye Res*, **67**, 179-191.
- 186 Sagara, T., Gatton, D.D., Lindsey, J.D., Gabelt, B.T., Kaufman, P.L. and Weinreb, R.N. (1999) Topical prostaglandin F2alpha treatment reduces collagen types I, III, and IV in the monkey uveoscleral outflow pathway. *Arch Ophthalmol*, **117**, 794-801.

- 187 Weinreb, R.N., Kashiwagi, K., Kashiwagi, F., Tsukahara, S. and Lindsey, J.D. (1997) Prostaglandins increase matrix metalloproteinase release from human ciliary smooth muscle cells. *Invest Ophthalmol Vis Sci*, **38**, 2772-2780.
- 188 Woodward, D.F., Nilsson, S.F., Toris, C.B., Kharlamb, A.B., Nieves, A.L. and Krauss, A.H. (2009) Prostanoid EP4 receptor stimulation produces ocular hypotension by a mechanism that does not appear to involve uveoscleral outflow. *Invest Ophthalmol Vis Sci*, **50**, 3320-3328.
- 189 Alvarado, J.A., Iguchi, R., Martinez, J., Trivedi, S. and Shifera, A.S. (2010) Similar effects of selective laser trabeculoplasty and prostaglandin analogs on the permeability of cultured Schlemm canal cells. *Am J Ophthalmol*, **150**, 254-264.
- 190 Brooks, A.M. and Gillies, W.E. (1992) Ocular beta-blockers in glaucoma management. Clinical pharmacological aspects. *Drugs Aging*, **2**, 208-221.
- 191 Trope, G.E. and Clark, B. (1982) Beta adrenergic receptors in pigmented ciliary processes. *Br J Ophthalmol*, **66**, 788-792.
- 192 Camras, C.B. and Podos, S.M. (1989) The role of endogenous prostaglandins in clinically-used and investigational glaucoma therapy. *Prog Clin Biol Res*, **312**, 459-475.
- 193 Toris, C.B., Camras, C.B. and Yablonski, M.E. (1999) Acute versus chronic effects of brimonidine on aqueous humor dynamics in ocular hypertensive patients. *Am J Ophthalmol*, **128**, 8-14.
- 194 Avila, M.Y., Carre, D.A., Stone, R.A. and Civan, M.M. (2001) Reliable measurement of mouse intraocular pressure by a servo-null micropipette system. *Invest Ophthalmol Vis Sci*, **42**, 1841-1846.
- 195 Overby, D.R., Bertrand, J., Schicht, M., Paulsen, F., Stamer, W.D. and Lutjen-Drecoll, E. (2014) The structure of the trabecular meshwork, its connections to the ciliary muscle, and the effect of pilocarpine on outflow facility in mice. *Invest Ophthalmol Vis Sci*, **55**, 3727-3736.
- 196 Li, G., Farsiu, S., Chiu, S.J., Gonzalez, P., Lutjen-Drecoll, E., Overby, D.R. and Stamer, W.D. (2014) Pilocarpine-induced dilation of Schlemm's canal and prevention of lumen collapse

at elevated intraocular pressures in living mice visualized by OCT. *Invest Ophthalmol Vis Sci*, **55**, 3737-3746.

197 Selbach, J.M., Gottanka, J., Wittmann, M. and Lutjen-Drecoll, E. (2000) Efferent and afferent innervation of primate trabecular meshwork and scleral spur. *Invest Ophthalmol Vis Sci*, **41**, 2184-2191.

198 Ito, T., Ohguro, H., Mamiya, K., Ohguro, I. and Nakazawa, M. (2006) Effects of antiglaucoma drops on MMP and TIMP balance in conjunctival and subconjunctival tissue. *Invest Ophthalmol Vis Sci*, **47**, 823-830.

199 Scherer, W.J. (2002) A retrospective review of non-responders to latanoprost. *J Ocul Pharmacol Ther*, **18**, 287-291.

200 Noecker, R.S., Dirks, M.S., Choplin, N.T., Bernstein, P., Batoosingh, A.L., Whitcup, S.M. and Bimatoprost/Latanoprost Study, G. (2003) A six-month randomized clinical trial comparing the intraocular pressure-lowering efficacy of bimatoprost and latanoprost in patients with ocular hypertension or glaucoma. *Am J Ophthalmol*, **135**, 55-63.

201 Gandolfi, S.A. and Cimino, L. (2003) Effect of bimatoprost on patients with primary open-angle glaucoma or ocular hypertension who are nonresponders to latanoprost. *Ophthalmology*, **110**, 609-614.

202 Lee, A.J. and McCluskey, P. (2010) Clinical utility and differential effects of prostaglandin analogs in the management of raised intraocular pressure and ocular hypertension. *Clin Ophthalmol*, **4**, 741-764.

203 Richter, G.M. and Coleman, A.L. (2016) Minimally invasive glaucoma surgery: current status and future prospects. *Clin Ophthalmol*, **10**, 189-206.

204 Melamed, S., Ben Simon, G.J. and Levkovitch-Verbin, H. (2003) Selective laser trabeculoplasty as primary treatment for open-angle glaucoma: a prospective, nonrandomized pilot study. *Arch Ophthalmol*, **121**, 957-960.

- 205 Latina, M.A. and de Leon, J.M. (2005) Selective laser trabeculoplasty. *Ophthalmology Clinics of North America*, **18**, 409-419, vi.
- 206 Leahy, K.E. and White, A.J. (2015) Selective laser trabeculoplasty: current perspectives. *Clin Ophthalmol*, **9**, 833-841.
- 207 Woo, D.M., Healey, P.R., Graham, S.L. and Goldberg, I. (2015) Intraocular pressure-lowering medications and long-term outcomes of selective laser trabeculoplasty. *Clin Exp Ophthalmol*, **43**, 320-327.
- 208 Weinand, F.S. and Althen, F. (2006) Long-term clinical results of selective laser trabeculoplasty in the treatment of primary open angle glaucoma. *Eur J Ophthalmol*, **16**, 100-104.
- 209 Cvenkel, B., Hvala, A., Drnovsek-Olup, B. and Gale, N. (2003) Acute ultrastructural changes of the trabecular meshwork after selective laser trabeculoplasty and low power argon laser trabeculoplasty. *Lasers Surg Med*, **33**, 204-208.
- 210 Kramer, T.R. and Noecker, R.J. (2001) Comparison of the morphologic changes after selective laser trabeculoplasty and argon laser trabeculoplasty in human eye bank eyes. *Ophthalmology*, **108**, 773-779.
- 211 Stein, J.D. and Challa, P. (2007) Mechanisms of action and efficacy of argon laser trabeculoplasty and selective laser trabeculoplasty. *Curr Opin Ophthalmol*, **18**, 140-145.
- 212 Guzey, M., Vural, H., Satıcı, A., Karadede, S. and Dogan, Z. (2001) Increase of free oxygen radicals in aqueous humour induced by selective Nd:YAG laser trabeculoplasty in the rabbit. *Eur J Ophthalmol*, **11**, 47-52.
- 213 Acott, T.S., Samples, J.R., Bradley, J.M., Bacon, D.R., Bylsma, S.S. and Van Buskirk, E.M. (1989) Trabecular repopulation by anterior trabecular meshwork cells after laser trabeculoplasty. *Am J Ophthalmol*, **107**, 1-6.

- 214 Alvarado, J.A., Chau, P., Wu, J., Juster, R., Shifera, A.S. and Geske, M. (2015) Profiling of Cytokines Secreted by Conventional Aqueous Outflow Pathway Endothelial Cells Activated In Vitro and Ex Vivo With Laser Irradiation. *Invest Ophthalmol Vis Sci*, **56**, 7100-7108.
- 215 Bradley, J.M., Anderssohn, A.M., Colvis, C.M., Parshley, D.E., Zhu, X.H., Ruddat, M.S., Samples, J.R. and Acott, T.S. (2000) Mediation of laser trabeculoplasty-induced matrix metalloproteinase expression by IL-1beta and TNFalpha. *Invest Ophthalmol Vis Sci*, **41**, 422-430.
- 216 Parshley, D.E., Bradley, J.M., Samples, J.R., Van Buskirk, E.M. and Acott, T.S. (1995) Early changes in matrix metalloproteinases and inhibitors after in vitro laser treatment to the trabecular meshwork. *Curr Eye Res*, **14**, 537-544.
- 217 Alvarado, J.A., Katz, L.J., Trivedi, S. and Shifera, A.S. (2010) Monocyte modulation of aqueous outflow and recruitment to the trabecular meshwork following selective laser trabeculoplasty. *Arch Ophthalmol*, **128**, 731-737.
- 218 Gedde, S.J., Herndon, L.W., Brandt, J.D., Budenz, D.L., Feuer, W.J., Schiffman, J.C. and Tube Versus Trabeculectomy Study, G. (2012) Postoperative complications in the Tube Versus Trabeculectomy (TVT) study during five years of follow-up. *Am J Ophthalmol*, **153**, 804-814 e801.
- 219 Cagini, C., Peruzzi, C., Fiore, T., Spadea, L., Lippera, M. and Lippera, S. (2016) Canaloplasty: Current Value in the Management of Glaucoma. *J Ophthalmol*, **2016**, 7080475.
- 220 Falkenberry, S.M. and Siegfried, C.J. (2009) Endocyclophotocoagulation. *Middle East Afr J Ophthalmol*, **16**, 130-133.
- 221 Francis, B.A., Berke, S.J., Dustin, L. and Noecker, R. (2014) Endoscopic cyclophotocoagulation combined with phacoemulsification versus phacoemulsification alone in medically controlled glaucoma. *J Cataract Refract Surg*, **40**, 1313-1321.
- 222 Lewis, R.A. (2014) Ab interno approach to the subconjunctival space using a collagen glaucoma stent. *J Cataract Refract Surg*, **40**, 1301-1306.

- 223 Hoeh, H., Ahmed, II, Grisanti, S., Grisanti, S., Grabner, G., Nguyen, Q.H., Rau, M., Yoo, S. and Ianchulev, T. (2013) Early postoperative safety and surgical outcomes after implantation of a suprachoroidal micro-stent for the treatment of open-angle glaucoma concomitant with cataract surgery. *J Cataract Refract Surg*, **39**, 431-437.
- 224 Siegel, M.J., Boling, W.S., Faridi, O.S., Gupta, C.K., Kim, C., Boling, R.C., Citron, M.E., Siegel, M.J. and Siegel, L.I. (2015) Combined endoscopic cyclophotocoagulation and phacoemulsification versus phacoemulsification alone in the treatment of mild to moderate glaucoma. *Clinical & Experimental Ophthalmology*, **43**, 531-539.
- 225 Voskanyan, L., Garcia-Feijoo, J., Belda, J.I., Fea, A., Junemann, A., Baudouin, C. and Synergy Study, G. (2014) Prospective, unmasked evaluation of the iStent(R) inject system for open-angle glaucoma: synergy trial. *Adv Ther*, **31**, 189-201.
- 226 Schmidt, W., Kastner, C., Sternberg, K., Allemann, R., Lobler, M., Guthoff, R. and Schmitz, K.P. (2013) New concepts for glaucoma implants--controlled aqueous humor drainage, encapsulation prevention and local drug delivery. *Curr Pharm Biotechnol*, **14**, 98-111.
- 227 Chen, P.P., Lin, S.C., Junk, A.K., Radhakrishnan, S., Singh, K. and Chen, T.C. (2015) The Effect of Phacoemulsification on Intraocular Pressure in Glaucoma Patients: A Report by the American Academy of Ophthalmology. *Ophthalmology*, **122**, 1294-1307.
- 228 Li, G., Mukherjee, D., Navarro, I., Ashpole, N.E., Sherwood, J.M., Chang, J., Overby, D.R., Yuan, F., Gonzalez, P., Kopczynski, C.C. *et al.* (2016) Visualization of conventional outflow tissue responses to netarsudil in living mouse eyes. *Eur J Pharmacol*, **787**, 20-31.
- 229 Ren, R., Li, G., Le, T.D., Kopczynski, C., Stamer, W.D. and Gong, H. (2016) Netarsudil Increases Outflow Facility in Human Eyes Through Multiple Mechanisms. *Invest Ophthalmol Vis Sci*, **57**, 6197-6209.

- 230 Wang, R.F., Williamson, J.E., Kopczynski, C. and Serle, J.B. (2015) Effect of 0.04% AR-13324, a ROCK, and norepinephrine transporter inhibitor, on aqueous humor dynamics in normotensive monkey eyes. *J Glaucoma*, **24**, 51-54.
- 231 Fukata, Y., Amano, M. and Kaibuchi, K. (2001) Rho-Rho-kinase pathway in smooth muscle contraction and cytoskeletal reorganization of non-muscle cells. *Trends Pharmacol Sci*, **22**, 32-39.
- 232 Goldhagen, B., Proia, A.D., Epstein, D.L. and Rao, P.V. (2012) Elevated levels of RhoA in the optic nerve head of human eyes with glaucoma. *J Glaucoma*, **21**, 530-538.
- 233 Rao, V.P. and Epstein, D.L. (2007) Rho GTPase/Rho kinase inhibition as a novel target for the treatment of glaucoma. *BioDrugs*, **21**, 167-177.
- 234 Wettschureck, N. and Offermanns, S. (2002) Rho/Rho-kinase mediated signaling in physiology and pathophysiology. *J Mol Med (Berl)*, **80**, 629-638.
- 235 Rao, P.V., Deng, P.F., Kumar, J. and Epstein, D.L. (2001) Modulation of aqueous humor outflow facility by the Rho kinase-specific inhibitor Y-27632. *Invest Ophthalmol Vis Sci*, **42**, 1029-1037.
- 236 Wang, S.K. and Chang, R.T. (2014) An emerging treatment option for glaucoma: Rho kinase inhibitors. *Clin Ophthalmol*, **8**, 883-890.
- 237 Riento, K. and Ridley, A.J. (2003) Rocks: multifunctional kinases in cell behaviour. *Nat Rev Mol Cell Biol*, **4**, 446-456.
- 238 Liu, X., Hu, Y., Filla, M.S., Gabelt, B.T., Peters, D.M., Brandt, C.R. and Kaufman, P.L. (2005) The effect of C3 transgene expression on actin and cellular adhesions in cultured human trabecular meshwork cells and on outflow facility in organ cultured monkey eyes. *Mol Vis*, **11**, 1112-1121.
- 239 Tian, B., Kiland, J.A. and Kaufman, P.L. (2001) Effects of the marine macrolides swinholide A and jasplakinolide on outflow facility in monkeys. *Invest Ophthalmol Vis Sci*, **42**, 3187-3192.

- 240 Bubb, M.R., Spector, I., Bershadsky, A.D. and Korn, E.D. (1995) Swinholidide A is a microfilament disrupting marine toxin that stabilizes actin dimers and severs actin filaments. *J Biol Chem*, **270**, 3463-3466.
- 241 Coue, M., Brenner, S.L., Spector, I. and Korn, E.D. (1987) Inhibition of actin polymerization by latrunculin A. *FEBS Lett*, **213**, 316-318.
- 242 Bubb, M.R., Senderowicz, A.M., Sausville, E.A., Duncan, K.L. and Korn, E.D. (1994) Jasplakinolide, a cytotoxic natural product, induces actin polymerization and competitively inhibits the binding of phalloidin to F-actin. *J Biol Chem*, **269**, 14869-14871.
- 243 Peterson, J.A., Tian, B., Geiger, B. and Kaufman, P.L. (2000) Effect of latrunculin-B on outflow facility in monkeys. *Exp Eye Res*, **70**, 307-313.
- 244 Okka, M., Tian, B. and Kaufman, P.L. (2004) Effect of low-dose latrunculin B on anterior segment physiologic features in the monkey eye. *Arch Ophthalmol*, **122**, 1482-1488.
- 245 Ethier, C.R., Read, A.T. and Chan, D.W. (2006) Effects of latrunculin-B on outflow facility and trabecular meshwork structure in human eyes. *Invest Ophthalmol Vis Sci*, **47**, 1991-1998.
- 246 Sabanay, I., Tian, B., Gabelt, B.T., Geiger, B. and Kaufman, P.L. (2006) Latrunculin B effects on trabecular meshwork and corneal endothelial morphology in monkeys. *Exp Eye Res*, **82**, 236-246.
- 247 Peterson, J.A., Tian, B., McLaren, J.W., Hubbard, W.C., Geiger, B. and Kaufman, P.L. (2000) Latrunculins' effects on intraocular pressure, aqueous humor flow, and corneal endothelium. *Invest Ophthalmol Vis Sci*, **41**, 1749-1758.
- 248 Rasmussen, C.A., Kaufman, P.L., Ritch, R., Haque, R., Brazzell, R.K. and Vittitow, J.L. (2014) Latrunculin B Reduces Intraocular Pressure in Human Ocular Hypertension and Primary Open-Angle Glaucoma. *Transl Vis Sci Technol*, **3**, 1.

- 249 Mitchell, C.H., Peterson-Yantorno, K., Carre, D.A., McGlenn, A.M., Coca-Prados, M., Stone, R.A. and Civan, M.M. (1999) A3 adenosine receptors regulate Cl⁻ channels of nonpigmented ciliary epithelial cells. *Am J Physiol*, **276**, C659-666.
- 250 Laties, A., Rich, C.C., Stoltz, R., Humbert, V., Brickman, C., McVicar, W. and Baumgartner, R.A. (2016) A Randomized Phase 1 Dose Escalation Study to Evaluate Safety, Tolerability, and Pharmacokinetics of Trabodenson in Healthy Adult Volunteers. *J Ocul Pharmacol Ther*, **32**, 548-554.
- 251 Myers, J.S., Sall, K.N., DuBiner, H., Slomowitz, N., McVicar, W., Rich, C.C. and Baumgartner, R.A. (2016) A Dose-Escalation Study to Evaluate the Safety, Tolerability, Pharmacokinetics, and Efficacy of 2 and 4 Weeks of Twice-Daily Ocular Trabodenson in Adults with Ocular Hypertension or Primary Open-Angle Glaucoma. *J Ocul Pharmacol Ther*, **32**, 555-562.
- 252 Zhong, Y., Yang, Z., Huang, W.C. and Luo, X. (2013) Adenosine, adenosine receptors and glaucoma: an updated overview. *Biochim Biophys Acta*, **1830**, 2882-2890.
- 253 Shearer, T.W. and Crosson, C.E. (2002) Adenosine A1 receptor modulation of MMP-2 secretion by trabecular meshwork cells. *Invest Ophthalmol Vis Sci*, **43**, 3016-3020.
- 254 Crosson, C.E., Sloan, C.F. and Yates, P.W. (2005) Modulation of conventional outflow facility by the adenosine A1 agonist N6-cyclohexyladenosine. *Invest Ophthalmol Vis Sci*, **46**, 3795-3799.
- 255 Chen, J., Runyan, S.A. and Robinson, M.R. (2011) Novel ocular antihypertensive compounds in clinical trials. *Clin Ophthalmol*, **5**, 667-677.
- 256 Cavet, M.E., Vollmer, T.R., Harrington, K.L., VanDerMeid, K. and Richardson, M.E. (2015) Regulation of Endothelin-1-Induced Trabecular Meshwork Cell Contractility by Latanoprostene Bunod. *Invest Ophthalmol Vis Sci*, **56**, 4108-4116.
- 257 Kalouche, G., Beguier, F., Bakria, M., Melik-Parsadaniantz, S., Leriche, C., Debeir, T., Rostene, W., Baudouin, C. and Vige, X. (2016) Activation of Prostaglandin FP and EP2

Receptors Differently Modulates Myofibroblast Transition in a Model of Adult Primary Human Trabecular Meshwork Cells. *Invest Ophthalmol Vis Sci*, **57**, 1816-1825.

258 Nilsson, S.F., Dreccoll, E., Lutjen-Dreccoll, E., Toris, C.B., Krauss, A.H., Kharlamb, A., Nieves, A., Guerra, T. and Woodward, D.F. (2006) The prostanoid EP2 receptor agonist butaprost increases uveoscleral outflow in the cynomolgus monkey. *Invest Ophthalmol Vis Sci*, **47**, 4042-4049.

259 Wang, J.W., Woodward, D.F. and Stamer, W.D. (2013) Differential effects of prostaglandin E2-sensitive receptors on contractility of human ocular cells that regulate conventional outflow. *Invest Ophthalmol Vis Sci*, **54**, 4782-4790.

260 Millard, L.H., Woodward, D.F. and Stamer, W.D. (2011) The role of the prostaglandin EP4 receptor in the regulation of human outflow facility. *Invest Ophthalmol Vis Sci*, **52**, 3506-3513.

261 Fujino, H., Xu, W. and Regan, J.W. (2003) Prostaglandin E2 induced functional expression of early growth response factor-1 by EP4, but not EP2, prostanoid receptors via the phosphatidylinositol 3-kinase and extracellular signal-regulated kinases. *J Biol Chem*, **278**, 12151-12156.

262 Zhong, J., Gencay, M.M., Bubendorf, L., Burgess, J.K., Parson, H., Robinson, B.W., Tamm, M., Black, J.L. and Roth, M. (2006) ERK1/2 and p38 MAP kinase control MMP-2, MT1-MMP, and TIMP action and affect cell migration: a comparison between mesothelioma and mesothelial cells. *J Cell Physiol*, **207**, 540-552.

263 Martinez, T., Jimenez, A.I. and Paneda, C. (2015) Short-interference RNAs: becoming medicines. *EXCLI J*, **14**, 714-746.

264 Moreno-Montanes, J., Sadaba, B., Ruz, V., Gomez-Guiu, A., Zarranz, J., Gonzalez, M.V., Paneda, C. and Jimenez, A.I. (2014) Phase I clinical trial of SYL040012, a small interfering RNA targeting beta-adrenergic receptor 2, for lowering intraocular pressure. *Mol Ther*, **22**, 226-232.

- 265 Datta, S., Baudouin, C., Brignole-Baudouin, F., Denoyer, A. and Cortopassi, G.A. (2017) The Eye Drop Preservative Benzalkonium Chloride Potently Induces Mitochondrial Dysfunction and Preferentially Affects LHON Mutant Cells. *Invest Ophthalmol Vis Sci*, **58**, 2406-2412.
- 266 Schehlein, E.M., Novack, G.D. and Robin, A.L. (2017) New classes of glaucoma medications. *Curr Opin Ophthalmol*, **28**, 161-168.
- 267 Rasmussen, C.A. and Kaufman, P.L. (2014) Exciting directions in glaucoma. *Can J Ophthalmol*, **49**, 534-543.
- 268 Liu, X., Brandt, C.R., Gabelt, B.T., Bryar, P.J., Smith, M.E. and Kaufman, P.L. (1999) Herpes simplex virus mediated gene transfer to primate ocular tissues. *Exp Eye Res*, **69**, 385-395.
- 269 Spencer, B., Agarwala, S., Miskulin, M., Smith, M. and Brandt, C.R. (2000) Herpes simplex virus-mediated gene delivery to the rodent visual system. *Invest Ophthalmol Vis Sci*, **41**, 1392-1401.
- 270 Loewen, N., Fautsch, M.P., Teo, W.L., Bahler, C.K., Johnson, D.H. and Poeschla, E.M. (2004) Long-term, targeted genetic modification of the aqueous humor outflow tract coupled with noninvasive imaging of gene expression in vivo. *Invest Ophthalmol Vis Sci*, **45**, 3091-3098.
- 271 Challa, P., Luna, C., Liton, P.B., Chamblin, B., Wakefield, J., Ramabhadran, R., Epstein, D.L. and Gonzalez, P. (2005) Lentiviral mediated gene delivery to the anterior chamber of rodent eyes. *Mol Vis*, **11**, 425-430.
- 272 Barraza, R.A., Rasmussen, C.A., Loewen, N., Cameron, J.D., Gabelt, B.T., Teo, W.L., Kaufman, P.L. and Poeschla, E.M. (2009) Prolonged transgene expression with lentiviral vectors in the aqueous humor outflow pathway of nonhuman primates. *Hum Gene Ther*, **20**, 191-200.

- 273 Budenz, D.L., Bennett, J., Alonso, L. and Maguire, A. (1995) In vivo gene transfer into murine corneal endothelial and trabecular meshwork cells. *Invest Ophthalmol Vis Sci*, **36**, 2211-2215.
- 274 Borrás, T., Tamm, E.R. and Zigler, J.S., Jr. (1996) Ocular adenovirus gene transfer varies in efficiency and inflammatory response. *Invest Ophthalmol Vis Sci*, **37**, 1282-1293.
- 275 Borrás, T., Gabelt, B.T., Klintworth, G.K., Peterson, J.C. and Kaufman, P.L. (2001) Non-invasive observation of repeated adenoviral GFP gene delivery to the anterior segment of the monkey eye in vivo. *J Gene Med*, **3**, 437-449.
- 276 Kee, C., Sohn, S. and Hwang, J.M. (2001) Stromelysin gene transfer into cultured human trabecular cells and rat trabecular meshwork in vivo. *Invest Ophthalmol Vis Sci*, **42**, 2856-2860.
- 277 Spiga, M.G. and Borrás, T. (2010) Development of a gene therapy virus with a glucocorticoid-inducible MMP1 for the treatment of steroid glaucoma. *Invest Ophthalmol Vis Sci*, **51**, 3029-3041.
- 278 Gerometta, R., Spiga, M.G., Borrás, T. and Candia, O.A. (2010) Treatment of sheep steroid-induced ocular hypertension with a glucocorticoid-inducible MMP1 gene therapy virus. *Invest Ophthalmol Vis Sci*, **51**, 3042-3048.
- 279 Borrás, T., Buie, L.K. and Spiga, M.G. (2016) Inducible scAAV2.GRE.MMP1 lowers IOP long-term in a large animal model for steroid-induced glaucoma gene therapy. *Gene Ther*, **23**, 438-449.
- 280 Manno, C.S., Pierce, G.F., Arruda, V.R., Glader, B., Ragni, M., Rasko, J.J., Ozelo, M.C., Hoots, K., Blatt, P., Konkle, B. *et al.* (2006) Successful transduction of liver in hemophilia by AAV-Factor IX and limitations imposed by the host immune response. *Nat Med*, **12**, 342-347.
- 281 Murphy, S.L. and High, K.A. (2008) Gene therapy for haemophilia. *Br J Haematol*, **140**, 479-487.

- 282 Colella, P., Ronzitti, G. and Mingozi, F. (2018) Emerging Issues in AAV-Mediated In Vivo Gene Therapy. *Mol Ther Methods Clin Dev*, **8**, 87-104.
- 283 McCarty, D.M., Monahan, P.E. and Samulski, R.J. (2001) Self-complementary recombinant adeno-associated virus (scAAV) vectors promote efficient transduction independently of DNA synthesis. *Gene Ther*, **8**, 1248-1254.
- 284 Buie, L.K., Rasmussen, C.A., Porterfield, E.C., Ramgolam, V.S., Choi, V.W., Markovic-Plese, S., Samulski, R.J., Kaufman, P.L. and Borras, T. (2010) Self-complementary AAV virus (scAAV) safe and long-term gene transfer in the trabecular meshwork of living rats and monkeys. *Invest Ophthalmol Vis Sci*, **51**, 236-248.
- 285 Bennett, J. (2017) Taking Stock of Retinal Gene Therapy: Looking Back and Moving Forward. *Mol Ther*, **25**, 1076-1094.
- 286 Javadi, M.A. and Feizi, S. (2011) Dry eye syndrome. *J Ophthalmic Vis Res*, **6**, 192-198.
- 287 Farid, M. (2015), in press.
- 288 Gupta, D., Wen, J.C., Huebner, J.L., Stinnett, S., Kraus, V.B., Tseng, H.C. and Walsh, M. (2017) Cytokine biomarkers in tear film for primary open-angle glaucoma. *Clin Ophthalmol*, **11**, 411-416.
- 289 Tong, Y., Zhou, Y.L., Zheng, Y., Biswal, M., Zhao, P.Q. and Wang, Z.Y. (2017) Analyzing cytokines as biomarkers to evaluate severity of glaucoma. *International Journal of Ophthalmology*, **10**, 925-930.
- 290 Khalef, N., Labib, H., Helmy, H., El Hamid, M.A., Moemen, L. and Fahmy, I. (2017) Levels of cytokines in the aqueous humor of eyes with primary open angle glaucoma, pseudoexfoliation glaucoma and cataract. *Electron Physician*, **9**, 3833-3837.
- 291 Kokubun, T., Tsuda, S., Kunikata, H., Yasuda, M., Himori, N., Kunimatsu-Sanuki, S., Maruyama, K. and Nakazawa, T. (2017) Characteristic Profiles of Inflammatory Cytokines in the Aqueous Humor of Glaucomatous Eyes. *Ocul Immunol Inflamm*, in press., 1-12.

- 292 Chua, J., Vania, M., Cheung, C.M., Ang, M., Chee, S.P., Yang, H., Li, J. and Wong, T.T. (2012) Expression profile of inflammatory cytokines in aqueous from glaucomatous eyes. *Mol Vis*, **18**, 431-438.
- 293 Taurone, S., Ripandelli, G., Pacella, E., Bianchi, E., Plateroti, A.M., De Vito, S., Plateroti, P., Grippaudo, F.R., Cavallotti, C. and Artico, M. (2015) Potential regulatory molecules in the human trabecular meshwork of patients with glaucoma: immunohistochemical profile of a number of inflammatory cytokines. *Molecular Medicine Reports*, **11**, 1384-1390.
- 294 Zhang, Y., Yang, Q., Guo, F., Chen, X. and Xie, L. (2017) Link between neurodegeneration and trabecular meshwork injury in glaucomatous patients. *BMC Ophthalmol*, **17**, 223.
- 295 Ahmad Sobhani, H.E., Ali ebrahimi, Mohammad Saadatnia, Heshmatallah Orooji, Ahmad Chitsaz. (2018) VCAM-1 as an Endothelial Factor for Diagnosis of Dementia in Parkinson's Disease. *Journal of Neurology and Neuroscience*, **9**, 243.
- 296 Foster, J.R. (2001) The functions of cytokines and their uses in toxicology. *Int J Exp Pathol*, **82**, 171-192.
- 297 Alexander, J.P., Samples, J.R. and Acott, T.S. (1998) Growth factor and cytokine modulation of trabecular meshwork matrix metalloproteinase and TIMP expression. *Curr Eye Res*, **17**, 276-285.
- 298 Micera, A., Quaranta, L., Esposito, G., Floriani, I., Pocobelli, A., Sacca, S.C., Riva, I., Manni, G. and Oddone, F. (2016) Differential Protein Expression Profiles in Glaucomatous Trabecular Meshwork: An Evaluation Study on a Small Primary Open Angle Glaucoma Population. *Adv Ther*, **33**, 252-267.
- 299 Li, G., Luna, C., Liton, P.B., Navarro, I., Epstein, D.L. and Gonzalez, P. (2007) Sustained stress response after oxidative stress in trabecular meshwork cells. *Mol Vis*, **13**, 2282-2288.

- 300 Liton, P.B., Challa, P., Stinnett, S., Luna, C., Epstein, D.L. and Gonzalez, P. (2005) Cellular senescence in the glaucomatous outflow pathway. *Exp Gerontol*, **40**, 745-748.
- 301 Blum, M.S., Toninelli, E., Anderson, J.M., Balda, M.S., Zhou, J., O'Donnell, L., Pardi, R. and Bender, J.R. (1997) Cytoskeletal rearrangement mediates human microvascular endothelial tight junction modulation by cytokines. *Am J Physiol*, **273**, H286-294.
- 302 Liton, P.B., Luna, C., Bodman, M., Hong, A., Epstein, D.L. and Gonzalez, P. (2005) Induction of IL-6 expression by mechanical stress in the trabecular meshwork. *Biochem Biophys Res Commun*, **337**, 1229-1236.
- 303 Alvarado, J.A., Alvarado, R.G., Yeh, R.F., Franse-Carman, L., Marcellino, G.R. and Brownstein, M.J. (2005) A new insight into the cellular regulation of aqueous outflow: how trabecular meshwork endothelial cells drive a mechanism that regulates the permeability of Schlemm's canal endothelial cells. *Br J Ophthalmol*, **89**, 1500-1505.
- 304 Eichler, W., Friedrichs, U., Thies, A., Tratz, C. and Wiedemann, P. (2002) Modulation of matrix metalloproteinase and TIMP-1 expression by cytokines in human RPE cells. *Invest Ophthalmol Vis Sci*, **43**, 2767-2773.
- 305 Li, D.Q., Meller, D., Liu, Y. and Tseng, S.C. (2000) Overexpression of MMP-1 and MMP-3 by cultured conjunctivochalasis fibroblasts. *Invest Ophthalmol Vis Sci*, **41**, 404-410.
- 306 Kirschner, N., Rosenthal, R., Furuse, M., Moll, I., Fromm, M. and Brandner, J.M. (2013) Contribution of tight junction proteins to ion, macromolecule, and water barrier in keratinocytes. *J Invest Dermatol*, **133**, 1161-1169.
- 307 Keaney, J., Walsh, D.M., O'Malley, T., Hudson, N., Crosbie, D.E., Loftus, T., Sheehan, F., McDaid, J., Humphries, M.M., Callanan, J.J. *et al.* (2015) Autoregulated paracellular clearance of amyloid-beta across the blood-brain barrier. *Science advances*, **1**, e1500472.
- 308 Campbell, M., Cassidy, P.S., O'Callaghan, J., Crosbie, D.E. and Humphries, P. (2018) Manipulating ocular endothelial tight junctions: Applications in treatment of retinal disease pathology and ocular hypertension. *Prog Retin Eye Res*, **62**, 120-133.

- 309 Nga, A.D., Yap, S.L., Samsudin, A., Abdul-Rahman, P.S., Hashim, O.H. and Mimiwati, Z. (2014) Matrix metalloproteinases and tissue inhibitors of metalloproteinases in the aqueous humour of patients with primary angle closure glaucoma - a quantitative study. *BMC Ophthalmol*, **14**, 33.
- 310 Tezel, G. (2011) The immune response in glaucoma: a perspective on the roles of oxidative stress. *Exp Eye Res*, **93**, 178-186.
- 311 Acott, T.S., Kelley, M.J., Keller, K.E., Vranka, J.A., Abu-Hassan, D.W., Li, X., Aga, M. and Bradley, J.M. (2014) Intraocular pressure homeostasis: maintaining balance in a high-pressure environment. *J Ocul Pharmacol Ther*, **30**, 94-101.
- 312 Nagase, H., Enghild, J.J., Suzuki, K. and Salvesen, G. (1990) Stepwise activation mechanisms of the precursor of matrix metalloproteinase 3 (stromelysin) by proteinases and (4-aminophenyl)mercuric acetate. *Biochemistry*, **29**, 5783-5789.
- 313 Nagase, H., Visse, R. and Murphy, G. (2006) Structure and function of matrix metalloproteinases and TIMPs. *Cardiovasc Res*, **69**, 562-573.
- 314 Clark, I.M. and Cawston, T.E. (1989) Fragments of human fibroblast collagenase. Purification and characterization. *Biochem J*, **263**, 201-206.
- 315 Rehnberg, M., Ammitzboll, T. and Tengroth, B. (1987) Collagen distribution in the lamina cribrosa and the trabecular meshwork of the human eye. *Br J Ophthalmol*, **71**, 886-892.
- 316 Medina-Ortiz, W.E., Belmares, R., Neubauer, S., Wordinger, R.J. and Clark, A.F. (2013) Cellular fibronectin expression in human trabecular meshwork and induction by transforming growth factor-beta2. *Invest Ophthalmol Vis Sci*, **54**, 6779-6788.
- 317 Hann, C.R., Springett, M.J., Wang, X. and Johnson, D.H. (2001) Ultrastructural localization of collagen IV, fibronectin, and laminin in the trabecular meshwork of normal and glaucomatous eyes. *Ophthalmic research*, **33**, 314-324.

- 318 Umihira, J., Nagata, S., Nohara, M., Hanai, T., Usuda, N. and Segawa, K. (1994) Localization of elastin in the normal and glaucomatous human trabecular meshwork. *Invest Ophthalmol Vis Sci*, **35**, 486-494.
- 319 Wirtz, M.K., Bradley, J.M., Xu, H., Domreis, J., Nobis, C.A., Truesdale, A.T., Samples, J.R., Van Buskirk, E.M. and Acott, T.S. (1997) Proteoglycan expression by human trabecular meshworks. *Curr Eye Res*, **16**, 412-421.
- 320 Murphy, G., Cockett, M.I., Stephens, P.E., Smith, B.J. and Docherty, A.J. (1987) Stromelysin is an activator of procollagenase. A study with natural and recombinant enzymes. *Biochem J*, **248**, 265-268.
- 321 Lijnen, H.R., Silence, J., Van Hoef, B. and Collen, D. (1998) Stromelysin-1 (MMP-3)-independent gelatinase expression and activation in mice. *Blood*, **91**, 2045-2053.
- 322 Ogata, Y., Enghild, J.J. and Nagase, H. (1992) Matrix metalloproteinase 3 (stromelysin) activates the precursor for the human matrix metalloproteinase 9. *J Biol Chem*, **267**, 3581-3584.
- 323 Rajashekhar, G., Shivanna, M., Kompella, U.B., Wang, Y. and Srinivas, S.P. (2014) Role of MMP-9 in the breakdown of barrier integrity of the corneal endothelium in response to TNF-alpha. *Exp Eye Res*, **122**, 77-85.
- 324 Bogner, B., Boye, S.L., Min, S.H., Peterson, J.J., Ruan, Q., Zhang, Z., Reitsamer, H.A., Hauswirth, W.W. and Boye, S.E. (2015) Capsid Mutated Adeno-Associated Virus Delivered to the Anterior Chamber Results in Efficient Transduction of Trabecular Meshwork in Mouse and Rat. *PLoS One*, **10**, e0128759.
- 325 Dong, B., Nakai, H. and Xiao, W. (2010) Characterization of genome integrity for oversized recombinant AAV vector. *Mol Ther*, **18**, 87-92.
- 326 Gray, S.J., Foti, S.B., Schwartz, J.W., Bachaboina, L., Taylor-Blake, B., Coleman, J., Ehlers, M.D., Zylka, M.J., McCown, T.J. and Samulski, R.J. (2011) Optimizing promoters for recombinant adeno-associated virus-mediated gene expression in the peripheral and central nervous system using self-complementary vectors. *Hum Gene Ther*, **22**, 1143-1153.

- 327 Plotkin, J.B., Robins, H. and Levine, A.J. (2004) Tissue-specific codon usage and the expression of human genes. *Proc Natl Acad Sci U S A*, **101**, 12588-12591.
- 328 Choi, V.W., McCarty, D.M. and Samulski, R.J. (2006) Host cell DNA repair pathways in adeno-associated viral genome processing. *J Virol*, **80**, 10346-10356.
- 329 Wu, Z., Asokan, A. and Samulski, R.J. (2006) Adeno-associated virus serotypes: vector toolkit for human gene therapy. *Mol Ther*, **14**, 316-327.
- 330 Agbandje-McKenna, M. and Kleinschmidt, J. (2011) AAV capsid structure and cell interactions. *Methods Mol Biol*, **807**, 47-92.
- 331 Pillay, S., Meyer, N.L., Puschnik, A.S., Davulcu, O., Diep, J., Ishikawa, Y., Jae, L.T., Wosen, J.E., Nagamine, C.M., Chapman, M.S. *et al.* (2016) An essential receptor for adeno-associated virus infection. *Nature*, **530**, 108-112.
- 332 Mowat, F.M., Gornik, K.R., Dinculescu, A., Boye, S.L., Hauswirth, W.W., Petersen-Jones, S.M. and Bartoe, J.T. (2014) Tyrosine capsid-mutant AAV vectors for gene delivery to the canine retina from a subretinal or intravitreal approach. *Gene Ther*, **21**, 96-105.
- 333 Warrington, K.H., Jr., Gorbatyuk, O.S., Harrison, J.K., Opie, S.R., Zolotukhin, S. and Muzyczka, N. (2004) Adeno-associated virus type 2 VP2 capsid protein is nonessential and can tolerate large peptide insertions at its N terminus. *J Virol*, **78**, 6595-6609.
- 334 Bartel, M.A., Weinstein, J.R. and Schaffer, D.V. (2012) Directed evolution of novel adeno-associated viruses for therapeutic gene delivery. *Gene Ther*, **19**, 694-700.
- 335 Schaffer, D.V. and Maheshri, N. (2004) Directed evolution of AAV mutants for enhanced gene delivery. *Conf Proc IEEE Eng Med Biol Soc*, **5**, 3520-3523.
- 336 Nass, S.A., Mattingly, M.A., Woodcock, D.A., Burnham, B.L., Ardinger, J.A., Osmond, S.E., Frederick, A.M., Scaria, A., Cheng, S.H. and O'Riordan, C.R. (2018) Universal Method for the Purification of Recombinant AAV Vectors of Differing Serotypes. *Mol Ther Methods Clin Dev*, **9**, 33-46.

- 337 Naso, M.F., Tomkowicz, B., Perry, W.L., 3rd and Strohl, W.R. (2017) Adeno-Associated Virus (AAV) as a Vector for Gene Therapy. *BioDrugs*, **31**, 317-334.
- 338 Mays, L.E., Wang, L., Lin, J., Bell, P., Crawford, A., Wherry, E.J. and Wilson, J.M. (2014) AAV8 induces tolerance in murine muscle as a result of poor APC transduction, T cell exhaustion, and minimal MHCI upregulation on target cells. *Mol Ther*, **22**, 28-41.
- 339 Basner-Tschakarjan, E. and Mingozzi, F. (2014) Cell-Mediated Immunity to AAV Vectors, Evolving Concepts and Potential Solutions. *Front Immunol*, **5**, 350.
- 340 Louis Jeune, V., Joergensen, J.A., Hajjar, R.J. and Weber, T. (2013) Pre-existing anti-Adeno-associated virus antibodies as a challenge in AAV gene therapy. *Hum Gene Ther Methods*, **24**, 59-67.
- 341 Stieger, K., Schroeder, J., Provost, N., Mendes-Madeira, A., Belbellaa, B., Le Meur, G., Weber, M., Deschamps, J.Y., Lorenz, B., Moullier, P. *et al.* (2009) Detection of intact rAAV particles up to 6 years after successful gene transfer in the retina of dogs and primates. *Mol Ther*, **17**, 516-523.
- 342 Petit, L., Khanna, H. and Punzo, C. (2016) Advances in Gene Therapy for Diseases of the Eye. *Hum Gene Ther*, **27**, 563-579.
- 343 Russell, S., Bennett, J., Wellman, J.A., Chung, D.C., Yu, Z.F., Tillman, A., Wittes, J., Pappas, J., Elci, O., McCague, S. *et al.* (2017) Efficacy and safety of voretigene neparvovec (AAV2-hRPE65v2) in patients with RPE65-mediated inherited retinal dystrophy: a randomised, controlled, open-label, phase 3 trial. *Lancet*, **390**, 849-860.
- 344 Anni Griswold, S.T. (2017), In *Comprehensive Ophthalmology, Retina/Vitreous* American Academy of Ophthalmology, Vol. 2017.
- 345 Konstas, A.G., Nakos, E., Tersis, I., Lallos, N.A., Leech, J.N. and Stewart, W.C. (2002) A comparison of once-daily morning vs evening dosing of concomitant latanoprost/timolol. *Am J Ophthalmol*, **133**, 753-757.

- 346 Badier-Commander, C., Verbeuren, T., Lebard, C., Michel, J.B. and Jacob, M.P. (2000) Increased TIMP/MMP ratio in varicose veins: a possible explanation for extracellular matrix accumulation. *The Journal of pathology*, **192**, 105-112.
- 347 Lutjen-Drecoll, E., Shimizu, T., Rohrbach, M. and Rohen, J.W. (1986) Quantitative analysis of 'plaque material' between ciliary muscle tips in normal- and glaucomatous eyes. *Exp Eye Res*, **42**, 457-465.
- 348 Rohen, J.W., Lutjen-Drecoll, E., Flugel, C., Meyer, M. and Grierson, I. (1993) Ultrastructure of the trabecular meshwork in untreated cases of primary open-angle glaucoma (POAG). *Exp Eye Res*, **56**, 683-692.
- 349 Parshley, D.E., Bradley, J.M., Fisk, A., Hadaegh, A., Samples, J.R., Van Buskirk, E.M. and Acott, T.S. (1996) Laser trabeculoplasty induces stromelysin expression by trabecular juxtacanalicular cells. *Invest Ophthalmol Vis Sci*, **37**, 795-804.
- 350 Takai, Y., Tanito, M. and Ohira, A. (2012) Multiplex cytokine analysis of aqueous humor in eyes with primary open-angle glaucoma, exfoliation glaucoma, and cataract. *Invest Ophthalmol Vis Sci*, **53**, 241-247.
- 351 Partridge, C.A., Jeffrey, J.J. and Malik, A.B. (1993) A 96-kDa gelatinase induced by TNF-alpha contributes to increased microvascular endothelial permeability. *Am J Physiol*, **265**, 438-447.
- 352 Si-Tayeb, K., Monvoisin, A., Mazzocco, C., Lepreux, S., Decossas, M., Cubel, G., Taras, D., Blanc, J.F., Robinson, D.R. and Rosenbaum, J. (2006) Matrix metalloproteinase 3 is present in the cell nucleus and is involved in apoptosis. *The American journal of pathology*, **169**, 1390-1401.
- 353 Garcia, A.J., Tom, C., Guemes, M., Polanco, G., Mayorga, M.E., Wend, K., Miranda-Carboni, G.A. and Krum, S.A. (2013) ERalpha signaling regulates MMP3 expression to induce FasL cleavage and osteoclast apoptosis. *Journal of bone and mineral research : the official journal of the American Society for Bone and Mineral Research*, **28**, 283-290.

- 354 Bradley, J.M., Kelley, M.J., Rose, A. and Acott, T.S. (2003) Signaling pathways used in trabecular matrix metalloproteinase response to mechanical stretch. *Invest Ophthalmol Vis Sci*, **44**, 5174-5181.
- 355 Gonzalez, P., Epstein, D.L. and Borrás, T. (2000) Genes upregulated in the human trabecular meshwork in response to elevated intraocular pressure. *Invest Ophthalmol Vis Sci*, **41**, 352-361.
- 356 Luna, C., Li, G., Liton, P.B., Epstein, D.L. and Gonzalez, P. (2009) Alterations in gene expression induced by cyclic mechanical stress in trabecular meshwork cells. *Mol Vis*, **15**, 534-544.
- 357 Vittitow, J. and Borrás, T. (2004) Genes expressed in the human trabecular meshwork during pressure-induced homeostatic response. *J Cell Physiol*, **201**, 126-137.
- 358 Lai, L., Lin, K., Foulks, G., Ma, L., Xiao, X. and Chen, K. (2005) Highly efficient ex vivo gene delivery into human corneal endothelial cells by recombinant adeno-associated virus. *Curr Eye Res*, **30**, 213-219.
- 359 Sharma, A., Ghosh, A., Hansen, E.T., Newman, J.M. and Mohan, R.R. (2010) Transduction efficiency of AAV 2/6, 2/8 and 2/9 vectors for delivering genes in human corneal fibroblasts. *Brain Res Bull*, **81**, 273-278.
- 360 Liu, J., Saghizadeh, M., Tuli, S.S., Kramerov, A.A., Lewin, A.S., Bloom, D.C., Hauswirth, W.W., Castro, M.G., Schultz, G.S. and Ljubimov, A.V. (2008) Different tropism of adenoviruses and adeno-associated viruses to corneal cells: implications for corneal gene therapy. *Mol Vis*, **14**, 2087-2096.
- 361 Bourne, W.M., Nelson, L.R. and Hodge, D.O. (1997) Central corneal endothelial cell changes over a ten-year period. *Invest Ophthalmol Vis Sci*, **38**, 779-782.
- 362 Kaufman, H.E., Capella, J.A. and Robbins, J.E. (1966) The human corneal endothelium. *Am J Ophthalmol*, **61**, 835-841.

- 363 Teichmann, J., Valtink, M., Nitschke, M., Gramm, S., Funk, R.H., Engelmann, K. and Werner, C. (2013) Tissue engineering of the corneal endothelium: a review of carrier materials. *Journal of Functional Biomaterials*, **4**, 178-208.
- 364 Borrás, T., Xue, W., Choi, V.W., Bartlett, J.S., Li, G., Samulski, R.J. and Chisolm, S.S. (2006) Mechanisms of AAV transduction in glaucoma-associated human trabecular meshwork cells. *J Gene Med*, **8**, 589-602.
- 365 Wang, L., Xiao, R., Andres-Mateos, E. and Vandenberghe, L.H. (2017) Single stranded adeno-associated virus achieves efficient gene transfer to anterior segment in the mouse eye. *PLoS One*, **12**, e0182473.
- 366 Herschler, J. (1976) Increased intraocular pressure induced by repository corticosteroids. *Am J Ophthalmol*, **82**, 90-93.
- 367 Mandapati, J.S. and Metta, A.K. (2011) Intraocular pressure variation in patients on long-term corticosteroids. *Indian Dermatology Online Journal*, **2**, 67-69.
- 368 Pleyer, U., Ursell, P.G. and Rama, P. (2013) Intraocular pressure effects of common topical steroids for post-cataract inflammation: are they all the same? *Ophthalmology and Therapy*, **2**, 55-72.
- 369 Clark, A.F., Steely, H.T., Dickerson, J.E., Jr., English-Wright, S., Stropki, K., McCartney, M.D., Jacobson, N., Shepard, A.R., Clark, J.I., Matsushima, H. *et al.* (2001) Glucocorticoid induction of the glaucoma gene MYOC in human and monkey trabecular meshwork cells and tissues. *Invest Ophthalmol Vis Sci*, **42**, 1769-1780.
- 370 Crowston, J.G., Aihara, M., Lindsey, J.D. and Weinreb, R.N. (2004) Effect of latanoprost on outflow facility in the mouse. *Invest Ophthalmol Vis Sci*, **45**, 2240-2245.
- 371 Gurney, K.J., Estrada, E.Y. and Rosenberg, G.A. (2006) Blood-brain barrier disruption by stromelysin-1 facilitates neutrophil infiltration in neuroinflammation. *Neurobiol Dis*, **23**, 87-96.

- 372 Johnson, T.V. and Tomarev, S.I. (2010) Rodent models of glaucoma. *Brain Res Bull*, **81**, 349-358.
- 373 Bouhenni, R.A., Dunmire, J., Sewell, A. and Edward, D.P. (2012) Animal models of glaucoma. *J Biomed Biotechnol*, **2012**, 692609.
- 374 Roy Chowdhury, U., Hann, C.R., Stamer, W.D. and Fautsch, M.P. (2015) Aqueous humor outflow: dynamics and disease. *Invest Ophthalmol Vis Sci*, **56**, 2993-3003.
- 375 Fernandes, K.A., Harder, J.M., Williams, P.A., Rausch, R.L., Kiernan, A.E., Nair, K.S., Anderson, M.G., John, S.W., Howell, G.R. and Libby, R.T. (2015) Using genetic mouse models to gain insight into glaucoma: Past results and future possibilities. *Exp Eye Res*, **141**, 42-56.
- 376 Libby, R.T., Anderson, M.G., Pang, I.H., Robinson, Z.H., Savinova, O.V., Cosma, I.M., Snow, A., Wilson, L.A., Smith, R.S., Clark, A.F. *et al.* (2005) Inherited glaucoma in DBA/2J mice: pertinent disease features for studying the neurodegeneration. *Vis Neurosci*, **22**, 637-648.
- 377 Anderson, M.G., Smith, R.S., Hawes, N.L., Zabaleta, A., Chang, B., Wiggs, J.L. and John, S.W. (2002) Mutations in genes encoding melanosomal proteins cause pigmentary glaucoma in DBA/2J mice. *Nat Genet*, **30**, 81-85.
- 378 Aihara, M., Lindsey, J.D. and Weinreb, R.N. (2003) Experimental mouse ocular hypertension: establishment of the model. *Invest Ophthalmol Vis Sci*, **44**, 4314-4320.
- 379 Moreno, M.C., Marcos, H.J., Oscar Croxatto, J., Sande, P.H., Campanelli, J., Jaliffa, C.O., Benozzi, J. and Rosenstein, R.E. (2005) A new experimental model of glaucoma in rats through intracameral injections of hyaluronic acid. *Exp Eye Res*, **81**, 71-80.
- 380 Morrison, J.C., Moore, C.G., Deppmeier, L.M., Gold, B.G., Meshul, C.K. and Johnson, E.C. (1997) A rat model of chronic pressure-induced optic nerve damage. *Exp Eye Res*, **64**, 85-96.
- 381 Shareef, S.R., Garcia-Valenzuela, E., Salierno, A., Walsh, J. and Sharma, S.C. (1995) Chronic ocular hypertension following episcleral venous occlusion in rats. *Exp Eye Res*, **61**, 379-382.

- 382 Jones, R., 3rd and Rhee, D.J. (2006) Corticosteroid-induced ocular hypertension and glaucoma: a brief review and update of the literature. *Curr Opin Ophthalmol*, **17**, 163-167.
- 383 Buchi, E.R. (1992) Cell death in rat retina after pressure-induced ischaemia-reperfusion insult: electron microscopic study. II. Outer nuclear layer. *Jpn J Ophthalmol*, **36**, 62-68.
- 384 Levkovitch-Verbin, H., Harris-Cerruti, C., Groner, Y., Wheeler, L.A., Schwartz, M. and Yoles, E. (2000) RGC death in mice after optic nerve crush injury: oxidative stress and neuroprotection. *Invest Ophthalmol Vis Sci*, **41**, 4169-4174.
- 385 Sun, Q., Ooi, V.E. and Chan, S.O. (2001) N-methyl-D-aspartate-induced excitotoxicity in adult rat retina is antagonized by single systemic injection of MK-801. *Exp Brain Res*, **138**, 37-45.
- 386 Fujimoto, T., Inoue, T., Inoue-Mochita, M. and Tanihara, H. (2016) Live cell imaging of actin dynamics in dexamethasone-treated porcine trabecular meshwork cells. *Exp Eye Res*, **145**, 393-400.
- 387 Yuan, Y., Call, M.K., Yuan, Y., Zhang, Y., Fischesser, K., Liu, C.Y. and Kao, W.W. (2013) Dexamethasone induces cross-linked actin networks in trabecular meshwork cells through noncanonical wnt signaling. *Invest Ophthalmol Vis Sci*, **54**, 6502-6509.
- 388 Underwood, J.L., Murphy, C.G., Chen, J., Franse-Carman, L., Wood, I., Epstein, D.L. and Alvarado, J.A. (1999) Glucocorticoids regulate transendothelial fluid flow resistance and formation of intercellular junctions. *Am J Physiol*, **277**, C330-342.
- 389 Harkness, K.A., Adamson, P., Sussman, J.D., Davies-Jones, G.A., Greenwood, J. and Woodroffe, M.N. (2000) Dexamethasone regulation of matrix metalloproteinase expression in CNS vascular endothelium. *Brain*, **123** (Pt 4), 698-709.
- 390 Yao, J., Yang, W., Liu, Y., Sun, Y.X. and Jiang, Q. (2012) Dexamethasone inhibits TGF-beta2-induced migration of human lens epithelial cells: implications for posterior capsule opacification prevention. *Molecular Medicine Reports*, **5**, 1509-1513.

- 391 Forster, C., Kahles, T., Kietz, S. and Drenckhahn, D. (2007) Dexamethasone induces the expression of metalloproteinase inhibitor TIMP-1 in the murine cerebral vascular endothelial cell line cEND. *J Physiol*, **580**, 937-949.
- 392 Resch, Z.T., Hann, C.R., Cook, K.A. and Fautsch, M.P. (2010) Aqueous humor rapidly stimulates myocilin secretion from human trabecular meshwork cells. *Exp Eye Res*, **91**, 901-908.
- 393 Joe, M.K., Sohn, S., Hur, W., Moon, Y., Choi, Y.R. and Kee, C. (2003) Accumulation of mutant myocilins in ER leads to ER stress and potential cytotoxicity in human trabecular meshwork cells. *Biochem Biophys Res Commun*, **312**, 592-600.
- 394 Kasetti, R.B., Maddineni, P., Millar, J.C., Clark, A.F. and Zode, G.S. (2017) Increased synthesis and deposition of extracellular matrix proteins leads to endoplasmic reticulum stress in the trabecular meshwork. *Sci Rep*, **7**, 14951.
- 395 Gaasterland, D. and Kupfer, C. (1974) Experimental glaucoma in the rhesus monkey. *Invest Ophthalmol*, **13**, 455-457.
- 396 Weber, A.J. and Zelenak, D. (2001) Experimental glaucoma in the primate induced by latex microspheres. *J Neurosci Methods*, **111**, 39-48.
- 397 Ward, K.W., Coon, D.J., Magiera, D., Bhadresa, S., Struharik, M. and Lawrence, M.S. (2009) Exploration of the African green monkey as a preclinical pharmacokinetic model: oral pharmacokinetic parameters and drug-drug interactions. *Xenobiotica*, **39**, 266-272.
- 398 Tuft, S.J. and Coster, D.J. (1990) The corneal endothelium. *Eye (Lond)*, **4 (Pt 3)**, 389-424.
- 399 Joyce, N.C. (2003) Proliferative capacity of the corneal endothelium. *Prog Retin Eye Res*, **22**, 359-389.
- 400 Schwartzkopff, J., Bredow, L., Mahlenbrey, S., Boehringer, D. and Reinhard, T. (2010) Regeneration of corneal endothelium following complete endothelial cell loss in rat keratoplasty. *Mol Vis*, **16**, 2368-2375.

- 401 Fathi, M., Barar, J., Aghanejad, A. and Omid, Y. (2015) Hydrogels for ocular drug delivery and tissue engineering. *Bioimpacts*, **5**, 159-164.
- 402 Hui, A. (2017) Contact lenses for ophthalmic drug delivery. *Clin Exp Optom*, **100**, 494-512.
- 403 Li, G., Gonzalez, P., Camras, L.J., Navarro, I., Qiu, J., Challa, P. and Stamer, W.D. (2013) Optimizing gene transfer to conventional outflow cells in living mouse eyes. *Exp Eye Res*, **109**, 8-16.
- 404 Hanemaaijer, R., Lent, N., Sorsa, T., Salo, T., Kontinen, Y.T. and Lindeman, J. (2001) Mark Nelson, W.H., Robert A. Greenwald (ed.), In *Tetracyclines in Biology, Chemistry and Medicine*. Birkhäuser Basel, Vol. 1, pp. 267.
- 405 Gause, S., Hsu, K.H., Shafor, C., Dixon, P., Powell, K.C. and Chauhan, A. (2016) Mechanistic modeling of ophthalmic drug delivery to the anterior chamber by eye drops and contact lenses. *Adv Colloid Interface Sci*, **233**, 139-154.
- 406 McDonnell, F., O'Brien, C. and Wallace, D. (2014) The role of epigenetics in the fibrotic processes associated with glaucoma. *J Ophthalmol*, **2014**, 750459.
- 407 Aihara, M., Lindsey, J.D. and Weinreb, R.N. (2002) Reduction of intraocular pressure in mouse eyes treated with latanoprost. *Invest Ophthalmol Vis Sci*, **43**, 146-150.
- 408 Ota, T., Murata, H., Sugimoto, E., Aihara, M. and Araie, M. (2005) Prostaglandin analogues and mouse intraocular pressure: effects of tafluprost, latanoprost, travoprost, and unoprostone, considering 24-hour variation. *Invest Ophthalmol Vis Sci*, **46**, 2006-2011.
- 409 Garway-Heath, D.F., Crabb, D.P., Bunce, C., Lascaratos, G., Amalfitano, F., Anand, N., Azuara-Blanco, A., Bourne, R.R., Broadway, D.C., Cunliffe, I.A. *et al.* (2015) Latanoprost for open-angle glaucoma (UKGTS): a randomised, multicentre, placebo-controlled trial. *Lancet*, **385**, 1295-1304.
- 410 Barker, S.E., Broderick, C.A., Robbie, S.J., Duran, Y., Natkunarajah, M., Buch, P., Balaggan, K.S., MacLaren, R.E., Bainbridge, J.W., Smith, A.J. *et al.* (2009) Subretinal delivery

of adeno-associated virus serotype 2 results in minimal immune responses that allow repeat vector administration in immunocompetent mice. *J Gene Med*, **11**, 486-497.

411 Li, Q., Miller, R., Han, P.Y., Pang, J., Dinculescu, A., Chiodo, V. and Hauswirth, W.W. (2008) Intraocular route of AAV2 vector administration defines humoral immune response and therapeutic potential. *Mol Vis*, **14**, 1760-1769.

412 Cone, R.E. and Pais, R. (2009) Anterior Chamber-Associated Immune Deviation (ACAID): An Acute Response to Ocular Insult Protects from Future Immune-Mediated Damage? *Ophthalmol Eye Dis*, **1**, 33-40.

413 Willett, K. and Bennett, J. (2013) Immunology of AAV-Mediated Gene Transfer in the Eye. *Front Immunol*, **4**, 261.

414 Stamer, W.D., Roberts, B.C., Howell, D.N. and Epstein, D.L. (1998) Isolation, culture, and characterization of endothelial cells from Schlemm's canal. *Invest Ophthalmol Vis Sci*, **39**, 1804-1812.

415 Perkumas, K.M. and Stamer, W.D. (2012) Protein markers and differentiation in culture for Schlemm's canal endothelial cells. *Exp Eye Res*, **96**, 82-87.

416 Heimark, R.L., Kaochar, S. and Stamer, W.D. (2002) Human Schlemm's canal cells express the endothelial adherens proteins, VE-cadherin and PECAM-1. *Curr Eye Res*, **25**, 299-308.

417 Stamer, W.D., Seftor, R.E., Williams, S.K., Samaha, H.A. and Snyder, R.W. (1995) Isolation and culture of human trabecular meshwork cells by extracellular matrix digestion. *Curr Eye Res*, **14**, 611-617.

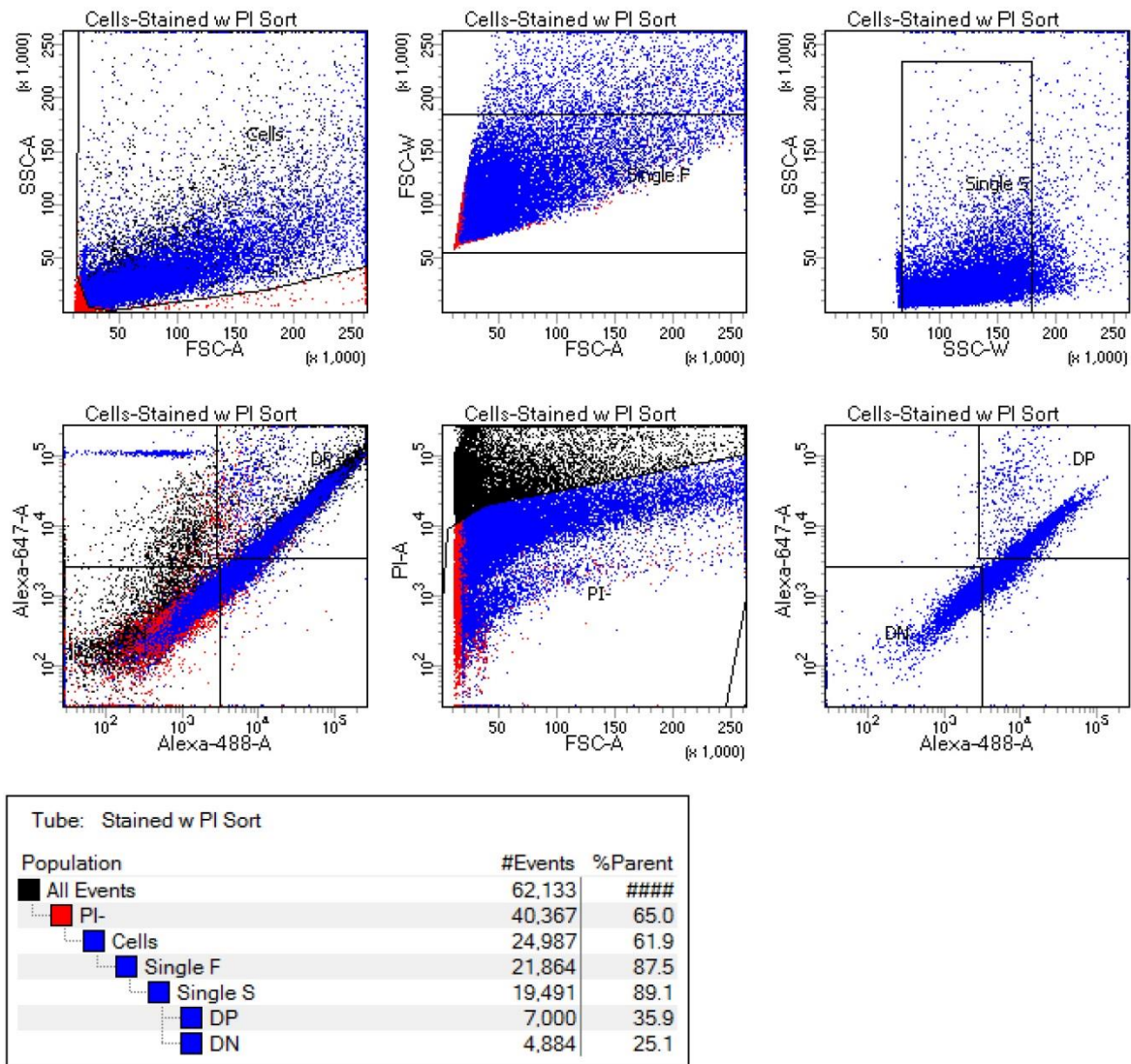
418 Stamer, W.D., Seftor, R.E., Snyder, R.W. and Regan, J.W. (1995) Cultured human trabecular meshwork cells express aquaporin-1 water channels. *Curr Eye Res*, **14**, 1095-1100.

419 Stamer, W.D., Huang, Y., Seftor, R.E., Svensson, S.S., Snyder, R.W. and Regan, J.W. (1996) Cultured human trabecular meshwork cells express functional alpha 2A adrenergic receptors. *Invest Ophthalmol Vis Sci*, **37**, 2426-2433.

- 420 Stamer, W.D. and Clark, A.F. (2017) The many faces of the trabecular meshwork cell. *Exp Eye Res*, **158**, 112-123.
- 421 Wallace, D.M., Clark, A.F., Lipson, K.E., Andrews, D., Crean, J.K. and O'Brien, C.J. (2013) Anti-connective tissue growth factor antibody treatment reduces extracellular matrix production in trabecular meshwork and lamina cribrosa cells. *Invest Ophthalmol Vis Sci*, **54**, 7836-7848.
- 422 Kohlbrenner, E., Henckaerts, E., Rapti, K., Gordon, R.E., Linden, R.M., Hajjar, R.J. and Weber, T. (2012) Quantification of AAV particle titers by infrared fluorescence scanning of coomassie-stained sodium dodecyl sulfate-polyacrylamide gels. *Hum Gene Ther Methods*, **23**, 198-203.

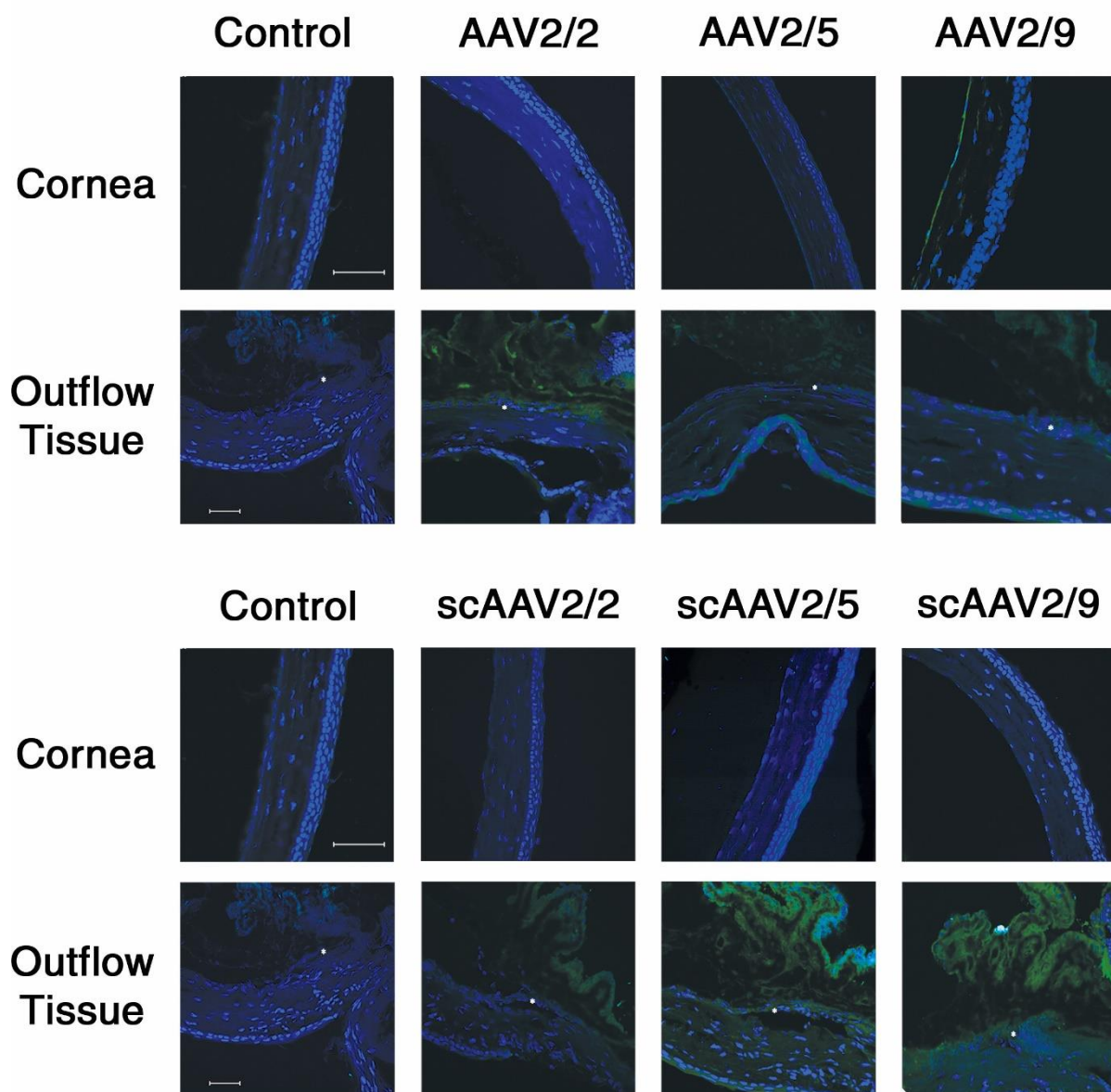
Appendix

Appendix 1: Supplementary Figures



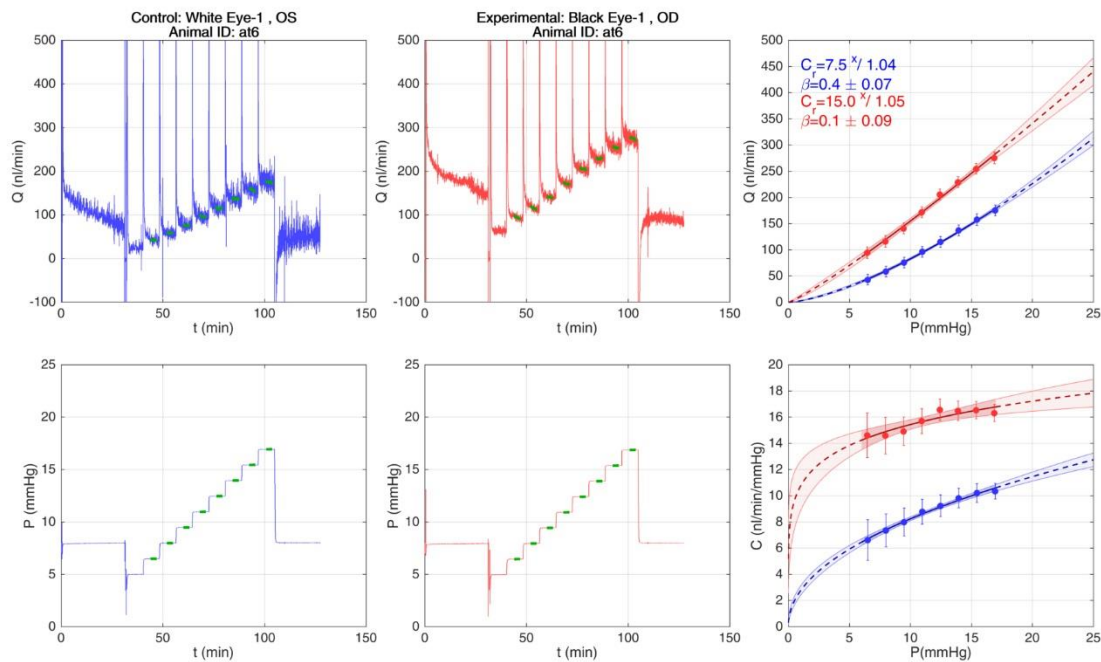
Supplementary Figure 1: Fluorescent-activated cell sorting of the mouse cornea

Gating strategy used in the attempt to isolate mouse Schlemm's canal cells from anterior segment dissections. Whole, live, single cells were isolated and observed for CD-31 and VEGF-R3 positive staining.



Supplementary Figure 2: Transfection of the anterior chamber with multiple AAVs.

AAV's of different serotype and strandedness were injected into the anterior chamber. Both the cornea and outflow tissues (asterisk) were examined for GFP expression. Interestingly, little to no expression was observed in the outflow tissues, and only autofluorescence was observed around the ciliary. Only single stranded AAV2/9 showed expression in the cornea, which was exclusive to the endothelial layer. Injections and staining were performed by Darragh Crosbie.



Supplementary Figure 3: Sample flow/pressure traces

Representative flow (Q), pressure (P) and facility (C) plots of a pair of contralateral eyes generated from MATLAB analysis as part of the iPerfusion system. Blue traces correspond to the control eye, and red traces correspond to the treated eye. When flow and pressure are plotted against each other, or when pressure and facility are plotted against each other (right column), it can be seen that the treated eye (red) has a higher flow and hence facility at each pressure step. A raw facility value is taken from the interpolation of C (bottom right) against a P of 8 mmHg, which is an approximation of the pressure drop across the Schlemm's canal in mice. This facility value is then weighted against system and biological uncertainties in statistical and paired analysis.

Appendix 2: MATLAB code for IOP analysis.

Import and process raw IOP data from excel

```
clear;clc;close all;
```

Import the data

```
[~, txt, raw] =  
xlsread('C:\Users\ocallaje\Desktop\Experiments  
\MYOC mice\MYOC.Induc.MMP3\MYOCmmp IOP  
interp_adjust.xlsx','Raw IOP','A1:CJ120');  
raw(cellfun(@(x) ~isempty(x) && isnumeric(x) &&  
isnan(x),raw)) = {''}; R = cellfun(@(x) ~isnumeric(x)  
&& ~islogical(x),raw); %Find non-  
numeric cells raw(R) = {NaN};  
%Replace non-numeric cells rawiopdata =  
reshape([raw{:}],size(raw));  
%Create output variable clearvars raw R;  
%clear temporary variables
```

Test for Outliers

```
%Does not account for values that could be outliers  
in one timepoint, but not in another dataVECTOR =  
rawiopdata;  
%Replicate vector for replacement  
dataVECTOR(:, [7:7:end,18:14:end])=NaN;  
%Replace timepoint and weight columns with NaN  
dataVECTOR(15,:)=NaN;  
%Replace reading number row with Nan outlierrowIOP =  
zeros(size(rawiopdata));  
%Initialise matrix for post outlier data  
hampelVECTOR=dataVECTOR;  
%Replicate vector for filtering  
hampelVECTOR=hampelVECTOR(:);  
%Convert to Column Vector  
  
hampelVECTOR(isnan(hampelVECTOR))=[];  
%Remove NaN's hampelx = 1:numel(hampelVECTOR);  
%Generate X axis for hampel filter  
  
[YY, I, Y0, LB, UB, ADX, NO] =  
hampel(hampelx,hampelVECTOR,numel(hampelVECTOR),4);  
%Perform Hampel filtering. Half-width of filter window  
should include all elements of data (the reason it  
%doesn't account for timepoint-dependant outliers).  
Threshold value of 4 means a value is an outlier if  
its  
%more than 4sigma from the median of data. figure(1)  
set(figure(1), 'Position', [100,350,1450,400])  
subplot(1,3,2) plot(hampelx,hampelVECTOR, 'b.');
```

```

on; %Plot Original
Data in blue plot(hampelx,hampelVECTOR, 'r');
%Plot Hampel Filtered Data in red
plot(hampelx(I), hampelVECTOR(I), 'ks');
%Plot Identified Outliers as boxes ylabel('Raw
IOP') xlabel('IOP Index') title('Filtered data')

outliers = hampelVECTOR(I);
%Vector containing Outliers

for e = 1:numel(dataVECTOR)
%For each element in matrix
if ismember(dataVECTOR(e),outliers) == 1
%If element equals outlier determined by HAMPEL
outlierrawIOP(e) = nanmedian(hampelVECTOR);
%Replace it with the data median
else outlierrawIOP(e) = dataVECTOR(e);
%Otherwise leave it as the original value
end end

noOUTLIERrawIOP = outlierrawIOP;
%Replicate outlier-replaced vector for re-inserting timepoint/
weight numericals
noOUTLIERrawIOP(:, [7:7:end,18:14:end])=rawiopdata(:,
[7:7:end,18:14:end]);
%Put back timepoints and weights
noOUTLIERrawIOP(15,:)=rawiopdata(15,:);
%Put back reading number row

```

Test for Normality

```

normVECTOR = rawiopdata;

normVECTOR(:, [7:7:end,18:14:end])=NaN;
%Replace timepoint and weight columns with NaN
normVECTOR(15,:)=NaN;
%Replace reading number row with Nan
normVECTOR(isnan(normVECTOR))=[];
%Remove non-numerical data from imported matrix (also
converts to a vector)
normVECTOR = normVECTOR(:);
%Convert to column vector
outlierrawIOP(isnan(normVECTOR))=[];
%Remove non-numerical data from imported matrix (also
converts to a vector)
outlierrawIOP = outlierrawIOP(:);
%Convert to column vector

[H1, Hp1] = swtest(normVECTOR, 0.05);
%Calls the Shapiro Wilks test function (saved in
the IOP folder)
[H2, Hp2] = swtest(outlierrawIOP, 0.05);
%Calls the Shapiro Wilks test function for outlier-
removed data

if H1 == 0
disp('Normal Distribution Detected')

```

```

subplot(1,3,1)      probplot(normVECTOR)
title('Raw Distribution')      x1 = max(normVECTOR)/2;
text(x1,-3,'Normal Distribution') else
disp('Non-Parametric Distribution Detected')
subplot(1,3,1)      probplot(normVECTOR)
title('Raw Distribution')      x1 = max(normVECTOR)/2;
text(x1,-3,'Non-Parametric Distribution') end

fprintf('Number of Outliers Detected = %i.\n',NO)
%Display number of outliers detected
disp('Removing Outliers...')
%Display "Removing Outliers..." in the command window

if H2 == 0
disp('Normal Distribution Detected After Outlier
Removal')
disp('Calculating Central Tendency of Tonometry
measurements from the mean')
subplot(1,3,3)      probplot(outlierrawIOP)
title('Outlier-Filtered Distribution')
x1 = max(outlierrawIOP)/1.7;
text(x1,-3,'Normal Distribution') else
disp('Non-Parametric Distribution Detected After
Outlier Removal')
disp('Calculating Central Tendency of Tonometry
measurements from the median')
      subplot(1,3,3)
probplot(outlierrawIOP)
title('Outlier-Filtered
Distribution')      x1 =
max(outlierrawIOP)/1.7;
text(x1,-3,'Non-Parametric
Distribution') end

```

Extract IOP data of each eye

```

IOPTimepoints = 8;
      %No. of IOP Timepoints
IOPanimals = 27;
      %No. of animals in timecourse

for i = 1:(IOPTimepoints),      for ii =
4:(IOPanimals)+3,      rawIOPmatrix{ii+1} =
noOUTLIERrawIOP(ii*4:ii*4+2,i*7:i*7+3);
%save each raw iop matrix into a cell array
newrawIOPmatrix =rawIOPmatrix(~cellfun('isempty',
rawIOPmatrix)); %remove empty cells in first level
all_IOP_Timepoints{1,i} = newrawIOPmatrix(:);      end
end

```

Interpolation

```

for x=1:length(all_IOP_Timepoints)
%each timepoint iteration for
n=1:cellfun('length', all_IOP_Timepoints) %each
mouse iteration a =
all_IOP_Timepoints{1,x}{n}; %Multi-
level indexing to retrieve an individual IOP matrix
from the timepoint cell within the all_IOP_Timepoint
cell %disp(a)
%remove comment to show each IOP matrix
IOptime = transpose(a(:,1));
%extract timepoints from IOP matrix

    if H1 == 0
average = nanmean(transpose(a(:,2:4)));
%average tonometer measurements using means if
data follows a normal distribution. Excludes NaN
values.
    else
average = nanmedian(transpose(a(:,2:4))); %middle
tonometer measurements using medians if data does not
follow a normal distribution. Excludes NaN values.
    end

    p = polyfit(IOptime, average, 1);
%compute linear regression (x, y, nth degree(1 for
linear)). Outputs a slope and intercept. xi
= 5; %Value
to interpolate from

    yfit = polyval(p, IOptime);
%line of fit from linear regression and x values
IOPEye=interp1(IOptime, yfit, xi, 'linear');
%Interpolate

    interpolatedeyes{1,x}{n,1} = IOPEye(:);
%Put each iteration of IOPEye into multi-level
array for each mouse and timepoint.

    if n==0
%Change value to display plot for specific mouse
iteration. Remove "if" statement to plot all
plot(IOptime, average)
hold on
plot(xi, IOPEye, '*')
plot(IOptime, yfit)
xlabel('Time (Minutes)')
ylabel('IOP (mmHg)')
axis([3, 8, 9, 18])
hold off pause(0.2)
disp(IOPEye); end end
letters = char(x+64);
%Convert the top level (timepoint) iteration into an
ASCII letter i.e. an excel column
%xlswrite('C:\Users\ocallaje\Desktop\Experiments
\Inducible_DOX\DexiMMP3\DM experiment outline
+macros.xlsm',interpolatedeyes{1,x},'IOP Matlab
Write',[letters num2str(3)]) end

```

```

interp_OUT=cell2mat(cellfun(@(x) cell2mat(x),
interpolatedeyes, 'un', 0)); %convert array to a
matrix for analysis

```

Extract weights

```

weightCOL = 18;

for wc = 1:(IOPtimepoints)-2, for wr =
4:(IOPanimals)+3, weightdata{wr+1} =
rawiopdata(wr*4,wc*14+4); %save each timepoint
weight into a cell array newweights
=weightdata(~cellfun('isempty', weightdata));
%remove empty cells in first level
all_weights{1,wc} = newweights(:); end end

weight_OUT=cell2mat(cellfun(@(x) cell2mat(x),
all_weights, 'un', 0));
%convert array to matrix

```

Extract names

```

[~, ~, txt] =
xlsread('C:\Users\ocallaje\Desktop\Experiments\MYOC
mice \MYOC.Induc.MMP3\MYOCmmp IOP
interp_adjust.xlsx', 'Raw IOP', 'F1:F144');
txt(cellfun(@(x) ~isempty(x) && isnumeric(x) &&
isnan(x),txt)) = {''}; cellVectors = txt(:,1);
%extract the column of interest containing names
namesCOL = cellVectors(:,1); clearvars raw cellVectors;
namedata = namesCOL(~cellfun('isempty', namesCOL));
%remove empty cells names_OUT= char(namedata);
%convert cells to character strings

```

Temperatures

```

%{

[~, txt, rawtemp] = xlsread('C:\Users\Jeff
Laptop\Documents\PhD work \MYOCmmp IOP
interp.xlsx', 'Room 2 Temps', 'A1:L200');
rawtemp(cellfun(@(x) ~isempty(x) && isnumeric(x) &&
isnan(x),rawtemp)) = {''};
R = cellfun(@(x) ~isnumeric(x) &&
~islogical(x),rawtemp);
%Find non-numeric cells rawtemp(R) =
{NaN};
%Replace non-numeric cells rawtempdata =
reshape([rawtemp{:}],size(rawtemp));
%Create output variable clearvars rawtemp
R;
%clear temporary variables

for t=1:12 tempdatamax{t} =
rawtempdata(t*8,5:11);

```

```

tempdatamin{t} =
rawtempdata((t*8)+1,5:11); end

tempmax_OUT=cell2mat(
tempdatamax);
tempmin_OUT=cell2mat(
tempdatamin); %}

```

Save data and figures

```

saveas (figure(1), 'C:\Users\ocallaje\Desktop\Experiment
s\MYOC mice \MYOC.Induc.MMP3\MATLAB IOP
exports\Dist.png')

clearvars -
except tempmax_OUT tempmin_OUT names_OUT weight_OUT interp_OUT
IOPanimals IOtimepo

```

Published with MATLAB® R2016a

IOP Analysis

```
close all;
```

EXCLUSIONS

Exclude 1 (Mouse 7.4)- bad IOP readings from the start

Compile treatment groups

```

%Positive Group
%Treated
TreatedOS = interp_OUT([3,4,8,11,14,16,18,19,20,26],[1:2:end]);
%eyes treated OS
TreatedOD =
interp_OUT([5,9,12,15,17,27],[2:2:end]);
%ex 25 %eyes treated OD
PosTreated_eyes = [TreatedOS;TreatedOD];
%Control
ControlOD = interp_OUT([3,4,8,11,14,16,18,19,20,26],[2:2:end]);
ControlOS =
interp_OUT([5,9,12,15,17,27],[1:2:end]);
PosControl_eyes = [ControlOD;ControlOS];

%Negative Group
%Treated
TreatedOS =
interp_OUT([7,13,21,24],[1:2:end]);
% ex 13

```

```

TreatedOD =
interp_OUT([1,2,6,10,22,23],[2:2:end]);
    %ex 1
NegTreated_eyes = [TreatedOS;TreatedOD];
    %Control
ControlOD =
interp_OUT([7,13,21,24],[2:2:end]);
ControlOS =
interp_OUT([1,2,6,10,22,23],[1:2:end]);
    %ex 1
NegControl_eyes = [ControlOD;ControlOS];

POS_Average =
[nanmean(PosTreated_eyes);nanmean(PosControl_eyes)]'
; NEG_Average =
[nanmean(NegTreated_eyes);nanmean(NegControl_eyes)]'
; xaxis1=(1:4)'; xaxis2=(1.12:1:4.12)';

```

Plot each animal

```

%{ figure(6) pte = 7; Labels1 = {'', 'Pre-Injection',
'Pre-Induction', 'Eye drops 1WK', 'Eye drops 2WK'};

set(figure(6), 'Position',
[800,200,400,400]) plot(xaxis1,
PosTreated_eyes(pte,:)) hold on
plot(xaxis2, PosControl_eyes(pte,:))
axis([0,5,7,20])
set(gca,'XTickLabel',Labels1)
set(gca,'XTickLabelRotation',45)
ylabel('IOP(mmHg)') legend('show')
legend({'AAV-iMMP-3','AAV-iGFP'},
'Location','northwest') title('MYOC (+)')
%}

```

Overdose Detection

```

%{ namenumbers =
[1:IOPanimals];
newnamenumbers =
zeros(1,IOPanimals);
weight_OUT(isnan(weight_
OUT)) = 0; for i
=1:IOPanimals
newnamenumbers(i) =
namenumbers(i); for
j =2:IOPtimepoints
if weight_OUT(i,j) < 0.9*weight_OUT(i,j-1) &
weight_OUT(i,j) <0.8*weight_OUT(i,1)
fprintf('Overdose in DEXM%i.\n',namenumbers(i))
newnamenumbers(i)=[]; else end end
end newnamenumbers =
newnamenumbers(newnamenumbers~=0)'; %}

```

Temperature Fluctuation


```

%{ alltemp =
vertcat(tempmax_OUT,tempmin_
OUT); tempaverage =
nanmean(alltemp);
templabels={'Dec 26th', 'Jan
2nd', 'Jan 9th', 'Jan 16th',
'Jan 23rd',
'Injection','Light cycle
fixed', 'Implantation', 'DEX
Week 1', 'DEX Week 2', 'DEX
Week 3', 'DEX Week 4'};

figure(6) plot(tempmax_OUT,'Color',[ 0.8 0 0]) hold on
plot(tempmin_OUT,'Color',[ 0 0 0.8])
plot(tempaverage,'Color',[0 0.8 0])
set(gca,'xtick',7:7:length(tempmax_OUT))
set(gca,'XTickLabel',templabels,
'XTickLabelRotation',45) legend('Temp Max', 'Temp
min', 'Temp Average', 'Location', 'northwest')
saveas(figure(6),'C:\Users\ocallaje\Desktop\Experiment
s\Inducible_DOX \DexiMMP3\IOP_temps.png')
%}

```

Non-Responder Detection

```

%{
orderanimals = [1,2,3,10,11,12,13,14,4,5,6,7,8,9,15];
QPplotpath
='C:\Users\ocallaje\Desktop\Experiments\ExVivo
Perfusions
\Jeff\Figures\Processing\Dex_all_eyes';
QPsavepath
='C:\Users\ocallaje\Desktop\Experiments\Inducible_DOX
\DexiMMP3';
Files =
{'Mouse_01','Mouse_02','Mouse_03','Mouse_04','Mouse_05','Mouse_06','
Mouse_07','Mou
load('C:\Users\ocallaje\Desktop\Experiments\ExVivo
Perfusions\MATLAB FACILITY VARIABLES\EyeFacilities\Dex_all_eyes');
Dex_all_eyesC = unweightedFacilities; clear unweightedFacilities
load('C:\Users\ocallaje\Desktop\Experiments\ExVivo
Perfusions\MATLAB FACILITY
VARIABLES\EyeFacilities\Dex_iMMP_Paired');
Dex_iMMP_PairedC = unweightedFacilities; clear
unweightedFacilities
load('C:\Users\ocallaje\Desktop\Experiments\ExVivo
Perfusions\MATLAB FACILITY
VARIABLES\EyeFacilities\NODEX_Paired'); NODEX_PairedC
= unweightedFacilities; clear unweightedFacilities
load('C:\Users\ocallaje\Desktop\Experiments\ExVivo
Perfusions\MATLAB FACILITY
VARIABLES\EyeFacilities\WT_iMMP_Paired');
WT_iMMP_PairedC = unweightedFacilities; clear
unweightedFacilities

Dex_all_eyesC(2,:) = NaN;
%Excluded pre-analysis, flow too high
Dex_all_eyesC(3,:) = NaN;

```

```

        %Excluded pre-analysis, flow too high
[~, ~, lower1, upper1,m1]
=confint(Dex_all_eyesC(:,1));
[~, ~, lower2, upper2,m2]
=confint(Dex_iMMP_PairedC(:,1));
[~, ~, lower3, upper3,m3]
=confint(NODEX_PairedC(:,1));
[~, uci, lower4, upper4,m4]
=confint(WT_iMMP_PairedC(:,1));
WTerror = m4+(1.5)*uci;

for i=1:IOptimepoints      if
PosControl_eyes(i,6)<PosControl_eyes(i,1)
% If animal is non-responder      fprintf('Non Responder
Detected in IOP of DEXM%i. \n',orderanimals(i))% Print the case in
the command window

        [~, idx] = ismember(orderanimals(i),
newnamenumbers);      % Cross reference order
of animals from OS/OD structure to order  of animals
perfused

        QPpath = fullfile(QPplotpath,Files{idx});
% Compile QP filepath of the non-responder
h = openfig(QPpath);
% Open the QP plot

        Labels3 = {'DEX Week 1', 'DEX Week 2', 'DEX
Week 3', 'DEX Week 4'};      subplot(2,3,4)
plot(PosControl_eyes(i,3:6), 'Color',[0 0 0.8])
ylabel('IOP(mmHg)')
set(gca,'XTickLabel',Labels3)
set(gca,'XTickLabelRotation',45)
hold on      xaxis = 3:6;      l =
polyfit(xaxis,PosControl_eyes(i,3:6),1);
ifit = polyval(l, xaxis);
plot(ifit,'Color',[ 0 0.8 0])

        subplot(2,3,5)
plot(PosTreated_eyes(i,3:6),'Color',[
0.8 0 0])      ylabel('IOP(mmHg)')
set(gca,'XTickLabel',Labels3)
set(gca,'XTickLabelRotation',45)
hold on      xaxis = 3:6;
l =
polyfit(xaxis,PosTreated_eyes(i,3:6),
1);      ifit = polyval(l, xaxis);
plot(ifit,'Color',[ 0 0.8 0])

        QPsavefolder = strcat(num2str(idx), '.png');
QPsave =
fullfile(QPsavepath,'nonresponders',QPsavefolder);
saveas(figure(1 ), QPsave);

        facilitycontrol = Dex_all_eyesC(idx,1);
facilitytreated = Dex_all_eyesC(idx,2);

```

```

        if facilitycontrol > upper1 &&
facilitycontrol > lower4 && facilitycontrol <
WTErrror          fprintf('Non Responder Detected
in Facility of DEXM%i.
\n',orderanimals(i))
            PosTreated_eyes(i,:)=NaN;
            % Exclude animal from further analysis
PosControl_eyes(i,:)=NaN;

        end
    close
end
end
end
%}

```

Generate Confidence Intervals

```

[CIDEXMMPn, CIDEXMMPp] =
confint(PosTreated_eyes);
[CIDEXGFPn, CIDEXGFPp] =
confint(PosControl_eyes);
[CIcycMMPn, CIcycMMPp] =
confint(NegTreated_eyes);
[CIcycGFPn, CIcycGFPp] =
confint(NegControl_eyes);

```

Plot IOP over time

```

figure(7)

Labels1 = {'', 'Pre-Injection', 'Pre-Induction', 'Eye drops
1WK', 'Eye drops 2WK'};

set(figure(7), 'Position', [100,60,1050,400])
subplot(1,2,1) errorbar(xaxis1,
(nanmean(PosTreated_eyes)), CIDEXMMPn, CIDEXMMPp)
hold on errorbar(xaxis2,
(nanmean(PosControl_eyes)), CIDEXGFPn, CIDEXGFPp)
axis([0,5,11,17]) set(gca,'XTickLabel',Labels1)
set(gca,'XTickLabelRotation',45)
ylabel('IOP(mmHg)') legend('show') legend({'AAV-
iMMP-3','AAV-iGFP'}, 'Location', 'northwest')
title('MYOC (+)')

subplot(1,2,2) errorbar(xaxis1,
(nanmean(NegTreated_eyes)), CIDEXMMPn, CIDEXMMPp)
hold on errorbar(xaxis2,
(nanmean(NegControl_eyes)), CIDEXGFPn, CIDEXGFPp)
axis([0,5,11,17]) set(gca,'XTickLabel',Labels1)
set(gca,'XTickLabelRotation',45)
ylabel('IOP(mmHg)') legend('show') legend({'AAV-
iMMP-3','AAV-iGFP'}, 'Location', 'northwest')
title('MYOC (-)')

saveas(figure(7), 'C:\Users\ocallaje\Desktop\Experiments\MYOC mice

```

```
\MYOC.Induc.MMP3\MATLAB IOP exports\IOP_time.png')
```

Plot IOP Changes

```
pos_wk1 =
[PosTreated_eyes(:,1),PosControl_eyes(:,
1)]; pos_wk4 =
[PosTreated_eyes(:,4),PosControl_eyes(:,
4)]; POS_IOPchange = pos_wk4-pos_wk1;

neg_wk1 =
[NegTreated_eyes(:,1),NegControl_eyes(:,
1)]; neg_wk4 =
[NegTreated_eyes(:,4),NegControl_eyes(:,
4)]; NEG_IOPchange = neg_wk4-neg_wk1;

Labels2 = {'AAV-iMMP-3', 'AAV-iGFP'};
W=0.5;
% Column half width
w=1.3; f8 = figure(8);
subplot(1,2,1) plot([0
1.8],[0
0], 'color',0.5*[1 1 1])
% plot zero line hold
all col={[0 0 1],[1 0
0]};
% base colour in RGB

for i=1:2
    z=POS_IOPchange(:,i);
    PRC=prctile(z,[5 25 50 75 95]);
    n=numel(z);

    x=linspace(i-0.5-W*w/2,i-
0.5+W*w/2,n);
% Define zx positions for scatter
    Order=SortBell(z,nanmedian(z));
% Calculate order, moving outfrom centre
    zo=z(Order);
% Reorder    x0=i-0.5;
% calculate LHS
    X=[x0-w/3.5 x0+w/3.5] ;
    % X value for box
    X2=[x0-w/6 x0+w/6] ;
% X for errorbar

    a=patch([X(1) X(1) X(2) X(2)], [PRC(2) PRC(4) PRC(4)
PRC(2)], col{i}); % plot 25/75 prctile box
    set(a, 'facealpha',0.15, 'edgecolor','k')
% make transparent
    plot(X2,PRC(1)*[1 1], 'color','k')
% lower EB
    plot(X2,PRC(5)*[1 1], 'color','k')
% upper EB
    plot(x0*[1 1],PRC([1 2]), 'k')
% connect lower EB    plot(x0*[1 1],PRC([4 5]), 'k')
    % Connect upper EB
    %plot(X,
```

```

[nanmean(DEX_IOPchange(:,i)),nanmean(DEX_IOPchange(:,i))],'color',0.
7*col{i},'linewidth' % plot midline      plot(X,PRC(3)*[1
1],'color',0.7*col{i},'linewidth',1.5)
plot(x,zo,'o','color',0.5*col{i},'markerfacecolor',0.8*col{i})
% plot data points end

set(gca,'fontsize',13.3) axis([0 2 -5 9])
% axis limits([lower-x upper-x lower-y upper-y])
h=my_xticklabels(gca,[0.5 1.5],Labels2);
set(h,'fontsize',13.3,'linewidth',0.75)
set(gca,'ytick', [-4 -2 0 2 4 6 8])
% y axis scale numbers (can enter each one ex. [0 2 4
6 8 10]) ylabel('Change in IOP (mmHg)', 'color', [0 0
0]) title('MYOC (+)')

W=0.5;
% Column half
width w=1.3;

subplot(1,2,2) plot([0
1.8],[0
0],'color',0.5*[1 1 1])
% plot zero line hold
all col={ [0 0 1],[1 0
0]};
% base colour in RGB for
i=1:2
    z=NEG_IOPchange(:,i);
    PRC=prctile(z,[5 25 50 75
95]);    n=numel(z);

    x=linspace(i-0.5-W*w/2,i-
0.5+W*w/2,n);
% Define zx positions for scatter
    Order=SortBell(z,nanmedian(z));
% Calculate order, moving outfrom centre

zo=z(Orde
r);
% Reorder
x0=i-0.5;
%
calculate
LHS
    X=[x0-w/3.5 x0+w/3.5] ;
    % X value for box
    X2=[x0-w/6 x0+w/6] ;
% X for errorbar

    a=patch([X(1) X(1) X(2)
X(2)], [PRC(2) PRC(4) PRC(4)
PRC(2)],col{i});    % plot 25/75 prctile
box
set(a,'facealpha',0.15,'edgecolor','k')
% make transparent      plot(X2,PRC(1)*[1
1],'color','k')

```

```

        % lower EB
        plot(X2,PRC(5)*[1 1], 'color','k')
% upper EB      plot(x0*[1 1],PRC([1 2]), 'k')
% connect lower EB      plot(x0*[1 1],PRC([4
5]), 'k')
% Connect upper EB      plot(X,PRC(3)*[1
1], 'color',0.7*col{i}, 'linewidth',1.5)
plot(x,zo, 'o', 'color',0.5*col{i}, 'markerfacecolor',
0.8*col{i})          % plot data points end

set(f8, 'position', [100 400 1000 370], 'color', 'w')
set(gca, 'fontsize',13.3) axis([0 2 -5 9])
% axis limits([lower-x upper-x lower-y upper-y])
h=my_xticklabels(gca, [0.5 1.5],Labels2);
set(h, 'fontsize',13.3, 'linewidth',0.75)
set(gca, 'ytick', [-4 -2 0 2 4 6 8])
% y axis scale numbers (can enter each one ex. [0 2 4
6 8 10]) ylabel('Change in IOP (mmHg)', 'color', [0 0
0]) title('MYOC (-)')

saveas (figure(8), 'C:\Users\ocallaje\Desktop\Experiments\MYOC mice
\MYOC.Induc.MMP3\MATLAB IOP exports\IOP_change.png')

```

Plot Final IOP

```

f9 = figure(9); subplot(1,2,1)
%Positive group plot([0 1.8],[0 0], 'color',0.5*[1
1 1])          % plot
zero line hold all
% base colour in RGB for i=1:2
z=pos_wk4(:,i);      PRC=prctile(z,[5 25 50 75
95]);      n=numel(z);

      x=linspace(i-0.5-W*w/2,i-
0.5+W*w/2,n);
% Define zx positions for scatter

Order=SortBell(z,nanmedian(z));
% Calculate order, moving
outfrom centre      zo=z(Order);
% Reorder      x0=i-0.5;
% calculate LHS
      X=[x0-w/3.5 x0+w/3.5] ;
      % X value for box
      X2=[x0-w/6 x0+w/6] ;
      % X for errorbar
      a=patch([X(1) X(1) X(2)
X(2)], [PRC(2) PRC(4) PRC(4)
PRC(2)], col{i}); % plot 25/75 prctile
box
set(a, 'facealpha',0.15, 'edgecolor', 'k')
% make transparent      plot(X2,PRC(1)*[1
1], 'color', 'k')
% lower EB      plot(X2,PRC(5)*[1
1], 'color', 'k')
% upper EB      plot(x0*[1 1],PRC([1

```

```

2]), 'k')
% connect lower EB      plot(x0*[1
1],PRC([4 5]), 'k')
% Connect upper EB
    %plot(X,
[nanmean(DEX_IOPchange(:,i)),nanmean(DEX_IOPchange(:,i))], 'color',0.
7*col{i}, 'linewidth' % plot midline      plot(X,PRC(3)*[1
1], 'color',0.7*col{i}, 'linewidth',1.5)
plot(x,zo, 'o', 'color',0.5*col{i}, 'markerfacecolor',0.8*col{i})
% plot data points end

set(gca, 'fontsize',13.3) axis([0 2 10 20])
% axis limits([lower-x upper-x lower-y upper-y])
h=my_xticklabels(gca,[0.5 1.5],Labels2);
set(h, 'fontsize',13.3, 'linewidth',0.75)
set(gca, 'ytick', [10 12 14 16 18 20])
% y axis scale numbers (can enter each one ex. [0 2 4 6
8 10]) ylabel('Final IOP (mmHg)', 'color', [0 0 0])
title('MYOC (+)')

subplot(1,2,2)
%Negative group plot([0 1.8],[0 0], 'color',0.5*[1
1 1]) % plot
zero line hold all
% base colour in RGB for i=1:2
z=neg_wk4(:,i);      PRC=prctile(z,[5 25 50 75
95]);      n=numel(z);

    x=linspace(i-0.5-W*w/2,i-
0.5+W*w/2,n);
% Define zx positions for scatter

Order=SortBell(z,nanmedian(z));
% Calculate order, moving
outfrom centre      zo=z(Order);
% Reorder      x0=i-0.5;
% calculate LHS
    X=[x0-w/3.5 x0+w/3.5] ;
    % X value for box
    X2=[x0-w/6 x0+w/6] ;
    % X for errorbar
    a=patch([X(1) X(1) X(2)
X(2)], [PRC(2) PRC(4) PRC(4)
PRC(2)],col{i}); % plot 25/75 prctile
box
set(a, 'facealpha',0.15, 'edgecolor', 'k')
% make transparent      plot(X2,PRC(1)*[1
1], 'color', 'k')
% lower EB      plot(X2,PRC(5)*[1
1], 'color', 'k')
% upper EB      plot(x0*[1 1],PRC([1
2]), 'k')
% connect lower EB      plot(x0*[1
1],PRC([4 5]), 'k')
% Connect upper EB
    %plot(X,

```

```

[nanmean(DEX_IOPchange(:,i)),nanmean(DEX_IOPchange(:,i))],'color',0.
7*col{i},'linewidth' % plot midline plot(X,PRC(3)*[1
1],'color',0.7*col{i},'linewidth',1.5)
plot(x,zo,'o','color',0.5*col{i},'markerfacecolor',0.8*col{i})
% plot data points end

set(gca,'fontsize',13.3) axis([0 2 10 20])
% axis limits([lower-x upper-x lower-y upper-y])
h=my_xticklabels(gca,[0.5 1.5],Labels2);
set(h,'fontsize',13.3,'linewidth',0.75)
set(gca,'ytick',[10 12 14 16 18 20])
% y axis scale numbers (can enter each one ex. [0 2 4 6
8 10]) ylabel('Final IOP (mmHg)','color',[0 0 0])
title('MYOC (-)')

set(f9,'position',[100 300 1000 370],'color','w')
saveas(figure(9),'C:\Users\ocallaje\Desktop\Experiments\MYOC mice
\MYOC.Induc.MMP3\MATLAB IOP exports\IOP_finalT.png')

```

Statistics

```

DCM = POS_IOPchange(:,1);
DCG = POS_IOPchange(:,2);
CCM = NEG_IOPchange(:,1);
CCG = NEG_IOPchange(:,2);

F1 = nanmedian(pos_wk4(:,1));
F2 = nanmedian(pos_wk4(:,2));
F3 = nanmedian(neg_wk4(:,1));
F4 = nanmedian(neg_wk4(:,2));

Finalmedians = horzcat(F1,F2,F3,F4);
finalmad1 =
mad(horzcat(pos_wk4(:,1),pos_wk4(:,2)),
1); finalmad2 =
mad(horzcat(neg_wk4(:,1),neg_wk4(:,2)),
1); if H1 == 0
% If Central Tendancy is the mean
[H3, ttest_Pvalue1] =
ttest(DCM,DCG); [H4,
ttest_Pvalue2] =
ttest(CCM,CCG);
pairedttest = horzcat(ttest_Pvalue1,ttest_Pvalue2)
% Paired Ttest

nanmean(POS_IOPchange); nanmean(NEG_IOPchange);
changemean =
horzcat(nanmean(POS_IOPchange),nanmean(NEG_IOPchange))
% Average IOP change t1s1 =ttest(DCM); t1s2
=ttest(DCG); t1s3 =ttest(CCM); t1s4
=ttest(CCG); Ttest_1Sample =
horzcat(t1s1,t1s2,t1s3,t1s4) %
1-Sample Ttest against a mean change of 0

```



```

    finalIOP1 =
ttest(pos_wk4(:,1),pos_wk4(:,2));
finalIOP2 =
ttest(neg_wk4(:,1),neg_wk4(:,2));

else
% If Central Tendancy is the median

    nanmedian(POS_IOPchange);
nanmedian(NEG_IOPchange);
changemedian =
horzcat(nanmedian(POS_IOPchange),nanmedian(NEG_IOPchange));
changemad1=mad(POS_IOPchange, 1);
% Median IOP change
changemad2=mad(NEG_IOPchange, 1);

    wc1 = signrank(DCM,0);    wc2 =
signrank(DCG,0);    wc3 =
signrank(CCM,0);    wc4 =
signrank(CCG,0);
wilcoxon_1sample =
horzcat(wc1,wc2,wc3,wc4);
% 1-Sample Wilcoxon against a median
change of 0

    wcp1 = signrank(DCM,DCG);
wcp2 = signrank(CCM,CCG);
wilcoxon_paired =
horzcat(wcp1,wcp2) ;
% Paired Wilcoxon signed rank
test

    finalIOP1 =
signrank(pos_wk4(:,1),pos_wk4(:,2));
finalIOP2 =
signrank(neg_wk4(:,1),neg_wk4(:,2));
finalIOPtest = horzcat(finalIOP1,
finalIOP2);

    %final MMPvsGFP
    % ranksum is the unpaired version of signed
rank
    %%ranksum is the unpaired version of signed rank
intergroupfinalIOP1 = ranksum(pos_wk4(:,1),
neg_wk4(:,2)); % POS_iMMP vs NEG_iGFP
(final IOP) %final GFP vs GFP
intergroupfinalIOP2 =
ranksum(pos_wk4(:,2),neg_wk4(:,2)); %
POS_iGFP vs NEG_iGFP (final IOP) %dex gfp change
vs control gfp change intergroupchangeIOP1 =
ranksum(POS_IOPchange(:,2),NEG_IOPchange(:,2)); %
POS_iGFP vs NEG_iGFP (change in IOP)

    % wc7 =
signrank(DEX_IOPchange2(:,1),DEX_IOPchange2(:,2)) %
wc8 =

```

```

signrank(cycloDEX_IOPchange2(:,1),cycloDEX_IOPchange2(:,2))

    nforpos=numel(PosTreated_eyes(:,1));
    nforneg=numel(NegTreated_eyes(:,1));

end

table1 = [changemedian;wilcoxon_1sample;Finalmedians]; table2 =
[wilcoxon_paired;finalIOPtest]; table3 =
[intergroupfinalIOP1;intergroupfinalIOP2;intergroupchangeIOP1;nfo
rpos;nforneg]; table4 =
[finalmad1;finalmad2;changemad1;changemad2];
xlswrite('C:\Users\ocallaje\Desktop\Experiments\MYOC mice
\MYOC.Induc.MMP3\MYOCmmp IOP interp_adjust.xlsx',table1,'IOP
Matlab Write','D4')
xlswrite('C:\Users\ocallaje\Desktop\Experiments\MYOC mice
\MYOC.Induc.MMP3\MYOCmmp IOP interp_adjust.xlsx',table2,'IOP
Matlab Write','D11')
xlswrite('C:\Users\ocallaje\Desktop\Experiments\MYOC mice
\MYOC.Induc.MMP3\MYOCmmp IOP interp_adjust.xlsx',table3,'IOP
Matlab Write','D15')
xlswrite('C:\Users\ocallaje\Desktop\Experiments\MYOC mice
\MYOC.Induc.MMP3\MYOCmmp IOP interp_adjust.xlsx',table4,'IOP
Matlab
Write','D24')

%close all;
disp('Analysis Complete')

```

Published with MATLAB® R2016a

Open-angle glaucoma: therapeutically targeting the extracellular matrix of the conventional outflow pathway

Jeffrey O'Callaghan , Paul S. Cassidy  and Pete Humphries

Ocular Genetics Unit, Smurfit Institute of Genetics, University of Dublin, Trinity College, Dublin, Ireland

ABSTRACT

Introduction: Ocular hypertension in open-angle glaucoma is caused by a reduced rate of removal of aqueous humour (AH) from the eye, with the majority of AH draining from the anterior chamber through the conventional outflow pathway, comprising the trabecular meshwork (TM) and Schlemm's Canal. Resistance to outflow is generated, in part, by the extracellular matrix (ECM) of the outflow tissues. Current pressure-lowering topical medications largely suppress AH production, or enhance its clearance through the unconventional pathway. However, therapies targeting the ECM of the conventional pathway in order to decrease intraocular pressure have become a recent focus of attention.

Areas covered: We discuss the role of ECM of the TM in outflow homeostasis and its relevance as a target for glaucoma therapy, including progress in development of topical eye formulations, together with gene therapy approaches based on inducible, virally-mediated expression of matrix metalloproteinases to enhance aqueous outflow.

Expert opinion: There remains a need for improved glaucoma medications that more specifically act upon sites causative to glaucoma pathogenesis. Emerging strategies targeting the ECM of the conventional outflow pathway, or associated components of the cytoskeleton of TM cells, involving new pharmacological formulations or genetically-based therapies, are promising avenues of future glaucoma treatment.

ARTICLE HISTORY

Received 16 June 2017
Accepted 26 September 2017

KEYWORDS

MMP; extracellular matrix; ECM; glaucoma; outflow facility; treatment; prostaglandin; AAV

1. Introduction

Glaucoma encompasses a range of eye disorders including pigmentary-, secondary-, and normal-tension forms of disease; however, the most prevalent are primary open-angle (POAG) and primary angle-closure glaucomas (PACG). POAG represents greater than 74% of all glaucoma cases [1]. In this form, the narrow angle between the cornea and iris leading to the conventional outflow tissues remains open, while the conventional outflow tissues themselves, the trabecular meshwork (TM) and Schlemm's canal (SC), retain only partial AH drainage function. In contrast, while these outflow tissues remain functional in PACG, flow of AH through them becomes physically blocked by the apposition of the iris against the cornea, often due to deformity of the iris. Thus, in both forms of disease, AH drainage becomes restricted, leading to increased intraocular pressure (IOP). Ocular hypertension is recognized as the major disease risk factor for vision loss in glaucoma, along with age, lifestyle, and gender [2,3]. As a result of elevations in IOP, the optic nerve head degenerates, visibly recognizable as receding, or 'cupping,' of the optic disc. This in turn places stress on the axons of the ganglion cells of the retina, ultimately resulting in a progressive loss of the visual fields. The disease, if left untreated, often leads to a complete loss of vision.

Glaucoma, in its various forms, is one of the most common causes of visual handicap in the world, rivaling cataract and infection. Glaucoma currently affects an estimated 70 million

people, with projections showing an increase to 76–79 million people in 2020 and nearly 120 million by 2040 [1,3]. Worldwide, approximately 10% of those suffering from glaucoma are bilaterally blind [1,4], with fewer than 50% of patients in developed countries being aware of having the disease until visual fields become significantly reduced [5].

2. Genes associated with POAG

POAG is a classically multifactorial disease in that, while there are familial tendencies, the vast majority of cases are of adult onset and are not inherited in a Mendelian sense. However, rare hereditary forms of disease do exist that segregate in families in an autosomal dominant fashion, and through genetic linkage studies, genes involved in such forms of disease were localized and characterized. Recent association studies have also highlighted an array of genes with moderate correlation to POAG [6].

The first gene to be identified through genetic linkage encoded a TM glucocorticoid response protein (TIGR), now known as myocilin. Most ocular tissues produce myocilin, but it is only secreted by some, including the TM [7,8]. Myocilin interacts with ECM components including fibronectin, laminin, and decorin [9,10]; however, the function of such interactions remain unknown. Current evidence suggests that mutant myocilin protein misfolds and aggregates in cells of the TM, rather than being secreted [11], leading to

Article highlights

- Glaucoma, a multifactorial disease, affects approximately 70 million people today. Several genetic components have been identified, with some variations indicating a link to ECM homeostasis.
- The ECM has a significant influence on the regulation of outflow resistance in the eye, and thus presents itself as an attractive therapeutic target.
- Commercially available medications do not significantly lower IOP over long periods of time, and often have indirect effects on the ECM.
- Medications in development have a greater focus on ECM modulation including cytoskeletal disorganisation, decreased cellular contractility and enhanced ECM turnover via MMPs, which are associated with improved efficacy.
- Recent gene therapy advancements allow for induced secretion of MMPs into the anterior chamber, resulting in significant decreases in IOP and increases in outflow facility.

This box summarizes key points contained in the article.

endoplasmic reticulum (ER) stress and dysfunction of TM cells. In TM cells expressing a dominant human Myocilin (Tyr437His) mutation, there is an intracellular build-up of ECM components and a decrease in secretion of matrix metalloproteinases [12]. Transgenic animals expressing this mutation exhibit elevated IOP and reduced outflow facility, characteristic of glaucoma [12,13].

The second gene to be mapped in POAG using genetic linkage studies encoded optic neuropathy-inducing protein, or optineurin. The gene is expressed in the TM, nonpigmented ciliary epithelium, retina, brain, and in other tissues [14]. Optineurin may play a neuroprotective role against TNF- α -mediated cytolysis, and translocates to the membrane in response to oxidative stress [14–16]. Most commonly associated with normal tension glaucoma, optineurin mutations have also been linked to POAG [17]. Together, mutations within the optineurin and myocilin genes have been encountered in up to 5% of adult-onset cases of POAG [18].

In regard to adult-onset disease, genome-wide association studies (GWAS) have implicated caveolins CAV1 and CAV2 in POAG. These proteins appear to affect the organization of collagen matrix fibers in lung tissue [19,20] and fibronectin, collagens, and α -SMA in murine mammary tumors [21], all of which are perturbed during fibrosis. Reduced expression of caveolins in glaucomatous tissues may be indicative of a pathological role for caveolins in POAG, such as their role in suppressing TGF- β 2 transcription, a known inducer of ECM expression [22,23]. Interestingly, it has recently been shown that lack of caveolae in the TM of mice results in ocular hypertension, with cells of the outflow tissues having a greater susceptibility to rupture through mechanical stress, indicating a possible genetic and functional link to glaucoma [24]. GWAS have resulted in the elucidation of additional glaucomatous or IOP-related susceptibility loci. Primary candidate genes related to both IOP and POAG include TMCO1, ABCA1, and GAS7 [25–27]. Their contributions to the pathogenesis of glaucoma are still unclear; however, basic functionalities have been established. TMCO1 encodes a transmembrane protein that functions as a calcium channel in response to excess calcium levels in the ER [28]. ABCA1 belongs to a family of transporters and

functions as a cholesterol efflux pump, and GAS7 may promote maturation and differentiation of neurons. Proteins encoded by these genes have been shown to be expressed in human ocular tissues [27].

While some of these high-penetrance glaucoma-causing genes are known to encode proteins that interact with ECM components, no genetic variants in ECM genes have as yet been significantly linked to POAG. There are, however, several genetic variants within the collagen genes that are significantly associated with glaucomatous endophenotypes such as maximum vertical cup-disc ratio, increased optic disc cup area and altered central corneal thickness [29–32]. Other mutations within fibrillin 1, latent-transforming growth factor beta-binding protein 2 and versican genes have been associated with glaucoma in humans [33–37]. These proteins constitute large ECM fibrils that have roles in cell adhesion within the matrix. Mutations in genes involved in the remodeling of the ECM, such as the ADAMTS proteins, members of the matrix metalloproteinase (MMP) family, are associated with increased vertical cup-disc ratio and reduced central corneal thickness [29,31,38]. Collectively, these data support the concept that genetic variations affecting ECM homeostasis may be related to the development of glaucomatous endophenotypes.

3. The ECM as a therapeutic target

3.1. ECM composition within the outflow tissues

The ECM of the conventional outflow tissues not only provides structural support, but is also involved in the regulation of a variety of cellular processes and functions. ECM within this region is comprised of a heterogeneous group of fibrous and matrical materials, including proteoglycans, collagens, fibronectin, laminin, elastin, and others, all of which contribute to its dynamic and complex function. The juxtacanalicular (JCT) region, adjoining the inner-most layer of the TM and the inner wall of the SC comprises cells resting on a basement membrane, surrounded by an amorphous ECM dispersed with open spaces, allowing aqueous egress [39,40]. The SC itself is a unique vessel in that it incorporates both blood and lymphatic endothelial cell phenotypes [41]. It is a continuous endothelial layer on a discontinuous basement membrane that facilitates flow in the basal to apical direction, differing from other vessels [42]. It is also distinct from other vessels in its ability to form giant vacuoles under high pressure and its unique tight junction profile including claudin-11 [43]. These features have allowed for new therapeutic opportunities to arise, such as the use of the VEGF family in outflow facility modulation [44,45]. The basement membrane is a fibrous layer of ECM material separating the endothelium from underlying connective tissues. It is discontinuous around the canal circumference tethering SC cells against large pressure gradients. As with other vascular endothelia, the basement membrane incorporates a lattice of collagen IV and laminin-511 along with collagen I, dystroglycans, and other laminin chains. Although these components are found throughout the ECM of the JCT, they are critical to basement function, in particular, the heterotrimer of laminin subunits with arms containing binding sites for SC cell surface receptors, integrins, and proteoglycans

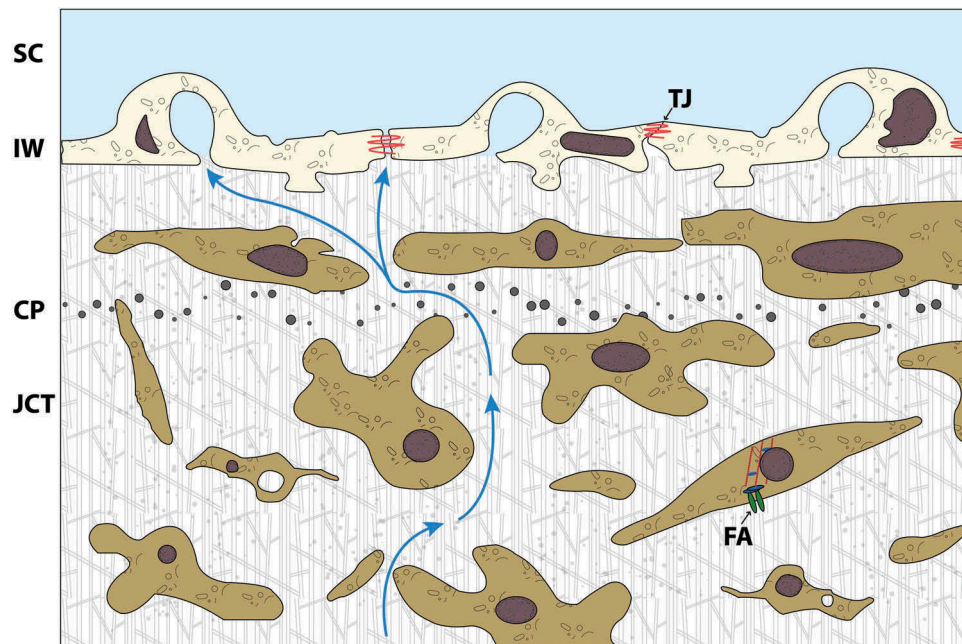


Figure 1. An expanded view of the JCT region.

Diagram depicting a cross section of the conventional outflow tissues including various ECM elements. AH traverses the TM, exiting the juxtacanalicular region (JCT) through the inner wall (IW) into the lumen of the Schlemm's canal (SC), via either the transcellular route, through transendothelial pores in giant vacuoles, or the paracellular route, through paracellular pores controlled by tight junctions (TJ). Cells are embedded in a structured ECM and adhesion to the matrix is facilitated by focal adhesions (FA) sites where integrins bind both extracellular material and the intracellular actin cytoskeleton (red). The cribriform plexus (CP) comprising elastin sheaths is predominantly found underlying the first sub-endothelial layer.

[46]. Colocalization studies show an overlap of laminin-511 and the integrin α_6 , expressed at the SC endothelial periphery and not the TM, indicating that this focal adhesion complex is involved in basement membrane-endothelial adhesion [47].

The ECM is formed by complex proteinaceous meshworks in the extracellular spaces throughout the JCT, which are regularly remodeled to retain porosity. Collagen fibers are irregularly orientated within the matrix of the JCT, which may provide an explanation as to why JCT cells are stationary while other cells in regularly orientated collagen matrices are migratory [39]. Fibronectin is a major ECM component, with the protein organizing into interwoven repeating chains that form extensible fibrils involved in the contractility of the TM in response to IOP. Alternative splicing of fibronectin occurs in the TM, and POAG patients are more likely to express key exons that promote assembly of fibronectin matrices which may decrease outflow facility [48]. Elastin is one of the core elements of the JCT, with elastin fibers forming the cribriform plexus, which runs tangential to the inner wall endothelium joining the basement material of the SC with the ciliary muscles. Elastin and its associated proteins react to muscle tension and thus induce widening or contraction of the SC lumen [49]. The binding of ECM to cell membranes is facilitated by integrin-ECM interactions at sites referred to as focal adhesions [50]. Transmembrane integrin subunits interact with the Arg-Gly-Asp domains of ECM proteins, while the cytoplasmic domain connects to actin-binding proteins [51–53]. Interaction between these proteins and the actin cytoskeleton reflect the importance of focal adhesions in regulating cellular function and response to environmental cues. In conjunction with integrins, inter-endothelial junctions maintain endothelial cell-

cell adhesion, regulating paracellular transport channels. These features are summarized in Figure 1.

The TM expresses MMP-2, tenascin-C, and α -SMA at consistently high levels, normally only expressed highly in cells undergoing remodeling, suggesting a constant remodeling process at the TM to maintain open-flow channels [46]. TGF- β_2 is a cytokine with an important regulatory role at the TM, inducing the expression of collagens, α -SMA, fibronectin, PAI-1 among others. TGF- β_2 signaling is mediated by elastic microfibrils, specifically the fibrillin component that confers ECM elasticity, which is critical to sequestration and activation of TGF- β_2 complexes [54]. Induction of ECM cross-linking by TGF- β_2 bears similarities to the cross linking observed in glaucomatous tissues, and may be a contributing factor to disease pathogenesis. Matricellular proteins are those described as nonstructural glycoproteins enabling communication between the cell and the surrounding ECM such as CTGF, SPARC, tenascin-C, thrombospondin, and others. These proteins are upregulated in response to TGF- β signaling, the levels of which are upregulated in POAG AH, and are associated with fibrosis and ECM deposition [55].

The ECM of glaucomatous tissues bears similarities to fibrotic tissue, in particular, excessive accumulation of ECM components such as α -SMA, progressing to a hardening or scarring of connective tissues [56,57]. The ECM at the glaucomatous JCT displays some hallmarks of fibrosis in the form of sheath-derived plaques, i.e. an increase in elastic fibril sheath size due to increased adherence of fibrils and other ECM components to the sheath, particularly in the aging TM [39,58].

3.2. ECM in outflow resistance

AH secreted from the ciliary body moves from the posterior chamber through the pupil and into the anterior chamber. From here it crosses the TM, its movement being facilitated by a pressure gradient, and is then directed toward the SC lumen. This pathway, known as the conventional outflow pathway, accounts for up to 90% of human aqueous drainage, especially in the elderly [59–61]. AH can also leave the eye through the unconventional pathway, where it flows between the ciliary muscle bundles into the supraciliary and suprachoroidal space (Figure 2). AH enters the SC either transcellularly, through pores in giant vacuoles formed in the endothelial cells lining the inner wall of the canal, or paracellularly, through the spaces between SC cells regulated by the inter-endothelial junctions [62–64]. AH then exits the lumen through collector channels into aqueous veins that discharge into the episcleral venous circulation. At lower IOP, the cross-sectional area of the SC lumen is too large to generate any significant outflow resistance. While canal collapse is seen to occur at high IOP, the resistance increase generated by lumen narrowing is not nearly as high as that observed in glaucomatous eyes. This indicates that although canal collapse could worsen the glaucomatous condition, it cannot be causative of it [65]. Regions of high flow are concentrated at collector channels, however, as is the case with the SC lumen, collector channels should not contribute significantly to resistance as their relatively large diameters suggests that resistance is again negligible [66,67]. After trabeculotomy 25% of outflow resistance remains, implicating the collector channels; however, such remaining resistance is not thought to be relevant to glaucoma as trabeculotomy also eliminates the elevated resistance observed in glaucoma [68,69]. This indicates that in glaucoma, the site of increased outflow resistance lies proximal to the collector channels, ruling out distal outflow pathway tissues as

potential therapeutic targets [65,68,70]. It is generally accepted that the majority of outflow resistance is generated at the JCT [42,66], in particular, at the ECM of the JCT [34,71–73]. Porous spaces within the ECM of this region allow AH to reach the endothelial lining of SC; however, proteoglycans, glycosaminoglycans, and other large ECM constituents can fill these spaces further increasing resistance to AH outflow [42,74–77]. Obstruction of AH flow through ECM components reducing ECM porosity is more likely in aged and glaucomatous tissue [75]. AH funnels from the full expanse of the TM/JCT to discrete pores in SC endothelium, leading to generation of outflow resistance through a bottleneck effect. As ECM accumulates, the extracellular space close to SCEC becomes more tortuous, leading to increased outflow resistance [42]. The effect that this ECM has on outflow resistance alone is difficult to measure; however, recent developments in measuring and modeling of perfusion data may lead to more accurate estimations of outflow facility [78].

In general, changes in ECM composition and turnover in the TM play an important role in outflow resistance, including dynamic reactions to environmental cues, such as mechanosensation of IOP [46,79].

3.3. Modulation of ECM turnover

Homeostatic ECM turnover plays an important role in the regulation of outflow resistance, turnover being triggered, for example, by stretch or distortion of TM cells, often as a result of elevated IOP [80]. JCT cells constitutively express a range of ECM proteins, with exposure to environmental stresses, synthetic agents, or laser trabeculoplasty surgeries invoking alterations in ECM gene expression profiles [81–84]. High gene expression levels are a reflection of the fact that regular ECM turnover, facilitated by proteinases that target ECM

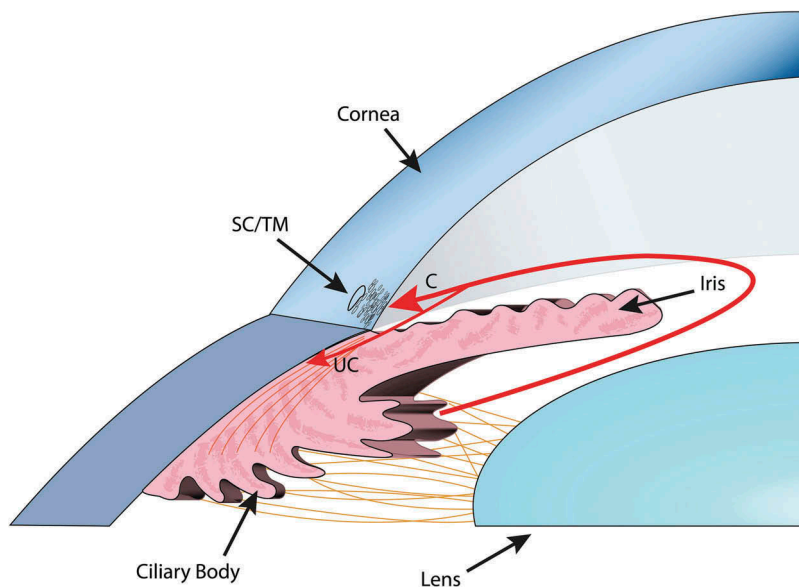


Figure 2. The route of aqueous humour.

Aqueous humour is secreted by the ciliary body and moves through the pupil, around the iris. A pressure gradient directs it toward the SC lumen, where most aqueous egresses (red arrow). This is termed the conventional pathway (C). The unconventional pathway (UC) involves the drainage of aqueous through the fibres of the ciliary body into the supraciliary and suprachoroidal spaces.

components, is essential to homeostasis [82]. Homeostatic proteinases include zinc-dependent proteinases – classical MMPs, adamalysins (ADAM and ADAMTS proteins), and other proteinases involved in plasminogen activation [85]. The MMP group of proteinases is secreted extracellularly in their inactive form, and require further processing for activation [86,87]. MMPs are constitutively expressed throughout the TM, expression profiles responding to various stimuli [88–90]. Tight regulation of proteinase expression within the ECM is required for effective control of outflow resistance. To this end, tissue inhibitors of metalloproteinases (TIMPs) are expressed in a manner similar to that of MMPs, while the ratios of MMP:TIMP determine the extent of ECM modulation [58,91]. Such ratios tend to be imbalanced in POAG [92–95], and may be indicative of dysfunctional ECM turnover. MMP proteins are often upregulated in glaucomatous AH; however, the activity of these proteins is reduced in comparison to cataract controls, likely reflective of MMP:TIMP imbalance [92,96–98]. Perfusion of ocular tissues with MMPs or MMP-activating compounds results in increased outflow facility, possibly the most convincing demonstration of ECM involvement in regulating outflow resistance [99–102]. Furthermore, recent studies on ECM characteristics, such as stiffness resulting from crosslinking, or caveolin-mediated matrix endocytosis, also highlight ECM influence on outflow facility [103,104].

ADAMs proteins have a similar domain structure to those of classic MMPs and also associate with ECM proteins and integrins [105]. As a result of MMP-related proteolysis, ECM remodeling can induce changes at the sites of focal (cell-matrix) adhesions. Disruption or inhibition of integrin-ECM linkages binding cells to the ECM, or ECM receptor inhibition has been associated with increases in endothelial permeability and transendothelial transport [52,106–108]. ECM remodeling at focal adhesions alters migration of fibers within the actin cytoskeleton, allowing F-actin and α -actinin to act as indicators of ECM turnover [48,109,110]. It is also worthy of note that ECM proteinases affect inter-endothelial SC junctions, providing an additional avenue for modulation of outflow resistance [43,111–113].

Newly emerging treatments, detailed below, have a greater focus on the conventional pathway, representing the major site of outflow resistance, often with direct or indirect effects on the ECM. This more targeted approach to glaucoma treatment will hopefully allow for the development of a new class of drugs that may prove to be more efficacious in arresting disease progression.

4. Traditional topical medications in the management of glaucoma

The primary standard of care for patients with open-angle glaucoma involves topically administered eye drops, surgery, or both, with the annual cost of such interventions in the USA having recently been estimated to amount to \$1.9 billion, 38–52% of which is related to topical pressure reducing medications [114]. Glaucoma management involves either reducing AH production at the ciliary body, or increasing AH outflow. A recent meta-analysis has confirmed that

prostaglandin analogs are the most effective in lowering IOP, a reflection of the fact that these compounds are the most commonly prescribed eye-drop [115]. Significant increases in unconventional outflow [116], and to a lesser extent, conventional outflow [117,118], are observed with such analogs. Prostaglandins are endogenously expressed in many tissues and throughout the anterior chamber [119], such expression being influenced by bioactive molecules, laser treatments, mechanical stress, or glucocorticoids, indicating their importance in homeostasis [120]. Extensive studies have demonstrated prostaglandin-related decreases in TM cell contractility and outflow resistance of organ-cultured anterior segments [121–123]. The overall mechanisms through which prostaglandins enhance AH outflow remain to be fully elucidated; however, it is widely accepted that remodeling of the ECM plays a part [124–127], and it is of note that upregulation in MMP expression, through activation of prostaglandin receptors, may be involved [89,128]. However, the unique receptor profile for each analog may induce ECM modulation via different cascade pathways. One EP4 receptor agonist in particular has been shown to induce an increase in conventional outflow facility specifically [129]. Comparisons have been made between the effects of laser treatment and prostaglandins in SC monolayer permeability. Cells treated by laser, media conditioned from lasered cells, or prostaglandins all show a reduction in levels of tight junctions and a concomitant increase in cell conductivity [130]. Modulation of SC permeability by prostaglandins further indicates an effect on enhancement of outflow through the conventional pathway.

Second-line medications include carbonic anhydrase inhibitors and β -blockers; however, the latter may have potentially dangerous off-target side effects. β -blockers inhibit either β_1 -, or both β_1 - and β_2 -adrenoceptors [131]. Since these receptors are abundantly expressed in the ciliary processes, this may result in an excess of noradrenaline, which may, in turn, induce vasoconstriction and decreases in blood supply to the ciliary body, aiding in the reduction of AH production [132]. Alpha2-adrenergic receptor agonists work in a similar way, but are not often used as topical medications owing to their side effects. These agents cause an initial decrease in aqueous production, and an increase in unconventional outflow after chronic exposure, likely due to elevated prostaglandin expression [133,134]. Carbonic anhydrase inhibitors also decrease AH production through chemical inhibition of bicarbonate formation [135].

Cholinergic drugs represent third-line medications that have seen a reduction in clinical use in recent years, primarily due to the frequency with which they need to be instilled (3–4 times per day). These drugs increase conventional outflow and decrease IOP [136,137] by inducing ciliary muscle contraction, increasing SC lumen area, in turn allowing for increased aqueous fluid transport across SC endothelial cells [138]. As previously mentioned, elastin fibers are responsible for the connection of the ciliary body to SC and associated muscle contractions. The ciliary muscles express cholinergic nerve terminals facilitating contraction, and it is presumed that the muscle is pulled back again by a recoil of the elastin net [137,139].

It is important to emphasize that these widely used topical medications predominantly target unconventional outflow and mostly only influence the conventional pathway by means of secondary or indirect responses. It is of interest to note, however, that administration of α/β -blockers, α_1 -blockers, α_2 -agonist-, and prostaglandin derivatives all upregulate MMPs and downregulate TIMPs, in contrast to the effects of β -blockers, suggesting at least some role in ECM modulation for these antiglaucoma drugs [140].

It should be noted that for the most commonly used prostaglandin analogs, between 25 and 50% of patients are suboptimally responsive, commonly defined as not achieving more than a 20% reduction in IOP [141,142]. Consequently, there continues to be a need for improved treatment methods, particularly targeting the conventional pathway.

5. Emerging medications

5.1. New classes of drug

A collective objective in developing new formulations is to increase conventional outflow via targeting of the JCT or cytoskeleton of cells of the outflow tissues. Rho kinase inhibitors, marine macrolides, adenosine- and prostanoid-receptor agonists together with siRNA formulations are all currently under evaluation. Arguably, the most advanced of these are rho kinase (ROCK) inhibitors that have already been approved for use in Japan and have completed phase III trials in the USA. IOP decrease in response to ROCK inhibitors is associated with enhanced outflow facility caused by expansion of the TM, JCT, and episcleral veins and increases in SC cross-sectional area [143,144]. Studies using a rho kinase inhibitor in conjunction with a norepinephrine transport inhibitor demonstrated similar results, but with the advantage of a dual mechanism of action that also decreases AH production [145]. Rho family GTPases are seen to be elevated in glaucomatous optic nerve heads, activating effector kinases to polymerize actin fibers and regulate smooth muscle contraction [146–149]. Decreases in myosin light-chain phosphorylation were observed in ROCK inhibitor-treated TM tissue, suggesting that outflow enhancement was facilitated by actomyosin cytoskeletal disorganization at the JCT/inner wall assembly [150,151]. ROCK effectors also indirectly stabilize filamentous actin, reducing cell migration and interact with actin-binding proteins. Depolymerization of filaments by ROCK inhibitors may further widen the empty spaces in the JCT and increase SC vacuoles, thereby increasing outflow facility [152,153]. Similarly, Rho GTPase inhibition via expression of exoenzyme C3 transferase has been shown to disrupt actin bundles in human TM cells, correlating with increased outflow facility in primates. Focal adhesions, as visualized through vinculin staining (involved in integrin-actin binding) were distinctly reduced, as was β -catenin, indicating a loss of intercellular junctions, reflected in the decrease in cellularity [154].

Marine macrolides, isolated from aquatic sponges, have antifungal, cytotoxic, and antiproliferative properties. Interactions of these compounds with actin are similar to those of the ROCK inhibitors. Macrolides have established functions in: (1) severing polymeric actin (F-actin) and

stabilizing dimeric actin, disrupting the cytoskeleton (swinholidide A); (2) sequestering actin monomers (G-actin) preventing their use in polymerization, thus disrupting filament organization as is the case with latrunculin-B; (3) competing for actin binding to induce and stabilize its polymerization (jasplakinolide) [155–158]. Macrolides have been shown to increase aqueous outflow facility in primate eyes, with the greatest focus appearing to have been placed on latrunculin-B [155,159–161]. Topical administration of latrunculin-B is sufficient to increase aqueous outflow facility and lower IOP [160], while in treated eyes, noticeable changes have been observed in the JCT region, including increased intercellular space and dilated SC, but with normal and intact corneoscleral regions [162]. Inter-endothelial junctions of primate SC endothelia appeared intact, although there was a loss of ordered alignment and integrity in actin filaments. Similar studies in human eyes have shown some focal SC inner wall separation from the ECM of the JCT [161]. Increased central corneal thickness and transient increase of corneal endothelium permeability was observed in one study, raising questions of safety issues in using macrolides in the anterior chamber [163]. Phase I trials have been conducted, however, and have reported few clinically significant adverse effects [164].

Adenosine receptor agonists have been shown to increase conventional outflow and lower IOP, with a similar mechanism to those of cholinergic agonists. A_3 agonists reduce AH flow by inhibiting chloride ion channels in ciliary epithelial cells [165]. An A_1 agonist in phase III trials has demonstrated favorable toxicity profiles, possible neuroprotective effects, and efficacious IOP lowering [166]. Receptor activation has also been shown to induce the secretion of MMPs, particularly MMP-2, probably the cause of reduced outflow resistance [167,168]. Increases in facility were negated by the addition of an MMP inhibitor, implicating ECM remodeling along with cell volume shrinkage as mediators of outflow enhancement [169,170].

Developments on prostanoid receptors have yielded agonists specific to individual receptor subtypes. Further understanding of the mechanism of action of the prostaglandin pathway has resulted in the development of drugs that include nitric oxide-donating prostaglandin F₂-analogs, which strongly increase fluid drainage across both pathways. Relaxation of TM cells as a result of a reduction of actin stress fibers and vinculin localization at focal adhesions was observed using such analogs [171]. Interest is increasing in the development of EP₂ and EP₄ receptor agonists for the treatment of POAG, with one such EP₂ agonist having been shown to reduce IOP by increasing both unconventional and conventional flow, facilitated by the relaxation of SC and by decrease in contractility and collagen deposition at the TM [172–174]. These effects are similar to those of traditional FP receptor agonists, however these, in contrast, may increase TM contractility. Furthermore, selective EP₄ agonists have also been shown to be efficacious in treatment of POAG. Both SC and TM cells express EP₄ receptors, and hypertension-lowering effects are believed to be primarily localized to the conventional pathway [129,175]. EP₄ receptors alone induce expression of early growth response factor-1, mediated by extracellular signal-regulated kinases [176], while these kinases

are also known to influence MMP expression [177]. These observations illustrate the unique modes of action of prosta-
noid receptors, and the potential that these drugs can be
tailored to have greater specificity and efficacy.

A number of siRNA therapies are in clinical trial for glau-
coma, some functioning in a similar manner to that of β -
blockers, inhibiting the B2-adrenergic receptors at the ciliary
body, thereby reducing AH production. Tolerability and safety
profiles indicate that siRNA was only present in ocular tissues,
providing a possible alternative form of therapy for patients
that may have asthma or congestive heart failure where the
use of traditional, nonselective beta blockers is limited
[178,179]. It is also interesting to note that a recent study in
rodents using siRNA targeting the tight junctions of the SC
reported increased outflow facility corresponding to additional
open clefts, indicating increased paracellular transport [43].

Since patient compliance is a major issue, the develop-
ment of longer-lasting medications could provide great
benefit to patients. Strategies for enhanced delivery
include drug reformulation into nanocapsules or nano-
spheres, reducing the amount of preservatives (which
may illicit side effects [180]), or modulation of solution
viscosity by incorporation of polymers, collagen shields,
gels, or liposomes. Such engineering allows greater cell
specificity and retention of stability. Slow-release implants
are also in development, including those designed for
sustained release of prostaglandin by an implant intro-
duced into the eye via intracameral injection. Other
devices include plugs or rings to deliver traditionally topi-
cal medications into the puntum or conjunctival fornices,
respectively [181,182]. A summary of traditional and emer-
ging formulations is provided in Table 1.

5.2. On the development of genetic therapies

Adenoviral (AV), Herpes simplex (HSV), Lentiviral, and Adeno-
associated viral (AAV) vectors have all been used in targeting
experimental gene therapies to the TM. There have also been
a limited number of early reports on the use of HSV vectors in
transfection of the TM, however, limited reporter gene expres-
sion and significant inflammatory responses were observed
[184,185]. Long-term expression in TM cells and in rodents
has been achieved with lentivirus following a single intracam-
eral inoculation [186,187]. The first demonstration of efficient
lentiviral transduction in primates reported well tolerated,
extensive viral expression with a mild inflammatory response
[188]. In early AV studies, gene expression was obtained in TM
cells of mice for up to 14 days following intracameral inocula-
tion of a replication-deficient AV vector expressing a LacZ
gene [189]. In practice, however, the feasibility of using AV
as a gene therapy vector is extremely limited owing to its
immunogenicity and the non-sustainability of viral expression;
however, AV has been a useful vector in demonstrating proof
of principle of gene therapy strategies [190–192]. In this
regard, an AV system in which MMP-1 expression could be
activated by a glucocorticoid-responsive promoter has been
developed. Corticosteroid treatments can result in elevations
in IOP in a significant number of individuals, thus steroid
induced expression of MMP-1 within the TM will result in a

Table 1. Comparison of traditional vs. emerging formulations in glaucoma treatment.

Class of medication	Clinical prevalence today	Primary mode of action	Mechanism	References
Traditional				
Prostaglandin F2 α Analog	1st line – Common	Increases unconventional and conventional outflow	Ciliary muscle relaxation, ECM remodeling by MMPs	[124–127]
β -blockers	2nd line – Uncommon	Reduces AH production	Block β 1/ β 2 adrenoceptors, vasoconstriction at ciliary body	[131,132]
Carbonic anhydrase inhibitors	2nd line – Uncommon	Reduces AH production	Inhibit bicarbonate formation	[135]
Cholinergics	3rd line – Uncommon	Increases conventional outflow	Ciliary muscle contraction	[136–138]
α 2-adrenergic receptor agonists	Rarely used due to side effects	Reduces AH production, increases unconventional outflow	Block α 2-adrenergic receptors, elevate prostaglandin expression	[133,134]
Emerging				
ROCK inhibitor	Approved in Japan, phase III trials in USA	Increases conventional outflow	Cytoskeletal disorganization, promotes cell migration	[143,144]
Macrolides	Phase I trials	Increases conventional outflow	Disruption of actin cytoskeleton	[155–164]
Adenosine receptor agonists (A ₁)	Phase III trials	Increases conventional outflow	ECM remodeling by MMPs	[165–170]
siRNA	Phase II trials	Reduces AH production	Inhibit β 2-adrenergic receptors at ciliary body	[178,179]
AAV	Predclinical development	Increases conventional outflow	ECM remodeling by MMPs	[98,183]

reduction in collagen type I, potentially preventing an increase in IOP [193]. This approach was subsequently extended to sheep, where steroid-induced expression of MMP-1 resulted in a decrease in IOP [194], and later deployed in a scAAV system more appropriate to human intervention [183].

AAVs are the most widely used gene therapy vector systems in use today. AAV is an innate human virus, integrated into the human genome on chromosome 19, and will only replicate in the presence of AV helper functions. It is minimally immunogenic even when used in high doses [195,196]. Moreover, AAV has been used extensively in human trials of gene therapy for retinopathies, particularly for Leber congenital amaurosis and retinitis pigmentosa. Conventional AAVs have a single-stranded DNA genome, which requires second strand synthesis by host DNA polymerases. By incorporating a second self-complementary DNA strand into these vectors (scAAV), these viruses have been shown to be significantly more efficient in transducing target cells, with the disadvantage of a reduction in the size of their DNA handling capacity [197]. While standard AAV constructs transfect but do not appear to be expressed in cells of the conventional outflow pathway, highly efficient expression has been demonstrated via the use of scAAV [198]. Rapid and widespread transfection of the TM has been demonstrated following intracameral inoculation of GFP-expressing scAAV2 constructs in both rats and nonhuman primates, with expression lasting in rats for greater than 3.5 months and in monkeys for at least 2.35 years.

In the case of glucocorticoid-inducible expression of MMP-1 previously mentioned, IOP was successfully reduced in sheep following intracameral inoculation of the AAV virus, with no localized or systemic negative effects [183]. This study was the first in which the feasibility of a gene therapy approach for steroid-induced IOP was demonstrated with a virus that could be deployed as a human therapy. The feasibility of controlled AAV-mediated expression of MMPs was further investigated in recent studies [98] in which a conventional AAV2/9 vector expressing a doxycycline-inducible MMP-3 gene was intracamerally inoculated into wild-type mice, with extensive transfection of the corneal endothelia being observed. As MMP-3 is a secretory protein, its expression in corneal endothelial cells resulted in secretion of the protease into the AH, where it traversed the anterior chamber with the natural flow of AH toward the outflow tissues. Here, the pro-peptide was initially cleaved by nonspecific proteases, allowing for further cleavage by MMP's, including other MMP-3 molecules themselves. ECM proteolysis ensued, reducing collagen and laminin contents, constriction of actin filaments and disorganization of fibronectin networks, resulting in elevated outflow facility and a reduction in IOP. Few adverse reactions were observed in the anterior chamber using this method, while ECM components were visibly modulated and greater intercellular spaces observed. Given the safety profile of AAV and its wide use in ocular gene therapy, having progressed through phase III trials for Leber congenital amaurosis and Leber hereditary optic neuropathy [199,200], AAV systems in which MMP expression can be periodically induced as indicated by IOP hold substantial promise as gene medicines.

6. Conclusion

The ECM is a dynamic structure capable of enhancing outflow resistance at the JCT region of the conventional outflow tissues. Normal responses to elevated IOP allow this structure to expand and alter its configuration to facilitate increased outflow facility, thus alleviating ocular hypertension. In open-angle glaucoma, however, hypertension remains through as of yet incompletely elucidated mechanisms. As lowering IOP remains the primary treatment for patients with this disease, medications and surgeries aim to do so via a variety of biological and mechanical interventions. New strategies in development target the conventional outflow pathway more specifically, many of which employ remodeling of the ECM. Re-organization of matrix components using MMPs, inhibition of focal adhesions, depolymerization of the actin cytoskeleton and deterioration of inter-endothelial junctions are such examples that provide a means by which AH outflow facility can be increased, ultimately leading to a reduction in IOP. Novel targeting approaches, together with advanced delivery systems and combination therapies, may assist in improving patient compliance, long-term cost, chronic reductions in IOP, and ultimately a reduction in vision loss.

7. Expert opinion

That the bulk of AH outflow is through the conventional pathway and that most of the medications in current clinical use do not primarily target this pathway will be a matter of intrigue to most nonspecialists. However, while many of the new formulations in development target pathological disease processes which are primarily located in the anterior part of the eye, death of the retina's output sensory neurons, the ganglion cells, is the final determinant of vision loss caused by elevated IOP. It is therefore not unreasonable to speculate that combinatorial therapies, simultaneously targeting outflow together with ganglion cell survival, may prove more highly efficacious than attempting to lower IOP singularly. Mediators of the cytoskeleton, focal adhesions, intercellular junctions, and ECM can all alter the architecture of the outflow tissues, including alterations in cell geometry, contractility, and migration, among other functions, leading to changes in outflow resistance. However, it remains to be determined whether such morphological changes are transient, and whether treated tissues will remain in their remodeled state if treatment is discontinued. To date, the underlying mechanisms by which current first-line medications act remain to be fully elucidated, although significant steps have been made in recent years. Emerging knowledge has led to the development of new formulations showing greater efficacy and safety than conventional medications, with many of these are currently in clinical trial. Many drugs, both old and new, target the conventional outflow pathway, in particular the ECM and cytoskeletal structures, but this is often secondary or indirect to their primary mode of action. Remodeling of the ECM has been shown to influence outflow resistance greatly, giving strength to the hypothesis that the ECM at the JCT contributes substantially to outflow resistance. Perfusion with compounds that activate

matrix modulators, such as MMPs, or even traditional medications, have been shown to increase outflow facility with simultaneous elevations in MMP expression. It is not surprising, however, that perfusion with purified MMPs alone significantly alters conventional outflow, in both its morphology and AH dynamics. Recent developments have demonstrated the efficacy of introducing MMP-1 and MMP-3 genes into the anterior chamber via AAVs. Implementing proteases directly modulating the ECM reduces the potential for unwanted off-target and downstream adversities in comparison to activators or inducers of such proteases; however, MMPs themselves also have downstream signaling cascades, thus selection of specific proteases is important and further development may see an even more specific use of metalloproteinases. For example, MMP-1 was chosen for glucocorticoid-induced expression as it is a well-documented MMP with a large target profile. MMP-3 was chosen for doxycycline eye-drop expression in the cornea due to its secretory domain, its ability to auto-activate and activate other MMPs, and for its target profile being similar to that of the composition of the ECM at the JCT. Similar selection must be undertaken for other drugs in development. ECM modulation by metalloproteinases should in theory be effective in targeting secondary glaucoma, including pseudoexfoliative, pigmentary, and uveitic glaucoma, which involve physical blockage of drainage channels. AAV used as a vector for gene delivery has an excellent safety and tolerability profile. External inducers of viral expression are avenues in themselves, response elements currently ranging from glucocorticoid responsive promoters to tetracycline responsive promoters. The tetracycline-inducible systems have been widely used in AAV expression; however, with them comes their own limitations including leaky promoters and potential toxicity of the inducer. In this regard, it is of note that doxycycline is commonly used as an antibiotic and is also approved for inhibition of select MMP expression. Alternative tetracycline derivatives could prove more efficacious, or the design of unique inducible elements may generate new means of controlling expression in disease states. Such therapies are still in proof-of-concept stages, however, and preclinical functional validation and safety in nonhuman primates will be required.

There is clearly an unmet need for novel glaucoma therapeutics which sufficiently demonstrates a long-term reduction of IOP with minimal side effects. Further elucidation of the exact mechanisms of open-angle glaucoma, and its treatments, may lead to medications that directly target the causative site, arresting disease progress and restoring function to existing tissues.

Funding

Glaucoma research at the Ocular Genetics Unit was supported by the European Research Council under grant [ERC-2012-AdG 322656-Oculus] and an equipment grant from Science Foundation Ireland under grant [12/ERC/B2539].

Declaration of Interest

The authors have no relevant affiliations or financial involvement with any organization or entity with a financial interest in or financial conflict with the subject matter or materials discussed in the manuscript. This includes

employment, consultancies, honoraria, stock ownership or options, expert testimony, grants or patents received or pending, or royalties.

ORCID

Jeffrey O'Callaghan  <http://orcid.org/0000-0001-8818-4331>

Paul S. Cassidy  <http://orcid.org/0000-0003-1454-0318>

References

Papers of special note have been highlighted as either of interest (*) or of considerable interest (***) to readers.

1. Quigley HA, Broman AT. The number of people with glaucoma worldwide in 2010 and 2020. *Br J Ophthalmol*. 2006;90:262–267.
2. Actis AG, Versino E, Brogliatti B, et al. Risk factors for primary open angle glaucoma (POAG) progression: a study ruled in Torino. *Open Ophthalmol J*. 2016;10:129–139.
3. Tham YC, Li X, Wong TY, et al. Global prevalence of glaucoma and projections of glaucoma burden through 2040: a systematic review and meta-analysis. *Ophthalmology*. 2014;121:2081–2090.
4. Quigley HA. Number of people with glaucoma worldwide. *Br J Ophthalmol*. 1996;80:389–393.
5. Sommer A, Tielsch JM, Katz J, et al. Relationship between intraocular pressure and primary open angle glaucoma among white and black Americans. The Baltimore eye survey. *Arch Ophthalmol*. 1991;109:1090–1095.
6. Abu-Amero K, Kondkar AA, Chalam KV. An updated review on the genetics of primary open angle glaucoma. *Int J Mol Sci*. 2015;16:28886–28911.
7. Hardy KM, Hoffman EA, Gonzalez P, et al. Extracellular trafficking of myocilin in human trabecular meshwork cells. *J Biol Chem*. 2005;280:28917–28926.
8. Hoffman EA, Perkumas KM, Highstrom LM, et al. Regulation of myocilin-associated exosome release from human trabecular meshwork cells. *Invest Ophthalmol Vis Sci*. 2009;50:1313–1318.
9. Peters DM, Herbert K, Biddick B, et al. Myocilin binding to hep II domain of fibronectin inhibits cell spreading and incorporation of paxillin into focal adhesions. *Exp Cell Res*. 2005;303:218–228.
10. Ueda J, Wentz-Hunter K, Yue BY. Distribution of myocilin and extracellular matrix components in the juxtacanalicular tissue of human eyes. *Invest Ophthalmol Vis Sci*. 2002;43:1068–1076.
11. Jacobson N, Andrews M, Shepard AR, et al. Non-secretion of mutant proteins of the glaucoma gene myocilin in cultured trabecular meshwork cells and in aqueous humor. *Hum Mol Genet*. 2001;10:117–125.
12. Kasetti RB, Phan TN, Millar JC, et al. Expression of mutant myocilin induces abnormal intracellular accumulation of selected extracellular matrix proteins in the trabecular meshwork. *Invest Ophthalmol Vis Sci*. 2016;57:6058–6069.
13. Zode GS, Kuehn MH, Nishimura DY, et al. Reduction of ER stress via a chemical chaperone prevents disease phenotypes in a mouse model of primary open angle glaucoma. *J Clin Invest*. 2011;121:3542–3553.
14. Rezaie T, Child A, Hitchings R, et al. Adult-onset primary open-angle glaucoma caused by mutations in optineurin. *Science*. 2002;295:1077–1079.
15. De Marco N, Buono M, Troise F, et al. Optineurin increases cell survival and translocates to the nucleus in a Rab8-dependent manner upon an apoptotic stimulus. *J Biol Chem*. 2006;281:16147–16156.
16. Gemenetzi M, Yang Y, Lotery AJ. Current concepts on primary open-angle glaucoma genetics: a contribution to disease pathophysiology and future treatment. *Eye (Lond)*. 2012;26:355–369.
17. Fuse N, Takahashi K, Akiyama H, et al. Molecular genetic analysis of optineurin gene for primary open-angle and normal tension glaucoma in the Japanese population. *J Glaucoma*. 2004;13:299–303.
18. Fingert JH. Primary open-angle glaucoma genes. *Eye (Lond)*. 2011;25:587–595.

19. Tourkina E, Gooz P, Pannu J, et al. Opposing effects of protein kinase Calpha and protein kinase Cepsilon on collagen expression by human lung fibroblasts are mediated via MEK/ERK and caveolin-1 signaling. *J Biol Chem.* 2005;280:13879–13887.
20. Del Galdo F, Lisanti MP, Jimenez SA. Caveolin-1, transforming growth factor-beta receptor internalization, and the pathogenesis of systemic sclerosis. *Curr Opin Rheumatol.* 2008;20:713–719.
21. Thompson C, Rahim S, Arnold J, et al. Loss of caveolin-1 alters extracellular matrix protein expression and ductal architecture in murine mammary glands. *PLoS One.* 2017;12:e0172067.
22. Surgucheva I, Surguchov A. Expression of caveolin in trabecular meshwork cells and its possible implication in pathogenesis of primary open angle glaucoma. *Mol Vis.* 2011;17:2878–2888.
23. Razani B, Zhang XL, Bitzer M, et al. Caveolin-1 regulates transforming growth factor (TGF)-beta/SMAD signaling through an interaction with the TGF-beta type I receptor. *J Biol Chem.* 2001;276:6727–6738.
24. Elliott MH, Ashpole NE, Gu X, et al. Caveolin-1 modulates intraocular pressure: implications for caveolae mechanoprotection in glaucoma. *Sci Rep.* 2016;6:37127.
25. Ozel AB, Moroi SE, Reed DM, et al. Genome-wide association study and meta-analysis of intraocular pressure. *Hum Genet.* 2014;133:41–57.
26. Burdon KP, Macgregor S, Hewitt AW, et al. Genome-wide association study identifies susceptibility loci for open angle glaucoma at TMCO1 and CDKN2B-AS1. *Nat Genet.* 2011;43:574–578.
27. Hysi PG, Cheng CY, Springelkamp H, et al. Genome-wide analysis of multi-ancestry cohorts identifies new loci influencing intraocular pressure and susceptibility to glaucoma. *Nat Genet.* 2014;46:1126–1130.
28. Wang QC, Zheng Q, Tan H, et al. TMCO1 Is an ER Ca(2+) load-activated Ca(2+) channel. *Cell.* 2016;165:1454–1466.
29. Lu Y, Vitart V, Burdon KP, et al. Genome-wide association analyses identify multiple loci associated with central corneal thickness and keratoconus. *Nat Genet.* 2013;45:155–163.
30. Springelkamp H, Hohn R, Mishra A, et al. Meta-analysis of genome-wide association studies identifies novel loci that influence cupping and the glaucomatous process. *Nat Commun.* 2014;5:4883.
31. Iglesias AI, Springelkamp H, Ramdas WD, et al. Genes, pathways, and animal models in primary open-angle glaucoma. *Eye (Lond).* 2015;29:1285–1298.
32. Springelkamp H, Mishra A, Hysi PG, et al. Meta-analysis of genome-wide association studies identifies novel loci associated with optic disc morphology. *Genet Epidemiol.* 2015;39:207–216.
33. Kloeckener-Gruissem B, Bartholdi D, Abdou MT, et al. Identification of the genetic defect in the original Wagner syndrome family. *Mol Vis.* 2006;12:350–355.
34. Keller KE, Bradley JM, Vranka JA, et al. Segmental versican expression in the trabecular meshwork and involvement in outflow facility. *Invest Ophthalmol Vis Sci.* 2011;52:5049–5057.
35. Jelodari-Mamaghani S, Haji-Seyed-Javadi R, Suri F, et al. Contribution of the latent transforming growth factor-beta binding protein 2 gene to etiology of primary open angle glaucoma and pseudoexfoliation syndrome. *Mol Vis.* 2013;19:333–347.
36. Kuchtey J, Chang TC, Panagis L, et al. Marfan syndrome caused by a novel FBN1 mutation with associated pigmentary glaucoma. *Am J Med Genet A.* 2013;161A:880–883.
37. Kuchtey J, Kuchtey RW. The microfibril hypothesis of glaucoma: implications for treatment of elevated intraocular pressure. *J Ocul Pharmacol Ther.* 2014;30:170–180.
38. Morales J, Al-Sharif L, Khalil DS, et al. Homozygous mutations in ADAMTS10 and ADAMTS17 cause lenticular myopia, ectopia lentis, glaucoma, spherophakia, and short stature. *Am J Hum Genet.* 2009;85:558–568.
39. Keller KE, Acott TS. The juxtacanalicular region of ocular trabecular meshwork: a tissue with a unique extracellular matrix and specialized function. *J Ocul Biol Dis Infor.* 2013;1:3.
 - **A comprehensive review of the JCT.**
40. Fuchshofer R, Welge-Lussen U, Lutjen-Drecoll E, et al. Biochemical and morphological analysis of basement membrane component expression in corneoscleral and cribriform human trabecular meshwork cells. *Invest Ophthalmol Vis Sci.* 2006;47:794–801.
41. Kizhatil K, Ryan M, Marchant JK, et al. Schlemm's canal is a unique vessel with a combination of blood vascular and lymphatic phenotypes that forms by a novel developmental process. *PLoS Biol.* 2014;12:e1001912.
42. Overby DR, Stamer WD, Johnson M. The changing paradigm of outflow resistance generation: towards synergistic models of the JCT and inner wall endothelium. *Exp Eye Res.* 2009;88:656–670.
 - **An important paper exploring the sites of resistance generation in the outflow tissue, and the ECM molecules that might be involved.**
43. Tam LC, Reina-Torres E, Sherwood JM, et al. Enhancement of outflow facility in the murine eye by targeting selected tight-junctions of schlemm's canal endothelia. *Sci Rep.* 2017;7:40717.
44. Reina-Torres E, Wen JC, Liu KC, et al. VEGF as a paracrine regulator of conventional outflow facility. *Invest Ophthalmol Vis Sci.* 2017;58:1899–1908.
45. Aspelund A, Tammela T, Antila S, et al. The Schlemm's canal is a VEGF-C/VEGFR-3-responsive lymphatic-like vessel. *J Clin Invest.* 2014;124:3975–3986.
46. Vranka JA, Kelley MJ, Acott TS, et al. Extracellular matrix in the trabecular meshwork: intraocular pressure regulation and dysregulation in glaucoma. *Exp Eye Res.* 2015;133:112–125.
47. VanderWyst SS, Perkumas KM, Read AT, et al. Structural basement membrane components and corresponding integrins in Schlemm's canal endothelia. *Mol Vis.* 2011;17:199–209.
48. Faralli JA, Schwinn MK, Gonzalez JM Jr., et al. Functional properties of fibronectin in the trabecular meshwork. *Exp Eye Res.* 2009;88:689–693.
49. Rohen JW, Futa R, Lutjen-Drecoll E. The fine structure of the cribriform meshwork in normal and glaucomatous eyes as seen in tangential sections. *Invest Ophthalmol Vis Sci.* 1981;21:574–585.
50. Burrige K, Fath K, Kelly T, et al. Focal adhesions: transmembrane junctions between the extracellular matrix and the cytoskeleton. *Annu Rev Cell Biol.* 1988;4:487–525.
51. Cheng YF, Kramer RH. Human microvascular endothelial cells express integrin-related complexes that mediate adhesion to the extracellular matrix. *J Cell Physiol.* 1989;139:275–286.
52. Lampugnani MG, Resnati M, Dejana E, et al. The role of integrins in the maintenance of endothelial monolayer integrity. *J Cell Biol.* 1991;112:479–490.
53. Geiger B, Bershadsky A, Pankov R, et al. Transmembrane crosstalk between the extracellular matrix–cytoskeleton crosstalk. *Nat Rev Mol Cell Biol.* 2001;2:793–805.
54. Han H, Wecker T, Grehn F, et al. Elasticity-dependent modulation of TGF-beta responses in human trabecular meshwork cells. *Invest Ophthalmol Vis Sci.* 2011;52:2889–2896.
55. Wallace DM, Murphy-Ullrich JE, Downs JC, et al. The role of matrix proteins in glaucoma. *Matrix Biol.* 2014;37:174–182.
56. Mutsaers SE, Bishop JE, McGrouther G, et al. Mechanisms of tissue repair: from wound healing to fibrosis. *Int J Biochem Cell Biol.* 1997;29:5–17.
57. Wight TN, Potter-Perigo S. The extracellular matrix: an active or passive player in fibrosis? *Am J Physiol Gastrointest Liver Physiol.* 2011;301:G950–G955.
58. Tektas OY, Lutjen-Drecoll E. Structural changes of the trabecular meshwork in different kinds of glaucoma. *Exp Eye Res.* 2009;88:769–775.
 - **A comparison of the TM in different types of glaucoma using electron microscopy.**
59. Alm A, Nilsson SF. Uveoscleral outflow—a review. *Exp Eye Res.* 2009;88:760–768.
60. Stamer WD. The cell and molecular biology of glaucoma: mechanisms in the conventional outflow pathway. *Invest Ophthalmol Vis Sci.* 2012;53:2470–2472.
61. Goel M, Picciani RG, Lee RK, et al. Aqueous humor dynamics: a review. *Open Ophthalmol J.* 2010;4:52–59.
62. Bill A, Svedbergh B. Scanning electron microscopic studies of the trabecular meshwork and the canal of Schlemm—an attempt to

- localize the main resistance to outflow of aqueous humor in man. *Acta Ophthalmol (Copenh)*. 1972;50:295–320.
63. Inomata H, Bill A, Smelser GK. Aqueous humor pathways through the trabecular meshwork and into Schlemm's canal in the cynomolgus monkey (*Macaca irus*). An electron microscopic study. *Am J Ophthalmol*. 1972;73:760–789.
 64. Johnstone MA, Grant WG. Pressure-dependent changes in structures of the aqueous outflow system of human and monkey eyes. *Am J Ophthalmol*. 1973;75:365–383.
 65. Johnson MC, Kamm RD. The role of Schlemm's canal in aqueous outflow from the human eye. *Invest Ophthalmol Vis Sci*. 1983;24:320–325.
 66. Johnson M. What controls aqueous humour outflow resistance? *Exp Eye Res*. 2006;82:545–557.
 67. Rosenquist R, Epstein D, Melamed S, et al. Outflow resistance of enucleated human eyes at two different perfusion pressures and different extents of trabeculotomy. *Curr Eye Res*. 1989;8:1233–1240.
 68. Grant WM. Experimental aqueous perfusion in enucleated human eyes. *Arch Ophthalmol*. 1963;69:783–801.
 69. Wise JB, Witter SL. Argon laser therapy for open-angle glaucoma. A pilot study. *Arch Ophthalmol*. 1979;97:319–322.
 70. Swaminathan SS, Oh DJ, Kang MH, et al. Aqueous outflow: segmental and distal flow. *J Cataract Refract Surg*. 2014;40:1263–1272.
 71. Tanihara H, Inatani M, Koga T, et al. Proteoglycans in the eye. *Cornea*. 2002;21:62–69.
 72. Floyd BB, Cleveland PH, Worthen DM. Fibronectin in human trabecular drainage channels. *Invest Ophthalmol Vis Sci*. 1985;26:797–804.
 73. Swaminathan SS, Oh DJ, Kang MH, et al. Secreted protein acidic and rich in cysteine (SPARC)-null mice exhibit more uniform outflow. *Invest Ophthalmol Vis Sci*. 2013;54:2035–2047.
 74. Keller KE, Bradley JM, Kelley MJ, et al. Effects of modifiers of glycosaminoglycan biosynthesis on outflow facility in perfusion culture. *Invest Ophthalmol Vis Sci*. 2008;49:2495–2505.
 75. Gong H, Freddo TF, Johnson M. Age-related changes of sulfated proteoglycans in the normal human trabecular meshwork. *Exp Eye Res*. 1992;55:691–709.
 76. Berggren L, Vrabec F. Demonstration of a coating substance in the trabecular meshwork of the eye and its decrease after perfusion experiments with different kinds of hyaluronidase. *Am J Ophthalmol*. 1957;44:200–208.
 77. Francois J. Corticosteroid glaucoma. *Ann Ophthalmol*. 1977;9:1075–1080.
 78. Sherwood JM, Reina-Torres E, Bertrand JA, et al. Measurement of outflow facility using ipefusion. *PLoS One*. 2016;11:e0150694.
 79. Vranka JA, Acott TS. Pressure-induced expression changes in segmental flow regions of the human trabecular meshwork. *Exp Eye Res*. 2016;158:67–72.
 - **This review describes the importance of the ECM at the TM in the homeostatic regulation of intraocular pressure.**
 80. Bradley JM, Kelley MJ, Zhu X, et al. Effects of mechanical stretching on trabecular matrix metalloproteinases. *Invest Ophthalmol Vis Sci*. 2001;42:1505–1513.
 - **This article describes how changes in the ECM induce responses in nearby cells, influencing the turnover rates of ECM. This feedback mechanism is fundamental to homeostatic regulation.**
 81. Zhao X, Ramsey KE, Stephan DA, et al. Gene and protein expression changes in human trabecular meshwork cells treated with transforming growth factor-beta. *Invest Ophthalmol Vis Sci*. 2004;45:4023–4034.
 82. Vittal V, Rose A, Gregory KE, et al. Changes in gene expression by trabecular meshwork cells in response to mechanical stretching. *Invest Ophthalmol Vis Sci*. 2005;46:2857–2868.
 83. Lo WR, Rowlette LL, Caballero M, et al. Tissue differential microarray analysis of dexamethasone induction reveals potential mechanisms of steroid glaucoma. *Invest Ophthalmol Vis Sci*. 2003;44:473–485.
 84. Izzotti A, Longobardi M, Cartiglia C, et al. Trabecular meshwork gene expression after selective laser trabeculoplasty. *PLoS One*. 2011;6:e20110.
 85. Keller KE, Aga M, Bradley JM, et al. Extracellular matrix turnover and outflow resistance. *Exp Eye Res*. 2009;88:676–682.
 86. Nagase H, Suzuki K, Enghild JJ, et al. Stepwise activation mechanisms of the precursors of matrix metalloproteinases 1 (tissue collagenase) and 3 (stromelysin). *Biomedica Biochimica Acta*. 1991;50:749–754.
 - **A detailed description of the mechanisms required to activate MMPs.**
 87. Chakraborti S, Mandal M, Das S, et al. Regulation of matrix metalloproteinases: an overview. *Mol Cell Biochem*. 2003;253:269–285.
 88. Alexander JP, Samples JR, Van Buskirk EM, et al. Expression of matrix metalloproteinases and inhibitor by human trabecular meshwork. *Invest Ophthalmol Vis Sci*. 1991;32:172–180.
 89. Oh DJ, Martin JL, Williams AJ, et al. Effect of latanoprost on the expression of matrix metalloproteinases and their tissue inhibitors in human trabecular meshwork cells. *Invest Ophthalmol Vis Sci*. 2006;47:3887–3895.
 - **An indication that MMP expression can be influenced by topical administration of medications.**
 90. Kelley MJ, Rose AY, Song K, et al. Synergism of TNF and IL-1 in the induction of matrix metalloproteinase-3 in trabecular meshwork. *Invest Ophthalmol Vis Sci*. 2007;48:2634–2643.
 91. Overby DR, Bertrand J, Tektas OY, et al. Ultrastructural changes associated with dexamethasone-induced ocular hypertension in mice. *Invest Ophthalmol Vis Sci*. 2014;55:4922–4933.
 92. Schlotzer-Schrehardt U, Lommatzsch J, Kuchle M, et al. Matrix metalloproteinases and their inhibitors in aqueous humor of patients with pseudoexfoliation syndrome/glaucoma and primary open-angle glaucoma. *Invest Ophthalmol Vis Sci*. 2003;44:1117–1125.
 93. Ronkko S, Rekonen P, Kaarniranta K, et al. Matrix metalloproteinases and their inhibitors in the chamber angle of normal eyes and patients with primary open-angle glaucoma and exfoliation glaucoma. *Graefes Arch Clin Exp Ophthalmol = Albrecht Von Graefes Archiv Fur Klinische Und Experimentelle Ophthalmologie*. 2007;245:697–704.
 94. Fountoulakis N, Labiris G, Aristeidou A, et al. Tissue inhibitor of metalloproteinase 4 in aqueous humor of patients with primary open angle glaucoma, pseudoexfoliation syndrome and pseudoexfoliative glaucoma and its role in proteolysis imbalance. *BMC Ophthalmol*. 2013;13:69.
 95. Ashworth Briggs EL, Toh T, Eri R, et al. TIMP1, TIMP2, and TIMP4 are increased in aqueous humor from primary open angle glaucoma patients. *Mol Vis*. 2015;21:1162–1172.
 96. Weinstein WL, Dietrich UM, Sapienza JS, et al. Identification of ocular matrix metalloproteinases present within the aqueous humor and iridocorneal drainage angle tissue of normal and glaucomatous canine eyes. *Vet Ophthalmol*. 2007;10(Suppl 1):108–116.
 97. Maatta M, Tervahartiala T, Vesti E, et al. Levels and activation of matrix metalloproteinases in aqueous humor are elevated in uveitis-related secondary glaucoma. *J Glaucoma*. 2006;15:229–237.
 98. O'Callaghan J, Crosbie DE, Cassidy PS, et al. The therapeutic potential of AAV-mediated MMP-3 secretion from corneal endothelium in treating glaucoma. *Hum Mol Genet*. 2017;26:1230–1246.
 - **This article demonstrated that virally expressed MMP-3 could be induced via eye drop to increase outflow facility and reduce IOP.**
 99. Bradley JM, Vranka J, Colvis CM, et al. Effect of matrix metalloproteinases activity on outflow in perfused human organ culture. *Invest Ophthalmol Vis Sci*. 1998;39:2649–2658.
 100. Pang IH, Fleenor DL, Hellberg PE, et al. Aqueous outflow-enhancing effect of tert-butylhydroquinone: involvement of AP-1 activation and MMP-3 expression. *Invest Ophthalmol Vis Sci*. 2003;44:3502–3510.
 101. Webb JG, Husain S, Yates PW, et al. Kinin modulation of conventional outflow facility in the bovine eye. *J Ocul Pharmacol Ther*. 2006;22:310–316.
 102. De Groef L, Van Hove I, Dekeyser E, et al. MMPs in the trabecular meshwork: promising targets for future glaucoma therapies? *Invest Ophthalmol Vis Sci*. 2013;54:7756–7763.

103. Aga M, Bradley JM, Wanchu R, et al. Differential effects of caveolin-1 and -2 knockdown on aqueous outflow and altered extracellular matrix turnover in caveolin-silenced trabecular meshwork cells. *Invest Ophthalmol Vis Sci.* 2014;55:5497–5509.
104. Yang YF, Sun YY, Acott TS, et al. Effects of induction and inhibition of matrix cross-linking on remodeling of the aqueous outflow resistance by ocular trabecular meshwork cells. *Sci Rep.* 2016;6:30505.
105. Huovila AP, Turner AJ, Pelto-Huikko M, et al. Shedding light on ADAM metalloproteinases. *Trends Biochem Sci.* 2005;30:413–422.
106. Stickel SK, Wang YL. Synthetic peptide GRGDS induces dissociation of alpha-actinin and vinculin from the sites of focal contacts. *J Cell Biol.* 1988;107:1231–1239.
107. Curtis TM, McKeown-Longo PJ, Vincent PA, et al. Fibronectin attenuates increased endothelial monolayer permeability after RGD peptide, anti-alpha 5 beta 1, or TNF-alpha exposure. *Am J Physiol.* 1995;269:248–260.
108. Wu MH, Ustinova E, Granger HJ. Integrin binding to fibronectin and vitronectin maintains the barrier function of isolated porcine coronary venules. *J Physiol.* 2001;532:785–791.
109. Tamm ER, Siegner A, Baur A, et al. Transforming growth factor-beta 1 induces alpha-smooth muscle-actin expression in cultured human and monkey trabecular meshwork. *Exp Eye Res.* 1996;62:389–397.
110. Schlunck G, Han H, Wecker T, et al. Substrate rigidity modulates cell matrix interactions and protein expression in human trabecular meshwork cells. *Invest Ophthalmol Vis Sci.* 2008;49:262–269.
111. Yang Y, Estrada EY, Thompson JF, et al. Matrix metalloproteinase-mediated disruption of tight junction proteins in cerebral vessels is reversed by synthetic matrix metalloproteinase inhibitor in focal ischemia in rat. *J Cereb Blood Flow Metab.* 2007;27:697–709.
112. Vermeer PD, Denker J, Estin M, et al. MMP9 modulates tight junction integrity and cell viability in human airway epithelia. *Am J Physiol Lung Cell Mol Physiol.* 2009;296:751–762.
113. Yamada H, Yoneda M, Inaguma S, et al. Infliximab counteracts tumor necrosis factor-alpha-enhanced induction of matrix metalloproteinases that degrade claudin and occludin in non-pigmented ciliary epithelium. *Biochem Pharmacol.* 2013;85:1770–1782.
114. Rylander NR, Vold SD. Cost analysis of glaucoma medications. *Am J Ophthalmol.* 2008;145:106–113.
115. Li T, Lindsley K, Rouse B, et al. Comparative effectiveness of first-line medications for primary open-angle glaucoma: a systematic review and network meta-analysis. *Ophthalmology.* 2016;123:129–140.
116. Mastropasqua R, Fasanella V, Pedrotti E, et al. Trans-conjunctival aqueous humor outflow in glaucomatous patients treated with prostaglandin analogues: an in vivo confocal microscopy study. *Graefes Arch Clin Exp Ophthalmol = Albrecht Von Graefes Archiv Fur Klinische Und Experimentelle Ophthalmologie.* 2014;252:1469–1476.
117. Toris CB, Gabelt BT, Kaufman PL. Update on the mechanism of action of topical prostaglandins for intraocular pressure reduction. *Surv Ophthalmol.* 2008;53(Suppl1):S107–S120.
- **This paper shows that prostaglandins can affect the conventional outflow pathway, not only the unconventional.**
118. Richter M, Krauss AH, Woodward DF, et al. Morphological changes in the anterior eye segment after long-term treatment with different receptor selective prostaglandin agonists and a prostamide. *Invest Ophthalmol Vis Sci.* 2003;44:4419–4426.
119. Goh Y, Urade Y, Fujimoto N, et al. Content and formation of prostaglandins and distribution of prostaglandin-related enzyme activities in the rat ocular system. *Biochim Biophys Acta.* 1987;921:302–311.
120. Wan Z, Woodward DF, Stamer WD. Endogenous bioactive lipids and the regulation of conventional outflow facility. *Expert Rev Ophthalmol.* 2008;3:457–470.
121. Bahler CK, Howell KG, Hann CR, et al. Prostaglandins increase trabecular meshwork outflow facility in cultured human anterior segments. *Am J Ophthalmol.* 2008;145:114–119.
122. Wan Z, Woodward DF, Cornell CL, et al. Bimatoprost, prostamide activity, and conventional drainage. *Invest Ophthalmol Vis Sci.* 2007;48:4107–4115.
123. Thieme H, Schimmat C, Munzer G, et al. Endothelin antagonism: effects of FP receptor agonists prostaglandin F2alpha and fluprostenol on trabecular meshwork contractility. *Invest Ophthalmol Vis Sci.* 2006;47:938–945.
124. Weinreb RN, Toris CB, Gabelt BT, et al. Effects of prostaglandins on the aqueous humor outflow pathways. *Surv Ophthalmol.* 2002;47 (Suppl 1):S53–S64.
125. Schachtschabel U, Lindsey JD, Weinreb RN. The mechanism of action of prostaglandins on uveoscleral outflow. *Curr Opin Ophthalmol.* 2000;11:112–115.
126. Ocklind A. Effect of latanoprost on the extracellular matrix of the ciliary muscle. A study on cultured cells and tissue sections. *Exp Eye Res.* 1998;67:179–191.
127. Sagara T, Gatton DD, Lindsey JD, et al. Topical prostaglandin F2alpha treatment reduces collagen types I, III, and IV in the monkey uveoscleral outflow pathway. *Arch Ophthalmol.* 1999;117:794–801.
128. Weinreb RN, Kashiwagi K, Kashiwagi F, et al. Prostaglandins increase matrix metalloproteinase release from human ciliary smooth muscle cells. *Invest Ophthalmol Vis Sci.* 1997;38:2772–2780.
129. Woodward DF, Nilsson SF, Toris CB, et al. Prostanoid EP4 receptor stimulation produces ocular hypotension by a mechanism that does not appear to involve uveoscleral outflow. *Invest Ophthalmol Vis Sci.* 2009;50:3320–3328.
130. Alvarado JA, Iguchi R, Martinez J, et al. Similar effects of selective laser trabeculoplasty and prostaglandin analogs on the permeability of cultured Schlemm canal cells. *Am J Ophthalmol.* 2010;150:254–264.
131. Brooks AM, Gillies WE. Ocular beta-blockers in glaucoma management. *Clinical pharmacological aspects. Drugs Aging.* 1992;2:208–221.
132. Trope GE, Clark B. Beta adrenergic receptors in pigmented ciliary processes. *Br J Ophthalmol.* 1982;66:788–792.
133. Camras CB, Podos SM. The role of endogenous prostaglandins in clinically-used and investigational glaucoma therapy. *Prog Clin Biol Res.* 1989;312:459–475.
134. Toris CB, Camras CB, Yablonski ME. Acute versus chronic effects of brimonidine on aqueous humor dynamics in ocular hypertensive patients. *Am J Ophthalmol.* 1999;128:8–14.
135. Beidoe G, Mousa SA. Current primary open-angle glaucoma treatments and future directions. *Clin Ophthalmol.* 2012;6:1699–1707.
136. Avila MY, Carre DA, Stone RA, et al. Reliable measurement of mouse intraocular pressure by a servo-null micropipette system. *Invest Ophthalmol Vis Sci.* 2001;42:1841–1846.
137. Overby DR, Bertrand J, Schicht M, et al. The structure of the trabecular meshwork, its connections to the ciliary muscle, and the effect of pilocarpine on outflow facility in mice. *Invest Ophthalmol Vis Sci.* 2014;55:3727–3736.
138. Li G, Farsiu S, Chiu SJ, et al. Pilocarpine-induced dilation of Schlemm's canal and prevention of lumen collapse at elevated intraocular pressures in living mice visualized by OCT. *Invest Ophthalmol Vis Sci.* 2014;55:3737–3746.
139. Selbach JM, Gottanka J, Wittmann M, et al. Efferent and afferent innervation of primate trabecular meshwork and scleral spur. *Invest Ophthalmol Vis Sci.* 2000;41:2184–2191.
140. Ito T, Ohguro H, Mamiya K, et al. Effects of antiglaucoma drops on MMP and TIMP balance in conjunctival and subconjunctival tissue. *Invest Ophthalmol Vis Sci.* 2006;47:823–830.
141. Scherer WJ. A retrospective review of non-responders to latanoprost. *J Ocul Pharmacol Ther.* 2002;18:287–291.
142. Noecker RS, Dirks MS, Choplin NT, et al. A six-month randomized clinical trial comparing the intraocular pressure-lowering efficacy of bimatoprost and latanoprost in patients with ocular hypertension or glaucoma. *Am J Ophthalmol.* 2003;135:55–63.

143. Li G, Mukherjee D, Navarro I, et al. Visualization of conventional outflow tissue responses to netarsudil in living mouse eyes. *Eur J Pharmacol.* **2016**;787:20–31.
144. Ren R, Li G, Le TD, et al. Netarsudil increases outflow facility in human eyes through multiple mechanisms. *Invest Ophthalmol Vis Sci.* **2016**;57:6197–6209.
145. Wang RF, Williamson JE, Kopczynski C, et al. Effect of 0.04% AR-13324, a ROCK, and norepinephrine transporter inhibitor, on aqueous humor dynamics in normotensive monkey eyes. *J Glaucoma.* **2015**;24:51–54.
146. Fukata Y, Amano M, Kaibuchi K. Rho-Rho-kinase pathway in smooth muscle contraction and cytoskeletal reorganization of non-muscle cells. *Trends Pharmacol Sci.* **2001**;22:32–39.
147. Goldhagen B, Proia AD, Epstein DL, et al. Elevated levels of RhoA in the optic nerve head of human eyes with glaucoma. *J Glaucoma.* **2012**;21:530–538.
148. Rao VP, Epstein DL. Rho GTPase/Rho kinase inhibition as a novel target for the treatment of glaucoma. *BioDrugs.* **2007**;21:167–177.
149. Wettschureck N, Offermanns S. Rho/Rho-kinase mediated signaling in physiology and pathophysiology. *J Mol Med (Berl).* **2002**;80:629–638.
150. Rao PV, Deng PF, Kumar J, et al. Modulation of aqueous humor outflow facility by the Rho kinase-specific inhibitor Y-27632. *Invest Ophthalmol Vis Sci.* **2010**;42:1029–1037.
151. Lu Z, Overby DR, Scott PA, et al. The mechanism of increasing outflow facility by rho-kinase inhibition with Y-27632 in bovine eyes. *Exp Eye Res.* **2008**;86:271–281.
152. Wang SK, Chang RT. An emerging treatment option for glaucoma: rho kinase inhibitors. *Clin Ophthalmol.* **2014**;8:883–890.
153. Riento K, Ridley AJ. Rocks: multifunctional kinases in cell behaviour. *Nat Rev Mol Cell Biol.* **2003**;4:446–456.
154. Liu X, Hu Y, Filla MS, et al. The effect of C3 transgene expression on actin and cellular adhesions in cultured human trabecular meshwork cells and on outflow facility in organ cultured monkey eyes. *Mol Vis.* **2005**;11:1112–1121.
155. Tian B, Kiland JA, Kaufman PL. Effects of the marine macrolides swinholide A and jaspilakinolide on outflow facility in monkeys. *Invest Ophthalmol Vis Sci.* **2001**;42:3187–3192.
156. Bubb MR, Spector I, Bershady AD, et al. Swinholide A is a microfilament disrupting marine toxin that stabilizes actin dimers and severs actin filaments. *J Biol Chem.* **1995**;270:3463–3466.
157. Coue M, Brenner SL, Spector I, et al. Inhibition of actin polymerization by latrunculin A. *FEBS Lett.* **1987**;213:316–318.
158. Bubb MR, Senderowicz AM, Sausville EA, et al. Jaspilakinolide, a cytotoxic natural product, induces actin polymerization and competitively inhibits the binding of phalloidin to F-actin. *J Biol Chem.* **1994**;269:14869–14871.
159. Peterson JA, Tian B, Geiger B, et al. Effect of latrunculin-B on outflow facility in monkeys. *Exp Eye Res.* **2000**;70:307–313.
160. Okka M, Tian B, Kaufman PL. Effect of low-dose latrunculin B on anterior segment physiologic features in the monkey eye. *Arch Ophthalmol.* **2004**;122:1482–1488.
161. Ethier CR, Read AT, Chan DW. Effects of latrunculin-B on outflow facility and trabecular meshwork structure in human eyes. *Invest Ophthalmol Vis Sci.* **2006**;47:1991–1998.
162. Sabanay I, Tian B, Gabelt BT, et al. Latrunculin B effects on trabecular meshwork and corneal endothelial morphology in monkeys. *Exp Eye Res.* **2006**;82:236–246.
163. Peterson JA, Tian B, McLaren JW, et al. Latrunculins' effects on intraocular pressure, aqueous humor flow, and corneal endothelium. *Invest Ophthalmol Vis Sci.* **2000**;41:1749–1758.
164. Rasmussen CA, Kaufman PL, Ritch R, et al. Latrunculin B reduces intraocular pressure in human ocular hypertension and primary open-angle glaucoma. *Transl Vis Sci Technol.* **2014**;3:1.
165. Mitchell CH, Peterson-Yantorno K, Carre DA, et al. A3 adenosine receptors regulate Cl⁻ channels of nonpigmented ciliary epithelial cells. *Am J Physiol.* **1999**;276:C659–C666.
166. Laties A, Rich CC, Stoltz R, et al. A randomized phase 1 dose escalation study to evaluate safety, tolerability, and pharmacokinetics of trabadenoson in healthy adult volunteers. *J Ocul Pharmacol Ther.* **2016**;32:548–554.
167. Zhong Y, Yang Z, Huang WC, et al. Adenosine, adenosine receptors and glaucoma: an updated overview. *Biochim Biophys Acta.* **2013**;1830:2882–2890.
168. Shearer TW, Crosson CE. Adenosine A1 receptor modulation of MMP-2 secretion by trabecular meshwork cells. *Invest Ophthalmol Vis Sci.* **2002**;43:3016–3020.
169. Crosson CE, Sloan CF, Yates PW. Modulation of conventional outflow facility by the adenosine A1 agonist N6-cyclohexyladenosine. *Invest Ophthalmol Vis Sci.* **2005**;46:3795–3799.
170. Chen J, Runyan SA, Robinson MR. Novel ocular antihypertensive compounds in clinical trials. *Clin Ophthalmol.* **2011**;5:667–677.
171. Cavet ME, Vollmer TR, Harrington KL, et al. Regulation of endothelin-1-induced trabecular meshwork cell contractility by latanoprostene bunod. *Invest Ophthalmol Vis Sci.* **2015**;56:4108–4116.
172. Kalouche G, Beguier F, Bakria M, et al. Activation of prostaglandin FP and EP2 receptors differently modulates myofibroblast transition in a model of adult primary human trabecular meshwork cells. *Invest Ophthalmol Vis Sci.* **2016**;57:1816–1825.
173. Nilsson SF, Drecoll E, Lutjen-Drecoll E, et al. The prostanoid EP2 receptor agonist butaprost increases uveoscleral outflow in the cynomolgus monkey. *Invest Ophthalmol Vis Sci.* **2006**;47:4042–4049.
174. Wang JW, Woodward DF, Stamer WD. Differential effects of prostaglandin E2-sensitive receptors on contractility of human ocular cells that regulate conventional outflow. *Invest Ophthalmol Vis Sci.* **2013**;54:4782–4790.
175. Millard LH, Woodward DF, Stamer WD. The role of the prostaglandin EP4 receptor in the regulation of human outflow facility. *Invest Ophthalmol Vis Sci.* **2011**;52:3506–3513.
176. Fujino H, Xu W, Regan JW. Prostaglandin E2 induced functional expression of early growth response factor-1 by EP4, but not EP2, prostanoid receptors via the phosphatidylinositol 3-kinase and extracellular signal-regulated kinases. *J Biol Chem.* **2003**;278:12151–12156.
177. Zhong J, Gencay MM, Bubendorf L, et al. ERK1/2 and p38 MAP kinase control MMP-2, MT1-MMP, and TIMP action and affect cell migration: a comparison between mesothelioma and mesothelial cells. *J Cell Physiol.* **2006**;207:540–552.
178. Martinez T, Jimenez AI, Paneda C. Short-interference RNAs: becoming medicines. *Excli J.* **2015**;14:714–746.
179. Moreno-Montanes J, Sadaba B, Ruz V, et al. Phase I clinical trial of SYL040012, a small interfering RNA targeting beta-adrenergic receptor 2, for lowering intraocular pressure. *Mol Ther.* **2014**;22:226–232.
180. Datta S, Baudouin C, Brignole-Baudouin F, et al. The eye drop preservative benzalkonium chloride potentially induces mitochondrial dysfunction and preferentially affects LHON mutant cells. *Invest Ophthalmol Vis Sci.* **2017**;58:2406–2412.
181. Schehlein EM, Novack GD, Robin AL. New classes of glaucoma medications. *Curr Opin Ophthalmol.* **2017**;28:161–168.
182. Rasmussen CA, Kaufman PL. Exciting directions in glaucoma. *Can J Ophthalmol.* **2014**;49:534–543.
183. Borrás T, Buie LK, Spiga MG. Inducible scAAV2.GRE.MMP1 lowers IOP long-term in a large animal model for steroid-induced glaucoma gene therapy. *Gene Ther.* **2016**;23:438–449.
- **This article was the first to show that an inducible virus expressing MMP in the anterior chamber could reduce IOP in an animal model.**
184. Liu X, Brandt CR, Gabelt BT, et al. Herpes simplex virus mediated gene transfer to primate ocular tissues. *Exp Eye Res.* **1999**;69:385–395.
185. Spencer B, Agarwala S, Miskulin M, et al. Herpes simplex virus-mediated gene delivery to the rodent visual system. *Invest Ophthalmol Vis Sci.* **2000**;41:1392–1401.
186. Loewen N, Fautsch MP, Teo WL, et al. Long-term, targeted genetic modification of the aqueous humor outflow tract coupled with noninvasive imaging of gene expression in vivo. *Invest Ophthalmol Vis Sci.* **2004**;45:3091–3098.

187. Challa P, Luna C, Liton PB, et al. Lentiviral mediated gene delivery to the anterior chamber of rodent eyes. *Mol Vis.* 2005;11:425–430.
188. Barraza RA, Rasmussen CA, Loewen N, et al. Prolonged transgene expression with lentiviral vectors in the aqueous humor outflow pathway of nonhuman primates. *Hum Gene Ther.* 2009;20:191–200.
189. Budenz DL, Bennett J, Alonso L, et al. In vivo gene transfer into murine corneal endothelial and trabecular meshwork cells. *Invest Ophthalmol Vis Sci.* 1995;36:2211–2215.
190. Borrás T, Tamm ER, Zigler JS Jr. Ocular adenovirus gene transfer varies in efficiency and inflammatory response. *Invest Ophthalmol Vis Sci.* 1996;37:1282–1293.
191. Borrás T, Gabelt BT, Klintworth GK, et al. Non-invasive observation of repeated adenoviral GFP gene delivery to the anterior segment of the monkey eye in vivo. *J Gene Med.* 2001;3:437–449.
192. Kee C, Sohn S, Hwang JM. Stromelysin gene transfer into cultured human trabecular cells and rat trabecular meshwork in vivo. *Invest Ophthalmol Vis Sci.* 2001;42:2856–2860.
193. Spiga MG, Borrás T. Development of a gene therapy virus with a glucocorticoid-inducible MMP1 for the treatment of steroid glaucoma. *Invest Ophthalmol Vis Sci.* 2010;51:3029–3041.
194. Gerometta R, Spiga MG, Borrás T, et al. Treatment of sheep steroid-induced ocular hypertension with a glucocorticoid-inducible MMP1 gene therapy virus. *Invest Ophthalmol Vis Sci.* 2010;51:3042–3048.
195. Manno CS, Pierce GF, Arruda VR, et al. Successful transduction of liver in hemophilia by AAV-Factor IX and limitations imposed by the host immune response. *Nat Med.* 2006;12:342–347.
196. Murphy SL, High KA. Gene therapy for haemophilia. *Br J Haematol.* 2008;140:479–487.
197. McCarty DM, Monahan PE, Samulski RJ. Self-complementary recombinant adeno-associated virus (scAAV) vectors promote efficient transduction independently of DNA synthesis. *Gene Ther.* 2001;8:1248–1254.
198. Buie LK, Rasmussen CA, Porterfield EC, et al. Self-complementary AAV virus (scAAV) safe and long-term gene transfer in the trabecular meshwork of living rats and monkeys. *Invest Ophthalmol Vis Sci.* 2010;51:236–248.
199. Bennett J. Taking stock of retinal gene therapy: looking back and moving forward. *Mol Ther.* 2017;25:1076–1094.
200. Spark Therapeutics 2017 [cited 2017 May 19]. Available from: <http://sparktx.com/>

ORIGINAL ARTICLE

Therapeutic potential of AAV-mediated MMP-3 secretion from corneal endothelium in treating glaucoma

Jeffrey O'Callaghan^{1,*}, Darragh. E. Crosbie¹, Paul. S. Cassidy¹, Joseph M. Sherwood², Cassandra Flügel-Koch³, Elke Lütjen-Drecoll³, Marian M. Humphries¹, Ester Reina-Torres¹, Deborah Wallace⁴, Anna-Sophia Kiang¹, Matthew Campbell¹, W. Daniel Stamer⁵, Darryl R. Overby², Colm O'Brien⁶, Lawrence C. S. Tam^{1,*,†} and Peter Humphries^{1,*,†}

¹Ocular Genetics Unit, Smurfit Institute of Genetics, University of Dublin, Trinity College, Dublin, D2, Ireland, ²Department of Bioengineering, Imperial College London, London, SW7 2BX, UK, ³Department of Anatomy II, University of Erlangen-Nürnberg, D-91054 Erlangen, Germany, ⁴Clinical Research Centre, UCD School of Medicine and Medical Science, University College Dublin, Belfield, Dublin 4, Ireland, ⁵Departments of Ophthalmology and Biomedical Engineering, Duke University, Durham, NC, USA and ⁶Department of Ophthalmology, Mater Misericordiae University Hospital, Dublin, D7, Ireland

*To whom correspondence should be addressed: Tel: 353 1 896 2164, 353 1 896 1547; Fax: 353 1 679 8558; E-mail: ocallaje@tcd.ie (J.O.), lawrencet@tcd.ie (L.C.S.T.), pete.humphries@tcd.ie (P.H.)

Abstract

Intraocular pressure (IOP) is maintained as a result of the balance between production of aqueous humour (AH) by the ciliary processes and hydrodynamic resistance to its outflow through the conventional outflow pathway comprising the trabecular meshwork (TM) and Schlemm's canal (SC). Elevated IOP, which can be caused by increased resistance to AH outflow, is a major risk factor for open-angle glaucoma. Matrix metalloproteinases (MMPs) contribute to conventional aqueous outflow homeostasis in their capacity to remodel extracellular matrices, which has a direct impact on aqueous outflow resistance and IOP. We observed decreased MMP-3 activity in human glaucomatous AH compared to age-matched normotensive control AH. Treatment with glaucomatous AH resulted in significantly increased transendothelial resistance of SC endothelial and TM cell monolayers and reduced monolayer permeability when compared to control AH, or supplemented treatment with exogenous MMP-3.

Intracameral inoculation of AAV-2/9 containing a CMV-driven MMP-3 gene (AAV-MMP-3) into wild type mice resulted in efficient transduction of corneal endothelium and an increase in aqueous concentration and activity of MMP-3. Most importantly, AAV-mediated expression of MMP-3 increased outflow facility and decreased IOP, and controlled expression using an inducible promoter activated by topical administration of doxycycline achieved the same effect. Ultrastructural analysis of MMP-3 treated matrices by transmission electron microscopy revealed remodelling and degradation of core extracellular

†These authors contributed equally to this work.

Received: December 9, 2016. Revised: January 17, 2017. Accepted: January 18, 2017

© The Author 2017. Published by Oxford University Press.

This is an Open Access article distributed under the terms of the Creative Commons Attribution Non-Commercial License (<http://creativecommons.org/licenses/by-nc/4.0/>), which permits non-commercial re-use, distribution, and reproduction in any medium, provided the original work is properly cited. For commercial re-use, please contact journals.permissions@oup.com

matrix components. These results indicate that periodic induction, via use of an eye drop, of AAV-mediated secretion of MMP-3 into AH could have therapeutic potential for those cases of glaucoma that are sub-optimally responsive to conventional pressure-reducing medications.

Introduction

The eye is pressurised by a balance in the production of aqueous humour (AH) by the ciliary processes and resistance to its drainage through the trabecular meshwork (TM) and Schlemm's canal (SC). Located at the apex of the iridocorneal angle, SC is a flattened circular vessel with an average meridional diameter of 233 μm in humans (1). AH exits the lumen of SC into collector channels and drains into the episcleral veins that are visible on the surface of the sclera. Precise regulation of aqueous inflow together with outflow resistance is critical in maintaining an average intraocular pressure (IOP) of approximately 16 mmHg in a normal functioning eye (2). In cases of primary open-angle glaucoma (POAG), so-called because the iridocorneal angle remains open without noticeable physical obstruction, resistance to AH drainage through the TM and SC is increased by mechanisms that have yet to be fully elucidated, resulting in elevated IOP (3). This, in turn, results in deformation of the lamina cribrosa—the tissue that structurally supports the optic nerve head—(often referred to as 'cupping' of the optic nerve head), damaging retinal ganglion cell axons, leading to ganglion cell degeneration and irreversible blindness.

Lowering IOP remains the only effective treatment for POAG. Topical pressure reducing medications either increase the rate of aqueous outflow through the conventional or unconventional pathway, or reduce aqueous production (3). The U.S. spends \$1.9 billion per annum to treat glaucoma, 38–52% of such costs being related to topical pressure reducing medications (4). However, such medications often do not reduce IOP to the desired target pressure and may induce side effects in certain patients. Such patients may then undergo surgical interventions, which have associated risks and complications. Hence, there remains an unmet clinical need for improved methods of disease treatment.

Functional studies have provided evidence that the generation of aqueous outflow resistance is most significant in the juxtacanalicular tissue (JCT—the outer layer of the TM) and inner wall endothelium of SC (5,6). In particular, the extracellular matrix (ECM) composition in the JCT region has been shown to influence outflow patterns and resistance generation (6–11). Competitive disruption or inhibition of integrin-ECM linkages that attach the cell to the ECM, or inhibition of ECM receptors have been associated with increases in endothelial monolayer permeability and transendothelial transport (12–15). This implicates features that are relevant to SC endothelial cells (SCEC) and their supporting basement membrane, such as integrin-ECM interactions, along with other inter-endothelial junctions that govern cell shape, in the control of endothelial paracellular permeability (16). TM cells play an integral role in modulating the ECM of the JCT to preserve AH flow pathways via continual and signal-initiated ECM remodelling (17). The ECM in the JCT region is comprised of a heterogeneous group of fibrous and matrical materials including collagen type IV, proteoglycans, laminin and fibronectin, all of which provide tensile strength and support to surrounding cells. The cribriform plexus, a structure composed of elastic fibres, connects the inner wall endothelium and the ciliary muscle, allowing for JCT expansion in response to IOP elevation (18). ECM reconditioning of these matrix networks can thus induce changes in the actin cytoskeleton through integrin-ECM linkages, enabling F-actin or alpha-

smooth muscle actin (α -SMA) to act as markers for active ECM remodelling (19–21). ECM turnover in the conventional outflow pathway is regulated by a family of zinc-dependent endopeptidases, the matrix metalloproteinases (MMPs). These secreted proteases are responsible for the degradation of ECM proteins and cell proliferation, and are thus key components in ECM remodelling and outflow tissue homeostasis (22). MMPs are secreted as inactive protein precursors and are activated when cleaved by extracellular proteinases and other MMPs (23). Levels of MMPs, along with TIMPs (Tissue Inhibitors of Metalloproteinases), have been shown to differ in glaucomatous AH and TM tissue as compared to those from normotensive individuals (24,25). Imbalance in MMP/TIMP ratios, and reduced MMP enzymatic activity, has been correlated with the accumulation of ECM materials in the TM that ultimately leads to an increase in outflow resistance (26,27). Therefore, reduction in ECM turnover within the TM and JCT region as a result of an imbalanced latent-to-activated MMP ratio can be a contributing factor to increased outflow resistance, as observed in glaucoma. It is therefore evident that increasing ECM turnover in outflow tissues may have therapeutic significance by reducing outflow resistance. Here, we set out to develop a gene-based therapy for the delivery of MMP targeting the conventional outflow tissues, with the primary aim of reducing both outflow resistance and IOP. Introduction of MMPs into the anterior chamber of the eye has previously been shown to increase outflow facility in organ-perfused cultures, indicating their therapeutic potential (28–31). Of the many classes of MMPs, MMP-3 (stromelysin-1) presents itself as an attractive candidate for targeting the ECM of outflow tissues. MMP-3 possesses a vast proteolytic target profile including type IV collagen, fibronectin, laminin, elastin, and proteoglycans, all of which are present in the meshwork and JCT regions of the outflow tissues, making this MMP of particular interest (32–36). In addition, MMP-3 can also activate other MMPs, including MMP-1 and MMP-9 (23,37–39), further assisting in the remodelling of ECM components (40–42).

Efficient gene delivery into the anterior segment of the eye is feasible through the use of adenoviral and adeno-associated viral (AAV) vectors. In particular, self-complementary AAV vectors have been shown to have such capability (43–46). Owing to the fact that MMP-3 is a secretory enzyme synthesised in the endoplasmic reticulum, transduction of tissues of the anterior segment with AAV expressing MMP-3 will result in the secretion of the protein into the AH. This will subsequently enable MMP-3 to be delivered into outflow tissues via conventional aqueous flow, potentially facilitating targeted degradation of ECM components and thus increasing aqueous outflow. In this regard, we observed highly efficient transduction of corneal endothelial cells following a single intracameral inoculation of AAV-2/9 expressing MMP-3, and both levels and activity of MMP-3 were significantly elevated in mouse AH following such inoculation. Importantly, AAV-mediated expression of MMP-3 in corneal endothelium, either from a CMV-, or doxycycline-inducible promoter, resulted in a marked increase in outflow facility and reduction in IOP. These observations correlated with structural alterations in the ECM of the outflow tissues, suggesting a mechanism of action for MMP-3 in modulating outflow resistance.

Results

Effects of glaucomatous aqueous humour on SC endothelial and TM cell monolayers

We treated cultured human SCEC monolayers with human glaucomatous (POAG) or control (cataract) AH for 24 h, and quantified levels of total secreted and activated MMP-3 in culture media. This was achieved by performing an ELISA and FRET assay, to monitor the degree of cleavage of an MMP-3 specific substrate, on cell media 24 h post-treatment. We did not observe a significant increase in the level of total (latent and active forms) secreted MMP-3 in culture media following treatment with POAG aqueous, with an increase of 0.15 [−0.35, 0.66] ng/ml (mean [95% confidence interval (CI)]) ($P=0.45$, $n=3$, Fig. 1A) over controls. However, activity assays indicated that the MMP-3 secreted in response to POAG aqueous had less enzymatic activity than that of cataract control AH, with an average change of -0.15 [−0.28, -0.02] mU/ml ($P=0.024$, $n=9$ cataract, $n=7$ POAG, Fig. 1B). These observations corroborate results obtained involving other members of the MMP family in POAG aqueous (24) in that the amount of secreted MMP may remain relatively unchanged but its proteolytic activity is reduced.

Effects of glaucomatous AH on the permeability of SCEC and human TM (HTM) monolayers were determined by trans-endothelial electrical resistance (TEER) and FITC-dextran flux assays. Treatment of cultured SCEC monolayers with POAG AH resulted in increased TEER by an average of 102% after 24-h treatment compared to control AH (−7%), displaying an average absolute increase of 19.82 [15.82, 23.81] $\Omega\cdot\text{cm}^2$ ($P<0.0001$, $n=6$ cataract, $n=12$ POAG, Fig. 1C). Similarly, HTM responded with an increase of 9.79 [5.55, 14.05] $\Omega\cdot\text{cm}^2$ in response to glaucomatous AH, ($P=0.0002$, $n=8$, Fig. 1D). Glaucomatous AH also reduced paracellular flux, as measured by permeability co-efficient (P_{app}), to dextran of 70 kDa as compared to cataract controls, with a mean difference of 0.14 [0.05, 0.22] $\text{cm/s} \times 10^{-8}$ ($P=0.009$, $n=3$ cataract, $n=3$ POAG, Fig. 1E). A reduction in HTM permeability was also observed with a mean difference of 0.17 [0.09, 0.23] $\text{cm/s} \times 10^{-9}$ ($P=0.005$, $n=8$ cataract, $n=7$ POAG, Fig. 1F).

Treatment of outflow cell monolayers with recombinant human MMP-3 increases permeability with concomitant reductions in TEER

In contrast to the negative effects of glaucomatous AH on SCEC and HTM permeability and resistance, we observed that treatment of cultured monolayers with 10 ng/ml of active recombinant human MMP-3 reduced TEER values on average by 5.62 [2.92, 8.32] $\Omega\cdot\text{cm}^2$ greater than inactivated MMP-3 controls over the course of 24 h for SCEC ($P<0.0001$, $n=8$, Fig. 2A) and by 4.29 [0.11, 8.48] $\Omega\cdot\text{cm}^2$ for HTM ($P=0.0137$, $n=8$, Fig. 2B) respectively. Permeability assays complemented these data as increases in paracellular flux of 70 kDa FITC-dextran by 0.14 [0.12, 0.18] $\text{cm/s} \times 10^{-9}$ ($P<0.0001$, $n=8$, Fig. 2C) were observed in SCEC, and 0.04 [0.01, 0.06] $\text{cm/s} \times 10^{-9}$ ($P<0.01$, $n=8$, Fig. 2D) in HTM monolayers when comparing treatments of MMP-3 to its inactivated counterpart control: TIMP-1 incubated with MMP-3. To rule out cytotoxicity as a reason for the observed changes in paracellular permeability, a cell viability assay was undertaken. Based on data shown in Figure 2E, for concentrations below 36 ng/ml MMP-3, the average SCEC cell viability for $n=3$ will exceed 85%. Greater tolerability was observed in HTM cases, retaining an average viability of at least 85% for MMP-3 concentrations up to 151 ng/ml ($n=3$, Fig. 2F).

Treatment of SCEC and HTM monolayers with active recombinant human MMP-3 induces remodelling and degradation of ECM components

In order to attribute increases in permeability to the ECM remodelling effects associated with MMP-3, SCEC and HTM monolayers were both treated as above with 10 mg/ml MMP-3 for 24 h. Following treatment, we observed changes in the staining pattern and intensity of a number of ECM proteins by immunocytochemistry. Specific collagen IV staining was localised to perinuclear areas and cytoplasm in both SCEC and HTM cells (Fig. 3A and B). In particular, we observed a decrease in the staining intensity around perinuclear areas in treated cells as compared to controls. α -SMA fibres facilitating cell-cell contacts in SCEC localised specifically to the cytoplasm and cytoskeleton, and MMP-3 treatment led to an attenuation of fibre bundles with thinning of intercellular connections (Fig. 3C). Fluorescent images of F-actin in HTM monolayers also revealed constricted actin bundles and a reduced tendency for bundle crossovers (Fig. 3D). Immunofluorescence staining of laminin in SCEC and HTM cells showed diminished cytoplasmic localisation and reduced network complexity and multiplicity in MMP-3 treated cells as compared to control staining intensity of laminin (Fig. 3E and F). To visualise fibronectin clearly without cellular interference, decellularisation was performed after MMP-3 treatment to isolate the ECM scaffold from the cell monolayer. Fluorescent images show significant perturbation of fibronectin network in treated cells as opposed to the linear cellular organisation observed in control cells (asterisk, Fig. 3G and H). To quantitatively demonstrate remodelling of these proteins, western blot analysis was performed on both cell lysate and media fractions of SC and HTM cell monolayers (Supplementary Material, Fig. S1). Specific bands were observed at 300 kDa for collagen IV, 42 kDa for α -SMA, 220 kDa for laminin and 290 kDa for fibronectin. A significant reduction of collagen IV ($P=0.01$, $P=0.01$) α -SMA ($P=0.04$, $P=0.04$) and laminin ($P=0.04$, $P=0.03$) were observed in SC and HTM whole cell lysate samples respectively ($n=4$ for all cases). Collectively, these data clearly illustrate that MMP-3 mediates remodelling of ECM components in both SCEC and HTM cell monolayers.

Intracameral inoculation of AAV-2/9 expressing a CMV-driven MMP-3 gene efficiently transduces corneal endothelium and results in elevated levels of MMP-3 in aqueous humour

AAV-mediated transduction of corneal endothelium could, in principle, serve as an efficient means of expressing and secreting MMP-3 into AH. The advantage of such an approach is that the natural flow dynamics of AH will allow transportation of secreted MMP-3 towards the outflow tissues (Fig. 4A). We evaluated the efficiency of a number of AAV serotypes with either single stranded or self-complementary genomes to deliver MMP-3 to the outflow tissues. 2 μl of viral particles (2×10^{12} vector genomes/ml) of each serotype, expressing a CMV-driven eGFP reporter gene (Fig. 4B) were intracamerally inoculated into wild type C57BL/6 mice and eyes examined via fluorescent microscopy at 3 weeks post-inoculation. Extensive expression of the reporter gene was observed in the corneal endothelium of eyes injected with non-self-complementary AAV-2/9 (Fig. 4C top), with no fluorescence being detectable in the outflow tissues themselves using this construct. Hence, the eGFP cDNA from AAV-2/9 was exchanged with murine MMP-3 cDNA to generate AAV-MMP-3, and similar inoculation resulted in MMP-3 expression that was prominently detected in the corneal

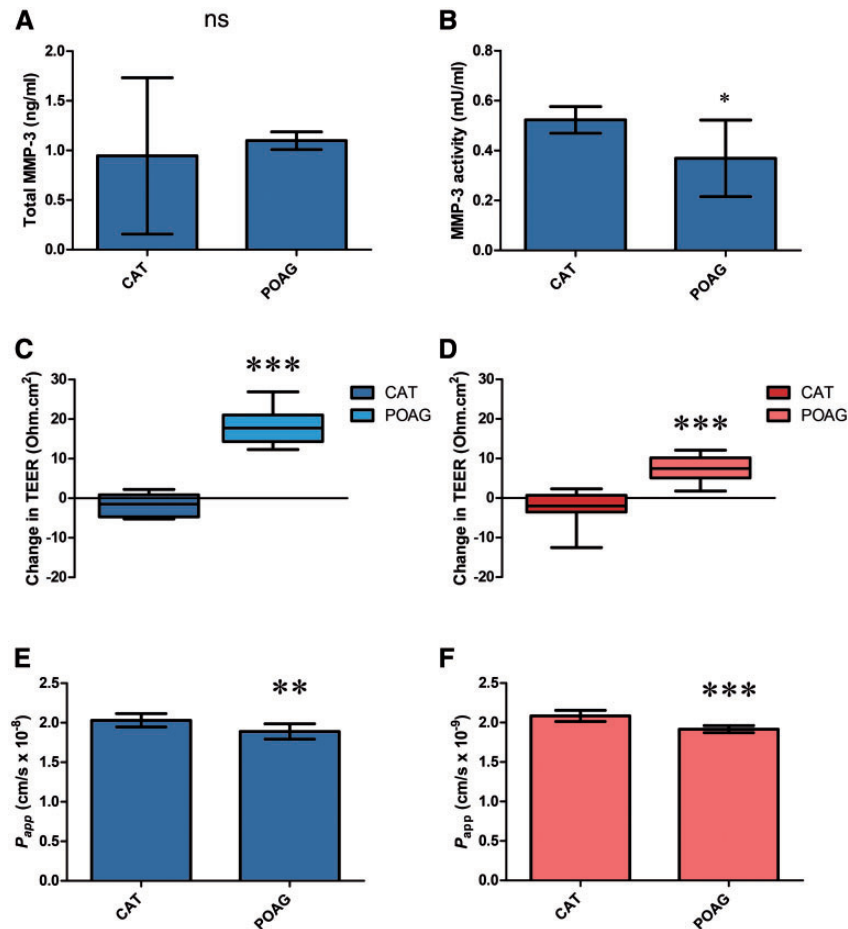


Figure 1. MMP-3 concentration in glaucomatous AH and the resulting effect on SCEC and HTM monolayers. (A) MMP-3 concentrations in the media of SCEC monolayers treated with either cataract (control) or POAG human AH showed no significant difference after 24 h. (B) POAG aqueous-treated SC media samples from (A) were found to have an average change in MMP-3 proteolytic activity of -0.15 [-0.28 , -0.02] mU/ml compared to control media. (C) Addition of POAG aqueous humour onto SC monolayers resulted in an average increase in TEER of 102% compared to controls. (D) Treatment of HTM cells with human aqueous also increased TEER value. (E,F) SCEC and HTM subjected to AH were tested for cellular permeability using a FITC-Dextran flux assay respectively. Decreased permeability to a 70 kDa dextran was observed in response to POAG rather than cataract AH. Graphs show mean with 95% CI error bars. CAT = cataract, POAG = primary open-angle glaucoma. Figures A-F were analysed with a Student's t-test. NS = non-significant. Symbols *, ** and *** denote P values of < 0.05 , < 0.01 and < 0.001 , respectively.

endothelium and not in null controls (Fig. 4C, bottom). No significant difference in central corneal thickness was detected following AAV inoculation between treated (116.7 [112.5 , 120.9] μm) and control eyes (116.4 [113.6 , 119.1] μm) ($n = 4$, Supplementary Material, Fig. S2). Corneas also appeared clear with no signs of cataracts upon visual inspection.

The level of total MMP-3 in the AH of twelve inoculated animals was quantified using enzyme-linked immunosorbent assay (ELISA), and we observed a significant average increase in total MMP-3 protein of 56%, 1.37 [0.89 , 1.84] ng/ml as compared to 0.87 [0.59 , 1.12] ng/ml for control AAV ($P = 0.016$, $n = 12$, Fig. 4D). The activity of AAV-mediated production of MMP-3 was also assessed using FRET, and a significant increase in activity of 34 [6.86, 61.14] % was observed, on average, in AAV-MMP-3 treated eyes compared to contralateral controls ($P = 0.0164$, $n = 17$, Fig. 4E).

Intracameral inoculation of AAV-2/9 expressing an MMP-3 gene increases outflow facility and reduces IOP in murine eyes

In order to determine the effect of AAV-mediated expression of MMP-3 from the corneal endothelium on aqueous outflow,

the conventional outflow facility was measured using the recently developed *iPerfusion* system designed specifically to measure conventional outflow facility in mice (47). Wild type mice were intracamerally injected with 1×10^{11} vector genomes of AAV-MMP-3, and contralateral eyes received the same quantity of AAV-Null. Four weeks post-inoculation, eyes were enucleated and perfused in pairs over incrementing steps in applied pressure. A representative flow-pressure plot provided in Supplementary Material, Figure S3A describes the relationship between flow rate (Q) at each pressure (P) step in both AAV-MMP-3 (red) and AAV-Null (blue) eyes. Furthermore, the relative percentage difference in facility within each data pair is depicted in Supplementary Material, Figure S3B (left). The resulting facility data presented in Figure 5A and B clearly illustrate that control eyes have an average facility of 8.44 [6.14 , 11.60] nl/min/mmHg with treated eyes having an average facility of 11.73 [8.05 , 17.08] nl/min/mmHg. There is, therefore, an average increase in outflow facility of 39 [19, 63] % between treated eyes and their contralateral controls ($P = 0.002$, $n = 8$ pairs).

As the major pathology in POAG is IOP elevation, and an increased outflow facility was observed, tonometric IOP

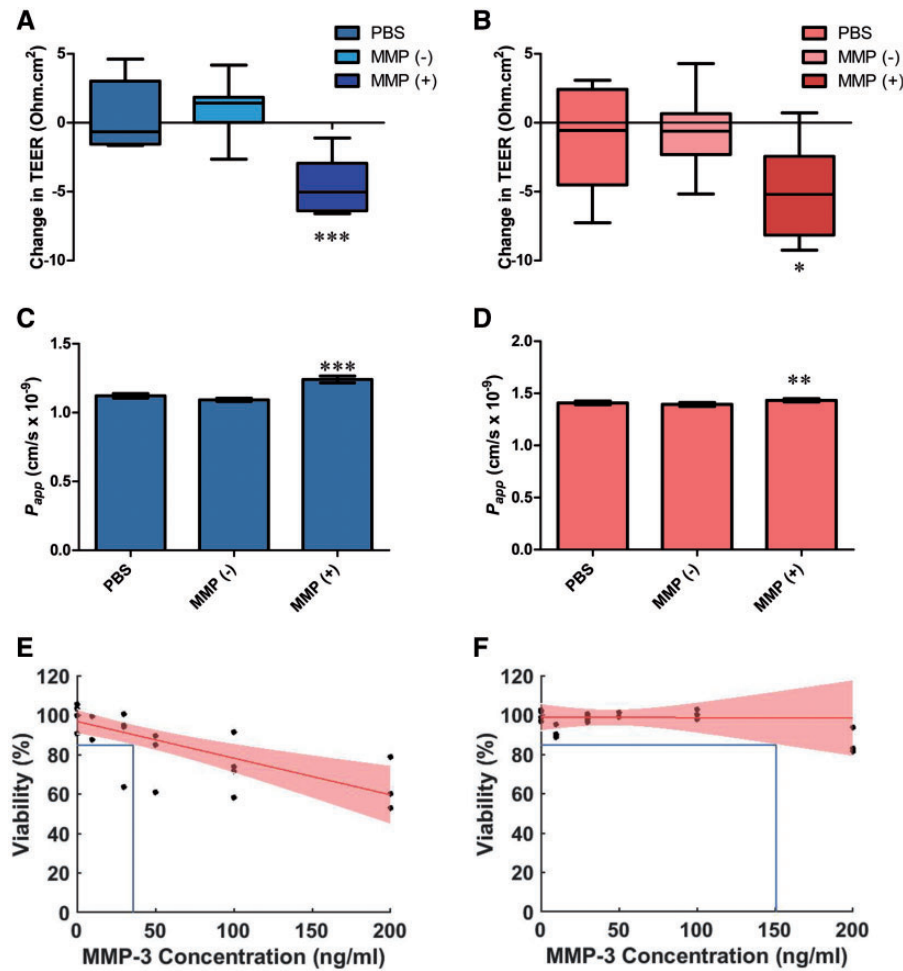


Figure 2. Effect of recombinant human MMP-3 on paracellular permeability in HTM and SCEC cell monolayers. SCEC and HTM cells were treated with 10 ng/ml recombinant MMP-3 for 24 h, using PBS and inactivated MMP-3 (incubation with TIMP-1, MMP(-)) as vehicle and negative controls respectively. (A) SCEC and (B) HTM both show reductions in TEER values after treatment of 4.6 [2.9, 6.2] and 5 [2.2, 7.8] Ohms.cm² respectively. Permeability to a 70 kDa dextran was increased in treated cells (MMP (+)) in both (C) SCEC and (D) HTM. (E) An average viability of 85% was expected for SCEC with MMP-3 concentrations up to 36 ng/ml. (F) 85% viability is retained on average in HTM cells at concentrations up to 151 ng/ml MMP-3. A, C and E in blue represent SCEC data, whereas B, D and F in red represent HTM data.

measurements were taken both immediately before (pre), and four weeks after (post) intracameral injection of AAV-2/9 expressing MMP-3 or a null vector in the case of the control. Differences between pre- and post-injection IOP were calculated using the non-parametric Wilcoxon matched-pairs signed rank test. Eyes treated with AAV-Null had no significant change in IOP -0.5 ± 2.9 mmHg (median \pm median absolute deviation (MAD), $P = 0.61$, $n = 7$, Wilcoxon signed-rank test with a theoretical median IOP change of 0) after treatment. In comparison, when treated with AAV-MMP-3, median IOP significantly decreased by 3.0 ± 2.9 mmHg ($P = 0.022$, $n = 7$, Fig. 5C). The IOP difference in AAV-MMP-3 treated eyes was significantly greater than the IOP difference in the contralateral AAV-Null treated eyes by 2.5 ± 0.7 mmHg ($P = 0.034$, $n = 7$, Fig. 5C).

Controlled periodic activation of MMP-3

To incorporate a control mechanism for the secretion of MMP-3 from corneal endothelium, we first introduced AAV-2/9 expressing eGFP under the control of a tetracycline-inducible promoter into the anterior chambers of both eyes of wild type mice. After 3 weeks, mice were treated with a regime of one drop of 0.2% doxycycline (a tetracycline derivative) two times

per day (approx. 8 h between each application) for 10–16 days in one eye only. PBS was administered onto the contralateral eye as a control. As illustrated in [Supplementary Material, Figure S4](#), extensive expression of the reporter gene was observed only in the corneal endothelium, and no expression was observed in the contralateral control. Following this, we replaced the reporter cDNA with murine MMP-3 cDNA and the resulting AAV (Induc. AAV-MMP-3) was injected into the anterior chambers of animals at 1×10^{11} viral genomes per eye. Using the inducible eGFP virus (Induc. AAV-eGFP) as a contralateral control, expression was induced by administering doxycycline (as above) to both eyes. Contralateral eyes were perfused as above, the control group exhibiting an average facility of 8.30 [5.75, 11.26] nl/min/mmHg and the MMP-3 treatment group resulting in a facility of 14.01 [11.09, 17.72] nl/min/mmHg. Paired, these eyes exhibit an average increase in outflow facility of 68 [24, 128] % ($P = 0.004$, $n = 11$, Fig. 5D and E). The relative difference in facility within individual pairs is presented in [Supplementary Material, Figure S3B](#) (right). This observation strongly supports the concept that MMP-3 expression could be induced in a controlled and reversible manner, with periodic IOP measurements utilised to guide the induction of expression.

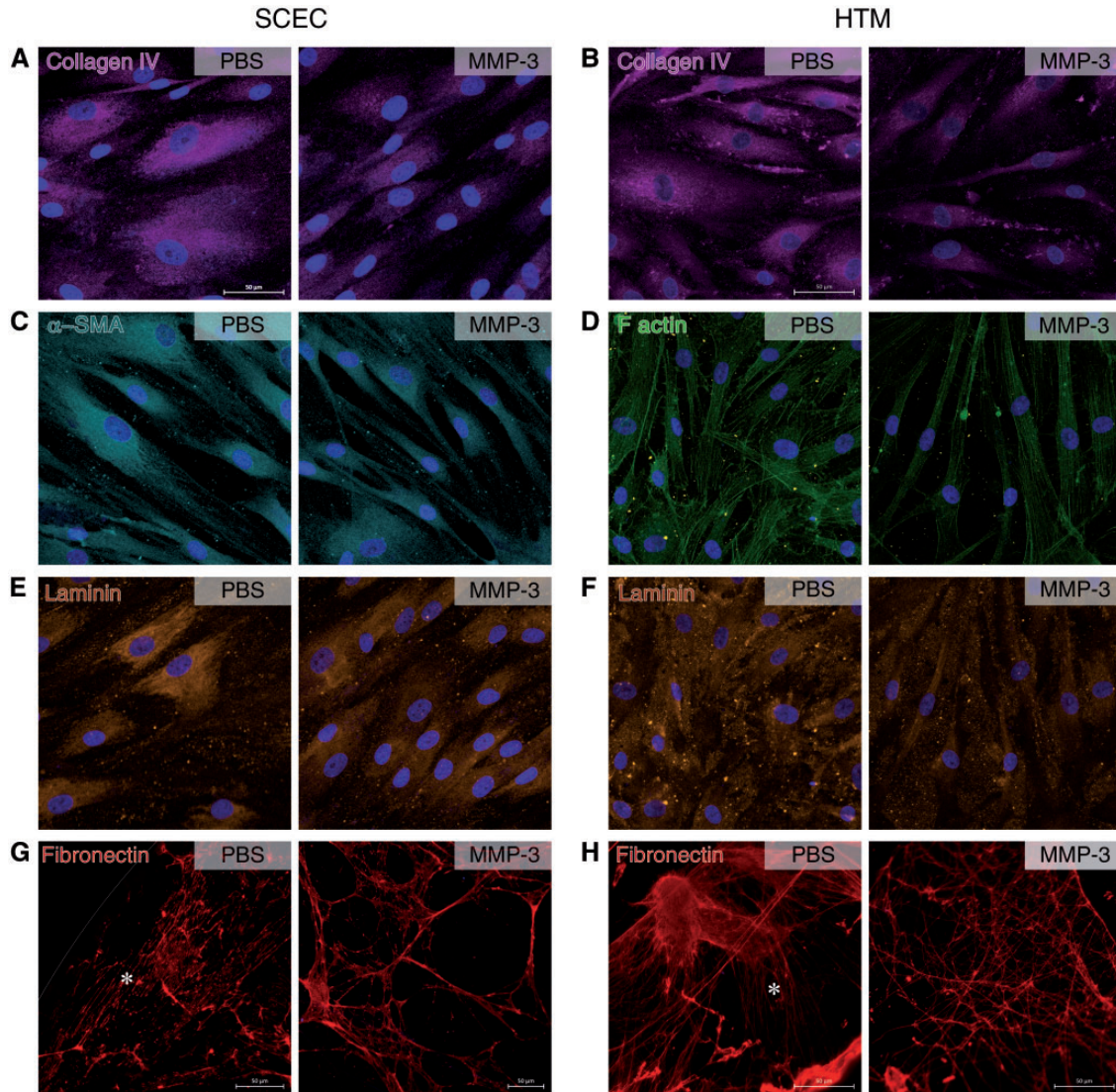


Figure 3. Remodelling of ECM components in SCEC and HTM cell monolayers. Immunocytochemistry shows various remodelling artefacts on core ECM components in SCEC and HTM cells in response to MMP-3 treatment. (A,B) Collagen IV appears to have reduced intensity in both cell types after treatment. Collagen IV is concentrated around cells in controls but shows reduced spread after treatment, fibrils barely protruding past the cell nuclei. (C) Alpha smooth muscle fibres extend the width of the cell towards a neighbouring cell. Treated samples show that these fibre bundles have constricted, leading to multiple thin connections between cells. (D) HTM F-actin staining depicts a slight thinning of filament bundles and a reduction of filament branching post MMP-3 treatment. (E,F) Laminin expression exhibits a modest reduction in staining intensity in both cell types, and a reduction in network complexity in TM cells. (G,H) Fibronectin was visualised after decellularisation, depicting linear and organised strands in PBS controls, as denoted by an asterisk. Treatment groups lacked a linear network, and instead showed a disjointed, porous network. Scale bars represent 50 μm . Left column pairs = SCEC, right column pairs = HTM.

Ultrastructural analysis of AAV-MMP-3 treated eyes

In order to evaluate whether the AAV-MMP-3 treatment affects the morphology of the eye and the TM including the inner wall of SC, ultrastructural investigation was performed in four pairs of mouse eyes. Corneas appeared translucent and healthy on visual inspection during enucleation. Semi-thin sections clearly demonstrated that there were no signs of an inflammatory reaction, either in the TM or in the cornea, uvea or retina (Fig. 6A and B). Ultrastructural analysis of control eyes revealed normal outflow structural morphology, cell-matrix attachments and cell-cell connections between the SC and TM. The inner wall endothelial cells formed foot-like connections with subendothelial TM cells, as well as connections to underlying elastic fibres and discontinuous basement membrane (Fig. 6C). However, in some

regions of treated eyes, especially those with a prominent SC lumen and scleral spur-like structure typical of the nasal quadrant (48), there appeared to be more optically empty space directly underlying the inner wall endothelium of SC, compared to AAV-Null controls (Fig. 6D). In these optically empty spaces, foot-like extensions of the inner wall to the sub-endothelial layer were absent or disconnected from the subendothelial cells or elastic fibres (Fig. 6D and E). Occasionally, we observed an accumulation of ECM clumps beneath the inner wall that were not observed within the controls (Fig. 6F) and may represent remnants of digested material.

We quantified the optically empty length directly underlying the inner wall of SC. In control eyes, the percent optically empty length in any one region ranged from 19 to 49% with an average of 37%. In the treated eyes, the equivalent range was

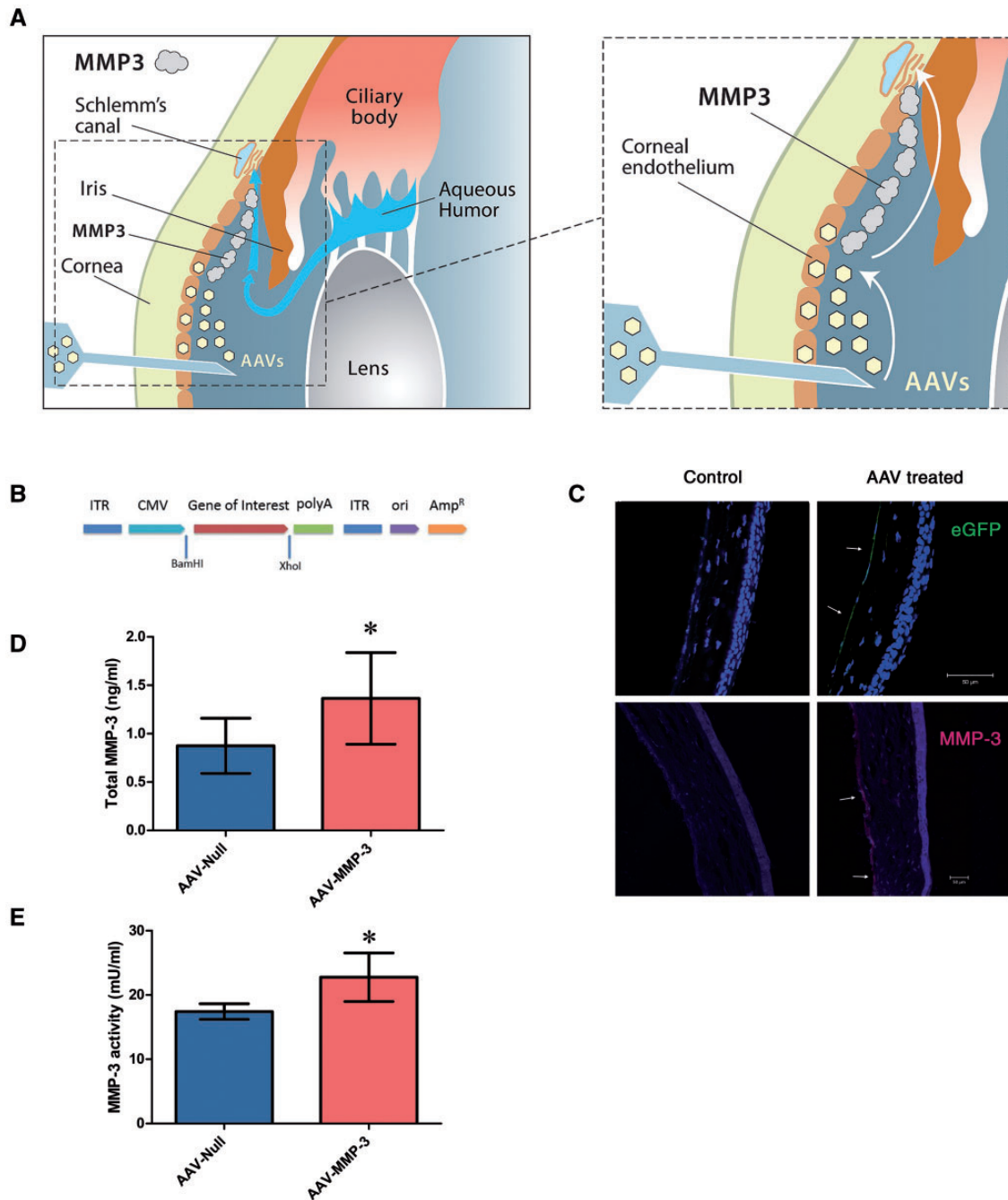


Figure 4. AAV-2/9 mediated MMP-3 expression in the corneal endothelium. (A) Diagrams illustrating the therapeutic concept addressed in this study. AAV-2/9 transduces the corneal endothelium upon intracameral inoculation (left). MMP-3 molecules are secreted into the AH from this location and are transported toward the outflow tissue by the natural flow of the aqueous (right). (B) A schematic diagram of the AAV-2/9 vector used for the expression of either eGFP or MMP-3. Murine MMP-3 cDNA was sub-cloned into the pAAV-MCS plasmid and constitutively driven by a CMV promoter (AAV-MMP-3). (C) Immunohistochemistry images of corneas from WT murine eyes intracamerally inoculated with AAV-2/9 expressing eGFP. AAV virus containing a CMV promoter demonstrates transduction and expression at the corneal endothelium (marked with arrows). Using the AAV-MMP-3 virus, MMP-3 was detected at the corneal endothelium in treated eyes only, denoted by arrows. (D) ELISA was performed on murine AH 4 weeks post-injection of virus. MMP-3 concentrations had increased by an average of 0.49 [0.11, 0.87] ng/ml in AAV-MMP-3 treated eyes (paired Student's t-test). (E) Aqueous MMP-3 activity was significantly increased by an average of 5.34 [1.12, 9.57] mU in AAV-MMP-3 treated eyes. Scale bars represent 50 μ m. Asterisk symbol denotes a P value of < 0.05.

39–76% with an average of 59% (Fig. 6G). The differences between control and experimental eyes for each pair ranged from 16 to 26%, which corresponded to a statistically significant increase in the proportion of open space underlying the inner wall with AAV-MMP-3 relative to AAV-Null ($P = 0.002$, $n = 4$; paired Student's t-test). These data indicate that reduced

ECM material in the TM and along the inner wall of SC is associated with AAV-MMP-3 treatment and may explain the enhanced outflow facility and IOP reduction. Furthermore, these morphological changes, because they were absent from controls, could not be attributed to an inflammatory or lytic response to AAV alone.

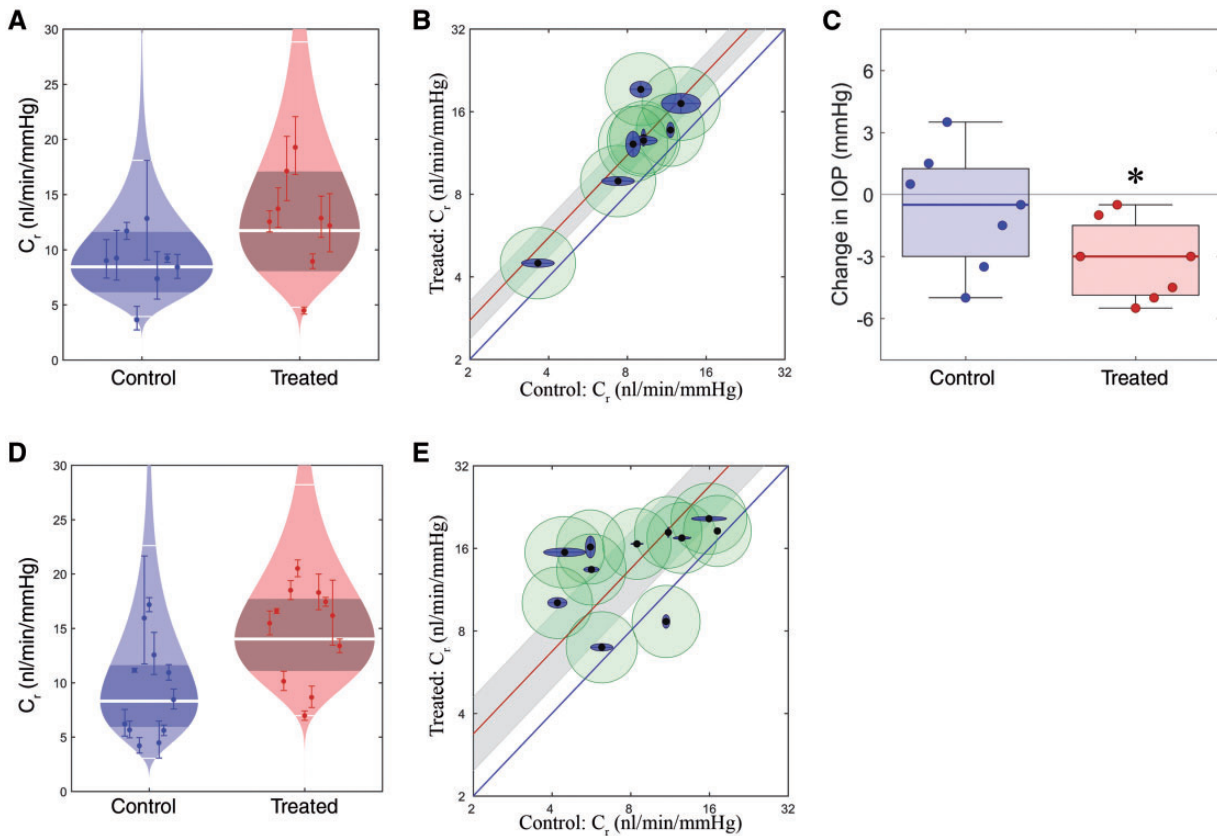


Figure 5. Effect of ECM remodelling on outflow facility and IOP. (A) 'Cello' plot depicting individual outflow facility values for eyes at 8 mmHg (C_r) and statistical distribution of both control (AAV-Null) and experimental (AAV-MMP-3) groups. Each point represents a single eye with 95% CI on C_r . Log normal distribution is shown, with the central white band showing the geometric mean and the thinner white bands showing two geometric standard deviations from the mean. The shaded region represents the 95% CI on the mean. (B) Paired outflow facility plot. Each inner point represents an eye pair, with log-transformed facilities of the control eye plotted on the x axis, and treated eye on the y axis. Outer blue and green ellipses show uncertainties generated from fitting the data to a model, intra-individual and cannulation variability respectively. Average increase is denoted by the red line, enclosed by a grey 95% CI, indicating significantly increased facility (does not overlap the blue unity line). (C) Box plots showing the change in IOP in treated and control eyes. Boxes show interquartile range and error bars represent the 5th and 95th percentiles. A significant reduction in IOP is observed in AAV-MMP-3 treated eyes (Wilcoxon signed-rank test). (D-E) Cello and paired facility plots for inducible AAV data sets.

Discussion

Matrix metalloproteinases are key regulators in the remodelling of extracellular matrices in the JCT region of the TM. Dysregulation of MMP expression and loss of MMP/TIMP homeostasis in glaucomatous AH have been associated with abnormal fibrillary ECM accumulation in the JCT region of POAG eyes (49–53). Furthermore, perfusion of anterior segments with purified MMPs increased outflow facility, while the use of metalloproteinase inhibitors (TIMP, minocycline) reduced outflow rates (30). Consistent with these findings, upregulation of MMPs following clinical laser treatment has been associated with the ocular hypotensive effect of trabeculoplasty (54,55). It is therefore apparent that the reduction in ECM turnover within the outflow tissues contributes to increased outflow resistance, and strategies specifically targeting outflow ECM may be effective in reducing outflow resistance. In this study, we focused on the development of a gene-based therapy for the delivery of MMP-3 into outflow tissues to facilitate aqueous outflow and reduce IOP.

It has been reported that the activity of a range of regulatory cytokines and growth factors found in AH directly impacts permeability in the outflow tissue, and many of these are known to be dysregulated in POAG AH (56,57). In particular, cytokines such as IL-1, TGF and TNF are known to influence the expression and secretion of ECM modulators, including MMPs in

outflow tissues (58–60). It was therefore of interest to assess how POAG AH may affect the MMP-3 secretion and their relative activity in outflow cell culture systems.

We performed permeability assays with AH-treated SCEC and HTM monolayers to demonstrate that dysregulated MMP's in POAG AH influence monolayer permeability via modified ECM remodelling. (12,61). SCEC monolayers showed decreased permeability *in vitro* in response to glaucomatous AH, and this decrease was associated with a reduction in extracellular MMP-3 activity. HTM cells exhibited similar reductions in permeability. In contrast, treatment of cell monolayers exclusively with recombinant MMP-3 elevated monolayer permeability in comparison to controls, suggesting that MMP-3 could correct the permeability lowering effects of POAG aqueous. Because MMP-3 has previously been associated with apoptotic behaviour in Chinese hamster ovary cells and osteoclasts (62,63), we evaluated the effect of a wide concentration range of MMP-3 on SCEC and HTM viability. This way, we confirm that increases in paracellular permeability were not related to an MMP-3 cytotoxic effect, but rather its proteolytic activities, which these data support. More importantly, even lower concentrations of MMP-3 were detected *in vivo* in murine AH after AAV-mediated MMP-3 secretion (1.37 [0.89, 1.84] ng/ml, Fig. 4D) than those used in *in vitro* experiments. Collectively, these results indicate that a

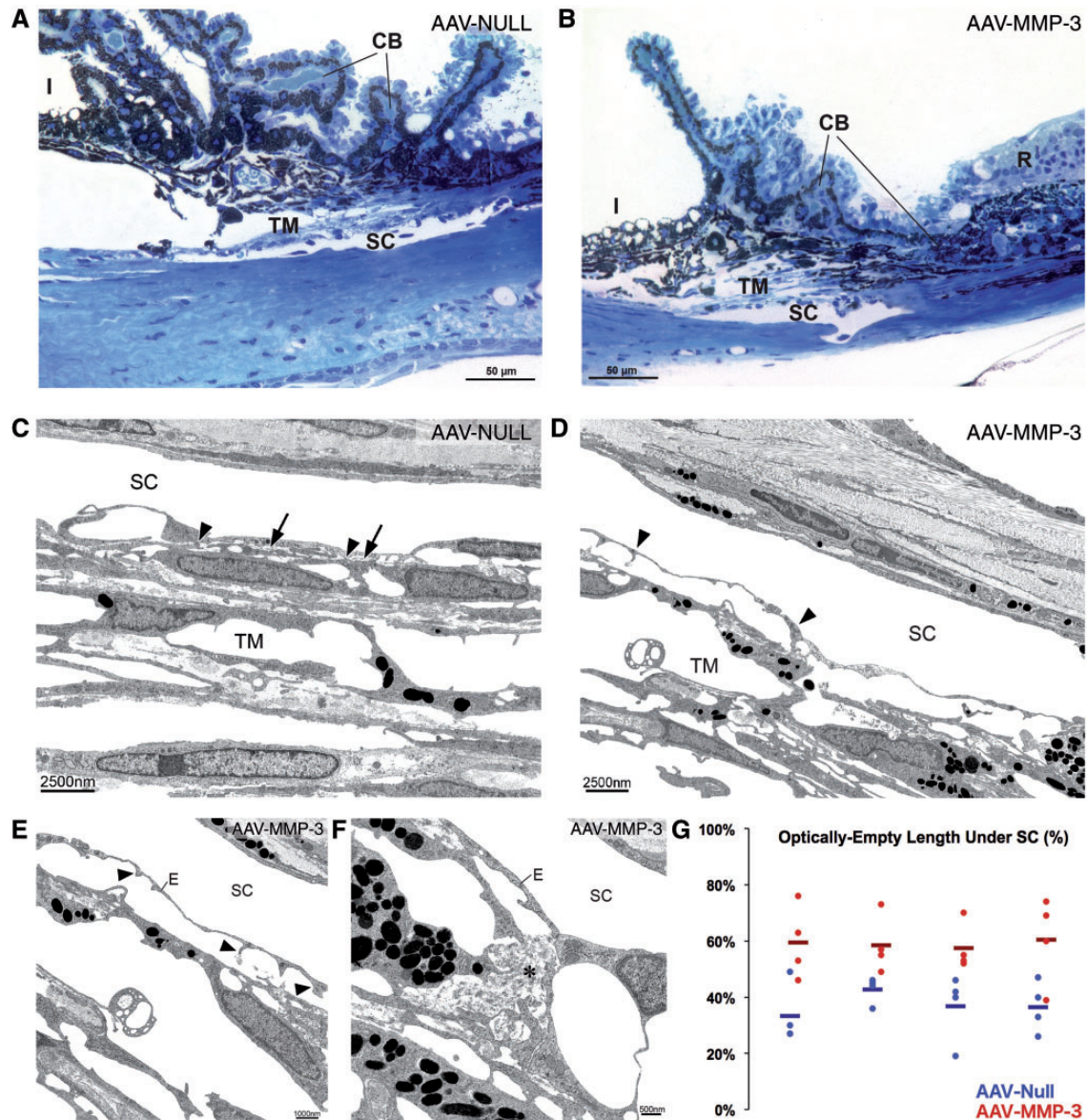


Figure 6. Transmission electron microscopy (TEM) analysis of ECM remodeling in outflow tissues. Semi-thin sections of the iridocorneal angle in mouse eyes treated with either (A) AAV-Null or (B) AAV-MMP-3. AAV-MMP-3 treated eyes show greater inter-trabecular spaces in outer trabecular meshwork (TM) than controls. Scale bar denotes 50 μ m. (C,D) Transmission electron micrograph of the inner wall of Schlemm's Canal (SC) and the outer TM. (C) Control eye illustrating normal attachment between foot-like extensions of the inner wall endothelium and subendothelial cells (arrowheads), as well as with the discontinuous basement-membrane material underlying the inner wall endothelium (arrows). (D) Representative TEM image of an MMP-3 treated eye showing a disconnection of the inner wall endothelium from the subendothelial cells and the ECM (arrowheads). The widened subendothelial region lacks basement-membrane material and other ECM components. (E,F) Higher magnification of the inner wall of a treated eye. (E) Foot-like extensions of the inner wall endothelium (E) have disconnected from the subendothelial cells and the ECM (arrowheads), and the lack of ECM in this region is shown. (F) In other regions of treated eyes, clumps of presumably degraded ECM-material are localised underneath the inner wall of SC (asterisk). Such clumps of ECM are not present in controls. Scale bars are denoted on each image. CB = ciliary body, I = iris, R = retina. (G). Morphometric measurements of the optically empty space immediately underlying SC from four regions of contralateral eyes treated with AAV-MMP-3 (red data points) or AAV-Null (blue data points). Bars indicate average values for each eye. Contralateral eyes are presented immediately next to one another.

plausible target for MMP-3 activity is likely to be the ECM of TM and the inner wall endothelium of SC. This further contributes to the body of evidence demonstrating that the molecular pathological effects of glaucomatous AH are due, in part, to dysregulations of MMP-mediated remodeling and that induced elevations in MMP-3 expression in outflow tissues will have an enhancing effect on increasing aqueous outflow.

Previously, perfusion of explants of human anterior segments with a mixture of MMP-3, -2, -9 has been shown to result in an increase in outflow facility to 160% of baseline level (30).

It has also been demonstrated that increases in IOP lead to an up-regulation of MMP-2, -3 and -14 through mechanical stretching of the TM and a reduction in TIMP2 (31,64–68). Such observations support the concept that controlled expression of MMPs within the anterior chamber holds therapeutic potential in regard to facilitating aqueous outflow. The inner wall endothelium of SC along with its basement membrane and JCT modulate the resistance to outflow. The interconnections between all components responsible for the outflow resistance generation is essential to maintain the homeostasis of outflow

drainage (11). Thus, targeting the ECM for remodelling in the JCT region using MMPs may effectively increase permeability of surrounding cells, thus increasing AH outflow rate and lowering IOP.

Owing to the fact that MMP-3 is a secretory enzyme, transduction of the corneal endothelium with AAV-MMP-3 will result in the secretion and delivery of the protein to the outflow tissues by following the natural flow of AH in the anterior chamber. *Ex vivo* studies in human corneas or corneal fibroblasts have demonstrated the potential and efficiency of delivering AAV to this tissue type (69,70). Successful transfection of different layers in the rabbit cornea by recombinant AAV further supports the potential of recombinant/exogenous protein delivery from corneal cells (71). Thus, it is likely that secreted MMP-3, expressed by corneal endothelia, will be directed toward the outflow tissue and activated with the aid of existing endogenous MMP-3 after which it will then be available for remodelling a range of ECM components. Attaining exclusive AAV expression in the cornea was obtained by using a single stranded AAV-2/9, as although single stranded AAV may enter other cells such as the TM, self-complementary viruses are required for sufficient DNA replication, and hence transduction of these cells (72).

The current data provide a direct proof of concept that AAV-mediated expression of MMP-3 from corneal endothelium decreases IOP with a concomitant increase in the rate of AH outflow through the drainage channels *ex vivo*. A number of parameters will require further refinement in order to address the translational feasibility of this approach. Although significant elevations in transient MMP-3 were found in murine AH post-treatment with AAV-MMP-3, these were well within tolerable limits as defined by our *in vitro* experiments (Fig. 2E and F). These MMP-3 elevations in AH (Fig. 4D), along with visually translucent corneas of normal thickness (Supplementary Material, Fig. S2), suggests that MMP-3 is preferentially secreted apically into the AH. MMP-3 expressed in the corneal endothelial cell layer is in the inactive form, which requires secretion for cleavage-induced activation, and is therefore unlikely to induce remodelling or damage to the endothelium itself. Activation is likely to occur in the AH after secretion, or extracellularly within the outflow tissues in the presence of other proteases. The observed elevation in aqueous MMP-3 activity indicates that activation at least begins in the AH (Fig. 4E). However, sustained expression of MMP-3, as would occur following permanent transfection of cells of the anterior chamber, could result in off-target proteolysis over time. A potentially more effective approach will be to employ an inducible promoter to drive MMP-3 expression on a periodic basis once the virus has been introduced into the anterior segment tissues of the eye. It is of note that the use of glucocorticoid-inducible promoters has been explored in this regard in adenoviral and AAV delivery systems to express MMP-1 in tissues of the TM (46). However, the use of a steroid response promoter may not be ideally suited from a therapeutic standpoint in humans, as activation of the promoter would require continuous exposure to steroid components, which can lead to abnormal IOP elevation (73–75). Glucocorticoids have also been shown to influence gene expression, which may play a pathogenic role in developing hypertension (76). Hence, we explored the effectiveness of a tetracycline-inducible system to express MMP-3 from the corneal endothelia, which allows for controllable and reversible activation by topically applied eye drops. We noted that activation of AAV for over 10 days was sufficient to significantly increase outflow facility *ex vivo* in mice and suggest that incorporation of other tetracycline derivatives may further enhance the

effectiveness of the promoter and hence MMP-3 production. Our observed increase in facility of 68 [24, 128] % rivals that of conventional prostaglandin analogues which are in current use to treat glaucoma, noted to have an increase of 56 [–4, 154] % in the case of PDA205, also using the iPerfusion system (47).

To date, in studies utilising MMPs for increasing outflow or reducing IOP little emphasis has been given to the mechanism of action. Here, we show that MMP-3-mediated remodelling of specific ECM components is likely responsible for increased outflow, and hence, decreased IOP. Reductions in intensity and distribution of core ECM materials including collagen IV and laminin were observed *in vitro*, along with the disorganisation of the fibronectin meshwork and constrictions in the actin skeleton. These modifications suggest the development of a porous nature within the ECM of these monolayers. Semi-quantitation via western blot analysis coincides with these results, showing significant reductions in collagen IV, α -SMA and laminin proteins in the cell lysate fraction, where ECM proteins are likely to reside as no significant changes were displayed in media samples. It is reasonable to assume that these extracellular changes contribute to the observed alterations in electrical resistance and paracellular flux. Ultrastructural analysis of AAV-MMP-3 treated mouse eyes also showed reductions in ECM material at the sub-endothelial/JCT region, including areas of degraded ECM and widened inter-trabecular spaces. Upon quantification, these areas optically lacking ECM material were found to be consistently increased in response to MMP-3 both between regions of the anterior chamber and between treated eyes. Tight junctions remained intact after incubation with AAV-MMP-3 (Supplementary Material, Fig. S5), contrary to previous studies which have shown tight junction degradation by MMPs (77,78); validating that MMP-3 may primarily augment cell monolayer permeability via other mechanisms such as alteration of ECM components. These data indicate that a reduction in ECM material in the TM and inner wall of SC is responsible for the enhancement of outflow facility and consequently lowering of IOP in the treated eyes. The data also show that the reduction in ECM is not due to an inflammatory response that secondarily induces lytic enzymes in the treated eyes but most likely to the induction of MMP-3 through the treatment directly.

We show here for the first time that a topical eye drop regime can control the expression of a gene therapy vector utilised to reduce outflow resistance and IOP through ECM remodelling. The current approach may hold substantial potential as an effective human therapy should long-term safety and efficacy prove successful in non-human primates.

Materials and Methods

Cell culture

Human SCEC were isolated, cultured and fully characterised according to previous protocols (79–81). Briefly, cells were isolated from the SC lumen of human donor eyes using a cannulation technique. Isolated cells were tested for positive expression of VE-cadherin and fibulin-2, but absence of myocilin induction upon treatment with 100nM dexamethasone for 5 days. Confluent cells displayed a characteristic linear fusiform morphology, were contact inhibited and generated a net transendothelial electrical resistance (TEER) greater than 10 Ω .cm². TEER values were confirmed again prior to MMP-3 treatments. SCEC strains used were SC82 and SC83 between passages 2 and 7. Dulbecco's modified eagle medium (Gibco, Life Sciences) 1%

Pen/Strep/glutamine (Gibco, Life Sciences) and 10% foetal bovine serum (FBS) performance plus (Gibco, Life Sciences) was used as culture media in a 5% CO₂ incubator at 37 °C. Cells were passaged with trypsin-EDTA (Gibco-BRL) and seeded into 12 well or 24 well transwell plates (Costar, Corning). Human trabecular meshwork (HTM) cells were isolated and fully characterised according to the procedures described in (82–85). TM tissue is removed from human donor eyes using a blunt dissection technique, and TM cells are dissociated from the tissue using a collagenase digestion protocol as previously described (82). Isolated cells are characterised by their dramatic induction of myocilin protein following treatment with dexamethasone (100 nM) for 5 days as detailed before (79). HTM123 and HTM134 cells were cultured similar to SCEC's and matured for one week in 1% FBS media prior to treatment.

Human AH samples (detailed below) were added 1:10 to fresh media for cellular treatment for use with TEER and permeability assays as described below.

Recombinant human active MMP-3 (ab96555, Abcam) was added to cell media at a concentration of 10 ng/ml for TEER, permeability assays, western blotting and immunocytochemistry as described below. Inactivated MMP-3 controls were achieved by incubating active MMP-3 (10 ng/ml) with recombinant human active TIMP-1 (100 ng/ml, ab82104, Abcam) in cell media for 1 h prior to treatment.

Animals

Animals and procedures used in this study were carried out in accordance with regulations set out by The Health Products Regulatory Authority (HPRA), responsible for the correct implementation of EU directive 2010/63/EU. 8–11-week-old male and female C57BL/6 mice were used in all experimentation outlined in this study. Animals were bred and housed in specific-pathogen-free environments in the University of Dublin, Trinity College and all injections and IOP measurements complied with the HPRA project authorisation number AE19136/P017.

Patient aqueous humour samples

Human aqueous was obtained from the Mater Misericordiae Hospital, Dublin, Ireland. Upon informed consent, AH samples were collected from both POAG and control patients undergoing routine cataract surgery. The criteria for POAG was defined as the presence of glaucomatous optic disc cupping with associated visual field loss in an eye with a gonioscopically open anterior drainage channel, with an intraocular pressure > 21 mmHg (86). The samples were taken immediately prior to corneal incision at the start of the procedure using a method described previously (87). Human AH collection conformed to the WMA Declaration of Helsinki and was approved by the Mater Misericordiae University Hospital Research Ethics Committee.

TEER measurement

Electrical resistance values were used as a representative of the integrity of the endothelial cell-cell junctions. Cells grown on Costar transwell-polyester membrane inserts with a pore size of 0.4 μm were treated with 10 ng/ml MMP-3 as described above. TEER readings were measured before and 24 h after treatment. An electrical probe (Millicell ERS-2 Voltohmmeter, Millipore) was placed into both the apical and basal chambers of the transwells and a current was passed through the monolayers,

reported as a resistance in Ω.cm². A correction was applied for the surface area of the membrane (0.33 cm²) and for the electrical resistance of the membrane (blank transwell).

Permeability assessment by FITC-dextran flux

The extent of monolayer permeability was assessed by the basal to apical movement of a tracer molecule through the monolayer. Measures of permeability were taken 24h after treatment immediately after TEER values, keeping experimental set-up identical to that of TEER readings. The permeability protocol was repeated as described in (88). A 70 kDa fluorescein isothiocyanate (FITC)-conjugated dextran (Sigma) was added to the basal compartment of the transwell. Fresh medium was applied to the apical chamber and aliquots of 100 μl were taken every 15 min for a total of 120 min, replacing with fresh media. Sample aliquots were analysed for FITC fluorescence (FLUOstar OPTIMA, BMG Labtech) at an excitation wavelength of 492 nm and emission wavelength of 520 nm. Relative fluorescent units (RFU) were converted to their corresponding concentrations by interpolating from a known standard curve. Corrections were made for background fluorescence and the serial dilutions generated over the experiments time course. P_{app} values were calculated representing the apparent permeability coefficient for control (PBS) and treatment (10 ng/ml MMP-3). This was achieved via the following equation:

$$P_{app}(cm/s) = (dM/dT)/(A \times C_0),$$

Where dM/dT is the rate of appearance of FITC-dextran (FD) (μg/s) in the apical chamber from 0 to 120 min after the introduction of FD into the basal chamber. A is the effective surface area of the insert (cm²) and C_0 is the initial concentration of FD in the basal chamber.

Cell viability

Cultured cells were treated with increasing concentrations of recombinant human MMP-3 (ab96555, Abcam) from 0 to 200 ng/ml. Cell viability was assessed 24 h post-treatment with MMP-3 using a CellTitre 96® Aqueous One Solution Cell Proliferation Assay (Promega). Cell media was aspirated and a 1 in 6 dilution of the supplied reagent in media was added to the cell surface. Cells were incubated at 37 °C for 1 h and the media/reagent was transferred to a 96-well plate for reading by spectrophotometry (Multiskan FC, Thermo Scientific) at 450 nm. Standard *in vitro* viability calculations fail to consider sample size and the biological significance of the data. Hence, a modified approach was taken to determine at which concentration SCEC's show a reduced tolerability to MMP-3. This was defined at an average of 85% viability over three cell samples. This conservative value ensures that a cell population would remain viable and still be able to proliferate. Anything lower should be regarded as MMP-3 intolerability i.e. reduced cell proliferation or cell death. Control samples (0 ng/ml MMP-3) were normalised to 100% viability and a linear model fitted to the normalised data. The MMP-3 concentration at which cells had an average of 85% viability was interpolated from the lower 95% confidence bound from this linear model. This value represents the concentration of MMP-3 at which the average of three cell samples would have a 97.5% chance of retaining a greater to or equal than 85% viability.

Immunocytochemistry (cell monolayers)

Immunocytochemistry was performed to visualise changes in ECM composition in response to MMP-3. Human SCEC and HTM were grown on chamber slides (Lab-Tek II) and fixed in 4% paraformaldehyde (pH 7.4) for 20 min at room temperature and then washed with PBS for 15 min. Cell monolayers were blocked in PBS containing 5% normal goat serum (10658654, Fischer Scientific) and 0.1% Triton X-100 (T8787, Sigma) at room temperature for 30 min. Primary antibodies of collagen IV (ab6586, Abcam), α -SMA (ab5694, Abcam), laminin (ab11575, Abcam) and F-actin (A12379, ThermoFisher Scientific) were diluted at 1:100 in blocking buffer and incubated overnight at 4°C. Secondary antibodies (ab6939, Abcam) were diluted at 1:500 in blocking buffer and then incubated for 2 h at room temperature. Following incubation, chamber slides were mounted with aquapoly-mount (Polyscience) after nuclei-counterstaining with DAPI. Fluorescent images of SCEC monolayers were captured using a confocal microscope (Zeiss LSM 710), and processed using imaging software ZEN 2012.

For clear fibronectin (ab23750, Abcam) staining, cells were grown on cover slips and subsequently decellularised, leaving only the ECM material. Round cover slips (15 mm Diameter, Sparks Lab Supplies) were silanised before cell seeding to enhance binding to ECM products. This was achieved by initially immersing slips in 1% acid alcohol (1% concentrated HCL, 70% ethanol, 29% dH₂O) for 30 mins. Slips were washed in running water for 5 min, immersed in dH₂O twice for 5 min, immersed in 95% ethanol twice for 5 min and let air dry for 15 min. Cover slips were then immersed in 2% APES (3-aminopropyl triethoxysilane (A3648, Sigma) in acetone (Fisher Chemical)) for 1 min. Slips were again washed twice in dH₂O for 1 min and dried overnight at 37°C. Cells were grown to confluency on these cover slips and, following treatment, were decellularised. This was achieved by consecutive washes in Hank's Balanced Salt Solution (HBSS), 20mM ammonium hydroxide (Sigma) with 0.05% Triton X-100, and finally HBSS again. Matrices were fixed and stained as described above with chamber slides.

Western blotting

Cells were treated with 10 ng/ml MMP-3 for 24 h in serum-free media. Media supernatants were aspirated and mixed 1:6 with StrataClean resin (Agilent). After centrifugation, the supernatant was removed and the pellet was resuspended in NP-40 lysis buffer containing 50 mM Tris pH 7.5, 150 mM NaCl, 1% NP-40, 10% SDS, 1X protease inhibitor (Roche). Cells were lysed using NP-40 lysis buffer for protein collection. Samples were centrifuged at 10,000 rpm for 15 min (IEC Micromax microcentrifuge) and supernatant was retained. Protein samples were loaded onto a 10% SDS-PAGE gel at 30–50 μ g per well. Proteins were separated by electrophoresis over the course of 150 min at constant voltage (120 V) under reducing conditions and subsequently electro-transferred onto methanol-activated PVDF membranes at constant voltage (12 V). Gels intended for use with Collagen IV antibodies were run under native conditions. Membranes were blocked for 1 h at room temperature in 5% non-fat dry milk and incubated overnight at 4°C with a rabbit primary antibodies to collagen IV, α -SMA, laminin and fibronectin as previously stated at concentrations of 1 in 1000 but 1 in 500 for laminin. Membrane blots were washed 3x5 min in TBS and incubated at room temperature for 2 h with horse radish peroxidase-conjugated anti-rabbit secondary antibody (Abcam). Blots were again washed and treated with a chemiluminescent

substrate (WesternBright ECL, Advansta) and developed on a blot scanner (C-DiGit, LI-COR). The membranes containing cell lysate samples were re-probed with GAPDH antibody (ab9485, Abcam) for loading control normalisation. Media samples were normalised against their total protein concentration as determined by a spectrophotometer (ND-1000, NanoDrop). A total of four replicate blots were quantified for each cell lysate sample antibody, and 2–3 replicates for a media sample. Band images were quantified using Image J software. Fold change in band intensity was represented in comparison to vehicle control treatments of PBS.

AAV

AAV-2/9 containing the enhanced green fluorescent protein (eGFP) reporter gene (Vector Biolabs) was initially used to assess viral transduction and expression in the anterior chambers of wild type mice (C57/BL6). Murine MMP-3 cDNA was incorporated into Bam HI/XhoI sites of the pAAV-MCS vector (Cell Biolabs Inc) for constitutive expression of MMP-3. A null virus was used as contralateral control using the same capsid and vector. The inducible vector was designed by cloning MMP-3 cDNA into a pSingle-tTS (Clontech) vector. This vector was then digested with BsrBI and BsrGI and the fragment containing the inducible system and MMP-3 cDNA was ligated into the NotI site of expression vector pAAV-MCS, to incorporate left and right AAV inverted terminal repeats (L-IRT and R-IRT). AAV-2/9 was generated using a triple transfection system in a stable HEK-293 cell line (Vector Biolabs). For animals injected with the inducible virus, after a 3-week incubation period, 0.2% doxycycline (D9891, Sigma) in PBS was administered twice daily to the eye for 10–16 days to induce viral expression. A similar inducible virus expressing eGFP was used as a control in the inducible study.

Intracameral injection

Animals were anaesthetised by intra-peritoneal injection of ketamine (Vetalar V, Zoetis) and domitor (SedaStart, Animalcare) (66.6 and 0.66 mg/kg, respectively). Pupils were dilated using one drop of tropicamide and phenylephrine (Bausch & Lomb) on each eye. 2 μ l of virus at a stock titre of 5×10^{13} vector genomes per ml was initially back-filled into a glass needle (ID1.0 mm, WPI) attached via tubing (ID-1.02 mm, OD-1.98 mm, Smiths) to a syringe pump (PHD Ultra, Harvard Apparatus). An additional 1 μ l of air was then withdrawn into the needle. Animals were injected intracamerally just above the limbus. Viral solution was infused at a rate of 1.5 μ l/min for a total of 3 μ l to include the air bubble. Contralateral eyes received an equal volume and titre of either AAV-MMP-3 or AAV-Null. The air bubble prevented the reflux of virus/aqueous back through the injection site when the needle was removed. Fucidic gel (Fucithalmic Vet, Dechra) was applied topically following injection as an antibiotic agent. To counter anaesthetic, Antisedan (atipamezole hydrochloride, SedaStop, Animalcare) was intra-peritoneally injected (8.33 mg/kg) and a carbomer based moisturising gel (Vidisic, Bausch & Lomb) was applied during recovery to prevent corneal dehydration.

Immunohistochemistry (mouse eyes)

Eyes were enucleated 4 weeks post-injection of virus and fixed in 4% paraformaldehyde overnight at 4°C. The posterior

segment was removed by dissection and anterior segments were washed in PBS and placed in a sucrose gradient of increasing sucrose concentrations containing 10%, 20% and finally 30% sucrose in PBS. Anterior segments were frozen in O.C.T compound (VWR Chemicals) in an isopropanol bath immersed in liquid nitrogen and cryosectioned (CM 1900, Leica Microsystems) at 12 μm thick sections. Sections were gathered onto charged Polysine[®] slides (Menzel-Gläser) and blocked for 1 h with 5% normal goat serum (10658654, Fischer Scientific) and 0.1% Triton X-100 in PBS. Slides were incubated overnight at 4 °C in a humidity chamber with a 1:100 dilution of primary antibody. Antibodies used were MMP-3 (ab52915, Abcam) and GFP (Cell Signalling). Sections were washed three times in PBS for 5 min and incubated with a Cy-3 conjugated anti-rabbit IgG antibody (ab6936, Abcam) at a 1:500 dilution for 2 h at 37 °C in a humidity chamber. Slides were washed as before and counter stained with DAPI for 30 s. Slides were mounted using Aquamount (Hs-106, National Diagnostics) with coverslips (Deckgläser) and visualised using a confocal microscope (Zeiss LSM 710).

Total MMP-3 quantification

MMP-3 concentration was quantified using enzyme-linked immunosorbent assay (ELISA) kits for both human SC monolayers (DMP300, R&D Systems) and murine aqueous (RAB0368-1KT, Sigma) according to the manufacturer's protocol. SC monolayers were cultured and treated with a 1 in 10 dilution of human cataract and POAG AH, a method previously described (87). Media was taken from the monolayers 24 h post-treatment and assayed for total MMP-3.

To measure the secretion of MMP-3 by AAV-2/9 into the AH, animals were inoculated with virus as described previously via intracameral injection. Four weeks post-injection, the animals were sacrificed and AH was collected. This was achieved by the cannulation of the cornea with a pulled glass needle (1B100-6, WPI) and gentle pressing of the eye until it was deflated. Aqueous was expelled from the needle (approximately 5 μl) by the attachment of a 25ml syringe connected via barb fitting and tubing (Smiths Medical) and a gradual push of the syringe plunger. Aqueous was assayed using the previously mentioned ELISA kit.

MMP-3 activity assay (FRET)

Enzymatic activity of secreted MMP-3 was quantified using fluorescence resonance energy transfer (FRET). A fluorescent peptide consisting of a donor/acceptor pair remains quenched in its intact state. This peptide contains binding sites specific to MMP-3. Once cleavage occurs through MMP-3 mediated proteolysis, fluorescence is recovered by the transfer of energy from the donor to the acceptor, resulting in an increase in the acceptor's emission intensity. Cleavage of substrate, and therefore fluorescence, was monitored on a FLUOstar OPTIMA (BMG Labtech) over the course of 2.5 h at 37 °C, to allow ample time for substrate cleavage. Media samples were collected from treated SC monolayers and combined with a 1:100 dilution of an MMP-3 specific substrate (ab112148, Abcam). Levels of active MMP-3 were interpolated from a standard curve defined by ELISA. For murine aqueous MMP-3 activity, aqueous was retrieved four weeks post-injection of AAV-MMP-3 or AAV-Null as described above. Aqueous samples were processed through an activity kit (abe3730, Source Bioscience), selected for its high

sensitivity and specificity, according to the manufacturer's protocol.

Enzymatic activity was calculated as described in MMP-3 activity Assay Kit's (ab118972, Abcam) protocol:

$$\text{MMP-3 Activity (nmol/min/ml)} = \frac{B \times \text{Dilution Factor}}{(T2 - T1) \times V}$$

Where B is the level of MMP-3 interpolated from the standard curve, T1 is the time (min) of the initial reading, T2 is the time (min) of the second reading and V is the sample volume (ml) added to the reaction well. The units 'nmol/min/ml' are equivalent to 'mU/ml'.

Measurement of outflow facility

Animals were sacrificed for outflow facility measurement 4 weeks after injection of virus. Eyes were enucleated for *ex vivo* perfusion using the iPerfusion[™] system as described in (47). Contralateral eyes were perfused simultaneously using two independent but identical iPerfusion systems. Each system comprises an automated pressure reservoir, a thermal flow sensor (SLG64-0075, Sensiron) and a wet-wet differential pressure transducer (PX409, Omegadyne), in order to apply a desired pressure, measure flow rate out of the system and measure the intraocular pressure respectively. Enucleated eyes were secured to a pedestal using a small amount of cyanoacrylate glue in a PBS bath regulated at 35 °C. Perfusate was prepared (PBS including divalent cations and 5.5mM glucose) and filtered (0.2 μm , GVS Filter Technology) before use. Eyes were cannulated using a bevelled needle (NF33BV NanoFil[™], World Precision Instruments) with the aid of a stereomicroscope and micromanipulator (World Precision Instruments). Eyes were perfused for 30 min at a pressure of ~8 mmHg in order to acclimatise to the environment. Incrementing pressure steps were applied from 4.5 to 21 mmHg, while recording flow rate and pressure. Flow (Q) and pressure (P) were averaged over 4 min of steady data, and a power law model of the form

$$Q = C_r \left(\frac{P}{P_r} \right)^\beta P$$

was fit to the data using weighted power law regression, yielding values of C_r , the reference facility at reference pressure $P_r = 8$ mmHg (corresponding to the physiological pressure drop across the outflow pathway), and β , a nonlinearity parameter characterising the pressure-dependent increase in facility observed in mouse eyes (47).

IOP

IOP measurements were performed by rebound tonometry (TonoLab, Icare) both prior to intracameral injection and 4 weeks post-injection. Readings, which were the average IOP values after five tonometric events, were taken 10 min after the intraperitoneal administration of mild general anaesthetic (53.28 mg/kg ketamine and 0.528 mg/kg domitor). Two readings were taken for one eye, then the other. This was repeated for a total of four readings per eye. Due to a minimum reading of 7 mmHg by the tonometer, a non-parametric approach was taken in the analysis of the readings. The median IOP was

calculated for each eye, and MAD (median absolute deviation) values were used as a measure of dispersion. For comparing median values in a paired population, the Wilcoxon matched-pairs signed-rank test was employed to test for changes in IOP pre- and post-injection, and also for changes between contralateral eyes.

Analysis of central corneal thickness

Enucleated mouse eyes transduced with AAV-MMP-3 or its contralateral control, AAV-Null, were fixed overnight in 4% PFA and washed in PBS. Posterior segments were removed by dissection under the microscope and anterior segments were embedded in medium (Tissue-Tek OCT Compound). Serial sectioning was performed on each eye and five frozen sections (12 µm) were transferred to a Polysine slide (Thermo Scientific) for staining with DAPI and mounted with aqua-polymount (Polyscience). Corneal sections were judged to be central by qualitatively taking the same distance from both iridocorneal angles. For quantitation, we measured the corneal thickness of sections on five consecutive slides by light and confocal microscopy (Zeiss LSM 710). A total of 25 measurements were taken from each eye to represent mean central corneal thickness (µm) using the NIH ImageJ software.

Transmission electron microscopy

Ultrastructural investigation was performed by transmission electron microscopy (TEM) in four pairs of mouse eyes. One eye of each pair was injected with AAV-Null, the other with AAV-MMP-3, as described above. Four weeks after injection, the eyes were enucleated and immersion fixed in Karnovsky's fixative (2.5% PFA, 0.1M cacodylate, 2.25% glutaraldehyde and dH₂O) for 1 h. Eyes were then removed from fixative and the cornea pierced using a 30-gauge needle (BD Microlance 3, Becton Dickinson). Eyes were placed back into fixative overnight at 4 °C, washed 3x10 min, stored in 0.1M cacodylate and sent to Erlangen.

Here the eyes were cut meridionally through the centre of the pupil, the lens carefully removed, and the two halves of each eye embedded in Epon. Semi-thin sagittal and then ultrathin sections of Schlemm's canal (SC) and trabecular meshwork (TM) were cut from one end of each half, and then the other approximately 0.2–0.3 mm deeper. The location of the superficial and deeper cut ends was alternated for the second half of the eye such that all four regions examined were at least 0.2–0.3 mm distant from one another. The ultrathin sections contained the entire anterior posterior length of the inner wall and the TM.

In four regions of each eye, we measured the length of optically empty space immediately underlying the inner wall endothelium of SC (Supplementary Material, Fig. S6). We also measured the inner wall length in contact with ECM, including basement membrane material, elastic fibres, or amorphous material. The optically empty length divided by the total length (optically empty + ECM lengths) was calculated and defined as the percentage of optically empty length for that region. All measurements were performed at 10,000x magnification, with each region including approximately 100 individual lengths of ECM or optically empty space. The measurements were performed by the two authors: ELD and CFK.

Statistical analysis

For TEER values, activity units (mU/ml) and concentrations (ng/ml), statistical differences were analysed by using unpaired two-tailed Student's t-tests. Differences in P_{app} values (cm/s) were determined by a one way ANOVA with Tukey's correction for multiple comparisons, where appropriate. ELISA standard curve concentrations were log-transformed and absorbance values were fitted to a sigmoidal dose response curve with variable slope for interpolation. Fold change of western blot data was log-transformed and investigated for significance using a one-sample t-test against a theoretical mean of 0. To measure MMP-3 concentration and activity in the AH of wild type (WT) mice, a paired two-tailed t-test was carried out for contralateral samples. Outflow facility was analysed using a weighted paired t-test performed in MATLAB as described in (47), incorporating both system and biological uncertainties. For IOP data, median values were obtained to reflect the non-parametric nature of the tonometer, and the Wilcoxon matched-pairs signed rank test was used to compare changes in paired populations. For morphology, the distribution of values representing the percent optically empty length was first examined using a Shapiro-Wilk and Anderson-Darling tests to detect for deviations from a normal distribution. The percent optically empty length between contralateral eyes was then analysed using a paired Student's t-test. Statistical significance was inferred when $P < 0.05$ in all experimentation. Results were depicted as 'mean, [95% Confidence Intervals]' unless otherwise stated in the results section.

Supplementary Material

Supplementary Material is available at HMG online.

Acknowledgements

We wish to acknowledge Caroline Woods and Charles Murray for animal husbandry. We would also like to thank Elke Kretzschmar, Britta Bäckermann and Andrea Eichhorn for preparing the semi- and ultrathin sections and Marco Gößwein for his assistance in finalizing the TEM images for publication.

Conflict of Interest statement. None declared.

Funding

Research at the Ocular Genetics Unit at the University of Dublin, Trinity College was supported by the European Research Council [ERC-2012-AdG 322656-Oculus]. We also acknowledge an equipment grant from Science Foundation Ireland in support of this project [12/ERC/B2539]. Research at Imperial College London was supported by the US National Institutes of Health (EY022359 and EY019696), the UK Engineering and Physical Sciences Research Council (EP/J010499/1), and Fight for Sight UK (Ref 1385). Work at Duke University was also supported by the US National Institutes of Health (EY022359). Funding to pay the Open Access publication charges for this article was provided by the European Research Council.

References

1. Yan, X., Li, M., Chen, Z., Zhu, Y., Song, Y. and Zhang, H. (2016) Schlemm's Canal and Trabecular Meshwork in Eyes with Primary Open Angle Glaucoma: A Comparative Study Using High-Frequency Ultrasound Biomicroscopy. *PLoS One*, **11**, e0145824.

2. Lanza, M., Iaccarino, S., Mele, L., Carnevale, U.A., Irregolare, C., Lanza, A., Femiano, F. and Bifani, M. (2016) Intraocular pressure evaluation in healthy eyes and diseased ones using contact and non contact devices. *Cont. Lens. Anterior. Eye*, **39**, 154–159.
3. Grant, W.M. (1951) Clinical measurements of aqueous outflow. *Am. J. Ophthalmol.*, **34**, 1603–1605.
4. Rylander, N.R. and Vold, S.D. (2008) Cost analysis of glaucoma medications. *Am. J. Ophthalmol.*, **145**, 106–113.
5. Hamanaka, T. and Bill, A. (1988) Effects of alpha-chymotrypsin on the outflow routes for aqueous humor. *Exp. Eye Res.*, **46**, 323–341.
6. Johnson, M. (2006) ‘What controls aqueous humour outflow resistance?’ *Exp. Eye Res.*, **82**, 545–557.
7. Tanihara, H., Inatani, M., Koga, T., Yano, T. and Kimura, A. (2002) Proteoglycans in the eye. *Cornea*, **21**, 62–69.
8. Floyd, B.B., Cleveland, P.H. and Worthen, D.M. (1985) Fibronectin in human trabecular drainage channels. *Invest. Ophthalmol. Vis. Sci.*, **26**, 797–804.
9. Keller, K.E., Bradley, J.M., Vranka, J.A. and Acott, T.S. (2011) Segmental versican expression in the trabecular meshwork and involvement in outflow facility. *Invest. Ophthalmol. Vis. Sci.*, **52**, 5049–5057.
10. Swaminathan, S.S., Oh, D.J., Kang, M.H., Ren, R., Jin, R., Gong, H. and Rhee, D.J. (2013) Secreted protein acidic and rich in cysteine (SPARC)-null mice exhibit more uniform outflow. *Invest. Ophthalmol. Vis. Sci.*, **54**, 2035–2047.
11. Overby, D.R., Stamer, W.D. and Johnson, M. (2009) The changing paradigm of outflow resistance generation: towards synergistic models of the JCT and inner wall endothelium. *Exp. Eye Res.*, **88**, 656–670.
12. Curtis, T.M., McKeown-Longo, P.J., Vincent, P.A., Homan, S.M., Wheatley, E.M. and Saba, T.M. (1995) Fibronectin attenuates increased endothelial monolayer permeability after RGD peptide, anti-alpha 5 beta 1, or TNF-alpha exposure. *Am. J. Physiol.*, **269**, 248–260.
13. Stickel, S.K. and Wang, Y.L. (1988) Synthetic peptide GRGDS induces dissociation of alpha-actinin and vinculin from the sites of focal contacts. *J. Cell Biol.*, **107**, 1231–1239.
14. Lampugnani, M.G., Resnati, M., Dejana, E. and Marchisio, P.C. (1991) The role of integrins in the maintenance of endothelial monolayer integrity. *J. Cell Biol.*, **112**, 479–490.
15. Wu, M.H., Ustinova, E. and Granger, H.J. (2001) Integrin binding to fibronectin and vitronectin maintains the barrier function of isolated porcine coronary venules. *J. Physiol.*, **532**, 785–791.
16. Mehta, D. and Malik, A.B. (2006) Signaling mechanisms regulating endothelial permeability. *Physiol. Rev.*, **86**, 279–367.
17. Keller, K.E. and Acott, T.S. (2013) The Juxtacanalicular Region of Ocular Trabecular Meshwork: A Tissue with a Unique Extracellular Matrix and Specialized Function. *J. Ocul. Biol. Dis. Infor.*, **1**, 3.
18. Rohen, J.W., Futa, R. and Lutjen-Drecoll, E. (1981) The fine structure of the cribriform meshwork in normal and glaucomatous eyes as seen in tangential sections. *Invest. Ophthalmol. Vis. Sci.*, **21**, 574–585.
19. Faralli, J.A., Schwinn, M.K., Gonzalez, J.M., Jr., Filla, M.S. and Peters, D.M. (2009) Functional properties of fibronectin in the trabecular meshwork. *Exp. Eye Res.*, **88**, 689–693.
20. Tamm, E.R., Siegner, A., Baur, A. and Lutjen-Drecoll, E. (1996) Transforming growth factor-beta 1 induces alpha-smooth muscle-actin expression in cultured human and monkey trabecular meshwork. *Exp. Eye Res.*, **62**, 389–397.
21. Schlunck, G., Han, H., Wecker, T., Kampik, D., Meyer-ter-Vehn, T. and Grehn, F. (2008) Substrate rigidity modulates cell matrix interactions and protein expression in human trabecular meshwork cells. *Invest. Ophthalmol. Vis. Sci.*, **49**, 262–269.
22. Acott, T.S., Kelley, M.J., Keller, K.E., Vranka, J.A., Abu-Hassan, D.W., Li, X., Aga, M. and Bradley, J.M. (2014) Intraocular pressure homeostasis: maintaining balance in a high-pressure environment. *J. Ocul. Pharmacol. Ther.*, **30**, 94–101.
23. Nagase, H., Suzuki, K., Enghild, J.J. and Salvesen, G. (1991) Stepwise activation mechanisms of the precursors of matrix metalloproteinases 1 (tissue collagenase) and 3 (stromelysin). *Biomed. Biochim. Acta*, **50**, 749–754.
24. Schlotzer-Schrehardt, U., Lommatzsch, J., Kuchle, M., Konstas, A.G. and Naumann, G.O. (2003) Matrix metalloproteinases and their inhibitors in aqueous humor of patients with pseudoexfoliation syndrome/glaucoma and primary open-angle glaucoma. *Invest. Ophthalmol. Vis. Sci.*, **44**, 1117–1125.
25. Ronkko, S., Rekonen, P., Kaamiranta, K., Puustjarvi, T., Terasvirta, M. and Uusitalo, H. (2007) Matrix metalloproteinases and their inhibitors in the chamber angle of normal eyes and patients with primary open-angle glaucoma and exfoliation glaucoma. *Graefes Arch. Clin. Exp. Ophthalmol.*, **245**, 697–704.
26. Tektas, O.Y. and Lutjen-Drecoll, E. (2009) Structural changes of the trabecular meshwork in different kinds of glaucoma. *Exp. Eye Res.*, **88**, 769–775.
27. Overby, D.R., Bertrand, J., Tektas, O.Y., Boussommier-Calleja, A., Schicht, M., Ethier, C.R., Woodward, D.F., Stamer, W.D. and Lutjen-Drecoll, E. (2014) Ultrastructural changes associated with dexamethasone-induced ocular hypertension in mice. *Invest. Ophthalmol. Vis. Sci.*, **55**, 4922–4933.
28. Pang, I.H., Fleenor, D.L., Hellberg, P.E., Stropki, K., McCartney, M.D. and Clark, A.F. (2003) Aqueous outflow-enhancing effect of tert-butylhydroquinone: involvement of AP-1 activation and MMP-3 expression. *Invest. Ophthalmol. Vis. Sci.*, **44**, 3502–3510.
29. Webb, J.G., Husain, S., Yates, P.W. and Crosson, C.E. (2006) Kinin modulation of conventional outflow facility in the bovine eye. *J. Ocul. Pharmacol. Ther.*, **22**, 310–316.
30. Bradley, J.M., Vranka, J., Colvis, C.M., Conger, D.M., Alexander, J.P., Fisk, A.S., Samples, J.R. and Acott, T.S. (1998) Effect of matrix metalloproteinases activity on outflow in perfused human organ culture. *Invest. Ophthalmol. Vis. Sci.*, **39**, 2649–2658.
31. De Groef, L., Van Hove, I., Dekeyser, E., Stalmans, I. and Moons, L. (2013) MMPs in the trabecular meshwork: promising targets for future glaucoma therapies?. *Invest. Ophthalmol. Vis. Sci.*, **54**, 7756–7763.
32. Rehnberg, M., Ammitzball, T. and Tengroth, B. (1987) Collagen distribution in the lamina cribrosa and the trabecular meshwork of the human eye. *Br. J. Ophthalmol.*, **71**, 886–892.
33. Medina-Ortiz, W.E., Belmares, R., Neubauer, S., Wordinger, R.J. and Clark, A.F. (2013) Cellular fibronectin expression in human trabecular meshwork and induction by transforming growth factor-beta2. *Invest. Ophthalmol. Vis. Sci.*, **54**, 6779–6788.
34. Hann, C.R., Springett, M.J., Wang, X. and Johnson, D.H. (2001) Ultrastructural localization of collagen IV, fibronectin, and laminin in the trabecular meshwork of normal and glaucomatous eyes. *Ophthalmic Res.*, **33**, 314–324.

35. Umihira, J., Nagata, S., Nohara, M., Hanai, T., Usuda, N. and Segawa, K. (1994) Localization of elastin in the normal and glaucomatous human trabecular meshwork. *Invest. Ophthalmol. Vis. Sci.*, **35**, 486–494.
36. Wirtz, M.K., Bradley, J.M., Xu, H., Domreis, J., Nobis, C.A., Truesdale, A.T., Samples, J.R., Van Buskirk, E.M. and Acott, T.S. (1997) Proteoglycan expression by human trabecular meshworks. *Curr. Eye Res.*, **16**, 412–421.
37. Murphy, G., Cockett, M.I., Stephens, P.E., Smith, B.J. and Docherty, A.J. (1987) Stromelysin is an activator of procollagenase. A study with natural and recombinant enzymes. *Biochem. J.*, **248**, 265–268.
38. Lijnen, H.R., Silence, J., Van Hoef, B. and Collen, D. (1998) Stromelysin-1 (MMP-3)-independent gelatinase expression and activation in mice. *Blood*, **91**, 2045–2053.
39. Ogata, Y., Enghild, J.J. and Nagase, H. (1992) Matrix metalloproteinase 3 (stromelysin) activates the precursor for the human matrix metalloproteinase 9. *J. Biol. Chem.*, **267**, 3581–3584.
40. Yang, Y., Estrada, E.Y., Thompson, J.F., Liu, W. and Rosenberg, G.A. (2007) Matrix metalloproteinase-mediated disruption of tight junction proteins in cerebral vessels is reversed by synthetic matrix metalloproteinase inhibitor in focal ischemia in rat. *J. Cereb. Blood Flow Metab.*, **27**, 697–709.
41. Yamada, H., Yoneda, M., Inaguma, S., Watanabe, D., Banno, S., Yoshikawa, K., Mizutani, K., Iwaki, M. and Zako, M. (2013) Infliximab counteracts tumor necrosis factor- α -enhanced induction of matrix metalloproteinases that degrade claudin and occludin in non-pigmented ciliary epithelium. *Biochem. Pharmacol.*, **85**, 1770–1782.
42. Rajashekar, G., Shivanna, M., Kompella, U.B., Wang, Y. and Srinivas, S.P. (2014) Role of MMP-9 in the breakdown of barrier integrity of the corneal endothelium in response to TNF- α . *Exp. Eye Res.*, **122**, 77–85.
43. Buie, L.K., Rasmussen, C.A., Porterfield, E.C., Ramgolam, V.S., Choi, V.W., Markovic-Plese, S., Samulski, R.J., Kaufman, P.L. and Borras, T. (2010) Self-complementary AAV virus (scAAV) safe and long-term gene transfer in the trabecular meshwork of living rats and monkeys. *Invest. Ophthalmol. Vis. Sci.*, **51**, 236–248.
44. Bogner, B., Boye, S.L., Min, S.H., Peterson, J.J., Ruan, Q., Zhang, Z., Reitsamer, H.A., Hauswirth, W.W. and Boye, S.E. (2015) Capsid Mutated Adeno-Associated Virus Delivered to the Anterior Chamber Results in Efficient Transduction of Trabecular Meshwork in Mouse and Rat. *PLoS One*, **10**, e0128759.
45. Gerometta, R., Spiga, M.G., Borras, T. and Candia, O.A. (2010) Treatment of sheep steroid-induced ocular hypertension with a glucocorticoid-inducible MMP1 gene therapy virus. *Invest. Ophthalmol. Vis. Sci.*, **51**, 3042–3048.
46. Borras, T., Buie, L.K. and Spiga, M.G. (2016) Inducible scAAV2.GRE.MMP1 lowers IOP long-term in a large animal model for steroid-induced glaucoma gene therapy. *Gene Ther.*, **23**, 438–449.
47. Sherwood, J.M., Reina-Torres, E., Bertrand, J.A., Rowe, B. and Overby, D.R. (2016) Measurement of Outflow Facility Using iPerfusion. *PLoS One*, **11**, e0150694.
48. Overby, D.R., Bertrand, J., Schicht, M., Paulsen, F., Stamer, W.D. and Lutjen-Drecoll, E. (2014) The structure of the trabecular meshwork, its connections to the ciliary muscle, and the effect of pilocarpine on outflow facility in mice. *Invest. Ophthalmol. Vis. Sci.*, **55**, 3727–3736.
49. Nga, A.D., Yap, S.L., Samsudin, A., Abdul-Rahman, P.S., Hashim, O.H. and Mimiwati, Z. (2014) Matrix metalloproteinases and tissue inhibitors of metalloproteinases in the aqueous humour of patients with primary angle closure glaucoma - a quantitative study. *BMC Ophthalmol.*, **14**, 33.
50. Ashworth Briggs, E.L., Toh, T., Eri, R., Hewitt, A.W. and Cook, A.L. (2015) TIMP1, TIMP2, and TIMP4 are increased in aqueous humor from primary open angle glaucoma patients. *Mol. Vis.*, **21**, 1162–1172.
51. Badier-Commander, C., Verbeuren, T., Lebard, C., Michel, J.B. and Jacob, M.P. (2000) Increased TIMP/MMP ratio in varicose veins: a possible explanation for extracellular matrix accumulation. *J. Pathol.*, **192**, 105–112.
52. Lutjen-Drecoll, E., Shimizu, T., Rohrbach, M. and Rohen, J.W. (1986) Quantitative analysis of 'plaque material' between ciliary muscle tips in normal- and glaucomatous eyes. *Exp. Eye Res.*, **42**, 457–465.
53. Rohen, J.W., Lutjen-Drecoll, E., Flugel, C., Meyer, M. and Grierson, I. (1993) Ultrastructure of the trabecular meshwork in untreated cases of primary open-angle glaucoma (POAG). *Exp. Eye Res.*, **56**, 683–692.
54. Parshley, D.E., Bradley, J.M., Samples, J.R., Van Buskirk, E.M. and Acott, T.S. (1995) Early changes in matrix metalloproteinases and inhibitors after in vitro laser treatment to the trabecular meshwork. *Curr. Eye Res.*, **14**, 537–544.
55. Parshley, D.E., Bradley, J.M., Fisk, A., Hadaegh, A., Samples, J.R., Van Buskirk, E.M. and Acott, T.S. (1996) Laser trabeculoplasty induces stromelysin expression by trabecular juxtacanalicular cells. *Invest. Ophthalmol. Vis. Sci.*, **37**, 795–804.
56. Takai, Y., Tanito, M. and Ohira, A. (2012) Multiplex cytokine analysis of aqueous humor in eyes with primary open-angle glaucoma, exfoliation glaucoma, and cataract. *Invest. Ophthalmol. Vis. Sci.*, **53**, 241–247.
57. Chua, J., Vania, M., Cheung, C.M., Ang, M., Chee, S.P., Yang, H., Li, J. and Wong, T.T. (2012) Expression profile of inflammatory cytokines in aqueous from glaucomatous eyes. *Mol. Vis.*, **18**, 431–438.
58. Kelley, M.J., Rose, A.Y., Song, K., Chen, Y., Bradley, J.M., Rookhuizen, D. and Acott, T.S. (2007) Synergism of TNF and IL-1 in the induction of matrix metalloproteinase-3 in trabecular meshwork. *Invest. Ophthalmol. Vis. Sci.*, **48**, 2634–2643.
59. Bradley, J.M., Anderssohn, A.M., Colvis, C.M., Parshley, D.E., Zhu, X.H., Ruddat, M.S., Samples, J.R. and Acott, T.S. (2000) Mediation of laser trabeculoplasty-induced matrix metalloproteinase expression by IL-1 β and TNF α . *Invest. Ophthalmol. Vis. Sci.*, **41**, 422–430.
60. Alexander, J.P., Samples, J.R. and Acott, T.S. (1998) Growth factor and cytokine modulation of trabecular meshwork matrix metalloproteinase and TIMP expression. *Curr. Eye Res.*, **17**, 276–285.
61. Partridge, C.A., Jeffrey, J.J. and Malik, A.B. (1993) A 96-kDa gelatinase induced by TNF- α contributes to increased microvascular endothelial permeability. *Am. J. Physiol.*, **265**, 438–447.
62. Si-Tayeb, K., Monvoisin, A., Mazzocco, C., Lepreux, S., Decossas, M., Cubel, G., Taras, D., Blanc, J.F., Robinson, D.R. and Rosenbaum, J. (2006) Matrix metalloproteinase 3 is present in the cell nucleus and is involved in apoptosis. *Am. J. Pathol.*, **169**, 1390–1401.
63. Garcia, A.J., Tom, C., Guemes, M., Polanco, G., Mayorga, M.E., Wend, K., Miranda-Carboni, G.A. and Krum, S.A. (2013) ER α signaling regulates MMP3 expression to induce FasL cleavage and osteoclast apoptosis. *J. Bone Miner. Res.*, **28**, 283–290.

64. Bradley, J.M., Kelley, M.J., Rose, A. and Acott, T.S. (2003) Signaling pathways used in trabecular matrix metalloproteinase response to mechanical stretch. *Invest. Ophthalmol. Vis. Sci.*, **44**, 5174–5181.
65. Bradley, J.M., Kelley, M.J., Zhu, X., Anderssohn, A.M., Alexander, J.P. and Acott, T.S. (2001) Effects of mechanical stretching on trabecular matrix metalloproteinases. *Invest. Ophthalmol. Vis. Sci.*, **42**, 1505–1513.
66. Gonzalez, P., Epstein, D.L. and Borrás, T. (2000) Genes upregulated in the human trabecular meshwork in response to elevated intraocular pressure. *Invest. Ophthalmol. Vis. Sci.*, **41**, 352–361.
67. Luna, C., Li, G., Liton, P.B., Epstein, D.L. and Gonzalez, P. (2009) Alterations in gene expression induced by cyclic mechanical stress in trabecular meshwork cells. *Mol. Vis.*, **15**, 534–544.
68. Vittitow, J. and Borrás, T. (2004) Genes expressed in the human trabecular meshwork during pressure-induced homeostatic response. *J. Cell. Physiol.*, **201**, 126–137.
69. Lai, L., Lin, K., Foulks, G., Ma, L., Xiao, X. and Chen, K. (2005) Highly efficient ex vivo gene delivery into human corneal endothelial cells by recombinant adeno-associated virus. *Curr. Eye Res.*, **30**, 213–219.
70. Sharma, A., Ghosh, A., Hansen, E.T., Newman, J.M. and Mohan, R.R. (2010) Transduction efficiency of AAV 2/6, 2/8 and 2/9 vectors for delivering genes in human corneal fibroblasts. *Brain Res. Bull.*, **81**, 273–278.
71. Liu, J., Saghizadeh, M., Tuli, S.S., Kramerov, A.A., Lewin, A.S., Bloom, D.C., Hauswirth, W.W., Castro, M.G., Schultz, G.S. and Ljubimov, A.V. (2008) Different tropism of adenoviruses and adeno-associated viruses to corneal cells: implications for corneal gene therapy. *Mol. Vis.*, **14**, 2087–2096.
72. Borrás, T., Xue, W., Choi, V.W., Bartlett, J.S., Li, G., Samulski, R.J. and Chisolm, S.S. (2006) Mechanisms of AAV transduction in glaucoma-associated human trabecular meshwork cells. *J. Gene Med.*, **8**, 589–602.
73. Herschler, J. (1976) Increased intraocular pressure induced by repository corticosteroids. *Am. J. Ophthalmol.*, **82**, 90–93.
74. Mandapati, J.S. and Metta, A.K. (2011) Intraocular pressure variation in patients on long-term corticosteroids. *Indian Dermatol. Online J.*, **2**, 67–69.
75. Pleyer, U., Ursell, P.G. and Rama, P. (2013) Intraocular pressure effects of common topical steroids for post-cataract inflammation: are they all the same? *Ophthalmol. Ther.*, **2**, 55–72.
76. Clark, A.F., Steely, H.T., Dickerson, J.E., Jr., English-Wright, S., Stropki, K., McCartney, M.D., Jacobson, N., Shepard, A.R., Clark, J.I., Matsushima, H., et al. (2001) Glucocorticoid induction of the glaucoma gene MYOC in human and monkey trabecular meshwork cells and tissues. *Invest. Ophthalmol. Vis. Sci.*, **42**, 1769–1780.
77. Gurney, K.J., Estrada, E.Y. and Rosenberg, G.A. (2006) Blood-brain barrier disruption by stromelysin-1 facilitates neutrophil infiltration in neuroinflammation. *Neurobiol. Dis.*, **23**, 87–96.
78. Vermeer, P.D., Denker, J., Estin, M., Moninger, T.O., Keshavjee, S., Karp, P., Kline, J.N. and Zabner, J. (2009) MMP9 modulates tight junction integrity and cell viability in human airway epithelia. *Am. J. Physiol. Lung Cell Mol. Physiol.*, **296**, 751–762.
79. Stamer, W.D., Roberts, B.C., Howell, D.N. and Epstein, D.L. (1998) Isolation, culture, and characterization of endothelial cells from Schlemm's canal. *Invest. Ophthalmol. Vis. Sci.*, **39**, 1804–1812.
80. Perkumas, K.M. and Stamer, W.D. (2012) Protein markers and differentiation in culture for Schlemm's canal endothelial cells. *Exp. Eye Res.*, **96**, 82–87.
81. Heimark, R.L., Kaochar, S. and Stamer, W.D. (2002) Human Schlemm's canal cells express the endothelial adherens proteins, VE-cadherin and PECAM-1. *Curr. Eye Res.*, **25**, 299–308.
82. Stamer, W.D., Seftor, R.E., Williams, S.K., Samaha, H.A. and Snyder, R.W. (1995) Isolation and culture of human trabecular meshwork cells by extracellular matrix digestion. *Curr. Eye Res.*, **14**, 611–617.
83. Stamer, W.D., Seftor, R.E., Snyder, R.W. and Regan, J.W. (1995) Cultured human trabecular meshwork cells express aquaporin-1 water channels. *Curr. Eye Res.*, **14**, 1095–1100.
84. Stamer, W.D., Huang, Y., Seftor, R.E., Svensson, S.S., Snyder, R.W. and Regan, J.W. (1996) Cultured human trabecular meshwork cells express functional alpha 2A adrenergic receptors. *Invest. Ophthalmol. Vis. Sci.*, **37**, 2426–2433.
85. Stamer, W.D. and Clark, A.F. (2016) The many faces of the trabecular meshwork cell. *Exp. Eye Res.*, in press.
86. Siah, W.F., Loughman, J. and O'Brien, C. (2015) Lower Macular Pigment Optical Density in Foveal-Involved Glaucoma. *Ophthalmology*, **122**, 2029–2037.
87. Wallace, D.M., Clark, A.F., Lipson, K.E., Andrews, D., Crean, J.K. and O'Brien, C.J. (2013) Anti-connective tissue growth factor antibody treatment reduces extracellular matrix production in trabecular meshwork and lamina cribrosa cells. *Invest. Ophthalmol. Vis. Sci.*, **54**, 7836–7848.
88. Keaney, J., Walsh, D.M., O'Malley, T., Hudson, N., Crosbie, D.E., Loftus, T., Sheehan, F., McDaid, J., Humphries, M.M., Callanan, J.J., et al. (2015) Autoregulated paracellular clearance of amyloid-beta across the blood-brain barrier. *Sci. Adv.*, **1**, e1500472.

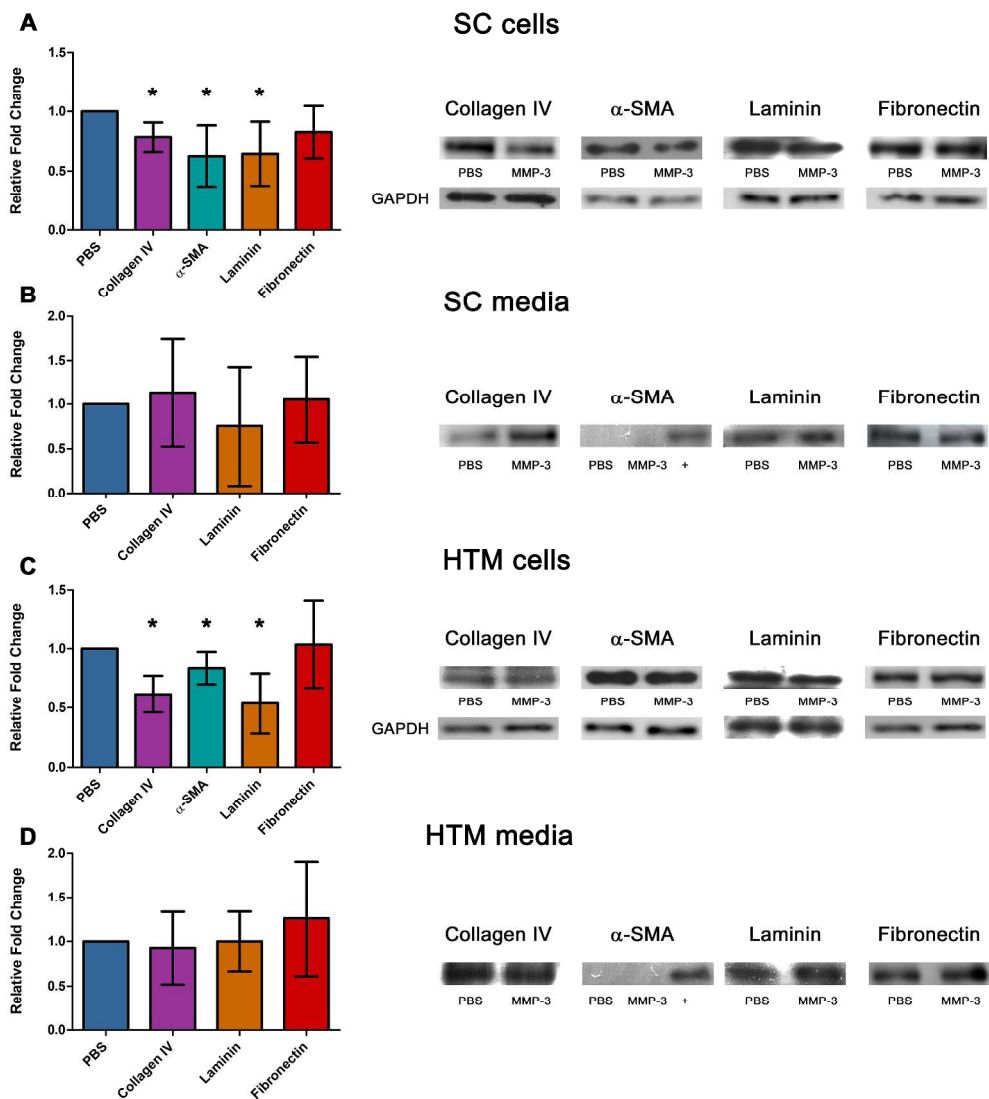


Fig.S1. Quantification of ECM remodelling and degradation. Western blot analysis was performed on PBS and MMP-3 treated samples of (A) SC cells, (B) SC media, (C) HTM cells and (D) HTM media. Significant degradation of collagen IV, α -SMA and laminin is apparent in cell lysates only. No α -SMA was detected in media samples. '+' denotes a positive control lane containing a cell lysate sample. Bars represent mean fold change with 95% confidence intervals.

Fig S1

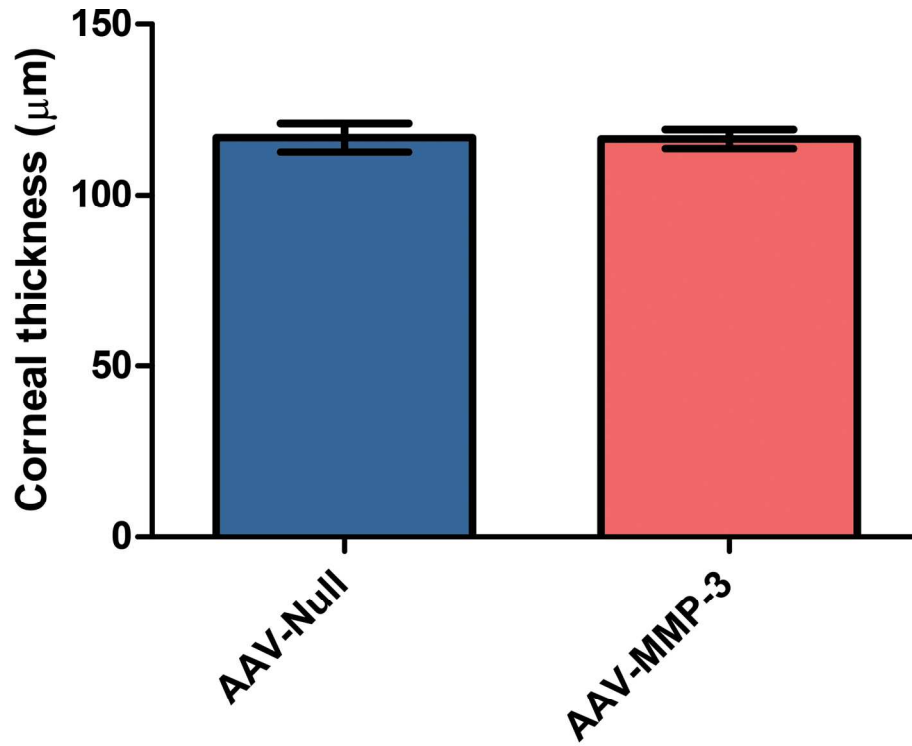


Fig.S2. Analysis of central corneal thickness. Central corneal thickness was quantified between AAV-MMP-3 injected eyes versus control. Average central corneal thickness (μm) between treatments was statistically compared by a paired Student's t-test. Error bars denote 95% CI. ($n = 4$ pairs of eyes).

Fig S2

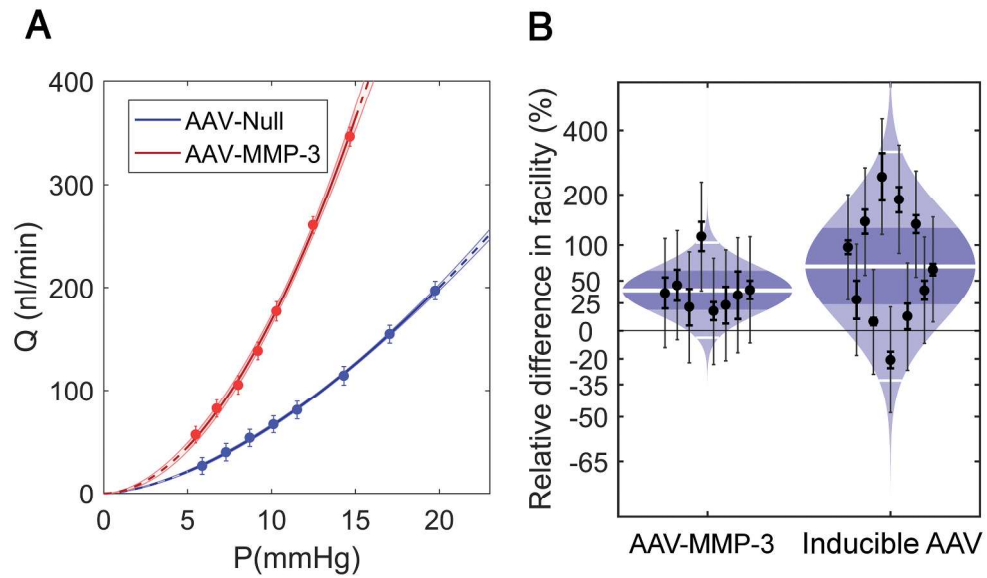


Fig.S3. Supplementary perfusion representations. (A) Plot depicting the relationship between flow (Q) and pressure (P) in a standard perfusion. As applied pressure increases, flow rate through the eye also increases. AAV-MMP-3 treated eyes have a greater response in flow to pressure increases compared to AAV-Null controls. (B) Relative differences in facility for paired eyes in both the constitutive and inducible viruses are depicted in the cello plot.

Fig S3

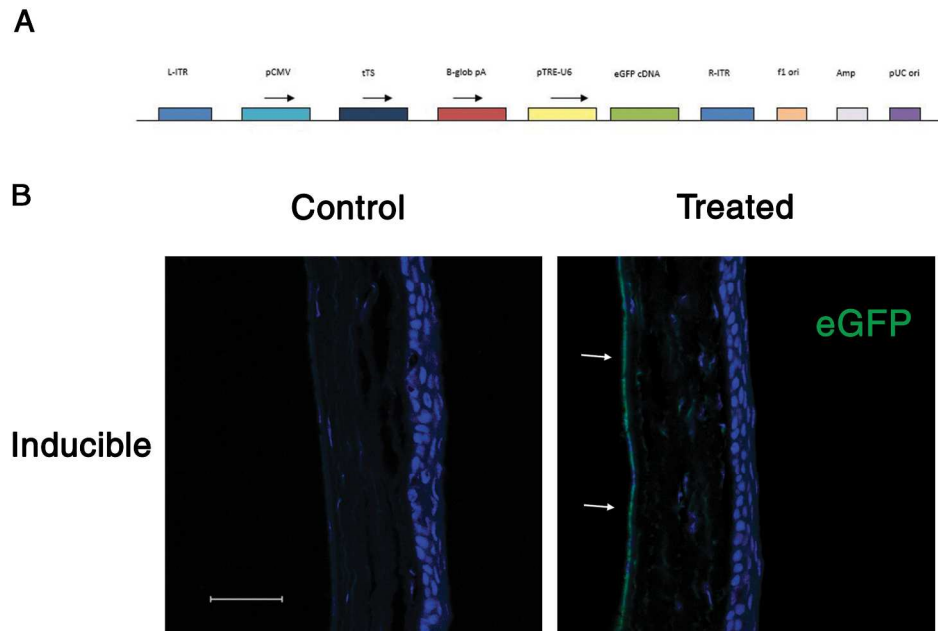


Fig.S4. Doxycycline induced expression of eGFP from corneal endothelium. (A) Illustration of the inducible vector construct. (B) AAV2/9 containing a tetracycline inducible promoter expressing eGFP was intracamerally inoculated into the anterior chamber. Expression patterns were similar to those obtained with constitutive expression of eGFP. Scale bar represents 50 μ m.

Fig S4

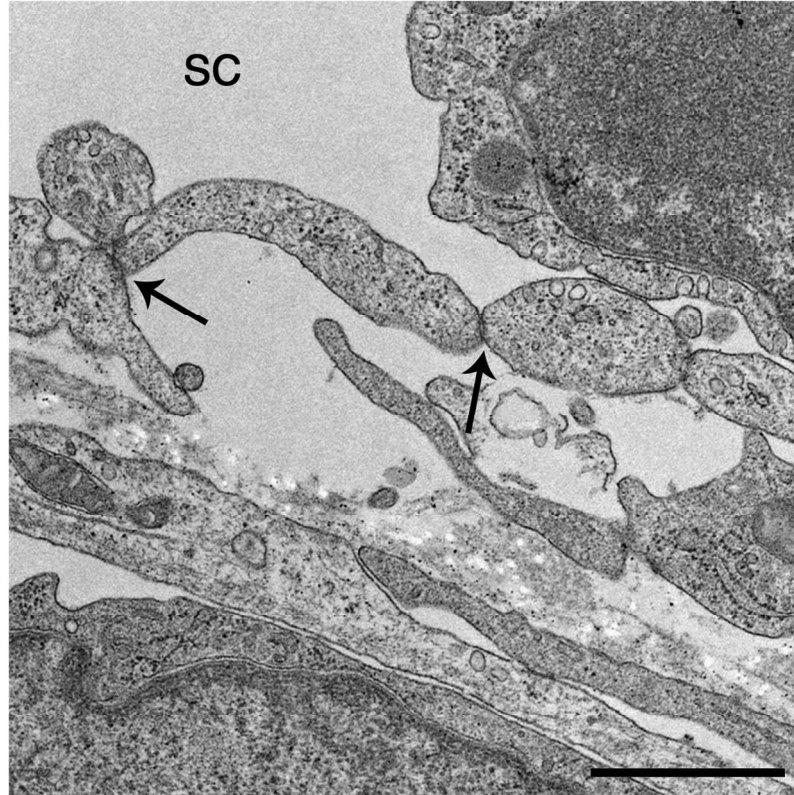


Fig. S5. TEM analysis of endothelial junctions. Ultrastructural analysis of Schlemm's Canal endothelium shows intact tight junctions between cells next to empty subendothelial regions in AAV-MMP-3 treated eyes. Scale bar represents 1 μ m.

Fig S5

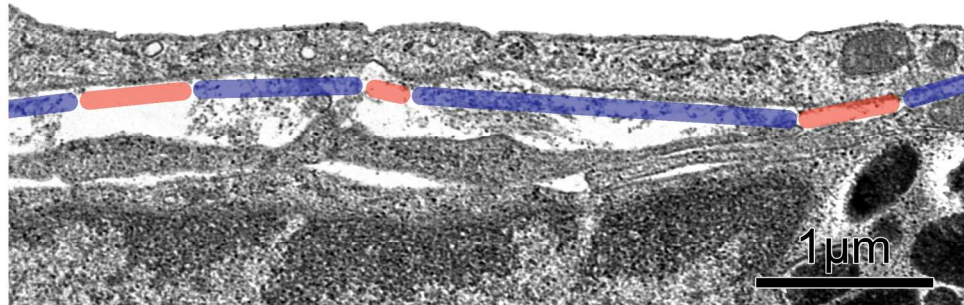


Fig. S6. Morphometric analysis of the optically empty space underlying the inner wall endothelium of SC. The anterior-posterior length of the inner wall was examined in 4 regions per eye at 10,000x magnification. Optically empty spaces (red zones) were identified, along with extracellular matrix (ECM) where the inner wall cell contacted basement membrane material, elastic fibres or amorphous material (blue zones). The ratio of optically empty length to total length (optically empty + ECM length) was defined as the percentage optically open length, as shown in Figure 6G.

Fig S6

Title

Intracameral Injection of AAV2/9 for Gene Delivery to Corneal Endothelium: a method for delivery of secretory proteins to the anterior chamber

Authors

Jeffrey O'Callaghan, Ocular Genetics Unit, Smurfit Institute of Genetics, University of Dublin, Trinity College, Dublin, D2, Ireland.

Matthew Campbell, Neurovascular Genetics Laboratory, Smurfit Institute of Genetics, University of Dublin, Trinity College, Dublin, D2, Ireland.

Peter Humphries, Ocular Genetics Unit, Smurfit Institute of Genetics, University of Dublin, Trinity College, Dublin, D2, Ireland.

Corresponding Author

Jeffrey O'Callaghan, ocallaje@tcd.ie, orcid ID = <https://orcid.org/0000-0001-8818-4331>

Intracameral Injection of AAV2/9 for Gene Delivery to Corneal Endothelium: a method for delivery of secretory proteins to the anterior chamber

Jeffrey O'Callaghan, Matthew Campbell, Peter Humphries.

ABSTRACT

AAV2/9 is expressed in a highly selective manner in the corneal endothelium of mice following intracameral inoculation into the anterior chamber of the eye, in principle, allowing genes encoding protein constituents of the secretome (representing up to 20% of the human proteome) to be delivered directly into the aqueous humour. From here the secreted protein moves with the natural flow of the aqueous humour via a pressure gradient, and is directed toward the outflow tissues. Such a delivery can be employed to modulate outflow facility and intraocular pressure through interactions at the trabecular meshwork and Schlemm's canal. We provide a protocol for the delivery of AAV to the corneal endothelium, using a CMV driven eGFP reporter gene as a marker.

Key Words

Intracameral injection, anterior chamber, protein secretion, corneal endothelium, outflow facility, intraocular pressure modulation, AAV transduction.

1. Introduction

The human secretome consists of a very large portfolio of proteins including cytokines, chemokines, proteolytic enzymes, extracellular matrix components, hormones and antimicrobial peptides synthesised in the endoplasmic reticulum [1].

These proteins could, in principle, be used in experimental therapeutic targeting of diseases of the anterior chamber of the eye including ophthalmitis, uveitis and glaucoma. As a pre-requisite, a means must be available for expression of such proteins in such a manner that they are able to gain immediate access to the aqueous humour. In this regard, the corneal endothelium, the single layer of cells lining the inner part of the cornea, represents an ideal target for such expression, since proteins can be secreted directly into the aqueous. The corneal endothelium is layer which retains proliferative capacity in humans but is maintained in a non-replicative state, rendering it an attractive cell type for long term AAV expression [2]. These cells, with an average cell density of 3200cells/mm² in subjects aged 50 and older, are entirely encompassed by the aqueous humour on the apical side, making it an available and readily accessible target for intracamerally injected AAV [3].

Disease pathology in primary open-angle glaucoma begins within the tissues of the conventional outflow pathway (the trabecular meshwork (TM) and Schlemm's canal), where, through as yet incompletely elucidated mechanisms, the natural flow of aqueous humour is impeded, resulting in elevated intraocular pressure and subsequent degeneration of the optic nerve head and retinal ganglion cells [4]. Interestingly, the pressure reducing medications routinely used in disease management largely either slow down aqueous humor production by the ciliary body, or increase aqueous humour drainage through the bundles of the ciliary muscles (the unconventional pathway for aqueous removal) [5]. Hence, pressure-reducing medications targeting conventional outflow are under active development. A recent gene therapy approach has been described targeting the TM in which AAV2/9 expressing a gene encoding matrix metalloproteinase-3 (MMP-3) was expressed in corneal endothelium following intracameral injection of the virus [6]. The AAV is selectively expressed in corneal

endothelium, resulting in secretion and activation of MMP-3 within the aqueous humour. This resulted in remodeling of the extracellular matrix of the TM, increasing aqueous outflow through the Schlemm's canal and reducing intraocular pressure. This method of delivery to the anterior chamber can also be used to routinely administer compounds including siRNAs or antibodies to the outflow tissues where AAV serotypes capable of transfecting cells of the TM other than, or in addition to corneal endothelium may be used [7-10]. A detailed and optimized protocol for AAV mediated delivery to corneal endothelium in mice using a CMV-driven eGFP reporter gene as a marker is described, utilizing a simple, single intracameral injection (Figure 1). This method involves a puncture into the anterior chamber to remove aqueous humour to allow for the infusion of viral solution from a guided syringe.

2. Materials

2.1 Preparation of virus

AAV2/9 containing an enhanced green fluorescent protein (eGFP) was purchased from Vector Biolabs to assess viral transduction and reporter gene expression in the anterior chamber of wild type mice (C57BL/6J). This AAV contains a capsid from AAV serotype 9 and ITR from AAV2. EGFP is expressed using the constitutive CMV promoter. A null virus, with the same capsid serotype with a null cassette containing the CMV promoter and no transgene, was used as contralateral control. Viral solutions were diluted to a working titre of 2×10^{12} vg/ml using nuclease free water.

2.2 *In vivo* procedures

1. Tools and equipment: 45° angled forceps, blunt forceps, micromanipulator, Hamilton syringes, hot bead sterilizer, U.V. sterilizer cabinet, surgical microscope, vertical micropipette puller, murine head holder and an anaesthesia system including vaporizer, scavenger, induction chamber and oxygen tank with regulator.
2. Consumables: 1mm diameter glass capillaries, sterile water, sterile drapes, parafilm.
3. Pharmaceuticals: Isoflurane, vidisic, fucithalamic, phenylephrine, tropicamide

2.3 Screening for eGFP

1. Tools and equipment: curved forceps, microdissection scissors, 25 gauge needle stereo microscope, cryostat, PAP pen, polylysine glass slides, coverslips, hydromount, Zeiss con focal microscope, imaging software.
2. Fixative: 4% paraformaldehyde in PBS
3. 10%, 20% and 30% sucrose solutions in PBS
4. Flash freezing tissues: OCT compound, small cryomoulds, isopropanol, liquid nitrogen.
5. Blocking buffer: 1% BSA, 5% normal goat serum and 0.1% Triton-X 100 in TBS.

6. Anti-eGFP rabbit primary antibody (cell signaling) and anti-rabbit cy-3 conjugated secondary antibody (Abcam).

7. Counterstaining solution: 1:5000 DAPI stain in TBS.

8. 1X TBS: 50mM Tris-Cl, pH 7.5, 150mM NaCl.

3. Methods

3.1 Needle preparation

1. Insert glass capillaries into the micropipette puller and set heater to 90°C. Once secured, allow the coil to heat up and the weight to pull the capillary into two needles automatically.

2. Place newly pulled needles into a clear petri dish and leave in a U.V. cabinet for 2-3 hours to sterilize needles. Place forceps in the hot bead sterilizer for 2-3 minutes, and let cool.

3. Place a sterile drape on workspace. Prior to injection, use a large, blunt forceps to break 1 mm off the tip of the needle to create an “injection needle”. On a separate needle, break approximately 3 mm off the tip of the needle to create the slightly larger in diameter “puncture needle”.

4. Insert the injection needle into the ferrule and then into the barrel of a Hamilton syringe and secure the compression fitting by tightening the locknut.

5. Place a few drops of sterile water onto a small sheet of parafilm. Withdraw this water into the needle, loosening and tightening the compression fittings as necessary, until the needle is filled and no air is present in the needle or syringe barrel.

6. Withdraw 2 μ l of air. Withdraw 1.5 μ l of virus. Withdraw a further 0.5 μ l of air.

3.2 Animal preparation

1. Expose the adult mouse to 2.5% isoflurane in oxygen at a flow rate of 1 litre/min in an induction chamber. After 2 minutes, transfer the animal to a head holder with a vaporizer/scavenger attachment. Animals should be placed on a heating pad atop a surgical drape.

3. Dilate the pupils by applying one drop of phenylephrine and tropicamide eye drops to each eye.

3. Adjust the micromanipulator to approximately 10° to the horizontal plane in a downward direction and secure the Hamilton syringe containing the virus.

4. Adjust the head holder in such a way that the animal is on its side so that the entire circumference of the eye can be seen through the surgical microscope. Dab any residual eye drops using tissue paper to remove them.

3.3 Intracameral injection

1. Using the angled forceps, secure the eye by gripping far and near sides of the sclera. Take the puncture needle and hold it at approximately 10° to match that of the micromanipulator.
2. Gently press the puncture needle through the cornea just above the limbus, taking care not to scratch the corneal surface or the lens. Due to the intraocular pressure, aqueous humour will enter the needle by capillary action. After 5-10 seconds, 2-3 μl will have entered the needle and it can be slowly removed, and the forceps can be released.
3. Align the micromanipulator to the puncture site on the corneal surface, adjusting to attain the same insertion angle as the puncture needle. Insert the injection needle into the puncture site 2-3mm so that the puncture site is sealed.
4. Slowly press on the syringe plunger to release the 0.5 μl air bubble and viral solution into the eye. Let sit for 1 minute to allow any increased intraocular pressure to disperse/equilibrate. Ensure that the air bubble lies near the puncture site.
5. Use the micromanipulator to slowly remove the needle from the eye. Apply a drop of fucithalamic antibacterial eye drop solution to the eye. Vidisic gel may also be applied during recovery to hydrate the eye if necessary.
6. Repeat the procedure for the other eye using a control virus, or remove the animal from the head holder and allow it to recover.

3.4 Tissue preparation

1. Animals are left for 4 weeks to allow for the virus fully transfect and express eGFP.

At this point, eyes are enucleated using a curved forceps and placed into fixative for 24 hours at 4°C.

2. Remove eyes from fixative and dissect under a stereo microscope. Using a 25 gauge needle or similar, pierce the sclera just below the limbus. Insert one blade of the microdissection scissors into this opening and cut around the circumference of the eye. This results in an anterior segment containing all of the cornea, iris and outflow tissues. Remove the lens before proceeding.

3. Place the anterior segment into a sucrose gradient (subsequent solutions of 10%, 20% and 30% sucrose) until the tissue sinks to the bottom.

4. Embed the tissue in OCT compound in a cryomould and place the mould into a container consisting of isopropanol. Flash freeze the tissue by placing this isopropanol bath into a trough of liquid nitrogen.

3.5 Detection of eGFP by immunohistochemistry

1. Attach the OCT block to the specimen disk with OCT compound. Place in the cryostat's object head and trim excess OCT from the block.

2. Section the tissue at a thickness of 12 μm and gather sections onto glass slides.

3. Draw around sections with a PAP pen and let dry.
4. Perform one wash with 1X TBS by dropping the TBS near the sections and after 5 minutes drain the TBS off the slide. Add blocking buffer and leave for 1 hour at room temperature.
5. Apply primary antibody (1:250 dilution in TBS) and place into a humidity chamber at 4°C overnight.
6. Wash slides 3 times for 5 minutes each in TBS. Drain and add secondary antibody (1:500 dilution) to the slides, with one slide getting no secondary antibody to serve as a negative control. Protect slides from light for 2 hours at room temperature.
7. Wash slides 2 times as before and add counterstaining solution for 30-60 seconds. Perform one final wash and remove all liquid from the slides. Apply hydromount medium and gently attach a coverslip.
8. Once mounting medium has dried, use a light microscope or confocal to determine the intensity of fluorescence. Imaging software can be employed to perform stitching, stacking or quantitative analysis across sections.

4. Notes

1. Filling the injection needle with water when in the syringe improves responsiveness for withdrawing small volumes as it removes air compression and expansion. Mineral

oil can also be used instead of the 2 μ l of air to prevent dilution or mixing of the virus and the water in the needle.

2. When puncturing the cornea, having the puncture needle at the same angle as the micromanipulator makes insertion of the injection needle easier. More than 2-3 μ l can be removed from the anterior chamber if it is intended that greater volumes be injected, however deflation of the eye can result in a depressed puncture site, making insertion of the injection needle difficult.

3. It is preferable for the air bubble to reside at the puncture site after injection to prevent reflux. The air bubble can be guided through the cornea using a forceps however it is recommended that the eye be tilted so that the bubble will naturally reside at the puncture site. A small amount (0.5-1 μ l) of reflux is tolerated with this method.

4. Fucithalamic eye drops may be applied before removal of the injection needle to further reduce reflux.

5. A syringe pump may be used in place of a Hamilton syringe. An infusion setting of 1-2 μ l can be used to minimize any sudden transient increases in intraocular pressure.

6. Care should be taken to avoid any scratches on any ocular surfaces. Aseptic technique should be employed to reduce the risk of infection or cataract. Needles should minimally penetrate the eye as to reduce the likelihood of infection or

haemorrhage. Puncturing too close to the limbus may result in piercing of the iris or an iris retraction into the wound site when healing.

7. Enucleated eyes can be transferred from fixative and stored in 0.01% sodium azide in PBS for longer term storage. Sections on slides may also be stored at 20°C prior to staining.

8. Glass needles are extremely brittle and care must be taken to preserve the tips. Blue tack can be used to secure needles in parallel along the diameter of a petri dish for storage and transport.

9. The length of time that phenylephrine and tropicamide eye drops should stay on the eye may vary between animals, but will take on average 3-5 minutes for the pupil to fully dilate. When these drops are removed from the first eye by gentle dapping of tissue paper, the drops on the other eye can be left until the first eye is injected so as to prevent dehydration.

10. This is an effective and repeatable method that takes less than 15 minutes for the inoculation of both eyes in the mouse from the onset of anaesthesia. Variations of this technique have also been described [9,10].

5. References

1. Sage H, Pritzl P, Bornstein P (1981) Secretory phenotypes of endothelial cells in culture: comparison of aortic, venous, capillary, and corneal endothelium.

Arteriosclerosis 1 (6):427-442

2. Joyce NC (2003) Proliferative capacity of the corneal endothelium. *Prog Retin Eye Res* 22 (3):359-389
3. Wilson RS, Roper-Hall MJ (1982) Effect of age on the endothelial cell count in the normal eye. *Br J Ophthalmol* 66 (8):513-515
4. Campbell M, Cassidy PS, O'Callaghan J, Crosbie DE, Humphries P (2018) Manipulating ocular endothelial tight junctions: Applications in treatment of retinal disease pathology and ocular hypertension. *Prog Retin Eye Res* 62:120-133. doi:10.1016/j.preteyeres.2017.09.003
5. O'Callaghan J, Cassidy PS, Humphries P (2017) Open-angle glaucoma: therapeutically targeting the extracellular matrix of the conventional outflow pathway. *Expert Opin Ther Targets* 21 (11):1037-1050. doi:10.1080/14728222.2017.1386174
6. O'Callaghan J, Crosbie DE, Cassidy PS, Sherwood JM, Flugel-Koch C, Lutjen-Drecoll E, Humphries MM, Reina-Torres E, Wallace D, Kiang AS, Campbell M, Stamer WD, Overby DR, O'Brien C, Tam LCS, Humphries P (2017) Therapeutic potential of AAV-mediated MMP-3 secretion from corneal endothelium in treating glaucoma. *Hum Mol Genet* 26 (7):1230-1246. doi:10.1093/hmg/ddx028
7. Tam LC, Reina-Torres E, Sherwood JM, Cassidy PS, Crosbie DE, Lutjen-Drecoll E, Flugel-Koch C, Perkumas K, Humphries MM, Kiang AS, O'Callaghan J, Callanan JJ, Read AT, Ethier CR, O'Brien C, Lawrence M, Campbell M, Stamer WD, Overby DR, Humphries P (2017) Enhancement of Outflow Facility in the Murine Eye by Targeting Selected Tight-Junctions of Schlemm's Canal Endothelia. *Sci Rep* 7:40717. doi:10.1038/srep40717
8. Raghuram A, Saravanan VR, Narendran V (2007) Intracameral injection of bevacizumab (Avastin) to treat anterior chamber neovascular membrane in a painful blind eye. *Indian journal of ophthalmology* 55 (6):460-462


9. Wang L, Xiao R, Andres-Mateos E, Vandenberghe LH (2017) Single stranded adeno-associated virus achieves efficient gene transfer to anterior segment in the mouse eye. PLoS One 12 (8):e0182473. doi:10.1371/journal.pone.0182473
10. Bogner B, Boye SL, Min SH, Peterson JJ, Ruan Q, Zhang Z, Reitsamer HA, Hauswirth WW, Boye SE (2015) Capsid Mutated Adeno-Associated Virus Delivered to the Anterior Chamber Results in Efficient Transduction of Trabecular Meshwork in Mouse and Rat. PLoS One 10 (6):e0128759. doi:10.1371/journal.pone.0128759

Figure 1 Caption

Figure 1: AAV-mediated GFP expression from the corneal endothelium.

GFP expression is observed in the murine eye 4 weeks post intracameral inoculation of AAV2/9 constitutively expressing eGFP. Expression is found to be exclusive to the corneal endothelium with AAV9 after immunostaining and con focal microscopy.

SCIENTIFIC REPORTS



OPEN

Enhancement of Outflow Facility in the Murine Eye by Targeting Selected Tight-Junctions of Schlemm's Canal Endothelia

Received: 05 August 2016
Accepted: 09 December 2016
Published: 16 January 2017

Lawrence C. S. Tam^{1,*}, Ester Reina-Torres^{1,2,*}, Joseph M. Sherwood², Paul S. Cassidy¹, Darragh E. Crosbie¹, Elke Lütjen-Drecoll³, Cassandra Flügel-Koch³, Kristin Perkumas⁴, Marian M. Humphries¹, Anna-Sophia Kiang¹, Jeffrey O'Callaghan¹, John J. Callanan⁵, A. Thomas Read⁶, C. Ross Ethier⁷, Colm O'Brien⁸, Matthew Lawrence⁹, Matthew Campbell¹, W. Daniel Stamer⁴, Darryl R. Overby² & Pete Humphries¹

The juxtacanalicular connective tissue of the trabecular meshwork together with inner wall endothelium of Schlemm's canal (SC) provide the bulk of resistance to aqueous outflow from the anterior chamber. Endothelial cells lining SC elaborate tight junctions (TJs), down-regulation of which may widen paracellular spaces between cells, allowing greater fluid outflow. We observed significant increase in paracellular permeability following siRNA-mediated suppression of TJ transcripts, claudin-11, zonula-occludens-1 (ZO-1) and tricellulin in human SC endothelial monolayers. In mice claudin-11 was not detected, but intracameral injection of siRNAs targeting ZO-1 and tricellulin increased outflow facility significantly. Structural qualitative and quantitative analysis of SC inner wall by transmission electron microscopy revealed significantly more open clefts between endothelial cells treated with targeting, as opposed to non-targeting siRNA. These data substantiate the concept that the continuity of SC endothelium is an important determinant of outflow resistance, and suggest that SC endothelial TJs represent a specific target for enhancement of aqueous movement through the conventional outflow system.

Under physiological conditions, the majority of aqueous humour (AH) exits the anterior chamber through the conventional outflow pathway in humans¹⁻³. In this pathway, AH filters sequentially through the trabecular meshwork (TM), including the juxtacanalicular tissue (JCT), and the endothelial lining of Schlemm's canal (SC) before entering the SC lumen and draining into the episcleral veins. Electron microscopic evidence has indicated that AH drainage across SC endothelium occurs through micron-sized pores that pass either through (transcellular) or between (paracellular) individual SC cells⁴⁻⁹. In particular, a significant fraction of AH crosses the inner wall of SC via paracellular pores¹⁰. Moreover, the presence of tight-, adherens- and gap-junctions in SC endothelial cells provides a mechanism by which the conventional outflow pathway is dynamically responsive to constantly changing physiological conditions while still preserving the blood-aqueous barrier¹¹⁻¹⁷. It has long been recognised that elevated intraocular pressure (IOP) associated with primary open-angle glaucoma (POAG) is due to elevated resistance to AH outflow through the conventional outflow pathway¹⁸, although the cause of elevated outflow resistance in glaucoma remains to be fully elucidated. Previous studies support the concept that outflow

¹Neurovascular Genetics, Smurfit Institute of Genetics, Trinity College, University of Dublin, Dublin 2, Ireland.

²Department of Bioengineering, Imperial College London, London, UK. ³Department of Anatomy, University of Erlangen-Nürnberg, Erlangen, Germany. ⁴Department of Ophthalmology, Duke University, Durham, NC, USA.

⁵Ross University School of Veterinary Medicine, P. O. Box 334, Basseterre, St. Kitts, West Indies. ⁶Department of Ophthalmology and Vision Sciences, University of Toronto, Canada. ⁷Coulter Department of Biomedical Engineering, Georgia Institute of Technology and Emory University, Atlanta, USA. ⁸Ophthalmology, Mater Hospital, UCD School of Medicine, Dublin, Ireland. ⁹RxGen, Hamden, CT, USA. *These authors contributed equally to this work.

Correspondence and requests for materials should be addressed to L.C.S.T. (email: lawrenc@tcd.ie) or W.D.S. (email: william.stamer@duke.edu) or P.H. (email: pete.humphries@tcd.ie)

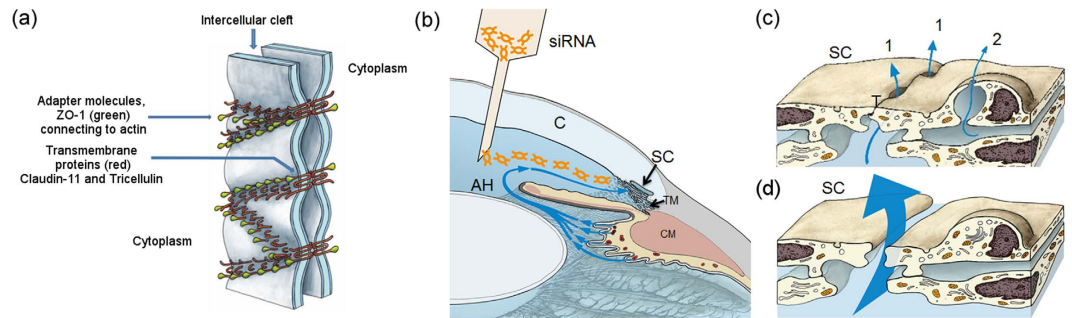


Figure 1. Schematic illustration of the therapeutic strategy addressed in this study. (a) Schematic representation of adapter molecules and transmembrane proteins connecting neighbouring SCEC.

(b) Intracameral delivery enables siRNAs to be transported towards the conventional outflow pathway by following the natural flow dynamics of aqueous humour in the anterior chamber. AH = aqueous humour; C = cornea; CM = ciliary muscle; SC = Schlemm's canal; TM = trabecular meshwork. (c) AH crosses the inner wall endothelium of SC via (1) the intercellular pathway through gaps in tight junctions (T) and, or via (2) the intracellular pathway through a giant vacuole with a pore. (d) siRNAs taken up by endothelial cells of the inner wall of SC elicit knockdown of tight junction proteins, resulting in the opening of intercellular clefts with concomitant increase in aqueous outflow facility.

resistance is modulated through a synergistic hydrodynamic interaction between JCT and SC endothelium such that inner wall pore density may influence outflow resistance generation by defining the regions of filtration through the JCT^{19–21}. As glaucomatous eyes have reduced SC inner wall pore density, decreased porosity of the inner wall appears to contribute to elevated outflow resistance and increased IOP^{22–24}.

Prolonged elevation of IOP results in progressive degeneration of retinal ganglion cell axons, and hence to irreversible vision loss. Treatment of POAG by lowering IOP remains the only approach to limiting disease progression. Topically applied medications that either reduce AH production or increase drainage through the unconventional (uveoscleral) outflow pathway are widely used in management of IOP in patients with POAG²⁵. However, a proportion of patients do not respond optimally to such medications and, therefore, there is a clear need to investigate novel approaches to reduce outflow resistance by identifying specific targets within the conventional outflow pathway through which this might be achieved. Owing to the fact that a major fraction of AH filtration at the level of SC appears to largely pass through paracellular routes¹⁰, strategies specifically targeting cell-cell junctions between endothelial cells of the inner wall of SC may be effective at decreasing outflow resistance. Hence, we hypothesised that down-regulation of selected tight junction (TJ) components of endothelial cells lining the inner wall of SC may increase the paracellular spaces between these cells, facilitating flow of AH across the inner wall into the SC (Fig. 1), thus reducing outflow resistance and IOP.

In this report, we have identified TJ components in human primary cultures of SC endothelial cells (SCEC), and also in mouse and non-human primate outflow tissues. We show that siRNA-mediated down-regulation of such components increases the paracellular permeability of human primary SCEC monolayers to 70 kDa FITC-dextran, and decreases transendothelial electrical resistance. Furthermore, intracameral delivery of siRNAs targeting selected TJ components is shown to increase intercellular open spaces between SC inner wall endothelial cells as observed by transmission electron microscopy (TEM) and elevates outflow facility (the mathematical inverse of outflow resistance) in normotensive mice. In summary, our findings clearly identify a specific approach to promoting AH outflow by direct manipulation of selected TJs within the conventional outflow pathway.

Results

Characterisation of tight junction expression in human SC endothelial cells. We examined the TJ expression profile in primary cultures of human SCEC isolated from four individual donors, with the objective of determining key junctional components that regulate permeability and selectivity of the inner wall of SC. The mean normalised expression ($2^{-\Delta\Delta Ct}$) of genes encoding claudin and adhesion junctional proteins from four different SCEC strains is shown in Fig. 2a. The complete expression pattern can be found as Supplementary Fig. S1. The expression profile shows that claudin-11 (or oligodendrocyte specific protein) was amongst the highest expressed claudin-based TJ protein in cultured SCEC (Fig. 2a). In addition, zonula-occludens-1 protein (ZO-1, also known as *TJPI*), a key component of junctional complexes that regulate TJ formation, was also expressed at high levels in cultured SCEC. The cell-cell adhesion molecule, junctional adhesion molecule-3 (JAM3) was also highly expressed in human SCEC monolayers. In contrast, occludin and claudin-5, which are major TJ components of human and mouse brain and inner retinal vascular endothelium^{26,27} were expressed at low levels in human SCEC. Collectively, these data indicate that claudin-11 is the dominant claudin in the TJs of cultured SCEC, and that ZO-1 is a major junctional associated protein of cultured SCEC. We also compared transcript levels of claudin-11 and ZO-1 in cultured monolayers of human SCEC (SC77) against those of human TM cells (TM93), and observed expression levels of claudin-11 to be 2.52-fold higher in SCEC than in TM cells (Supplementary Fig. S2). However, no significant difference in ZO-1 transcript expression was observed between TM and SCEC.

Claudin-11 and ZO-1 protein expression was detected in cultured SCEC by Western blot (Fig. 2b). In addition, we also detected expression of another TJ protein, tricellulin (also known as MARVELD2) in cultured SCEC,

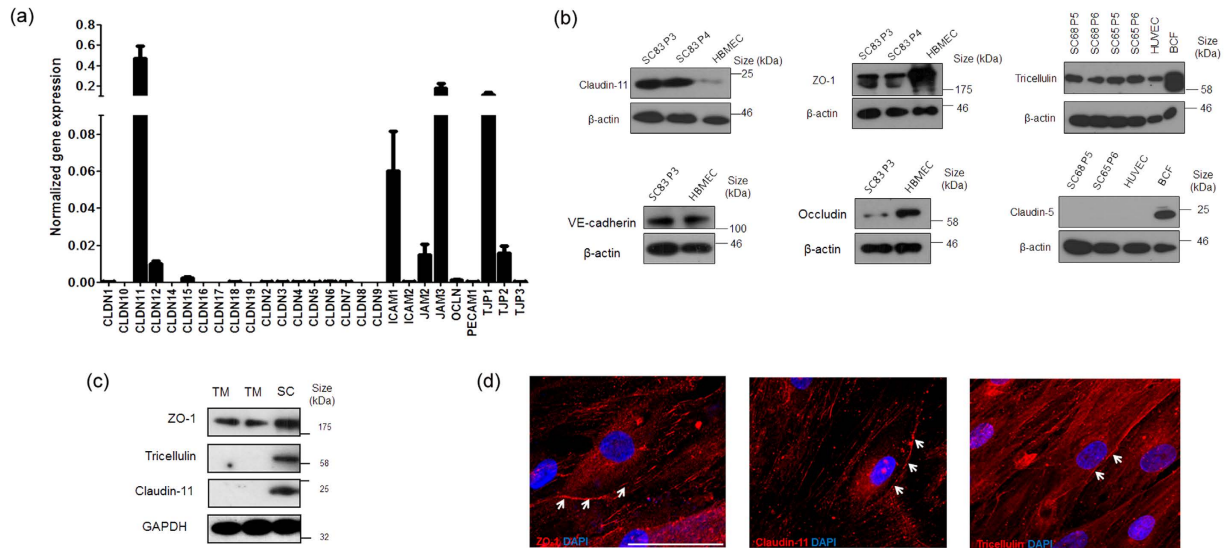


Figure 2. Characterisation of tight junction expression in human Schlemm's canal endothelial cells.

(a) The human TJs RT² Profiler PCR array was used to profile the expression of claudin and adhesion junctional proteins. Bar graphs illustrate average relative gene expression ($2^{-\Delta CT}$) normalised to 5 housekeeping genes from 4 different human SCEC strains. Data are mean \pm s.e.m. Note the break in scale for normalised gene expression. **(b)** Protein analysis of claudin-11, ZO-1, tricellulin, VE-cadherin, occludin and claudin-5 in cultured human SCEC. HBMEC = human brain microvascular endothelial cells; BCF = Mouse brain capillary fraction; B-actin as loading control. Different SCEC strains are denoted followed by passage (P) number. **(c)** Tight junction protein expression in TM (TM120 and TM130) and SCEC. GAPDH as loading control. **(d)** White arrow heads illustrate immuno-detection of ZO-1, claudin-11 and tricellulin (Cy3) in cultured human SCEC. Blue = DAPI nuclei staining. Scale bar, 50 μ m.

which was not included in the PCR array. Consistent with previous studies^{14,28}, expression of vascular endothelial (VE)-cadherin was also identified in cultured SCEC (Fig. 2b). However, we did not detect claudin-5 protein expression in cultured SCEC, and only low levels of occludin protein expression were detected, an observation consistent with the PCR array data. Furthermore, we did not detect claudin-11 and tricellulin expression in TM cells (TM120 and 130), whereas both TM and SCEC (SC82) were shown to express ZO-1 protein (Fig. 2c). This is consistent with a previous finding showing that both TM and SCEC express the junction-associated protein, ZO-1²⁹. Immunocytochemistry was then undertaken to examine the expression patterns of TJ proteins in confluent SCEC monolayers. We observed discontinuous membrane-specific staining patterns for ZO-1, claudin-11 and tricellulin in cultured SCEC monolayers (Fig. 2d).

Characterisation of expression of tight junction and tight junction associated components in mouse and non-human primate outflow tissues. We performed immunohistochemistry (IHC) on frozen sections of mouse anterior segments to localise the expression of TJ proteins in the outflow region comprising the TM and the inner wall of SC. Immunofluorescent images show tricellulin and ZO-1 staining predominantly localising in the inner wall endothelium of SC (Fig. 3a). In particular, we observed ZO-1 staining to be diffusely distributed in the cytoplasm of SCEC. In regions where part of the endothelium was cut obliquely to the inner wall of SC, continuous junctional strands were displayed around SCEC margins. ZO-1 and tricellulin staining were also detected in the TM region and in the outer wall. In both regions the endothelial cells were connected by TJs. However, we did not detect claudin-11 or claudin-5 staining in the inner wall of SC and TM with the antibodies used in this study (Supplementary Fig. S3). These data indicate that murine outflow tissues may possess a different junctional composition at the inner wall of SC as compared to humans, with the possible absence of claudin-based tight junctional proteins in TM and SCEC. However, the presence of ZO-1 and tricellulin along the inner wall in mice indicates that these proteins may be suitable targets for assessment of effects of TJ down-regulation in mice.

IHC was performed on paraffin sections of African green monkey anterior segments to identify the junctional composition of the outflow region. Hematoxylin and eosin staining (H&E) of the anterior chamber clearly identified the iridocorneal angle and conventional outflow tissues (Fig. 3b). Superimposed immunofluorescent imaging showed strong continuous claudin-11 staining along the endothelial cell margins of the inner wall of SC, highly indicative of TJ barrier function (Fig. 3b). Claudin-11 immunostaining was also present along the outer wall of SC and between TM cells. Similarly, ZO-1 and tricellulin staining were observed in the inner wall endothelium of SC. All three TJ proteins were present between TM endothelial cells, but the staining was less intense than in the inner wall endothelium. In addition, we did not detect claudin-5 expression in SCEC isolated from non-human primates (Supplementary Fig. 4). These data indicate that SCEC in non-human primates possess a similar TJ barrier composition to that found in humans.

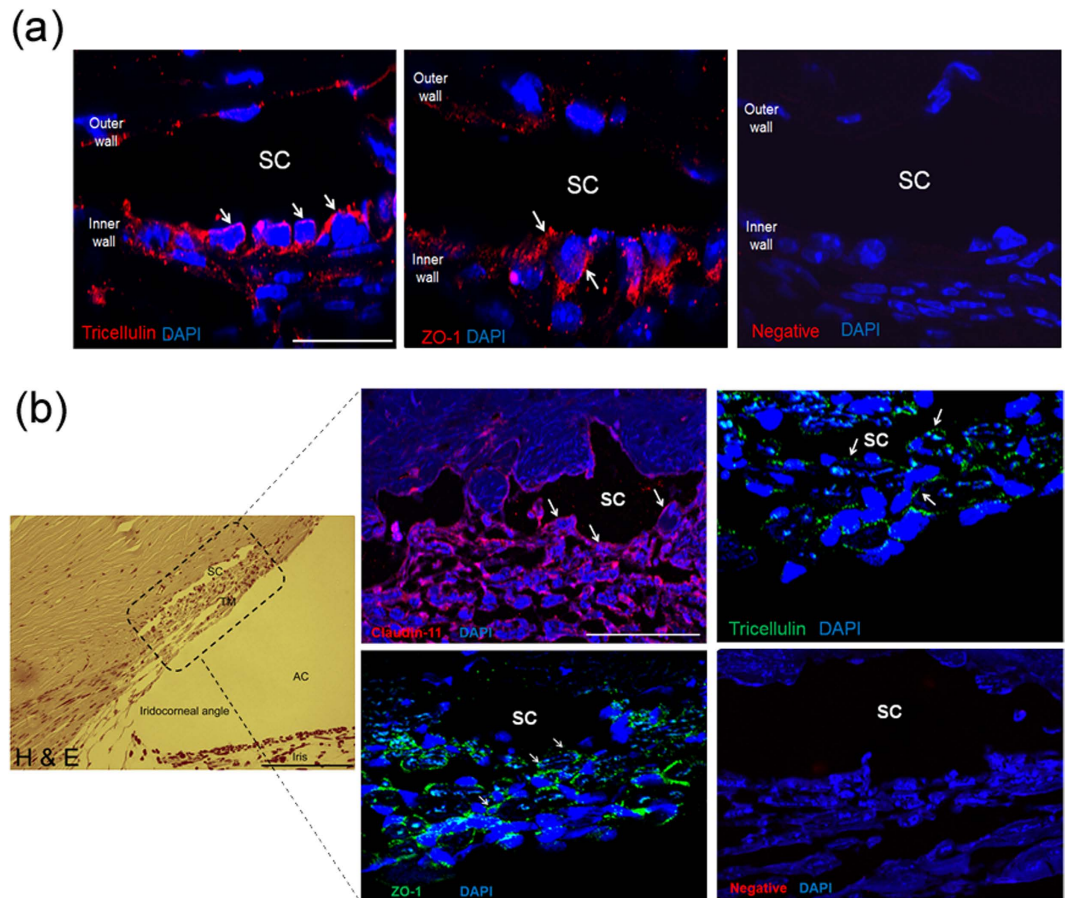


Figure 3. Characterisation of tight junction expression in mouse and non-human primate outflow tissues. (a) Immunostaining of tricellulin and ZO-1 in frozen sections of mouse anterior segments. ZO-1 and tricellulin = Cy3 (red); DAPI = blue; SC = Schlemm's canal lumen. Scale bar, 50 μ m. (b) H&E staining of paraffin monkey anterior segments (left panel). Boxed area depicts superimposed regions shown in immunofluorescence images. AC = anterior chamber; SC = Schlemm's canal lumen; TM = trabecular meshwork. Scale bar, 200 μ m. Immunofluorescent images of claudin-11, ZO-1 and tricellulin staining in the inner wall endothelium of SC. White arrows indicate detection of corresponding tight junctions at the inner wall of SC endothelium. Negative = no primary antibody. Scale bar, 50 μ m.

Validation of tight junction siRNAs. In order to validate the suppression efficiency of pre-designed siRNAs targeting the human transcripts of claudin-11, ZO-1 and tricellulin, cultured SCEC were separately transfected with 40 nM of each siRNA, and levels of endogenous TJ expression were assessed in a time-dependent manner by Western blot. Time-dependent down-regulation of claudin-11 expression to $5 \pm 3\%$ ($p < 0.0001$), $11 \pm 1\%$ ($p < 0.0001$) and $9 \pm 4\%$ ($p < 0.0001$) (mean \pm s.e.m.), was achieved at 24, 48 and 72 h post-transfection respectively, as compared to non-targeting (NT) siRNA (Fig. 4a). ZO-1 expression was reduced to $72 \pm 3\%$ ($p = 0.005$), $64 \pm 4\%$ ($p = 0.0004$) and $49 \pm 18\%$ ($p = 0.02$) at 24, 48 and 72 h post-transfection respectively (Fig. 4b). Furthermore, tricellulin expression was reduced to $75 \pm 0.2\%$ ($p = 0.002$), $81 \pm 6\%$ ($p = 0.012$) and $87 \pm 8\%$ ($p > 0.05$) at 24, 48 and 72 h respectively following siRNA treatment (Fig. 4c). The difference in knock-down efficiencies likely indicates that ZO-1 and tricellulin have slower protein turnover rates than claudin-11 in cultured SCEC. A cell viability assay was performed on transfected SCEC and no change in viability due to siRNA treatment was detected when cells were treated with either 40 or 200 nM of siRNA (Supplementary Fig. S5). siRNAs targeting mouse ZO-1 and tricellulin were also validated and show efficient knockdown of gene expression *in vitro* (Supplementary Fig. S6).

The efficacy of siRNA inhibition *in vivo* was tested in retinas from mice injected intravitreally with siRNA against ZO-1 and tricellulin. RT-PCR carried out on RNA extracted from mouse retinas showed that 12 h post-injection, tricellulin RNA was significantly reduced to 0.32 fold ($p = 0.049$; Supplementary Fig. S7) compared to eyes injected with NT-siRNA while ZO-1 was reduced to 0.57 fold ($p = 0.048$; Supplementary Fig. S7). This approach using retina was taken because of the difficulty in isolating SC endothelium from mouse eyes to perform a reliable quantification analysis.

We performed cell death assays to assess SCEC viability following siRNA inoculation *in vivo* in mouse outflow tissues. Immunohistochemistry was performed on eyes 48 hours post injection with either targeting or NT siRNA. Approximately 30–40 μ m sections were each stained by TUNEL and complemented by cleaved

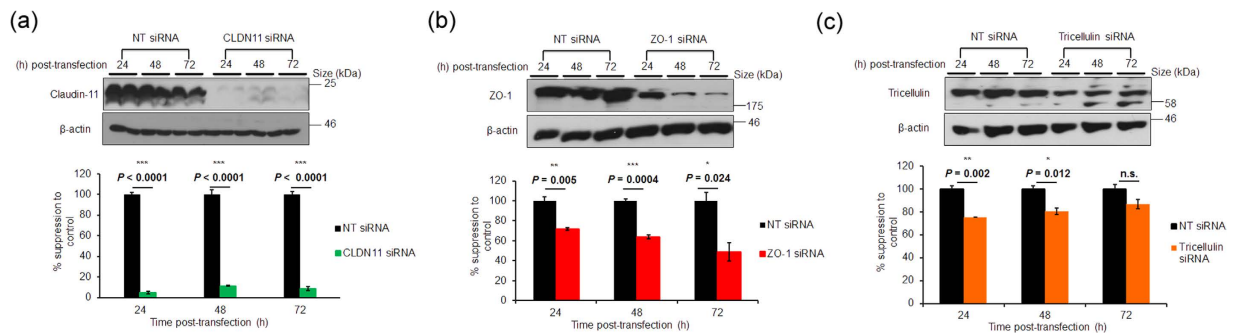


Figure 4. siRNA-mediated down-regulation of tight junction RNA transcripts in cultured human SCEC.

Representative Western blots of (a) claudin-11, (b) ZO-1 and (c) tricellulin knockdown in cultured human SCEC over a 72 h period. Corresponding bar graphs depict densitometric analysis of percentage protein normalised to β-actin. NT siRNA = non-targeting siRNA. Data are mean \pm s.e.m.; n.s. = $P \geq 0.05$ (n = 4, unpaired *t*-test).

caspace-3 staining as markers of apoptosis for representatives of targeting and non-targeting siRNA. For TUNEL staining, most sections displayed some apoptotic damage in the corneal epithelium. Parts of the ciliary body were also the site of minor labelling, regardless of treatment received. Closer inspection of the angle and outflow tissue itself provided no evidence of any apoptotic cell death in either targeting or NT controls. Cleaved caspace-3 was sparsely detected in the ciliary body, and effectively absent in the angle or outflow tissue in either treatment, correlating with observations by TUNEL (Supplementary Fig. S8).

Effect of down-regulation of tight junctions on SCEC monolayer permeability. In order to address the hypothesis that down-regulation of TJ components in SCEC could be used as a means of modulating the resistance of SC inner wall, transendothelial electrical resistance (TEER) was measured to assess changes in endothelial barrier function in confluent SCEC monolayers following TJ knockdown. SCEC monolayers transfected with claudin-11 or ZO-1 siRNAs showed significant reduction in TEER compared to NT siRNAs at 48 and 72 h post-transfection ($p < 0.001$; Fig. 5a). Furthermore, transfection with a combination of claudin-11 and ZO-1 siRNAs elicited a significant decrease in TEER, and the magnitude of decrease was more profound than those treated with single siRNAs at 48 h post-transfection ($p < 0.001$, Fig. 5a). Similarly, treatment with tricellulin siRNA alone also showed significant reduction of TEER at 48 h post-transfection, and the effect was sustained up to 72 h ($p < 0.001$, Fig. 5b). We next treated SCEC monolayer simultaneously with a combination of three siRNAs targeting claudin-11, ZO-1 and tricellulin, and observed significant reduction in TEER from 24 to 72 h post-transfection as compared to control ($p < 0.001$, Fig. 5c). Measured TEER values can be seen in Supplementary Table S1.

The effect of TJ down-regulation on endothelial permeability was tested in confluent SCEC monolayers using non-ionic macromolecular tracer, FITC-dextran (FD), which can only transverse via the paracellular route. To investigate the size selectivity of paracellular permeability in SCEC monolayers, we first determined the flux of 4, 70 and 150 kDa FD in the basal to apical direction following treatment of monolayers with siRNAs targeting tricellulin. At 24 h post-transfection, we observed no difference between control and treated in apparent permeability co-efficient (P_{app}) to the 4 kDa FD ($\approx 3.66 \times 10^{-6}$ cm/s), which readily passes through the monolayer. In contrast, the 150 kDa FD did not readily cross the monolayer ($\approx 1.23 \times 10^{-8}$ cm/s). The largest decrease in barrier tightness as measured by P_{app} was observed with the 70 kDa FD ($p < 0.0001$, Fig. 5d). These data indicate that down-regulation of tricellulin in SCEC monolayers selectively opens the paracellular route to macromolecules of 70 kDa. Following this, we treated SCEC monolayers with siRNAs targeting other TJs, and observed that down-regulation of claudin-11 ($p < 0.0001$), ZO-1 ($p < 0.0001$), as well as tricellulin ($p < 0.0001$) significantly increased paracellular flux of 70 kDa FD, as compared to controls (Fig. 5e,f). In addition, P_{app} (70 kDa FD) was observed to be significantly greater in monolayers treated singly with a combination of ZO-1 and tricellulin siRNAs than control ($p < 0.0001$), and compared to those treated singly with either ZO-1 or tricellulin siRNA ($p < 0.001$) (Fig. 5f). Furthermore, treatment with a combination of siRNAs targeting three TJs simultaneously also increased P_{app} of SCEC to 70 kDa FD ($p = 0.0004$ vs. control; Fig. 5g). We used primary SCEC strains from different donor eyes for flux assays in Fig. 5e–g, and as a consequence, we observed natural variability in baseline P_{app} values and responses to TJ down-regulation from different strains. Collectively, these data demonstrate that claudin-11, ZO-1 and tricellulin contribute to the barrier function of cultured human SCEC, and that siRNA-mediated down-regulation of these cellular junctional proteins significantly alters endothelial cell barrier integrity and permeability.

Ultrastructural analysis of the inner wall endothelium of SC following treatment with siRNAs.

To examine how siRNA treatment affects the continuity of the inner wall of SC, ultrastructural investigation of TJs between SC cells was performed by TEM. Six wild type C57BL/6J mice were intracamerally injected with a combination of 1 μ g ZO-1 siRNA and 1 μ g of tricellulin siRNA, and contralateral eyes were injected with 2 μ g of NT siRNA. 48 h post-injection, all animals were sacrificed with eyes enucleated immediately after death and immersed for TEM investigation. As can be seen in Fig. 6a,b, the inner wall of SC in both treated and control

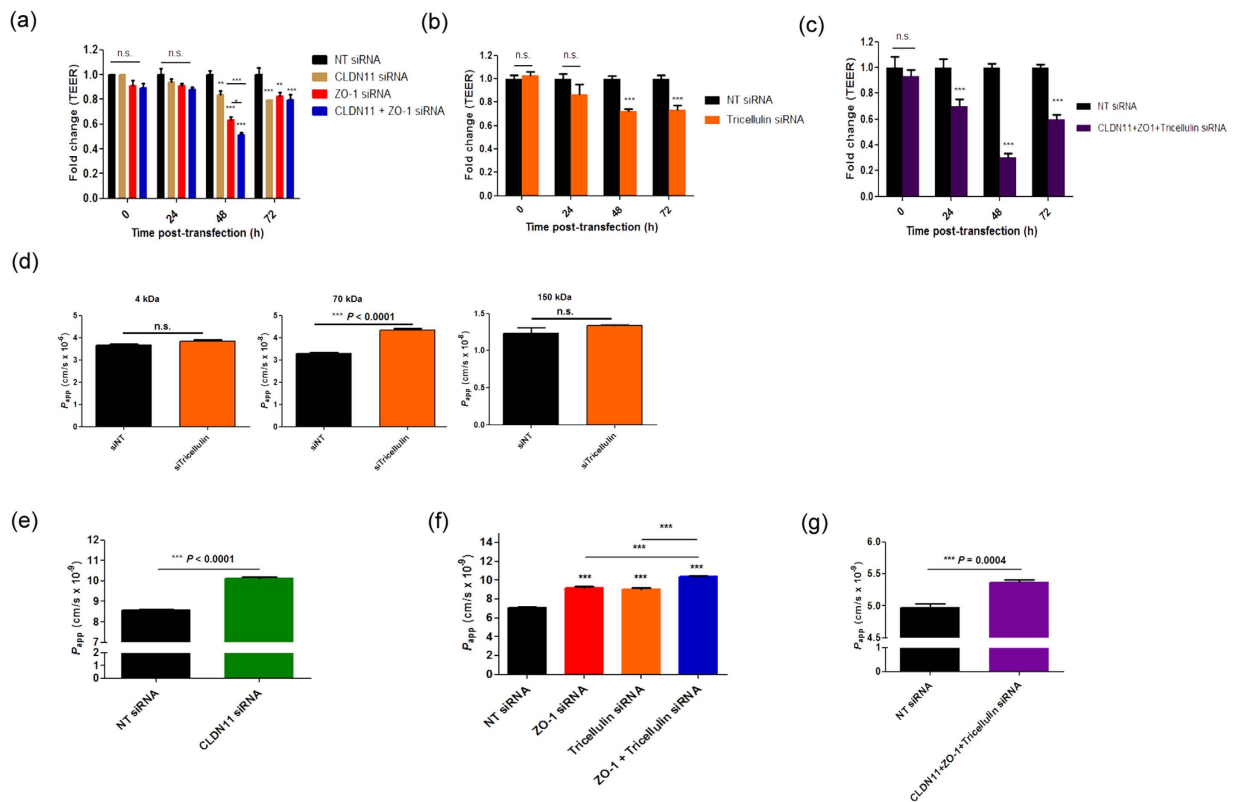


Figure 5. siRNA-mediated down-regulation of tight junction RNA transcripts modulates TEER and paracellular permeability in cultured SCEC monolayers. (a) Effect of siRNA-mediated knockdown of TJ RNA transcripts on TEER across human SCEC monolayers. 40 nM of siRNA targeting claudin-11, ZO-1, or in combination were transfected into human SCEC, and TEER was measured 24, 48 and 72 h post-transfection. * $P < 0.05$, ** $P < 0.01$, *** $P < 0.001$, n.s. $P \geq 0.05$ ($n = 3$ separate cell transfection, two way analysis of variance (ANOVA) followed by Bonferroni's multiple comparison post-tests). Data are fold change \pm s.e.m. (b) TEER measurements following treatment with tricellulin siRNAs in cultured SCEC monolayers ($n = 5$ separate cell transfections, two way ANOVA followed by Bonferroni's multiple comparison post-tests). *** $P < 0.0001$. Data are fold change \pm s.e.m. (c) TEER measurements following treatment of SCEC monolayers with a combination of claudin-11, ZO-1 and tricellulin siRNAs ($n = 7$ separate cell transfections, two way ANOVA followed by Bonferroni's multiple comparison post-tests). *** $P < 0.001$. n.s. = $P > 0.05$. (d) Cultured SCEC monolayers demonstrate size selectivity. Apparent permeability co-efficient (P_{app} , cm/s) of 4, 70 and 150 kDa FITC dextrans was determined following treatment with siRNAs targeting tricellulin. (*** $p < 0.0001$; $n = 3$). n.s. = $P \geq 0.05$ (e,f,g) P_{app} of 70 kDa FITC-dextran through human SCEC monolayers following treatment with claudin-11, ZO-1 and tricellulin siRNAs, or in combination. NT = non-targeting. Data are mean \pm s.e.m. Note the break in scale for P_{app} (e,f). (e) *** $P < 0.0001$, $n = 6$. (f) (*** $P < 0.0001$, $n = 4$). (g) *** $P = 0.0004$, $n = 6$. (unpaired Student's t -test for left and right bar graphs; one way ANOVA followed by Bonferroni's *post hoc* test for middle bar graphs).

eyes appeared similar. The inner wall was continuous without loss of cells or apparent cellular damage, and in both control and treated eyes there were no swollen cells that would indicate necrosis. There were also no cellular extensions and nuclear densifications or fragmentations that would indicate apoptosis.

To more clearly visualize cell membranes and junctions, sections were stained with UAR-EMS rather than uranyl acetate (see materials and methods). This staining allowed better visualization of the intercellular junctions and revealed that intercellular clefts between neighbouring SC cells were more often open in eyes treated with targeting siRNAs than in controls, indicating an absence or weakening of the TJ complexes. Open clefts exhibited a typical width of 10–20 nm without any contact between neighbouring cell membranes, while closed clefts exhibited a focal fusion between neighbouring cell membranes often surrounded by small cytoplasmic filaments (Fig. 6c,d). Quantification of intercellular junctions was performed by 2 independent observers, who examined TEM sections at 80,000x along the anterior-posterior extent of the inner wall from 4 regions of each eye ($n = 6$ treated and 5 control eyes; one control eye was removed as, for technical reasons, not all 4 regions could be evaluated). Each section contained between 10–30 cells, and each region was separated from another by at least several hundred microns, such that each region could be considered an independent sample. This quantification revealed that approximately 33% of intercellular junctions were open in eyes treated with targeting siRNA (Table 1). In contrast, only approximately 2% of intercellular junctions were open in contralateral eyes treated with non-targeting siRNA (Table 2), and this difference was statistically significant ($p = 0.004$, unpaired Student's

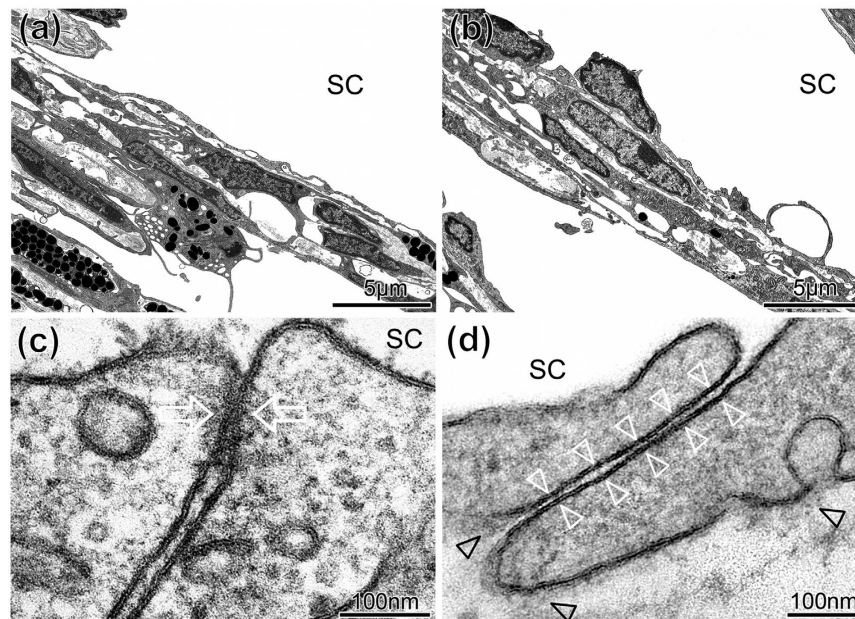


Figure 6. Transmission electron microscopic analysis of sagittal sections of the inner wall of SC following siRNA treatment. (a,b) Representative sagittal sections through the inner wall of Schlemm's canal (SC) and outer trabecular meshwork (TM) of a mouse eye treated with (a) non-targeting (NT) or (b) targeting (T) siRNA illustrating intact cells and an intact and continuous inner wall endothelium that appeared similar in both cases. The inner wall endothelium is connected to the underlying ECM so that no ballooning was visible. (c,d) High magnifications of sagittal sections through intercellular clefts along the inner wall endothelium of SC showing examples for junctions quantitatively evaluated as closed (c) with fusion between the neighbouring cell membranes (arrows) or open clefts (d) where the cell membranes of adjacent endothelial cells were clearly separated along the entire cleft length (white arrowheads). Despite the open clefts, adhesions to subendothelial matrix (black arrowheads) were preserved. The number of open intercellular clefts was quantified (see Tables 1 and 2).

Sample	Region 1		Region 2		Region 3		Region 4		% open
	N total	N open	N total	N open	N total	N open	N total	N open	
C4 NEP T	15	4	17	3	21	5	24	9	27%
C4 REP T	18	15	14	3	22	17	10	5	63%
C4 LEP T	9	5	26	1	18	9	12	3	28%
C5 LEP T	26	10	15	3	24	4	20	4	25%
C6 LEP T	25	11	31	11	15	4	18	2	31%
C6 NEP T	25	2	29	9	16	4	30	8	23%
								Average	33%
								SD	25%

Table 1. Quantification of total and open intercellular clefts along the inner wall in treated eyes that were immersion fixed immediately after death.

t-test). These data reveal that the siRNA treatment is opening intercellular clefts along the inner wall of SC *in vivo*, presumably by affecting TJs.

It is feasible that siRNA treatment may also have affected adherens or cell-matrix junctions that provide mechanical support between endothelial cells and to the subendothelial tissue. Indeed, TJs and adherens junctions are coupled, and disassembly of adherens junctions often leads to disassembly of TJ³⁰. To determine whether siRNA had affected these other junctional types, we examined for disconnections between the inner wall and subendothelial tissue that typically leads to inner wall 'ballooning' as observed following treatment with Na₂-EDTA^{31,32}. In none of the 4 regions examined per eye in either case, did we observe any ballooning of the inner wall (Fig. 6a,b). Even in areas with open intercellular clefts, the basal cell membranes of the endothelial cells were still attached to the underlying extracellular matrix (ECM) (Fig. 6d). This implies that the cell-matrix adhesions remained intact. We also examined for adhered platelets, which is a sign of inner wall damage, as platelets often seal endothelial gaps where ECM is exposed to the lumen of SC^{31,32}. No adhering platelets were observed in any region of any eye.

Sample	Region 1		Region 2		Region 3		Region 4		% open
	N total	N open	N total	N open	N total	N open	N total	N open	
C4 NEP NT	8	0	22	0	17	2	28	0	3%
C4 REP NT	17	1	20	0	13	0	18	0	1%
C5 LEP NT	21	0	26	0	14	0	19	0	0%
C6 LEP NT	11	1	30	0	26	0	9	0	1%
C6 NEP NT	20	1	17	0	29	0	31	1	2%
								Average	2%
								SD	1%

Table 2. Quantification of total and open intercellular clefts along the inner wall in control eyes that were immersion fixed immediately after death.

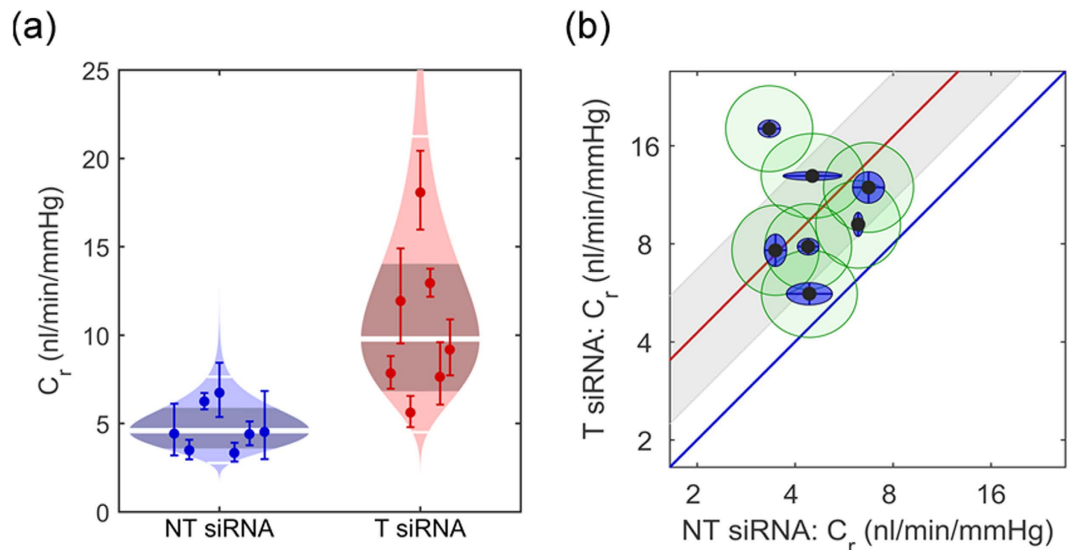


Figure 7. Effect of down-regulation of tight junction RNA transcripts on outflow facility *ex vivo*. (a) ‘Cello’ plots showing the individual values and statistical distribution of outflow facility at 8 mmHg (C_r) for eyes treated with either non-targeting (NT) siRNA or a combination of ZO-1 and tricellulin targeting (T) siRNA. Each individual point represents a single eye, with error bars showing the 95% confidence intervals on C_r , arising from the regression analysis. For each condition, the predicted log-normal distribution is shown, with the thick central white band showing the geometric mean and the thinner white bands showing two geometric standard deviations from the mean. The shaded central region indicates the 95% confidence interval on the mean. (b) Paired facility plot: each data point represents one pair of eyes, with C_r for the treated T siRNA eye on the Y-axis and the C_r for contralateral control NT-siRNA eye on the X-axis. The red line shows the average difference between contralateral eyes, with its confidence interval in grey, whilst the blue line represents the case of identical facility between contralateral eyes, corresponding to no effect due to T siRNA. All data points are above the blue unity line, indicating that the facility was higher in the treated eyes compared to the controls; $n = 7$, $p = 0.006$. Inner blue ellipses show the 95% confidence intervals on C_r , arising from the regression analysis, whilst the green outer ellipses show additional uncertainty due to variability between contralateral eyes, estimated from 10 pairs of C57BL/6J eyes perfused only with glucose supplemented PBS³⁶.

Effect of down-regulation of tight junctions on outflow facility *ex vivo*. In order to evaluate whether down-regulation of TJs increases outflow facility, studies were performed in mouse eyes since the conventional outflow pathway of mice resembles that of human morphologically, physiologically and pharmacologically^{33–35}. We targeted ZO-1 and tricellulin based on the IHC data obtained in Fig. 3a. Seven wild type C57BL/6J mice were intracamerally injected with a combination of 1 μ g ZO-1 siRNA and 1 μ g of tricellulin siRNA, and contralateral eyes were injected with 2 μ g of NT siRNA. 48 h post-injection, all animals were sacrificed and enucleated eyes were perfused in pairs using the recently developed *iPerfusion*³⁶ system to measure outflow facility, calculated from the flow measured over multiple pressure steps (Supplementary Fig. S9). Outflow facility in the siRNA treated eyes was increased compared to eyes receiving NT siRNA (Fig. 7a). Figure 7b shows the paired facility data where the facility of the treated eye is plotted against that of the contralateral control eye. In all cases, the facility of the treated eye was elevated compared to control ($n = 7$ pairs), exhibiting an average facility increase of 113% (confidence interval [35, 234]%, $p = 0.0064$, facility values for each pair of eyes are provided in Supplementary Table S2). These data demonstrate that down-regulation of TJ components within the

conventional outflow pathway significantly increases conventional outflow facility in mouse eyes *ex vivo*. To investigate the long-term effect of TJ down-regulation, we perfused eyes from animals 8 weeks post-injection and we observed no difference in outflow facility between treated and control eyes (average facility increase of 9.2%, confidence interval $[-14.22, 32.62]\%$, $p > 0.05$, $n = 4$ pairs, facility values for each pair of eyes are provided in Supplementary Table S2). This observation indicates that a single injection of siRNAs enables transient and reversible modulation of outflow facility in the anterior chamber of murine eyes.

Discussion

AH exiting the anterior chamber via the conventional outflow pathway passes through the tissues of the TM and into the SC lumen by crossing its endothelial barrier. Conceptually, loosening the TJs that bind endothelial cells could render the barrier more permeable resulting in reduced outflow resistance. However, this targeted approach has not been previously assessed in regard to AH outflow. The current study focused on identifying TJ components present in human, murine and non-human primate outflow tissues that might serve as plausible targets for siRNA-mediated down-regulation. A number of such targets were identified in primary cultures of human SCEC, disruption of which has previously been associated with altering endothelial cell permeability in other cell systems^{37–39}.

The TJ profile found in human SCEC identifies claudin-11 and tricellulin as SC specific TJ related proteins not present in TM cells, while ZO-1 has been found to be present in both SCEC and TM cells as previously reported^{29,40}. Previous studies have also reported the identification of specific protein markers that are either exclusively expressed in the inner wall endothelium of SC, or differ appreciably in their expression from TM cells^{14,28,41,42}. Owing to the high level of claudin-11 expression found in SCEC as compared to TM cells, this claudin-based TJ may also be used as a specific marker for identifying SC cells.

The association of both claudin-11 and tricellulin with SCEC is of significance because both TJs have been associated with maintenance of barrier function. Several studies on paracellular tightness have demonstrated that claudin-11 modulates paracellular cation permeability^{39,43,44} and its knockdown increases TEER in human corpus cavernosum endothelial cells⁴⁵. On the other hand, transcript knockdown studies have shown that the inhibition of tricellulin leads to instability of TJs⁴⁶, whereas tricellulin overexpression is associated with reduced permeability to macromolecules⁴⁷. Accordingly, we observed that siRNA-mediated knockdown of selected TJ decreases transendothelial resistance and increases permeability to 70 kDa FD in cultured human SC cell monolayers. In particular, these effects were more profound when a combination of siRNAs was used, suggesting a synergistic effect in increasing paracellular permeability following down-regulation of a range of TJs.

Paracellular pathways have been well established to possess defined values of electrical conductance as well as charge and size selectivity⁴⁸. For example, the junctional complexes comprising of tight and adherens junctions between cerebral endothelial cells enable the blood-brain barrier to regulate the entry of blood-borne molecules and preserve ionic homeostasis within the brain microenvironment⁴⁹. Our size selectivity data indicate that SC endothelial barriers have restrictive properties to regulate paracellular passage, and direct alteration of TJ complex only allows the passage of dextrans of up to 70 kDa, representing a biologically relevant size comparable to albumin (66 kDa), which does not cross the paracellular route readily in unperturbed endothelial monolayers⁵⁰. We have shown that TJ barriers are formed and localised along the endothelial cells of the inner wall of SC *in vivo*. In conjunction with *in vitro* permeability data, TJs in the inner wall endothelium of SC are identified as possibly playing a pivotal role in contributing to paracellular movement of AH and solutes across the endothelial layer. Similarly to human SCEC, non-human primates also express ZO-1, claudin-11 and tricellulin in the inner wall of SC. However, we did not detect claudin-11 expression in the mouse outflow pathway, which suggests differential expression patterns between species.

In order to prove the efficacy of the siRNA in an *in vivo* system, ZO-1 and tricellulin siRNA were injected into the anterior chambers of mice. We show that knockdown of transcripts encoding TJs in the conventional outflow pathway increases AH outflow facility in wild type mice, and that this effect is associated with the presence of an increased number of open intercellular clefts between SCEC. It is therefore reasonable to infer that opening of intercellular clefts is responsible for the increased outflow facility measured *ex vivo*. In contrast to studies using EDTA to disrupt cellular junctions along the inner wall^{31,32}, no eyes treated with siRNA exhibited signs of necrosis or apoptosis, and there were no platelets adhering to the inner wall. This indicates that the endothelial cell membranes remained intact and the subendothelial ECM was not exposed to the lumen of SC.

Our *in vivo* data also reinforce that the hydraulic conductivity of the inner wall endothelium of SC is maintained by the adhesive forces produced at the endothelial cell-cell junctions between TJ proteins^{14,28}. It is therefore correct to propose that factors which change the adhesive properties of TJ proteins in the inner wall of SC may alter the existing behaviour of the outflow pathway. To illustrate this point, we have preliminary data demonstrating higher claudin-11 and ZO-1 expression in glaucomatous SCEC monolayers as compared to healthy controls (Supplementary Fig. S10a). In addition, cultured glaucomatous SCEC strains displayed higher TEER values than healthy strains (Supplementary Fig. S10b). The increase in TJ expression found in glaucomatous SCEC suggests that altered barrier function in the inner wall of SC may negatively impact on conventional outflow behaviour.

While conventional adeno-associated viruses (AAV) have been shown to be inefficient in transducing cells of the outflow tissues, self-complementary AAV have been reported to be effective in such transduction^{51,52}. It is of note that AAV expressing inducible short hairpin RNAs (shRNA) targeting claudin-5, or a combination of claudin-5 and occludin have been used to transfect cerebral and retinal tissues, and that down-regulation of these TJ vascular endothelial cell components renders the blood-brain and inner blood-retina barriers reversibly permeable to compounds up to 1 kDa, or 5 kDa respectively^{53,54}. Should it prove possible using this technique to periodically activate virus expressing shRNAs within SCEC using an inducible promoter, expression of such shRNA could in principle be used as a means of periodically increasing outflow facility in cases of POAG in which patients fail to achieve target IOP with conventional medications. Alternatively, episcleral delivery of

siRNA, where materials can be delivered non-invasively into the outflow tissues in a retrograde fashion as an outpatient procedure⁵⁵, might represent an attractive alternative, thus avoiding the necessity of introducing a viral vector into the anterior chamber to secure viral-mediated shRNA expression. To explore the feasibility of an episcleral delivery approach, we have successfully achieved delivery of biotin conjugated tracer molecules to the conventional outflow pathway via the episcleral route in mice. Taken together, results from this study support the concept that endothelial TJs of the inner wall of SC are an attractive target upon which to base future attempts to increase AH outflow in cases of ocular hypertension.

Materials and Methods

Cell Culture. Human SCEC and TM cells were isolated, cultured and characterised as previously described^{56,57}. SCEC strains used in this study were SC65, SC68, SC73, SC76, SC77, SC82 and SC83. TM93 was used for RNA analysis, whereas TM120 and TM130 were used for protein analysis. All SCEC and TM cells were used between passages 2 and 6. SCEC were cultured in low glucose Dulbecco's modified Eagle medium (Gibco, Life Sciences) supplemented with 10% *Performance Plus* foetal bovine serum (FBS) (Gibco, Life Sciences), 1% Pen/Strep glutamine (Gibco, Life Sciences), in a 5% CO₂ incubator at 37°C. TM cells underwent a differentiation step by plating at full confluency for one week in media containing 10% FBS, and changed over to media containing 1% FBS for an additional week prior to experimentation. Cultured cells were passaged with trypsin-EDTA (Gibco-BRL) to maintain exponential growth.

Human tight junction PCR array. The human TJ RT² Profiler PCR array (PAHS-143ZA, Qiagen) was used to profile the expression of 84 key genes encoding proteins that form selective barriers between epithelial and endothelial cells to regulate size selectivity, polarity, proliferation and differentiation. Total RNA was extracted from four different human SCEC strains (SC65, 68, 76 and 77) at passages 3 to 5 using RNEasy Mini Kit (Qiagen) according to manufacturer's protocol. Genomic DNA contamination was eliminated by DNase treatment. Total RNA was reverse-transcribed into cDNA using RT² First Strand Kit (Qiagen). The Threshold cycle (Ct) values of different passage numbers from each SCEC strain were determined and averaged using ABI Prism 7700 Sequence Detector. The mean normalised expression ($2^{-\Delta Ct}$) of genes encoding claudin and adhesion junctional proteins was determined and analysed using the online Qiagen RT² Profiler PCR Array Data Analysis software. Normalised gene expression was calculated by using the equation: $2^{-\Delta Ct} = 2^{-[Ct(\text{gene of interest}) - Ct(\text{Housekeeping genes})]}$. Normalisation was carried out with five housekeeping genes (*ACTB*, *B2M*, *GAPDH*, *HPRT1* and *RPLP0*) included in the PCR array. The $2^{-\Delta\Delta Ct} = 2^{-\Delta Ct \text{ treated}} / 2^{-\Delta Ct \text{ control}}$ method was used to calculate fold changes for each gene as difference in gene expression⁵⁸.

Western Blot. Protein lysates were isolated from cultured cells in protein lysis buffer containing 1 M Tris pH 7.5, 1 M NaCl, 1% NP-40, 10% SDS, 1X protease inhibitor cocktail (Roche). The homogenate was centrifuged at 10,000 r.p.m. (IEC Micromax microcentrifuge, 851 rotor) at 4°C for 20 min and the supernatant was stored at -80°C until use. Protein concentration was determined by BCA Protein assay kit (Pierce, IL, USA) with bovine serum albumin (BSA) at 2 mg/ml as standards on 96-well plates according to the manufacturer's protocol. 30–50 µg of total protein was loaded in each lane. Protein samples were separated by electrophoresis on 7.5–10% SDS-PAGE under reducing conditions and electro-transferred to PVDF membranes. After blocking with 5% blotting grade blocker non-fat dry milk in TBS for 1 h at room temperature, membranes were incubated overnight at 4°C with the following Rabbit polyclonal primary antibodies: anti-oligodendrocyte specific protein antibody (1:500; Abcam); anti-ZO-1 antibody (1:250; Invitrogen), anti-tricellulin C-terminal antibody (1:125; Invitrogen), anti-occludin antibody (1:500; Invitrogen) and anti-VE-cadherin antibody (1:1000; Abcam). Blots were washed with TBS and incubated with horse radish peroxidase-conjugated polyclonal rabbit IgG secondary antibody (Abcam). The blots were developed using enhanced chemiluminescent kit (Pierce Chemical Co.) and exposed to Fuji X-ray film. Each blot was stripped with Restore Western Blot Stripping Buffer (Pierce) and probed with rabbit polyclonal to β-actin or GAPDH (Abcam) as loading controls. Protein band intensities were quantified by scanning with a HP Scanjet Professional 10000 Mobile Scanner and analysed using *Image J* (Version 1.50c). The percentage reduction in band intensity was calculated relative to the control non-targeting siRNA, which was standardised to represent 100% and normalised against β-actin.

Immunocytochemistry. Human SCEC were grown on Lab-Tek II chamber slides and fixed in 4% paraformaldehyde (pH 7.4) for 20 min at room temperature and then washed with PBS for 15 min. Cell monolayers were blocked in PBS containing 5% normal goat serum and 0.1% Triton X-100 at room temperature for 20 min. Primary antibodies were diluted at 1:100 in blocking buffer and incubated overnight at 4°C. Secondary antibodies diluted at 1:500 were then incubated for 2 h at room temperature in a humidity chamber. Following incubation, chamber slides were mounted with aqua-polymount (Polyscience) after nuclei-counterstaining with DAPI. Fluorescent images of SCEC monolayers were captured using a confocal microscope (Zeiss LSM 710), and processed using imaging software ZEN 2012.

Immunohistochemistry for frozen sections. Eucleated mouse eyes were fixed in 4% paraformaldehyde (pH 7.4) overnight at 4°C on a rotating device. Posterior segments of the eye and the lens were removed and anterior segments were then washed with PBS for 15 min and sequentially submerged in 10, 20 and 30% sucrose. Dissected anterior segments were then suspended in specimen blocks with OCT solution (Tissue-Tek) and frozen in a bath of isopropanol submerged in liquid nitrogen. Frozen anterior segments were sectioned using a cryostat (Leica CM 1900) to 12 µm thickness. Sections were collected on Polysine[®] slides (Menzel-Glazer). To detect TJ proteins, sections were blocked for 20 min at room temperature in PBS containing 5% goat serum and 0.1% Triton-X, and incubated with the corresponding antibodies at 1:100 dilutions overnight at 4°C in a humidity chamber. All sections were then washed three times in PBS and incubated with Cy-3 labelled anti-rabbit IgG

antibody at 1:500 (Abcam) for 2 h at room temperature in a humidity chamber. Following incubation, sections were washed with PBS and mounted with aqua-polymount (Polyscience) after nuclei-counterstaining with DAPI. Anterior segments were visualised using a confocal microscope (Zeiss LSM 710).

Immunohistochemistry for paraffin embedded sections. Paraffin sections of African green monkey (*Chlorocebus Sabeus*) anterior segments were rehydrated by immersion in the following solutions: twice for 2 min each in Histoclear solution; 100% ethanol for 1 min; 95% ethanol for 1 min; 70% ethanol for 1 min; deionised water for 1 min; washing twice for 5 min in PBS. For antigen retrieval, paraffin sections were heated to 95 °C for 10 min in citrate buffer (Sodium citrate, pH 6). Paraffin sections were then blocked and stained as described above.

siRNAs. All *in vivo* pre-designed siRNAs used in this study were synthesised by Ambion and reconstituted as per manufacturer's protocol. siRNA identification numbers are as follows: human claudin-11 siRNA (ID number: s9925), human ZO-1 siRNA (ID number: s14156), human MARVELD2 siRNA (ID number: s45794), mouse ZO-1 siRNA (ID number: s75175), mouse MARVELD2 siRNA (ID number: ADCSU2H). Silencer Negative control siRNA (Ambion) was used as a non-targeting control in knockdown studies.

Cell viability assay. SCEC were grown to confluency on a 96-well plate. Cells were transfected with siRNA in quadruplicate using Lipofectamine RNAiMax reagent as outlined by the manufacturer (Life Technologies) at both 1 pmol/well (40 nM) and 5 pmol/well (200 nM). Cells were left for 48 hours, apart from a media change after 24 hours. CellTitre 96 Aqueous One Solution Reagent (Promega) was thawed and mixed with culture medium at a 1:5 dilution. Cells were incubated with this mixture for a period of 2 hours, before transferring the media to a fresh 96-well plate. Absorbance of each well was recorded at 450 nm on a spectrophotometer (Multiskan FC, Thermo Scientific). After blanking against wells with reagent and no cells, each treatment group was presented relative to a negative control containing no siRNA. A positive control was achieved by incorporating 1% SDS into the media-reagent mixture. A one-way ANOVA with a Tukey's post-test was performed on the data set.

Measurement of SCEC monolayer transendothelial electrical resistance (TEER). TEER was used as a measure of TJ integrity by the human SCEC monolayers as previously described⁵⁴. In brief, human SCEC (1×10^4 cells per well) were grown to confluency on Costar HTS Transwell-polyester membrane inserts with a pore size of 0.4 µm. The volume of the apical side (inside of the membrane inserts) was 0.1 ml and that of the basal side (outside of the membrane inserts) was 0.6 ml. Confluent cells were then transfected in triplicates with 40 nM of claudin-11, ZO-1 and tricellulin siRNAs, or in combination, using Lipofectamine RNAiMax reagent as outlined by the manufacturer (Life Technologies). Non-targeting siRNA was used as a control. 48 h post-transfection, TEER values were determined using an EVOM resistance meter with Endohm Chamber (World Precision Instruments) and a Millicell-Electrical Resistance System. For measurement of TEER, both the apical and basolateral sides of the endothelial cells were bathed in fresh growth medium at 37 °C, and a current was passed across the monolayer with changes in electrical resistance, which was reported as $\Omega \cdot \text{cm}^2$ after correcting for the surface area of the membrane (1.12 cm). Electrical resistance was measured in triplicate wells, and the inherent resistance of a blank transwell was subtracted from the values obtained for the endothelial cells.

Cell permeability assay using FITC-dextran. Human SCEC were prepared and treated using the same method for TEER measurement as described above. Transwell permeability assays were carried out as previously described⁵⁴. In brief, 4 kDa, 70 kDa and 150 kDa fluorescein isothiocyanate (FITC)-conjugated dextran (FD) (Sigma) was applied at 1 mg/ml to the basal compartment of the transwells. Sampling aliquots of 0.1 ml were collected every 15 min for a total of 120 min from the apical side for fluorescence measurements and the same volume of culturing media was added to replace the medium removed. FITC fluorescence was determined using a spectrofluorometer (Optima Scientific) at an excitation wavelength of 485 nm and an emission wavelength of 520 nm. Relative fluorescence units (RFU) were converted to values of nanograms per millilitre using FITC-dextran standard curves, and were corrected for background fluorescence and serial dilutions over the course of the experiment. The apparent permeability co-efficient (P_{app} , cm/s) for each treatment was calculated using the following equation:

$$P_{app} = (dM/dt)/(A \times C_0),$$

where dM/dt (µg/s) is the rate of appearance of FD on the apical side from 0 min to 120 min after application of FD. C_0 (µg/ml) is the initial FD concentration on the basal side, and A (cm²) is the effective surface area of the insert. dM/dt is the slope calculated by plotting the cumulative amount of (M) versus time.

Animal Husbandry. The use of animals and injections carried out in this study were in accordance with the European Communities Regulations 2002 and 2005 and the Association for Research in Vision and Ophthalmology statement for the use of Animals in Ophthalmic and Vision Research, and was approved by the institutional Ethics Committee. In this case, all procedures carried out at Imperial College London and Trinity College Dublin were approved by the UK Home Office and by the Health Products Regulatory Authority of the Irish Medicines Board (project authorisation AE19136/P017) respectively. Male C57BL/6J mice (Charles River Laboratories, UK) of age 10 to 12 weeks were used. *Ex vivo* perfusions and intracameral injections were done under the UK Home Office Project at Imperial College London. Animals were brought into the animal facility one week prior injections for an acclimatisation period. Mice were housed in individually ventilated cages with 5 mice per cage. They were provided with food and water *ad libitum* and were under 12 h light/dark cycles (7 am to 7 pm) at 21 °C.

Intracameral injection. Adult C57BL/6J mice of 10 to 12 weeks of age were anaesthetised by intra-peritoneal injection of medetomidine hydrochloride (Domitor) and ketamine (0.66 and 66.6 mg/kg body weight, respectively). Pupils were dilated with 2.5% tropicamide and 2.5% phenylephrine eye drops. Glass micro-capillaries (outer diameter = 1 mm, inner diameter = 0.58 mm; World Precision Instruments) were pulled using a micro-pipette puller (Narishige PB-7). Under microscopic control, a pulled blunt-ended micro-glass needle (tip diameter ~100 µm) was first used to puncture the cornea to withdraw AH. Immediately after puncture, a pulled blunt-ended micro-glass needle attached to a 10 µl syringe (Hamilton, Bonaduz) was inserted through the puncture, and 1.5 µl of PBS containing 1 µg of ZO-1 siRNA and 1 µg of tricellulin siRNA was administered into the anterior chamber to give a final concentration of 16.84 µM. Contralateral eyes received an identical injection of 1.5 µl containing the same concentration of NT siRNA. Following surgery, a reversing agent (1.5 mg/kg body weight, atipamezole hydrochloride) was delivered by intra-peritoneal injection. Fusidic gel was applied topically to the eye as antibiotic and Vidisic gel was also applied topically as a moisturiser. Furthermore, 5 mg/kg enrofloxacin antimicrobial (Baytril; Bayer Healthcare) was injected subcutaneously.

Apoptosis markers staining. IHC was performed on perfused eyes 48 hours post injection with either targeting or non-targeting siRNA. Approximately 30–40 12 µm sections were each stained by TUNEL and complemented by cleaved caspase-3 staining as markers of apoptosis for representatives of targeting and non-targeting siRNA. Eyes were fixed and prepared for cryosectioning as described before. TUNEL staining was performed as per manufacturers protocol (*in situ* Cell Death Detection Kit, POD, Roche), for positive controls, slides treated with Dnase-1 for 10 minutes at room temperature after permeabilisation and prior to antibody labelling. Cleaved caspase-3 staining was performed as described before using cleaved caspase 3 marker antibody (#9661, Cell Signalling Technology), positive controls were obtained by perfusing wild type eyes *ex vivo* for 24 hours at 35 °C with 200 ng/ml of mouse IL-1B and 100 ng/ml of human TNF-α in DMEM to induce apoptosis.

Transmission electron microscopy (TEM). All eyes were immersion fixed in Karnovsky's solution initially and post-fixed in Ito's solution. The eyes were embedded in Epon and semi-thin sagittal sections were cut through the whole globe. Ultrathin sections of SC and TM were cut sagittally from one side of the eye first, and then another ultrathin section approximately 1mm deeper was cut. If possible, this section was taken from the other side of the eye. In the small mouse eye, this process could be repeated four times. In this way, different parts of the circumference of the eye were evaluated. Different staining methods were investigated to visualise cell membranes, and the best results were obtained using UAR-EMS (Science Services, Munich, Germany). In ultrathin sections of the entire anterior posterior length of the inner wall from all four regions of treated eyes and their controls, we investigated whether there was any ballooning of the inner wall endothelium, necrosis or apoptosis of endothelial cells or adherence of platelets to the inner wall endothelium. Intercellular gaps were counted at magnifications of 80,000x by two independent observers (ELD and CFK).

Outflow facility measurements. Mouse eyes were perfused *ex vivo* to measure outflow facility using the *iPerfusion* system³⁶. Mice were culled by cervical dislocation and the eyes were enucleated within 10 min post mortem and stored in PBS at room temperature to await perfusion (~20 min). Both eyes were perfused simultaneously using two independent perfusion systems as described previously³⁶. Briefly, each eye was affixed to a support using a small amount of cyanoacrylate glue and submerged in a PBS bath regulated at 35 °C. The eye was cannulated via the anterior chamber with a 33-gauge bevelled needle (NanoFil, #NF33BV-2, World Precision Instruments) under a stereomicroscope using a micromanipulator. The *iPerfusion* system comprises an automated pressure reservoir, a thermal flow sensor (SLG64-0075, Sensirion) and a wet-wet pressure transducer (PX409, Omegadyne) in order to apply a desired pressure, measure flow rate out of the system and measure the intraocular pressure respectively. The perfusate was DBG (PBS including divalent cations and 5.5 mM glucose), and was filtered through a 0.22 µm filter (VWR international) prior to use.

Following cannulation, eyes were perfused for 30 min at ~8 mmHg to allow the eye to acclimatise to the environment. Subsequently, nine discrete pressure steps were applied from 4.5 to 21 mmHg, while flow and pressure were recorded. Stability was defined programmatically, and data were averaged over 4 min at steady state. A non-linear model was fit to flow-pressure data to account for the pressure dependence of outflow facility in mouse eyes. This model was of the form $Q = C_r P (P/P_r)^\beta$, where Q and P are the flow rate and pressure respectively, and C_r is the outflow facility at reference pressure P_r , which is selected to be 8 mmHg (the approximate physiological pressure drop across the outflow pathway). The power law exponent β quantifies the non-linearity in the Q - P response and thus the pressure dependence of outflow facility. The data analysis methodology described previously³⁶ was applied in order to analyse the treatment effect, whilst accounting for measurement uncertainties and statistical significance was evaluated using the paired weighted t -test described therein.

Statistical analysis. For real-time PCR, TEER and paracellular permeability measurements, Student's t -tests and ANOVA with Bonferroni post-test were carried out using GraphPad Prism 5.0. For *ex vivo* perfusions, a paired weighted t -test was performed using MATLAB as described³⁶. For open clefts quantification, an unpaired t -test was performed. Statistical significance was indicated by $p \leq 0.05$.

References

1. Bill, A. The aqueous humor drainage mechanism in the cynomolgus monkey (*Macaca irus*) with evidence for unconventional routes. *Invest Ophthalmol Vis Sci* **4**, 911–919 (1965).
2. Toris, C. B., Yablonski, M. E., Wang, Y. L. & Camras, C. B. Aqueous humor dynamics in the aging human eye. *Am J Ophthalmol* **127**, 407–412 (1999).
3. Bill, A. & Phillips, C. I. Uveoscleral drainage of aqueous humour in human eyes. *Exp Eye Res* **12**, 275–281 (1971).

4. Holmberg, A. The fine structure of the inner wall of Schlemm's canal. *AMA Arch Ophthalmol* **62**, 956–958 (1959).
5. Tripathi, R. C. Ultrastructure of Schlemm's canal in relation to aqueous outflow. *Exp Eye Res* **7**, 335–341 (1968).
6. Bill, A. & Svedbergh, B. Scanning electron microscopic studies of the trabecular meshwork and the canal of Schlemm—an attempt to localize the main resistance to outflow of aqueous humor in man. *Acta Ophthalmol (Copenh)* **50**, 295–320 (1972).
7. Grierson, I. & Lee, W. R. Pressure effects on flow channels in the lining endothelium of Schlemm's canal. A quantitative study by transmission electron microscopy. *Acta Ophthalmol (Copenh)* **56**, 935–952 (1978).
8. Epstein, D. L. & Rohen, J. W. Morphology of the trabecular meshwork and inner-wall endothelium after cationized ferritin perfusion in the monkey eye. *Invest Ophthalmol Vis Sci* **32**, 160–171 (1991).
9. Ethier, C. R., Coloma, F. M., Sit, A. J. & Johnson, M. Two pore types in the inner-wall endothelium of Schlemm's canal. *Invest Ophthalmol Vis Sci* **39**, 2041–2048 (1998).
10. Braakman, S. T., Read, A. T., Chan, D. W., Ethier, C. R. & Overby, D. R. Colocalization of outflow segmentation and pores along the inner wall of Schlemm's canal. *Exp Eye Res* **130**, 87–96 (2015).
11. Raviola, G. & Raviola, E. Paracellular route of aqueous outflow in the trabecular meshwork and canal of Schlemm. A freeze-fracture study of the endothelial junctions in the sclerocorneal angle of the macaque monkey eye. *Invest Ophthalmol Vis Sci* **21**, 52–72 (1981).
12. Bhatt, K., Gong, H. & Freddo, T. F. Freeze-fracture studies of interendothelial junctions in the angle of the human eye. *Invest Ophthalmol Vis Sci* **36**, 1379–1389 (1995).
13. Ye, W., Gong, H., Sit, A., Johnson, M. & Freddo, T. F. Interendothelial junctions in normal human Schlemm's canal respond to changes in pressure. *Invest Ophthalmol Vis Sci* **38**, 2460–2468 (1997).
14. Perkumas, K. M. & Stamer, W. D. Protein markers and differentiation in culture for Schlemm's canal endothelial cells. *Exp Eye Res* **96**, 82–87 (2012).
15. Braakman, S. T. *et al.* Biomechanical strain as a trigger for pore formation in Schlemm's canal endothelial cells. *Exp Eye Res* **127**, 224–235 (2014).
16. Braakman, S. T., Moore, J. E. Jr., Ethier, C. R. & Overby, D. R. Transport across Schlemm's canal endothelium and the blood-aqueous barrier. *Exp Eye Res* **146**, 17–21 (2015).
17. Stamer, W. D. *et al.* Biomechanics of Schlemm's canal endothelium and intraocular pressure reduction. *Prog Retin Eye Res* **44**, 86–98 (2015).
18. Grant, W. M. Clinical measurements of aqueous outflow. *Am J Ophthalmol* **34**, 1603–1605 (1951).
19. Johnson, M., Shapiro, A., Ethier, C. R. & Kamm, R. D. Modulation of outflow resistance by the pores of the inner wall endothelium. *Invest Ophthalmol Vis Sci* **33**, 1670–1675 (1992).
20. Lütjen-Drecoll, E. Structural factors influencing outflow facility and its changeability under drugs. A study in *Macaca arctoides*. *Invest Ophthalmol Vis Sci* **12**, 280–294 (1973).
21. Overby, D. R., Stamer, W. D. & Johnson, M. The changing paradigm of outflow resistance generation: towards synergistic models of the JCT and inner wall endothelium. *Exp Eye Res* **88**, 656–670 (2009).
22. Allingham, R. R. *et al.* The relationship between pore density and outflow facility in human eyes. *Invest Ophthalmol Vis Sci* **33**, 1661–1669 (1992).
23. Johnson, M. *et al.* The pore density in the inner wall endothelium of Schlemm's canal of glaucomatous eyes. *Invest Ophthalmol Vis Sci* **43**, 2950–2955 (2002).
24. Overby, D. R. *et al.* Altered mechanobiology of Schlemm's canal endothelial cells in glaucoma. *Proc Natl Acad Sci USA* **111**, 13876–13881 (2014).
25. Zhang, K., Zhang, L. & Weinreb, R. N. Ophthalmic drug discovery: novel targets and mechanisms for retinal diseases and glaucoma. *Nat Rev Drug Discov* **11**, 541–559 (2012).
26. Morita, K., Sasaki, H., Furuse, M. & Tsukita, S. Endothelial claudin: claudin-5/TMVCF constitutes tight junction strands in endothelial cells. *J Cell Biol* **147**, 185–194 (1999).
27. Campbell, M. *et al.* An experimental platform for systemic drug delivery to the retina. *Proc Natl Acad Sci USA* **106**, 17817–17822 (2009).
28. Heimark, R. L., Kaochar, S. & Stamer, W. D. Human Schlemm's canal cells express the endothelial adherens proteins, VE-cadherin and PECAM-1. *Curr Eye Res* **25**, 299–308 (2002).
29. Underwood, J. L. *et al.* Glucocorticoids regulate transendothelial fluid flow resistance and formation of intercellular junctions. *Am J Physiol* **277**, C330–342 (1999).
30. Gumbiner, B., Stevenson, B. & Grimaldi, A. The role of the cell adhesion molecule uvomorulin in the formation and maintenance of the epithelial junctional complex. *J Cell Biol* **107**, 1575–1587 (1988).
31. Bill, A., Lütjen-Drecoll, E. & Svedbergh, B. Effects of intracameral Na₂EDTA and EGTA on aqueous outflow routes in the monkey eye. *Invest Ophthalmol Vis Sci* **19**, 492–504 (1980).
32. Hamanaka, T. & Bill, A. Morphological and functional effects of Na₂EDTA on the outflow routes for aqueous humor in monkeys. *Exp Eye Res* **44**, 171–190 (1987).
33. Bărăny, E. H. Simultaneous measurement of changing intraocular pressure and outflow facility in the vervet monkey by constant pressure infusion. *Invest Ophthalmol Vis Sci* **3**, 135–143 (1964).
34. Overby, D. R. *et al.* The structure of the trabecular meshwork, its connections to the ciliary muscle, and the effect of pilocarpine on outflow facility in mice. *Invest Ophthalmol Vis Sci* **55**, 3727–3736 (2014).
35. Li, G. *et al.* Pilocarpine-induced dilation of Schlemm's canal and prevention of lumen collapse at elevated intraocular pressures in living mice visualized by OCT. *Invest Ophthalmol Vis Sci* **55**, 3737–3746 (2014).
36. Sherwood, J. M., Reina-Torres, E., Bertrand, J. A., Rowe, B. & Overby, D. R. Measurement of outflow facility using iPerfusion. *Plos One* **11**, e0150694 (2016).
37. Van Itallie, C. M., Fanning, A. S., Bridges, A. & Anderson, J. M. ZO-1 stabilizes the tight junction solute barrier through coupling to the perijunctional cytoskeleton. *Mol Biol Cell* **20**, 3930–3940 (2009).
38. Ikenouchi, J., Sasaki, H., Tsukita, S., Furuse, M. & Tsukita, S. Loss of occludin affects tricellular localization of tricellulin. *Mol Biol Cell* **19**, 4687–4693 (2008).
39. Gow, A. *et al.* CNS myelin and sertoli cell tight junction strands are absent in *Osp/claudin-11* null mice. *Cell* **99**, 649–659 (1999).
40. Alvarado, J. A., Betanzos, A., Franse-Carman, L., Chen, J. & Gonzalez-Mariscal, L. Endothelia of Schlemm's canal and trabecular meshwork: distinct molecular, functional, and anatomic features. *Am J Physiol Cell Physiol* **286**, C621–634 (2004).
41. Park, D. Y. *et al.* Lymphatic regulator PROX1 determines Schlemm canal integrity and identity. *J Clin Invest* (2014).
42. Kizhatil, K., Ryan, M., Marchant, J. K., Henrich, S. & John, S. W. Schlemm's canal is a unique vessel with a combination of blood vascular and lymphatic phenotypes that forms by a novel developmental process. *PLoS Biol* **12**, e1001912 (2014).
43. Van Itallie, C., Rahner, C. & Anderson, J. M. Regulated expression of claudin-4 decreases paracellular conductance through a selective decrease in sodium permeability. *J Clin Invest* **107**, 1319–1327 (2001).
44. Morita, K., Sasaki, H., Fujimoto, K., Furuse, M. & Tsukita, S. Claudin-11/OSP-based tight junctions of myelin sheaths in brain and Sertoli cells in testis. *J Cell Biol* **145**, 579–588 (1999).
45. Wessells, H. *et al.* Transcriptional profiling of human cavernosal endothelial cells reveals distinctive cell adhesion phenotype and role for claudin 11 in vascular barrier function. *Physiol Genomics* **39**, 100–108 (2009).
46. Ikenouchi, J. *et al.* Tricellulin constitutes a novel barrier at tricellular contacts of epithelial cells. *J Cell Biol* **171**, 939–945 (2005).

47. Krug, S. M. *et al.* Tricellulin forms a barrier to macromolecules in tricellular tight junctions without affecting ion permeability. *Mol Biol Cell* **20**, 3713–3724 (2009).
48. Bazzoni, G. Endothelial tight junctions: permeable barriers of the vessel wall. *Thromb Haemost* **95**, 36–42 (2006).
49. Stamatovic, S. M., Keep, R. F. & Andjelkovic, A. V. Brain endothelial cell-cell junctions: how to “open” the blood brain barrier. *Curr Neuropharmacol* **6**, 179–192 (2008).
50. Johnstone, M. A. In *Becker-Shaffer's Diagnosis and Therapy of the Glaucomas* (8th Edition) (eds Marc F. Lieberman & Michael V. Drake) 25–46 (Mosby, 2009).
51. Buie, L. K. *et al.* Self-complementary AAV virus (scAAV) safe and long-term gene transfer in the trabecular meshwork of living rats and monkeys. *Invest Ophthalmol Vis Sci* **51**, 236–248 (2010).
52. Bogner, B. *et al.* Capsid mutated adeno-associated virus delivered to the anterior chamber results in efficient transduction of trabecular meshwork in mouse and rat. *Plos One* **10**, e0128759 (2015).
53. Campbell, M. *et al.* Systemic low-molecular weight drug delivery to pre-selected neuronal regions. *EMBO Mol Med* **3**, 235–245 (2011).
54. Keaney, J. *et al.* Autoregulated paracellular clearance of amyloid-beta across the blood-brain barrier. *Sci Adv* **1**, e1500472 (2015).
55. Morrison, J. C. *et al.* A rat model of chronic pressure-induced optic nerve damage. *Exp Eye Res* **64**, 85–96 (1997).
56. Stamer, W. D., Roberts, B. C., Howell, D. N. & Epstein, D. L. Isolation, culture, and characterization of endothelial cells from Schlemm's canal. *Invest Ophthalmol Vis Sci* **39**, 1804–1812 (1998).
57. Stamer, W. D., Seftor, R. E., Williams, S. K., Samaha, H. A. & Snyder, R. W. Isolation and culture of human trabecular meshwork cells by extracellular matrix digestion. *Curr Eye Res* **14**, 611–617 (1995).
58. Schmittgen, T. D. & Livak, K. J. Analyzing real-time PCR data by the comparative C(T) method. *Nat Protoc* **3**, 1101–1108 (2008).

Acknowledgements

Work at the Ocular Genetics Unit at the University of Dublin, Trinity College, was supported by the European Research Council ERC-2012-AdG. The Unit also receives support from Science Foundation Ireland. Work at Duke University was supported by grants from the US National Institutes of Health (EY022359 and EY019696) and at Imperial College London by Fight for Sight UK (Ref 1385), the US National Institutes of Health (EY022359 and EY019696), and the UK Engineering and Physical Sciences Research Council (EP/J010499/1). We would like to thank C. Woods and C. Murray for animal husbandry. We thank Elke Kretshmar, Hong Nguyen and Britta Bäckermann for their technical assistance with TEM, Jörg Pekarsky for preparing the schematic drawing and Marco Gößwein for preparing the final version of Figure 1.

Author Contributions

All authors reviewed the manuscript. L.C.S.T. performed PCR arrays, RNAi knockdown, gene expression analysis in SCEC, IHC, TEER and *Papp* measurements, and wrote the main manuscript text; E.R.-T. performed mouse intracameral injections, iPerfusion, gene expression analysis in TM cells and contributed to manuscript preparation; J.M.S. contributed to experimental design, performed statistical analysis for iPerfusion and contributed to manuscript preparation; P.C. performed RNAi knockdown, mouse intracameral injection and assisted with iPerfusion; D.C. performed mouse IHC and protein inhibition analysis in mouse; E.L.-D. performed TEM; C.F.-K. performed TEM; K.P. provided SCEC lines; M.M.H. performed gene sequencing and contributed to siRNA design; A.-S.K. assisted with PCR array analysis and contributed to manuscript preparation; J.O'C assisted with iPerfusion and performed cell viability experiments; J.J.C. provided non-human primate anterior segment paraffin sections; A.T.R. contributed to the interpretation of physiological data and statistical analysis, and provided revisions to the manuscript; C.R.E. contributed to the interpretation of physiological data and statistical analysis, and provided revisions to the manuscript; C.O'B. contributed to manuscript preparation; M.L. contributed to manuscript preparation; M.C. contributed to manuscript preparation; W.D.S. conceived the concept and assisted with experimental design, provided cell lines and contributed to manuscript preparation; D.R.O. assisted with experimental design, iPerfusion and contributed to manuscript preparation; P.H. conceived the concept and contributed to experimental design and writing of the manuscript.

Additional Information

Supplementary information accompanies this paper at <http://www.nature.com/srep>

Competing financial interests: The authors declare no competing financial interests.

How to cite this article: Tam, L. C. S. *et al.* Enhancement of Outflow Facility in the Murine Eye by Targeting Selected Tight-Junctions of Schlemm's Canal Endothelia. *Sci. Rep.* **7**, 40717; doi: 10.1038/srep40717 (2017).

Publisher's note: Springer Nature remains neutral with regard to jurisdictional claims in published maps and institutional affiliations.



This work is licensed under a Creative Commons Attribution 4.0 International License. The images or other third party material in this article are included in the article's Creative Commons license, unless indicated otherwise in the credit line; if the material is not included under the Creative Commons license, users will need to obtain permission from the license holder to reproduce the material. To view a copy of this license, visit <http://creativecommons.org/licenses/by/4.0/>

© The Author(s) 2017

ENHANCEMENT OF OUTFLOW FACILITY IN THE MURINE EYE BY TARGETING SELECTED TIGHT-JUNCTIONS OF SCHLEMM'S CANAL ENDOTHELIA

Lawrence C.S. Tam^{1*+}, Ester Reina-Torres^{1,2+}, Joseph M. Sherwood², Paul S. Cassidy¹, Darragh E. Crosbie¹, Elke Lütjen-Drecoll³, Cassandra Flügel-Koch³, Kristin Perkumas⁴, Marian M. Humphries¹, Anna-Sophia Kiang¹, Jeffrey O'Callaghan¹, John J. Callanan⁵, A. Thomas Read⁶, C. Ross Ethier⁷, Colm O'Brien⁸, Matthew Lawrence⁹, Matthew Campbell¹, W. Daniel Stamer^{4*}, Darryl R. Overby², Pete Humphries^{1*}

¹Ocular Genetics Unit, Institute of Genetics, Trinity College, University of Dublin, Dublin 2, Ireland.

²Department of Bioengineering, Imperial College London, London, UK.

³Department of Anatomy, University of Erlangen-Nürnberg, Erlangen, Germany. ⁴Department of Ophthalmology, Duke University, Durham, NC, USA.

⁵Ross University School of Veterinary Medicine, P. O. Box 334, Basseterre, St. Kitts, West Indies.

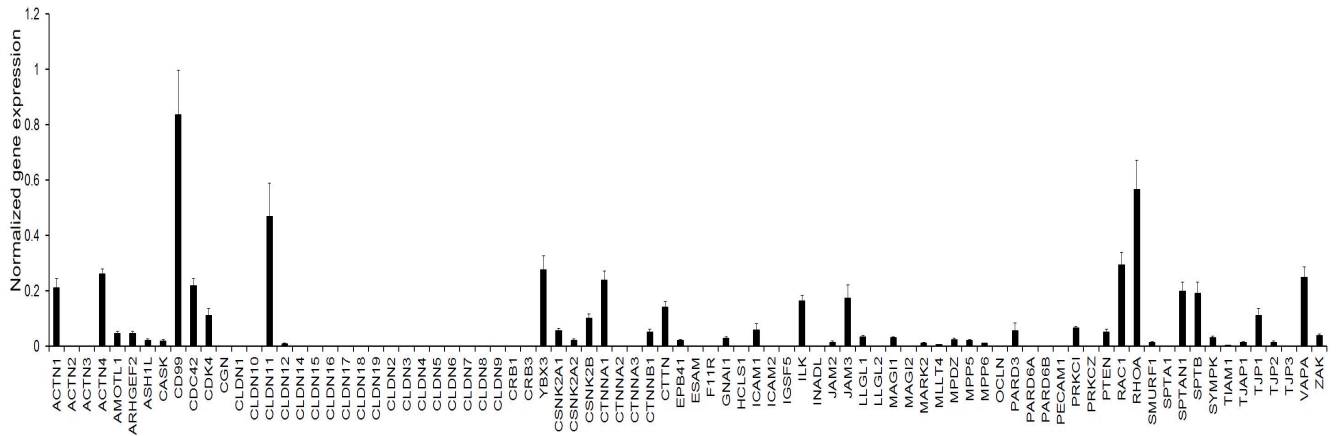
⁶Department of Ophthalmology and Vision Sciences, University of Toronto, Canada. ⁷Coulter Department of Biomedical Engineering, Georgia Institute of Technology and Emory University, Atlanta, USA.

⁸Ophthalmology, Mater Hospital, UCD School of Medicine, Dublin, Ireland.

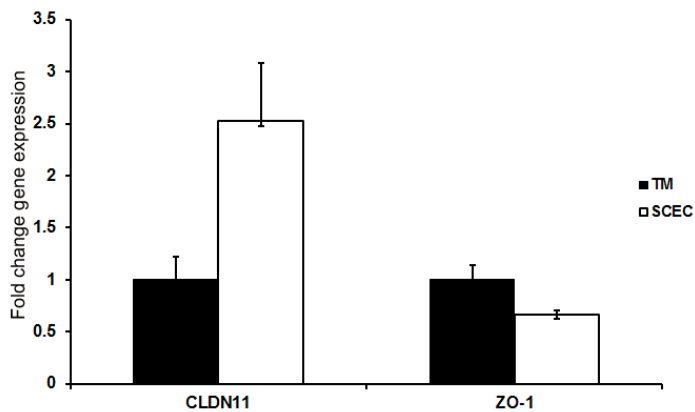
⁹RxGen, Hamden, CT, USA.

*Correspondence should be addressed to L.C.S.T (lawrenct@tcd.ie), P.H. (pete.humphries@tcd.ie) or W-D.S (william.stamer@duke.edu)

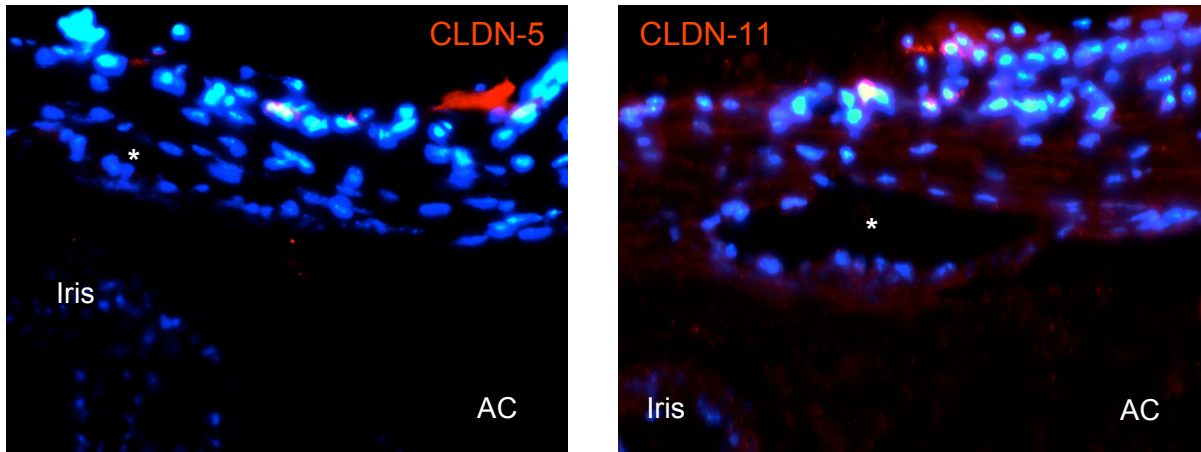
⁺These authors contributed equally to this work.



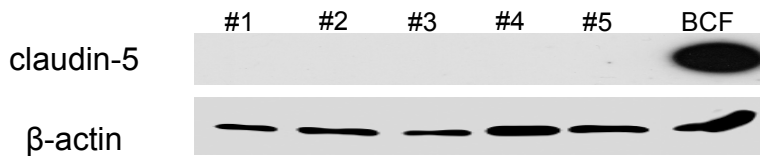
Supplementary Figure S1: A complete normalised gene expression pattern of human TJs in cultured human SCEC. SC65, 68, 76 and 77 SCEC strains were used for this study. Data are mean \pm s.e.m.



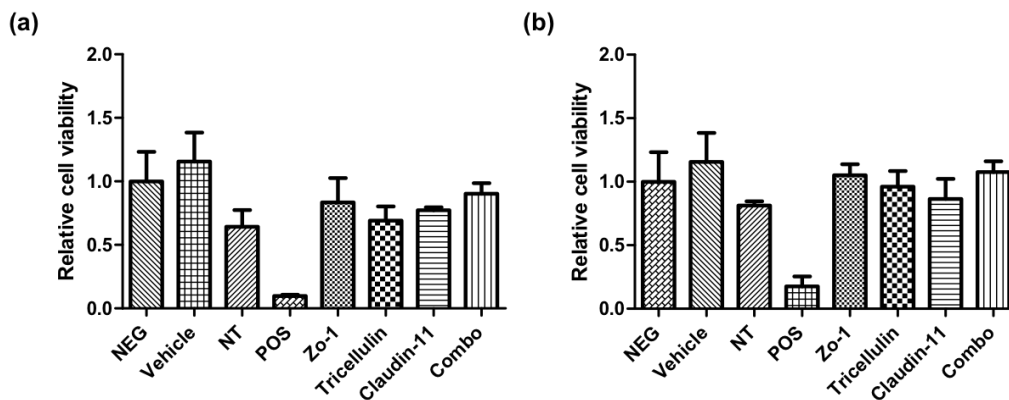
Supplementary Figure S2: Comparison of claudin-11 and ZO-1 gene expression between cultured human TM and SCEC. Fold change in gene expression was determined by the $2^{-\Delta\Delta Ct}$ method. Data represent mean fold change of SC77 and TM93 cell strains at two-passage numbers \pm s.e.m (n = 2).



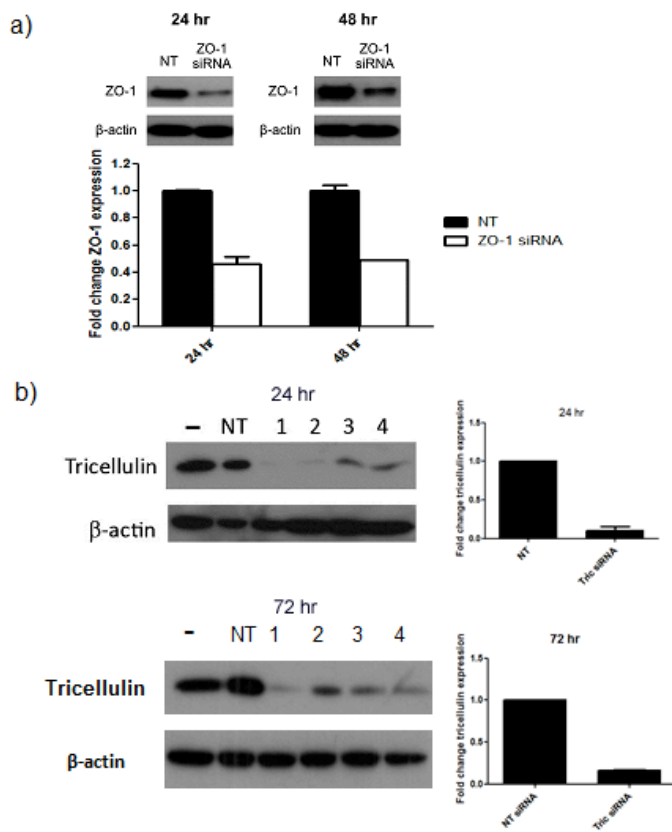
Supplementary Figure S3: Immunostaining of claudin-5 and claudin-11 in frozen sections of mouse anterior segments. claudin-5 and claudin-11 = Cy3 (red); DAPI = blue; * = Schlemm's canal lumen.



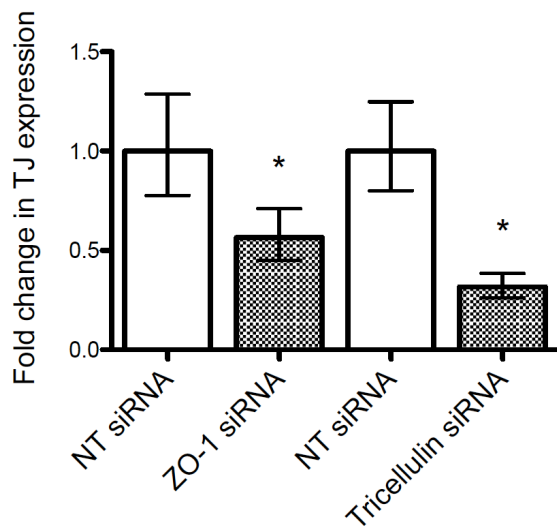
Supplementary Figure S4: Western blot for claudin-5 in Schlemm's canal endothelial cells dissected from five different non-human primates. BCF = mouse brain capillary fraction as positive control.



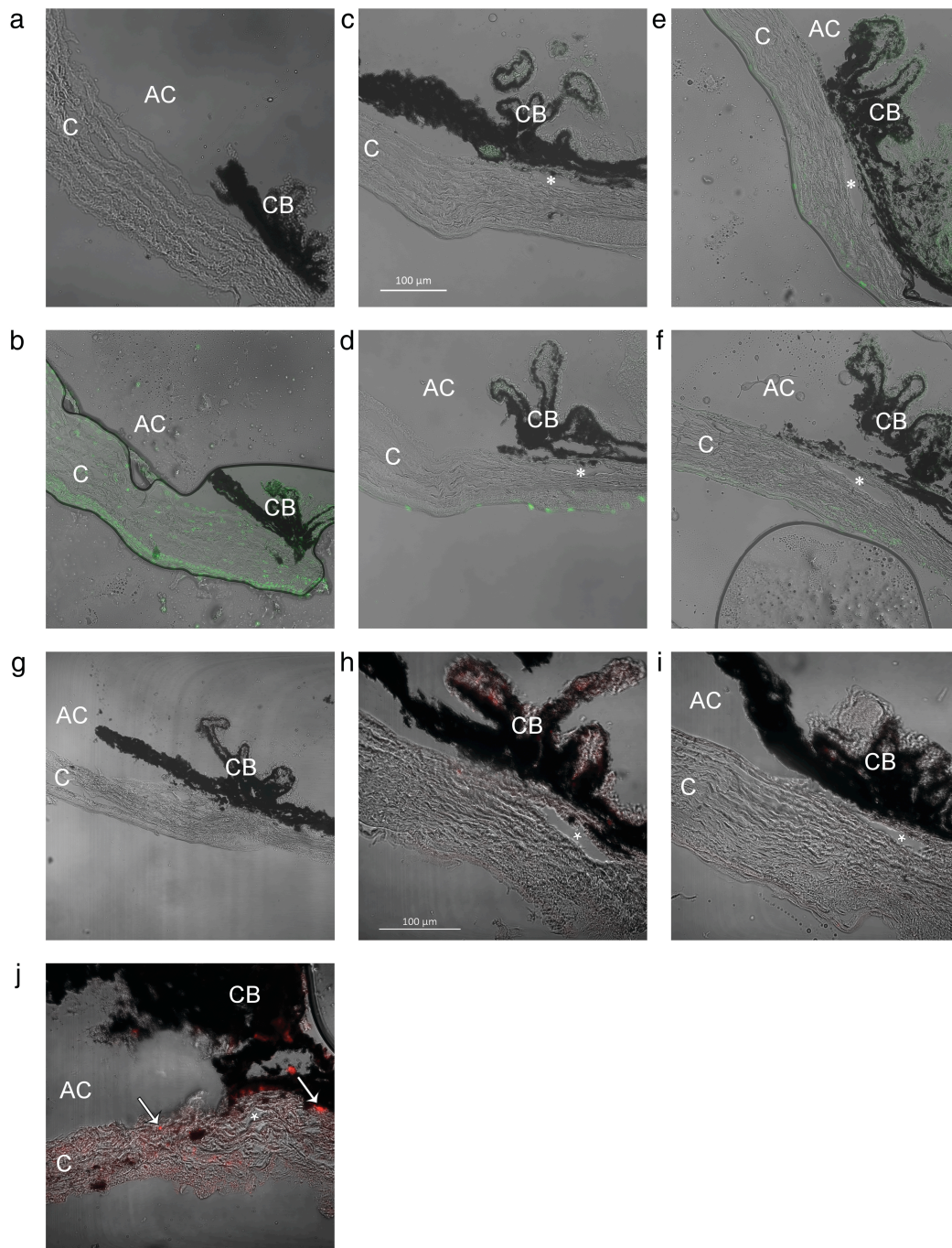
Supplementary Figure S5: Cell viability assay on cultured SCEC treated with (a) 40 nM siRNA or (b) 200 nM siRNA. No significant difference was found between the negative control and any of the siRNA treated samples (n=4; one-way ANOVA with a Tukey's post-test). NEG = negative control; Vehicle = transfection reagents alone; NT = non-targeting siRNA; POS = positive control; Combo = combination of ZO-1, claudin-11 and tricellulin.



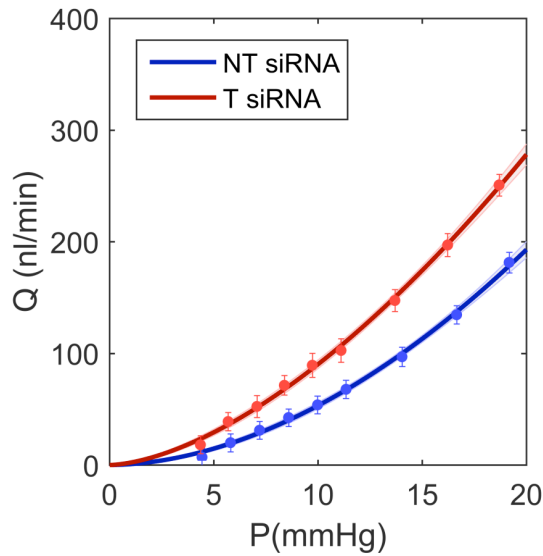
Supplementary Figure S6: a) Western blot analysis illustrating knockdown of ZO-1 in mouse brain endothelial cells (bEND3) 24 and 48 hr post-transfection. Data show average \pm s.e.m. (n=2). **b)** Western blot analysis illustrating knockdown of tricellulin in HEK293 cells transfected with mouse tricellulin cDNA 24 and 72 hr post-siRNA transfection (n=4). NT: non-targeting siRNA.



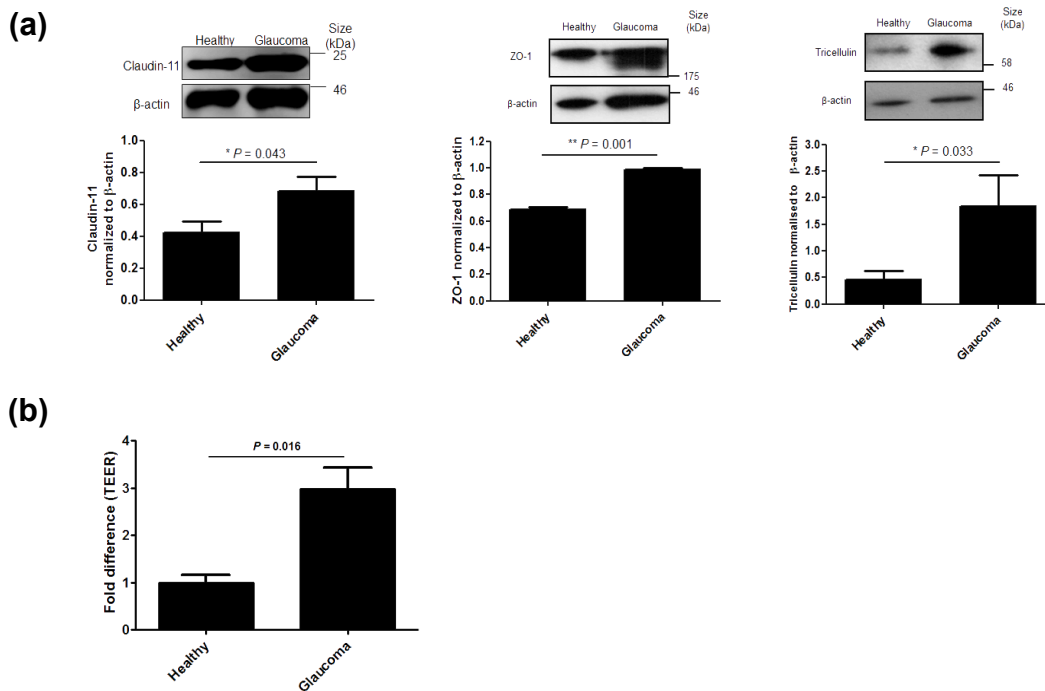
Supplementary Figure S7: Quantitative RT-PCR analysis illustrating knockdown of ZO-1 and tricellulin transcript levels at 12 hrs post siRNA delivery in the mouse retina. n = 3, *P \leq 0.05. Data is mean fold change with max and min from $\Delta\Delta$ Ct standard deviations.



Supplementary Figure S8. (a-f) IHC based TUNEL staining. (a) Negative control. (b) DNAase1 treated positive control. (c-d) Representative non-targeting images showing minor fluorescence in the corneal epithelium and ciliary body. (e-f) Representative targeting images showing similar staining patterns to that of non-targeting controls. (g-i) Cleaved caspase-3 staining. (g) Negative control. (h) Non-targeting staining shows little to no signal in outflow tissues, and minor signal in the ciliary. (i) Similar staining was observed in targeting sections as a whole. (j) Caspase-3 positive control. Representative scale bars denote 100 μm . Arrows = high incidence of apoptosis; Asterisk = SC lumen; C = cornea; AC = anterior chamber; CB = ciliary body.



Supplementary Figure S9: Representative flow (Q) vs. pressure (P) plot for a pair of eyes. Each data point shows the average of 4 min of stable flow at each pressure step, and error bars represent 95% confidence intervals. A power-law model (see Methods) is fit to the data and the 95% confidence bounds of the fit are represented by the shaded areas.



Supplementary Figure S10. (a) Western blots comparing Claudin-11, ZO-1 and Tricellulin protein expression between cultured healthy and glaucomatous SCEC monolayers. Histograms depict relative densitometric changes in protein expression from four independent experiments. **(b)** TEER values were measured in cultured glaucomatous SCEC strain (SC57g) and healthy SCEC strain (SC68) after one week of confluency was reached. Data represented as mean \pm s.e.m. (unpaired Student's t test).

Time post-transfection (hr)	NT siRNA ($\Omega \cdot \text{cm} \pm \text{s.e.m.}$) n=6	CLDN11 siRNA ($\Omega \cdot \text{cm} \pm \text{s.e.m.}$) n=6	ZO-1 siRNA ($\Omega \cdot \text{cm} \pm \text{s.e.m.}$) n=6	CLDN11 + ZO-1 siRNA ($\Omega \cdot \text{cm} \pm \text{s.e.m.}$) n=6
0	10.64 \pm 0.33	11.48 \pm 0.28	10.64 \pm 0.33	10.36 \pm 0.55
24	14.56 \pm 0.00	12.60 \pm 0.28	10.64 \pm 1.00	12.88 \pm 0.33
48	15.96 \pm 0.55	12.60 \pm 0.28	11.76 \pm 1.00	7.84 \pm 0.00
72	15.12 \pm 0.66	12.88 \pm 0.00	10.08 \pm 1.00	4.20 \pm 0.55

Time post-transfection (hr)	NT siRNA ($\Omega \cdot \text{cm} \pm \text{s.e.m.}$) n=4	Tricellulin siRNA ($\Omega \cdot \text{cm} \pm \text{s.e.m.}$) n=4
0	13.22 \pm 0.38	13.66 \pm 0.33
24	13.66 \pm 0.57	11.87 \pm 1.09
48	15.12 \pm 0.30	10.98 \pm 0.28
72	15.57 \pm 0.48	11.42 \pm 0.57

Time post-transfection (hr)	NT siRNA ($\Omega \cdot \text{cm} \pm \text{s.e.m.}$) n=6	CLDN11+ZO-1+Tric siRNA ($\Omega \cdot \text{cm} \pm \text{s.e.m.}$) n=6
0	16.32 \pm 1.42	15.26 \pm 0.79
24	15.75 \pm 1.74	7.77 \pm 1.44
48	14.88 \pm 1.49	5.88 \pm 0.91
72	16.00 \pm 1.49	10.50 \pm 1.54

Supplementary Table S1: Raw values from TEER measurements following treatment of SCEC monolayers with claudin-11, ZO-1, tricellulin, claudin-11 + ZO-1 siRNA or a combination of the three siRNAs. Data are $\Omega \times \text{cm}^2 \pm \text{s.e.m.}$

Mouse	NT siRNA		T siRNA	
	Cr (nl/min/mmHg)	χ^2 / ME95	Cr (nl/min/mmHg)	χ^2 / ME95
1	4.5	1.23	12.9	1.03
2	3.5	1.08	7.6	1.12
3	6.3	1.04	9.2	1.09
4	6.7	1.12	11.9	1.12
5	4.4	1.08	7.8	1.06
6	4.4	1.18	5.6	1.08
7	3.3	1.08	18.1	1.06

Supplementary Table S2: Facility values (Cr) for each pair of eyes together with the margin of error at 95% confidence level (ME95) measured 48 hr post-injection.

	NT siRNA		T siRNA	
Mouse	Cr (nl/min/mmHg)	^x / ME95	Cr (nl/min/mmHg)	^x / ME95
1	10.2	1.18	10.8	1.11
2	13.0	1.02	11.7	1.06
3	12.6	1.08	14.8	1.04
4	13.7	1.04	16.9	1.11

Supplementary Table S3: Facility values (Cr) for each pair of eyes together with the margin of error at 95% confidence level (ME95) measured 8 weeks post-injection.



Manipulating ocular endothelial tight junctions: Applications in treatment of retinal disease pathology and ocular hypertension



Matthew Campbell^{**}, Paul S. Cassidy, Jeffrey O'Callaghan, Darragh E. Crosbie, Pete Humphries^{*}

Smurfit Institute of Genetics, Lincoln Place Gate, Trinity College Dublin, Dublin 2, Ireland

ARTICLE INFO

Article history:

Received 3 July 2017

Received in revised form

1 September 2017

Accepted 20 September 2017

Available online 22 September 2017

Keywords:

Tight junctions

RNAi

Blood-retina barrier (BRB)

Schlemm's canal

Endothelium

Retinal degeneration

ABSTRACT

Protein levels of endothelial tight-junctions of the inner retinal microvasculature, together with those of Schlemm's canal, can be readily manipulated by RNA interference (RNAi), resulting in the paracellular clefts between such cells to be reversibly modulated. This facilitates access to the retina of systemically-deliverable low molecular weight, potentially therapeutic compounds, while also allowing potentially toxic material, for example, soluble Amyloid- β 1-40, to be removed from the retina into the peripheral circulation. The technique has also been shown to be highly effective in alleviation of pathological cerebral oedema and we speculate that it may therefore have similar utility in the oedematous retina. Additionally, by manipulating endothelial tight-junctions of Schlemm's canal, inflow of aqueous humour from the trabecular meshwork into the Canal can be radically enhanced, suggesting a novel avenue for control of intraocular pressure. Here, we review the technology underlying this approach together with specific examples of clinical targets that are, or could be, amenable to this novel form of genetic intervention.

© 2017 The Authors. Published by Elsevier Ltd. This is an open access article under the CC BY-NC-ND license (<http://creativecommons.org/licenses/by-nc-nd/4.0/>).

Contents

1. Introduction	121
2. Structure and organization of endothelial tight junctions of cerebral and inner retinal vasculatures	121
3. Structure and organization of Schlemm's canal endothelial tight junctions	122
4. Induction of inner retinal microvessel permeability: validation of the concept as a potentially therapeutic modality	123
5. Site-specific modulation of the iBRB	124
6. On the potential therapeutic utility of manipulation of iBRB permeability	124
6.1. Experimentally enhancing macular pigment (MP) access to retina	124
6.2. Alleviation of retinal oedema	125
6.3. Enhancing clearance of soluble amyloid β 1-40 from glaucomatous retinas	128
6.4. Targeting oxidative stress	129
6.5. Targeting unique IRD molecular pathologies	129
7. Targeting Schlemm's canal endothelial tight junctions: a novel process for enhancement of aqueous outflow through the conventional outflow pathway	130
8. Future prospects	131
Acknowledgement	131
References	131

* Corresponding author.

** Corresponding author.

E-mail addresses: matthew.campbell@tcd.ie (M. Campbell), pete.humphries@tcd.ie (P. Humphries).

1. Introduction

Endothelial cells lining the cerebral and inner retinal microvasculatures, together with those of the Canal of Schlemm, possess tight-junctions. In the brain and retina, tight junctions form an exceedingly tight seal, with very low rates of fluid-phase transcytosis. Such junctions, constituting the blood-brain and inner blood-retina barriers (BBB/iBRB), prevent potentially noxious materials, including for example, low molecular weight blood-borne enzymes, anaphylatoxins, antibodies etc., from entering and damaging neurological tissues (Hawkins and Davis, 2005; Abbott et al., 2010; Campbell et al., 2011, 2012; Campbell and Humphries, 2012). Additionally, in the anterior segment of the eye, Schlemm's Canal (SC) constitutes part of the conventional aqueous humour outflow pathway, aqueous produced by the ciliary body passing into the anterior chamber of the eye and then into the trabecular meshwork, from where it filters into the canal across its endothelial barrier (Stamer and Clark, 2017). While weaker and less well characterised than their counterparts of the inner retinal vessels, the tight junctions of canal endothelia are dynamically responsive to fluctuations in intraocular pressure (see Figs. 1 and 2) (Ye et al., 1997). Since it is well proven and within our capabilities to artificially modulate levels of transcript encoding tight-junctions, a means exists to enhance the permeability of the inner retinal vessels and the Canal for potentially therapeutic purposes.

Here, we provide an overview of the structure of tight junctions and of how levels of transcripts encoding tight junction components can be reversibly modulated both in retinal and SC endothelial cells. We provide examples of how low molecular weight compounds can be systemically delivered to the retina in its 'barrier modulated' state, and speculate on those degenerative retinal conditions in which oedema accumulates in the presence of an essentially intact iBRB and which could, in principle, be targeted using this approach. In the context of glaucoma, up to six percent of cases of open-angle disease are bilaterally sub-optimally

responsive to standard topically-applied pressure-reducing medications (Kass et al., 2002) and for the most commonly used prostaglandin analogue, Latanoprost, between 25 and 50% of patients do not achieve greater than a 20% reduction in intraocular pressure (Scherer, 2002; Noecker et al., 2003). These topical formulations act largely by inhibiting aqueous secretion by the ciliary body or to increase aqueous outflow through the unconventional drainage pathway. Down regulation of SC endothelial tight junctions has been shown to increase aqueous humour outflow in experimental animal model systems (Tam et al., 2017) and could form the basis of a radical therapeutic approach targeting the major aqueous humour outflow system of the eye.

2. Structure and organization of endothelial tight junctions of cerebral and inner retinal vasculatures

Tight junctions (TJs), are essentially contact points between the plasma membranes of adjacent cells, or indeed the point where one endothelial cell contacts itself in a microvessel. TJs are located at the apical periphery of the plasma membrane, and each TJ is paired to and associates with another TJ on the membrane of the adjacent cell. TJs have numerous functions and can act as sites for vesicle targeting, proliferation, transcription signals, mediating cell polarity. Given their molecular complexity, TJs also act as a physical barrier to limit paracellular diffusion of solutes across the BBB/iBRB and indeed the endothelium of Schlemm's canal.

Typically, each TJ consists of at least three different types of protein; 1) occludin, 2) junction adhesion molecule (JAM) family of proteins, and 3) claudin proteins (Ben-Yosef et al., 2003). However, the TJ itself can consist of over 40 individual proteins between support proteins, structural proteins, transport proteins, and other more unique proteins such as tricellulin, a homologue of occludin that concentrates when three cells come together (Anderson and Van Itallie, 2008). In addition, the actin cytoskeleton of the cell is critical for TJ formation, as actin strands bind the PDZ-domain containing scaffolding proteins ZO-1, ZO-2, ZO-3, MAGI-1, PatJ, PALS1 and MUPP1, which can subsequently bind to the TJ proteins that can mediate extracellular interaction with adjacent TJ proteins.

During the assembly stage of the TJ, the proteins Par3, Par6 and aPKC are critical and the TJ is also important for the function of the basolateral-located adherens junctions, which are largely cadherin based junctions. Indeed, the protein VE-cadherin can act as a mediator of intracellular signalling via its interaction with phosphatidylinositol-3-OH kinase or other growth factor receptors. For example, VE-cadherin has been shown to interact directly with β -catenin, which can subsequently regulate cellular homeostasis or responses to cellular stress (Taddei et al., 2008). Paracellular transport of molecules from blood to retina or across the Schlemm's canal endothelium is exclusively passive, driven predominantly by concentration gradients (Van Itallie and Anderson, 2004).

The molecular composition and indeed the overt permeability of TJs varies considerably amongst different tissue types. For example, some tissues display variable electrical conductance, charge selectivity, non-charged solute permeability, and size selectivity, and this is reflected to a large degree on the density of claudin proteins present in their TJs. Importantly, TJs are distinguished from adherens junctions (AJs) in that they are located at the apical periphery of the contact point of endothelial cells, with AJs expressed below them. Additionally, AJs have a different molecular composition, being enriched with cadherins, catenins and nectin amongst others.

Structurally claudins are integral membrane proteins with four transmembrane domains and two extracellular and one intracellular loop. In the first extracellular loop claudins have a common WGLWCC motif, and they also possess a C-terminus PDZ domain. This region binds to the PDZ domains of the TJ support proteins,

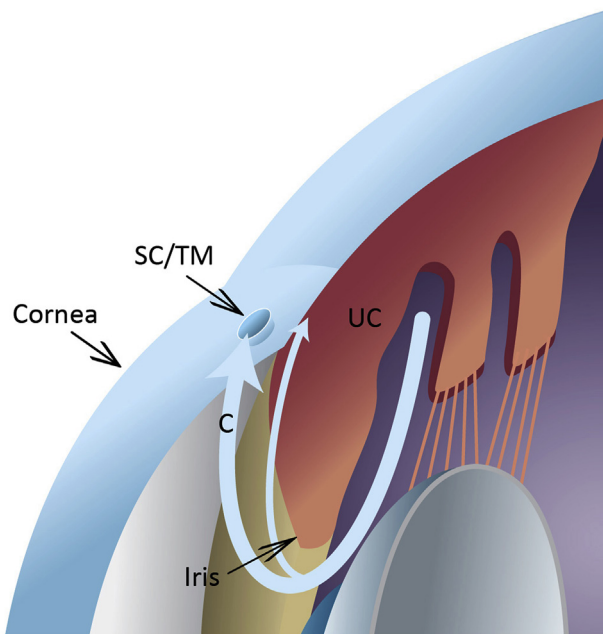


Fig. 1. Aqueous humour is secreted by the ciliary body and moves through the pupil, around the iris. A pressure gradient directs it toward the SC lumen, where most aqueous egresses (red arrow). This is termed the conventional pathway (C). The unconventional pathway (UC) involves the removal of aqueous through the fibres of the ciliary body into the supraciliary and suprachoroidal spaces.

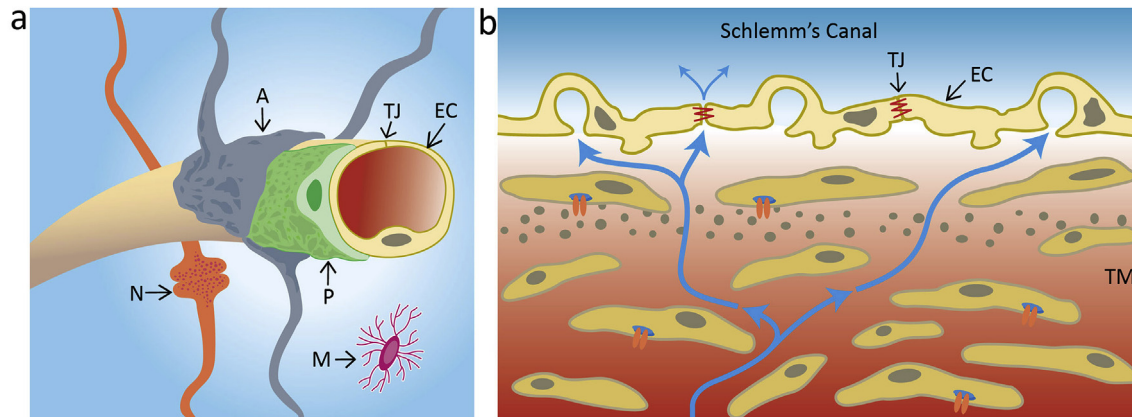


Fig. 2. **a)** Structure of the neurovascular unit of the inner blood retina barrier (iBRB) comprising endothelial cells (EC), pericytes (P) and astrocyte foot processes (A). The contacting point of an iBRB EC is where the tight junction (TJ) is formed. Neurons (N) and microglia (M) are located on the retina aspect of the iBRB. **b)** Schlemm's canal endothelial cells contain TJs but also manifest giant vacuoles to allow for aqueous humour movement (see arrows for directionality of flow) into Schlemm's canal via the trabecular meshwork (TM).

such as ZO-1, ZO-2, ZO-3 (Itoh et al., 1999) and MUPP-1 (Hamazaki et al., 2002). The C-terminus tail, is also the region which confers stability to claudins, and swapping the C-terminus tails has been found to coincide with a reversal of protein half-lives (Van Itallie et al., 2004).

Various post-translational modifications have also been implicated in claudin function. For example, phosphorylation has been shown to increase claudin1-4 permeability to chloride ions (Yamauchi et al., 2004), and loss of palmitoylation sites on claudin-14 results in reduced localization of the protein to the membrane (Van Itallie et al., 2005).

Some claudins, such as claudin-1, are widely expressed (Van Itallie and Anderson, 2004), whereas other claudin proteins are expressed only in certain cell types or during embryonic development (Turksen and Troy, 2001). This, suggests that claudins play various roles not necessarily limited to the TJs.

Various studies expressing combinations of different claudins in Madin-Darby canine kidney (MDCK) cells found that over-expression of claudin-7 increased paracellular permeability to cations, while reducing it to anions. Additionally, over-expression of claudin-4, -8 and -14 reduced permeability to cations but not anions, while over-expression of claudin-2 decreased barrier integrity without reducing the number of TJ strands (Ben-Yosef et al., 2003; Furuse and Tsukita, 2006).

The finding that claudin-14 reduces permeability to cations aligns with its abundant *in vivo* expression in the outer hair cells of the cochlea in the ear. Here TJs function to separate the K^+ -rich endolymph and Na^+ -rich perilymph, a separation essential for optimal hearing. The importance of claudin-14 for this role is observed in the deafness observed in mice and humans with claudin-14 mutations (Ben-Yosef et al., 2003). Claudin-11-null mice also exhibit deafness, and this is due to a similar role of claudin-11 in maintaining the endocochlear potential in the ear (Kitajiri et al., 2004).

Indeed, mutations in the claudin-16 gene, expressed in the thick ascending limb of the nephron, cause Mg^{2+} reabsorption in humans and cattle, resulting in deficiency of the ion. Claudin-16 contains a number of negatively charged residues in its first extracellular loop, which appear to electrostatically interact with soluble ions, enabling or inhibiting their passage (Simon et al., 1999). Detailed in Table 1, are some key properties of the claudins listed in this section.

As well as mediating selective ion transport across the paracellular pathway, claudins also play a central role in determining

the maximum size of molecules that diffuse across an endothelial cell layer. Claudin-1 knockout mice, for example, die within one day of birth due to excessive water loss across the skin. Additionally, mutations in claudin-1 are associated in humans with ichthyosis – a condition manifested by skin dehydration (Hadj-Rabia et al., 2004). These observed phenotypes in humans and other animals lacking claudin proteins demonstrate their importance in regulating TJ function and in controlling passive paracellular diffusion of materials across the TJ. Claudins are distinguished from other tight junction proteins such as occludin in that their extracellular domains have a certain degree of homology and mediate size selectivity and ion flux across the various barriers. Occludin appears to have a more regulatory role at the tight junction.

3. Structure and organization of Schlemm's canal endothelial tight junctions

The endothelial tight junctions of Schlemm's Canal differ from those seen in vascular endothelia in several ways. Early studies using electron microscopy showed electron dense junctions present between endothelial cells of Schlemm's Canal similar to those seen in vascular endothelia (Vege, 1967). Subsequent freeze fracture studies showed that Schlemm's Canal endothelial cells TJs were composed of parallel junctional strands with minimal branching which did not form complex bi-dimensional networks. The lack of branching between TJ strands in SC endothelial cells leads to the formation of channels between junction strands that are continuous from the juxtacanalicular tissue to the SC lumen. These channels were identified as a potential paracellular route for AH outflow in to the SC lumen through intercellular clefts in the SC inner wall endothelium (Raviola and Raviola, 1981; Bhatt et al., 1995). Early tracer studies using cationised ferritin showed staining of cell membranes lining channels between tight junctions in the SC inner wall endothelium, showing therefore that these channels represented a paracellular pathway across the SC inner wall. Further, these channels were of greater size and number in eyes that were fixed at elevated pressure, (Epstein and Rohen, 1991). Additionally, endothelial tight junctions in perfused human donor eyes were shown by freeze fracture to exist in single and double stranded forms at the majority of TJs, with a minority of TJs having three or more junctional strands. The complexity of these junctions was shown to be responsive to applied pressure in the eye, with the number of junctional strands decreasing as perfusion pressure increased, (Ye et al., 1997). The above features are in

Table 1
Relevant claudins and their chromosomal and tissue expression pattern.

Gene	Protein name	Chromosome	Tissue expression (protein)
CLDN1	claudin 1	3q28	Heart, brain, lung, liver testis
CLDN2	claudin 2	Xq22.3	Liver, kidney
CLDN3	claudin 3	7q11.23	Lung, liver, kidney, testis
CLDN4	claudin 4	7q11.23	Lung, kidney
CLDN5	claudin 5	22q11.21	Brain, heart, lung, liver, kidney, testis, endothelial cells in general
CLDN6	claudin 6	16p13.3	Embryonic tissues
CLDN7	claudin 7	17p13.1	Lung, kidney, testis
CLDN8	claudin 8	21q22.11	Lung, liver, kidney, testis
CLDN10	claudin 10	13q32.1	Liver
CLDN11	claudin 11	3q26.2	Brain, testis
CLDN14	claudin 14	21q22.13	Liver, kidney, ear
CLDN16	claudin 16	3q28	Kidney

contrast to TJs of the inner retinal vascular endothelium, which are composed of complex networks of multiple TJ strands, and do not exhibit dynamic regulation in response to pressure, with no changes to TJ strand structure in response to perfusion pressure (Fujimoto, 1995; Schneeberger and Karnovsky, 1976).

Schlemm's canal endothelial cells also differ from inner retinal vascular endothelial cells in that they have remarkably high hydraulic conductivity, with Schlemm's canal having a hydraulic conductivity of $4000\text{--}9000 \times 10^{-11} \text{ cm}^2 \text{ s/g}$, significantly higher than other ocular barriers, and possibly one of the highest hydraulic conductivities of all body vessel linings (Johnson, 2006). The inner wall endothelium of SC is also permeable to higher molecular weight tracer molecules than other endothelial cells of the eye, with labelled ferritin, 450 kDa, staining the interior of paracellular pores, while the inner blood-retinal barrier (iBRB) excludes molecules as small as 500 Da (Epstein and Rohen, 1991; Campbell et al., 2009). It must be noted that these differences in endothelial permeability cannot be solely apportioned to differences in TJ structure and organization as, in addition to TJ mediated paracellular pores between cells, SCECs possess giant vacuoles containing large intracellular pores. These intracellular pores have an average pore size of approximately 1 μm in diameter, with pores greater than 3 μm reported (see Fig. 3 for an overview of the differences in iBRB and SC endothelia) (Sit et al., 1997).

Human SC endothelial cells have differing TJ protein expression

profiles than is seen other endothelial cells. For example, at the iBRB, ZO-1, occludin and claudin-5 are instrumental in maintaining barrier function, with claudin-5 being particularly important in controlling paracellular permeability (Campbell and Humphries, 2012; Morita et al., 1999). Contrastingly, recent studies have shown a more simplistic TJ composition in human SC endothelial cells, with claudin-11 and ZO-1 being the major TJ proteins present, and claudin-5 and occludin being expressed at low levels only (Tam et al., 2017).

4. Induction of inner retinal microvessel permeability: validation of the concept as a potentially therapeutic modality

In the original experimental approach (Campbell et al., 2008, 2009) targeting both the BBB and iBRB simultaneously, 20 μg of siRNA targeting Claudin-5 was hydrodynamically injected into the tail veins of mice in a volume of 10% of the body weight of the animal, a procedure that was well tolerated given the overtly high volumes. Using this approach, maximum suppression of claudin-5 was observed approximately 48 h after each tail injection, levels of claudin-5 returning to normal by 72 h post inoculation. During this period, both the BBB and iBRB became permeable to the perfused nuclear stain, Hoechst H33342 (molecular weight, 563Da). In cryosections of the retina, staining of the inner nuclear

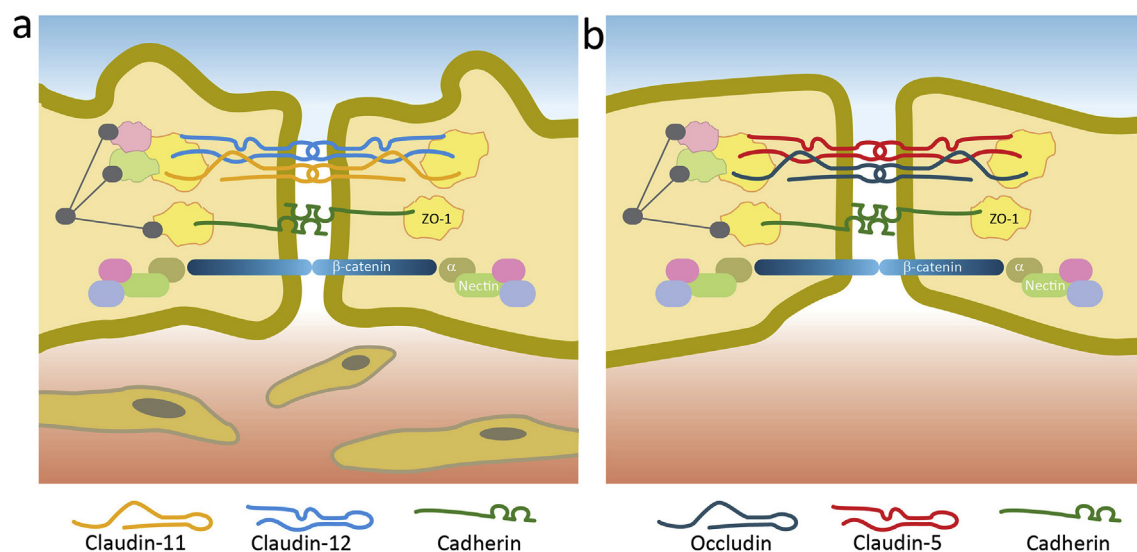


Fig. 3. a) Molecular architecture of the Schlemm's canal endothelial cells shows an enrichment of claudin-11 and claudin-12 at the tight junction. b) Tight junctions of endothelial cells associated with the inner blood retina barrier (iBRB) show an enrichment of claudin-5 and occludin at the tight junction.

layer (INL) was evident 24 h post-siRNA injection, while staining of the outer nuclear layer (ONL) became evident at 48 h. However, 72 h after siRNA inoculation, no staining could be detected in any of the nuclear layers (Fig. 4). Under the same conditions, systemically administered FITC-labelled dextran, FD-4 (MW 4,400Da), showed no evidence of being able to access any of the nuclear layers of the retina, these data indicating that down-regulation of claudin-5 facilitates a transient and size-selective enhancement of permeability at the iBRB to compounds of at least 563 Da, but not to those of higher molecular weight. In subsequent studies (Campbell et al., 2012), tail injections were undertaken with siRNA complexed with a clinically enabled polyethylene imine (PEI) carrier, *in vivo*-JetPEI (Polyplus Transfection). 20 µg of claudin-5 siRNA injected in a volume of 0.4 ml with this carrier was shown to be as effective as the hydrodynamic approach in down-regulation of claudin-5. While these initial experiments validated barrier modulation technology as an enabling system for enhancing drug delivery to neural tissues, it was unable to selectively target the retina while leaving the BBB intact.

5. Site-specific modulation of the iBRB

In order to selectively target the retina, claudin-5 shRNA was incorporated into an AAV-2/9 vector, inducible by doxycycline (Campbell et al., 2011). A single once off sub-retinal injection of this vector was required, provision of doxycycline in drinking water (2 mg/ml) being used to induce claudin-5 shRNA expression (viral constructs are now available that are capable of accessing the retina following intravitreal inoculation and there is no reason not to assume that such constructs will act in a similar manner, providing they have tropism for vascular endothelia). The efficacy of this system was initially validated in a light-induced murine model of apoptotic photoreceptor degeneration, in which it has been firmly established that death of photoreceptor cells is calpain-dependent (Perche et al., 2007). N-Acetyl-L-leucyl-L-methionine; calpain inhibitor II (ALLM), molecular weight 401Da is a potent calpain inhibitor. Albino mice given doxycycline in drinking water, were treated IP with 20 mg/kg ALLM followed by exposure to 7900 lux of white light. After 24 h, photoreceptor cell death was assessed by TUNEL staining of retinal cryosections. As illustrated in Fig. 5, photoreceptor cell viability was extensively preserved in animals systemically treated with the drug which, under conditions where permeability of the iBRB had not been modulated, could not gain sufficiently effective access to the retina to provide therapeutic benefit.

Validating this approach, a murine model of the exudative form of age-related macular degeneration (AMD) was also used (Campbell et al., 2011). Wild type C57BL/6J mice were sub-retinally

inoculated in one eye with an AAV-2/9 expressing claudin-5 shRNA and the other eye with an AAV-2/9 expressing a non-targeting shRNA as control. Animals were administered doxycycline (2 mg/kg) for 3 weeks prior to induction of laser burns to the RPE/Bruch's membrane, inducing localized expression of vascular endothelial growth factor (VEGF) and choroidal neovascularisation (CNV) at the site of laser burns. During an interval of 14 days subsequent to laser treatment, mice were administered two systemic (IP) doses either of 17-AAG (30 mg/kg), or sunitinib malate (20 mg/kg), both well characterised and potent inhibitors of VEGFR-2. As shown in Fig. 6, animals having received a claudin-5 targeting vector showed highly significant suppression of CNV compared to the contralateral eye receiving a non-targeting vector.

It is of interest also to note that endothelial tight junctions at the iBRB can be further manipulated in order to increase barrier permeability beyond that achievable using claudin-5 alone. In this regard, Keaney et al. (2015), demonstrated that co-suppression of transcripts encoding claudin-5 and occludin rendered the iBRB reversibly permeable to systemically administered compounds up to approximately 4 kDa in molecular weight. While manipulating permeability to this extent runs the risk of admission into the retina (or brain) of potentially damaging low molecular weight materials such as anaphylatoxins, or low molecular weight enzymes, no observable negative physiological consequences of such modulation were noted. The possible therapeutic implications of this observation will be considered later in this review.

6. On the potential therapeutic utility of manipulation of iBRB permeability

6.1. Experimentally enhancing macular pigment (MP) access to retina

The macular pigments, lutein, zeaxanthin and mesozeaxanthin, act protectively within the retina, acting as filters for short wavelength blue light and also as scavengers of reactive oxygen species (Whitehead et al., 2006). Potentially beneficial effects of dietary supplementation have been investigated in a number of scenarios, including for example, inherited retinal degenerations, specifically retinitis pigmentosa and Usher syndrome (Aleman et al., 2001) and in patients with AMD (Ma et al., 2012; Liu et al., 2014). In the study by Aleman et al. (2001), there was a trend toward more severe progression of disease in those patients who had lower retinal MP levels. In the study by Ma et al. (2012), abnormalities in central retinal function in early AMD were reported to be improved and in the study reported by Liu et al. (2014,2015), a meta-analysis of 1176 AMD patients, both visual acuity and contrast sensitivity were found to improve with supplementation. However, it is well

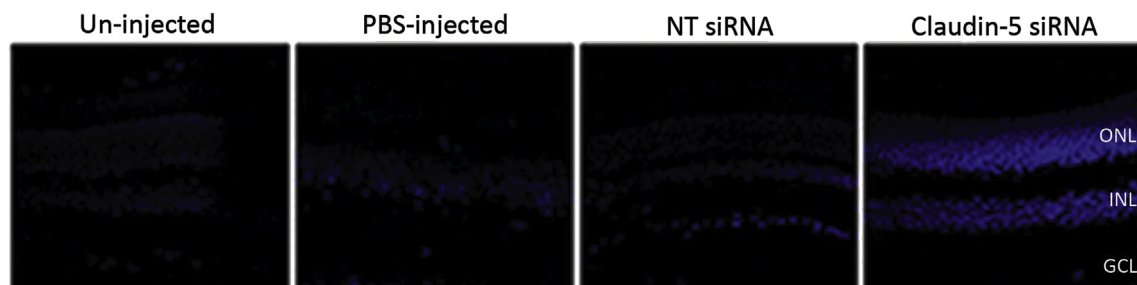


Fig. 4. Extravasation of Hoechst H33342 from the retinal microvessels was manifested by distinct staining of nuclei in the inner nuclear layer (INL) and outer nuclear layer (ONL) 48 h post delivery of claudin-5 siRNA when compared to control groups.

This is part of figure 6 from our paper, Campbell et al., J. Gene Medicine 2008 Aug; 10(8) 930–47

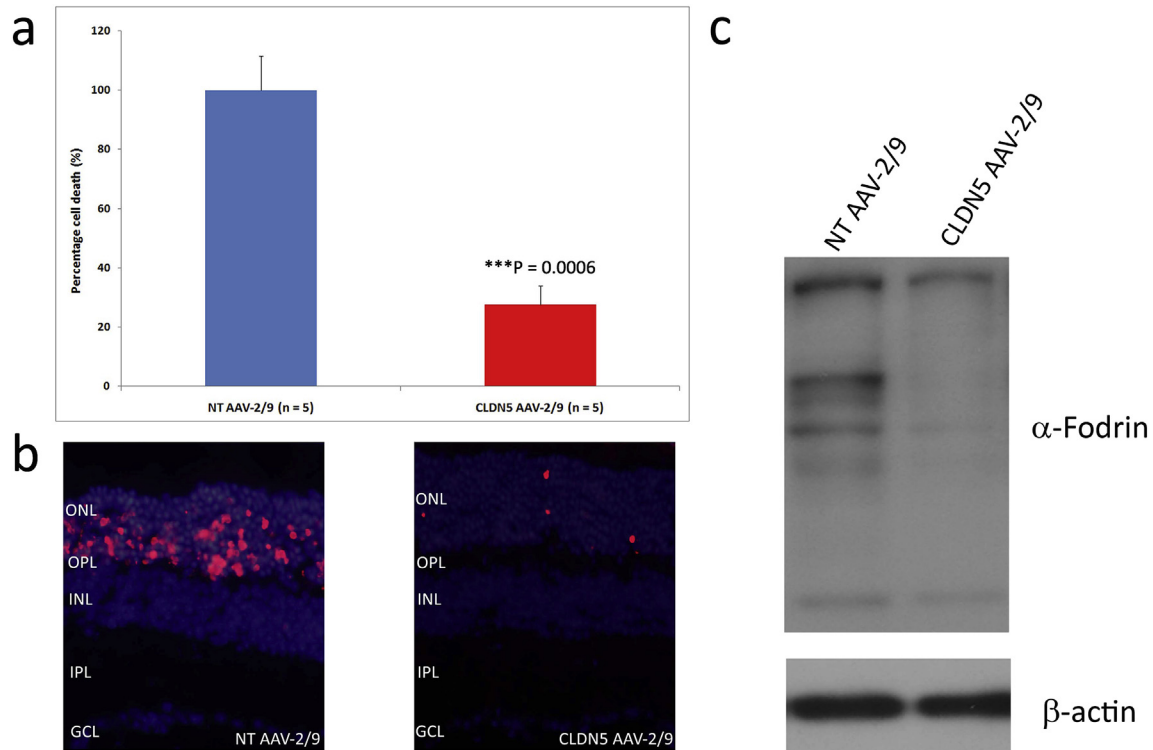


Fig. 5. (a) Albino Balb/c mice were inoculated sub-retinally with either the NT AAV-2/9 in their left eye or the CLDN5 AAV-2/9 in their right eye. Significant protection of photoreceptor cells was observed in the right eyes (CLDN5 AAV-2/9) of mice compared to the left eyes (NT AAV-2/9) (***P = 0.0006). (b) TUNEL positive cells were shown to be consistently localized in large numbers to the outer nuclear layer (ONL) of NT AAV-2/9 injected retinas compared to CLDN5 AAV-2/9 injected retinas. Outer plexiform layer (OPL), inner nuclear layer (INL), inner plexiform layer (IPL), ganglion cell layer (GCL). (c) Extensive cleavage of the calpain substrate α -fodrin was observed in mice receiving the NT AAV compared to mice receiving the CLDN5 AAV with ALLM prior to light ablation.

This is figure 4 from our paper, Campbell et al., EMBO Molecular Medicine 2011, 3, 235–245.

recognised that not all on supplementation show increases in MP density within the retina, a probable reflection of variability in carotenoid transporter efficiency (40, 43, 44).

While mice do not possess a macula, they nevertheless could represent a highly cost efficient avenue for study of the physiological effects of MPs in normal and degenerating retinas. However, wild type mice do not accumulate these carotenoids within retinal tissues even when supplemented in their diet. Recent studies however, have shown that mice with targeted disruptions of β -carotene oxygenases 1 and 2 (*Bco2*^{-/-} in particular) are able to accumulate MPs within the retina (Li et al., 2017). However, a very large amount of carotenoid ~2.6 mg per mouse per day, equivalent to an average human dose of about 635 mg per day, was required to achieve measurable levels of MP within these retinas. Controlled modulation of the permeability of the iBRB of *Bco2*^{-/-} mice, would enable very much smaller systemic doses of MP to be required in order to achieve elevated MP levels within retinal tissues. Given the fact that lutein and zeaxanthin have molecular weights (569Da), well below the cut off for systemic delivery following transient down regulation of claudin-5, *Bco2*^{-/-} mice would likely be rendered a more versatile and useful model for studies of the physiological or protective effects of MPs within the retina. The same system could be used to experimentally enhance MP uptake in primates.

6.2. Alleviation of retinal oedema

Previous studies from this laboratory (Campbell et al., 2012) have shown that siRNA-mediated down regulation of claudin-5 is highly effective in reducing pathological cerebral oedema in a

murine model of traumatic brain injury (TBI). In this model, a small ultra-cold probe is placed for a short period of time onto the skulls of anaesthetised animals. This induces a focal necrotic cerebral lesion and breakdown of the BBB, with extensive extravasation of fluid from the cerebral capillaries into the parenchyma of the brain. The barrier then reforms, pathological oedema remaining within penumbral region of the brain, adjacent to the injury site. [It is of interest to note that TBI accounts for about 1% of all adult mortality worldwide and cerebral oedema induced by out-of-hospital cardiac arrest is similarly prevalent. Treatments involving injection of the osmotic diuretic, mannitol, are archaic and inefficient if oedema persists beyond 24 h. This treatment paradigm has hardly changed in over 80 years]. In the current approach, claudin-5 siRNA complexed with the carrier agent *in-vivoJetPEI* was systemically administered. The transiently modulated BBB allowed efficient fluid drainage from the brain, reducing lesion volumes and improving cognitive function (Fig. 7).

It is of interest to note in the above context, that a number of well-defined retinal conditions are characterised by a build-up of intra-retinal oedema and could be targetable using this approach. In general, retinal oedema as a co-morbidity of a range of retinal conditions will involve vasogenic oedema as the initial insult, i.e., oedema derived from a vascular source, with extravasation of fluid from blood to neural tissues. Vasogenic oedema will lead to acute pressure changes within neural tissue and will lead to eventual cytotoxic oedema, where cells within the penumbral region of injury/damage will gradually decline. Bearing in mind that the retina is simply an extension of the central nervous system (CNS), we speculate that in such conditions, it may be possible to counterbalance fluid exudation into retinal tissues, by enhancing fluid

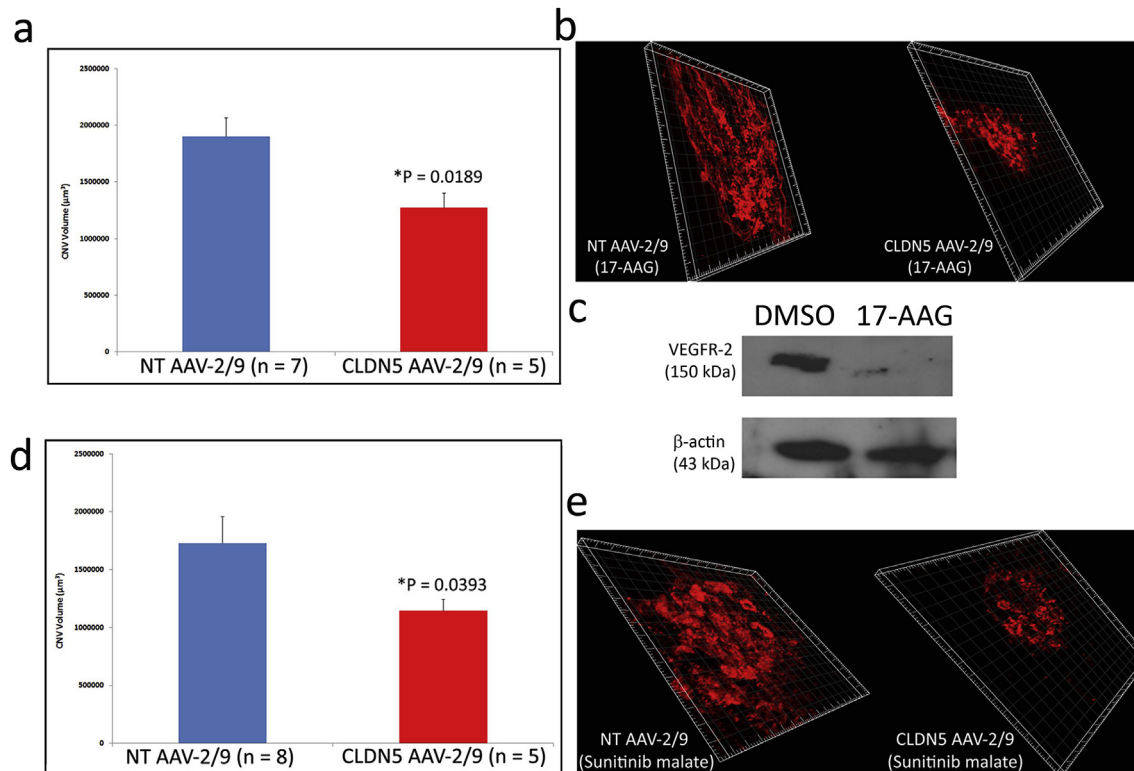


Fig. 6. (a) Albino BalB/c mice were inoculated sub-retinally with either the NT AAV-2/9 in their left eye or the CLDN5 AAV-2/9 in their right eye. Significant protection of photoreceptor cells was observed in the right eyes (CLDN5 AAV-2/9) of mice compared to the left eyes (NT AAV-2/9) ($***P = 0.0006$). (b) TUNEL positive cells were shown to be consistently localized in large numbers to the outer nuclear layer (ONL) of NT AAV-2/9 injected retinas compared to CLDN5 AAV-2/9 injected retinas. Outer plexiform layer (OPL), inner nuclear layer (INL), inner plexiform layer (IPL), ganglion cell layer (GCL). (c) Extensive cleavage of the calpain substrate α -fodrin was observed in mice receiving the NT AAV compared to mice receiving the CLDN5 AAV with ALLM prior to light ablation.

This is part of Figure 5 from our paper, Campbell et al., EMBO Molecular Medicine 2011, 3, 235–245.

resorption into the inner retinal vasculature by manipulating iBRB permeability. While this may appear counter-intuitive, the approach is now validated in murine models of TBI, where BBB breakdown is a hallmark pathology. The same will apply to retinal oedematous conditions, where penumbral regions are at risk of perpetuating neural damage. Such conditions include, *inter alia*, Non-arteritic Anterior Ischaemic Optic Neuropathy (NAION), characterised by axoplasmic flow stasis and extracellular oedema at the optic nerve head and X-linked Juvenile Retinoschisis, in which fluid-filled cavities develop as the retina splits, cavities largely forming in the outer/inner plexiform and inner nuclear layers of the retina (fundus images of these conditions, clearly revealing the presence of retinal oedema are shown in Fig. 8). NAION is caused by reduced blood flow in the posterior ciliary artery, which causes ischaemia in the anterior part of the optic nerve head, resulting in a vasogenic oedema and axoplasmic flow stasis in ganglion cell axons, causing them to swell and become damaged (Hayreh, 2013). It is a major cause of visual handicap in older people, with approximately 6000 cases per year in US (the prevalence is higher in diabetics). 25% of patients experience NAION in contralateral eye within five years of developing the disease and loss of vision is often permanent. Most importantly, there are no effective treatments (Hayreh, 2014). Animal models of NAION are controversial. However, given the impelling data that exist on efficient clearance of oedema from the brain, we suggest that claudin-5 suppression within the inner retinal endothelial vasculature could represent a plausible means of alleviation of optic nerve head swelling. In this regard, we tested the efficacy of intravitreal inoculation of GLP grade claudin-5 siRNA in the Vervet (African Green) monkey.

Tissues at the optic nerve head were dissected and subjected to RT-PCR analysis. Clearly, claudin-5 levels can be reduced using this approach (see Fig. 9). In the current context it is of note that intravitreal inoculation is widely accepted in routine ophthalmic practice (some patients have now received several hundred intravitreal injections of Lucentis). Moreover, therapy could readily be packaged as lyophilized compound, reconstituted and administered in outpatient facilities and readout of efficacy over days/weeks following therapy would be rapid, using standard clinical techniques (fluorescein angiography, visual acuity, OCT, ERG).

X-linked juvenile retinoschisis, caused by recessive mutations within the RS1 (Retinoschisin) gene, is characterised by splitting of the retina, particularly in the region of the macula, largely occurring in the OPL, INL and IPL layers (Gerth et al., 2008; Yu et al., 2010; Gregori et al., 2009). Retinoschisin is an extracellular matrix (ECM) protein secreted from a number of retinal cell types including photoreceptors, bipolar, amacrine and ganglion cells, and binding strongly to the membranes of photoreceptors and bipolar cells, stabilizing retinal cellular architecture (Vijayasarathy et al., 2012; Molday et al., 2012). AAV-mediated therapeutic intervention involving either CMV or endogenous promoter-driven expression of the RS1 gene, has now progressed from murine models (Zeng et al., 2004; Bush et al., 2016; Byrne et al., 2014; Dalkara et al., 2013) into clinical evaluation (ClinicalTrials.gov.NCT02416622; NCT0231787). It is also of note that regression of retinal cysts in one patient with juvenile XL retinoschisis was induced by oral administration (500 mg/day over four days) of the carbonic anhydrase inhibitor, acetazolamide (Zhang et al., 2015). The latter is used as a topical medication for open angle

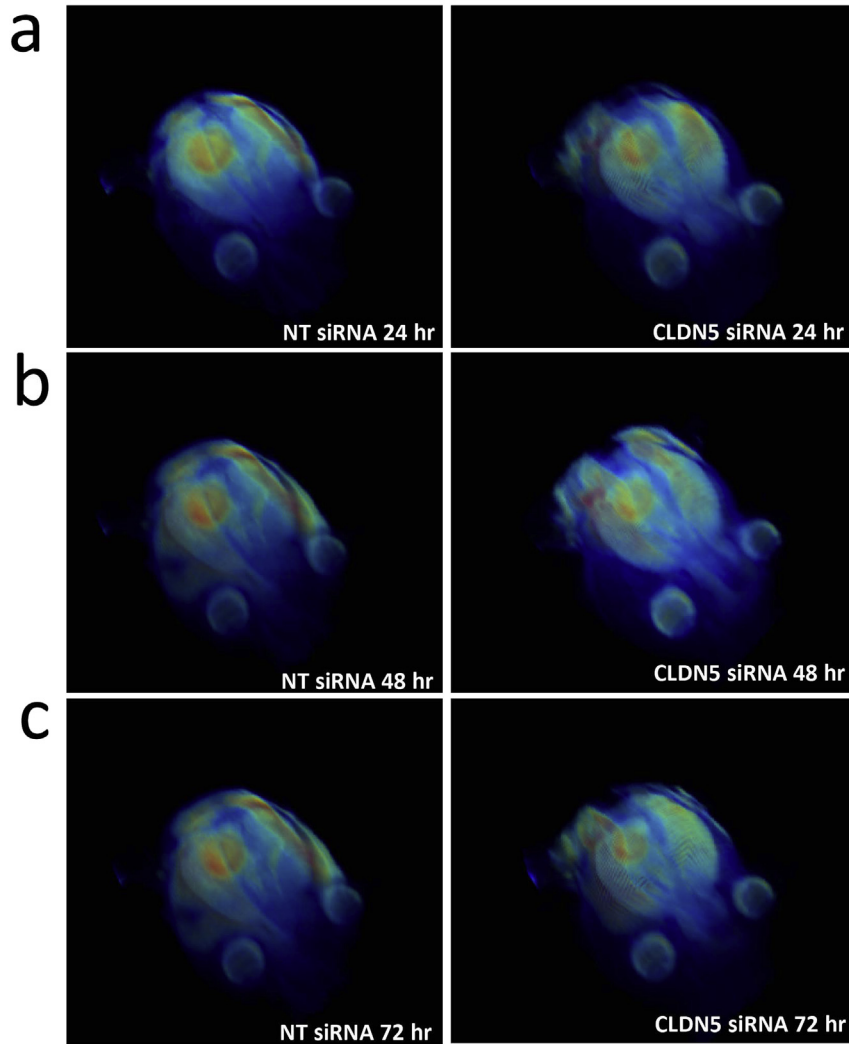


Fig. 7. Three-Dimensional volumetric rendering of MRI data showed lesion volume in red (pseudocolor) with NT siRNA injected mice in the left column and claudin-5 siRNA injected mice in the right column. **a)** NT siRNA and claudin-5 siRNA 24 h post injury. **b)** 48 h post injury. **c)** 72 h post injury. This is a small part of figure 4 from our paper, Campbell et al., Nature Communications 2012 May 22; 3: 849.

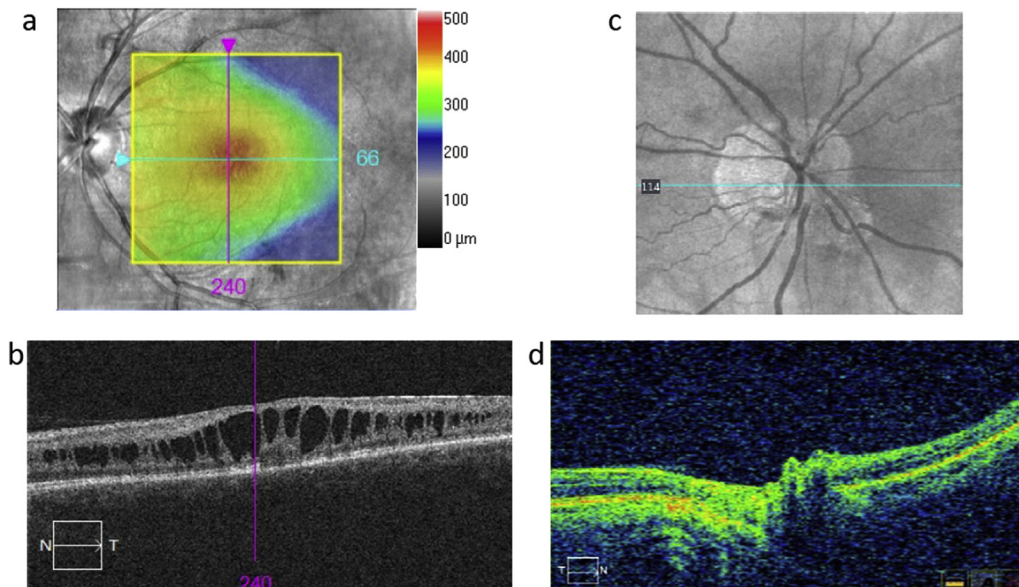


Fig. 8. **a)** and **b)** Optical coherence tomography (OCT) analysis of X-linked retinoschisis. **c)** and **d)** OCT analysis of non-arteritic ischemic optic neuropathy (NAION).

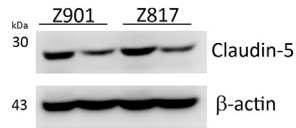


Fig. 9. Claudin-5 suppression in the vasculature associated with the optic nerve head in African green monkeys 48 h post injection of claudin-5 siRNA.

glaucoma and acts by enhancing aqueous outflow through the uveoscleral route. However, it also enhances the pumping activity of the RPE enabling excess fluid accumulating in intra-retinal cysts to be transported into the choroidal circulation. In view of the fact that the inner retinal microvessels innervate the layers of the retina in which schisis most frequently occurs, we speculate that modulation of the permeability of the inner retinal vessels may assist in facilitating fluid clearance from the large cysts that occur within these retinal layers. In this regard, it is noteworthy that intravitreal inoculation is an accepted mode of delivery of siRNA, the following trials serving as an indication: QPI-1007 (Quark): siRNA targeting caspase-2 for suppression of apoptosis in NAAION; AGN211745 (siRNA/Allergan): siRNA targets VEGFR1 (AMD); Bevasiranib (Opko Health): siRNA targets VEGF (diabetic macular oedema); PF-04523655 (Quark): siRNA targets RTP801/REDD1 apoptotic stress response gene; ALY040012 (Sylentis): siRNA targeting ocular hypertension. (Bevasiranib was initially withdrawn from trial owing to lack of efficiency in suppressing VEGF activity. Note however, that in the scenario described above, only partial knockdown of claudin-5 transcript is required to enhance iBRB permeability). This approach could also be envisaged as an adjunct to AAV-mediated therapeutic intervention, where AAV expressing an inducible claudin-5 shRNA is used in conjunction with gene replacement.

6.3. Enhancing clearance of soluble amyloid β 1-40 from glaucomatous retinas

Evidence has accumulated over a number of years to suggest a pathological role for amyloid- β ($A\beta$) in degenerative retinopathies, including AMD and glaucoma. Co-localization of $A\beta$ and drusen in post-mortem human AMD eyes has been observed in a number of studies, including those reported by Dentchev et al. (2003), Anderson et al. (2004) and Johnson et al. (2002), such studies suggesting $A\beta$ as a putative activator of complement cascades. Further evidence for a pathological role for $A\beta$ in AMD was reported by Ding et al. (2011) and Liu et al. (2015). In the former study, systemic anti- $A\beta$ antibody treatment of APOE4 mice, fed on a high fat diet to induce AMD-like retinal symptoms, resulted in an alleviation of disease pathology, while in the latter, sub-retinal inoculation of $A\beta$ into wild type mice produced pathological changes in RPE and photoreceptors. In optic nerve head post mortem tissue from individuals with glaucoma, Gupta et al. (2016) detected elevated levels of soluble $A\beta$, which has also been detected in aqueous humour from up to 40% of patients with glaucoma (Janciauskiene and Krakau, 2001).

These, and many other studies, strongly suggest that suppression of $A\beta$ accumulation within retinal tissues may be protective in AMD, glaucoma and possibly in inherited retinal degenerations. In this regard, our own studies (Keaney et al., 2015) have shown that siRNA-mediated down regulation of endothelial tight junction transcripts encoding claudin-5 together with occludin, allowed paracellular transport of a soluble $A\beta$ 1-40 monomer (MW 4.3 kDa), modified with proline at position 19 and not prone to aggregation into higher molecular weight structures, to readily diffuse across brain endothelial cell monolayers *in vitro*. However, a dityrosine cross-linked $A\beta$ 1-40 dimer (MW 8.6 kDa) did not diffuse in such a

manner, these data demonstrating that the paracellular spaces between brain endothelial cells can be widened sufficiently by down regulation of two tight junction components to allow soluble $A\beta$ 1-40 dimers to diffuse across them. These observations were confirmed *in vivo* in wild type mice and in a murine AD model (Tg2576) expressing a mutated form of APP, where it was shown that tail vein co-inoculation of claudin-5 and occludin siRNAs rendered the BBB reversibly permeable to biotinylated dextran of 3kD but not of 10kD. Periodic intravenous inoculation of claudin-5

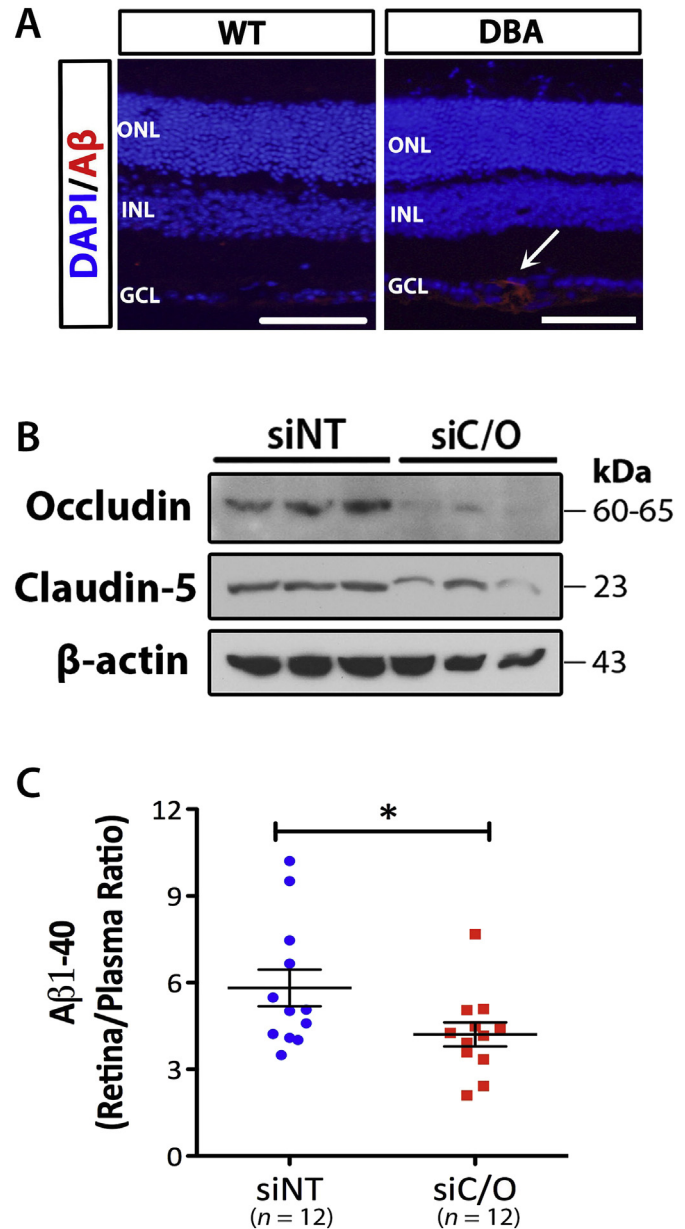


Fig. 10. $A\beta$ in retinas of 8-month old siRNA-treated DBA/2J mice. **a)** $A\beta$ immunostaining in the ganglion cell layer of wild-type (WT) and DBA/2J mouse retinas (ONL: outer nuclear layer, INL: inner nuclear layer, GCL: ganglion cell layer. Scale bar = 50 μ m). **b)** Western blot analysis of claudin-5 and occludin in retinas of DBA/2J mice following systemic administration of non-targeting (NT) or claudin-5 and occludin (C/O) siRNAs. **c)** Retina/plasma ratios of $A\beta$ (1-40) (pg/g soluble retina $A\beta$ (1-40) to pg/ml plasma $A\beta$ (1-40)) in DBA/2J mice after a single round of siRNA administration (unpaired Student's *t*-test, $n = 12$ animals per experimental group, $*P = 0.045$. Data are means \pm s.e.m.). This is supplementary Figure 10 from our paper, Keaney et al., Sci. Adv. 2015 Sep; 1(8) e1500472.

and occludin siRNAs every 21 days into AD mice for a period of 9 months resulted during this period in a significant induction of movement of soluble A β 1–40 from brain tissue into the peripheral circulation. Furthermore, in a murine model of pseudoexfoliative glaucoma, the DBA/2J mouse, in which A β 1–40 was clearly detectable in retinal sections, a single intravenous injection of claudin-5 and occludin siRNAs resulted in retina:plasma ratios of A β 1–40 being significantly reduced (Fig. 10).

These data raise the distinct possibility for an avenue of clearance of neurotoxic A β 1–40 from retinal tissues as a means of protecting against ganglion cell death in glaucoma. It will be of interest in this context to assess such an approach in additional models more accurately resembling the primary open-angle form of glaucoma, for example in transgenic mice expressing a C437H mutation within the human myocilin gene, a model mimicking primary open angle glaucoma in which there is an intracellular accumulation of ECM material within cells of the Trabecular meshwork, and a decrease in secretion of MMPs, favouring an extracellular accumulation of ECM materials, these animals classically displaying elevations in IOP and reduced outflow facility, with concomitant demise of retinal ganglion cells (Zode et al., 2011).

6.4. Targeting oxidative stress

The brain and retina account for approx. 20% of the body's oxygen consumption, which generates appreciable levels of reactive oxygen species and peroxides, contributing to neurological and retinal degeneration (Ott et al., 2007). For example, oxygen free radicals interact with membrane phospholipids generating MDA (malondialdehyde; HOCH=CH-CHO, or C₃H₄O₂). This compound is pro-inflammatory, and has been recently shown (Weismann et al., 2011) to be normally sequestered by complement factor H (CFH). CFH is an inhibitor of the alternative complement pathway and a mutation, His402Tyr within the SCR-7 domain of the protein was the first to be strongly associated with AMD. The risk variant, CC has been shown to have a very much lower affinity for MDA than the non-risk variant TT. People with AMD who are heterozygous for the normal and risk variants have a compromised ability to bind MDA, presumably increasing the risk of disease progression. The Authors conclude: 'We report the identification of CFH as a hitherto unrecognized innate defence protein against MDA, which is a ubiquitously generated pro-inflammatory product of lipid peroxidation'. Reactive oxygen species are also similarly important in contributing to disease pathology in IRDs and in diabetic retinopathy (Kiang et al., 2014).

Mitochondria are a major site of generation of oxygen free radicals in the retina. A recently developed oxygen free radical scavenger, XJB -5-131 (4-hydroxy-2,2,6,6-tetramethyl piperidine-1-oxyl nitroxide chemically linked to a mitochondrial targeting peptide, Leu-D-Phe-Pro-Val-Orn), enables the systemically-administered drug to become localized in the membranes of the mitochondria and it has been shown to be protective against neurological degeneration in a murine model of Huntington's disease (Xun et al., 2012). While this drug, with a molecular weight of 959 Da, can access the brain in the Huntington model, it's systemic access to the retina could be radically enhanced (with concomitant reduction in systemic dosage) by periodic manipulation of iBRB permeability, possibly representing an approach to slowing disease progression in a manner independent of primary mutations in IRDs or other retinopathies.

6.5. Targeting unique IRD molecular pathologies

With over 260 genes having so far been identified in IRDs, with 70 in retinitis pigmentosa, the molecular pathologies associated

with these conditions are clearly of immense diversity, genes encoding proteins, or enzymes involved in transport processes, protein deglutamylation, membrane trafficking, ciliogenesis, calcium-sensitive chloride channels, proteins with protective function against apoptosis/oxidative stress, retinal neurotransmission, photoreceptor morphogenesis, fatty acid and steroid metabolism, extracellular proteins of the retina, retinal adhesion proteins, phagocytosis of rod outer segments, transcription factors and activators, semaphorins, protein ubiquitination, actin binding proteins, pre-mRNA processing, the rate-limiting step of the alternative pathway of guanine nucleotide biosynthesis, and about every gene encoding proteins or enzymes of the visual transduction and retinoid cycles, and indeed many more (Jane Farrar et al., 2017). In some cases, molecular pathologies specific to only one, or a limited number of genetic subtypes of disease may offer opportunities to target such uniqueness by systemic drug treatment.

The RP10 form of RP is arguably one of these, accounting for at least 5% of autosomal dominant cases of RP (perhaps 25–30,000 cases world-wide). It is an early onset, aggressive retinopathy, symptoms manifesting within the first decade. The disease is caused by mutations within the inosine monophosphate dehydrogenase 1 (IMPDH1) gene (Jordan et al., 1993; Kennan et al., 2002; Aherne et al., 2004), which, together with IMPDH2, are the rate-limiting enzymes of *de novo* guanine nucleotide biosynthesis. While each enzyme performs the same role in converting IMP to XMP, which is then converted to GMP, levels of expression between tissues vary considerably, the predominant enzyme within the murine retina being IMPDH1 (Aherne et al., 2004). IMPDH1–/– mice (hence having little or no IMPDH activity because of minimal expression of IMPDH2) have only a very slow deterioration in retinal function, the outer nuclear layer (ONL) of these animals remaining largely intact (Aherne et al., 2004). Since both IMPDH1 and IMPDH2 are minimally expressed in these retinas, retinal function appears to be maintained with a sufficient supply of guanine nucleotides generated by the salvage pathway of guanine nucleotide biosynthesis. Mutations identified in RP10, occur within the CBS domain of the IMPDH1 enzyme, a binding site for GDP/GTP inhibition, indicating that mutations within the IMPDH1 gene result in constitutive activation of the enzyme, disturbing guanine nucleotide pools within the retina and thus causing loss of photoreceptor function (Buey et al., 2015). Interestingly however, OCT imaging (unpublished data) of severely affected individuals reveals a remarkably intact outer nuclear retinal layer, indicating that while visual function is lost, photoreceptors appear to remain viable (Fig. 11), thus providing a potentially very robust window of opportunity for therapeutic intervention. These data suggest that suppression of IMPDH in dominant RP10 could result in a restoration of visual function. A number of FDA-approved IMPDH inhibitors (inhibiting both IMPDH1 and 2) are available, including CellCept, Mizorbine and VX-497 and these have been used as

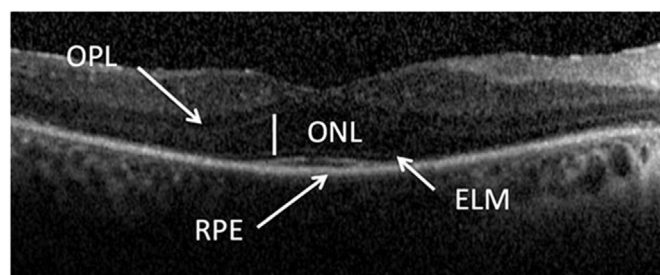


Fig. 11. Preserved outer nuclear layer (ONL) in a patient with the RP10 form of retinitis pigmentosa.

effective immunosuppressive agents (B and T lymphocytes are highly dependent upon the alternative, rather than the salvage pathway of guanine nucleotide biosynthesis). The concept of repositioning such agents as orally-available therapeutics for an IRD, delivery of which could be enhanced (thus reducing systemic dosage) by manipulating ocular endothelial tight junctions is a provocative but potentially realistic concept, dependent on long term tolerability. Given the ease with which systemically-deliverable compounds can access the retina (Fig. 3), tolerable doses may be achievable.

The gene encoding Bestrophin, a calcium-gated chloride channel located in the basolateral region of RPE cells, is mutated in the ciliopathy, autosomal recessive bestrophinopathy (Johnson et al., 2017). Mutated proteins have been shown to mis-localise and end up in proteasomes in the cytoplasm and are degraded (Uggetti et al., 2016). These authors have shown in vitro that proteasomal inhibitors, Bortezomib and 4-phenylbutyrate (4PBA), both approved proteasomal inhibitors, effectively restore the location of mutant bestrophins to the RPE and restore Cl⁻ conductance of the channels in vitro. The Authors comment: "The functional rescue achieved with 4PBA is significant because it suggests that this drug, which is already approved for long-term use in infants and adults, might represent a promising therapy for the treatment of ARB and other bestrophinopathies resulting from missense mutations in BEST1". Again, the degree of enhancement of systemic drug uptake by claudin-5 modulated iBRB could render such compounds (MW 4-PBA 186Da; MW Bortezomib 384Da) systemically tolerable over prolonged periods.

7. Targeting Schlemm's canal endothelial tight junctions: a novel process for enhancement of aqueous outflow through the conventional outflow pathway

Glaucoma in its various forms represents the second most common blinding disease on a global basis after cataract, elevations in IOP being the greatest risk factor (Quigley and Broman, 2006; Tham et al., 2014; Actis et al., 2016). Aqueous humour leaves the eye through the so-called conventional and un-conventional outflow pathways located close together in the periphery of the anterior chamber, at the apex of the narrow angle formed between the iris and the cornea. The conventional outflow pathway comprises the trabecular meshwork, which, as the name suggests, is an interlaced structure of cells embedded in a pressure-responsive ECM through which aqueous flows into the Canal of Schlemm both through paracellular gaps or through cellular pores in the canal's endothelial lining. While a number of genes have been firmly associated with open-angle glaucoma susceptibility, a robust understanding of the molecular pathology of the disease remains to be determined. It should be highlighted, that a balance in the production of matrix metalloproteinases (MMPs) and their tissue inhibitors within the trabecular meshwork is a significant factor in the maintenance of physiological IOP at between 12 and 22 mmHg (De Groef et al., 2013). From the canal, fluid flows through collector channels and eventually into the episcleral veins. Some aqueous also leaves the eye through the bundles of the ciliary muscles – the so-called un-conventional or uveoscleral route. Interestingly, currently used topical medications (including prostaglandin analogues, carbonic anhydrase inhibitors and β -blockers) either slow up aqueous production by the ciliary body, or enhance its clearance via the uveoscleral route, none of these formulations directly and primarily targeting the conventional pathway. Since an appreciable number of those with open angle disease do not respond adequately to currently available pressure-reducing drugs, a large amount of research in recent years has gone into the development of medicines capable of enhancing aqueous outflow through the

conventional route. These include Rho kinase inhibitors (Li et al., 2016; Ren et al., 2016), adenosine receptor agonists (Laties et al., 2016; Myers et al., 2016), marine macrolides (Ethier et al., 2006), prostanoid receptor agonists (Kalouche et al., 2016) and AAV-mediated gene therapies involving enhanced MMP expression to remodel the ECM within the Trabecular meshwork (Spiga and Borrás, 2010; Gerometta et al., 2010; Borrás et al., 2016; O'Callaghan et al., 2017).

The bulk of outflow resistance in the conventional pathway is generated within the juxtacanalicular tissues and the endothelial cells of the canal itself. Aqueous enters Schlemm's canal either through the formation of intra-endothelial fluid-filled vacuoles (so called 'giant' vacuoles) or through the paracellular route, where it passes through pores left between the endothelial tight junctions. Less is known of the nature of the tight junctions joining SC endothelia than those of the cerebral and inner retinal vasculatures. Interestingly claudin-5, a major component of the tight junctions of the cerebral and inner retinal vascular endothelia, is absent from human SC endothelial cells (Tam et al., 2017). However, as outlined earlier, ZO-1, tricellulin and claudin-11 are prominently expressed TJ proteins. In order to explore the hypothesis that down-regulation of SC endothelial TJs might result in an increase in the permeability of the canal, Tam et al. (2017) intracamerally injected siRNA validated against tricellulin and ZO-1 into wild type mice. Injected material followed the natural flow of aqueous through the trabecular meshwork and into the canal's endothelial cells. As illustrated in Fig. 12, transmission electron microscopy revealed reversible opening of the paracellular clefts between endothelial cells as a result of such down-regulation. This was accompanied by a significant elevation in outflow facility in treated eyes *ex vivo*.

In translational terms, a major factor to be considered in this approach is the mode of siRNA delivery. Recent reports have indicated that siRNA can be effectively delivered to the eye in the form of topical drops to the cornea. However, in this approach, while the siRNA (SYLO40012, targeting the β 2-adrenoceptor) was able to efficiently access the ciliary body which was the primary site of action, little siRNA was found in the aqueous humour using this technique (Martinez et al., 2014; Moreno-Montanes et al., 2014). While periodic intracameral injection of siRNA as indicated by IOP is a realistic option, an alternative and less invasive procedure would involve retrograde introduction of siRNA into Schlemm's canal via the episcleral veins and a device facilitating this approach has been manufactured (Retioject Inc, NC). An alternative would be the use of AAV as a delivery vehicle for shRNAs. While single stranded AAV particles will not transfect tissues of the trabecular meshwork, self-complementary AAV have been reported to do so with high efficiency (Buie et al., 2010). However, it is unclear from this work as to whether AAV directly transfects SC endothelial cells. If this can be demonstrated, an AAV expressing shRNAs under the control of a promoter inducible by a topical eye drop could in principle be used. In this regard, it is of interest to note in a recently reported experimental system, that AAV transfecting the corneal endothelium can be activated to express MMP3 via the use of doxycycline applied to the cornea, the enzyme then being secreted from the corneal endothelia in to the TM, where re-modelling of the ECM resulted in increased outflow facility and decreased IOP in wild type mice (O'Callaghan et al., 2017). Since an inducing agent will travel with the natural flow of aqueous toward Schlemm's canal, there is reason to believe that AAVs transfecting SC endothelia could be periodically activated using such a procedure. A combinatorial AAV-mediated approach, targeting ECM remodelling together with incrementing SC permeability, is a realistic possibility based on observations to date.

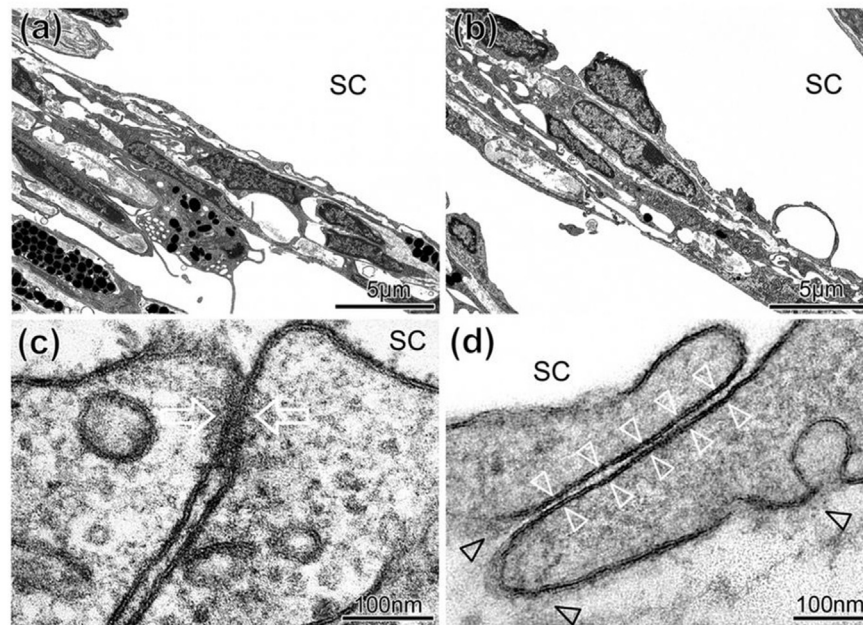


Fig. 12. Representative sagittal sections through the inner wall of Schlemm's canal (SC) and outer trabecular meshwork (TM) of a mouse eye treated with (a) non-targeting (NT) or (b) targeting (T) siRNA illustrating intact cells and an intact and continuous inner wall endothelium that appeared similar in both cases. The inner wall endothelium is connected to the underlying ECM so that no ballooning was visible. (c, d) High magnifications of sagittal sections through intercellular clefts along the inner wall endothelium of SC showing examples for junctions quantitatively evaluated as closed (c) with fusion between the neighbouring cell membranes (arrows) or open clefts (d) where the cell membranes of adjacent endothelial cells were clearly separated along the entire cleft length (white arrowheads). Despite the open clefts, adhesions to sub-endothelial matrix (black arrowheads) were preserved.

This is Figure 6 from our paper Tam et al., Scientific Reports 2017; 7: 40717 (pbl on line Jan 16 2017).

8. Future prospects

Retinal endothelial barrier modulation technologies are, in principle, deployable in a stand-alone sense, or in combination with gene and other molecular therapeutic approaches. There is a significant need for a therapy for one of the more common idiopathic retinopathies, NAION, which is currently incurable and can lead to irreversible blindness. Clearance of oedema from the optic nerve head by intravitreal injection of siRNA targeting claudin-5 could well be effective in this scenario. It is also of note that as yet there are no medicines available for the most common (non-exudative) form of AMD, and yet, clearance of A β , or drug-mediated suppression of oxidative stress within the retina, could have utility in slowing down disease progression in this, and indeed other forms of retinal degeneration including glaucoma. It will also be of interest to assess the efficacies of gene therapy for XL-retinoschisis *vis-à-vis* direct facilitation of fluid egress from intraretinal cysts, perhaps the two approaches, each using AAV could be used in a combinatorial sense. Repositioning approved drugs for use as therapies in early stage IRDs where the iBRB is essentially intact, is an interesting possibility, several scenarios having been outlined, including the possibility of IMPDH1 suppression in the RP10 form of RP and the use of proteasome inhibitors for at least one form of bestrophinopathy, but there will be many other examples based on the very extensive range of molecular pathologies that are involved, low molecular weight drug-mediated inhibition of protein misfolding for example, being one. Improved treatment regimens for open-angle glaucoma continue to be a priority. As outlined, much research is currently being directed toward the development of topical formulations targeting the major (conventional) outflow pathway. The fact that siRNA could periodically be delivered in a retrograde fashion into Schlemm's canal endothelia through the episcleral veins, obviating a requirement for intracameral

inoculation, is an interesting concept which, in principle, could be deployed as an outpatient procedure. In summary, we suggest that direct manipulation of permeability of both the inner retinal microvasculature and the Canal of Schlemm, may have significant potential clinical utility.

Acknowledgement

We thank Blanca Garcia Sandoval and Carmen Ayuso for provision of unpublished OCT images of RP10; Matthew Lawrence for provision of dissected primate tissues from the optic nerve head and David Keegan for OCT and fundus images of NAION and XL-retinoschisis. Research on modulation of permeability at the blood-brain and inner blood-retina barriers has been supported by grants from the Wellcome Trust, Science Foundation Ireland, the Health Research Board of Ireland, Enterprise Ireland, Bright Focus Foundation and the US Department of Defense. Studies on enhancement of aqueous outflow by modulation of permeability at SC endothelia is supported by the European Research Council (ERC-2012-AdG 322656-Oculus). Primate studies on claudin-5 suppression were supported by the St. Kitt's Medical Research Foundation.

References

- Abbott, N.J., Patabendige, A.A., Dolman, D.E., Yusof, S.R., Begley, D.J., 2010. Structure and function of the blood-brain barrier. *Neurobiol. Dis.* 37, 13–25.
- Actis, A.G., Versino, E., Brogliatti, B., Rolle, T., 2016. Risk factors for primary open angle glaucoma (POAG) progression: a study ruled in Torino. *Open Ophthalmol. J.* 10, 129–139.
- Aherne, A., Kennan, A., Kenna, P.F., McNally, N., Lloyd, D.G., Alberts, I.L., Kiang, A.S., Humphries, M.M., Ayuso, C., Engel, P.C., Gu, J.J., Mitchell, B.S., Farrar, G.J., Humphries, P., 2004. On the molecular pathology of neurodegeneration in IMPDH1-based retinitis pigmentosa. *Hum. Mol. Genet.* 13, 641–650.
- Aleman, T.S., Duncan, J.L., Bieber, M.L., de Castro, E., Marks, D.A., Gardner, L.M., Steinberg, J.D., Cideciyan, A.V., Maguire, M.G., Jacobson, S.G., 2001. Macular pigment and lutein supplementation in retinitis pigmentosa and Usher

- syndrome. *Invest Ophthalmol. Vis. Sci.* 42, 1873–1881.
- Anderson, J.M., Van Itallie, C.M., 2008. Tight junctions. *Curr. Biol.* 18, R941–R943.
- Anderson, D.H., Talaga, K.C., Rivest, A.J., Barron, E., Hageman, G.S., Johnson, L.V., 2004. Characterization of beta amyloid assemblies in drusen: the deposits associated with aging and age-related macular degeneration. *Exp. Eye Res.* 78, 243–256.
- Ben-Yosef, T., Belyantseva, I.A., Saunders, T.L., Hughes, E.D., Kawamoto, K., Van Itallie, C.M., Beyer, L.A., Halsey, K., Gardner, D.J., Wilcox, E.R., Rasmussen, J., Anderson, J.M., Dolan, D.F., Forge, A., Raphael, Y., Camper, S.A., Friedman, T.B., 2003. Claudin 14 knockout mice, a model for autosomal recessive deafness DFNB29, are deaf due to cochlear hair cell degeneration. *Hum. Mol. Genet.* 12, 2049–2061. [Epub 2003/08/13](#).
- Bhatt, K., Gong, H., Freddo, T.F., 1995. Freeze-fracture studies of interendothelial junctions in the angle of the human eye. *Invest Ophthalmol. Vis. Sci.* 36, 1379–1389.
- Borras, T., Buie, L.K., Spiga, M.G., 2016. Inducible scAAV2.GRE.MMP1 lowers IOP long-term in a large animal model for steroid-induced glaucoma gene therapy. *Gene Ther.* 23, 438–449.
- Buey, R.M., Ledesma-Amaro, R., Velazquez-Campoy, A., Balsera, M., Chagoyen, M., de Pereda, J.M., Revuelta, J.L., 2015. Guanine nucleotide binding to the Bateman domain mediates the allosteric inhibition of eukaryotic IMP dehydrogenases. *Nat. Commun.* 6, 8923.
- Buie, L.K., Rasmussen, C.A., Porterfield, E.C., Ramgolam, V.S., Choi, V.W., Markovic-Plese, S., Samulski, R.J., Kaufman, P.L., Borras, T., 2010. Self-complementary AAV virus (scAAV) safe and long-term gene transfer in the trabecular meshwork of living rats and monkeys. *Invest Ophthalmol. Vis. Sci.* 51, 236–248.
- Bush, R.A., Zeng, Y., Colosi, P., Kjellstrom, S., Hiriyanna, S., Vijayarathay, C., Santos, M., Li, J., Wu, Z., Sieving, P.A., 2016. Preclinical dose-escalation study of intravitreal AAV-RS1 gene therapy in a mouse model of X-linked retinoschisis: dose-dependent expression and improved retinal structure and function. *Hum. Gene Ther.* 27, 376–389.
- Byrne, L.C., Ozturk, B.E., Lee, T., Fortuny, C., Visel, M., Dalkara, D., Schaffer, D.V., Flannery, J.G., 2014. Retinoschisis gene therapy in photoreceptors, Muller glia or all retinal cells in the Rs1h^{-/-} mouse. *Gene Ther.* 21, 585–592.
- Campbell, M., Humphries, P., 2012. The blood-retina barrier: tight junctions and barrier modulation. *Adv. Exp. Med. Biol.* 763, 70–84.
- Campbell, M., Kiang, A.S., Kenna, P.F., Kerskens, C., Blau, C., O'Dwyer, L., Tivnan, A., Kelly, J.A., Brankin, B., Farrar, G.J., Humphries, P., 2008. RNAi-mediated reversible opening of the blood-brain barrier. *J. Gene Med.* 10, 930–947.
- Campbell, M., Nguyen, A.T., Kiang, A.S., Tam, L.C., Gobbo, O.L., Kerskens, C., Ni Dhubbghaill, S., Humphries, M.M., Farrar, G.J., Kenna, P.F., Humphries, P., 2009. An experimental platform for systemic drug delivery to the retina. *Proc. Natl. Acad. Sci. U. S. A.* 106, 17817–17822.
- Campbell, M., Humphries, M.M., Kiang, A.S., Nguyen, A.T., Gobbo, O.L., Tam, L.C., Suzuki, M., Hanrahan, F., Ozaki, E., Farrar, G.J., Kenna, P.F., Humphries, P., 2011. Systemic low-molecular weight drug delivery to pre-selected neuronal regions. *EMBO Mol. Med.* 3, 235–245.
- Campbell, M., Hanrahan, F., Gobbo, O.L., Kelly, M.E., Kiang, A.S., Humphries, M.M., Nguyen, A.T., Ozaki, E., Keane, J., Blau, C.W., Kerskens, C.M., Cahalan, S.D., Callanan, J.J., Wallace, E., Grant, G.A., Doherty, C.P., Humphries, P., 2012. Targeted suppression of claudin-5 decreases cerebral oedema and improves cognitive outcome following traumatic brain injury. *Nat. Commun.* 3, 849.
- Dalkara, D., Byrne, L.C., Klimczak, R.R., Visel, M., Yin, L., Merigan, W.H., Flannery, J.G., Schaffer, D.V., 2013. In vivo directed evolution of a new adeno-associated virus for therapeutic outer retinal gene delivery from the vitreous. *Sci. Transl. Med.* 5, 189ra76.
- De Groef, L., Van Hove, L., Dekeyser, E., Stalmans, I., Moons, L., 2013. MMPs in the trabecular meshwork: promising targets for future glaucoma therapies? *Invest Ophthalmol. Vis. Sci.* 54, 7756–7763.
- Dentchev, T., Milam, A.H., Lee, V.M., Trojanowski, J.Q., Dunaief, J.L., 2003. Amyloid-beta is found in drusen from some age-related macular degeneration retinas, but not in drusen from normal retinas. *Mol. Vis.* 9, 184–190.
- Ding, J.D., Johnson, L.V., Herrmann, R., Farsi, S., Smith, S.G., Groelle, M., Mace, B.E., Sullivan, P., Jamison, J.A., Kelly, U., Harrabi, O., Bollini, S.S., Dilley, J., Kobayashi, D., Kuang, B., Li, W., Pons, J., Lin, J.C., Bowes Rickman, C., 2011. Anti-amyloid therapy protects against retinal pigmented epithelium damage and vision loss in a model of age-related macular degeneration. *Proc. Natl. Acad. Sci. U. S. A.* 108, E279–E287.
- Epstein, D.L., Rohen, J.W., 1991. Morphology of the trabecular meshwork and inner-wall endothelium after cationized ferritin perfusion in the monkey eye. *Invest Ophthalmol. Vis. Sci.* 32, 160–171.
- Ethier, C.R., Read, A.T., Chan, D.W., 2006. Effects of latrunculin-B on outflow facility and trabecular meshwork structure in human eyes. *Invest Ophthalmol. Vis. Sci.* 47, 1991–1998.
- Fujimoto, K., 1995. Freeze-fracture replica electron microscopy combined with SDS digestion for cytochemical labeling of integral membrane proteins. Application to the immunogold labeling of intercellular junctional complexes. *J. Cell Sci.* 108 (Pt 11), 3443–3449.
- Furuse, M., Tsukita, S., 2006. Claudins in occluding junctions of humans and flies. *Trends Cell Biol.* 16, 181–188.
- Gerometta, R., Spiga, M.G., Borras, T., Candia, O.A., 2010. Treatment of sheep steroid-induced ocular hypertension with a glucocorticoid-inducible MMP1 gene therapy virus. *Invest Ophthalmol. Vis. Sci.* 51, 3042–3048.
- Gerth, C., Zawadzki, R.J., Werner, J.S., Heon, E., 2008. Retinal morphological changes of patients with X-linked retinoschisis evaluated by Fourier-domain optical coherence tomography. *Arch. Ophthalmol.* 126, 807–811.
- Gregori, N.Z., Berruol, A.M., Gregori, G., Murray, T.G., Knighton, R.W., Flynn Jr., H.W., Dubovy, S., Puliafito, C.A., Rosenfeld, P.J., 2009. Macular spectral-domain optical coherence tomography in patients with X linked retinoschisis. *Br. J. Ophthalmol.* 93, 373–378.
- Gupta, V., Gupta, V.B., Chitranshi, N., Gangoda, S., Vander Wall, R., Abbasi, M., Golzan, M., Dheer, Y., Shah, T., Avolio, A., Chung, R., Martins, R., Graham, S., 2016. One protein, multiple pathologies: multifaceted involvement of amyloid beta in neurodegenerative disorders of the brain and retina. *Cell Mol. Life Sci.* 73, 4279–4297.
- Hadj-Rabia, S., Baala, L., Vabres, P., Hamel-Teillac, D., Jacquemin, E., Fabre, M., Lyonnet, S., De Prost, Y., Munnich, A., Hadchouel, M., Smahi, A., 2004. Claudin-1 gene mutations in neonatal sclerosing cholangitis associated with ichthyosis: a tight junction disease. *Gastroenterology* 127, 1386–1390.
- Hamazaki, Y., Itoh, M., Sasaki, H., Furuse, M., Tsukita, S., 2002. Multi-PDZ domain protein 1 (MUPP1) is concentrated at tight junctions through its possible interaction with claudin-1 and junctional adhesion molecule. *J. Biol. Chem.* 277, 455–461.
- Hawkins, B.T., Davis, T.P., 2005. The blood-brain barrier/neurovascular unit in health and disease. *Pharmacol. Rev.* 57, 173–185.
- Hayreh, S.S., 2013. Ischemic optic neuropathies - where are we now? *Graefes Arch. Clin. Exp. Ophthalmol.* 251, 1873–1884.
- Hayreh, S.S., 2014. Ocular vascular occlusive disorders: natural history of visual outcome. *Prog. Retin Eye Res.* 41, 1–25.
- Itoh, M., Furuse, M., Morita, K., Kubota, K., Saitou, M., Tsukita, S., 1999. Direct binding of three tight junction-associated MAGUKs, ZO-1, ZO-2, and ZO-3, with the COOH termini of claudins. *J. Cell Biol.* 147, 1351–1363.
- Janciauskiene, K., Krakau, T., 2001. Alzheimer's peptide: a possible link between glaucoma, exfoliation syndrome and Alzheimer's disease. *Acta Ophthalmol. Scand.* 79, 328–329.
- Jane Farrar, G., Carrigan, M., Dockery, A., Millington Ward, S., Palfi, A., Chadderton, N., Humphries, M., Kiang, A.S., Kenna, P.F., Humphries, P., 2017 Aug 1. Toward an elucidation of the molecular genetics of inherited retinal degenerations. *Hum. Mol. Genet.* 26 (R1), R2–R11.
- Johnson, M., 2006. 'What controls aqueous humour outflow resistance?'. *Exp. Eye Res.* 82, 545–557.
- Johnson, L.V., Leitner, W.P., Rivest, A.J., Staples, M.K., Radeke, M.J., Anderson, D.H., 2002. The Alzheimer's A beta -peptide is deposited at sites of complement activation in pathologic deposits associated with aging and age-related macular degeneration. *Proc. Natl. Acad. Sci. U. S. A.* 99, 11830–11835.
- Johnson, A.A., Guziewicz, K.E., Lee, C.J., Kalathur, R.C., Pulido, J.S., Marmorstein, L.Y., Marmorstein, A.D., 2017. Bestrophin 1 and retinal disease. *Prog. Retin Eye Res.* 58, 45–69.
- Jordan, S.A., Farrar, G.J., Kenna, P., Humphries, M.M., Sheils, D.M., Kumar-Singh, R., Sharp, E.M., Soriano, N., Ayuso, C., Benitez, J., et al., 1993. Localization of an autosomal dominant retinitis pigmentosa gene to chromosome 7q. *Nat. Genet.* 4, 54–58.
- Kalouche, G., Beguier, F., Bakria, M., Melik-Parsadaniantz, S., Leriche, C., Debeir, T., Rostene, W., Baudouin, C., Vige, X., 2016. Activation of prostaglandin FP and EP2 receptors differently modulates myofibroblast transition in a model of adult primary human trabecular meshwork cells. *Invest Ophthalmol. Vis. Sci.* 57, 1816–1825.
- Kass, M.A., Heuer, D.K., Higginbotham, E.J., Johnson, C.A., Keltner, J.L., Miller, J.P., Parrish 2nd, R.K., Wilson, M.R., Gordon, M.O., 2002. The Ocular Hypertension Treatment Study: a randomized trial determines that topical ocular hypotensive medication delays or prevents the onset of primary open-angle glaucoma. *Arch. Ophthalmol.* 120 (701–13), 829–830 discussion.
- Keane, J., Walsh, D.M., O'Malley, T., Hudson, N., Crosbie, D.E., Loftus, T., Sheehan, F., McDaid, J., Humphries, M.M., Callanan, J.J., Brett, F.M., Farrell, M.A., Humphries, P., Campbell, M., 2015. Autoregulated paracellular clearance of amyloid-beta across the blood-brain barrier. *Sci. Adv.* 1, e1500472.
- Kennan, A., Aherne, A., Palfi, A., Humphries, M., McKee, A., Stitt, A., Simpson, D.A., Demtrodter, K., Orntoft, T., Ayuso, C., Kenna, P.F., Farrar, G.J., Humphries, P., 2002. Identification of an IMPDH1 mutation in autosomal dominant retinitis pigmentosa (RP10) revealed following comparative microarray analysis of transcripts derived from retinas of wild-type and Rho(-/-) mice. *Hum. Mol. Genet.* 11, 547–557.
- Kiang, A.S., Humphries, M.M., Campbell, M., Humphries, P., 2014. Antioxidant therapy for retinal disease. *Adv. Exp. Med. Biol.* 801, 783–789.
- Kitajiri, S., Miyamoto, T., Mineharu, A., Sonoda, N., Furuse, K., Hata, M., Sasaki, H., Mori, Y., Kubota, T., Ito, J., Furuse, M., Tsukita, S., 2004. Compartmentalization established by claudin-11-based tight junctions in stria vascularis is required for hearing through generation of endocochlear potential. *J. Cell Sci.* 117, 5087–5096.
- Laties, A., Rich, C.C., Stoltz, R., Humbert, V., Brickman, C., McVicar, W., Baumgartner, R.A., 2016. A randomized phase 1 dose escalation study to evaluate safety, tolerability, and pharmacokinetics of trabadenosin in healthy adult volunteers. *J. Ocul. Pharmacol. Ther.* 32, 548–554.
- Li, G., Mukherjee, D., Navarro, I., Ashpole, N.E., Sherwood, J.M., Chang, J., Overby, D.R., Yuan, F., Gonzalez, P., Kopczyński, C.C., Farsi, S., Stamer, W.D., 2016. Visualization of conventional outflow tissue responses to netarsudil in living mouse eyes. *Eur. J. Pharmacol.* 787, 20–31.
- Li, B., Vachali, P.P., Shen, Z., Gorusupudi, A., Nelson, K., Besch, B.M., Bartschi, A., Longo, S., Mattinson, T., Shihab, S., Polyakov, N.E., Suntsova, L.P., Dushkin, A.V., Bernstein, P.S., 2017. Retinal accumulation of zeaxanthin, lutein, and beta-

- carotene in mice deficient in carotenoid cleavage enzymes. *Exp. Eye Res.* 159, 123–131.
- Liu, R., Wang, T., Zhang, B., Qin, L., Wu, C., Li, Q., Ma, L., 2014. Lutein and zeaxanthin supplementation and association with visual function in age-related macular degeneration. *Invest. Ophthalmol. Vis. Sci.* 56, 252–258.
- Liu, C., Cao, L., Yang, S., Xu, L., Liu, P., Wang, F., Xu, D., 2015. Subretinal injection of amyloid-beta peptide accelerates RPE cell senescence and retinal degeneration. *Int. J. Mol. Med.* 35, 169–176.
- Ma, L., Dou, H.L., Huang, Y.M., Lu, X.R., Xu, X.R., Qian, F., Zou, Z.Y., Pang, H.L., Dong, P.C., Xiao, X., Wang, X., Sun, T.T., Lin, X.M., 2012. Improvement of retinal function in early age-related macular degeneration after lutein and zeaxanthin supplementation: a randomized, double-masked, placebo-controlled trial. *Am. J. Ophthalmol.* 154, 625–634 e1.
- Martinez, T., Gonzalez, M.V., Roehl, I., Wright, N., Paneda, C., Jimenez, A.I., 2014. In vitro and in vivo efficacy of SYLO40012, a novel siRNA compound for treatment of glaucoma. *Mol. Ther.* 22, 81–91.
- Molday, R.S., Kellner, U., Weber, B.H., 2012. X-linked juvenile retinoschisis: clinical diagnosis, genetic analysis, and molecular mechanisms. *Prog. Retin Eye Res.* 31, 195–212.
- Moreno-Montanes, J., Sadaba, B., Ruz, V., Gomez-Guiu, A., Zarranz, J., Gonzalez, M.V., Paneda, C., Jimenez, A.I., 2014. Phase I clinical trial of SYLO40012, a small interfering RNA targeting beta-adrenergic receptor 2, for lowering intraocular pressure. *Mol. Ther.* 22, 226–232.
- Morita, K., Sasaki, H., Furuse, M., Tsukita, S., 1999. Endothelial claudin: claudin-5/TMVC constitutes tight junction strands in endothelial cells. *J. Cell Biol.* 147, 185–194.
- Myers, J.S., Sall, K.N., DuBiner, H., Slomowitz, N., McVicar, W., Rich, C.C., Baumgartner, R.A., 2016. A dose-escalation study to evaluate the safety, tolerability, pharmacokinetics, and efficacy of 2 and 4 Weeks of twice-daily ocular trabendosin in adults with ocular hypertension or primary open-angle glaucoma. *J. Ocul. Pharmacol. Ther.* 32, 555–562.
- Noecker, R.S., Dirks, M.S., Choplin, N.T., Bernstein, P., Batoosingh, A.L., Whitcup, S.M., 2003. Bimatoprost/Latanoprost Study G. A six-month randomized clinical trial comparing the intraocular pressure-lowering efficacy of bimatoprost and latanoprost in patients with ocular hypertension or glaucoma. *Am. J. Ophthalmol.* 135, 55–63.
- O'Callaghan, J., Crosbie, D.E., Cassidy, P.S., Sherwood, J.M., Flugel-Koch, C., Lutjen-Drecoll, E., Humphries, M.M., Reina-Torres, E., Wallace, D., Kiang, A.S., Campbell, M., Stamer, W.D., Overby, D.R., O'Brien, C., Tam, L.C.S., Humphries, P., 2017. Therapeutic potential of AAV-mediated MMP-3 secretion from corneal endothelium in treating glaucoma. *Hum. Mol. Genet.* 26, 1230–1246.
- Ott, M., Gogvadze, V., Orrenius, S., Zhivotovskiy, B., 2007. Mitochondria, oxidative stress and cell death. *Apoptosis* 12, 913–922.
- Perche, O., Doly, M., Ranchon-Cole, I., 2007. Caspase-dependent apoptosis in light-induced retinal degeneration. *Invest. Ophthalmol. Vis. Sci.* 48, 2753–2759.
- Quigley, H.A., Broman, A.T., 2006. The number of people with glaucoma worldwide in 2010 and 2020. *Br. J. Ophthalmol.* 90, 262–267.
- Raviola, G., Raviola, E., 1981. Paracellular route of aqueous outflow in the trabecular meshwork and canal of Schlemm. A freeze-fracture study of the endothelial junctions in the sclerocorneal angle of the macaque monkey eye. *Invest. Ophthalmol. Vis. Sci.* 21, 52–72.
- Ren, R., Li, G., Le, T.D., Kocpczynski, C., Stamer, W.D., Gong, H., 2016. Netarsudil increases outflow facility in human eyes through multiple mechanisms. *Invest. Ophthalmol. Vis. Sci.* 57, 6197–6209.
- Scherer, W.J., 2002. A retrospective review of non-responders to latanoprost. *J. Ocul. Pharmacol. Ther.* 18, 287–291.
- Schneeberger, E.E., Karnovsky, M.J., 1976. Substructure of intercellular junctions in freeze-fractured alveolar-capillary membranes of mouse lung. *Circ. Res.* 38, 404–411.
- Simon, D.B., Lu, Y., Choate, K.A., Velazquez, H., Al-Sabban, E., Praga, M., Casari, G., Bettinelli, A., Colussi, G., Rodriguez-Soriano, J., McCredie, D., Milford, D., Sanjad, S., Lifton, R.P., 1999. Paracellin-1, a renal tight junction protein required for paracellular Mg²⁺ resorption. *Science* 285, 103–106.
- Sit, A.J., Coloma, F.M., Ethier, C.R., Johnson, M., 1997. Factors affecting the pores of the inner wall endothelium of Schlemm's canal. *Invest. Ophthalmol. Vis. Sci.* 38, 1517–1525.
- Spiga, M.G., Borrás, T., 2010. Development of a gene therapy virus with a glucocorticoid-inducible MMP1 for the treatment of steroid glaucoma. *Invest. Ophthalmol. Vis. Sci.* 51, 3029–3041.
- Stamer, W.D., Clark, A.F., 2017. The many faces of the trabecular meshwork cell. *Exp. Eye Res.* 158, 112–123.
- Taddei, A., Giampietro, C., Conti, A., Orsenigo, F., Breviario, F., Pirazzoli, V., Potente, M., Daly, C., Dimmeler, S., Dejana, E., 2008. Endothelial adherens junctions control tight junctions by VE-cadherin-mediated upregulation of claudin-5. *Nat. Cell Biol.* 10, 923–934.
- Tam, L.C., Reina-Torres, E., Sherwood, J.M., Cassidy, P.S., Crosbie, D.E., Lutjen-Drecoll, E., Flugel-Koch, C., Perkumas, K., Humphries, M.M., Kiang, A.S., O'Callaghan, J., Callanan, J.J., Read, A.T., Ethier, C.R., O'Brien, C., Lawrence, M., Campbell, M., Stamer, W.D., Overby, D.R., Humphries, P., 2017. Enhancement of outflow facility in the murine eye by targeting selected tight-junctions of Schlemm's canal endothelium. *Sci. Rep.* 7, 40717.
- Tham, Y.C., Li, X., Wong, T.Y., Quigley, H.A., Aung, T., Cheng, C.Y., 2014. Global prevalence of glaucoma and projections of glaucoma burden through 2040: a systematic review and meta-analysis. *Ophthalmology* 121, 2081–2090.
- Turksen, K., Troy, T.C., 2001. Claudin-6: a novel tight junction molecule is developmentally regulated in mouse embryonic epithelium. *Dev. Dyn.* 222, 292–300.
- Uggetti, C., Briant, K., Streit, A.K., Thomson, S., Koay, Y.H., Baines, R.A., Swanton, E., Manson, F.D., 2016. Restoration of mutant bestrophin-1 expression, localisation and function in a polarised epithelial cell model. *Dis. Model Mech.* 9, 1317–1328.
- Van Itallie, C.M., Anderson, J.M., 2004. The molecular physiology of tight junction pores. *Physiol. (Bethesda)* 19, 331–338.
- Van Itallie, C.M., Colegio, O.R., Anderson, J.M., 2004. The cytoplasmic tails of claudins can influence tight junction barrier properties through effects on protein stability. *J. Membr. Biol.* 199, 29–38. Epub 2004/09/16.
- Van Itallie, C.M., Gambling, T.M., Carson, J.L., Anderson, J.M., 2005. Palmitoylation of claudins is required for efficient tight-junction localization. *J. Cell Sci.* 118, 1427–1436. Epub 2005/03/17.
- Vegge, T., 1967. The fine structure of the trabeculum cribriforme and the inner wall of Schlemm's canal in the normal human eye. *Z. Zellforsch. Mikrosk. Anat.* 77, 267–281.
- Vijayasathya, C., Ziccardi, L., Sieving, P.A., 2012. Biology of retinoschisin. *Adv. Exp. Med. Biol.* 723, 513–518.
- Weismann, D., Hartvigsen, K., Lauer, N., Bennett, K.L., Scholl, H.P., Charbel Issa, P., Cano, M., Brandstatter, H., Tsimikas, S., Skerka, C., Superti-Furga, G., Handa, J.T., Zipfel, P.F., Witztum, J.L., Binder, C.J., 2011. Complement factor H binds malondialdehyde epitopes and protects from oxidative stress. *Nature* 478, 76–81.
- Whitehead, A.J., Mares, J.A., Danis, R.P., 2006. Macular pigment: a review of current knowledge. *Arch. Ophthalmol.* 124, 1038–1045.
- Xun, Z., Rivera-Sanchez, S., Ayala-Pena, S., Lim, J., Budworth, H., Skoda, E.M., Robbins, P.D., Niedernhofer, L.J., Wipf, P., McMurray, C.T., 2012. Targeting of XJB-5-131 to mitochondria suppresses oxidative DNA damage and motor decline in a mouse model of Huntington's disease. *Cell Rep.* 2, 1137–1142.
- Yamauchi, K., Rai, T., Kobayashi, K., Sahara, E., Suzuki, T., Itoh, T., Suda, S., Hayama, A., Sasaki, S., Uchida, S., 2004. Disease-causing mutant WNK4 increases paracellular chloride permeability and phosphorylates claudins. *Proc. Natl. Acad. Sci. U. S. A.* 101, 4690–4694.
- Ye, W., Gong, H., Sit, A., Johnson, M., Freddo, T.F., 1997. Interendothelial junctions in normal human Schlemm's canal respond to changes in pressure. *Invest. Ophthalmol. Vis. Sci.* 38, 2460–2468.
- Yu, J., Ni, Y., Keane, P.A., Jiang, C., Wang, W., Xu, G., 2010. Foveomacular schisis in juvenile X-linked retinoschisis: an optical coherence tomography study. *Am. J. Ophthalmol.* 149, 973–978 e2.
- Zeng, Y., Takada, Y., Kjellstrom, S., Hiriyanna, K., Tanikawa, A., Wawrousek, E., Smaoui, N., Caruso, R., Bush, R.A., Sieving, P.A., 2004. RS-1 gene delivery to an adult Rs1h knockout mouse model restores ERG b-wave with reversal of the electronegative waveform of X-linked retinoschisis. *Invest. Ophthalmol. Vis. Sci.* 45, 3279–3285.
- Zhang, L., Reyes, R., Lee, W., Chen, C.L., Chan, L., Sujirakul, T., Chang, S., Tsang, S.H., 2015. Rapid resolution of retinoschisis with acetazolamide. *Doc. Ophthalmol.* 131, 63–70.
- Zode, G.S., Kuehn, M.H., Nishimura, D.Y., Searby, C.C., Mohan, K., Grozdanic, S.D., Bugge, K., Anderson, M.G., Clark, A.F., Stone, E.M., Sheffield, V.C., 2011. Reduction of ER stress via a chemical chaperone prevents disease phenotypes in a mouse model of primary open angle glaucoma. *J. Clin. Invest.* 121, 3542–3553.